Impacts of climate change on water resources of global dams

Van Soesbergen, Arnout

Awarding institution:
King's College London

Impacts of climate change on water resources of global dams

By

Arnout Johannes Jacobus van Soesbergen

April 2013

A thesis submitted to King's College London
for the degree of Doctor of Philosophy

Department of Geography
King's College London

"When archaeologists from some other planet sift through the bleached bones of our civilization, they may well conclude that our temples were dams. Imponderably massive, constructed with exquisite care, our dams will outlast anything else we have built – skyscrapers, cathedrals, bridges, even nuclear power plants. When forests push through the rotting streets of New York and the Empire State Building is a crumbling hulk, Hoover Dam will still sit astride the Colorado River much as it does today – intact, formidable, serene.

The permeance of our dams will merely impress the archaeologists, their numbers will leave them in awe. ..."

Risner, M. 1993 Cadillac Desert: The American West and its Disappearing Water. Penguin, New York, chapter 3, p.104

Abstract

This thesis aims to assess the effects of climate change mediated through the watersheds of global dams on water resources delivered to those dams. Dams and reservoirs play an important role in social and economic development contributing water for 12-16% of global food production and providing around 20% of the world's energy supply through hydropower. The first part of this research has been dedicated to the further development of the first global geo-referenced database of dams (KCL GOOD^2) that allows for modelling the impacts of land use and climate changes on water supplies. More than 36,000 dams were identified in a collaborative effort using an open source database (GEOWIKI) and Google Earth. This database was then used to extract all individual dam watersheds. These watersheds combined make up around 18% of global land mass which means that impacts of climate change can have profound impacts on the water resources delivered to dams.

By combining the calculated watersheds of dams with climate model projections from the IPCC AR4, changes in the water balance in the catchments of these dams were calculated and changes in reservoir water level were estimated for a range of large dams. The AguaAndes/WaterWorld spatial hydrological model using a multi-GCM scenario was then applied to three case study dams in different climate regions around the world to evaluate directional changes in water and sediment supply. Sensitivity to climate and land cover changes of the basins containing the dams was assessed by running the model for a range of scenarios.

The final part of this thesis describes the application of the AguaAndes/WaterWorld model to the Santa basin in Peru to assess the impacts of climate change on a small hydroelectric plant using several multi-GCM scenarios to address uncertainty in the projections.

Acknowledgments

Even though it feels like it sometimes, writing a thesis is not something you do all by yourself. I could not have done it without the help of many people. So I would like to take this opportunity to thank a number of people (and groups of people) in particular. Firstly, I would like to acknowledge my supervisor, dr. Mark Mulligan who nearly five years ago pointed me to the topic of dams and the existing knowledge (and data) gap. With the dam database turning into a damned database many times, Mark was always there to help out and resolve issues. I am very grateful for his guidance, patience and support throughout the course of my PhD as well as for his resourcefulness in finding financial support to fund this study.

That brings me to my next round of acknowledgments. I would like to thank Google.org for their generous grant that kept me going in the first 2 years. Also many thanks to CPWF COMPANDES that provided me with funding as well as the opportunity to be part of a really interesting project. The trip to the Andes is not one that I will forget easily and gave me an on the ground insight into the problems with sharing water resources.

I would also like to thank the department of Geography at King's for giving me the opportunity to top up my funding and gain experience as a teaching assistant. I learned a lot helping out on various courses and it made me feel very included in the department.

Many thanks also to the PhD community at King's. From day one I have felt included and throughout the last 4 years I have gained many friends. It has been a pleasure to be involved and helping out with organising coffee mornings, Christmas and summer parties, seminars and other events. In particular and at the risk of offending people for leaving them out I'd like to acknowledge Tom, Duick, Fabian, Faith, Briony, Kate, Leo Z and 'Team A' for their friendship and support.

I also like to thank my friends back home in The Netherlands who haven't forgotten about me since moving to the UK and who have been (and continue to be) a huge support to me even though I don't see them as often as I'd like to.

My biggest thank you goes out to my wonderful family and in particular my parents. Mum, dad, thank you for always being there for me and encouraging and supporting me to continue with my education. Without your help I wouldn't have been able to finish this thesis. Thanks also to my brothers and sister who have always been a great support to me.

Last but definitely not least I like to thank Trish. You have been a massive support to me, particularly these last few months when the deadline was approaching fast. Thanks for your encouragement and patience.

Abbreviations

AET	- Actual Evapo-Transpiration
AOGCM	- Atmosphere Ocean General Circulation Model
ASCII	- American Standard Code for Information Interchange
AR4	- IPCC 4th Assessment Report
CGIAR	- Consultative Group on International Agricultural Research
CIAT	- International Center for Tropical Agriculture
CIESIN	- Center for International Earth Science Information Network
COV	- Coefficient Of Variation
CPWF	- Challenge Program on Water and Food
DEM	- Digital Elevation Model
ESRI	- Environmental Systems Research Institute
FAO	- Food and Agriculture Organization
FEMA	- Federal Emergency Management Agency (USA)
FIESTA	- Fog Interception for the Enhancement of Streamflow in Tropical Areas
GCM	- General Circulation Model
GDP	- Gross Domestic Product
GIS	- Geographical Information System
GLOF	- Glacial Lake Outburst Flood
GLWD	- Global Lakes and Wetland Database
GRAnD	- Global Reservoir and Dam database
GRDC	- Global Runoff Data Centre
HEP	- Hydro-Electric Power
HydroSHEDS	-Hydrological data and maps based on SHuttle Elevation Derivatives at multiple Scales
ICOLD	- International Panel on Climate Change
IPCC	- International Panel on Climate Change
IPCC DDC	- Data Distribution Centre of the IPCC
ITCZ	- Intertropical Convergence Zone

KCL GOOD^2 - Kings College London GlObal geO-referenced Database of Dams

KCL GTDD - Kings College London Geo-referenced Tropical Dams Database

KML - Keyhole Markup Language

LAI - Leaf Area Index

LDD - Local Drain Direction

LANDSAT ETM+ - LANDSAT Enhanced Thematic Mapper Plus

LANDSAT MSS - LANDSAT Multi Spectral Scanner

LANDSAT TM - LANDSAT Thematic Mapper

MASL - Metres Above Sea Level

MODIS - MODerate resolution Imaging Spectroradiometer

MRC - Mekong River Commission

NID - National Inventory of Dams (USA)

NOAA - National Oceanic and Atmospheric Administration (USA)

PE - Potential Evapotranspiration

PET - Potential Evapo-Transpiration

RCM - Regional Climate Model

RCP - Representative Concentration Pathways

SD - Standard Deviation

SPOT - Système Pour l'Observation de la Terre

SRES - Special Report on Emission Scenarios

SRTM - Shuttle Radio Topography Mission

STARDEX - Statistical and Regional Dynamical Downscaling of EXtremes for European regions

SWBD - SRTM Water Body Dataset

TRMM - Tropical Rainfall Measuring Mission

USACE - United States Army Corps of Engineers

VCF - Vegetation Continuous Fields

VUA - VU University Amsterdam

WCD - World Commission on Dams

Table of contents

List of figures

Chapter 2 Background

Chapter 3: Development of a geo-referenced global database of dams

Chapter 4 Climate change impacts on global catchments of dams

Chapter 5 Hydrological impacts of climate change on large dam catchments

Chapter 6 Case study basins sensitivity analysis using AguaAndes/WaterWorld

List of tables

Chapter 6 Case study basins sensitivity analysis using AguaAndes/WaterWorld

Chapter 7 Impacts of climate change on Cañón del Pato HEP station, Santa basin, Peru

1. Research goals and objectives

1.1. Introduction to research problem

Dams and their reservoirs play an important role in social and economic development as they supply water, generate energy, and provide security and consumption needs. Half of the world's large dams were built primarily for irrigation and are estimated to contribute water for 12-16% of global food production. Furthermore, 19% of the world's energy supply is provided by hydropower plants (World Commission on Dams, 2000). The total capacity of artificial storage by dams is estimated to be around 7200 km^3, which is twice the global annual fresh water withdrawal (Oki and Kanae, 2006). In contrast, the global contribution of groundwater to freshwater resources is estimated at 734 km^3 (Wada et al., 2010) and desalination from salt water at 14.6 km^3 (Schiermeier, 2008).

However, dams also cause serious damage to freshwater ecosystems, affecting both nature and people. The construction of dams and reservoirs disconnects floodplains and wetlands and requires large areas of land to be flooded with associated losses of agricultural land and displacements of communities. For instance, the Three Gorges Dam Project in China alone has an official displacement figure of up to 1.2 million people (WWF, 2004). Due to increased demands for energy, water storage and flood control, especially in developing countries, more and larger dams are being constructed, often in a single basin. For example, nearly 50 dams are being planned or constructed on the Yangtze River in China and 29 on the La Plata River Basin in South America (WWF, 2004; Reidy Liermann, 2007).

Effects of a changing climate on dams can lead to a range of environmental and socio-economic impacts. The reliability of reservoirs will be affected by changes in river inflows and lake evaporation. Safety of dams is affected by changes in the intensity and frequency of extreme precipitation events (World Commission on Dams, 2000). While changes in the frequency and magnitude of extreme precipitation events caused

by global warming are uncertain, such events are likely to become more frequent and intense (Kundzewicz *et al.,* 2007). An increase in water flow due to climate change can reduce the lifespan of dams as a result of increased sedimentation and erosion which can amplify flood risk and risk of breaches or dam failure leading to a potential loss of lives and high economic costs (Palmer *et al.,* 2008). A decrease in water flow on the other hand can lead to increased water temperature and deteriorating water quality. Changing flow regimes can also lead to changes in hydroelectric power generation, with financial performance being sensitive to precipitation change and rising temperature (Harrison *et al.,* 2003)

Because of the large impact that dams have on both humans and the environment, a thorough understanding of effects of climate change on dams is required. This understanding will help in devising more adaptive, flexible and sustainable water management schemes to cope with the increased pressures and challenges posed by climate change. Moreover, a better understanding of dam functioning under climate change can support upstream watershed management and conservation efforts.

1.2. Aims and objectives

With dams playing such an important role in water supply and energy generation in many countries, it is critical to have a thorough understanding of effects of future climate change on dams and reservoirs. However, as of yet there is no definitive spatially referenced database of dams with which it is possible to model impacts of land use and climate changes on water supplies. The scope of this study is to contribute to the realization of such a database which can then be combined with other spatial data and hydrological models to understand the impacts of climate change on water resources at dams on a global scale, as well as to assess the implications of these changes in more detail for a selection of case studies. A better understanding of the relationship between climate change and dam functioning could help with devising more adaptive, flexible and sustainable water management

schemes to cope with the increased pressures and challenges posed by climate change.

1.2.1. Aim

The broad aim of this study is to assess the effects of climate change in the watersheds of global dams on water resources delivered to those dams and then to examine the implications of climate change for a number of these dams in more detail, with specific focus on the Andes mountain range in South America

1.2.2. Objectives

In order to achieve the stated aim for this research, three main objectives have been identified:

1) To contribute to the mapping of global dams, extract the watersheds of these dams and study trends and variability in projections for future climate change in these watersheds in order to evaluate the potential implications for water and sediment delivery to dams.

2) To use an existing hydrological model (AguaAndes/WaterWorld) to simulate the hydrological baseline and the hydrological impacts of a range of climate model projections for rainfall and temperature on a number of major dams in order to evaluate directional changes in water and sediment supply and implications for hydroelectric power generation and water resource availability.

3) To assess the impacts of projected climate change in terms of water supply and sediment input of a small dam located in the Santa basin, Peru and examine the likely impact for the basin and its peoples and the uncertainty associated with this impact

1.2.3. Specific objectives

More specifically this thesis aims to:

- help complete a global geo-referenced database of dams and extract the individual hydrologically correct watersheds of those dams
- create global high resolution multi-model climate change grids for temperature and precipitation for two different emission scenarios for the 2050s
- assess the impact of projected climate change (temperature and precipitation) on the watersheds of global dams in terms of changes in available water
- model the impact of climate change on a number of large dams in different climate regions using the WaterWorld model (Mulligan, 2012d)
- Test the sensitivity of this model for a number of model outputs and inputs
- Compare the model against the best available field data for baseline (current) conditions
- Apply the model to the Santa basin in Peru to assess the impacts of climate change on a small hydro-electric power plant

1.3. Contribution

The research presented in this thesis consists of empirical work (the dam database) and analyses using mainly free (global) datasets and free modelling systems. The use of consistent global data sources and methods allows for easy inter-comparison across sites but also means that the methodologies are replicable and the modelling as presented in the case studies can be carried out for dams in other parts of the world with relative ease, in contrast to existing data sets and assessment methods.

Specific contributions of this thesis to the academic and wider community are:

- The co-development of the first global geo-referenced database of dams using innovative techniques that can be used for a multitude of research including impacts of climate change on those dams and their contributing watersheds (this thesis) but also impacts of land use and land cover change as well as any other global or local study into dams.
- The assessment of impacts of climate change on the watersheds of global dams under two projected future scenarios highlights those dam impacted areas around the world that are most sensitive to changes in climate in terms of

water provision which is valuable information to dam operators, water resource managers and those interested in adaptation to climate change through for example ecosystem based adaptation in the watersheds of dams.

- The testing and validating of results from the web-based modelling system AguaAndes/WaterWorld (see section 2.7.3) provides important information on the performance of this model in different climatic areas and the sensitivity of model input datasets, that is useful to the growing number of users of the tool around the world as well as for optimisation and further development of the model.

1.4. Overview of this thesis/outline

This document contains 8 chapters. An overview of what can be found in each chapter is given below.

1.4.1. Chapter 1

Chapter one, this chapter states the research goals and objectives. A short introduction to the research problem is given and the specific aims and objectives of the research are described along with a general layout of this document.

1.4.2. Chapter 2

Chapter two gives an overview of the current state of knowledge and a background literature review of this PhD study. This will be described in terms of significance of dams, their environmental and social impacts, both positive and negative, the general implications of climate change and more specifically the impacts of climate change on dams around the world. Furthermore, the distribution of dams around the world and the availability and development of dam databases will be discussed. Finally a overview of modelling impacts of climate change on freshwater resources and dams in particular will be presented. The chapter concludes with a overview of other water resource models.

1.4.3. Chapter 3

This chapter will describe the development of the KCL GlObal geO-referenced Database of Dams (GOOD^2). A global spatially geo-referenced database of dams is necessary to be able to model the hydrological impacts of climate change and land use changes on water inputs into global dams. The database presented in this chapter is built using a GEOWIKI approach in which anyone with an internet connection and Google Earth installed can contribute. Visible dams in Google Earth were digitised and named and as much additional information as possible about the dam was given. Furthermore, catchments for these dams were calculated using spatial analysis techniques. The full methodology will be described and results presented on the distribution of dams around the world and the associated dam catchments.

1.4.4. Chapter 4

This chapter aims to assess the impacts of climate change on the catchments of dams on a global scale. Using the calculated dam catchment areas from the GOOD^2 database as described in chapter 3, in combination with general circulation model output from the latest available IPCC Assessment Report (AR4), an assessment of changes in water provision as a result of climate change within dam catchments will be presented. This involves the creation of multi-model mean global climate change grids for temperature and precipitation on a common resolution from the outputs of the various General Circulation Models that are available in the AR4 along with some uncertainty metrics such as range, and coefficient of variation. Changes in water balance over the dam catchments between the baseline and A1B and A2A scenarios for the 2050s are calculated using a temperature based approach for the evapo-transpiration calculation and remotely sensed data on soil moisture. Furthermore, changes in reservoir water level under these climate change scenarios are estimated for a range of large dams using the SWBD (Farr and Kobrick 2000; NASA 2005) database to locate the dams with the largest reservoirs. Finally the impact of these projected climate changes on agriculture and human population within the dam catchments were assessed.

1.4.5. Chapter 5

In chapter 5 a spatial hydrological model is utilised to characterise and quantify hydrological changes as a result of changes in climatic inputs (precipitation and temperature) within three case study basins in different climatic areas that are heavily impacted by dams. These basins are the Guadalquivir basin in Spain, the Maputo basin in Swaziland and South Africa and the Savannah basin in the United States. Within each basin a major dam is selected and simulated changes in sediment and water inputs into the dams are assessed. The hydrological model used is the FIESTA model (Mulligan and Burke, 2005: Bruijnzeel *et al.,* 2011; Mulligan, 2012d) which is used within the framework of the policy support system AguaAndes/Waterworld (Waterworld, 2012) which is an online policy support system initially developed for the Challenge Programme on Water and Food (CPWF) in the Andes. However, this system of models can be applied anywhere in the world because all necessary data is contained in a global database called SimTerra (Mulligan, 2009).

1.4.6. Chapter 6

Chapter 6 explores several features of the AguaAndes/WaterWorld modelling system to assess the sensitivity of the case study basins presented in chapter 5 as well as the sensitivity of the modelling system to changes in input data. Sensitivity of basins to climate change is assessed by applying simple climate change scenarios and examining the outputs. Furthermore, to highlight how differences in basin geography such as terrain, vegetation and baseline climate affect the outcomes of the *same* climate change, an analysis is carried out whereby the same climate change (i.e. the same delta's) will be applied to the different basins. This analysis helps in determining which characteristics of basins make them more or less sensitive to a given climate change and thus can be instrumental in devising adaptation measures in basins. Also, some model experiments have been carried out on changing land use with the use of the land use change scenario functionality in the modelling system to simulate possible ecosystem based management interventions that can be taken in the river basins to mitigate the impacts of climate change. Finally, some model experiments have been

carried out whereby only one input variable is changed at a time in order to assess the sensitivity of the output to changes in the various input data parameters.

1.4.7. Chapter 7

Chapter 7 describes the application of the AguaAndes/WaterWorld model to the Santa river basin in the Peruvian Andes. This basin is studied as part of the Challenge Program on Water and Food (CPWF, www.benefitsharing.net) project that aims to develop mechanisms for benefit sharing that can improve productivity and reduce water conflicts. The first part of this chapter will describe the application of AguaAndes to assess the potential impacts of a range of climate change scenarios on the Cañón del Pato hydroelectric power station located in the Santa basin.

1.4.8. Chapter 8

Even though chapters 3 to 7 incorporate discussion and conclusions, these are synthesized in chapter 8 as the overall concluding chapter. Furthermore, this chapter describes to what extent the objectives for the research have been met and provides recommendations for future research.

2. Background

2.1. Introduction

Dams and reservoirs play an important role in social and economic development as they store water for supply, generate energy, and provide safety barriers for potential flooding. Half of the world's approximately 50,000 large dams were built primarily for irrigation, which is estimated to represent 12-16% of global food production. Furthermore, 19% of the world's electricity supply is provided by hydropower plants (World Commission on Dams, 2000). Increasing global population and increased demand for energy is resulting in more and larger dams being constructed, especially in developing countries. Moreover, hydropower is a (low carbon) renewable resource making it a relevant option for reducing carbon emissions, particularly in the face of new international climate agreements.

Effects of a changing climate on dams can lead to a range of environmental and socio-economic impacts. The reliability of reservoirs will be affected by changes in river inflows and lake evaporation. Safety of dams is affected by changes in the intensity and frequency of extreme precipitation events (World Commission on Dams, 2000). Changes in extreme precipitation events caused by global warming are uncertain, but they are likely to become more frequent and intense (Kundzewicz *et al.,* 2007). This chapter will describe the significance of dams and their global distribution. Furthermore, the issue of climate change and its impacts on water resources will be discussed along with the current state of knowledge on climate change impacts modelling in relation to dams. Finally, the aim and objectives for this study will be described and an outline of this report will be given.

2.2. Significance of dams

2.2.1. Environmental impacts of dams

The purpose of a dam is to store water for energy generation, water supply, irrigation, flood control, recreation, navigation or a combination of these. These functions are particularly important in highly seasonal environments or those with infrequent storms producing runoff. In a 2005 global overview of dam-based impacts on global river systems it was shown that more than half of the 192 world's largest river systems are affected by dams (Nilsson *et al.,* 2005) and that all large dams in the world combined are capable of holding back around 15% of global annual river runoff. It was also shown that dam-impacted basins experience about 25 times more economic activity per unit of water than unaffected basins. Hydropower regulates around 12% of the world's rivers fluvial volume and irrigation water withdrawals account for almost 70% of global water withdrawals (Sternberg, 2009). Large dams therefore play an important role in the distribution and utilisation of the world's water resources. Their environmental and socio-economic impact however remains an issue of contention.

Dams impact river ecosystems as they constitute man-made obstacles that limit free flow of water and nutrient fluxes. River systems are extremely complex interlinked systems that support an enormous biodiversity that is maintained by the changes in the flow of the river, including floods. With almost half (42%) of all known fish species and a quarter of all mollusc species (25%) occurring in freshwater (Darwall *et al.,* 2005), any obstruction in the free flow of fluxes can have a significant environmental impact. The physical, chemical and biological components of the river ecosystem are controlled by the frequency of flow extremes such as floods and droughts. In unregulated rivers, channel shapes are determined by flooding while floods also provide the floodplain with nutrients and sediments with the resulting floodplain forming a habitat for many river species, including fish. Changes in flow can be important for the life cycles of certain species e.g. fish spawning that coincides with optimal flow and temperature conditions (McCartney and King, 2011).

Petts, (1984) and McCartney and King (2011) describe the impacts of dams on river ecosystems as a hierarchy of interconnected effects with first, second and third order impacts (figure 2.1) with first order impacts being changes in the physical driving variables such as hydrology, water quality and sediment. These impacts can also effect the terrestrial environment, e.g. as a result of reduced flooding and nutrient deposition on floodplains. The second-order impacts are the result of the changes in the first-order impacts and third-order impacts similarly are the result of changes in second-order impacts. This chain of effects makes prediction of higher order impacts increasingly difficult.

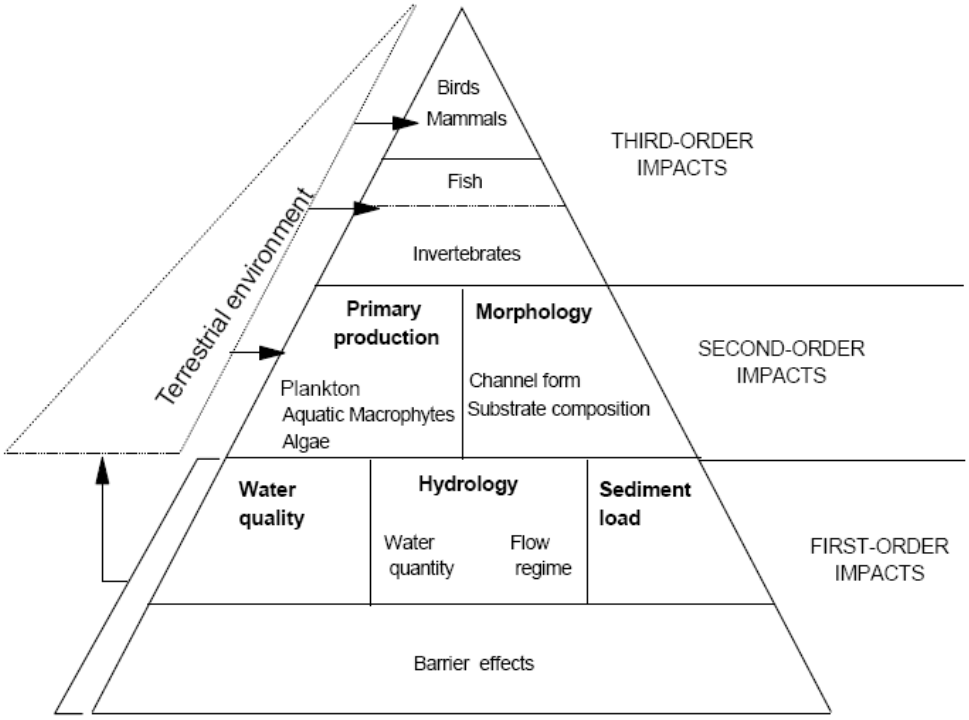

Figure 2.1 The impact of dams on river ecosystems (source: McCartney and King, 2011)

Dams can alter the pattern of flow as well as the total annual volume of flow depending on their storage capacity and the operational type of the dam. Hydropower generation can cause rapid flow fluctuations occurring at unnatural rates. With very large dam reservoirs such as the Three Gorges dam in China, filling up the reservoir for the first time can take years, reducing the annual flow greatly. In addition, water abstraction for irrigation and water supply reduce the flow further.

2.2.1.1. Impacts on sediment

As a result of the reduced flow velocity in reservoirs, more sedimentation occurs, filling up the reservoir. Sedimentation rates are dependent on characteristics of the catchment, land use practises and the operation of the dam and vary largely between different areas in the world but can be extremely high (McCartney and King, 2011). For instance, the High Aswan dam on the Nile captures more than 98% of the sediment transported by the Nile resulting in a decreased deposition of nutrient-rich soils on the downstream floodplains and delta (Stanley and Warne, 1998). Furthermore, the reduced sedimentation can have severe impacts on the downstream rivers and delta's as it can cause increased erosion of river banks and beds and loss of floodplain (McCartney and King, 2011).

2.2.1.2. Impacts on water quality

Storing water in reservoirs has an effect on water temperature, oxygen levels and nutrient levels with a top-down gradient so that there are differences between water released from near the surface (well oxygenated, warm and nutrient-depleted) and the bottom of the reservoir (cold, oxygen-depleted and nutrient-rich) that can impact downstream flora and fauna. Furthermore, eutrophication can occur in reservoirs leading to algal blooms that can be toxic for freshwater species as well as humans.

2.2.1.3. Impacts on organisms

As is clear from the above, dams have a direct impact on river ecosystems and water quality that in turn impacts the flora and fauna both upstream and downstream of the dam. As a direct effect they can block the movement of species, such as salmon for instance but most effects are secondary, with changes in turbidity, flow, sediment, water quality and water temperature all impacting on the habitat of fresh water species. The world commission on dams in its 2000 report stated that at least 20% of the world's freshwater fish have become extinct, threatened or endangered in recent years (World Comission on Dams, 2000).

2.2.1.4. Cumulative impacts

Since dams are often built in the same catchment on different tributaries (parallel) or on the same river (series) the cumulative impact can be greater than the sum of the individual ones (McCartney and King, 2011). When a dam alters certain river characteristics, the self-correcting nature of the river will lead to a return to normal levels downstream. However, if there are other dams downstream, they will start with a different than normal situation and altering it even further.

2.2.1.5. Impacts on atmosphere

Some large reservoirs in tropical areas emit significant amounts of greenhouse gases, specifically methane as a result of rotting vegetation in the reservoir. The exact quantity of these emissions is uncertain as research into these emissions is still fairly recent and remain largely controversial (Fearnside and Pueyo, 2012). However, estimates by Fearnside (2012) indicate that the cumulative emissions of large tropical dams in the Amazon exceed those of fossil-fuel generation for time-periods up to several decades (Fearnside, 2012)

2.2.2. Social impacts of dams

Dam projects are often initiated from a development perspective. Hence, there is a large socio-economic impact on human communities. Some of these impacts are apparent from the purpose of the dam itself such as provision of irrigation water for agriculture, flood control and providing electricity. However, there can be competing interests. For example, keeping reservoir levels high to maintain energy production can cause a shortage of water downstream or reduce the capacity to retain floodwater. The largest social impact surrounding dams is associated with the construction of the dam when populations are displaced and areas of land are flooded. It is estimated that between 40 and 80 million people globally have been displaced as a result of dam construction (World Commission on Dams, 2000). The downstream impacts of dams on people are not widely understood and depend on a complex set of impacts that in

turn depend on the amounts and timings of water flows as well as the hydrological links between the river and the floodplain (World Commission on Dams, 2000)

2.2.2.1. Socio-economic benefits of dams

There is no doubt that dams can have a positive impact on the socio-economic position of communities. If designed and operated well, they are capable of ensuring a reliable supply of water to benefit agriculture, industrial and domestic users. Furthermore through the generation of electricity, they can increase industrial output, create jobs and thereby increase per capita income. Storing water in reservoirs and irrigation diversions can also increase agricultural output and increase food security (World Commission on Dams, 2000). Another aspect of dams is that they are able to regulate flows which means they have the capability of mitigating droughts and to some extent also control floods. McCartney and King (2011) list some examples of the services and benefits generated by seven large dams in Africa with the clearest example being the High Aswan dam in Egypt that economically faired so well that its costs were recovered within 2 years of construction. Furthermore, it provided 50% of Egypt's electricity production in its first few years and provides irrigation for nearly all of the country's agriculture (McCartney and King, 2011).

2.2.2.2. Displacement and resettlement

In many cases, new dams require the resettlement of people living in the area that will be inundated by the reservoir. Estimates of global displacement by dams vary widely between 40 to 80 million up to the year 2000 (World Comission on Dams, 2000) with the Three Gorges dam in China reported to have the highest number of people displaced: 1.3 million. The livelihoods of people in terms of its economic and social values before displacement is often underestimated. After relocation, people might not only lose land but they also lose access to resources. It is found that displaced people experience higher levels of landlessness, unemployment, indebtedness and hunger than before displacement (McCartney and King, 2011). Also, the more people are displaced, the fewer the chances that the resettlement is a success. Scudder (2005)

in a study of affected communities for 44 large dams around the world found that in only three cases, living standards were improved and in only five cases it was restored.

2.2.2.3. Loss of downstream resources and livelihoods

Many people, particularly in Africa, rely on the floodplains for their livelihood using it for agriculture, fishing, grazing and wild plant gathering. The economic value of these activities can be significant (World Comission on Dams, 2000) and sometimes higher than benefits arising from diverting water for irrigation (Barbier and Thompson, 1998). Through modification of flow regimes, dams have an impact on the natural resources provided by these floodplains. Furthermore, as a result of a reduction in natural flooding, the floodplains can get more populated increasing the risk of agricultural losses and lives lost when dams have to suddenly release water in extremely wet periods (McCartney and King, 2011)

2.2.2.4. Health impacts

In general, dams contribute to better health by providing higher food security and increased income. However, some adverse health impacts, particularly in Africa have been shown by Keiser *et al*. (2005) that relate to the intensified transmission of malaria and schistosomiasis as a result of an increased abundance of disease vectors such as mosquitoes and snails.

2.3. Distribution of dams around the world

According to current figures, there are more than 50,000 large dams around the world, with large dams being defined as those greater than 15 m in height or having a storage capacity greater than three million cubic metres (World Commission on Dams, 2000, Reidy Liermann, 2007). Data on new dams is difficult to obtain but most new dams are being built in the developing world where growth of water and electricity demand is strongest. Currently the most important dam building nation in the world is China, where in 2008 more than 200 hydropower dams were planned or under construction. Moreover, more than 80% of new hydro-electric systems in 2008 were located in Asia

(Sternberg, 2009). On the other hand an increasing number of dams is being removed, particularly in the United States where over 400 dams have intentionally been removed in the last three decades as a result of new perspectives on ecological, social and economic aspects as well as safety risks due to ageing of the structures (Heinz Center, 2003)

2.3.1. Dam databases

Various dam databases exist around the world and cover differing spatial extents. An overview of dam data sources is given in Reidy-Liermann (2007). Generally none of these databases are comprehensive or fully global in extent. Also, many databases are not digital and/or geo-referenced (e.g. (ICOLD, 2003) making it difficult to use these databases for hydrological modelling where the characteristics of the dam watershed need to be known. Databases can also be inaccessible or not published such as the database compiled by the University of Yamanashi, Japan (Magome *et al.,* 2006). Recently though, a international collaborative effort published the GRAnD (Global Reservoir and Dam Database, (Lehner *et al.,* 2011) that is global in scale and geo-referenced. However, this database contains information for only 6,862 dams.

2.4. Climate change and its impacts on water resources

There is now a wealth of evidence pointing to a warming of our planet over the last 200 years (Mann and Jones, 2003) with continuing climate change expected to have major impacts on river systems around the world, causing changes in discharge and flood frequency. These changes in the hydrological regimes can have both positive and negative impacts although overall a net negative impact on realisable water resources is projected globally. Areas with a projected decline in runoff will see a reduction in value provided by water resources and areas with increased runoff will experience more variability in precipitation and shifts in seasonal runoff leading to higher flood risk and a less insecure water supply (Kundzewicz *et al.,* 2007)

2.4.1. Observed climate change

Key questions when examining evidence for climate change are: is there an increase in global temperature, have the precipitation patterns changed? A number of studies have focused on showing the evidence for this.

2.4.1.1. Temperature

Global mean surface temperatures have risen by between 0.5°C and 0.9°C between 1906 and 2005 with a rate of warming that has almost doubled (0.13°C ± 0.03°C vs. 0.07°C ± 0.02°C per decade) in the last 50 years compared to the first 50 years of that period (Trenberth *et al.,* 2007). Figure 2.1. shows the measured annual global land surface air temperature relative to 1961-1990 from various data interpretations with small differences mainly due to spatial averaging techniques. Warming has been strongest over continental Asia and the northern part of North-America while cooling has only been observed in the northern North Atlantic.

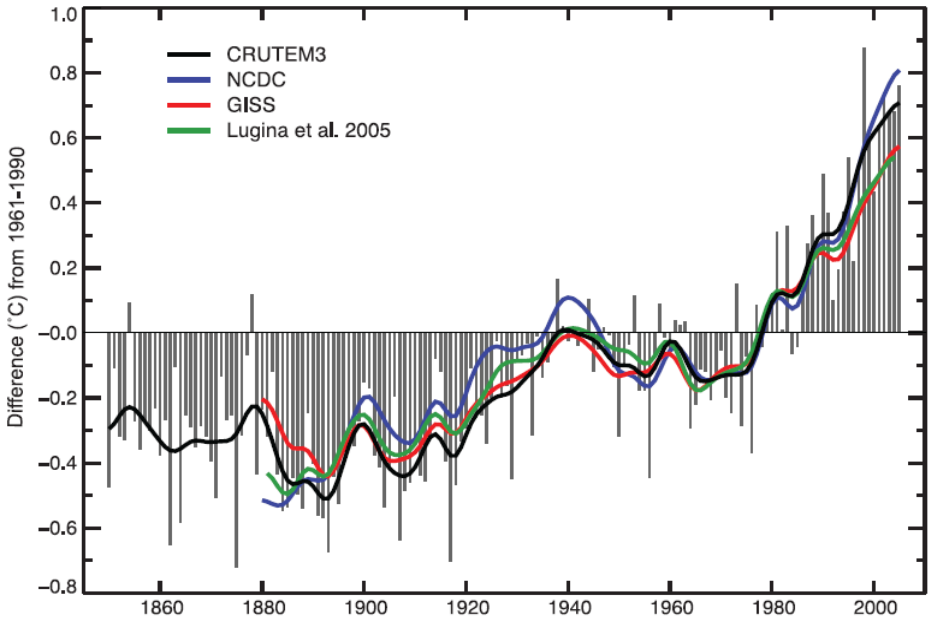

Figure 2.2 Annual anomalies of land surface air temperature (°C), 1850 to 2005 relative to the 1961-1990 mean. Smooth curves show decadal variations. Source: (Trenberth *et al.,* 2007)

2.4.1.2. Precipitation

Observations of precipitation show changes in amount, intensity, frequency and type of precipitation (Trenberth *et al.,* 2007). Significant wetting has been observed in eastern North and South America, northern Europe and northern and central Asia while drying has occurred in the Sahel, Southern Africa, the Mediterranean and Southern Asia. Changes have also been observed in the frequency of heavy precipitation events. These changes are associated with rising temperatures, particularly in the world's oceans leading to increased water vapour in the atmosphere.

2.4.1.3. Variability and extremes

Evidence for changes in inter-annual variability of temperature is sparse (Scherrer *et al.,* 2005) but significant decreases in the annual occurrence of cold nights and increase in occurrence of warm nights has been shown over the period since 1946 for more than 70% of global land area (Alexander *et al.*, 2006); Caesar and Alexander 2006) implying that daily minimum temperatures around the globe are increasing. Generally there is an increase in the amount of heavy daily precipitation events leading to floods. Also, evidence suggests an increase in tropical storm and hurricane frequencies since the 1970s (Trenberth *et al.,* 2007)

2.5. Climate change projections and impacts on water resources

Given the evidence for climate change over the last century it is important to understand how climate will change in the future and the effects such a change will have on water resources. The main drivers for water availability are precipitation, temperature and evaporative demand. Projections from the latest IPCC (IPCC, 2007) assessment report (AR4) indicate an increase in global mean surface temperature in the range of 1.1-6.4°C by the end of the 21st century, relative to 1980-1990, with a best estimate of 1.8 - 4.0°C and also an increase in frequency and intensity of heavy precipitation events (Meehl *et al.,* 2007). Figure 2.2 shows the temperature

projections to 2100 based on various emission scenarios and models. Constant CO_2 assumes stabilized levels of CO_2 at year 2000 levels.

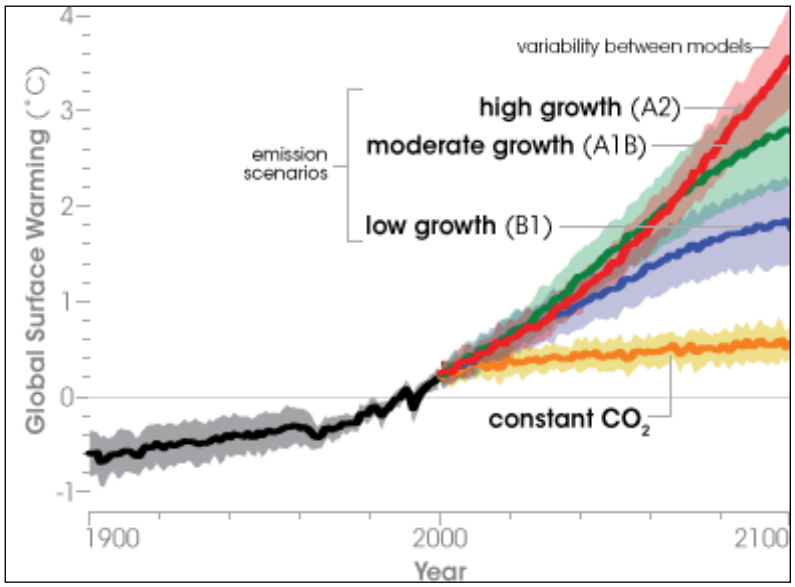

Figure 2.3 Global temperature projections to 2100. Source: NASA Earth Observatory, based on IPCC AR4 (IPCC, 2007).

According to a review by Kundzewicz et al., (2007), the changes in temperatures and precipitation will result in impacts on runoff, leading to a likely increase by 10% to 40% from 2050 in the high latitudes, and decrease by 10% to 30% in the mid-latitudes

2.5.1. Emission scenarios

In order to carry out climate change modelling, scenarios of global emission, population growth, energy use and economic development need to be available. For the 4th assessment report of the IPCC a range of such scenarios was developed in the Special Report on Emission Scenarios (SRES, Nakicenovic *et al.,* 2000). The SRES report comprises 40 scenarios that are grouped into four different storylines with each storyline detailing different developmental pathways that lead to different emission scenarios for atmospheric concentrations of greenhouse gases and aerosols. There are

six marker scenarios in the SRES (A1F1, A1B, A1T, A2, B1 and B2) and these were used by the different modelling groups to drive the global climate models and develop a range of climate scenarios. Figure 2.4 Shows the four storylines and the direction of development they represent.

Figure 2.4 Main direction of the four SRES storylines. source:
http://www.bom.gov.au/info/climate/change/gallery/images/74.gif

The A1 storyline represents a future world of rapid economic growth, global population with a peak in 2050 and a decline after that. It also anticipates a rapid introduction of new and more efficient technologies. There are three main variants to this scenario that make different assumptions about sources of energy. A1F is a fossil intensive world, A1T assumes no fossil fuels and A1B has a balanced mix across all sources. The A2 storyline represents a heterogeneous world where the population

continuously increases throughout the century but where economic growth is more regionally oriented, more fragmented and slower than the other storylines. The B1 storyline represents a convergent world with similar population growth as the A1 storyline but with rapid changes in economic structures focused on a service and information economy. Furthermore, a reduction in material intensity and introduction of clean and resource efficient technologies. Finally the B2 storyline represents a world that has a continuously (but lower than A2) growing population but is focused on local solutions to economic, social and environmental sustainability and has intermediate economic development.

As well as the SRES emission scenarios, other scenarios have been developed. For example the EU ensembles climate prediction project developed the E1 scenario which is the first scenario to incorporate an aggressive mitigation policy where CO2 levels stabilize at 440 ppm in the 22nd century (Lowe *et al.,* 2009).

2.5.1.1. Emission scenario uncertainty

Since there are so many factors that influence emissions there is a large uncertainty surrounding the emission scenarios. This uncertainty naturally increases more when the projection is farther into the future. The SRES scenarios for example do not take into account 'disaster' scenarios such as the melting of the Greenland ice sheet and associated rising of sea levels or climate mitigation policies that may be enacted by the international community. Furthermore, land cover trends in the scenarios are found to be inconsistent with current global land use developments (Arnell*,* 2004). Therefore, Arnell, (2004) recommends the use of a wider range of scenarios for studying future climate change impacts to better estimate the range of those impacts.

For the 5th IPCC assessment report that is due in 2014, new emission scenarios will be used that are being developed in a parallel process. In this process, radiative forcing characteristics for modelling of climate are identified first, after which Representative Concentration Pathways (RCPs) are selected from published literature. Then, in parallel

with the development of climate scenarios based on the RCPs, new socio-economic scenarios will be developed in order to explore socio-economic uncertainties that affect adaptation and mitigation. Finally, the new socio-economic scenarios will be integrated with the new climate scenarios and used to study adaptation, mitigation and impacts (Moss *et al.,* 2010) This approach has the advantage that it is much quicker and reactive than the earlier approach where emission scenarios were developed first and after that climate scenarios. It also allows for exploring additional issues and uncertainties as there will be a whole range of new scenarios that have different radiative forcing pathways (Moss *et al.,* 2010).

Pattern scaling approaches can be used to study uncertainties associated with choice of emission scenario or to provide climate change projections for time periods and emission scenarios not simulated by GCMs. By constraining individual models to reproduce the same global temperature, information about differences in model predictions such as those to do with differences in response in atmospheric circulation to global radiative forcing are preserved.

An example of such a pattern scaling approach are the Climgen scenarios developed by CRU-UEA. Climgen uses global mean temperature change to generate spatial scenarios (Todd *et al.,* 2010) with the assumption that the pattern of climate change is relatively constant for a given GCM (Arnell and Osborn*.,* 2006). With this approach the pattern of climate change for a GCM can then be rescaled to any global average temperature change in order to explore specific thresholds of global climate change (Kingston and Taylor*.,* 2010).

2.5.2. GCMs and RCMs

The most complex general circulation models or GCMs are the AOGCMs which are coupled atmosphere/ocean models. These models divide the atmosphere and ocean into grid cells, and include interactive land-surface and biophysical processes. Typically, GCMs have a horizontal resolution of between 250 and 600 km with anything between

10 to 20 vertical layers in the atmosphere and up to 30 layers in the oceans. (IPCC, 2007). Many physical processes, such as cloud formation take place at smaller scales and are therefore averaged in these models. Regional climate models or RCMs have a much finer resolution (typically 25 to 40 km) and focus on sub-continental scale geographies. The boundary conditions for RCMs are given by the GCM that they derive from after which the local impacts are calculated based on finer scale information on land use and orography. RCMs generally do not include ocean components.

2.5.2.1. GCM and RCM uncertainty

Since there are many atmospheric processes with dimensions smaller than GCM model resolution, these processes need to be parameterized in the models (e.g. variations in solar radiation, volcanic eruptions and anthropogenic greenhouse gas emissions). This means that it is difficult to address GCM uncertainty, since it can derive from the unpredictability of the climate system itself or the different parameter values and model structures of the climate models (Tebaldi and Knutti, 2007). Another source of uncertainty is in the feedback mechanisms in models that deal with water vapour and warming, clouds and radiation, ocean circulation and ice and snow albedo. As a result of these processes, different GCMs can produce very different responses despite having the same forcing due to the way these processes and feedbacks are modelled (IPCC, 2007). Another limitation to GCMs is that they are not capable of capturing so called tipping points in the earth system. Lenton et al (2008) describe a number of such tipping points of which the Indian Summer Monsoon (ISM) is the most important in terms of water resources as it potentially leads to a decrease in precipitation and possible drought in areas that are currently projected to have an increase in precipitation.

2.5.3. Downscaling

Due to the very coarse spatial resolution of GCMs (typically grids of 2.5° latitude by 2.5° longitude or 2.5° latitude by 3.75° longitude or 150-300 km^2) it is often necessary for hydrological impact modelling to downscale the output of the GCM spatially. This

can be done with either dynamical downscaling techniques, which use physical relationships between large-scale and small-scale models or statistical downscaling techniques that use empirical relationships between large-scale climate variables and observed weather variables (Wilby *et al.,* 2004). Recently more and more impact studies use regional climate models (RCMs) that have a much higher spatial resolution making them more useful and accurate for predicting climate change on a smaller scale (see Teutschbein, 2010 for a review). The advantage of these models is that they produce high resolution (20km to 60km) data that takes into account local and regional topography. A disadvantage of RCMs, however, is that they are nested in GCMs, where boundary condition data is provided by the GCM making them subject to the biases present in the GCM (Fowler *et al.,* 2007). Moreover, they require a high level of computational resources and lots of expertise in climate modelling.

2.5.3.1. Downscaling uncertainty

The main uncertainty with either downscaling technique is that they propagate the uncertainties contained in the GCM that they are derived from plus additional intrinsic uncertainty in the RCM itself. With statistical downscaling, the main assumption is that statistical correlations between climate variables derived from observational data are valid under a changed climate (Wilby *et al.,* 2004). They also assume that predictor variables used for the downscaling are adequately simulated by the GCMs (Fealy and Sweeney, 2007). The Statistical and Regional Dynamical Downscaling of Extremes for European regions or STARDEX project has attempted to compare both methods and found that generally for both methods, the models perform better in downscaling temperature than precipitation and were better able to capture means rather than extremes (STARDEX, 2006)

Another issue with GCM data in relation to hydrological modelling is temporal resolution. Many hydrological models, particularly those designed for flood modelling need daily time series as input. However, GCM data are usually only available as monthly means necessitating the need for temporal downscaling. The most common

technique of deriving daily time series of climate variables from monthly values is by using a stochastic weather generator which is a statistical model that replicates time series of climate variables based on the same statistical characteristics as observation data. The main assumption being that statistical correlations between climate variables derived from observational data are valid under a changed climate (Wilby *et al.,* 2004).

2.5.4. Uncertainty and climate change impact modelling

Predicting future climate is a very complex exercise fraught with uncertainty. This uncertainty propagates and intensifies through all the stages of climate change prediction from projections of future socio-economic development paths through to the regional stage to local climate change impacts leading to a cascade of uncertainty (Schneider, 1983; Jones, 2000; Wilby, 2005). Figure 2.5 illustrates this cascade of uncertainty.

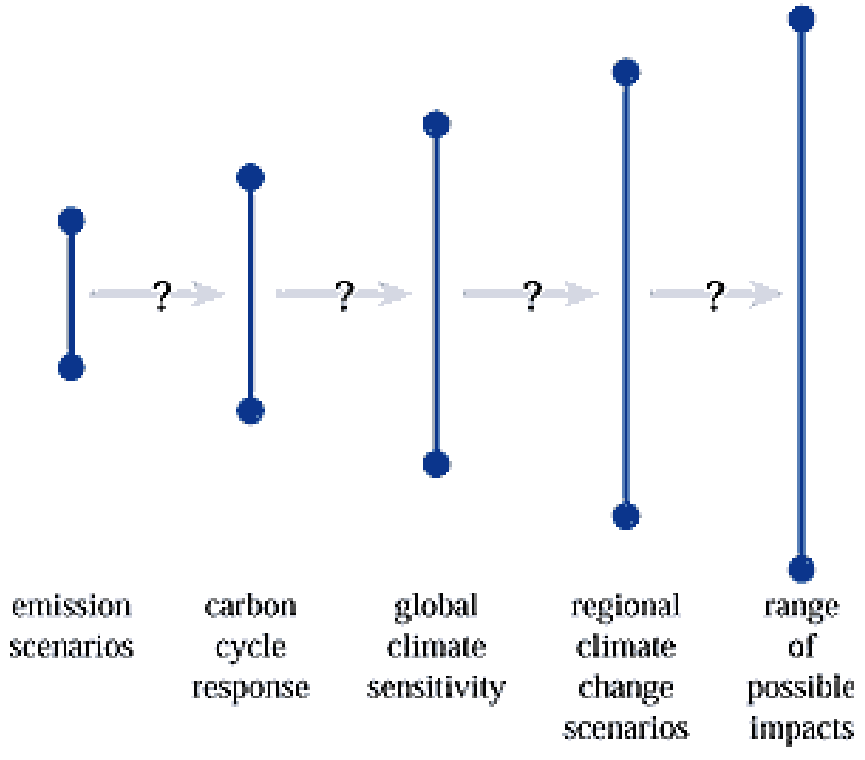

Figure 2.5 Cascade of uncertainty in climate projections for impact modelling (source: Murphy, 2010)

Furthermore, some climate systems are still poorly understood or difficult to model such as cloud behaviour and regional weather patterns. To quantify some of this

uncertainty in impact analysis, multi-model ensembles can be used. This approach is sometimes called the 'one model one vote' approach as it is very useful to convey the message of climate change to a wider audience, particularly when there is no specific regional focus (Tebaldi, 2010). Indeed it has been found that the central tendency of all models in the AR4 compared to observational records outperforms any single model simulation (Reichler and Kim*.,* 2008) and no model outperforms all others (Gleckler *et al*., 2008). This is also found for statistics of variability (Pierce *et al*., 2009). Therefore multi-model means are generally considered a safer bet than single model output (Tebaldi, 2010).

2.6. Climate sensitivity of dams

With expected changes in floods and droughts as a result of climate change, there will be an impact on dams and reservoirs whatever the direction of the change. Therefore, during their lifetime, existing as well as new dams will likely be exposed to different climatic conditions than those experienced in the recent past and for which they were designed and engineered. There are four key issues surrounding dams and reservoirs that are affected by climate change. These are safety, reservoir yield and reliability, reservoir operation and reservoir sedimentation.

2.6.1. Safety

Dam spillways are generally capable of discharging high flows with a return period in excess of 1000 years so the structure of the dam is not compromised. Generally these design flows are based on past stream flows. However, as a result of climate change, extreme floods exceeding the design flow become a possibility.

2.6.2. Reservoir yield and reliability

Perhaps the most important impact of climate change on a dam is its effect on the yield and reliability of the reservoir. Changing stream flow patterns and the more frequent occurrence of extreme rainfall-runoff events can have significant effects on the management of a dam. Reliability of a reservoir is determined as its ability to meet

the demands that are placed on it and is therefore a function of inputs into the reservoir, evaporative outputs and characteristics of the reservoir such as its storage capacity and release capacity (Arnell and Hulme, 2000).

2.6.3. Reservoir operation

Reservoir management is determined by the demand on the reservoir such as to provide enough water for hydroelectric power generation or storage of water for drier periods. This means that operational management is highly dependent on timing and volume of inflows. For instance, many dams in the northern hemisphere depend on snowmelt for filling of their reservoir. If temperatures in these regions increase this could lead to earlier spring floods and higher winter flows resulting in a need for a change in management practice.

2.6.4. Reservoir sedimentation

Sediment delivery into a reservoir depends on the flow regime of the rivers that feed into it. It is common practice to design and operate reservoirs to allow them to fill with sediment making their operational life subject to a finite period of time. Already under current climate, many large dams fill up with sediment before the end of their designed lifetime leading to substantial costs (Palmieri *et al.,* 2001). As a result of changing inflow patterns, particularly with extreme rainfall events more sediment could be deposited in the reservoir as a result of the higher erodibility under these conditions. This reduces the lifespan of the dam even quicker but can also amplify flood risk and risk of breaches or dam failure leading to a potential loss of lives and associated high economic costs (Palmer *et al.,* 2008).

The above mentioned effects are all direct hydrological impacts as a result of changing temperature and rainfall. However, there are several other effects that are mediated through the resulting impacts of climate change on the land surface such as the response of land use and land management to climate.

2.7. Modelling impacts of climate change on freshwater resources

2.7.1. Modelling impacts of climate change on freshwater resources

Many studies have been devoted to the impact of climate change on the hydrological regimes of large river basins around the world. However, a large portion of these have focused on river basins in the United States, Europe and Australasia using a variety of hydrological models, projections, scenarios and downscaling techniques. A few examples of basin-wide studies include the Columbia river basin (Hamlet and Lettenmaier, 1999) Colorado river basin (Christensen *et al.,* 2004, Christensen and Lettenmaier, 2006), Rhine basin (Middelkoop *et al.,* 2001) and Blue Nile (Elshamy *et al.,* 2008). Furthermore, a few studies have assessed the impact of climate change on river basins on a global scale covering a range of geographic and climatic conditions. Nijssen *et al.,* (2001) used 4 different General Circulation Models (GCMs) to assess climate sensitivity of nine continental river basins and Arora (2000) simulated stream flow for 23 major river basins around the world using one GCM and a flow-routing algorithm by Arora and Boer (1999). Overall, the results of these basin-wide studies indicate that warming will lead to changes in the seasonality of river flows in cases where the bulk of the precipitation falls as snow.

Uncertainties in predictions related to these experiments are mainly to do with uncertainties in the hydrological model on the short to medium time horizon. For the longer-term projections, uncertainty relates more to the emission scenario chosen. In a GCM intercomparison project carried out by Covey *et al.,* (2003) that analysed outputs of 18 models it was shown that GCMs agree reasonably well with observations for temperature but not so much for precipitation. Overall uncertainty in climate change impact studies on water resources are first and foremost due to the GCM used, followed by the chosen emission scenario(s) and finally the type of hydrological modelling undertaken (Kundzewicz *et al.,* 2007). Many impact studies adjust observed climate values with GCM output in order to get scenarios that are consistent with current conditions (the delta method). This methodology is applied in many studies

with the aim to minimise GCM error assuming that the biases in the climate model are of a similar magnitude for current as well as the projected climate. It also has the advantage that it can be used with relative ease making it very useful for studies in which a variety of projections and scenarios are utilised.

2.7.2. Modelling impacts of climate change on dams

Generally, climate change impact studies on stream flow for a particular basin incorporate one or more climate change projections from GCMs into a hydrological model. There are fewer studies however that have looked at the actual impact of hydrological changes on dam reservoir operation and management. In a study using one GCM and two moderate scenarios by Lehner *et al.,* (2005) it was found that climate change can lead to a reduction in hydroelectricity production of up to 25% by the 2070s in Europe and even more for Southern and South-eastern European countries. Using two different GCMs and two emission scenarios, Harrison (2002a) found that hydroelectricity production for the Zambezi basin in Africa declined by up to 32%. Markoff and Cullen (2008) also found a decrease in hydropower for a majority of climatic projections for the Columbia River basin.

Most studies however assume no change to operational practice despite the long-term window over which the changes are modelled. One study that does take into account a change in operational practice was carried out by Minville *et al.,* (2009). Using a regional climate model forced with a single emission scenario, hydropower production was found to first decrease but then significantly increase as a result of adapted operating rules. However, reliability of the reservoir was found to decrease and vulnerability increased with changing climate. Table 2.1 gives a summary of studies that have looked at the effects of a changing climate on hydropower generation, which indicates the range of different studies in terms of models and emission scenarios used.

Table 2.1 Studies into the effects of changing climate on hydropower generation

Author (s)	**Year**	**Basin**	**projections and nr. of emission scenarios used**
Markoff and Cullen	2008	Columbia	7 GCM 6 scenarios
Harrison and Whittington	2002	Zambezi	2 GCM, 3 scenarios
Munoz and Sailor	1998	Sacramento, Eel and Russia (northern California)	3 GCM multi-scenario
Minville *et al.*	2009	Peribonka river (Canada)	RCM (CGCM3) SRES A2 scenario
Payne *et al.*	2004	Columbia	RCM, GCM, 5 scenarios
Christensen and Lettenmaier	2006	Colorado	11 GCM 2 scenarios (SRES A2 and B1)
VanRheenen *et al.*	2004	Sacramento-San Joaquin	RCM, GCM, 5 scenarios
Vicuna *et al.*	2008	Upper American river (California)	2 GCM, 2 scenarios
Schaefli *et al.*	2007	Mauvoisin (Switzerland)	RCM, 1 scenario
Mimikou and Baltas	1997	Polyfyto (Greece)	GCM, 3 scenarios
Lehner *et al.*	2005	Europe	2 GCM, 2 scenarios
Maurer et al.	2009	Rio Lempa (Central America)	16 GCM, 2 scenarios

From table 2.1 it can be seen that most studies have focused on river basins in North-America, with far less studies in Europe, Africa, Asia and South-America. Considering the large number of existing and projected dams and the projected changes in hydrological regimes as a result of climate change on the latter continents this is an important gap in existing knowledge.

The above studies nearly all focus on modelling of hydropower production and associated revenue changes. Very few studies focus on the impact of climate change

on other functions of dams such as water supply despite the significant number of irrigation dams around the world and the likely impacts that climate change will have on these dams. It is estimated that an increase in temperature and an increase in variability of precipitation will generally lead to a higher demand for irrigation, water supply and also hydropower. Globally the net irrigation requirements are expected to increase by 1 to 3% by the 2020s and between 2 and 7% by the 2070s (Kundzewicz *et al.,* 2007). While there are studies that look into the effects of a changing climate on agricultural production and irrigation water demand (Rosenzweig *et al.*, 2004, Jones, 2000), very few of these actually take into account the role of dams in provisioning of this water under climate change scenarios. One of the few studies that have looked into impacts of climate change on irrigation supply through dams was carried out by Block *et al.,* (2007), who modelled irrigation and hydropower output for four dams in the Blue Nile basin under increased El Niño and La Niña scenarios and concluded that there is a potential for cost-benefit increase under climate change but there are also possible significant decreases due to increased variability in stream flow.

2.7.3. Water resource models

In order to model impacts of climate change on the water resources of dams, a hydrological model is required that includes the capability of implementing scenarios of land use and climate change. A number of hydrological models exists at a range of temporal and spatial resolutions. The choice of model is therefore highly dependent on the application. Spatially distributed models allow for simulation of land use changes and use of spatially distributed data such as remotely sensed data which has the advantage that these models are easier to implement in ungauged basins. Table 2.2 gives an overview of some of the most widely used and/or most suitable spatially distributed hydrological models and their main characteristics.

Table 2.2 spatially distributed hydrological models and main characteristics

Model	**Primary reference**	**Freely available?**	**Primary application**	**Typical time for setup**
SHETRAN	Ewen, 2000	Yes (max 50x50 grid)	Stream flow simulation, Water management	1-2 weeks
MIKE-SHE	DHI Software, 2007	No	Forecasting, design, water management	1 day
SWAT	Neitsch *et al.,* 2005	Yes	Land management/agricultural	1 day
WetSpa	Wang *et al.,* 1996	Yes	Flood prediction	1 day
AguaAndes/WaterWorld (FIESTA)	Mulligan and Burke, 2005)	Yes	Land use/climate change scenario analysis	10 minutes

This list of models is by no means exhaustive and a range of other spatially distributed hydrological models are available e.g. STREAM (Aerts*.,* 1999), WaterGap (Alcamo *et al.,* 2003), VIC (GAO *et al.,* 2010), DHSVM (Wigmosta *et al.,* 1994) and LISFLOOD (de Roo *et al.,* 2000) which are not considered for use in this thesis.

Another important distinction between hydrological models is whether they are transient (i.e. dynamic) or equilibrium (i.e. static) models. Dynamic models use time-series data and update at every time-step whereas equilibrium models, calculate a state for a given time-period. For the modelling carried out in this chapter, only equilibrium models have been considered since the focus is on the relative change in water resources of dams between a future period and a baseline period on a global scale. Furthermore, given the uncertainties in climate change projections, using a long term climatological mean for projections as well as the baseline provides a better estimate of total water resources available for a given time-period.

To be able to make a decision on the most suitable model to be applied for this thesis, the following criteria and considerations were taken into account:

- The model should be spatially distributed in order to simulate land use changes;
- The model has to be able to simulate the impacts of changes in climatic conditions and be applicable in un-gauged basins, so a purely empirical rainfall/runoff model would be inappropriate;
- For the purposes of this study, a monthly time-step is sufficient since our focus is long term water resource not short term flood dynamics;Since this thesis looks at global dams, a model is required that can be applied globally and without the need for extensive data gathering;
- The model should allow for easy implementation of land use and climate change scenarios;
- The model should be applicable to large river basins but also small dam catchments.

A short description of each of the models listed in table 2.2 is given below as well as their suitability for the modelling purposes in this thesis with regard to the criteria listed above.

SHETRAN

SHETRAN is a physically-based distributed rainfall-runoff model system that can simulate water flow, sediment and solute transport in river catchments (Ewen *et al.,* 2000). The model includes hydrological components that can simulate rainfall interception by vegetation, evaporation and transpiration; snowpack formation and snowmelt; overland and channel flow; saturated subsurface flow; and river/aquiver interactions (Birkinshaw, 2010). Flow and transport are calculated using partial differential equations on a finite difference grid. The model uses text-based input and output files and uses time-series data for rainfall and evaporation. The original model requires very detailed physical information about the catchment and often requires weeks of preparatory work before any simulation can be run (Birkinshaw, 2010). A more recent version of the model includes a graphical user interface (GUI) that allows

for a much easier and quicker setup that can serve as a starting point for a more detailed setup. However, since the GUI uses a minimum of input-data (only a DEM, and vegetation and soil parameters from a library are required), this feature limits the capabilities of the model (Birkinshaw, 2010). To optimally use SHETRAN, detailed parameterisation of soil and vegetation parameters would be necessary. For the analysis in this thesis, a number of scenarios will be implemented in different geographical areas which would require a considerable data gathering and pre-processing effort. Furthermore, the freely downloadable windows version of the model only allows for modelling in small catchments (50x50 grid cells) whereas some of the case study basins are much larger than that. A version of the model that is capable of running more grid cells is available on request but only for experienced users (as it is the more complicated full model) and in collaboration with the developers. These restrictions and the difficulty in setting up this model resulted in this model not being considered for use in this thesis.

MIKE-SHE

MIKE-SHE is a integrated hydrological modelling system that has been in development since the 1980s by the Danish Hydraulic Institute (DHI Water and Evironment). The model includes process models for evapo-transpiration, overland flow, groundwater flow and channel flow (Graham and Butts, 2005) and has been used throughout the World for a range of applications including flood studies, wetland management studies and impacts of land use and climate change studies. The model has its own graphical user interface (GUI) and links with GIS software such as ESRI Arcmap. The model is a commercial product mainly used by consultancies and comes at considerable cost (~€10,000). The high cost and significant data requirement made it not feasible to apply this model for this thesis.

WetSpa

WetSpa is a GIS-based distributed watershed model originally developed by Wang (1996) and later adapted to include flood prediction (deSmedt *et al.,* 2000; Liu *et al.,*

2002) and is maintained by the Vrije Universiteit Brussels. More recently, the model has been developed as an ArcGIS module (Chormanski and Michalowski, 2011). The model has mostly been applied in eastern European catchments such as Poland (Poretta-Brandyk *et al.,* 2011) and Slovakia (Bahremand *et al.,* 2006). Since the model is mostly used for flood prediction, it runs on daily or hourly time-scales. The model requires spatial data on land use and soil types as well as daily hydro-meteorological data such as rainfall and potential evapo-transpiration and discharge at the basin outlet for calibration purposes. Optionally, PET can be calculated using a Penman-Monteith equation but this then requires daily data for air temperature, short wave radiation, relative humidity and wind speed. Since daily data is not available for most of the climate change scenarios as well as the case study basins, applying this model would require the temporal downscaling of hydro-meteorological data. Furthermore, considerable cost and effort would have to be put in preparing the land use and soil data. Overall, this model would be a good choice when looking at short term flood dynamics but since the interest for this thesis is on long-term water resources the model will not be used.

SWAT

The Soil and Water Assessment (SWAT) model is a physically based, continuous-time hydrological model that can be applied at basin scale at a daily or sub-daily time step (Gassman *et al*., 2007). It was developed to predict the impact of land management on water, sediment and agricultural chemical yields in ungauged watersheds (Neitsch *et al.,* 2005; Gassman *et al.,* 2007) but can also be applied for assessing impacts of climate change. The model runs in a GIS environment (ESRI Arcmap) and although computationally efficient, requires quite extensive user input. SWAT operates by dividing a watershed into multiple sub-watersheds, that are further sub-divided into hydrologic response units or HRU's. These HRU's are theoretically homogenous in land use, land management and soil characteristics. The number of HRU's depends on the level of detail of the land use, soil and land management. The model is freely available and has been applied for various applications throughout the world (Gassmann *et al.,*

2007). Similar to the WetSpa model, SWAT requires daily or sub-daily data which is difficult to obtain in some of the regions studied for this thesis and requires temporal downscaling of GCM output. Moreover, the significant effort required to prepare the datasets for the hydrologic response units make this model a less ideal choice for the analysis in this thesis since modelling will be carried out for a number of case studies.

AguaAndes/WaterWorldAguaAndes/WaterWorldAguaAndes/WaterWorld is a policy support system that was initially developed as the FIESTA model for UK DfID and then made available as a web based tool for the CGIAR Basin Focal Project for the Andes (AguaAndes) but can be applied at global scales (as WaterWorld). The system is a web-based water resources policy support tool that that can be used to test the consequences of implementing land and water related policies. The system can be applied globally and runs on either 1-square km or 1-hectare resolution using an extensive global detailed spatial database and spatial models as well as scenarios for climate, land use and economic change. The underlying hydrological model in the system is the FIESTA model (Mulligan and Burke, 2005) which is a spatially explicit model designed to calculate a water balance for tropical mountain areas using physically based representations of wind driven rainfall, cloud water interception and evapo-transpiration. The model uses some 130 input data layers which include terrain (SRTM, Farr and Kobrick, 2000), climate (WorldClim, Hijmans *et al.,* 2005) and land cover (MODIS vegetation continuous fields VCF2000; Hansen *et al.,* 2006). Climate variables are incorporated as long term (50 year) monthly means and a water balance is calculated for a total of 48 time steps for twelve months with 4 time steps in each month representing a diurnal cycle. Finally the water balance is accumulated downstream along a stream flow network to obtain potential runoff.

The AguaAndes/WaterWorld PSS has the advantage that it enables users without specific technical hydrological or GIS skills to use a sophisticated spatial hydrological model like FIESTA without the need for obtaining and preparing the extensive datasets required. Moreover, it is the only such model system to allow users to apply

downscaled climate scenaria from the IPCC to simulate hydrological changes under climate change scenarios. Given the criteria for model selection described above, the AguaAndes/WaterWorld model was therefore chosen as the most appropriate model for the analysis in this thesis.

2.7.4. Tools for modelling freshwater service flows

As well as spatially distributed hydrological models, there are models and model systems that are widely used in the assessment of changes in land use and climate and hydropower and reservoir sedimentation. Two of such models are INVEST by the Natural Capital Project which is a joint venture among Stanford University's Woods institute for the environment, University of Minnesota's institute on the environment, The Nature Conservancy and the World Wildlife Fund and WEAP, developed by the Stockholm Environment Institute (SEI). Both models are described below.

INVEST

InVEST is a collection of models for quantifying and mapping the values of multiple ecosystem services based upon ecological production functions and economic valuation methods (Tallis and Polasky, 2009). The aim of the models is to enable better consideration of natural capital in decision making (Tallis *et al.* 2008). InVEST allows users to visualize the impacts of potential land management decisions, identifying tradeoffs and compatibilities between likely environmental, economic and social benefits (Tallis *et al*. 2008; Nelson *et al*. 2009). InVEST includes a suite of simple model components that include carbon sequestration, pollination of crops, managed timber production, water pollution regulation and sediment retention for reservoir maintenance. It also includes a biodiversity component so analysis of tradeoffs between biodiversity and ecosystem services can be analysed. Moreover, InVEST 1.003 (beta) includes two additional model components, namely: avoided reservoir sedimentation and reservoir hydropower production. InVEST has a tiered design, in which each model component would include a simple and a complex version that provides users the option to be able to run a model with different data availability

levels. The model components realised in InVEST 1.003 (beta) are all simple versions only (the sophisticated models are yet to be developed, Tallis *et al.,* 2008). InVEST is aimed at government agencies, conservation organizations and corporations, among others, that often have to evaluate tradeoffs between natural resource management and environmental protection or conservation (Tallis *et al*. 2008).

WEAP

WEAP is a water planning and water allocation modelling tool that can be applied at multiple scales from small watersheds to basins that is designed to evaluate user-developed scenarios that accommodate changes in the bio-physical and socio-economic conditions of watersheds over time (Yates *et al.,* 2005). The model includes limited physical processes and is mainly focused on evaluating different water allocation schemes subject to water demand and associated priorities. Hydrology is calculated by using a semi-distributed water balance approach and the model can dynamically be linked to groundwater, water quality and optimization models (Sieber and Purkey, 2007). The software has an inbuilt module to simulate reservoirs and power production. The financial planning module of WEAP can calculate costs and revenues associated with scenarios. WEAP uses a GIS-like graphical interface where a user can build a system using a link node structure that describes water demands and pollutant sources. The time step can range from days to seasons with time horizons from single years to a maximum of 100 years. Demand sites are given a user defined priority ranking and water allocation is solved in an iterative, linear programming approach. The model is widely used around the world for a range of different applications. Since the hydrology component of WEAP is rather limited, as the model focuses on water allocation rather than hydrology, this model was not considered for use in this thesis.

3. Development of a geo-referenced global database of dams

3.1. Introduction

This chapter will describe the development of a GlObal geO-referenced Database of Dams (GOOD^2). This database has been developed using a so-called Google Earth GEOWIKI approach, which is an open source database that allows anyone with an internet connection and Google Earth installed to contribute to the development of the database. Building a dam database using Google Earth and GEOWIKI started in 2006 and the database has been in development since. Additions can still be made online at the following weblink:

http://geodata.policysupport.org/dams

In order to model the hydrological impacts of climate change and land use changes on water inputs into global dams, it is necessary to have a global spatially geo-referenced database. Visible dams in Google Earth were digitised and named and as much additional information as possible about the dam was given. As anyone can access and add to the database, the development is a collaborative effort. However, most dams were digitised by Leo Saénz, Arnout van Soesbergen and Mark Mulligan. Leo Saénz did most of the digitising in the tropical and subtropical region between 23.5° North and 35.5° South as his PhD dealt with the impacts of land use change on dams in the pan tropics (Saénz, 2011) and Arnout van Soesbergen did most of the area north and south of this region with additions from Mark Mulligan at various locations throughout the globe. Furthermore, a number of dams were digitised by master students from the Environmental Monitoring, Modelling and Management course *Environmental GIS* and some attributions from elsewhere. The pantropical dam database or KCL Geo-referenced Tropical Dams Database (KCL GTDD) has been published separately (Saénz, 2011; Saénz and Mulligan, 2012) hence this chapter has some commonality with those publications as the global database is an extension of the pan-tropical dam database.

3.2. Background

The total number of large dams (dams with a dam wall above 15m height) around the world is estimated to be around 50,000 (ICOLD, 2003, World Commission on Dams, 2000) with an additional 800,000 smaller ones (McCully, 1996). To date, around 120-320 new large dams are built every year (McCully, 1996) with a particular boom in dam building in the 1950s and 1960s in the US, the 1970s in Asia and 1980s in Africa. Currently, around two thirds of the largest dams are found outside the developed world and most new dams are planned or being built in the developing world particularly in India, China, Brazil and Turkey. Of the estimated 800,000 smaller dams around the world, around 70,000 can be found in the US (Graf, 1999) and around 60,000 in China. These smaller dams play a large role in local scale water supply schemes, often in rural areas but there is a need to monitor them for engineering safety evaluations -especially in meteorologically and tectonically hazardous areas- because of the downstream risk they represent to human communities in the event of failure (Graf, 1999). Whilst the population of these small dams is larger and potentially more impacting than the population of large dams around the world, these smaller dams are the least well documented.

Due to the ability of dams to store water for energy generation, water supply, irrigation, flood control, recreation and navigation, they have a significant impact on the hydrological and biogeochemical water cycles which influences many aspects of economy, ecology and human welfare (Lehner and Döll, 2004). Information on the distribution of dams is therefore of interest to many disciplines of science. Despite these significant impacts and demand for improved datasets to facilitate research, very few comprehensive datasets exist that take into account precise location of dams on a global scale. Whilst there are a number of local to national scale datasets it is particularly the global distribution of dams that is of interest for assessment of land use and climate change modelling and large-scale studies of their role in fresh water productivity. A global geo-referenced census of dams combined with scenarios of land use and climate change is therefore critical in understanding future water supplies for

both humans and the environment and for investigating the potential outcomes of policy and engineering interventions to mitigate the impacts.

Various databases of dams exist around the world but most of these are only partial, covering different spatial extents or lack spatial information making them of limited use for spatial analysis. The most comprehensive dataset on a global scale is the world register of dams published by the International Commission on Large Dams (ICOLD, 2003) whose latest publication (2011) contains 37,626 dams. Even though this database is comprehensive in that it contains many attributes of the reported dams such as use and type of dam and storage capacities amongst others, there is no geo-spatial location information on the dams. Moreover, the database is not freely available and incomplete for a number of fields particularly for developing countries. The database only reports large dams where such a dam is defined as dams with a structural dam height of no less than 15m or a storage capacity greater than 3 million cubic metres. The information in the database is gathered through official enquiry and literature review amongst its 82 ICOLD member countries and 58 non-member countries. As such, data for some countries (most notably the member countries) is better than for other countries. The type of data gathering also carries the risk with it that there are differences in the way dams and their attributes are reported between countries. Also, if countries failed to respond to the data request, information was taken from the earlier version of the database (ICOLD, 2003). However, on a global scale, the database is the most comprehensive and it provides information on important dam features such as catchment area sizes that can be used to validate the database described in this chapter. The recently completed international collaborative GRAnD (Global Reservoir and Dam Database) dam database is the first geo-referenced database that is global in extent. This database currently contains only 6862 dams but is freely available for non commercial use (Lehner *et al.,* 2011).

The most comprehensive regional dataset is the National Inventory of Dams of the United States compiled by the US Army corps of Engineers (USACE, 2006) and the

Federal Emergency Management Agency (FEMA), collectively known as NID (NID, 2007). This database is geo-referenced and contains around 75,000 dams that are of "environmental consequence". Dams are defined as artificial barriers with a minimum height of 2m and a storage volume of more than 61,700 cubic metres.

FAO, through its Information System on Water and Agriculture (AQUASTAT) hosts a geo-referenced database of dams on the African continent (AQUASTAT 2006). This database holds around 1300 dams in total and is collated using information gathered from a variety of sources including ICOLD, national reports and internet sources. Most dams in the database are large dams as defined by ICOLD but there are also some smaller dams included if data were available. The precision of the geo-referenced dams however is shown to contain errors. Saénz (2011) carried out a validation of a sample of 100 dams in the database against Google Earth imagery and found that nearly half of the dams were poorly geo-referenced and not in the right location with a mean geo-referencing error of 2200 m latitude and 4000 m longitude. This means that using this database geo-referenced attributes for derivation of dam catchments within the proposed methodology (see section 3.2) is not feasible.

Other national or regional dam databases are the National Register of large dams in India which reports dams in the same standard as ICOLD and contains (as of 2009) 4710 dams, the Brazilian Committee on Dams (CBDB, 2008), the Venezuelan Committee on large dams (COVENPRE, 2008) and the Mekong River Commission main streams dam map (MRC, 2008). Furthermore there are a few datasets compiled for research purposes that are global or nearly global in extent such as Rödel, (2005) which is a dataset mostly based on geo-referencing dams from the ICOLD database and McKercher (2005) which is a comprehensive dataset for New Zealand. Finally, there are also databases of lakes and reservoirs that are indicative of dam locations such as the reservoir database by Vörösmarty *et al*, (2003) which is global in extent but only includes reservoirs with more than 0.5 km^3 of storage and the Global Lakes and

Wetland database (GLWD) by Lehner and Döll (2004) which is a very comprehensive global dataset of natural and artificial reservoirs.

Many of these databases are particularly useful for studies with a more regional context and or studies that require additional attributes on dam information. However, for the purposes of hydrological modelling of climate change on water inputs into global dams, a consistent, global and precisely geo-referenced database is necessary. Therefore, the KCL pantropical dam database was extended to the global scale using the same methodology as applied to the pantropical dam database (Saenz and Mulligan, 2007).

3.3. Methodology

3.3.1. Dams

3.3.1.1. Digitising global dams

Dams were digitised by scanning through one by one degree tiles on the Google Earth geobrowser (Google Earth, 2009) using a variety of imagery sources such as LANDSAT Geocover (GLCF, 2007), QUICKBIRD (Digitalglobe, 2010) and aerial photographic imagery that are available in Google Earth. To be able to identify likely locations of dams based on their reservoirs, a Google Earth visualisation of the SRTM Water Body Dataset (SWBD) (Farr and Kobrick 2000) by Mulligan (2006e) was used as a guide in the digitising process. The GEOWIKI works as a collection of kml layers where, if a dam is identified, double clicking the arrow opens up a web browser where additional information about the dam and the name of the person digitising can be filled in. Once the imagery throughout the 1-degree tile has been visually scanned for dams, an arrow in the centre of the tile is clicked and information on the digitiser can be filled in. Once submitted, the square becomes red, indicating the tile is complete. This means that multiple users can add to the database without interfering with each other's efforts and users can clearly identify which areas are left to scan. Figure 3.1 shows how dams are being digitised for high-resolution (Quickbird, IKONOS, SPOT, Aerial, 1m resolution)

and low-resolution (LANDSAT Geocover 2000, 15m resolution) imagery in Google Earth and figure 3.2 shows screenshots of the Google Earth GEOWIKI for dams at various zoom levels.

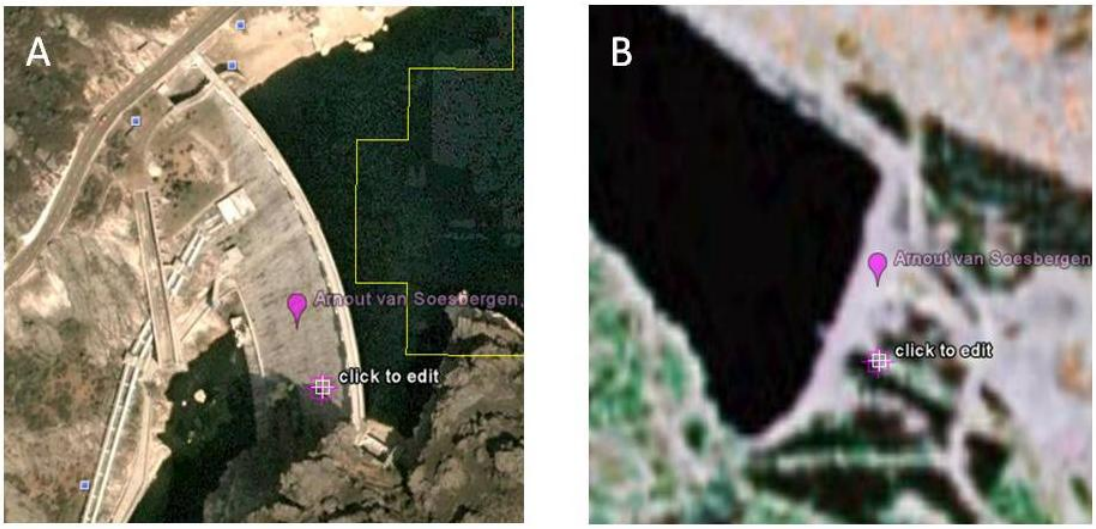

Figure 3.1 Difference between high-resolution (A) and low-resolution imagery (B) for dam digitising in Google Earth (Image A: Digitalglobe 2010, Camporredondo dam Spain. Image B: Terametrics 2010, Karlgard, Sweden)

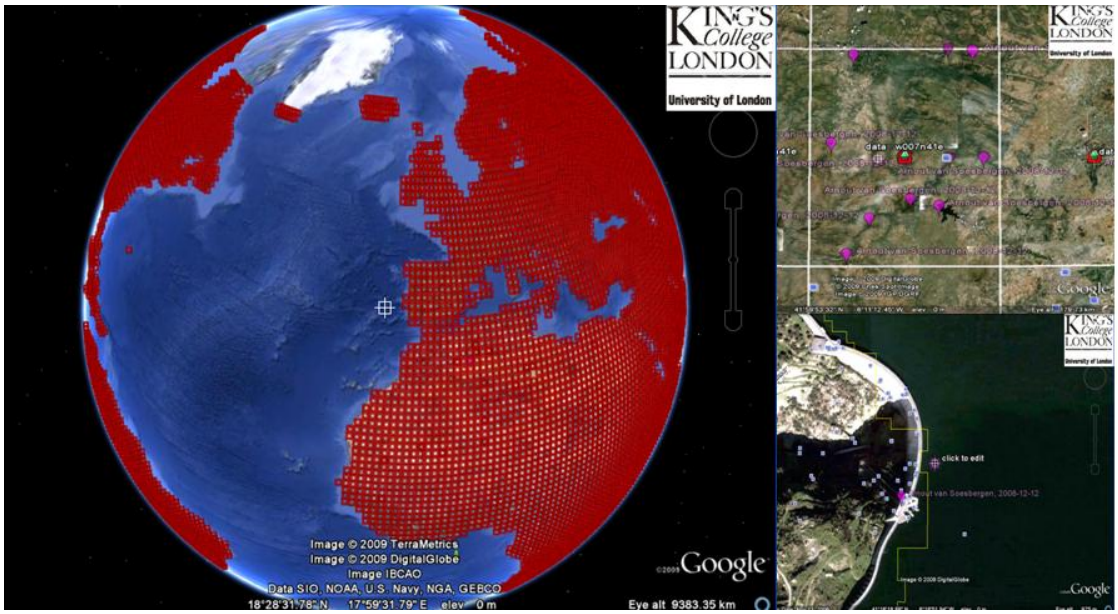

Figure 3.2 Screenshots of various zoom levels for dam digitising using the Google Earth GEOWIKI (Google Earth 5.1; Mulligan, 2008)

3.3.1.2. Minimum dam size criteria

Since Google Earth imagery resolution differs for different areas around the world and at different periods in time, a minimum dam size for inclusion in the dam database had to be established, defined as the minimum size that could still be identified as a dam with low (LANDSAT Geocover 2000) resolution imagery. Saénz (2011), assessed the dimensions of the length of the dam wall and maximum length of the dam reservoir perpendicular to the dam wall as the dimensions that could be identified based on the values of these on a sample of 100 small dams from the NID (2007) database. This resulted in a reservoir length of 500 metres and dam wall length of 150 metres for small dams that could be identified with certainty from low resolution imagery available in Google Earth.

3.3.1.3. Supporting sources

A number of supporting sources were used to more easily find locations of dams or to verify and validate the catchment of the dam. These sources included geo-referenced digital information, lists and printed documentation. Included in the GEOWIKI on Google Earth are the SRTM SWBD (see section 3.2.1.1. and the Gazetteer place names database, Mulligan, (2006c) which is a geographic feature database containing more than 4 million features globally compiled from the US National Geospatial Intelligence Agency GEONET Names Server database (GNS). The World Register of Dams (ICOLD, 2003) was used to find dams more easily in areas with low resolution imagery on Google Earth (e.g. Russia) by matching place names from Gazetteer with the location attribute listed in the ICOLD database such as nearest village or name of dam. Furthermore, the geo-referenced database by the US Army corps of Engineers (USACE, 2006) was used as an overlay in Google Earth to locate dams in the US. Similary, Saénz (2011) used the FAO AQUASTAT (AQUASTAT, 2006) database to locate dams on the African continent. Other sources that were used included information from the World Commission on Dams (World Commission on Dams, 2000), the Brazilian Committee on Dams (CBDB, 2008), the Venezuelan Committee on Dams, (COVENPRE, 2008), the Mekong River Commision main streams dam map (MRC, 2008), the Global Lakes and

Wetlands Database (Lehner and Döll, 2004), the National Register of Large Dams in India (2009) and the SEPREM, Spanish Association on Dams and Reservoirs (SEPREM, 2010). Many of these sources were also used to validate the calculated dam catchment areas as discussed in section 3.2.3.4.

3.3.1.4. Validation: Image resolution, cloud cover and contributors

The spatial resolution of imagery in Google Earth ranges from around 1m based on IKONOS, Quickbird, SPOT and aerial photography to around 15m based on Landsat Geocover Mosaics from the 2000s. The higher resolution imagery is generally found in urban areas and developed countries whereas lower resolution imagery is found in developing countries and more remote areas such as northern Canada and Siberia. Even though the imagery in Google Earth is continuously updated, there are still large areas of the globe that only have the lower (15m) resolution. Since the visual identification of dams depends on the spatial resolution of the imagery, geographical variation in image spatial resolution will lead to differences in number of dams identified.

To account for the possible underestimation of the number of dams in areas with low resolution imagery, a number of areas have been digitised twice using the historical imagery feature of Google Earth (available from version 5.1). A number of 1-degree tiles previously digitised in high resolution imagery areas that contain dams were randomly selected for this procedure. The tiles were re-digitised using older Landsat geocover mosaic (circa 2000) imagery. The difference between both sets of dams can then be used as an indicator of the potential number of dams that are not represented in the database for areas still under low resolution imagery. This procedure has been applied to 4 locations of 4 1-degree tiles in both high dam density areas and low dam density areas. Only 4 tiles were chosen for this analysis as this work builds on earlier work by Saénz (2011) who carried out a similar exercise for 14 frames around the pantropics giving a sufficiently large sample of dams to be validated (~5% of the total

population of dams). Table 3.1 presents the results of this validation process for the 4 tiles.

Table 3.1 Ratios of underestimation of nr of dams found for different imagery resolutions

Location[1]		Date imagery	Nr of dams	Date Imagery	Nr of dams	Ratio
LatLL	LongLL					
41.00	08.00	01/02/2000	0	30/07/2005	45	0
41.00	121.00	01/11/2000	7	05/03/2005	9	0.8
22.00	76.00	18/01/2003	34	15/01/2004	70	0.5
47.00	06.00	31/10/2002	2	05/11/2006	10	0.2

[1]Lower left latitude and longitude of 2 x 2 degree grid

It is clear from the small sample displayed in table 3.1 that the level of underestimation can be quite high in certain areas, with the maximum number of dams found in the low resolution imagery amounting to eighty percent of those found independently in the high resolution imagery (i.e. an underestimation of 20%). The 14 frames sampled by Saénz (2011) yielded better results with an average underestimation of 21% for all frames. The extent to which this underestimation will lead to underestimation in the global database is most likely to be less though as the areas with low resolution are generally confined to more remote and uninhabited areas that have fewer dams anyway, such as Siberia and North-Canada. Human modified landscapes that have most of the world's dams tend to be covered by high resolution imagery.

Another source of potential error related to imagery comes from cloud cover. Some areas, particularly in the tropical mountains are obscured by heavy cloud cover in the native Google Earth imagery which makes it virtually impossible to locate a dam. To be able to find dams in cloud affected regions, Terrascope imagery (Mulligan, 2007) was used. Terrascope is a Google Earth implementation of the LANDSAT MSS, TM and ETM+ ortho mosaics for the 1970s, circa 1990 and circa 2000. These images have been converted to superoverlays with resolutions ranging from 57 metres/pixel for the 1970s (MSS) to 14.25 metres/pixel for circa 2000 (based on ETM+). Particularly the

1990s imagery can be very useful in detecting dams under cloud affected imagery in Google Earth native imagery (which uses Geocover 2000s).

Finally, a potential error in the number of dams identified for a region exists because of the GEOWIKI approach in which any user can contribute to the database. Different users may have different interpretations of what constitutes a dam or should be included in the database (see section on minimum size dam criteria, 3.2.1.2). To be able to account for any potential differences between various contributors, a number of 1-degree tiles were digitised twice, making sure the imagery used in the digitisation process was the same by looking at the date when the tile was finished and if necessary setting the imagery date on Google Earth to the imagery available at that time. Table 3.2 presents the descriptive results for this procedure.

Table 3.2 Validation of number of dams found between different contributors

Country/Continent	LatLL	LongLL	Initial	Re-digitised	% overlap
China	30N	105E	242	212	87.6
India	19N	77E	94	90	87.6
Africa	26S	29E	93	66	70.9
South America	07S	50W	6	8	100.0
South America	06S	75W	5	3	60.0
North America	27N	100W	190	188	98.9
South America	10N	67W	89	55	61.8

LatLL and LongLL are the Lower left latitude and longitude of 1 x 1 degree grid

From table 3.2 it can be seen that the number of dams found between two contributors can differ somewhat although on average more than 80% of dams were found by both contributors, so differences are less than 20%. Since most dams are to be found in the watersheds of other dams these kinds of errors probably have little impact on the watersheds which are the prime analytical property used in this research. Also the largest watersheds will tend to be dammed by the larger dams so that the majority of watersheds should be definable from digitizing the largest dams.

3.3.2. Catchment areas

To be able to understand impacts of land use and climate change on water and sediment loads arriving at dams, it is necessary to accurately derive the watersheds that contribute to each dam. The methodology to calculate contributing watersheds to dams consists of calculating a hydrologically correct stream flow network (based on a digital elevation model, DEM) which can be overlaid with dam locations which are then snapped to occur on the correct flowline. Using common GIS techniques, one can then derive the watershed that contributes flow to that particular dam.

3.3.2.1. DEM, LDD and Stream Flow network

The first step in deriving a stream flow network is to have a digital elevation model (DEM). The DEM used in this study is the freely available HydroSheds (Lehner *et al.,* 2008a) elevation model at 30-arc second or ~ 1 km resolution, available as continental .BIL files. This DEM is derived from elevation data from the SRTM space shuttle mission (NASA, 2009) reprocessed to fill voids using a combination of two algorithms developed by CIAT (Jarvis *et al.,* 2008) and HydroSheds (Lehner,(2008b), and is a seamless, nearly global void-filled DEM that is particularly useful for hydrological modelling. A more technical description of this DEM is given in Lehner *et al.,* (2008a). As the SRTM DEM only covers the globe between latitudes of 60 degrees south and 60 degrees north, another DEM had to be used for the land masses in the most northern regions (Scandinavia, North Russia, Canada, Alaska). The DEM used for these regions is the global Hydro1K at 30 arc second (~ 1km) resolution which is available on a continental scale. The necessary region (above 60 degrees north) was clipped and mosaiced with the SRTM DEM using ArcMap 9.3 GIS software (ESRI, 2010) resulting in six continental tiles as described in table 3.3. Note that the extents of the continents are overlapping. This is to ensure that if there are dams on the border of a continental tile, their catchments will be calculated correctly on either of the two overlapping tiles depending on the DEM in that area.

Table 3.3 Continental tiles and extents

Continent	**Resolution**	**Latitude**		**Longitude**	
		From	To	From	To
North America	1 km	90 North	0 North	-180 West	-50 West
South America	1 km	20 North	-60 South	-90 West	- 30 West
Africa	1 km	- 40 South	40 North	- 20 West	60 East
Europe	1 km	90 North	10 North	-30 West	70 East
Asia	1 km	80 North	0 South	50 East	180 East
Australasia	1 km	30 North	-30 South	-180 West	-130 West

These continental DEMs were subsequently used to derive a stream flow network using the PCRaster Environmental Modelling Language (Wesseling *et al.,* 1996) and standard PCRaster operators. The reason for using PCRaster derived stream flow networks and not the stream flow networks that are part of the Hydrosheds distribution is to ensure consistency with the earlier (PCRaster) derived stream flow networks for the pantropical dam database as carried out by Saénz (2011) as well as to ensure a consistent approach to the derivation of a stream flow network for the areas above 60 degrees North. The first step in the analysis was to calculate a Local Drain Direction map or LDD. A LDD map indicates the direction of flow of material (e.g. water or sediment) from one cell to its immediate steepest down slope neighbouring cell (PCRaster, 2008). The LDD map was calculated using the D8 algorithm (O'Callaghan and Mark, 1984) with the PCRcalc (PCRaster calculator engine) operator *lddcreate*, using 1e31 as the parameter value for outflow depth, core volume, core area and catchment precipitation. This means that all pits in the LDD will be removed. Pits are sinks in the system where flow of material would stop in the stream network. Hence pit cells can receive flow from upstream cells but do not contribute to downstream cells. Erroneous pits therefore produce errors when flows will be accumulated downstream. This algorithm is discussed in more detail in Van Deursen (1995). To create the ldd map, the

continental DEMs as created in ArcMap 9.3, first had to be exported as ASCII files and converted to .map format in PCRaster after which the following syntax was used:

pcrcalc ldd.map = lddcreate (dem.map, 1e31, 1e31, 1e31, 1e31) (3.1)

Subsequently, a stream order network was calculated using the method of Strahler (Strahler, 1952) and the PCRcalc operator *streamorder* using the following syntax:

pcrcalc streamorder.map = streamorder(ldd.map) (3.2)

Since the SRTM elevation model is derived from radar data, the data is influenced by vegetation and surface effects such as roughness, wetness, open water surfaces and radar shadow (Freeman, 1996). Therefore, the derived river network can also be affected by these errors. This is particularly the case for flat regions such as deltas where relief is not well-defined. For the purpose of calculating the catchments of dams this is not a major problem as dams are typically found in areas where there is strong relief.

3.3.2.2. Verification and relocation on the river network

In order to be able to calculate the catchments associated with the dams, it is necessary that the dam locations spatially overlay the correct stream flow lines. Even though the spatial location of the digitised dams in Google Earth is highly accurate relative to the image locations of the dams, this does not mean they will always overlay the representation of the stream flow network on the stream order map derived from the DEM because of the relatively coarse resolution of 1-km. To align the dams with the stream flow lines, the stream order map as calculated in section 3.2.1.1 was overlaid with the shapefile of dams as digitised in Google Earth and locations of dams were manually spatially adjusted in a GIS using ArcMap 9.3 so they overlay the stream flow lines (see figure 3.3a and 3.3b).

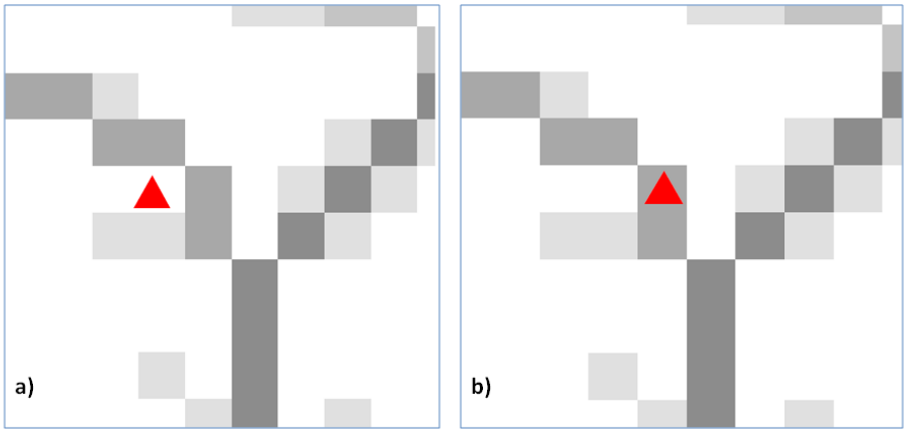

Figure 3.3 (a) Dam out of place in relation to calculated flow network at 1km resolution and (b) dam adjusted.

3.3.2.3. Calculation of catchment areas

When all dams are accurately aligned with the stream flow network derived from the DEM at 1km resolution, the upstream catchment areas of dams can then be calculated. The catchments were calculated using the PCRaster operator *subcatchment*. This function will dedicate all contributing area pixels on a given flow network as indicated by the LDD map above a catchment outflow point or a given pixel of interest such as a dam (PCRaster, 2008). In order to use this function in PCRaster, the dam point shapefile was first converted to a raster and subsequently exported as an ARCASCII file using ArcMap 9.3 making sure that cell size and number of columns and rows were identical to that of the continental LDD maps. This resulted in six dam ASCII raster files. These were converted to .map using PCRasters asc2map function. Finally, the catchments of the dams were calculated using the following syntax:

pcrcalc subcatchment.map = subcatch (ldd.map, dams.map) (3.3)

The continental maps of catchment areas were then opened in ArcMap 9.3 and converted to kml files so they could be visually inspected in Google Earth in order to check if the derived catchments were of the expected size and shape. For instance, if a dam is placed on the wrong stream flow line during the spatial adjustment process it

may be calculated to have a much smaller or larger catchment than expected. If a dams' catchment was found to be erroneous, the dam was subsequently moved to the correct location on the stream flow network and a new catchment map was calculated using the procedure above.

3.3.2.4. Validation

To verify the accuracy of the calculated catchment areas, the derived values were compared against reported figures available from the World Register of Dams (ICOLD, 2003), the United States National Inventory of Dams (NID, 2007) and other supporting sources as described in section 3.2.1.3. In total, a random sample of 358 large dams (171 for the tropical region (Saénz, 2011) and 187 for the rest of world) - for which catchment areas were available in the literature - were compared against the calculated derived catchment areas. Appendix I shows all the dams that have been used in this process and figure 3.4 shows the result of this verification procedure. The graph shows that there is a good correlation between calculated catchment size and reported size for most of the dams (R^2 = 0.98). The average difference between calculated and reported catchment area amounts to 8.8%. However, some larger differences were found for specific dams. When looking into those specific cases, errors were found in the supporting sources used for validation. For instance, for the La Miel dam in Colombia, the reported catchment area is almost ten times larger than the calculated area but also nearly eight times larger than the river basin in which the dam is located (Saénz, 2011). This points to a large error in the reported catchment size. Other such cases were also found for the La Honda dam in Venezuela and the Segredo and Embarracoda dams in Brazil (Saénz and Mulligan, 2012).

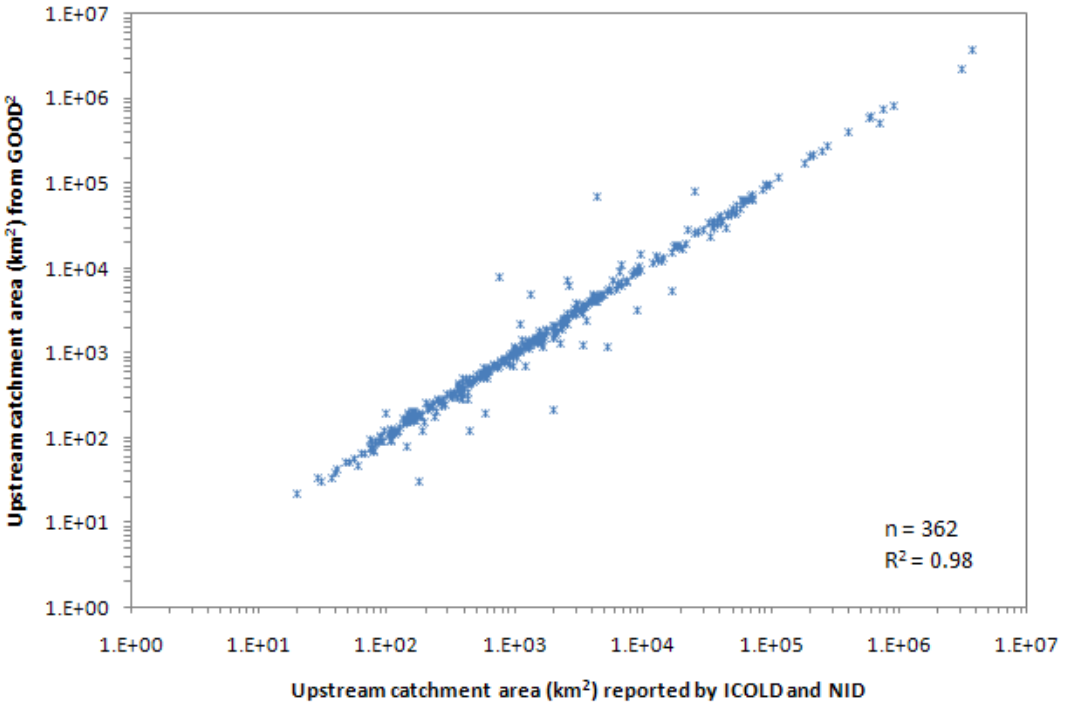

Figure 3.4 Log log correlation between dam catchment areas derived from GOOD[2] and ICOLD (2003) and NID (2006) reported areas in km^2 . Source: author with data contribution from Saénz (2011).

3.4. Results

3.4.1. Dam census

The database to date holds 36,194 dams with 18,742 dams in the tropical and subtropical zone between 23.5 degrees north and 35.5 degrees south and 17,112 dams above that in the northern hemisphere and 339 dams below 35.5 degrees south. Figure 3.5 shows the distribution of dams around the world in the three different zones. On a continental basis, 50% of all dams are found in Asia (18,066 dams), 6.5 % in Europe (2,335 dams), 15.4% in North-America (5,562 dams), 17.1% in South-America (6,203 dams), 9.2 % in Africa (3,347dams) and 1.6% in Australia (583). As discussed in section 3.2.1.4, with relatively large areas having lower imagery resolution at the time of digitising, some areas can be underrepresented though this is not likely to have large effects on the calculated watersheds of dams since the missed dams will be the smallest.

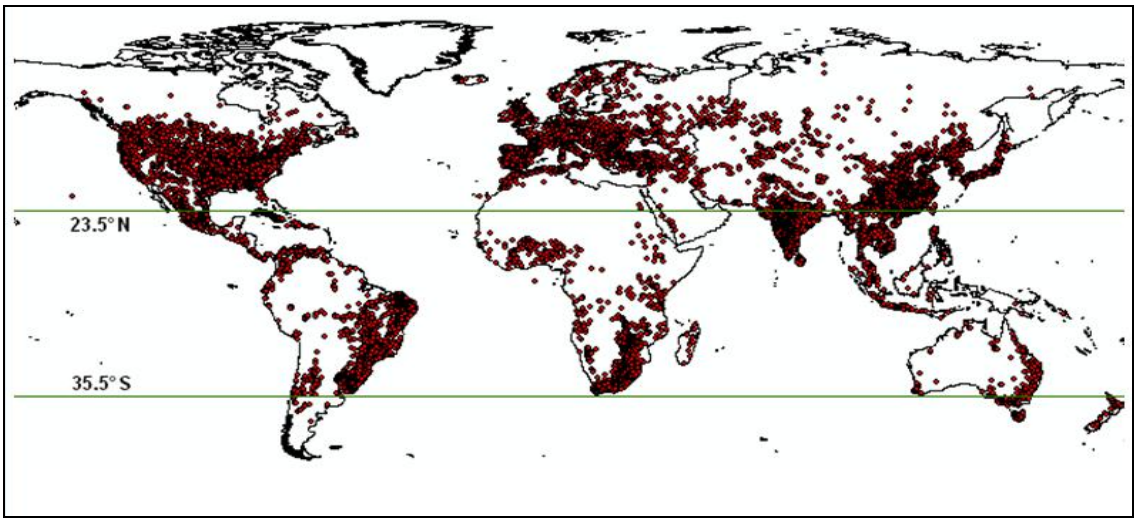

Figure 3.5 Global distribution of dams in GOOD^2 database

3.4.1.1. Dams per country

Figure 3.6 shows a map of the number of dams per country around the world. It can be seen that the lowest number of dams per country are found on the African continent and the highest density is found in Asia. The country with most dams is China with 8,742 dams, followed by India with 6,665 dams, Brazil with 5,305 dams, the United States with 4,014 dams and South Africa with 1,355 dams. In total there are 157 countries around the world that have at least 1 dam. The full list of countries with number of dams can be found in Appendix II.

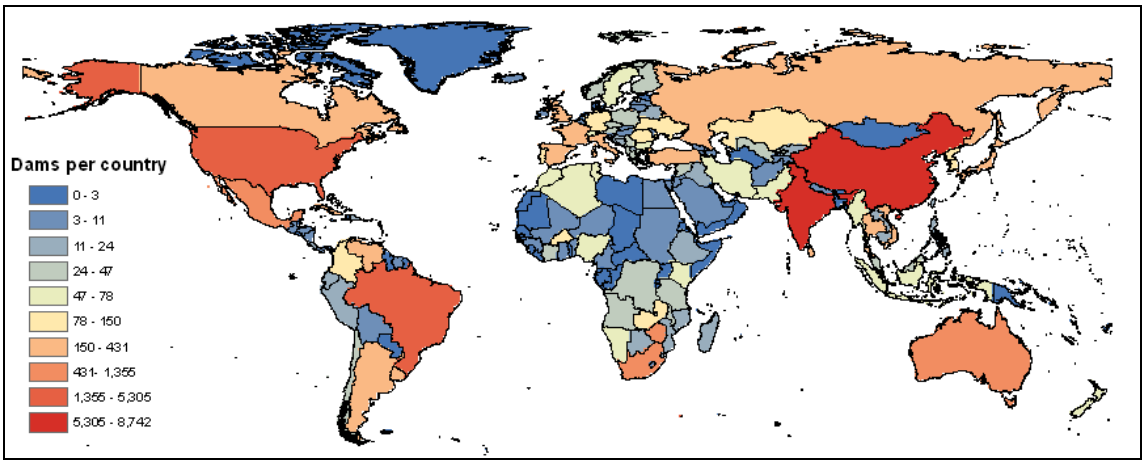

Figure 3.6 Number of dams per country

Table 3.4 lists the above mentioned 5 countries with number of dams in the GOOD^2 database compared to the ICOLD database and other sources. It should be noted that

this edition of the ICOLD database (2003) contains known errors for some countries. For instance, approximately 17,000 dams between 15 and 30 metres in height in China are not included in the 2003 edition (ICOLD, 2003).

Table 3.4 Countries with most large dams in GOOD^2 and compared with other databases

Country	GOOD^2	ICOLD	Other Sources[1]
China	8742	4688	-
India	6665	4636	4710
Brazil	5380	635	-
United States	4014	9265	8122
South Africa	1355	915	-

[1]National Register of Large dams, India (2009) NID, USA (2007)

The 2009 inventory of large dams in India by the National Register of Large dams reports 4,710 large dams and another 390 dams under construction in India in January 2009. ICOLD (2003) has only 635 dams reported in Brazil whereas within the GOOD^2 database 5,380 dams are identified. The main reason for this discrepancy is the inclusion of many small dams in the GOOD^2 database that are not reported in the ICOLD (2003) database as this includes only large dams. Furthermore, ICOLD reports 9,265 dams in the United States with only 4,014 dams identified in GOOD^2. A main reason for this is the exclusion of industrial and mines tailing dams in GOOD^2 as these are not significant for the purpose of water resources modelling.

3.4.1.2. Dam densities

Figure 3.7 shows a map of the density of dams per 10,000 km^2 on a country basis. This representation gives a better idea of how large the impacts of dams are on a national basis. It shows that the countries with the highest population as described in section 3.3.1.1. are not necessarily those with the most dams per unit area. For instance, Brazil ranks third in terms of number of dams but for density it ranks 12th. Most notable are the smaller nations such as Cuba, Puerto Rico, and Singapore with 21, 16 and 18 dams

per 10,000 km^2 respectively. India still ranks highest meaning this country is significantly impacted by dams.

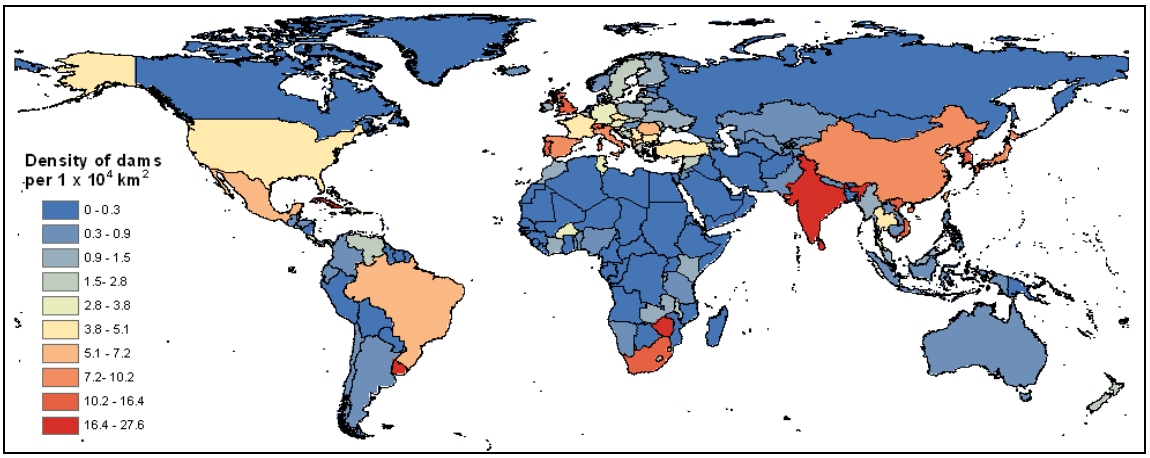

Figure 3.7 Density of dams per 1 x 10^4 km^2 of area on a country basis.

To get a better idea of the density of dams on a global scale without undue weighting by areas such as deserts and wilderness areas where dams do not occur, figure 3.8 shows the density of dams per 10,000 km^2 but only taking into account those one degree tiles that contain at least 1 dam. This way of representing has the advantage of showing a more accurate representation of dam densities as it only focuses on those areas that are affected by dams because it leaves out uninhabited areas.

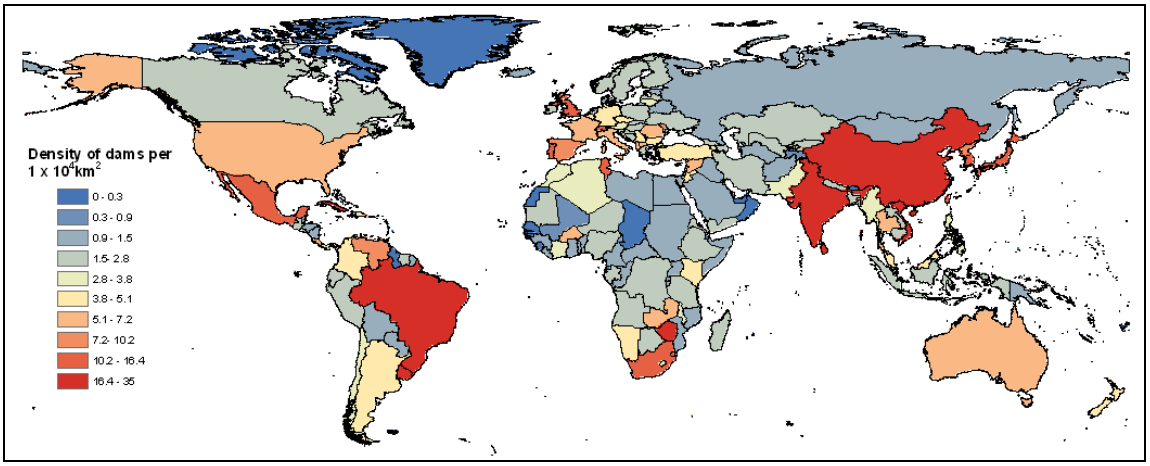

Figure 3.8 Density of dams per 1 x 10^4 km^2 of area on a country basis only considering non-zero one degree tiles.

In this representation Brazil, India and China rank highest with 20, 33 and 22 dams per 10,000 km^2 respectively.

3.4.1.3. Dams in large river basins

Figure 3.9 shows the population of dams in large river basins around the world as defined by the Global Runoff Data Centre (GRDC) large river basins dataset. This dataset contains the 405 largest river basins around the world derived from the flow direction data set of the HYDRO1k Elevation Derivative Database (GRDC, 2007). The three most dam populated river basins in the world are the Yangtze river in China (5,017 dams), the Mississippi river in the United States (1,557 dams) and the Krishna river in India with 1,527 dams. The most populated river basin in South-America is the trans-national river basin of the Uruguay river with 1,484 dams. It should be pointed out that the GOOD^2 database mostly contains reservoir dams with only a few run-of-river dams that are found for example in the Mekong river basin. Due to the lack of reservoir these dams are less easy to identify but are also less relevant in terms of water resources.

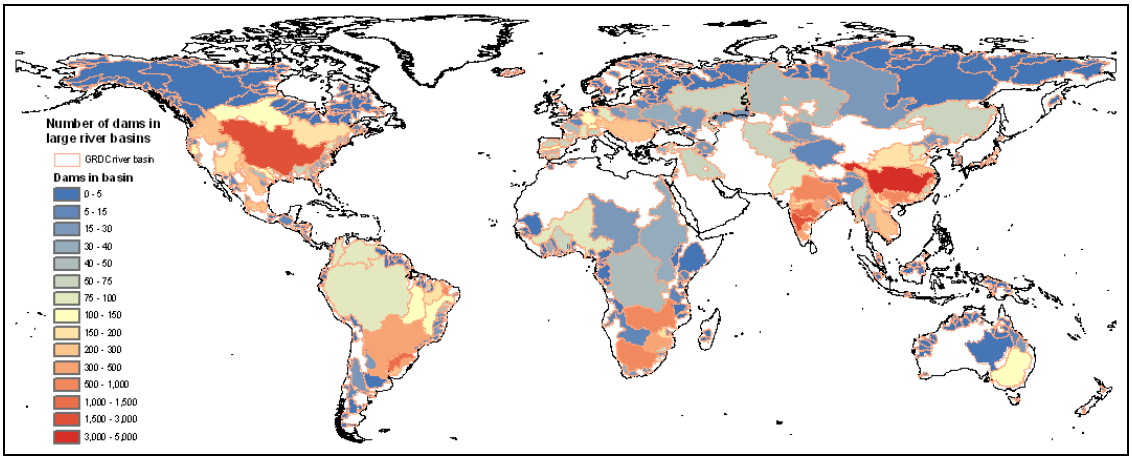

Figure 3.9 Number of dams per large river basin (GRDC)

3.4.2. Catchment areas of dams

Figure 3.10 shows the total land mass covered by dam catchments. In total, around 18% of all global land area and around 32% of all tropical land area (Saénz 2011) drains into a dam. The continental areas affected by dam catchments are also shown in figure 3.10 with the largest dam watersheds found in Africa. However, as can be seen on the

map, these percentages are calculated based on the total continental land mass which means that for instance North America and Asia seem to be less affected due to their vast uninhabited northern areas (e.g. Northern Canada, Alaska and Siberia).

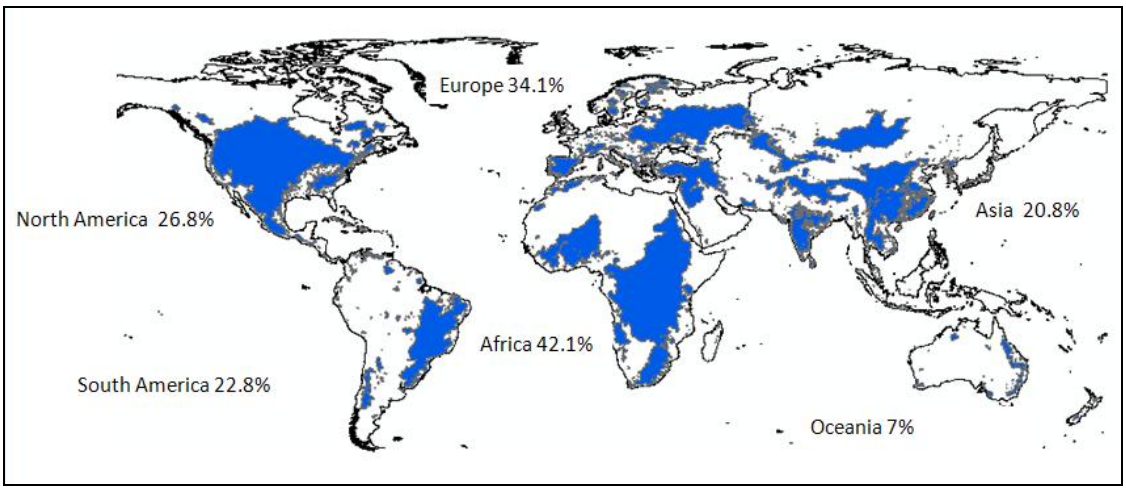

Figure 3.10 Dam catchments and continental area affected by dams

Figure 3.11 shows the individual catchment areas by size (km^2). The largest single dam catchments are found in Africa with the Inga dams in the Congo DRC creating the single largest dam catchment with a calculated area of 3,270 000 km^2 followed by the Kainji catchment in Nigeria. The Inga dams (Inga I and II) are located next to each other on the Inga falls, the world's largest waterfalls on the Congo river. The Kainji dam in Nigeria is a reservoir dam that creates Kainji lake. Other large catchments are mostly found in the Northern hemisphere with some large catchments in Canada such as the AC Bennet dam, and Russia (Volga and Bratsk).

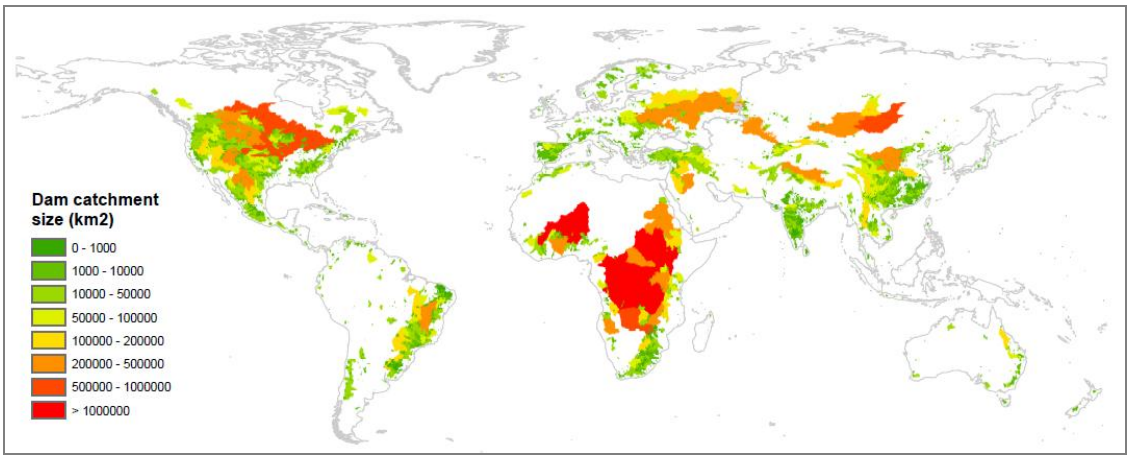

Figure 3.11 Dam catchment size (km^2) in $GOOD^2$ database

3.4.2.1. Proportion of national territory draining into dams

Figure 3.12 shows the percentage of the area of individual countries that drains into a dam. This is a measure of how much of a countries land surface affects the inputs of water to its dams. Some of the countries with the greatest areas can be found in Africa with Congo, Zambia, Burkina Faso and Malawi all having more than 80% of their country area draining into dams. These are mostly because of a few very large dams. In Europe, Spain is the most affected with 73% of its land area draining into dams. From the top 5 countries in terms of dam numbers from table 3.4, South Africa has the largest area draining into dams (57%) followed closely by the United States with 56% , India and China with 46% each and finally Brazil with 39%. It should be noted that some large dam catchment areas are trans-national which could mean that part of some countries land mass drains into downstream dams that are outside their national borders. Appendix III gives the full list of all countries and their numbers of dams and country area draining into dams by percentage.

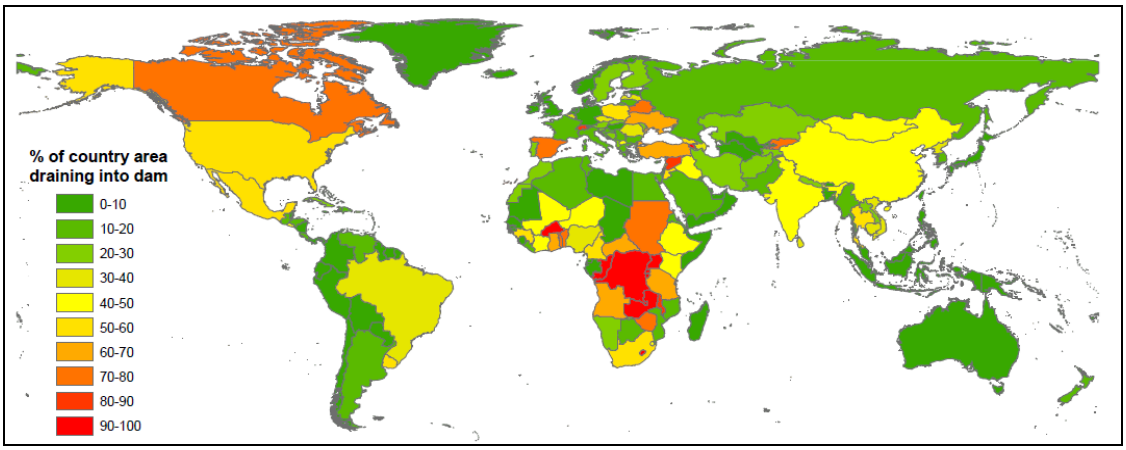

Figure 3.12 Catchment areas that contribute flow to dams generated with GOOD[2]

3.4.2.2. Downstream affected river reaches

Figures 3.13 to 3.18 show the number of upstream dams for river reaches by continent. The most impacted river system in the world is the Yangtze river in China with a total of 5,017 dams upstream (see figure 3.14). Some of the most affected rivers in the world are also found in Asia such as the Ganges (742 dams), Krishna(1,527 dams), and Godavari river (1,463) systems in India and the Xi Jiang (1,013 dams) in China. In Europe, the most affected river is the Danube with 287 dams upstream, followed by the Tejo river in Spain with 108 dams and the Rhine in the Netherlands with 96 dams upstream. Considering the relative small country sizes in Europe compared to the river systems, many of these basins are trans-national with downstream people affected by dams found outside their country borders.

In Africa, the most affected river systems can be found in South East Africa with the Zambezi (870 dams upstream) and Limpopo (412 dams upstream) in Mozambique the most affected. Further South and draining towards the west is the Oranje river on the border between Namibia and South Africa with 535 dams upstream. The Nile is an example of a very large river basin where a small number of upstream dams (34) can propagate effects far downstream on the main stem river.

In North America the Mississippi, the largest drainage basin also has the most upstream dams (1,557). The highest density of dams in the United States can be found

in the South East. In many cases these are smaller dams though. Some of the largest dams are found in the South West, the largest and most affected river system here is the Colorado river with 187 dams upstream.

In South America, most dams are found in Brazil and the most affected river system is the Uruguay, with 1,488 dams draining south between Uruguay and Argentina. Other river systems that have many dams upstream are the Jaguaribe with 521 dams and Acarau with 574 dams. These rivers are also found in Brazil. The world's largest river, the Amazon is relatively little impacted with 90 dams found in its upstream reaches.

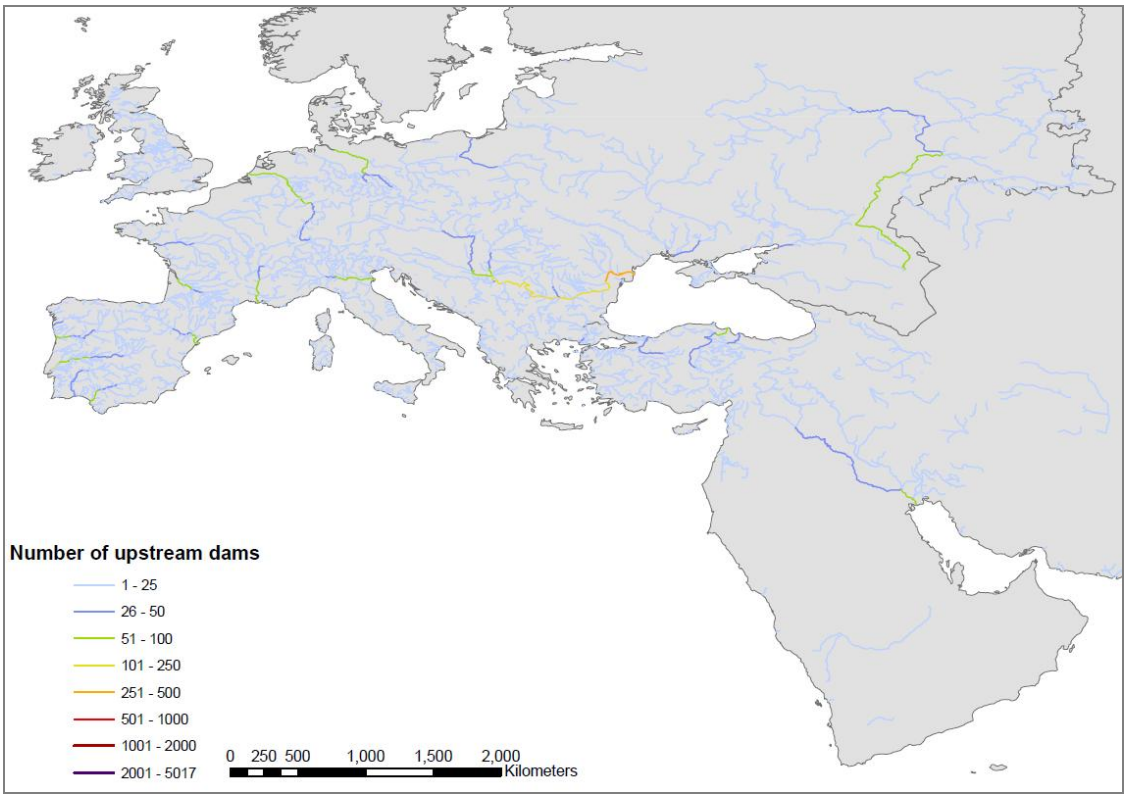

Figure 3.13 Downstream affected river reaches in Europe by number of upstream dams

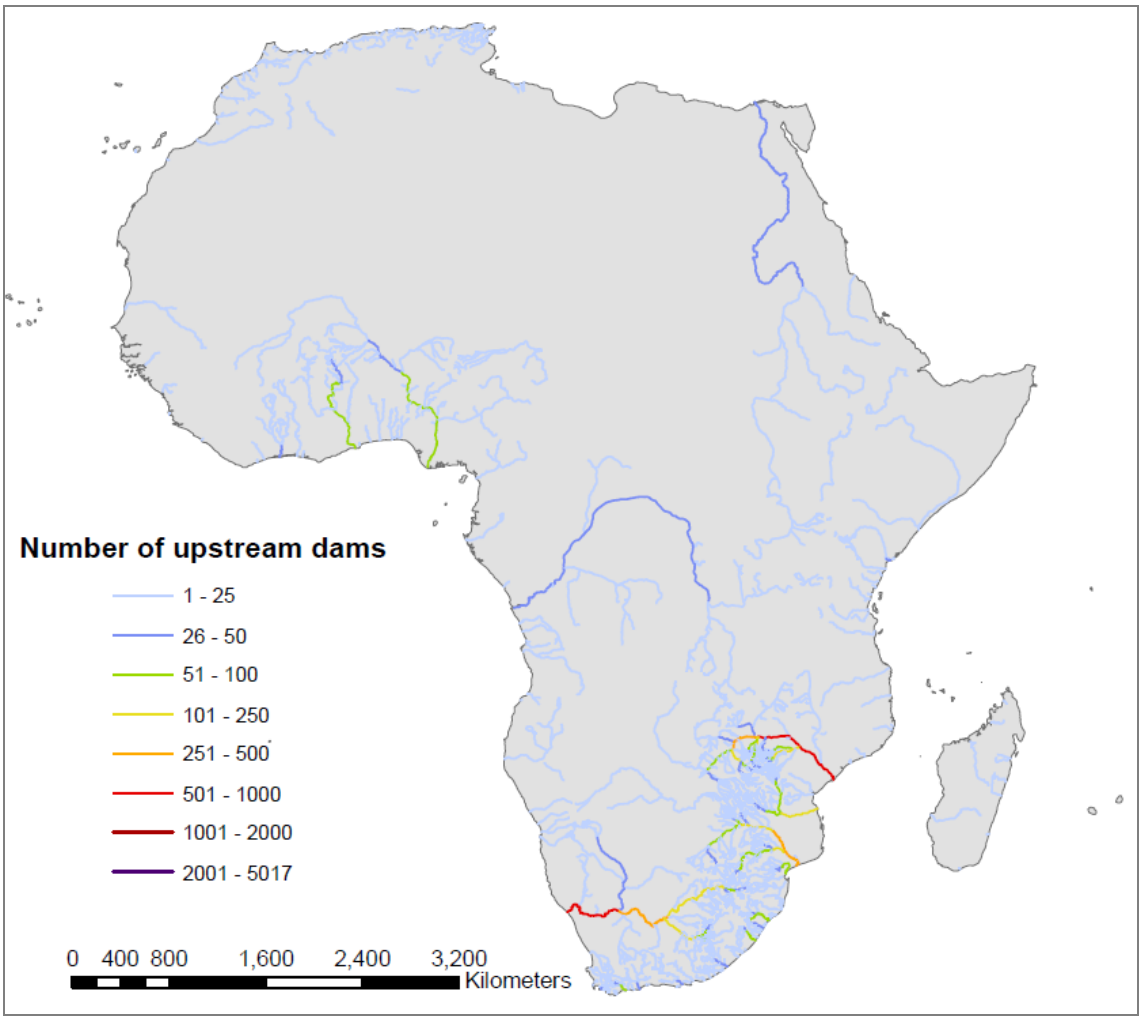

Figure 3.14 Downstream affected river reaches in Africa by number of upstream dams

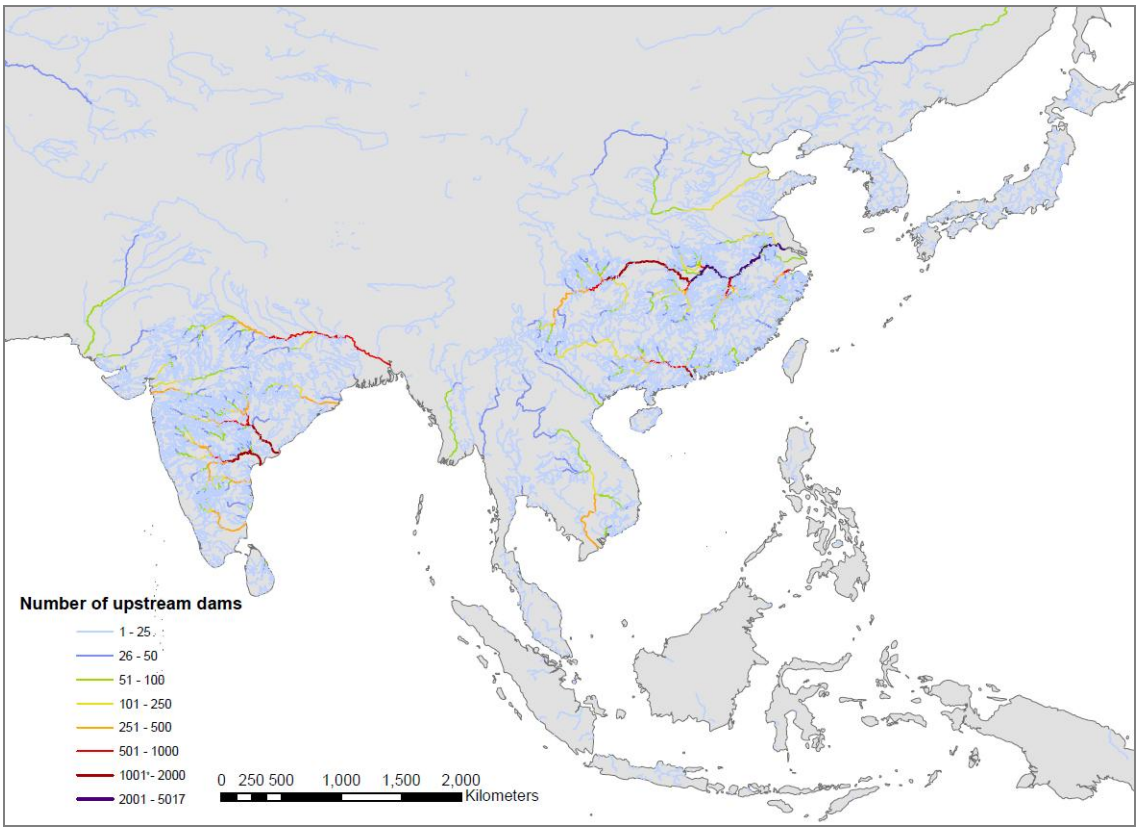

Figure 3.15 Downstream affected river reaches in Asia by number of upstream dams

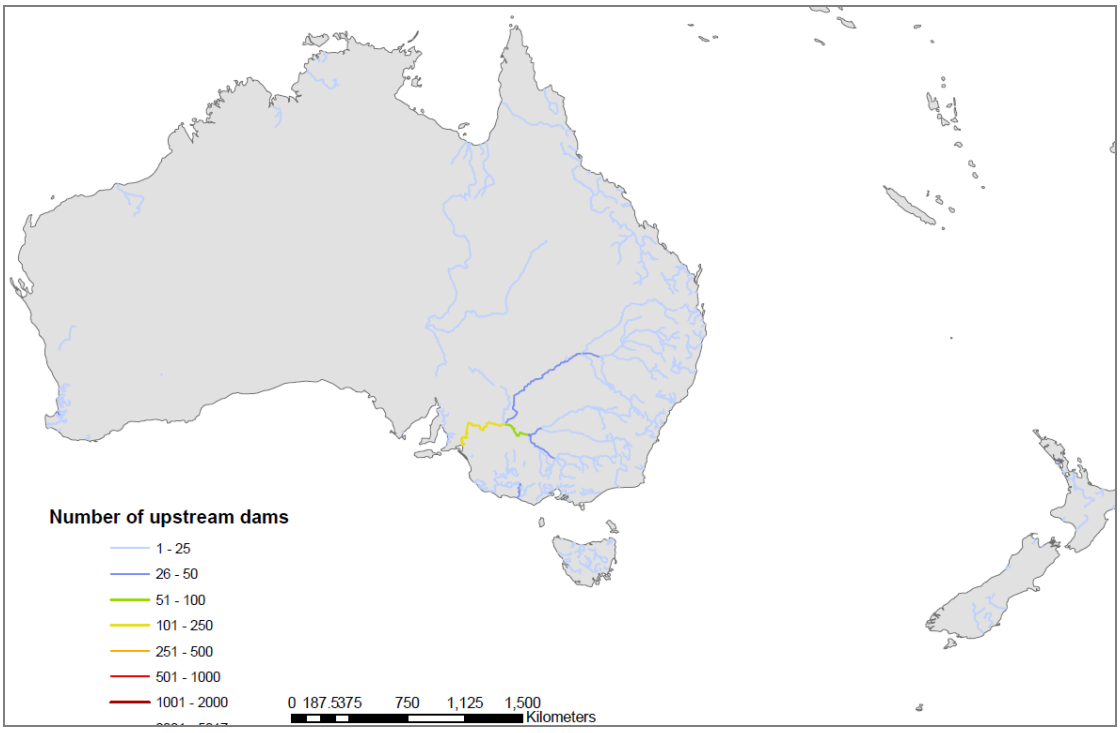

Figure 3.16 Downstream affected river reaches in Oceania by number of upstream dams

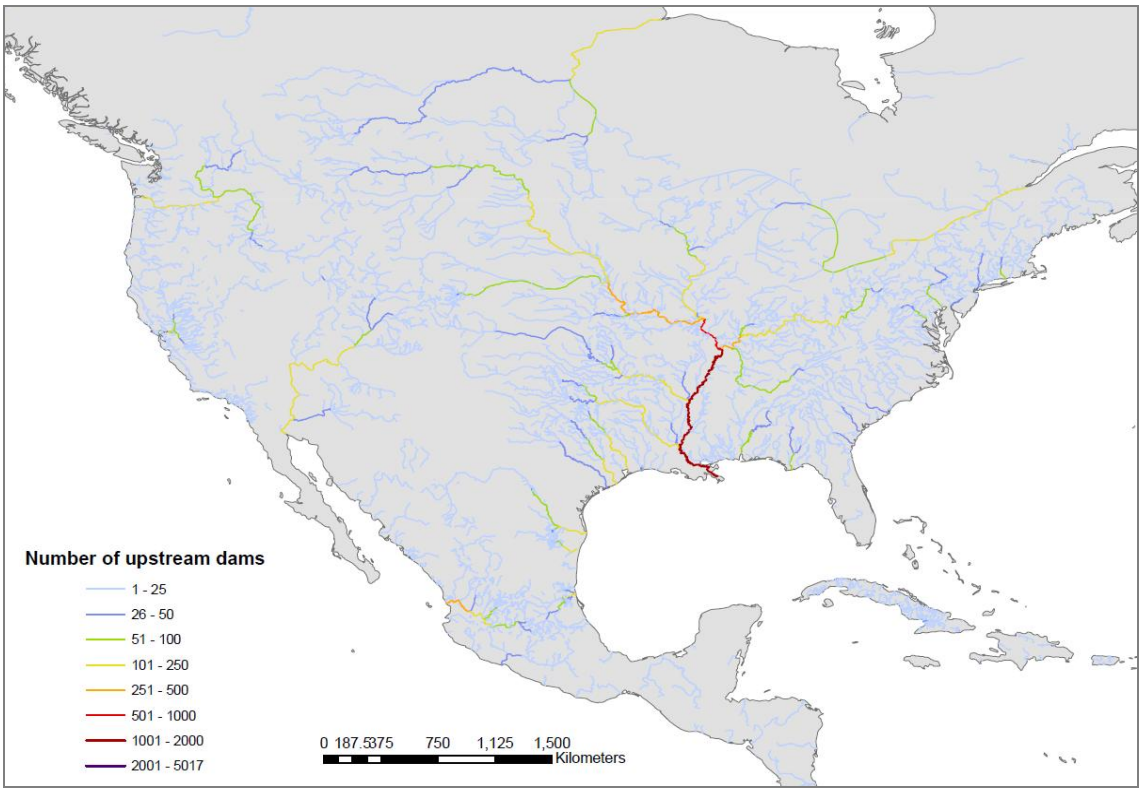

Figure 3.17 Downstream affected river reaches in North America by number of upstream dams

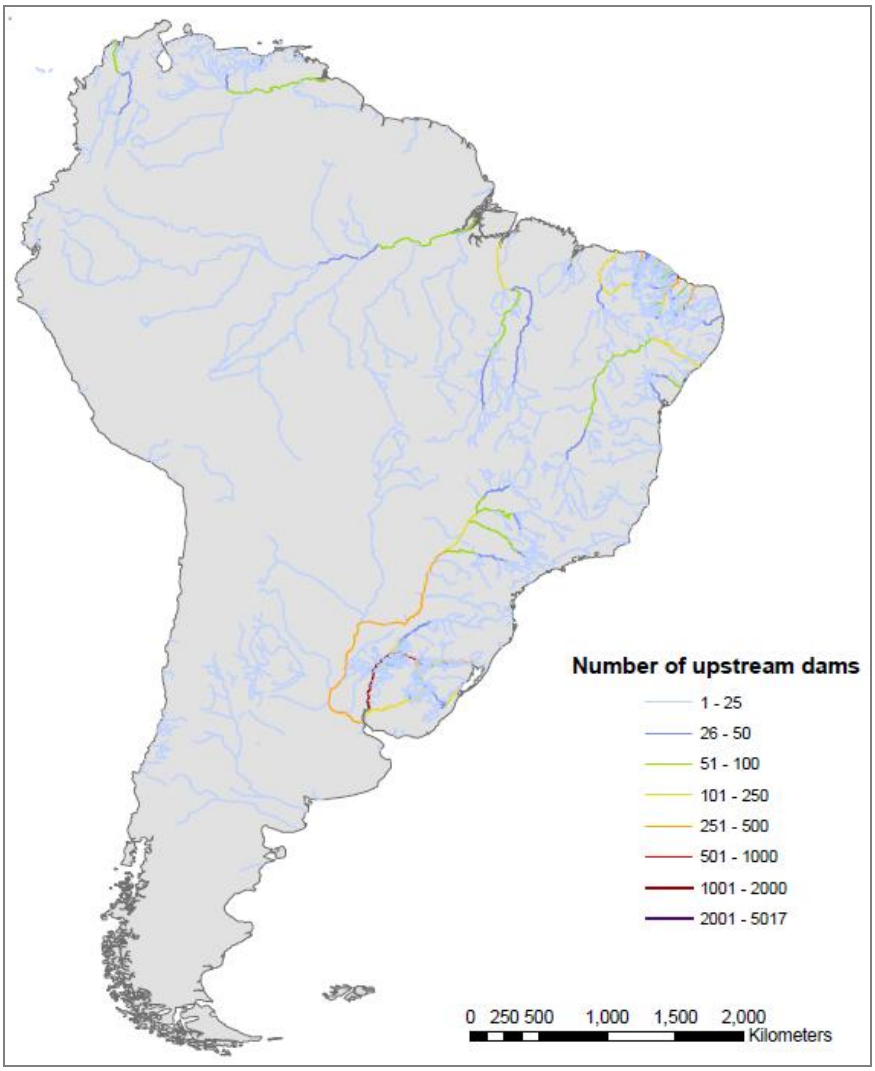

Figure 3.18 Downstream affected river reaches in South America by number of upstream dams

3.4.2.3. Country dependency on dams

Table 3.5 shows the percentage of irrigated cropland and percentage of total electricity production made up by hydroelectric power as a measure of the dependency of individual countries on dams based on data from the UN energy statistics database (UN, 2012) and the World Development Indicator Database (Worldbank, 2012). The table shows the top 20 countries with a full list available in Appendix III. Countries are ranked by their highest combined fractions for both irrigated cropland and percentage HEP. Tajikistan ranks first in this list, even though the country only has 5 dams according to the GOOD^2 database although some of these are very large, including the tallest dam in the world (Nurek dam) which is over 300 m

tall and has an installed capacity of 3,000 MW (Ghasimi, 1994). The list further includes countries from different continents with the number of dams within their borders ranging from only 1 to a 105, most of these are considered developing countries. Countries ranking high in this list can be considered more sensitive to impacts of climate change on dams as they are more dependent on them for their energy security.

Table 3.5 Top 20 country dependency on dams in terms of percentage of total cropland irrigated and percentage of total electricity production generated by hydroelectric power. A list of all countries is available in Appendix III

Rank	Country	% Irrigated cropland	% HEP	Nr of dams
1	Tajikistan	68.3	98.1	5
2	Kyrgyzstan	75.9	90.4	16
3	Albania	50.5	98.1	29
4	Nepal	47.1	99.6	11
5	Suriname	75.0	53.9	4
6	Georgia	44.0	84.8	8
7	Bhutan	23.5	100.0	1
8	Chile	82.4	40.5	35
9	Pakistan	82.0	30.3	63
10	Egypt	99.9	10.9	4
11	Uzbekistan	84.9	23.0	27
12	Colombia	24.0	82.8	105
13	Laos	16.5	86.2	13
14	Zambia	2.9	99.7	104
15	Mozambique	2.6	99.9	24
16	Paraguay	2.1	100.0	3
17	Lesotho	0.9	100.0	6
18	Afghanistan	33.8	67.0	5
19	Burundi	1.6	98.2	3
20	Congo, DR	0.1	99.4	36

3.5. Discussion and limitations

Despite the high accuracy in the geo-referencing of dams and the calculations of the catchment areas there are still some limitations to the KCL GOOD^2 database. Firstly,

there is a probable lack of representation for small dams which is mostly due to the geographical differences in image resolution and the presence of cloud cover in the Google Earth imagery at the time of digitising. The results of a validation exercise shown in table 3.1 show that this under-representation can be fairly high in certain areas, however, the extent to which this will lead to underestimation in the global database is most likely to be less as the areas with low resolution are generally confined to more remote and uninhabited areas that have few dams such as Siberia and North-Canada. Furthermore, many of the missing dams will be smaller dams with small catchments that have less impact on calculated watershed areas. Since the dams GEOWIKI remains active, the database can and should be updated regularly with more and more areas of the globe now under high resolution imagery on Google Earth. Regularly updating will also allow for the inclusion of all newly built dams in the meantime as the database only accounts for existing dams at the time of collection (between 2006-2010).

Currently the database holds 36,194 large dams. Compared to reported figures and estimates of the number of dams to range between 40,000 - 50,000 (World Commission on Dams, 2000; ICOLD, 2003; Lehner and Döll, 2004) this means most large dams will be captured in this database. However, as there are an estimated 800,000 smaller dams in the world (McCully, 1996) and many dams in the GOOD^2 database will be smaller than the dams as defined by ICOLD (2003), this means that some large dams may have not be included. This can partly be explained by the differences in image resolution and cloud cover as discussed above and by the presence of run of river schemes that are rarely captured using our method (except for the largest of these). Another explanation for this discrepancy can be found in reporting techniques as discussed in section 3.1. For instance the reported figure for dams in the US is around 75,000 (Graf, 1999) whereas in GOOD^2 only 4,014 dams have been identified. Even though GOOD^2 includes both large and small dams, many dams were not included because they are run of the river dams, auxiliary dams (dams built to confine reservoirs created by a primary dam) or mining or tailings dams that are not

relevant to water resources assessment. It is assumed that this also explains discrepancies between reported figures and the GOOD^2 database in other areas of the globe.

Another limitation to the study is the use of a digital elevation model (DEM) that has a spatial resolution of 1 km. This means that even though the dams have initially been geo-referenced highly accurately in Google Earth, many of them have to be shifted somewhat to make sure they intersect with the stream flow network derived from this DEM. This is not so much a problem in areas with low dam densities as dams can easily be attributed to the correct river. However, in areas with high dam densities, dams can be as close to each other as a few kilometres making it more difficult to distinguish them. Furthermore, by using such a relatively coarse DEM, small catchments (generally below 10 km^2) tend to show a larger error in their derived catchment size as compared to the reported areas. Another issue with the use of the 1km SRTM DEM is that when it is used for catchment area delineations in flat areas, its uncertainty tends to be higher (Jarvis *et al.,* 2008). This could be a reason for differences in calculated catchment areas and reported dam catchment areas for dams located in relatively flat areas. In addition, the inconsistencies found in the supporting sources used in the validation of the calculated catchment areas (see section 3.2.2.4) could account for part of this error as well.

A main limitation to the database is that there is no distinction being made between run of the river dams or reservoir dams. This means that some of the large catchments could be the result of run of-the-river dams while these dams have no reservoir and do not hold back all of the flow. The extent to which this is a limitation depends on the type of study though as this is an important distinction for studies into freshwater reservoirs but in hydrological terms the contributing area to this dam remains correct. Also, while run-of-the river dams may not be as relevant as reservoir dams for water resources impacts of climate change (since most run-of-the river dams are for HEP)

they may be so for sediment delivery impacts. Therefore, for future updates it is recommended that these attributes are added to the database.

3.6. Conclusion

Using a Google Earth GEOWIKI in combination with supporting layers such as the Gazetteer and SWBD has proven to be a excellent tool to compile a database such as the GOOD^2 database. This resulted in the first consistent global geo-referenced database of dams currently containing 36,194 dams with 18,742 dams in the tropical and subtropical zone between 23.5 degrees north and 35.5 degrees south and 17,112 dams above 23.5 degrees north.

The database includes large dams as defined by ICOLD (2003) as well as a large number of smaller dams. It has therefore a high representation of all current existing dams around the world. Most dams exist in countries with strong upcoming economies such as China with 8,742 dams, India with 7,159 dams and Brazil with 5,176 dams. These countries have large potential for hydropower and have high energy needs to keep their economies growing. It is therefore also these countries that show the highest rates of dam building. The United States which ranks fourth with 4,014 large dams contained in the database had its dam boom in the 1950s and 1960s and is currently decommissioning a number of dams. On a continental scale, Asia has by far the largest population of dams with 18066 dams, followed by South America with 6,203 dams and North America with 5,562 dams.

Using GIS techniques, catchment areas for all these dams were calculated and these have proven to be highly accurate when compared to reported figures from a variety of sources. These catchments cover around 18% of the total global land mass with 32% of all tropical land mass contributing to flow into dams. Countries that are most affected by dams, i.e. have the highest percentage of their land area flow into dams are mostly found in Africa with some countries completely covered by dam catchments such as Burundi, Uganda and Rwanda even though the number of dams is relatively

low in these countries (5, 8 and 5 dams respectively). National dependence on dams was assessed by looking at the hydroelectric production as a percentage of total electricity production and percentage of irrigated agriculture. For large river basins, it was found that the most affected river basins in terms of number of dams are the Yangtze in China with 4,763 dams, the Mississippi in North America with 1,557 dams and the Krishna river basin in India with 1,527 dams.

In conclusion, this chapter has presented the development of the first geo-referenced *global* dataset of dams using innovative techniques based on freely available datasets and the Google Earth geo browser. This database can be used to model the potential impacts of land use and climate change on the access and supply of freshwater as well as the potential interventions to mitigate such impacts.

4. Climate change impacts on global catchments of dams

4.1. Introduction

This chapter will assess the impacts of projected climate change on the catchments of dams on a global scale, using the calculated dam catchment areas from the KCL GOOD^2 database as described in chapter 3, in combination with general circulation model output from the latest IPCC Assessment Report (AR4) to calculate a change in water balance in the catchments of these dams. The first step in this analysis was to create multi-model mean global climate change grids for temperature and precipitation on a common resolution from the outputs of five General Circulation Models that are available in the AR4 along with some inter-model uncertainty metrics such as standard deviation, range, and coefficient of variation. Once this was completed, changes in water balance over the dam catchments between the baseline and A1B and A2A scenarios for the 2050s were calculated using a temperature based approach for the calculation of evapo-transpiration and remotely sensed data on soil moisture. Changes in reservoir water level under these climate change scenarios are estimated for a range of large dams by combining dam locations with the SWBD (Farr and Kobrick, 2000; Mulligan, 2006e) database to locate the dams with the largest reservoirs. These changes in reservoir level can have a direct influence on the potential hydroelectric power output of these dams or their capacity to provide freshwater for irrigation or other purposes. Finally, an assessment is made of the impacts of the projected climate changes on the water available for domestic use (according to population) and croplands (according to agriculture) within the dam catchments.

4.2. Methodology

4.2.1. Creating multi-model mean climate change grids

The general circulation models and scenarios used in this study are the set of model outputs that were developed for the fourth assessment report of the IPCC (AR4, IPCC, 2007). These model results are available through the Data Distribution Centre (DDC) of the IPCC. Since GCMs run on coarse resolutions, ranging from 1.875° latitude by 1.875° longitude or 2.5° latitude by 3.75° longitude (e.g. HADCM3 model by the Hadley Centre in the UK), they need to be downscaled to a common and finer resolution before they can be combined to create multi model ensemble means for regional application. It is necessary to use downscaled GCM input for hydrological impact analysis since the coarse resolution of GCMs do not take into account significant sub-grid scale features such as topography, clouds and land use (Fowler *et al.,* 2007). In order to simulate monthly flows in mountainous river basins larger than 10,000 km^2 in size, the minimum spatial resolution for temperature and precipitation should therefore be no more than 0.125° latitude and longitude (Salathé, 2003). A more in-depth discussion of GCM downscaling and uncertainties is provided in section 2.5.3.

CIAT (2010) provides freely available downscaled GCM model output for 24 GCMs from the AR4 on a global scale downscaled to 1 km resolution for monthly mean, maximum and minimum temperature and monthly total precipitation as well as other bioclimatic variables. This database is still in development with more and more data becoming available over time and can be accessed through the following link: http://ccafs-climate.org/

The downscaling method used for these datasets is the delta method which is a statistical downscaling technique that uses empirical relationships between large-scale climate variables and observed weather variables (Wilby *et al.,* 2004). Essentially, this method takes the GCM model output for both the future period and the baseline period and produces the deltas or anomalies as the differences between the projected climate and the current observed climate. This field is then smoothed (interpolated) to

remove edge effects and applied to the high resolution monthly baseline climate data, in this case from WorldClim (Hijmans *et al.,* 2005). The main assumptions of this method are that changes in climate at coarse scales represent those occurring also at finer scales and that the spatial variability of climate surfaces at the sub-grid scale will be similar in future climates as to those today. It is argued though that these assumptions - while true in some cases - might be wrong in others, particularly when landscapes are highly heterogeneous and considerable variation is caused by topographic conditions over relatively small distances (Ramirez and Jarvis, 2010). A more in-depth discussion of different downscaling techniques is given in section 2.5.3.

Using long-term climatic means also means that extremes and temporal variability is not taken into account. Therefore, extremes such as droughts are not reflected in the projections. The IPCC in its Special Report on Extremes (SREX) (IPCC, 2012) highlights that there is medium confidence that droughts will intensify in the 21st century for a number of regions, most notably the Mediterranean. However, in many other regions, there is low confidence as a result of inconsistency in projections. A number of studies have attempted to model future drought (e.g. Lehner et al.,2006; Burke et al., 2006; Blenkinsop and Fowler, 2007; Hirabayashi et al., 2008). However all these studies are limited by the uncertainties in projections of precipitation by GCM. Downscaled GCM data for two IPCC SRES emission scenarios were downloaded; the A1B and A2A scenarios. The A1B scenario assumes a rapid economic growth with rapid introduction of more efficient technologies balanced across fossil intensive and non-fossil energy sources while the A2A scenario assumes a heterogeneous world with slower technological change resulting in higher emissions, particularly towards the second half of the 21st century. Section 2.2 gives a more detailed overview of these emission scenarios. These scenarios were chosen as at the time when this analysis was carried out, these were the only ones that had output of several models downscaled already. The data can be downloaded either as zipped Arc ASCII files or zipped ArcGIS GRID files and are available on four different resolutions, 10 arc minutes, 5 arc minutes, 2.5 arc minutes and finally 30 arc seconds. In total, output of 5 models for A2A and 5 models

for A1B were downloaded for the 2050s period which is calculated as a 30-year mean for the period 2041-2060. This time period was chosen because it is the most relevant time period to use in impact analysis with regards to dams, which have a limited lifespan and since they represent the climate to which adaptation must be most focused upon.

The five models were chosen on the basis of availability of results for both of the two scenarios assuring a consistent approach to the climate change analysis. Model output for all 5 models for the A1B scenario was available for the whole globe up to 90 degrees North whereas for the A2A scenario, model output was only available up to 60 degrees North, leaving out some areas where dams are found such as Canada, Scandinavia and Russia. Table 4.1 gives an overview of the GCMs used.

Table 4.1 Overview of GCM used in analysis

Model	**Resolution**		**Developed by**
	Longitude	**Latitude**	
CCCMA_CGCM_31	2.8	2.8	Canadian Center for Climate Modelling and Analysis
CSIRO_MK30	1.875	1.875	Australia's Commonwealth Scientific and Industrial Research Organisation
IPSL_CM4	3.75	2.5	Institut Pierre Simon Laplace France
MPI_ECHAM5	1.875	1.875	Max-Planck-Institut for Meteorology Germany
UKMO_HADCM3	3.75	2.5	UK Met. Office

After all of the files were downloaded, they where then unzipped and an ArcGIS python script was used to calculate mean monthly values for the scenarios and annual means for temperature and annual mean sum for precipitation. To assess the uncertainty between the models, the inter-model, range and directional agreement were also calculated on a monthly and annual basis along with the monthly coefficient

of variation for precipitation and monthly standard deviation for temperature. Finally, anomalies were calculated using the baseline climate data available from WorldClim (Hijmans *et al.,* 2005) for the time period 1960-1999. In order to be consistent in methodology, WorldClim climate data is used throughout this thesis.

4.2.2. Uncertainty in climate change modelling

Uncertainty with respect to GCM modelling experiments has been described in much more detail in section 2.5 with uncertainty introduced at the level of emission scenarios, the GCM and the downscaling. In order to deal with some of these uncertainties, particularly on a global scale, it is advisable to use multi model ensembles rather than individual GCM results. For some studies results are presented for all models in the ensemble but for spatial studies this becomes very challenging and difficult to communicate so some measure of the overall tendency of the ensemble such as the mean (Tebaldi, 2010; Knutti et al., 2010) should be used. In this chapter, the ensemble mean is used. Buytaert *et al.,* (2009) and Stainforth *et al.,* (2007) note that using a range of GCM models provides a climate change envelope that is considered to be a sensible way to provide this uncertainty information to stakeholders. However, using the multi-model mean has the disadvantage of averaging out extremes. Because of the increased performance in predicting current climate by multi-model means they are often applied in hydrological impact studies. For example, RCMs from the UK Climate Projections project (UKCP09) have been used in various impact studies. In order to improve precipitation predictions (important for flood studies) in many cases the precipitation fields are bias corrected whereby the mean is corrected using relatively arbitrary methods such as cut-off thresholds, distribution corrections or variance increase (Yang et al., 2010; Wetterhal., 2012; Cloke et al., 2012). Recently, alternative approaches to assess climate risks based on sensitivity analysis have been suggested where, rather than a GCM driven analysis, GCM projections are used to inform in a user-led approach (Brown and Wilby, 2012).

For reasons of differences in availability of downscaled GCM models for the chosen SRES emission scenarios and time periods, no more than 5 GCM have been used in this analysis. To assess the uncertainty in the annual multi-model climate grids, the inter-model range (precipitation and temperature) and the number of models that agree on the direction of the change with regard to the WorldClim baseline (precipitation only) was calculated. This gives an indication of the geographical distribution and magnitude of the uncertainty. Figures 4.1 to 4.4 give the results for this analysis.

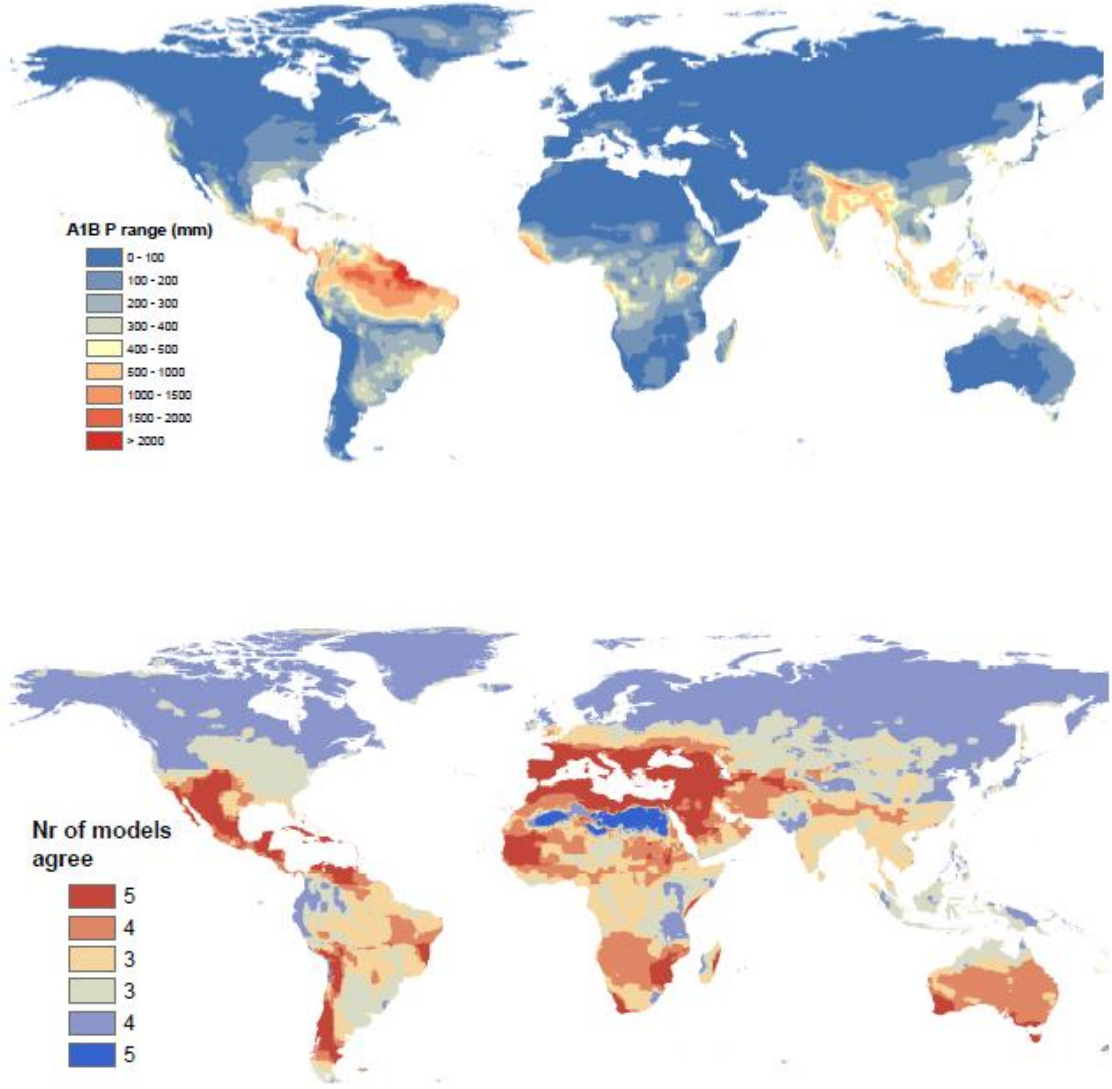

Figure 4.1 Range of precipitation projections for 5 GCM for A1B scenario (top) and the number of models that agree on the direction of the change with respect to the WorldClim baseline climatology, red is drier and blue is a wetter direction of change (bottom)

Figure 4.1 shows the range of precipitation projections and the number of models that agree on the direction of the change with respect to the WorldClim baseline. The greatest disagreement between the models can be found in the humid tropics, most notably in the Amazon and South East Asia. Also, large parts of the eastern United States and eastern South America have projected differences of up to 400 mm a year between models. Under this scenario, almost all of the world up to around 60 degrees North dries, with parts of northern Africa a notable exception. All 5 models agree on a drying in the Mediterranean and large parts of the Middle East.

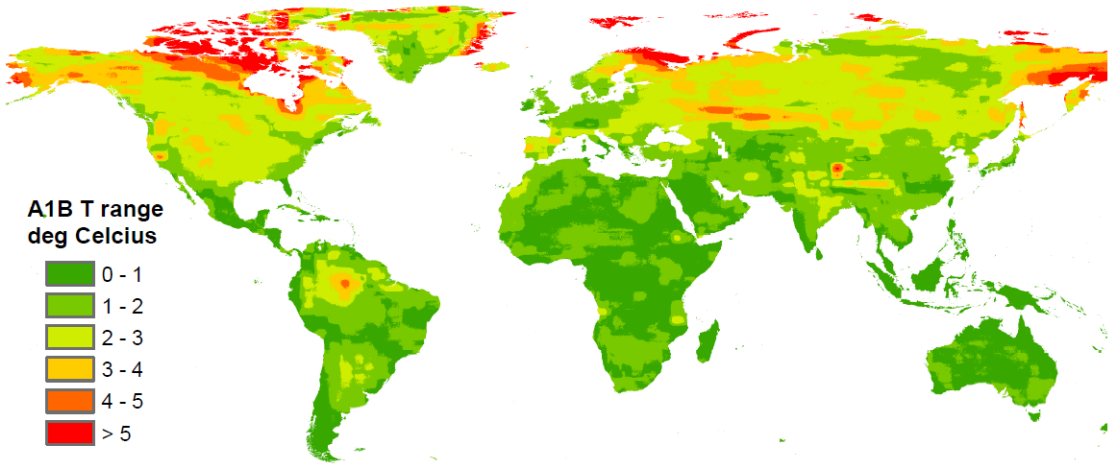

Figure 4.2 Range of temperature projections for 5 GCM for A1B scenario for the 2050s

Figure 4.2 shows the range of temperature projections for the A1B scenario for the 2050s. All models project a warming. However, the range of temperature projections for the 5 GCMs under the A1B scenario show the greatest disagreement between models in the northern hemisphere with projections differing between 2 to 4 or even 5 degrees Celsius. The highest agreement can be found for the African continent, the Middle East, Australia and parts of South East Asia where the range is no more than 2 degrees Celsius.

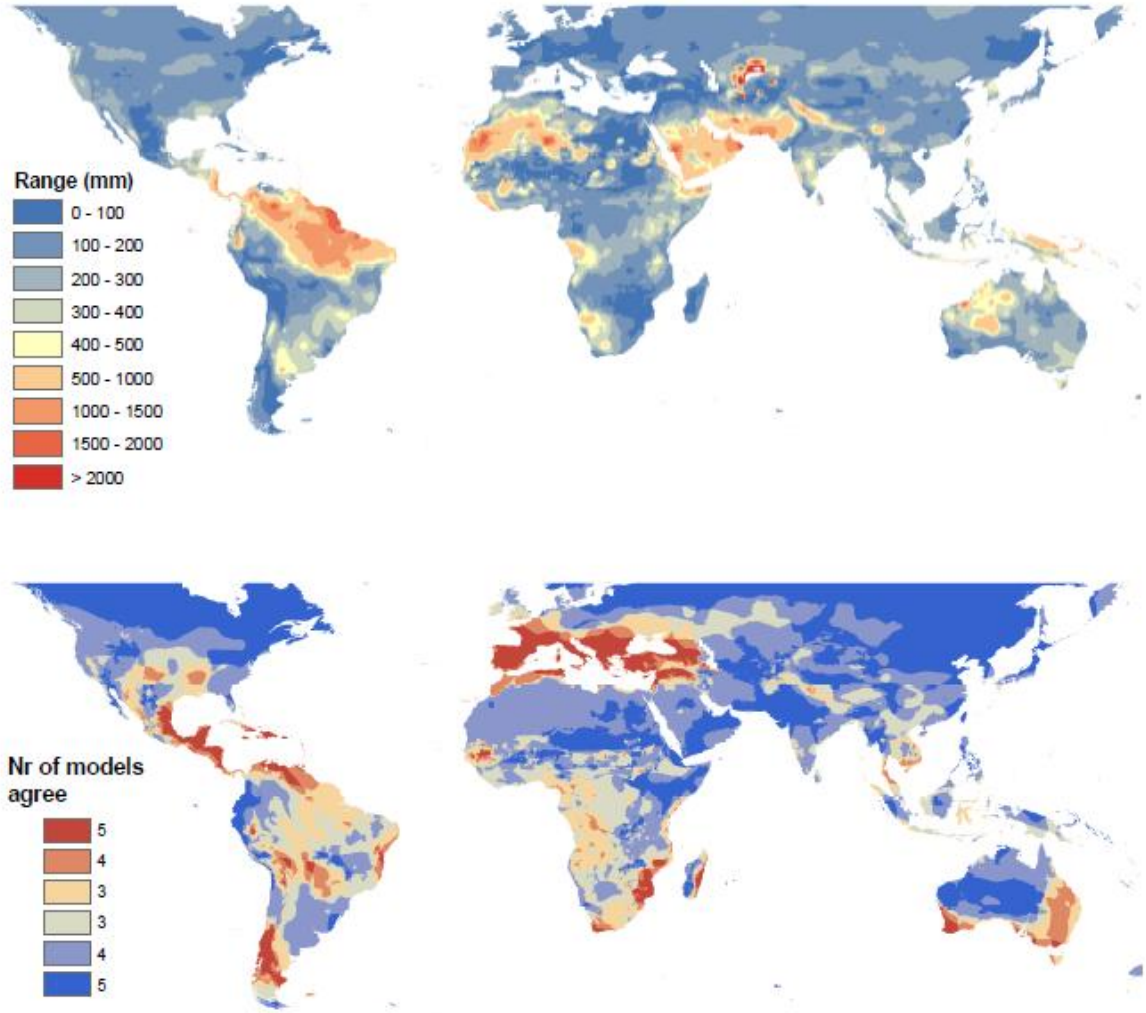

Figure 4.3 Range of precipitation projections for 5 GCM for A2A scenario (top) and the number of models that agree on the direction of the change with respect to the WorldClim baseline climatology, red is drier and blue is wetter (bottom)

As can be seen from figure 4.3, the range of projected precipitation for the A2A scenario is greatest in the Amazon basin, northern Africa, the Middle East and parts of western Australia. When looking at the agreement between models, it shows that all models agree on a drying in the Mediterranean and Central America and wetting generally in the more northern latitudes which is similar to the projections of these models for the A1B emission scenario.

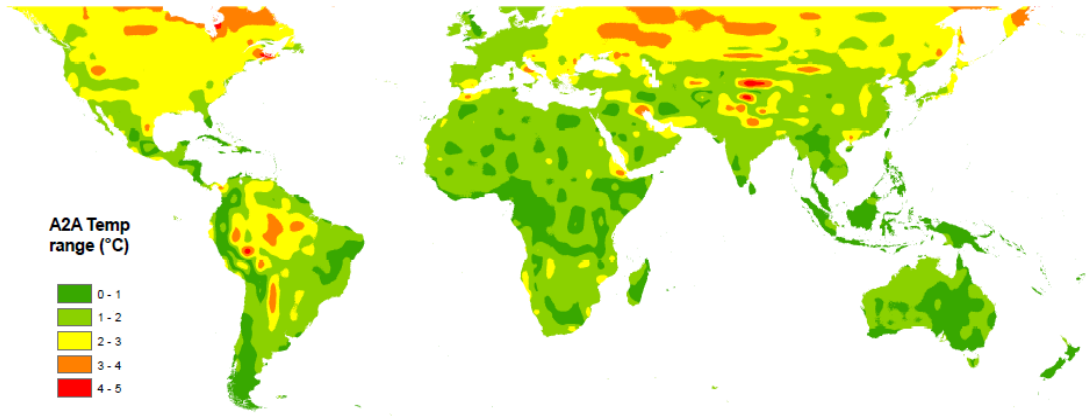

Figure 4.4 Range of temperature projections for 5 GCM for A2A scenario for the 2050s.

The range of temperature projections for the A2A scenario shows a similar pattern as the A1B scenario in figure 4.2. Similarly, for almost all of Africa and Australia the maximum range between models is 2 degrees Celsius. For South America however, the models range up to 4 degrees warming for the central parts of the continent.

To quantify some of the seasonal uncertainty in the multi-model climate grids that are described in this chapter, the monthly coefficient of variation for precipitation was calculated. For temperature, the monthly standard deviation was calculated as a measure of uncertainty as a CV of temperature in degrees C would be meaningless since temperature can be negative (Livers, 1942). Alternatively, temperature can be expressed in degrees K which allows for the calculation of a CV. This approach has not been applied though. The coefficient of variation is the ratio of the inter model standard deviation to the multi model mean and is a good measure of uncertainty when looking at seasonal differences as the probability distribution is normalised. Figure 4.5 shows the monthly CV for precipitation for the South American continent for the 5 GCMs used while figure 4.6 shows the monthly inter-model standard deviation for temperature. There is a high level of disagreement for precipitation in the Andes mountain range, but also for the Amazon rain forest biome where precipitation is very high. Buytaert *et al.,* (2010) using the full range of IPCC models in a multi model GCM study for part of the Andes also found considerable differences between model projections that are most likely attributable to the differing coarse resolutions

between models that fail to accurately take into account elevation gradients and thus neglect orographic precipitation events.

Disagreement between models for temperature is seasonally variable with high levels of disagreement from January to May centrally on the continent (northern Argentina, Paraguay and Bolivia) and throughout the year in the Amazon biome but particularly from July to December in Colombia, Venezuela and western Brazil.

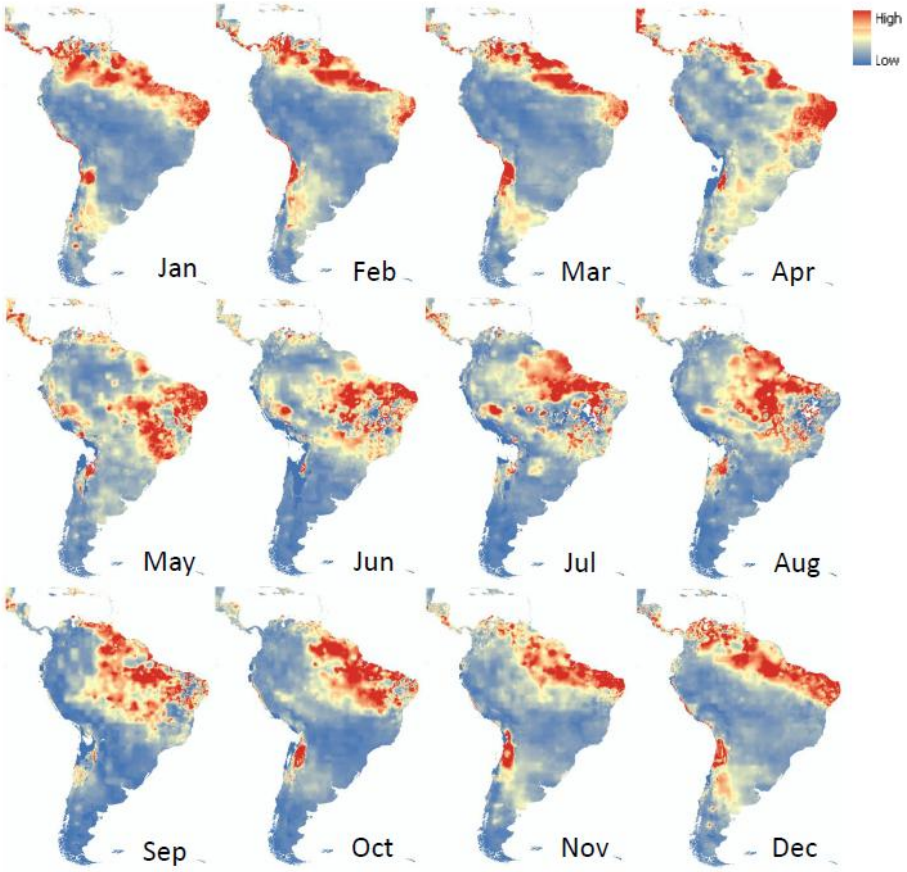

Figure 4.5 CV of precipitation for A1B scenario for 2050s for South America. GCMs used: CCCMA_CGCM31, CSIRO_MK30, IPSL_CM4, MPI_ECHAM5, UKMO_HADCM3

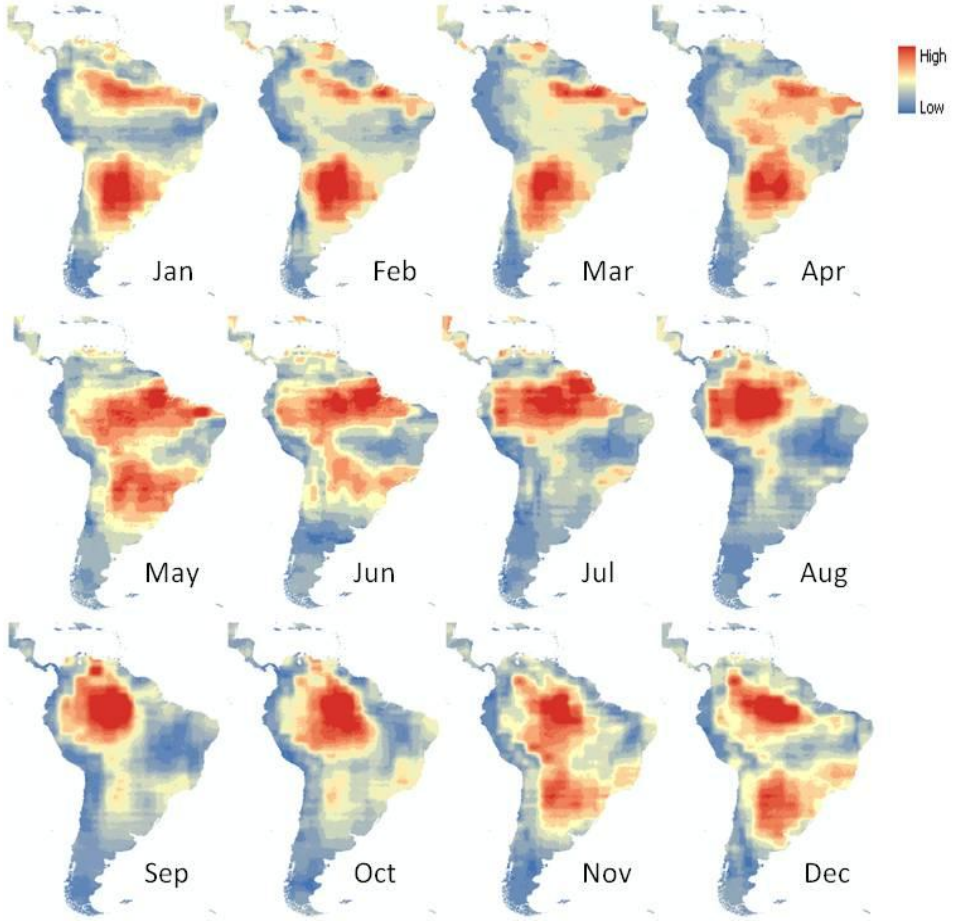

Figure 4.6 Inter-model temperature standard deviation for 5 GCM for A1B scenario for 2050s for South America. GCMs used: CCCMA_CGCM31, CSIRO_MK30, IPSL_CM4, MPI_ECHAM5, UKMO_HADCM3

4.2.3. Estimating PET for global water balance

The water balance of any catchment is equal to the input precipitation minus the water loss through evaporation with the remainder either stored in the surface and subsurface or leaving the catchment as runoff. Potential evapo-transpiration is defined as 'the amount of water that would evaporate if sufficient water were available' (Kay and Davies, 2008, p222). The food and agricultural organisation (FAO) defines PET as the ET of a reference crop under optimal conditions, with the characteristics of well watered grass with an assumed height of 12 centimetres, a surface resistance of 70 seconds per meter and an albedo of 0.23 (Allen *et al*, 1998).

There is a variety of ways with varying complexity that can be used to calculate PET. Some methods only need one atmospheric input variable such as temperature (e.g.

Thorntwaite 1948, Hargreaves, 1975 and Kharrufa, 1985), while others require a number of variables such as relative humidity, wind speed and solar radiation (e.g. Penman 1948, Priestley and Taylor 1972). For current climate, estimating PET based on these formulae can be done using observed data. However, climate models do not always provide all of the necessary variables for these calculations. Since the climate scenarios used in this chapter are downscaled multi-model means for monthly precipitation and temperature, PET must be calculated on the basis of temperature alone. In order to calculate the change in water balance over the global catchments of dams a consistent approach that can be applied to current baseline and future projected change is necessary.

The method used to estimate PET in this chapter is based on a simple, temperature based approach by Oudin *et al*, (2005b). This method is based on a study of the performance of more than 25 existing PE formulations used as input for hydrological models for more than 300 catchments (Oudin, 2005a). Kay and Davies (2008) have compared this method with the more physically based and well established Penman-Monteith PE approach (Monteith, 1965) and found that the T-based PE approach performed better when compared to a gridded ET dataset based on weather observations for the UK (Kay and Davies, 2008). The temperature based PE formulation is given by:

$$PE_T = \begin{cases} \frac{R_e}{\lambda_w}\frac{T_a+5}{100} & if\ T_a + 5 > 0, \\ 0 & otherwise, \end{cases} \qquad (4.1)$$

Where is the latent heat flux taken equal to 2.45 x 10^6 J/Kg and w is the density of water with a value of 1.00 kg/m^3. R_e is extraterrestrial radiation (J/m2/s) which depends on latitude and Julian day. Finally, T_a represents the daily air temperature (°C) yielding a PET in m/s. The formula was initially developed for long term mean daily data but it has been proven that monthly data can be used without significantly affecting the results (Federer *et al.,* 1996; Kay and Davies, 2008).

Data for extraterrestrial radiation was obtained from the CGIAR CSI global aridity and PET database which is a database of high-resolution potential evapo-transpiration and global aridity. Part of this database is the global ET solar radiation which reports the radiation at the top of the atmosphere expressed in mm/day as equivalent of evaporation (CGIAR-CSI, 2010). Values are provided for the 15th day of each month to describe averages for each month using the method of Allen *et al.,* (1998). Monthly values were obtained by multiplying these values with the number of days for each month. Using these values, the monthly PET can then be calculated as follows:

$$PET = R_e \left(\frac{mm}{month}\right) * \left(\frac{T_a + 5}{100}\right) \quad (4.2)$$

Giving a PET in mm/month. This method was then applied to the WorldClim baseline monthly temperature data and the mean monthly temperature data for the A1B and A2A multi-model scenarios to obtain PET values for the climate change projections.

4.2.4. Comparing PET with other datasets

To assess whether the baseline calculated PET (WC PET) yielded reasonable results, the values were compared with other global gridded PET datasets estimated using different formulae and a MODIS remotely sensed estimation. All these datasets were then compared against a common database of ET estimations derived from the FAO CLIMWAT dataset (FAO, 2009). The global gridded PET datasets that were obtained are the CIAT (GLOBAL-PET) dataset based on Hargreaves method and using long term monthly means from 1950-2000 (CGIAR-CSI, 2010), MODIS estimated PET (Mulligan, 2012c) developed from Mu *et al.,* (2011) for the period 1986-2000, and finally a medium resolution (10') grid from FAO based on the Penman-Monteith estimation using long-term monthly means from the CRU CL 1.0 Global Climate dataset (New *et al.,* 1999) for 1950-2000 (FAO, 2004). The MODIS PET dataset has been validated against eddy covariance flux tower data from 46 towers around North, Central and South America with measured data for the years 2000-2006 which yielded a correlation coefficient of 0.55 (Mu *et al.,* 2011). The CIAT-PET dataset was validated by

comparing the monthly values of PET based on Hargreaves method with a Penman-Monteith application to observed station data for 2288 stations in Africa and South America from the FAOCLIM2 database (Allen *et al.,* 1998) yielding mean differences of 30 mm for the month of January (SD 18) and 24 mm for the month of July (SD 17). Information on validation of the FAO-PET dataset could not be obtained. According to the background documentation (Allen *et al.,* 1998) users should validate the data for their area of interest. The CLIMWAT dataset against which the values are compared, is based on the Penman-Monteith model that is applied to daily direct observations of climatic variables such as wind speed, air temperature, relative humidity and solar radiation using the method described by Allen *et al.,* (1998). The dataset is available for more than 5000 stations worldwide for the time-period of 1971-2000 or if this time period was not available, for another period of at least 15 years between 1950-2000. More information about this data is given in Appendix IV. Since both the CIAT PET and the WC PET datasets are based on WorldClim temperature data, they cannot be compared against all CLIMWAT data points as the latter data might be based on the same temperature observations as the WorldClim data. To ensure they are based on independent observations, only those stations in the CLIMWAT dataset located more than 5 km from a WorldClim temperature data station were included in the comparison, this yielded 310 stations, equally distributed on all continents, except the United States where the WorldClim station density is so high that independent stations could not be identified. Table 4.2 shows the mean difference between the CLIMWAT PET values and the four PET datasets as the mean difference between the points on an annual basis and for the months of January and July.

It can be seen from table 4.2 that all temperature based PET estimations (CIAT PET, PET FAO and WC PET) have a negative annual mean difference with the CLIMWAT data, while the MODIS estimation shows a positive mean difference. However, there are seasonal differences in over- and underestimations as the MODIS estimation is negative for the mean of points for both January and July. Overall, the CIAT-PET estimation based on Hargreaves method yields the best results although the difference

with the WC PET and PET FAO estimations are small on an annual basis (24 and 10 mm respectively).

Table 4.2 Specifics about PET datasets and comparison of 4 different PET estimations with common PET dataset.

	MODIS PET		**CIAT PET**		**PET FAO**		**WC PET**	
Method used	Penman-Monteith		Hargreaves		Penman-Monteith		Temp-PE (oudin *et al.,* 2005b)	
Time period data	**1984-2000**		**1950-2000**		**1961-90**		**1950-2000**	
Resolution	8 km		~1 km		10 arc minute		~1 km	
Data requirements	MODIS data (land cover, albedo, LAI, EVI) Air pressure Air temperature Humidity Solar radiation		Air temperature Daily temperature range Solar radiation		CRU data: Air temperature Relative humidity Wind Speed Solar radiation		Air temperature Solar radiation	
	Mean difference (mm)	Stdev	Mean difference (mm)	Stdev	Mean difference (mm)	Stdev	Mean difference (mm)	Stdev
Annual	402	742	-116	582	-126	591	-240	602
January	-51.5	96	-13	63	-57	92	-24	66
July	-55	72	2.8	54	-84	57	-15	53

Figure 4.7 shows the estimated annual PET for the four datasets. While the total annual PET differs between the datasets it shows that the spatial pattern is largely the same. Particularly between the CIAT PET estimation and the temperature based PET method applied in this chapter since they are based on the same station data. The 10' FAO PET dataset shows lower values for the Southern Hemisphere, particularly for South America, Southern Africa and South East Asia. The annual MODIS based PET estimation shows higher values mainly for the Arabian peninsula and Australia but much lower for the Amazon which is the result of high cloud cover which reduced solar loads.

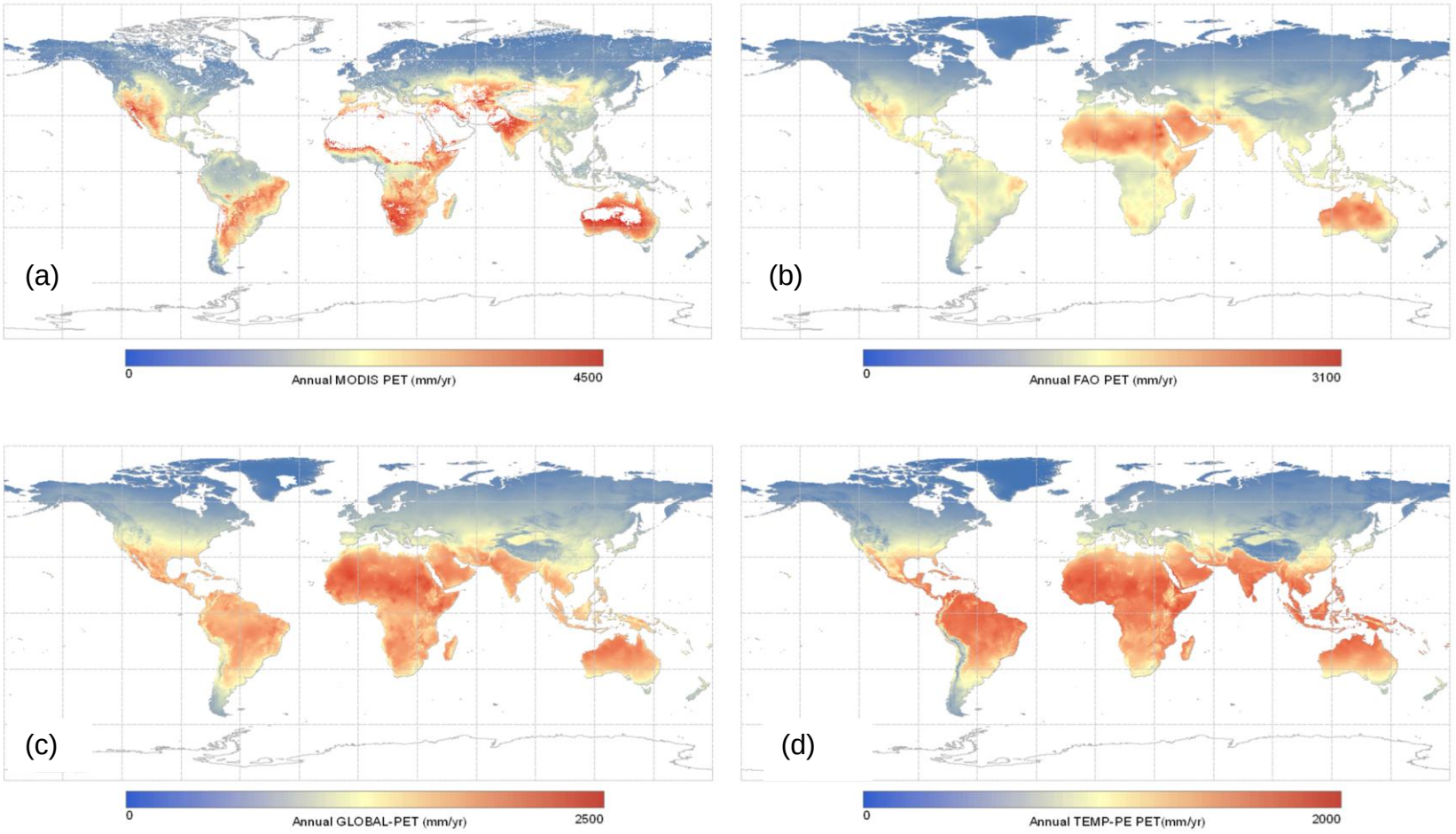

Figure 4.7 Comparison of four different PET estimations. (a) MODIS PET (Mulligan, 2012c; Mu *et al.,* 2011), (b) FAO PET (FAO, 2004), (c) CIAT PET (CGIAR-CSI,2010), (d) TEMP-PE PET (author)

4.2.5. Calculating global water balance

Since the WC PET yielded good results compared to other PET datasets and can be calculated based on mean monthly temperature alone - making it possible to calculate PET for the climate change scenarios (see section 4.2.3) - this dataset will be used for estimation of global water balances for the WorldClim baseline and the A1B and A2A scenario projections. This will allow for the assessment of changes in water yield for all dam catchments as a result of climate change. However, using the calculated PET values for water loss to evapo-transpiration would yield in a overestimation of this water loss as PET assumes unlimited soil water availability. In reality though, actual evapo-transpiration is limited by soil water availability and vegetation cover and properties as well as local climate effects including wind speed and humidity. To obtain more realistic results for water loss through evaporative processes, actual evapo-transpiration was calculated on a monthly basis using remotely sensed soil moisture data. These data were obtained from the VUA soil moisture dataset (Owe *et al.,* 2008) which is a consistent 30 year multi-sensor daily remotely sensed soil moisture product on a 0.25 degree resolution reprocessed into a mean monthly soil moisture climatology for the entire period by Mulligan (2012b) with values given as soil moisture fractions. To obtain monthly global AET grids, the calculated baseline and climate change PET grids were then multiplied with these soil moisture fraction datasets assuming a linear relationship between fractional soil moisture and AET/PET. Using baseline soil moisture data for future projections is a major limitation to the model. However, there is currently no available data on future soil moisture conditions globally. Since the soil moisture fractions do not change between the baseline and future timeperiods, changes in AET are solely driven by changes in PET.

Another limitation to this method is the relatively low resolution of the soil moisture data at 0.25 degree. However, for the purpose of calculating impacts of ET this is considered sufficient given no higher resolution dataset is available.

Precipitation inputs for the baseline water balance calculation were based on the high resolution WorldClim rainfall dataset and for the climate change projections the data

described in section 4.2.1 was used. Finally, changes in water balance between the baseline and climate change scenarios were calculated on a monthly basis and clipped to the dam catchments.

To assess whether the calculated baseline water balances are in the correct range, they were compared with estimates of the long-term river discharge as provided by the Global Runoff Data Centre (GRDC, 2007). Long term runoff data from the gauging station closest to the outlet of 405 major river basins was converted to mm equivalent using the GRDC reported basin area to which the outlet belongs and compared with the calculated water balance, thus 'closing' the balance. This method assumes that all of the water balance generates runoff rather than contributing to changes in soil and groundwater storage which is reasonable given the 50 year time-period being analysed but could also explain some of the differences. The analysis revealed that in only 10% of the basins was water balance lower than the measured runoff, almost all of them above 60 degrees North. This indicates that precipitation inputs for these 10% of catchments are likely underestimated or that runoff is sustained by groundwater storage or flows from neighbouring basins as the AET for these areas is very low. All the other basins (92 % of all basins) showed measured runoff close to water balance or lower, indicating losses to terrestrial water storage or errors in estimation of AET, the high resolution precipitation fields or in the runoff data.

4.2.6. Seasonality

Since most dams would be more affected by changes in the seasonal distribution of water rather than changes in total annual yield, an assessment of the seasonality of water balance was carried out for all dam catchments. Dry periods were defined as the three driest consecutive months and similarly wet periods were defined as the three wettest consecutive months. For each dam catchment, these values were calculated for the baseline as well as for the climate change scenarios and differences were plotted and analysed.

4.2.7. Within-catchment variability

For simplicity, the water balances for dam catchments are averaged over the dam catchments for the analyses in this chapter. However, precipitation and ET can be significantly different within catchments, particularly for very large dam catchments. This variability can be as great as the variability between catchments. While this spatial variability is very important for water users *within* the catchments, the amount of water reaching the dam integrates these differences.

4.2.8. Individual dams

To illustrate the impacts of climate change on dams, the water yield for fifty nine individual dam catchments around the world were calculated using the water balances as described in section 4.2.5. The selection of dams was based on reservoir size (large reservoirs), representation on all continents and the type of dam (only reservoir dams were used). Along with estimates of derived surface area for the reservoirs for these catchments (Mulligan, 2012a) a quantitative indication of the change in reservoir level and thus hydraulic head can be given which has implications for the hydroelectric power production potential and irrigation water output.

For this analysis, the first step consisted of matching the dams in the global dam database with the nearest polygon in the SWBD dataset to assess the reservoir sizes of the individual dams. The areas of these polygons were then calculated and ranked from large to small. The dams were then linked to the catchment area polygon using the unique ID and catchment areas for each dam were obtained. Along with the mean changes in water balance under the two climate change scenarios, a total water yield for each dam catchment could then be calculated and, with the known surface area of the reservoir within the catchment, changes in annual and seasonal average water level in the individual reservoirs could be calculated assuming the full water yield is routed through the catchment to the reservoir. This method assumes that there are no water releases from the dam (i.e. to maintain flow downstream) as relative impacts would be greater if the same releases had to be maintained with less water provided in

the catchment of the dam. Another assumption to this method is that all reservoirs are assumed to be extended vertically in a rectangular like way as reservoir bathymetry for the individual dams is not known. For all calculated water yields, a manual check on the catchment areas was carried out as some dam catchments are fragmented into sub-catchments by upstream dams. Moreover, in some cases, the automated matching of the dams with the SWBD polygons lead to errors when there is a high dam density further necessitating the need for manual checks.

4.2.9. Projecting impacts of climate change on human activity supported by dams

In most cases dams are designed to provide energy or to provide freshwater for irrigation or other consumptive uses. They are usually located in more populated areas, not least since these are typically found on large rivers and supply agricultural and urban areas. Therefore, any changes to the water provision to dams as a result of climate change is most likely to affect the nearby population dependent on those dams the most. These include the people living in the catchments whose irrigation may be supplied as well as those located immediately downstream whose flows may be affected. To assess how the impacts of the projected climate changes in the dam catchments affect humans in terms of their freshwater provision, the maps of projected changes in water balance as a result of climate change were combined with global maps of population density based on gridded population data developed by CIESIN (2005) and estimates of human water consumption based on country wide estimates from AQUASTAT (AQUASTAT, 2006). This analysis thus highlights those dams in which climate change will have significant impacts on populations and agriculture. Since dam beneficiaries are also found downstream of dams or outside their catchment (depending on water and energy distribution networks) , a buffer of 50 km around large dams (defined as having a catchment area of more than 10,000 km^2) and a 25 km buffer around medium sized dams (with catchment area of more than 1000 km^2) was applied to analyse the population and agricultural beneficiaries and dependence upon these dams in relation to the projected climate change that they will undergo.

The analysis consisted of calculating the current total of water produced in each dam (m^3) catchment using the baseline water balance as described in section 4.2.5. Then the gridded population data was multiplied with the per-country estimates of domestic water consumption in m^3 per year from AGUASTAT (2006) thus yielding a annual human water consumption for each grid cell in m^3 per year. The water supply calculated from the baseline water balance was then combined with this assessment of demand to assess the water surplus or deficit. This activity was then repeated for the water balances for both the climate change projections keeping population and average water consumption initially the same. Differences between the baseline and projections were calculated and averaged over the dam catchments plus the buffer areas. Finally, a scenario analysis was carried out where projected increase in country-wide population until 2050 was taken into account by multiplying the mean catchment wide population with the projected population growth for the country in which most of the catchment can be found. This way, the spatial differences between population growth and thus increased human water use can be accounted for. Data for country wide population growth rate was obtained from the UN population division (UN, 2012). The changes in human water consumption per dam catchment thus only take into account those attributable to the increase of population and do not account for changes in per capita water use.

4.2.10. Impacts of climate change on croplands within dam catchments

Similar to the assessment of impact on human population, an analysis was carried out into the impacts on croplands. Total water use by cropping within dam catchments was calculated by combining the calculated per pixel actual evapo-transpiration as described in section 4.2.5 and the Ramankutty (2008) dataset that represents total cropland as per pixel fractional areas. This yielded global per pixel maps of water use by cropland for the baseline and for both the climate change scenarios assuming the areas of agriculture remain the same. Since the AET maps for the baseline as well as the climate change scenarios in this assessment are based on the same soil moisture data, this means that crop AET only changes as a result of a change in temperature and

not as a result of available soil water. Finally, to obtain the proportion of water used by crops as percentage of total available water the following equation was used:

$$\frac{CROP-AET_{sc}}{Water\ balance_{sc}}\ x\ 100 \qquad (4.3)$$

Where *sc* denotes the scenario (baseline, and climate change scenarios). As with the assessment of impact on domestic water consumption, these maps were clipped to the dam catchment plus buffer areas to limit the analysis to the influence zone of dams and averaged over these areas. Figure 4.8 shows an example of such a dam with buffer area. The final results are given as the relative change in use of water by croplands within these areas. This analysis serves to highlight the dam catchments that are under most water stress from climate change in terms of their agricultural production.

Figure 4.8 Example of dam catchment with dam buffer used in analysis

4.3. Results

4.3.1. Changes under A1B 2050s scenario

Figures 4.9, 4.11 and 4.12 show the relative changes in water balance for all dam catchments as annual change, change in dry season and change in wet season between the baseline and the A1B 2050s scenario while figure 4.10 shows the absolute change (mm/yr) for the Mediterranean and northern India.

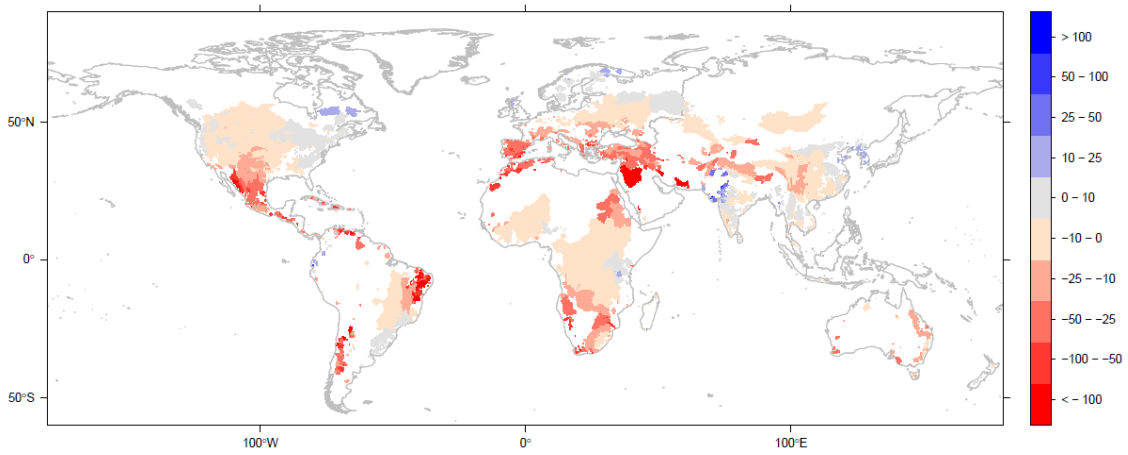

Figure 4.9 Percentage change in water balance (Precip-AET) for all dam catchments between A1B 2050s scenario and Worldclim baseline (%)

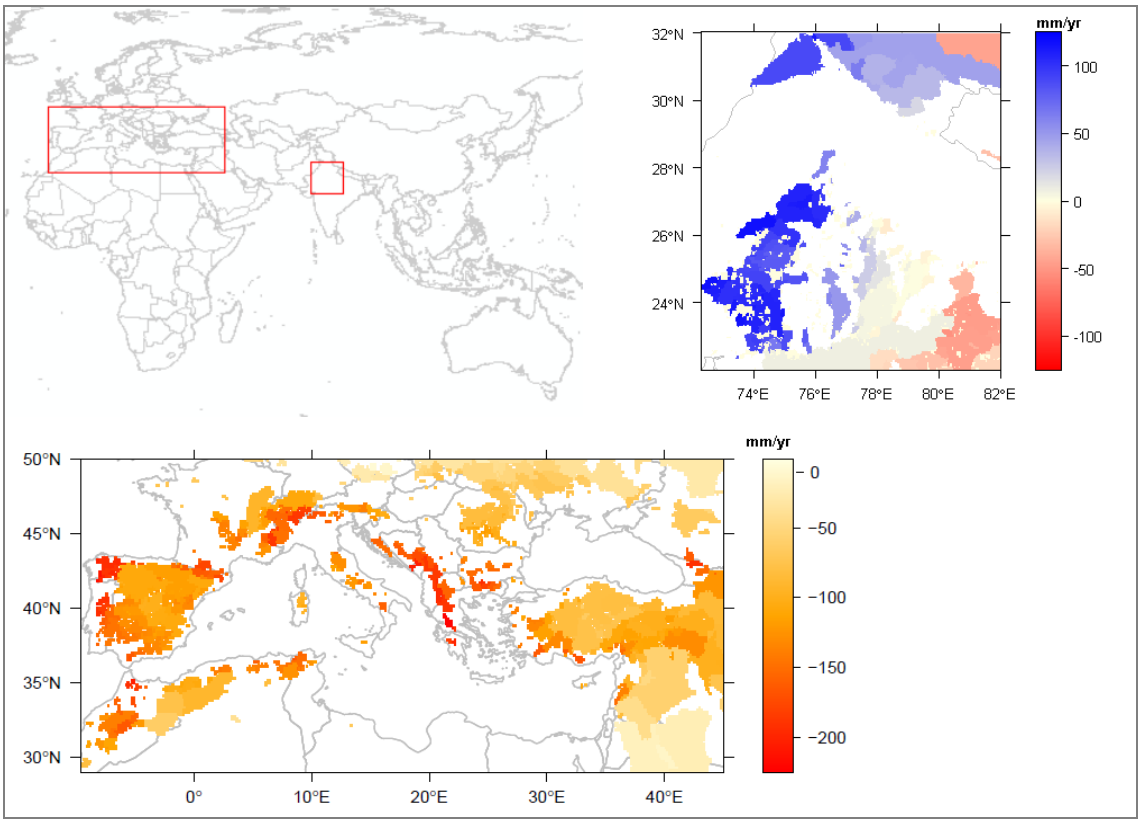

Figure 4.10 Absolute change in water balance (Precip-AET) for dam catchments in the Mediterranean and northern India between A1B 2050s scenario and WorldClim baseline (mm/yr)

The annual results show that a large number of global dam catchments are projected to be drier under the A1B 2050s scenario with some catchments, mainly in Europe and the Mediterranean seeing changes of more than -100% of annual water balance. Most notable positive changes in water balance are for a number of large catchments in India which is the result of increases in precipitation since glacial melting is not incorporated in this global analysis. Figure 4.11 and 4.12 show the relative changes for the wet season and dry season (defined as the three wettest and three driest consecutive months in a year respectively) showing significant drying in the dry season for most dam catchments and also a drying in the wet season for pan-tropical catchments. Changes for the wet season are more moderate than changes in the dry season though with about half of all dam catchments showing no more than 10 percent change, either drying or wetting. Dam catchments above around 50 degrees North show a wetting in the wet season. Overall though, these results show that

climate changes for the relatively moderate A1B emission scenario have significant impacts for the available water resources of most dam catchments.

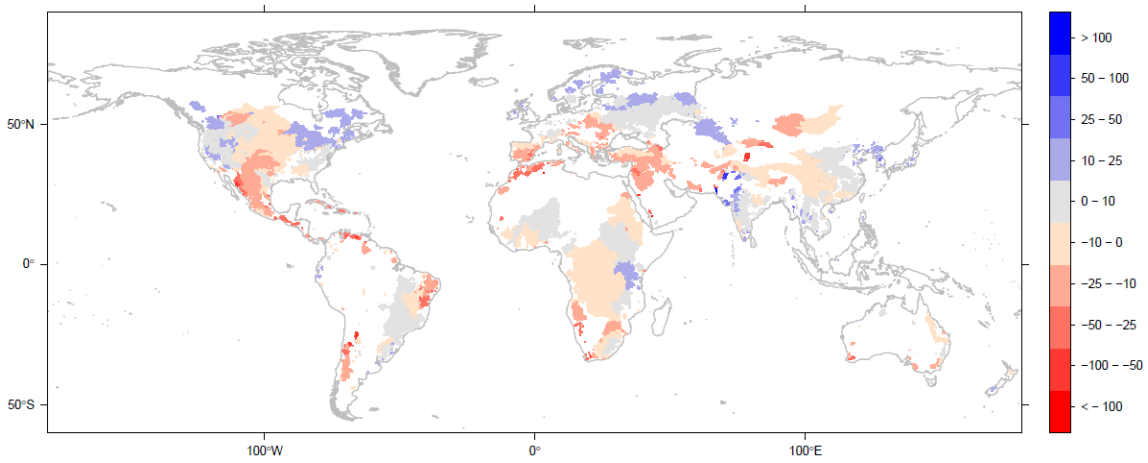

Figure 4.11 Percentage change in wet season water balance (Precip-AET) for all dam catchments between A1B 2050s scenario and WorldClim baseline.

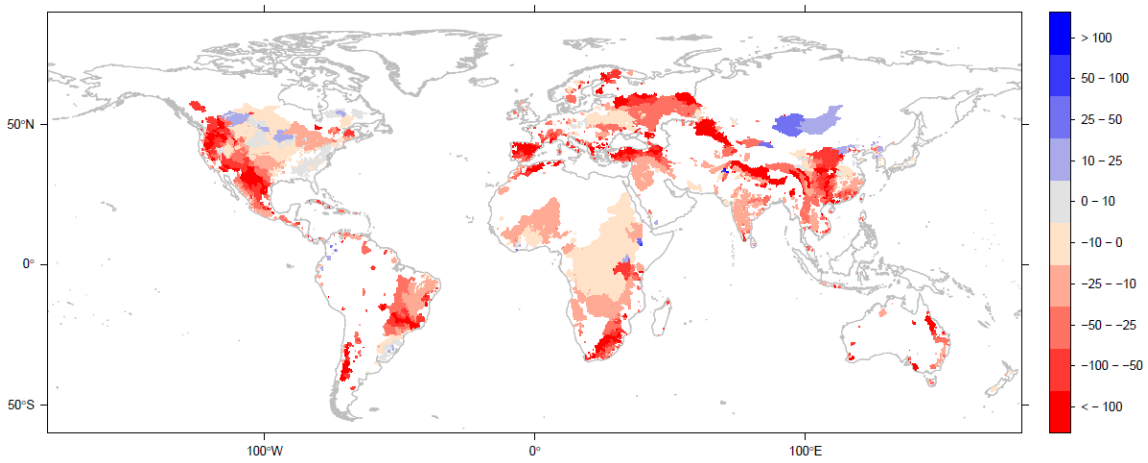

Figure 4.12 Percentage change in dry season water balance (Precip-AET) for all dam catchments between A1B 2050s scenario and WorldClim baseline

4.3.2. Changes under A2A 2050s scenario

Figure 4.13 shows the relative change in annual water balance for all dam catchments for the A2A 2050s climate change scenario and figure 4.14 shows the absolute change (mm/yr) for the Mediterranean and northern India. This scenario shows more spatially variable results with a large number of dam catchments having an annual increase in water yield but also many dam catchments having less water annually, mostly in the Mediterranean, Southern Africa and southern United States.

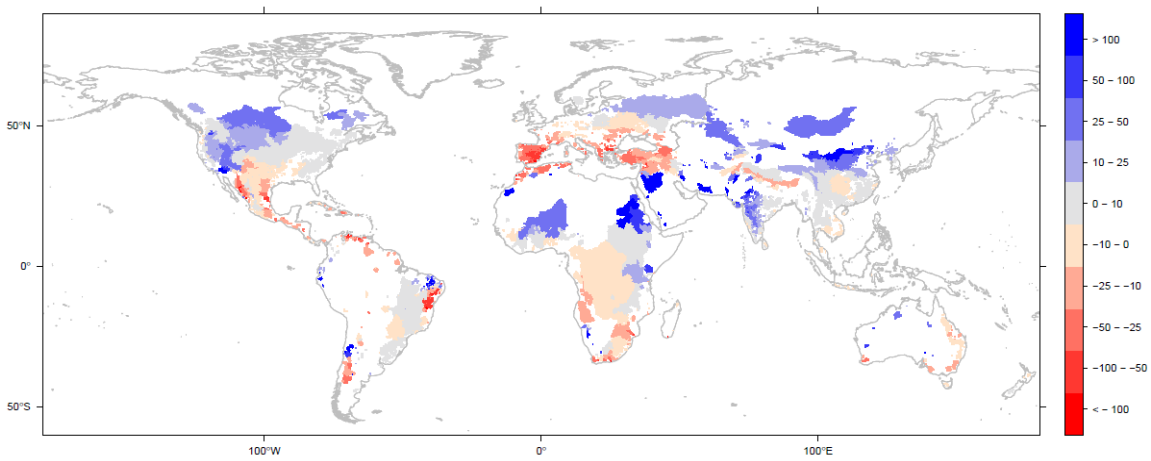

Figure 4.13 Percentage change in annual water balance (Precip-AET) for all dam catchments between A2A 2050s scenario and WorldClim database

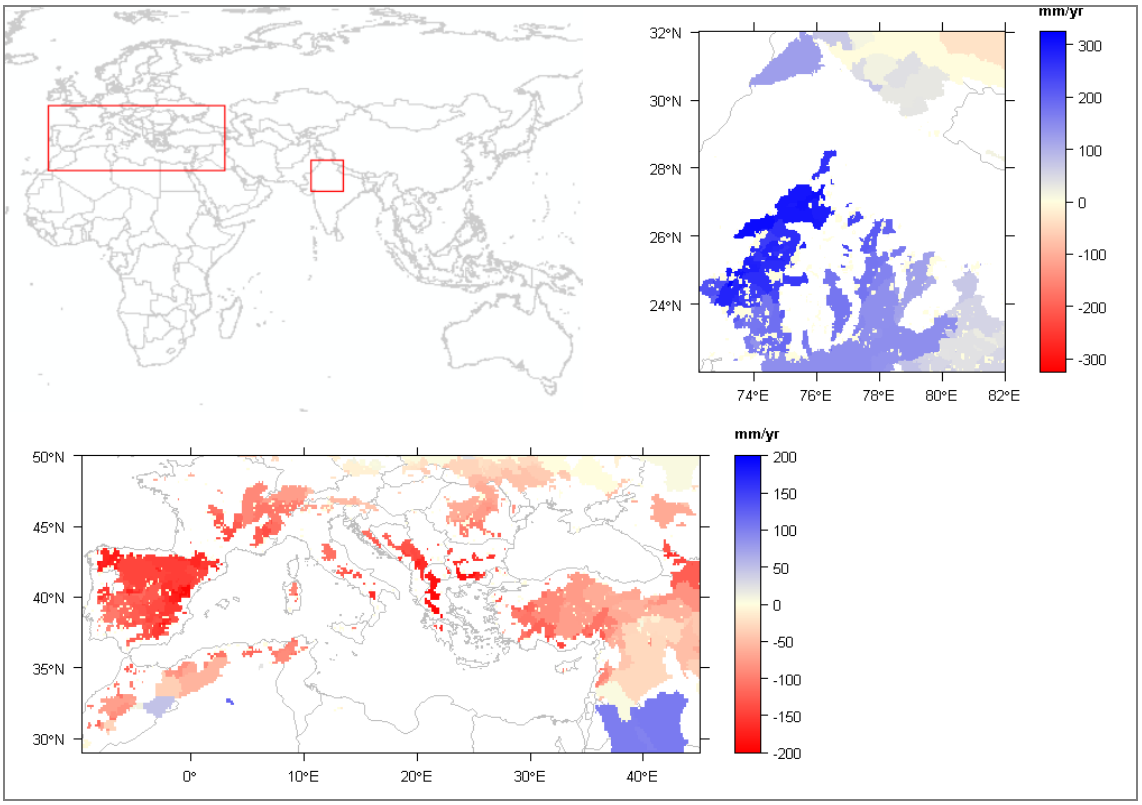

Figure 4.14 Absolute change in water balance (Precip-AET) for dam catchments in the Mediterranean and northern India between A2A 2050s scenario and WorldClim baseline (mm/yr)

Examining the maps of changes in the wet and dry seasons (figures 4.15 and 4.16), the most notable change is the increase in catchment water balance in the dry season for a large number of catchments, particularly in Africa which could be beneficial for some

of the dams located in these areas. It should be noted however that these are relative changes with regards to the baseline water balance, hence if these areas are already very dry the changes may not be high on an absolute scale. This is particularly true for the African catchments. Indeed, whilst these catchments are drier in the wet season by about the same percentage as in the dry season, the overall annual change is a drying of the catchment (see figure 4.13). Overall, there is a notable shift in hydrological seasonality (current wet season dries and current dry season wets) under this scenario which could have consequences for the management of dams in these areas.

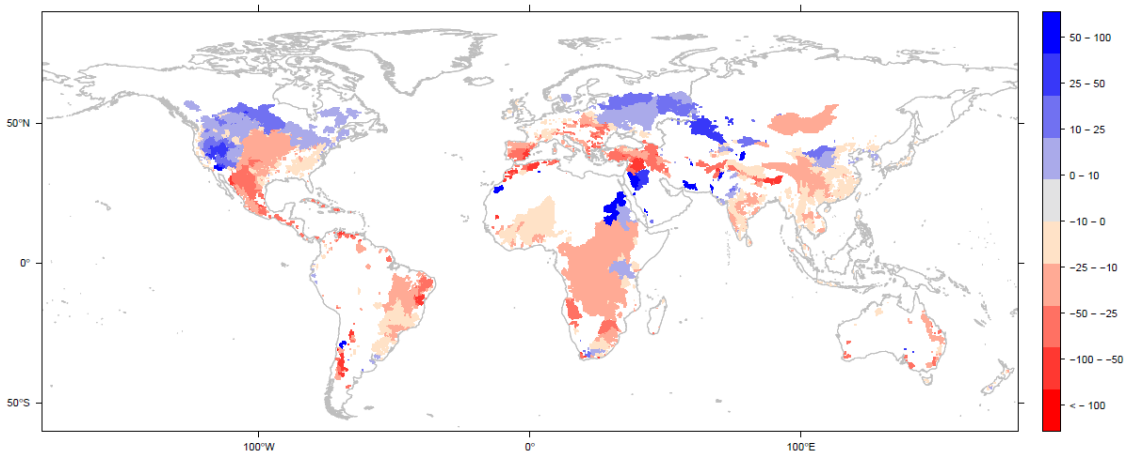

Figure 4.15 Percentage change in wet season water balance (Precip-AET) for all dam catchments between A2A 2050s scenario and WorldClim database

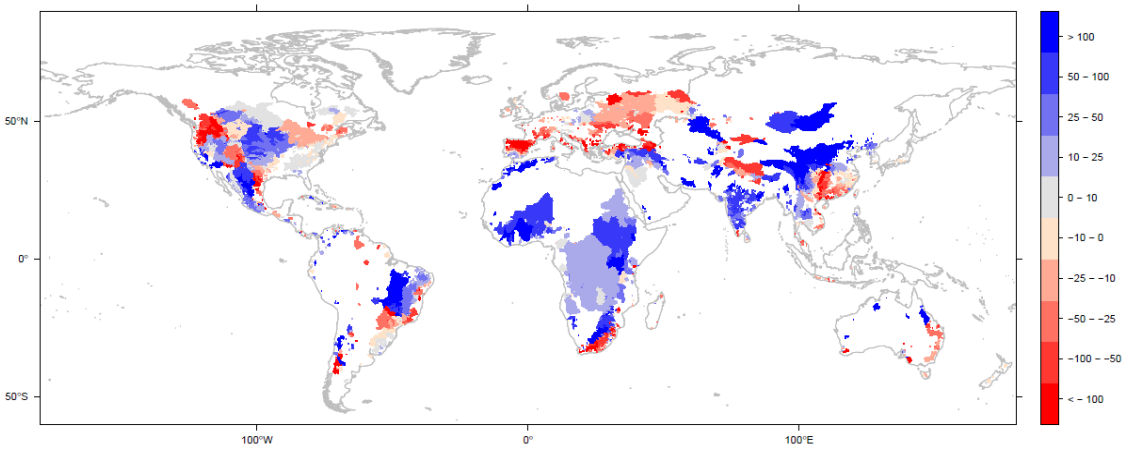

Figure 4.16 Percentage change in dry season water balance (Precip-AET) for all dam catchments between A2A 2050s scenario and WorldClim database

4.3.3. Seasonality

Figure 4.17 shows the percentage of dam catchments in each category of relative change of water balance on an annual basis for the two climate change scenarios. Figures 4.18 and 4.19 show these results for the dry and wet seasons. The A1B scenario annually results in much drier conditions in the catchments with nearly 70% of catchments drier than the baseline. For the A2A scenario, 41% of catchments are drier annually, thus more catchments see an increase in their water budget. Looking more at specific cohorts, both A1B and A2A scenarios have around 20% of catchments showing a change of more than 25% with just under 8% of catchments showing an annual decrease or increase in water budget of more than 50% for both scenarios. When looking at the changes in dry and wet season, it can clearly be seen that for the A1B scenario, almost all catchments become drier (88%) in the dry season whereas for the A2A scenario only 40% of catchments become drier. Changes in the wet season are almost equal between the two scenarios with around 50% of all catchments becoming drier and the same number becoming wetter.

Under the A1B scenario, 27% of dam catchments see a change in the start month of their dry season, with 7% of catchments having a shift of more than 3 months. In the wet season, 21% of the catchments see a change in the timing of the start of the season with less than 1% shifting more than 3 months. For the A2A scenario, nearly 50% of all catchments show a change in the start of the dry season with 7% of catchments shifting more than 3 months. In the wet season, 23% of catchments see a change in the start month of the season with 4% of catchments shifting more than 3 months.

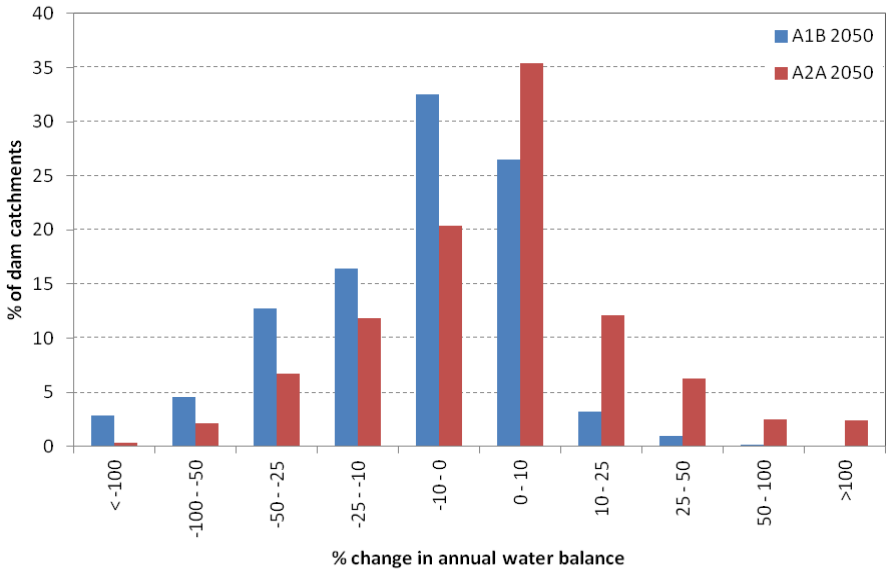

Figure 4.17 Percentage of total global dam catchments in classes of change in annual water balance between two climate change scenarios

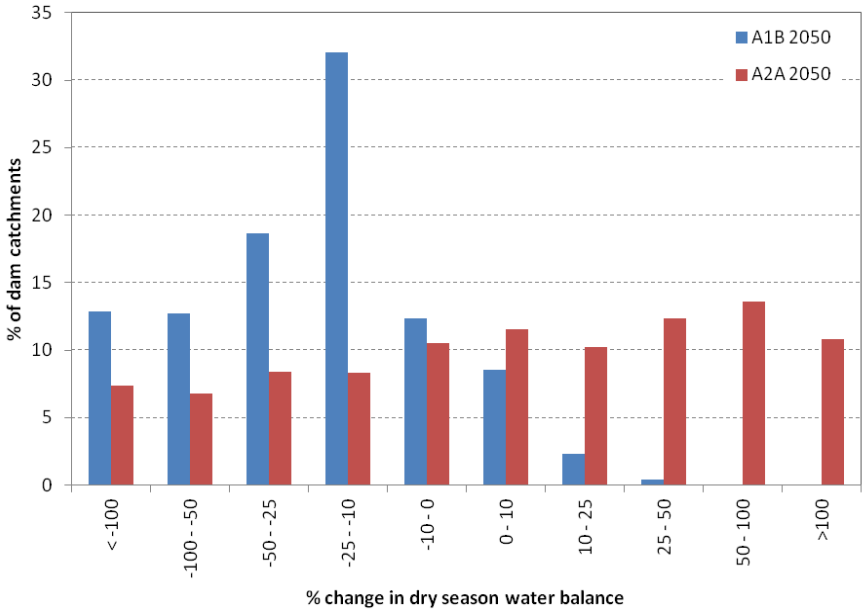

Figure 4.18 Percentage of total global dam catchments in classes of change in dry season water balance between two climate change scenarios

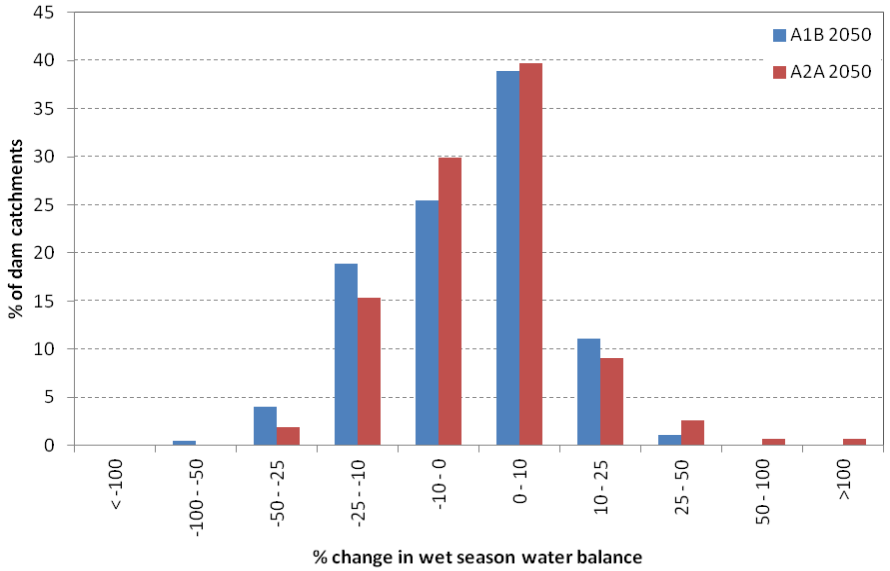

Figure 4.19 Percentage of total global dam catchments in classes of change in wet season water balance between two climate change scenarios

4.3.4. Individual dams

Table 4.3 shows the projected changes in reservoir level (m) for 59 large dams located throughout the world for annual and seasonal changes between the A1B and A2A climate scenarios and the WorldClim baseline.

Table 4.3 Projected change in reservoir level (m) for 60 large dams for A1B and A2A 5 GCM scenarios for the 2050s. Annual changes (positive and negative) of more than 10 metres for either or both of the scenarios are indicated in grey. Agree indicates the number of GCM agreeing on the direction of change

Dam name	**Country**	**Catchment area (km^2)**	**Reservoir area**	**Change in reservoir level (m) by scenario**							
				A2A	A2A	A2A	Agree	A1B	A1B	A1B	Agree
Kerr	United Sates	22240	486	1.1	-1.6	1.4	4	-0.8	-1.1	0.6	3
Gardiner	Canada	126000	390	35.5	6.4	5.9	5	-0.1	1.6	-3.2	3
Robert	Canada	93569	2586	5.4	0.0	1.5	5	2.1	0.0	1.1	4
Outardes 4	Canada	18530	414	3.9	-0.3	1.6	5	2.6	-0.4	1.3	4
Daniel	Canada	29241	1617	2.0	-0.1	0.6	5	1.3	-0.1	0.5	4
Guri	Venezuela	85000	3656	-6.7	-0.7	-2.2	4	-9.2	-0.9	-3.9	4
Buyo	Cote D'Ivoire	47689	508	3.8	4.4	1.2	4	-2.3	-0.3	0.7	3
High Aswan	Egypt	2849000	5377	37.7	1.1	26.6	5	-4.3	-1.1	-1.4	4
Cheboksary	Russia	354048	1008	16.6	-2.7	10.1	5	-4.2	-4.9	3.3	4

Table 4.3 continued

A.C. Bennet	Canada	72000	1622	2.6	-0.5	1.3	5	0.0	-1.1	1.1	4
Hoover	United States	435000	640	35.6	1.8	19.4	3	-10.1	-8.2	4.1	5
Eufala	USA	36471	355	-0.1	1.1	-1.6	3	-6.1	-1.3	-2.7	3
Le Grande-4	Canada	35854	749	7.4	1.1	1.7	5	3.5	0.7	1.2	4
El Chocon	Argentina	19730	711	-0.9	0.0	-0.6	3	-1.4	-0.4	-0.5	5
Balbina	Brazil	16638	2300	-1.5	-0.7	-0.2	3	-0.5	-0.7	0.1	3
Yacyreta	Argentina	970000	1110	10.0	-12.8	5.8	4	20.5	-13.8	-0.9	3
La Rincon del	Uruguay	25309	718	1.7	0.3	0.7	4	2.3	0.6	0.7	3
Sergio Motta	Brazil	108598	1202	-2.7	-1.1	0.1	4	-3.9	-3.3	1.6	3
Sao Simano	Brazil	45740	583	2.3	1.5	1.2	5	-1.0	-1.6	3.4	3
Marimbondo	Brazil	11529	349	0.6	0.2	0.2	4	-0.3	-0.7	1.1	3
Itumbiara	Brazil	18682	333	3.5	1.8	0.6	4	-0.1	-1.0	2.8	3
Serra da	Brazil	767000	1784	46.1	42.2	6.9	4	-6.5	-5.9	16.6	3
Sobradinho	Brazil	498425	2060	3.7	9.0	-1.8	3	-16.1	-2.8	-5.2	3
Manantali	Mali	27800	478	-3.4	2.0	-1.5	4	-	-0.45	-3.4	5
Selingue	Mali	31911	335	1.0	5.1	0.5	3	-7.4	-0.5	-0.9	5
Kossu dam	Cote D'Ivoire	29565	500	3.7	4.6	0.4	3	-3.4	-0.1	-0.7	4
Akosombo	Ghana	385180	6037	2.6	2.9	0.1	5	-2.4	0.0	0.0	4
Kariba	Zambia	663000	5270	-3.2	1.3	-2.6	5	-11.6	-1.4	-3.6	3
Dnieper	Ukraine	504000	2090	-0.5	-1.9	4.5	3	-9.1	-0.9	1.8	4
Kaniv	Ukraine	330000	469	-1.4	-5.7	13.2	4	-26.4	-2.7	5.3	4
Mtera	Tanzania	69995	443	6.7	-0.2	1.1	4	3.5	-1.2	5.9	5
Tabqa	Syria	4941	636	-0.3	0.0	-0.2	5	-0.5	-0.1	-0.2	5
Ataturk	Turkey	99084	660	0.0	0.0	0.0	3	-0.1	0.0	0.0	5
Haditha	Iraq	158061	339	-14.0	1.9	-	3	-26.8	-1.9	-9.7	5
Keban	Turkey	7251	398	-10.7	3.8	-2.7	3	-18.1	-3.7	-3.3	5
Krasnoyarsk	Russia	288200	2251	0.6	-3.1	2.5	3	-3.7	-2.2	1.2	4
Volga	Russia	1340000	2607	2.2	-12.5	10.0	4	-14.8	-8.7	4.8	4
Mingachevir	Azerbaijan	17444	415	-4.8	-3.7	-1.3	5	-5.5	-3.1	-1.8	5
Zhiguli	Russia	1200000	2021	36.7	-2.1	20.4	5	1.3	-8.4	7.5	3
Votkinsk	Russia	180000	841	13.9	-1.3	7.9	5	1.8	-3.4	3.5	4
Kairakum	Azerbaijan	51615	429	5.3	0.4	3.4	5	-3.2	-1.7	-0.2	4
Kaptai	Bangladesh	11444	326	2.8	1.4	0.9	3	4.8	-0.5	2.9	3
Srinagarind	Thailand	6428	345	1.2	0.3	0.1	4	0.1	-0.6	1.4	3
Sultan	Malaysia	2561	325	-0.8	-0.5	-0.1	3	-0.7	-0.8	0.0	3
Nam Ngum	Lao PDR	8410	436	0.6	0.0	0.3	4	0.0	-0.4	0.9	3
Irkutsk HEP	Russia	604300	31932	1.7	0.3	0.0	5	-0.3	0.0	-0.2	4
Corra Linn	Canada	45584	412	1.9	-5.1	3.6	4	0.5	-5.0	4.4	4
Garrison	USA	317400	1125	14.3	-0.7	4.2	4	-1.3	-0.1	0.4	3
Salto Grande	Argentina	110783	533	2.4	-3.1	1.4	3	4.9	-3.3	-0.2	3
Itaipu	Paraguay	150734	1155	-5.7	-7.4	2.4	3	-6.8	-5.9	1.8	3
Agua	Brazil	20903	506	0.3	-0.1	0.2	5	-0.7	-0.9	1.3	3
Tucuri	Brazil	182075	2346	1.5	8.1	-1.4	4	-9.1	-1.3	1.0	4
Tres marias	Brazil	37711	799	1.5	0.6	1.5	3	0.6	-0.8	2.1	3
Itezhi tezhi	Zambia	103098	328	-4.4	2.0	-4.0	3	-20.0	-3.1	-3.4	4

Table 4.3 continued

Ukai	India	19130	370	7.6	1.6	0.8	5	2.2	-0.4	3.3	3
Kapchagay	Kazakhstan	124569	1205	3.3	-2.8	2.6	4	-2.0	-1.8	-1.0	3
Rihand	India	11194	398	1.5	0.6	-0.4	4	-1.2	-0.2	-0.9	3
Hsin-an	China	4377	424	0.2	0.0	0.1	4	-0.1	-0.2	0.1	5
Lake Argyle	Australia	46100	828	9.1	3.0	0.7	4	-0.6	-0.3	0.5	3

A total of seventeen dams have projected changes (positive and negative) in their reservoir water level of more than 10 metres. For eleven dams this occurs under the A2A scenario, while this is the case for ten dams under the A1B scenario. Four dams see these changes under both scenarios. The highest projected changes occur for the Sera da Mesa dam in Brazil with an increase in reservoir level of more than 46 metres (dam wall 154 metres high) under the A2A scenario and the High Aswan dam in Egypt with an increase in reservoir level of nearly 38 metres under the A2A scenario (dam wall 111 metres high). For the Sera da Mesa dam however, the change is reversed under the A1B scenario. For nine of the dams with greatest change, the direction of the change differs between both scenarios indicating how sensitive the results are to the chosen scenario. Since these are multi-model scenarios, it is not known how sensitive these results are to the multi-model mean. This would have to be assessed by doing the analysis with individual climate models to test if changes in direction and magnitude exist between models which could be the scope of future work.

In terms of differences between wet and dry seasons, the dam with the greatest change in difference between seasons is the Serra da Mesa dam in Brazil with an additional difference of more than 30 metres under A2A scenario. This dam also shows the greatest change in seasonal difference under the A1B scenario with 35 metres difference although baseline difference in seasonal water levels is also high with 85 metres. The high Aswan dam also shows considerable change in seasonality under A2A scenario with an additional wet-dry difference of more than 25 metres compared to a seasonal difference of 52 metres under the baseline. Other dams showing great changes in seasonal differences are the Hoover dam in the United States (17 metre for baseline), Zhiguli (70 metres for baseline) and Volga dams in Russia (62 metres for

baseline) and the Haditha dam in Iraq (8 metres for baseline). Some of the most dramatic changes occur where large reservoirs are fed by small or dry catchments. This is particularly the case for the dams with the greatest changes as described above such as the Serra de Mesa dam in Brazil. However, this does highlight the specific vulnerability of these dams to changes in climate and thus water balance within their catchments. Figure 4.20 shows a scatter plot of the reservoir to catchment ratio (%) versus the change in water level for individual reservoirs for both scenarios making it clear that the largest changes occur for dams that have a small reservoir relative to their catchment . Any dam with a high reservoir to catchment ratio is more vulnerable to climate changes. One example is the Guri dam in Venezuela with a reservoir of over 4% the size of its catchment, changes in the water balance in its catchment have a greater impact on the water levels in the reservoir. Moreover, this dam provides 73% of Venezuela's electricity, making this country especially vulnerable to climate change (Power technology, 2012). The results in table 4.3 show that even dams with large reservoir areas compared to their catchments still have projected changes of up to a few metres which may still have significant impact on the operation of the dam.

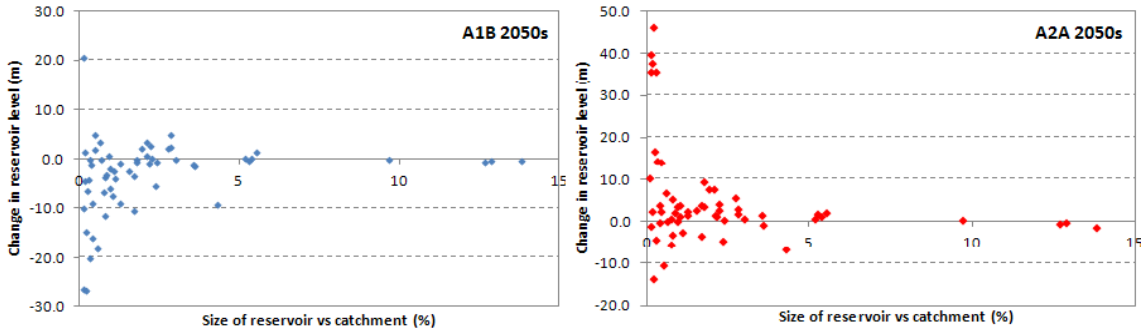

Figure 4.20 Scatter plots of reservoir to catchment ratio (%) versus change in water level for individual reservoirs for A1B 2050s and A2A 2050s

Figures 4.21 and 4.22 show the annual changes in reservoir level of the individual dams for both the A1B and A2A climate change scenarios as well as the number of GCM that agree on the direction of change in precipitation as an indication of uncertainty underlying the model since precipitation is the largest input in the water balance equation.

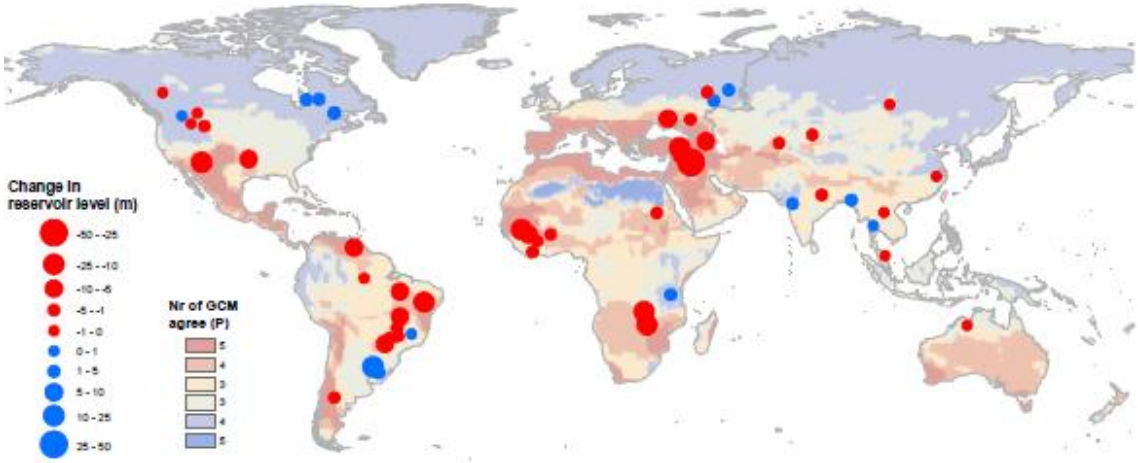

Figure 4.21 Projected changes in reservoir water level (m) for large dams and precipitation uncertainty as number of GCM agree on direction of change for A1B scenario for the 2050s

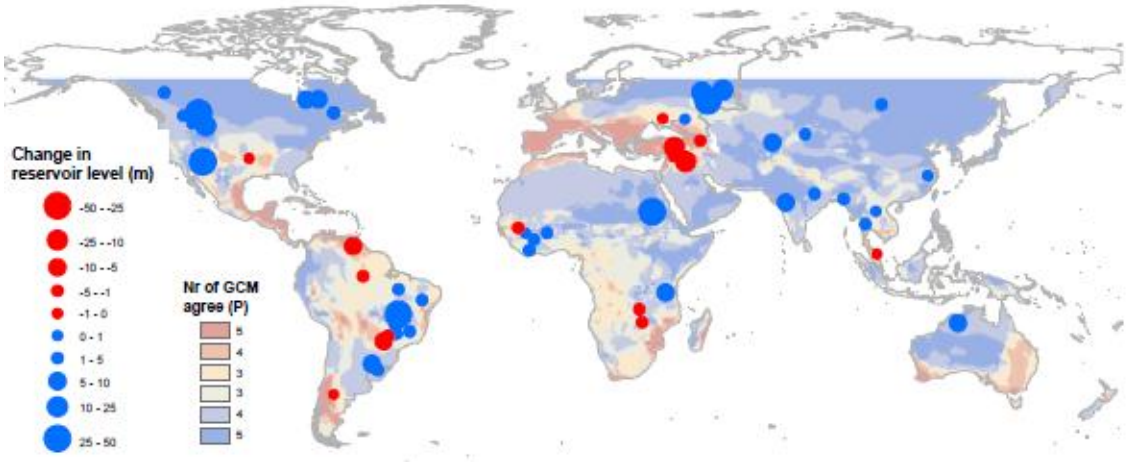

Figure 4.22 Projected changes in reservoir water level (m) for large dams and precipitation uncertainty as number of GCM agree on direction of change for A2A scenario for the 2050s

It should be noted that this analysis is a rather crude estimation of the potential changes in reservoir level since it does not take into account the difference between open reservoir and land evaporation as reservoir areas change which could be

significant considering the size of these reservoirs. Moreover, the assumption that total water yield in the catchment area is routed down to the reservoir does not take into account the complex processes of water production and runoff generation as well as sub surface storage processes. Furthermore, assumptions have been made on reservoir volume, water releases and timing effects (see section 4.2.8). These assumptions are warranted since the analysis is based on monthly means rather than on individual events. However, the methodology can serve as a rapid approach to assessing the potential for change in freshwater provision and hydropower production under different climate change projections as well as an indication of the vulnerability to climate change of individual dams and should be robust for examining relative changes between different dams.

4.3.5. Projecting impacts of climate change on human activity supported by dams

Figure 4.23 shows the baseline human water consumption as proportion of the total available water (based on the water balance) within the catchments as a measure of current water stress. It can be seen that most large catchments are relatively resilient to climate change as their size to population ratio's are much greater therefore the human water consumption is low relative to the total amount of water produced. Note that this analysis does not take into account other water uses such as industrial use nor the fact that water is often re-used multiple times. Some small catchments were calculated to have higher human water use than the total amount of water produced. This concerns only a handful of small catchments though that possibly import water from other sources or basins or have significant treatment and reuse.

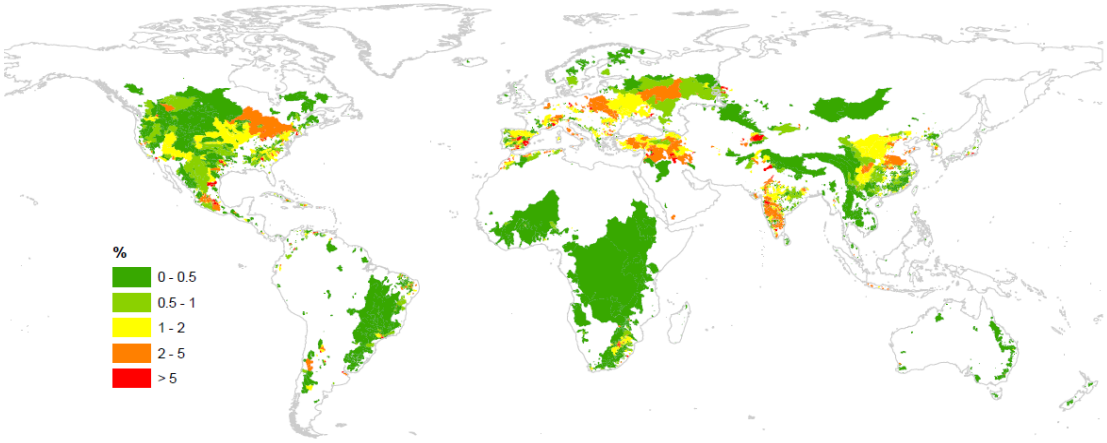

Figure 4.23 Baseline human water consumption as a proportion of available water (based on water balance) for dam catchment areas

Figure 4.24 and 4.25 show the relative change in human non-consumptive water use as a proportion of available water within dam catchments between the baseline and the climate change scenarios assuming no population growth. Clearly under the A1B scenario, more people are negatively affected by having a greater proportion of water used within their catchments with Mediterranean catchments affected the most. Under the A2A scenario, a large number of dam catchments have more water available with the most notable exception the Mediterranean area.

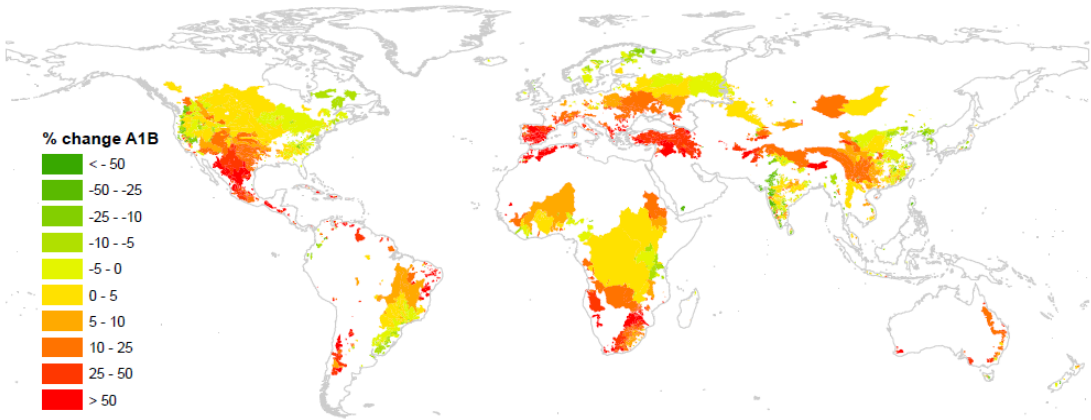

Figure 4.24 Relative change in human water use as a proportion of available water within dam catchments under A1B scenario for the 2050s

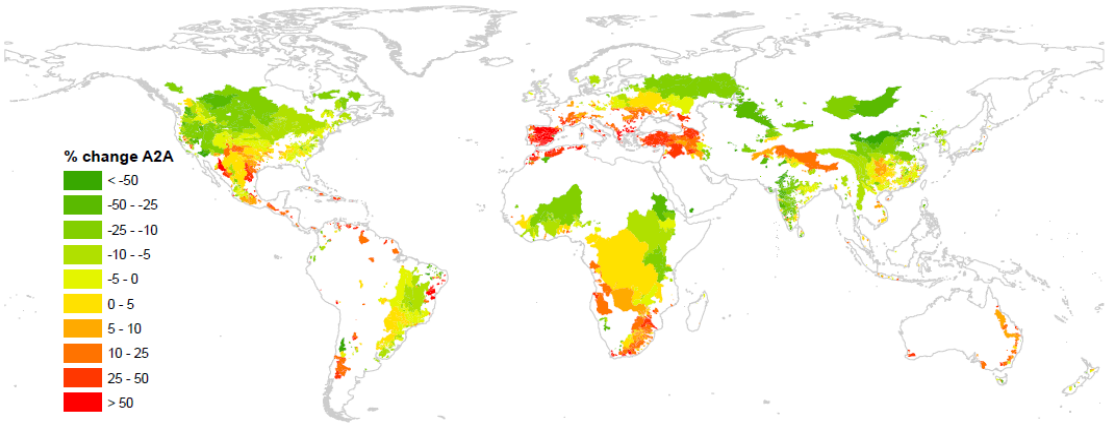

Figure 4.25 Relative change in human water use as a proportion of available water within dam catchments under A2A scenario for the 2050s

Figure 4.26 and 4.27 show the relative changes in human water consumption as a proportion of available water within dam catchments between the climate change scenarios and the baseline but in this case combined with scenarios of population change until 2050. Since almost all countries are expected to have positive population growth, it is not surprising that the human water consumption compared to applying only the climate change scenarios (figures 4.24 and 4.25) will increase, leading to a higher demand in dam catchments. Exceptions include some eastern European and Scandinavian catchments that have negative population growth rates. Since population growth is very high for some African countries, almost all African dam catchments see a change of more than 50% in the proportion of water used for human consumption compared to the baseline. Even though some of these actually have more water available as a result of climate change (see figure 4.25).

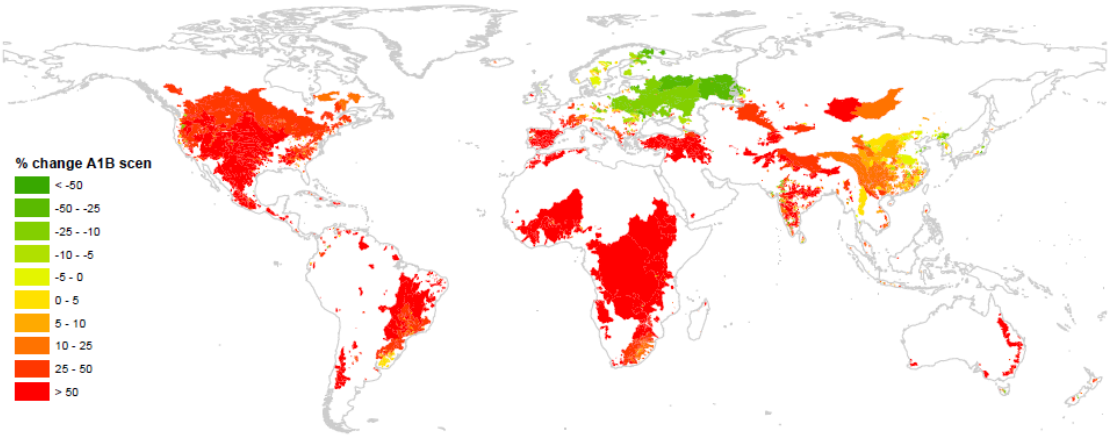

Figure 4.26 Relative change in human water use as a proportion of available water within dam catchments for A1B scenario combined with population change scenario for the 2050s

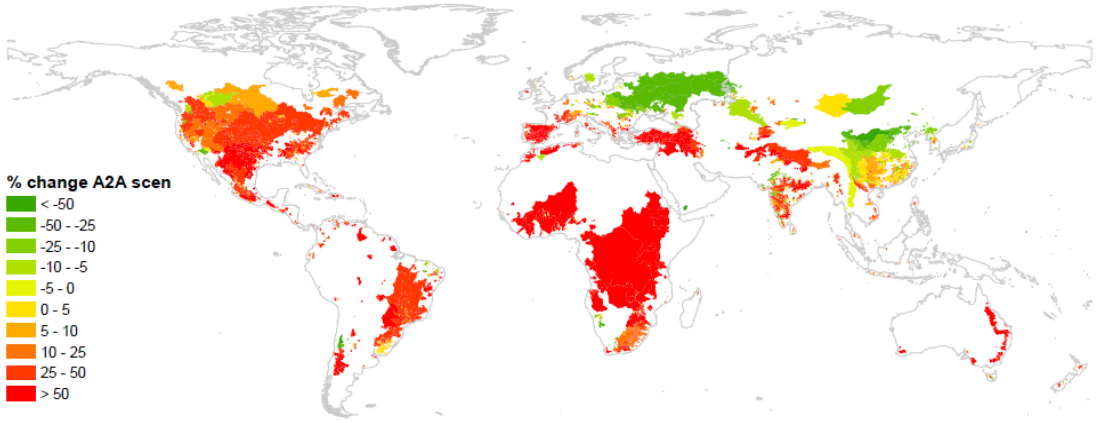

Figure 4.27 Relative change in human water use as a proportion of available water within dam catchments for A2A scenario combined with population change scenario for the 2050s

Overall these results show that more of the available water is consumed under the A1B scenario but less under the A2A scenario for a large number of catchments, except the Mediterranean that has more of the available water consumed under both scenarios. Combined with population growth projections though, almost all dam catchments have more of the available water consumed under both climate change scenarios apart from eastern Europe, Scandinavia and parts of Asia. Under these projections, a total of 740 million people based on current population are affected by drying for the A1B scenario and 423 million by wetting. For the A2A scenario, a total of 788 million are affected by wetting and 370 million by drying.

4.3.6. Impacts of climate change on croplands within dam catchments

Figure 4.28 shows the crop water use for the baseline as a percentage of the total amount of water available within dam catchment areas. The highest demand for water for crop production takes place in parts of India where in many catchments crop production uses more than half of the total amount of water available.

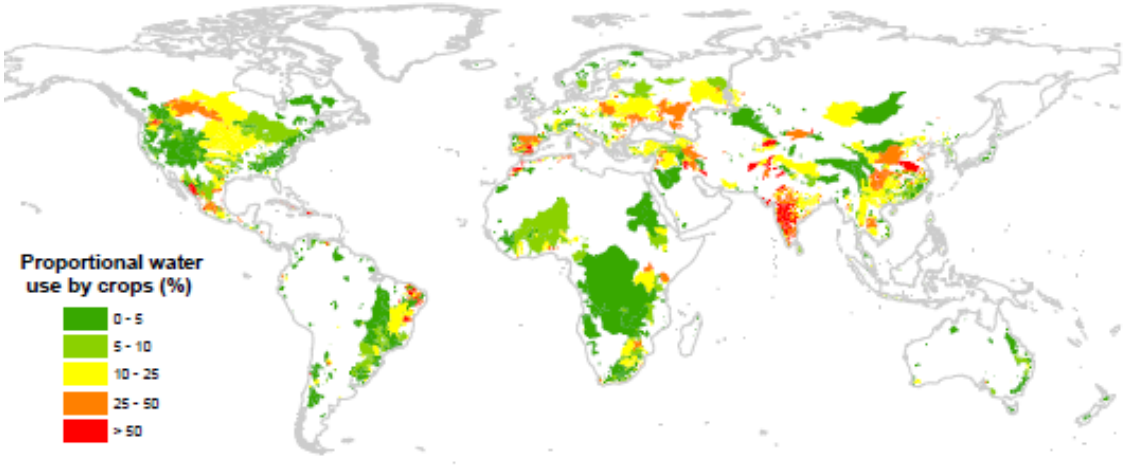

Figure 4.28 Baseline crop water use as proportion of available water for all dam catchments

Figure 4.29 shows the relative change between proportion of total available water used by crops for the baseline and the A1B scenario when cropping area remains the same. It is evident that almost all dam catchments show a higher proportional use because of the reduced water balance meaning that crop demand for water becomes larger than supply of water in the dam catchment. This is due to decreases in overall water balance (change in rainfall + AET). The assumption of keeping soil moisture conditions the same means the overall AET increases due to higher temperatures even if rainfall declines. Nevertheless, the figure shows that intensive cropping areas as seen in India are not significantly affected with some catchments even having less crop water use under the projected climate.

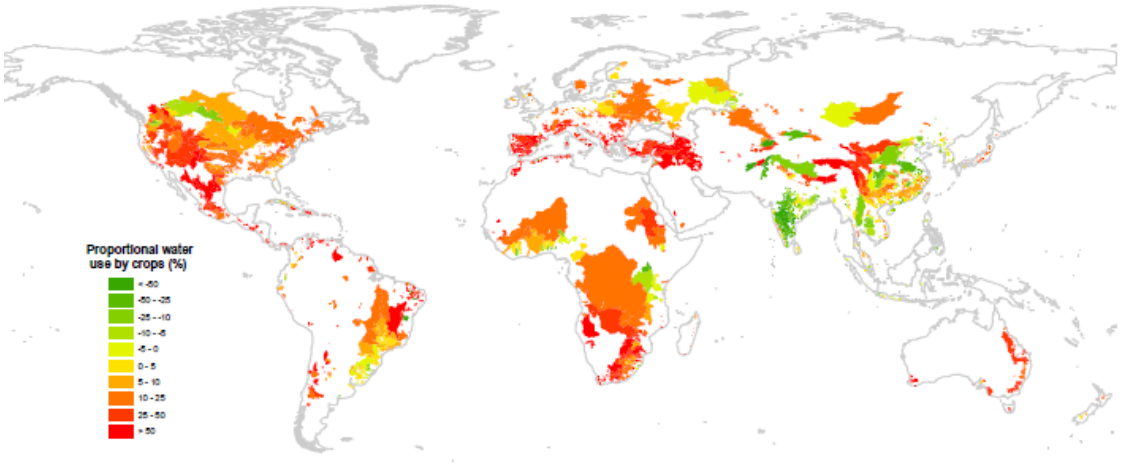

Figure 4.29 Relative change in crop water use as proportion of available water in dam catchments under A1B scenario for the 2050s

Figure 4.30 shows the percentage change for the A2A scenario where it can be seen that under this scenario, nearly half of the total global dam catchments see a decrease in proportion of available water used by crops as a result of increases in water balance. Examining the difference between the two climate change scenarios it becomes clear that the Mediterranean, particularly Spain have significantly less water under both scenarios while already having high crop water use for the baseline. The same is true for some large catchments in China.

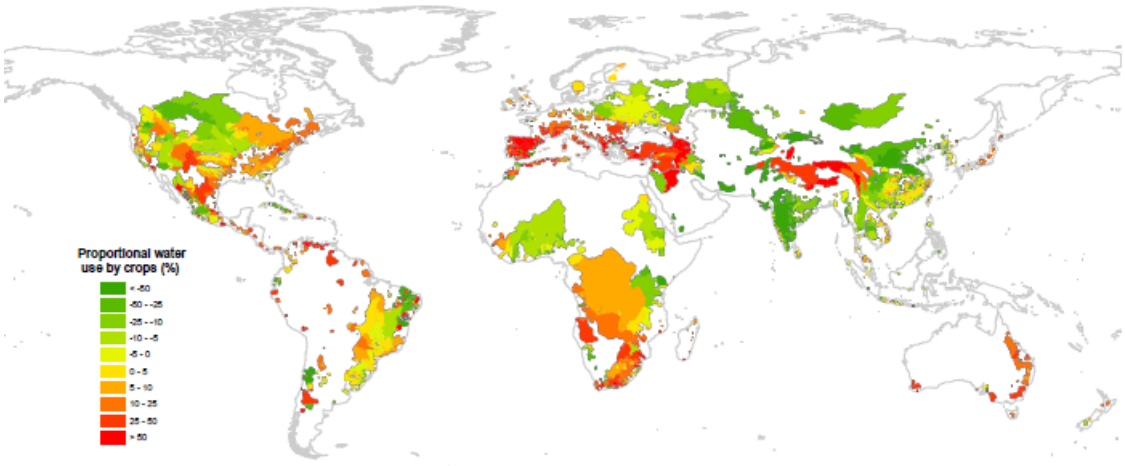

Figure 4.30 Relative change in crop water use as a proportion of available water in dam catchments under A2A scenario for the 2050s

The most impacted dam catchments from the individual dams as described in table 4.3, are the Tabqa dam in Syria, Haditha dam in Iraq and Ataturk dam in Turkey for both A1B and A2A scenarios. The least impacted catchments are the Mtera dam catchment in Tanzania and Kaptai dam in Bangladesh for the A1B scenario and Sobradinho and Sera da Mesa dams in Brazil for the A2A scenario. The Srinagarind and Nam Ngum dam catchments in Thailand and Lao PDR respectively are also not highly impacted under both scenarios. Under the A1B scenario, 20% of agriculture in dam affected areas is projected to experience wetting and 72% will dry with the remainder not seeing much change. For the A2A scenario, 62% of agriculture in dams is projected to be wetter and 29% drier.

4.4. Discussion

4.4.1. Climate change projections

All climate change impact modelling studies suffer from a number of uncertainties. Precipitation projections as calculated by different general circulation models show large differences as is displayed by the coefficient of variation for precipitation in figure 4.5, particularly in areas with high precipitation and in areas with large altitudinal gradients. Furthermore, downscaling the coarse GCM output to finer scale resolution can add uncertainty as it evens out finer scale terrain properties that can have completely different rainfall characteristics. For instance, at the original GCM resolution the Andes mountain range in most cases is represented by a single grid cell. Temperature projections between models tend to be more in agreement although their performance is also reduced in mountainous areas. As the literature suggests (Buytaert, 2009; Tebaldi, 2010), one way to deal with GCM uncertainty is to use more than one GCM in impact analysis. As discussed in section 2.5, the central tendency of a range of models outperforms any one single model when compared to observational records for the AR4 scenarios (Reichler and Kim*.,* 2008) therefore this metric was chosen to use in the impact analysis here. For reasons of data availability this resulted in using 5 GCMs and taking into account uncertainties in future emission pathways by

using two different emission scenarios. While it is acknowledged that there is a range of uncertainties with regards to the GCMs, the downscaling and the application of climate projections, the focus of this chapter is not to provide quantitative assessments of changes but rather show the projected direction and general trends of changes, geographic patterns of relative change as well as spatial sensitivity to climate changes and the individual dam sensitivity to these changes for two possible futures.

4.4.2. Global water balance

Creating the global water balance was limited by the climate variables available in the climate change projections. To assure a consistent approach, only temperature could be used in calculating the potential evapo-transpiration for the baseline and both the climate change scenarios. Using a temperature based approach however has proven to yield satisfactory results when compared to observational data as well as more physically based approaches to ET calculations (Kay and Davies, 2008) and performs well when used as input for hydrological models in areas throughout the world (Oudin *et al.,* 2005b). This approach can also be used with monthly data without significantly affecting results. Furthermore, comparing the obtained PET values using the temperature based method with other PET calculation approaches and observational data (see table 4.2) yielded satisfying results.

In order to obtain a realistic water balance it was necessary to convert the PET values to actual evapo-transpiraton values (AET) to reflect the limits to water loss by the process of evapo-transpiration imposed by the soil water availability. The best available global data on soil water availability at reasonable resolution are remotely sensed datasets. For this analysis, the VUA daily long term soil moisture dataset was used (Owe *et al.,* 2008) as it provides a consistent approach to deriving soil moisture values from 4 different sensors which gives it the advantage of being the only long term (30 years) global observed soil moisture record. The limitation of this dataset is that it comes at 0.25 degrees resolution (~30 km) and is therefore coarser than any of the other datasets used in the calculation of global water balance. However, for the purpose of the assessment in this chapter this resolution is sufficient. Another

limitation to this dataset is that, since it is based on remote sensing, it does not provide values in areas that are heavily vegetated (such as the rainforests) where the soil cannot be 'seen' through the vegetation. It also provides only surface soil moisture within the first few mm of the soil which may not be reflective of available water for ET in areas with deep rooting vegetation and significant groundwater. This potentially limits its usability in deriving AET values for dam catchments that are found in those areas. From assessing the available data it was found that the only large dam catchment affected by significant rainforest presence is the Inga dam in The DRC. Moreover, using the observed soil moisture data to calculate projected AET for the 2050s assumes that there will be no changes in the soil moisture characteristics between the baseline and the projected climate.

Finally, since rainfall is the most dominant variable in determining a water balance, uncertainties in the water balance in most cases can be attributed to uncertainty in the rainfall data. The WorldClim high resolution spatial rainfall data is considered one of the best and most widely used available global spatial rainfall datasets with a high resolution. However, there are some limitations of the dataset, particularly in areas where there is a low density of climate stations, regions of very high precipitation and in mountainous environments. Similarly, the precipitation for the scenarios suffers from the same uncertainties as they are based on the delta downscaling method and thus applied to the WorldClim dataset. Moreover, the scenario precipitation fields are subject to GCM uncertainties as described in section 4.2.2. Nevertheless, spatial representation of rainfall at the global scale is captured well within WorldClim (Hijmans *et al.,* 2005) and with agreement on the direction of changes in the precipitation fields for the scenarios as discussed above, at the scale of this analysis, the water balances should be indicative of changes that could happen.

4.4.3. Impacts of climate change on dams

In the analysis of climate change impacts on dam catchments, mean changes in water balance were calculated for every catchment. This means that spatial variability of AET

and precipitation are not taken into account. This variability can be very important for water users within the catchment but since the dams are located at the outflow point of the catchment, changes in dam outputs integrate these effects. Dam catchments are individually assessed on the projected changes in water balance within their catchment. However, many dams fall within single large river basins hence if a upstream dam is more impacted by climate change in terms of reduced or increased water supply and that effects the regime of water releases or side flows from that dam, downstream dams may be impacted more severely as well independently of the climate change effects within their own catchments. Examining the annual changes in water balance for catchments for the two scenarios (figures 4.9 and 4.13), 33% of large river basin areas affected by dams are projected to have positive as well as negative changes in water balance for the A1B scenario while for the A2A scenario, this figure is 31%. This means that for most dam catchments (~70%) the impacts of climate change between upstream and downstream catchments are more likely to amplify than each other cancel out.

The analysis of potential changes in reservoir level is a rather crude estimation as it does not take into account differences between reservoir bathymetries, sideflows and releases, open reservoir and land evaporation for their (mostly very large) reservoirs. It also assumes that the total water yield within the catchments are routed down to the reservoir which does not allow for sub surface storage processes. However, given that long-term climatologies are applied, storage terms are likely to be evened out. Only a small number of large dams are included in this analysis and some large reservoirs are not included such as the Three Gorges dam reservoir. This is because the SWBD dataset that was used to derive the locations of large reservoirs stems from a date prior to the development of the dam and the filling up of the reservoir. Future work could add these reservoirs by digitizing them from imagery.

As with all climate change impact analyses, the results should be interpreted with caution, particularly with quantitative predictions such as with the changes in large

reservoirs. The results of this analysis only represent two possible futures. However, the methodology can serve as a rapid assessment of the potential for change in freshwater provision and hydropower production under different climate change projections as well as an indication of the vulnerability to climate change of individual dams.

4.4.4. Impacts of climate change on humans and agriculture within dam catchments

It is difficult to understand which of the changes in these dams may have the most serious impacts on water availability for agricultural and domestic use. Therefore a simple analysis was conducted on people and agriculture contained within the dam catchments. This has the limitation that it assumes that beneficiaries of a particular dam are within its catchment which might not be the case for many dams, especially those which supply water transfer schemes or energy through hydropower. An attempt was made to address this issue by creating buffers around dams so as to include those people and agricultural areas that are within a reasonable distance for water to be transferred by pipeline and are thus still influenced by the dam. Another limitation to the analysis is that the scenarios of human water consumption are based on population and population growth projections only. While this is probably a good way of indicating where current and future domestic demand is and will be, it does not account for differences or changes in water use efficiency and water re-use. Changes in per-capita water use can potentially offset changes in total water available for human water consumption for a given dam catchment. However, both analyses do highlight the potential and projected stresses or opportunities for humans and agricultural production systems and can therefore serve as guidance in policy considerations regarding planning of new dams or location of intensive agriculture

4.5. Conclusion

This chapter assessed impacts of climate change on catchments of dams on a global scale using the derived catchment areas from the KCL GOOD^2 database described in chapter 3. Multi-model mean climate change scenarios were created based on the

output of 5 GCM from the AR4 on a global scale at 1 km resolution for two different emission scenarios. Between-model uncertainty was assessed by looking at the range of projections for precipitation and temperature for all 5 models and the number of models that agree on the direction of the change with respect to the WorldClim baseline. Results for precipitation show that the greatest disagreement between models can be found in the humid tropics for both emission scenarios. Both scenarios, generally show drying in the Mediterranean with all models agreeing and wetting in the more northern latitudes with all models agreeing. These results agree with the literature e.g. Gao *et al.,* (2006), Meehl *et al.,* (2007) and Giorgi and Lionello (2008). Furthermore, the coefficients of variation for precipitation for the South American continent showed that between model differences for precipitation are mostly found in areas with a strong altitudinal gradient or in high precipitation areas such as the Amazon basin. For temperature projections there is more agreement between models with most differences also occurring in mountainous areas such as the Andes mountain range in South America. The climate change scenarios were then used to estimate a global water balance using a temperature based method to estimate evapo-transpiration combined with observed remotely sensed soil moisture data and the high resolution WorldClim dataset for precipitation. This method yielded satisfactory results for the baseline water balance when compared to the GRDC large river runoff dataset. Applying the temperature based PET method to the projected temperature data of the two climate change scenarios yielded global projected water balances that were then used to calculate differences with the baseline for all dam catchments annually and for dry and wet seasons. The results showed that nearly all dam catchments are affected by climate change with nearly 70% of dam catchments drier than the baseline for the A1B scenario and more than 40% of catchments drier than the baseline for the A2A scenario. There are also significant seasonal changes expected with most catchments under the A1B scenario becoming even drier in the dry season. Under the A2A scenario many catchments will receive relatively more water in the dry season, however many of these currently have low water yield for this season meaning the total volume of water may not increase much.

To assess the impacts on individual dams, 59 large dams were selected based on the size of their reservoirs and changes in the dam reservoir level were calculated assuming no water losses to storage within the catchment or to releases. The results show that under the A2A scenario the average change in reservoir level is -3.8 metres for dam catchments that are projected to have a decrease in their water budgets and +8 metres for those that have a projected increase in their budgets. For the A1B scenario these values are -6 and +3.1. Seventeen of the large dams are projected to have changes in their reservoir level of more than 10 metres with some large dams such as the Serra da Mesa dam in Brazil and the High Aswan dam in Egypt showing very large changes (46 and 37 metres respectively) for the A2A scenario. For the A1B scenario, 42 dams are projected to become drier and 17 wetter while for the A2A scenario 16 dams are projected to become drier and 43 dams wetter. Some of these changes can partly be explained by the fact that the reservoir size for these dams is small compared to their catchments which makes these dams particularly vulnerable to climate change.

While this assessment has only been carried out for 59 of the estimated 40-50 000 large dams in the world, the methodology has proven to be very useful in quickly assessing the potential for change in freshwater provision and hydropower production under different climate change projections. Furthermore, the methodology can serve as an indication of the vulnerability to climate change of individual dams and can easily be extended and applied to the other dams contained in the GOOD^2 database, although some of these dams will not have their own reservoir in which case the impacts of climate change are more dependent on the changes in stream flow as a results of these climate changes. To assess the detailed impacts at individual dams -also incorporating the effects of snow and ice-, it is necessary to apply a spatial hydrological model as will be the focus of the following chapter.

Finally, an assessment was made of the impact of the projected climate change for both scenarios on humans and cropping agriculture within the dam catchments. The

results show that humans consume more of the available water for domestic use under the A1B scenario but less under the A2A scenario for a large number of catchments, except the Mediterranean where the proportion of water used by humans in dam catchments increases under both scenarios. Combined with population growth projections though, almost all dam catchments show increases in the proportion of the available water consumed under both climate change scenarios apart from eastern Europe, Scandinavia and parts of Asia. In terms of use of water by croplands, the results show that under the A1B scenario, nearly all dam catchments use more of the available water for cropland compared with the baseline. Whereas, under the A2A scenario, this is the case for about half of all dam catchments. Catchments in which most of the available water is used are those that already have high crop water use in their catchments combined with a decrease in total available water as a result of climate change such as those in the Mediterranean. However, some large catchments in India where crop water use is high under the baseline are projected to have more water available under both climate change scenarios.

5. Hydrological impacts of climate change on large dam catchments

5.1. Introduction

The assessment of impacts of climate change on global dam catchments carried out in chapter 4, highlighted those dam catchments and areas that are most vulnerable to changes in climate based on two scenarios for the 2050s. However, since this assessment was carried out on a global scale, the approach was based on limited input data and relatively coarse resolution, mainly focusing on very large dams. Furthermore, changes in reservoir level at individual dams were calculated based on the assumption that the full water budget -modelled simply as rainfall minus actual evapo-transpiration- within catchments would be accumulated up to the dam point. However, the hydrological processes within a catchment are much more complex and spatially variable. Therefore, to assess whether projected changes in climatic inputs (precipitation and temperature) into the system will lead to changes in inflow of water and sediment into the reservoirs of these dams, a more sophisticated spatial hydrological modelling approach is necessary. In this chapter, a hydrological model will be applied to three basins that are heavily affected by dams in different climatic areas of the world. Within each basin, a large dam is then selected and changes in inflow into the reservoir between a baseline and a climate change scenario will be simulated. Applying the model at the basin scale in which the dam catchment can be found allowed for validating some of the input and output data as this proved very difficult at the scale of the dam catchment. Moreover, a model sensitivity analysis is carried out at the scale of these basins in the following chapter. The hydrological model that will be used is the FIESTA (Mulligan and Burke, 2005; Bruijnzeel *et al.,* 2011) spatial hydrological model which is used within the framework of the policy support system AguaAndes/Waterworld (Mulligan, 2012d) which is an online policy support system initially developed for the Challenge Programme on Water and Food (CPWF) in the

Andes. However, this system of models can be applied anywhere in the world since all necessary data is provided in a global database called SimTerra (Mulligan, 2009).

5.2. Methodology

5.2.1. Case study basins

The selection of the case study basins for hydrological modelling was based on a number of criteria using the number of dams from the GOOD^2 database introduced in chapter 3 that are contained in the GRDC large river basins (see figure 3.9) as a basis. A sub-selection of river basins was then made by selecting basins whose watersheds are fully contained within 10 degree latitude and longitude tiles as at the current time, the WaterWorld model has no capabilities of running across the 10 degree square tiles that it uses (neighbouring tiles would have to be run individually and then results exported to GIS for further analysis). This filtering yielded a subset of 82 river basins that could be used. Then, a selection was made of basins that are heavily impacted by dams as simulated impacts on one dam within a basin are likely to be similar within the same (medium sized) river basin and thus can be up-scaled for the basin. Basins heavily impacted by dams was defined as basins that have more than 20 dams and have more than 25% of their area draining into dams which yielded 22 basins. To narrow the selection down further, the degree of projected impact of climate change was assessed in order to select case studies that reflect a range from low projected impact to high projected impact. This was done by combining the mean basin-wide projected changes in precipitation and temperature under the A1B scenario for 5 GCMS (CCCMA_CGCM31, CSIRO_MK30, IPSL_CM4, MPI_ECHAM5, UKMO_HADCM3) for the 2050s. These were then normalised on a 0-1 scale with changes in precipitation normalised irrespective of direction of change as both wetting and drying can have serious impacts on dams. The final scores were then ranked into high, medium and low impact based on equal classes. For each class a basin was then selected within each of the impact classes based on a preliminary search of availability of ground-measured parameterisation and validation data.

5.2.1.1. Basins

Based on the above selection criteria, the following three basins on three different continents were selected:

- Guadalquivir river basin, Spain (high impact of climate change)
- Savannah river basin, USA (medium impact of climate change)
- Maputo river basin, South Africa (low impact of climate change)

The Guadalquivir basin in Spain has a catchment area of 57,017 square kilometres and is located in southern Spain. The basin is drained by the Guadalquivir river that extends westerly and is 640 km long (Bhat and Blomquist*.,* 2004) Long term mean precipitation in the basin is 571 mm but is highly variable over space and time with less than 400 mm per year in the eastern area that has low elevation and up to more than 1500 mm per year in the mountains. Most precipitation falls in the winter months from November to March. The basin is heavily modified and contains 64 dams with 74% of the basin area draining into dams. Figure 5.1 shows a map of the basin and the location of the dams while table 5.1 summarizes the key basin characteristics for all three case study basins.

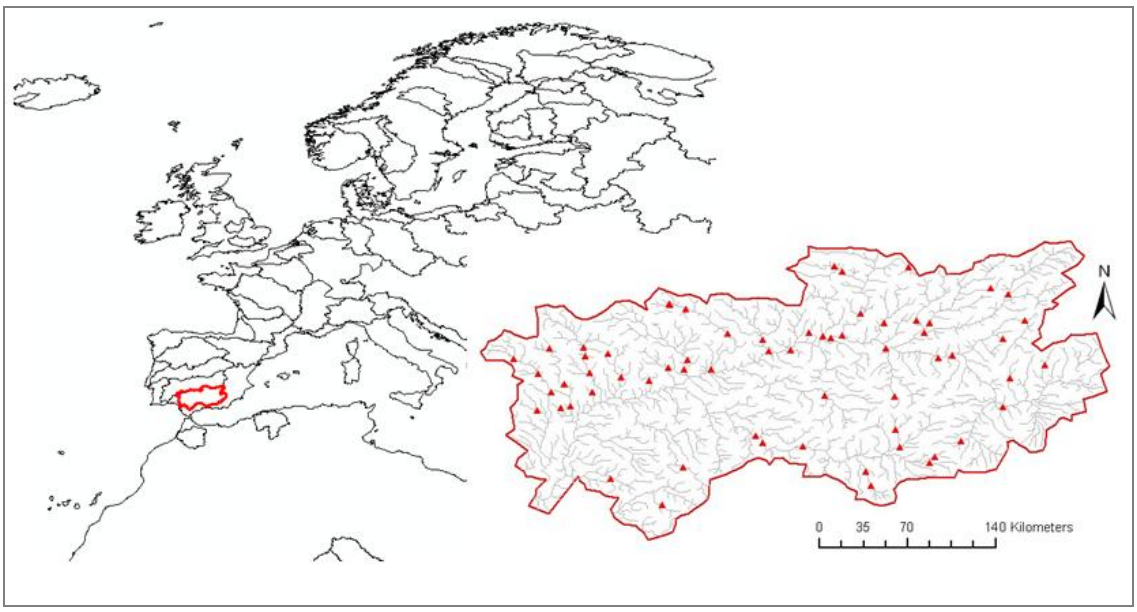

Figure 5.1 Guadalquivir basin, Spain with locations of dams.

The Savannah basin is a large river basin in the South East of the United States with a drainage area of just over 25,000 square kilometres. The main river is the Savannah river that originates in the Appalachian mountains in the state of North Carolina, and runs eastward through Georgia and South Carolina where it broadens into an estuary before flowing into the Atlantic ocean. The basin contains 31 dams and over 70% of the basin drains into a dam. Long term mean precipitation for the area is 1288 mm per year that is more or less evenly distributed over the basin with the exception of the headwaters in the mountains that receive considerably more precipitation. A small amount of runoff comes from snow melt in winter. Figure 5.2 shows a map of the Savannah basin and location of the dams.

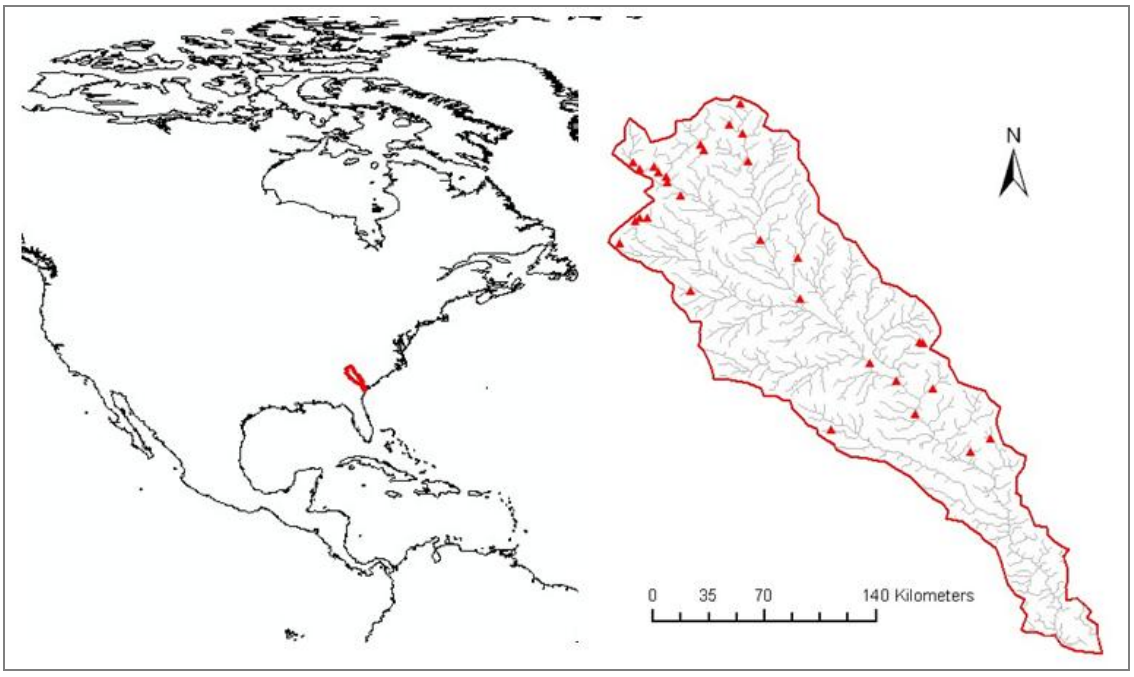

Figure 5.2 Savannah basin, USA with locations of dams.

The Maputo basin is located in East Southern Africa and is a shared basin between South Africa, Swaziland and Mozambique. It has a total area of 29,970 square kilometres and consists of three sub basins, the Usuthu, Pongola and Maputo. The upstream countries, South Africa and Swaziland account for most of the basin while only around 5% of the basin area falls in Mozambique (Kramer, 2003). The basin is fed by rainfall and land drainage so that highest discharge is recorded in and shortly after the rainy season between January and April (Langedijk, 1984). The Maputo basin has

two seasons with the rainy season from October to March and a mean annual precipitation of 815 mm a year. In total there are 21 dams in the basin with four large dams on the Usuthu basin that transfer water to the Upper Vaal and Upper Olifants basin in South Africa, which is used mainly for power generation (Kramer, 2003). The main dam on the Pongola river is the Phongolapoort dam that is described in more detail in section 5.2.1.2. Figure 5.3 shows a map of the basin and location of dams.

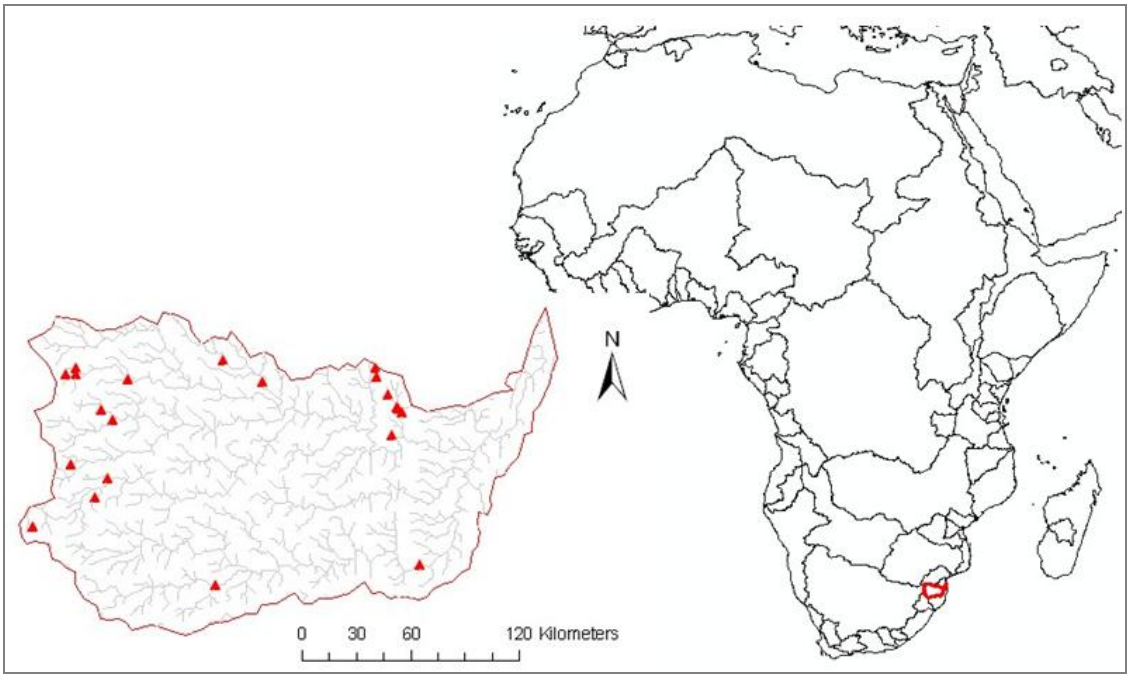

Figure 5.3 Maputo basin, South Africa with locations of dams.

Table 5.1 shows the characteristics for these basins and figure 5.4 shows digital elevation models for each basin.

Table 5.1 Basin characteristics

Basin	**Drainage area (km^2)**	**Mean T[1] 1950-2000 (°C)**	**Mean P[1] 1950-2000 (mm/yr)**	**Mean AET[2] (mm/yr)**	**Number of dams in basin**	**% of basin draining into dams**
Guadalquivir	57,017	16	571	399	64	74
Savannah	25,511	16	1288	741	31	70.5
Maputo	30,375	19	815	519	21	44.5

[1] based on WorldClim climate data (Hijmans *et al.,* 2006)

[2] based on WaterWorld model (WaterWorld, 2012)

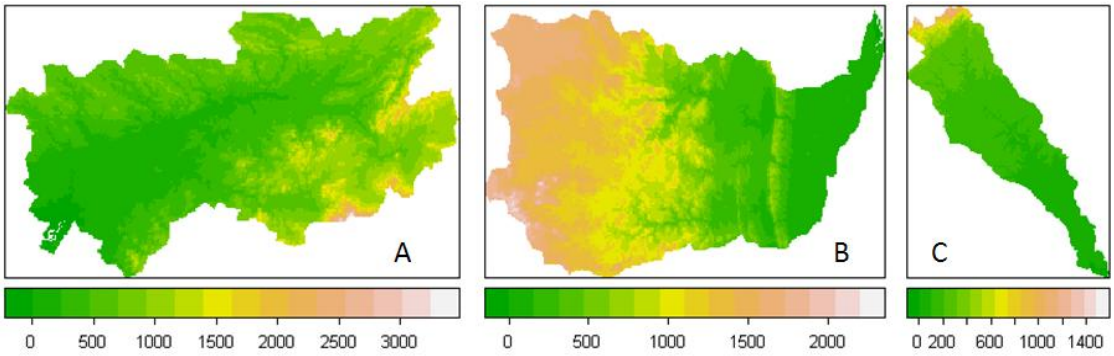

Figure 5.4 Digital Elevation Models (SRTM) for A: Guadalquivir basin, B: Maputo basin and C: Savannah basin (m.a.s.l.)

5.2.1.2. Dams

For each case-study basin, a major dam was then selected as the point at which changes in inflow of water and sediment as a result of projected climate change can be calculated. The hydrological modelling assessment used in this chapter is an equilibrium assessment in which the baseline climate and runoff is compared to projected future climate and associated runoff for the 2050s. Since the spatial model used is a process-based, un-calibrated model, the purpose of this modelling exercise is not to closely model current inflows into dams but rather provide information on the possible relative magnitudes, spatial pattern and direction of changes.

The selected dam for the Guadalquivir basin simulation in Spain is the Tranco de Beas dam, which is an irrigation dam with an average output of 1.5 Million m^3 a day and a catchment area of 550 km^2. The dam was built in 1944. Figure 5.5 shows a picture of the dam and the location of the dam in the Guadalquivir basin.

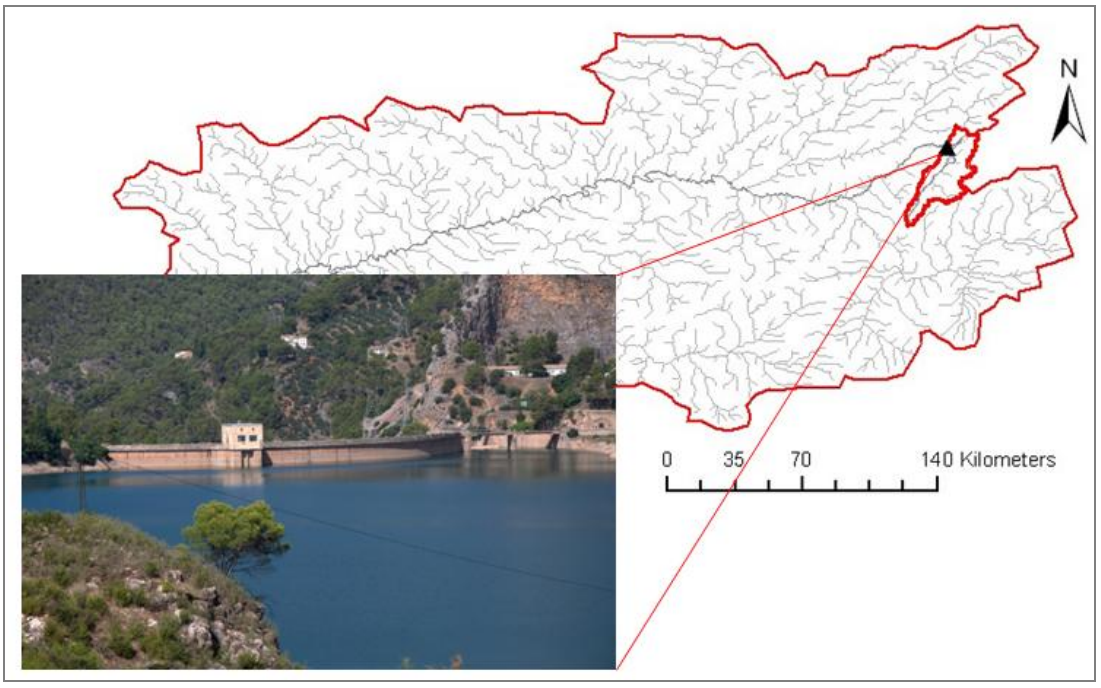

Figure 5.5 Picture, location and catchment area of Tranco de Beas dam in Guadalquivir catchment, Spain. Picture source: http://www.andaluciarustica.com

The selected dam for the Savannah basin is the J. Strom Thurmond dam which is also known as the Clarks Hill dam. This dam was built between 1946 and 1954 and is one of three major dams that impound the Savannah river. The dam's purpose is flood control and hydropower generation and has a total output capacity of 380 MW. Figure 5.6 shows a picture and the location and catchment area of the dam within the Savannah river basin.

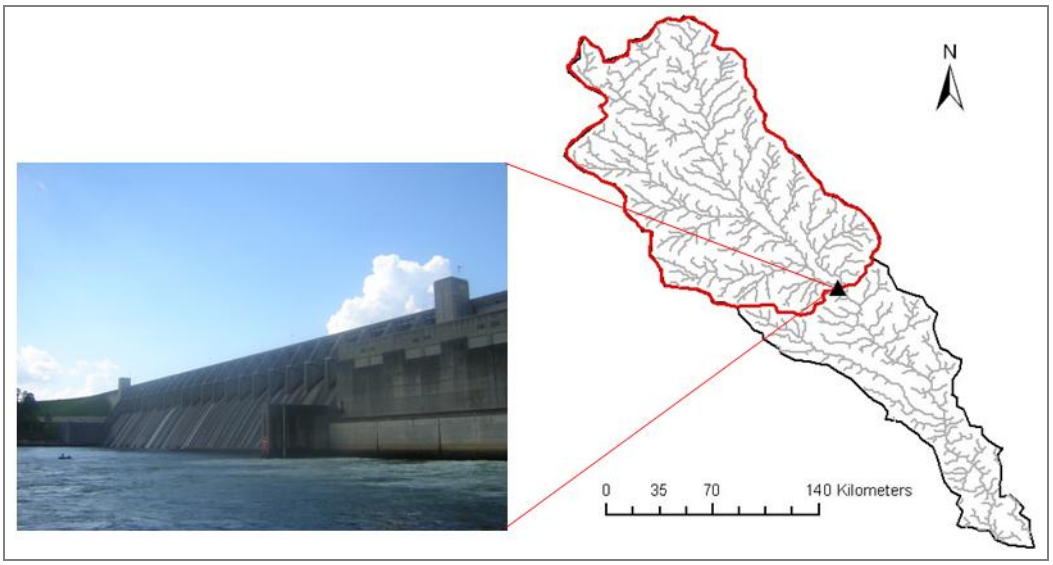

Figure 5.6 Picture, location and catchment area of J. Strom Thurmond dam in Savannah basin, USA. Picture source: J. Stephen Conn

The Phongolapoort dam (formerly Jozini), is located in the Maputo basin and is one of the five largest dams in South Africa, mainly used for irrigation and domestic uses (50 and 16 million m^3/yr respectively). Figure 5.7 shows a picture and the location and catchment area of the dam within the Maputo river basin.

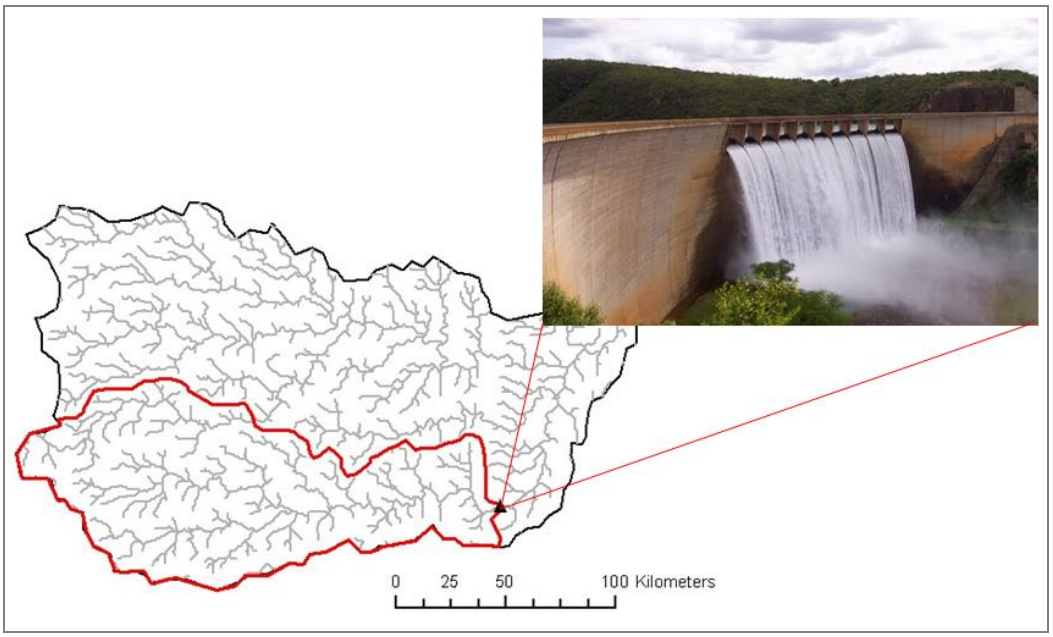

Figure 5.7 Picture, location and catchment area of Phongolapoort dam, South Africa. Picture source: Panoramio.com

Table 5.2 summarizes the main dam statistics.

Table 5.2 Dam and river statistics

Dam	Purpose	Output	River	Dam catchment area (km^2)	In operation since	Volume reservoir (Mm^3)	Elevation masl	Dam height
Tranco de Beas	Irrigation	1.5 Mm^3/d	Guadalquivir	550	1944	500	650	93
J. Strom Thurmond	HEP	380 MW	Savannah	15,910	1954	4712	55	61
Jozini/ Phongolapoort	Irrigation	6.2 Mm^3/d	Maputo	6121	1970	2267	68	89

5.2.1.3. Projected climate change

The modelling in this chapter is carried out using the multi-model mean scenario based on 5 GCMs for the A1B scenario as described in chapter 4. The A1B scenario assumes a rapid economic growth that is increasingly globalised, a general wealth increase, convergence between regions and a reduction in differences between regional incomes. Energy sources to fuel this growth are balanced between fossil and non-fossil sources assuming similar improvement rates of all energy supply and end-use technologies (Arnell *et al.,* 2004). The SRES scenarios are discussed in more detail in section 2.5.3 while a more in-depth discussion of the multi-model mean scenarios, the downscaling method and GCM uncertainty is given in section 4.2.1.

Table 5.3 shows the descriptive statistics for temperature and precipitation change for climate projections for this scenario for the three case study basins for mean change between the 1950-2000 WorldClim baseline and the 2050s scenario projection.

Table 5.3 Change in temperature and precipitation for three case study basins from 1950-2000 to 2050 under the A1B emissions scenario and the standard deviation between GCM projections for 5 GCMs

	Temperature				**Precipitation**			
Full basin	*Min*	*Max*	*Mean*	*SD*	*Min*	*Max*	*Mean*	*SD*
Guadalquivir	2.7	3.1	2.9	3.6	-131	-78	-97	165
Maputo	2.5	2.9	2.7	1.2	-54	0	-15	275
Savannah	2.5	2.7	2.6	4.5	25	74	45	480
Dam catchment								
Tranco de Beas	2.9	3.0	3.0	0.01	-86	-79	-83	1.56
Phongolopoort	2.5	2.8	2.7	0.07	-17	0	-8	4.56
J. Strom Thurmond	2.6	2.7	2.7	0.02	33	74	51	9.15

Figure 5.8 and 5.9 show the frequency histograms for precipitation and temperature change respectively for this climate change scenario for the case study basins drawn to the same horizontal scale and frequencies expressed as percent of basin area. These frequency distributions show the range and spatial variability within and between the basins indicating that the Maputo basin has the least variability in precipitation change with a distribution centred around -25 mm a year and Guadalquivir and Savannah basins both having a wider range of distribution with decreases in the Guadalquivir and increase in the Savannah basin.

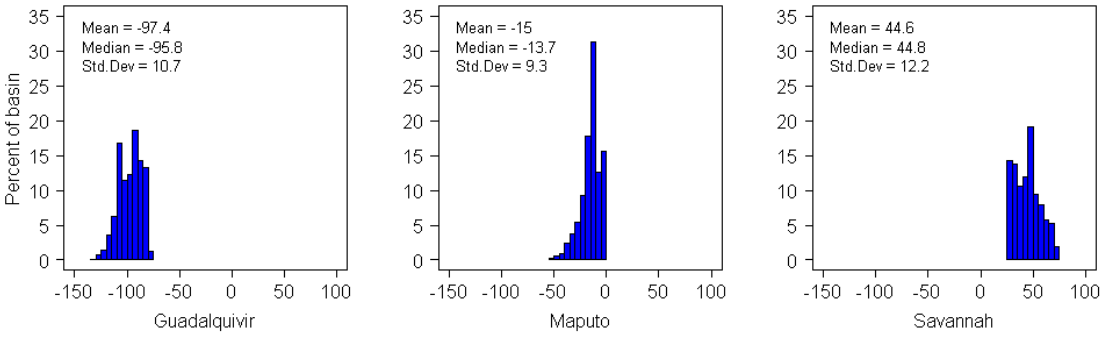

Figure 5.8 Frequency histograms for precipitation change for the case study basins based on the mean of 5 GCM under the A1B scenario for the 2050s (mm/yr)

The frequency distributions for temperature change indicate that the Savannah basin has the least variability with a range between 2.4 and 2.7 degrees Celsius centred

around 2.6 degrees while the Maputo basin has a more evenly distributed temperature change over the basin between 2.5 and 2.9 degrees. Guadalquivir basin shows the highest projected temperature change that centres around 3 degrees Celsius.

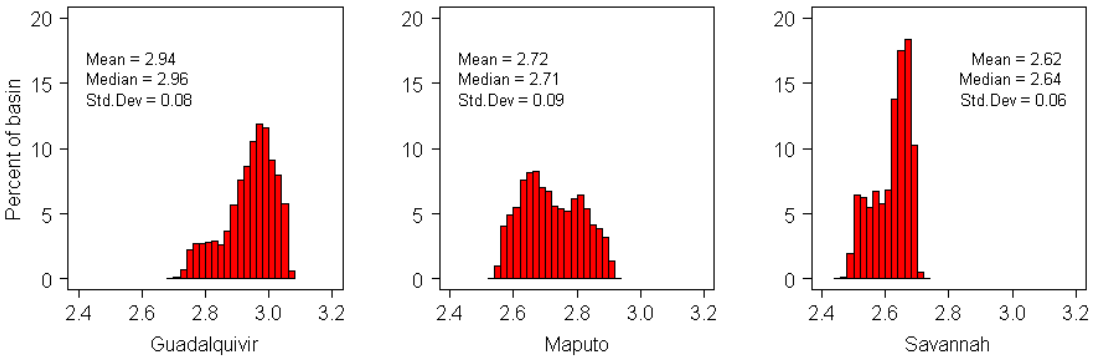

Figure 5.9 Frequency histograms for temperature change for the case study basins based on the mean of 5 GCM under the A1B scenario for the 2050s (°C/yr).

5.2.2. Climate change projections for dam catchments

Figure 5.10 shows the projected monthly changes in temperature and precipitation for the three case study dam catchments as the change between the mean of 5 GCM for the A1B scenario for the 2050s and the WorldClim baseline. Mean precipitation for the Tranco de Beas dam catchment is projected to decrease with 16.5% and become significantly more seasonal. Mean temperature on average increases with 2.9 degrees Celsius. Mean annual precipitation in the Phongolapoort dam catchment in the Maputo basin is projected to become slightly drier with an overall decrease in precipitation of 3.7%, mainly due to a sharp increase in wet season precipitation. Mean annual temperature is projected to rise with 2.7 degrees Celsius. Finally, precipitation in the J. Strom Thurmond dam catchment in the Savannah basin is projected to increase with 3.8% with an average annual temperature increase of 2.6 degrees Celsius. The Phongolapoort dam catchment shows much greater seasonal changes for precipitation than the other two catchments with a substantial decrease in the dry season and minor increases for the wet season. Temperature changes are much more

seasonal in the Tranco de Beas dam catchment with a difference of nearly 2 degrees Celsius between the winter and summer months.

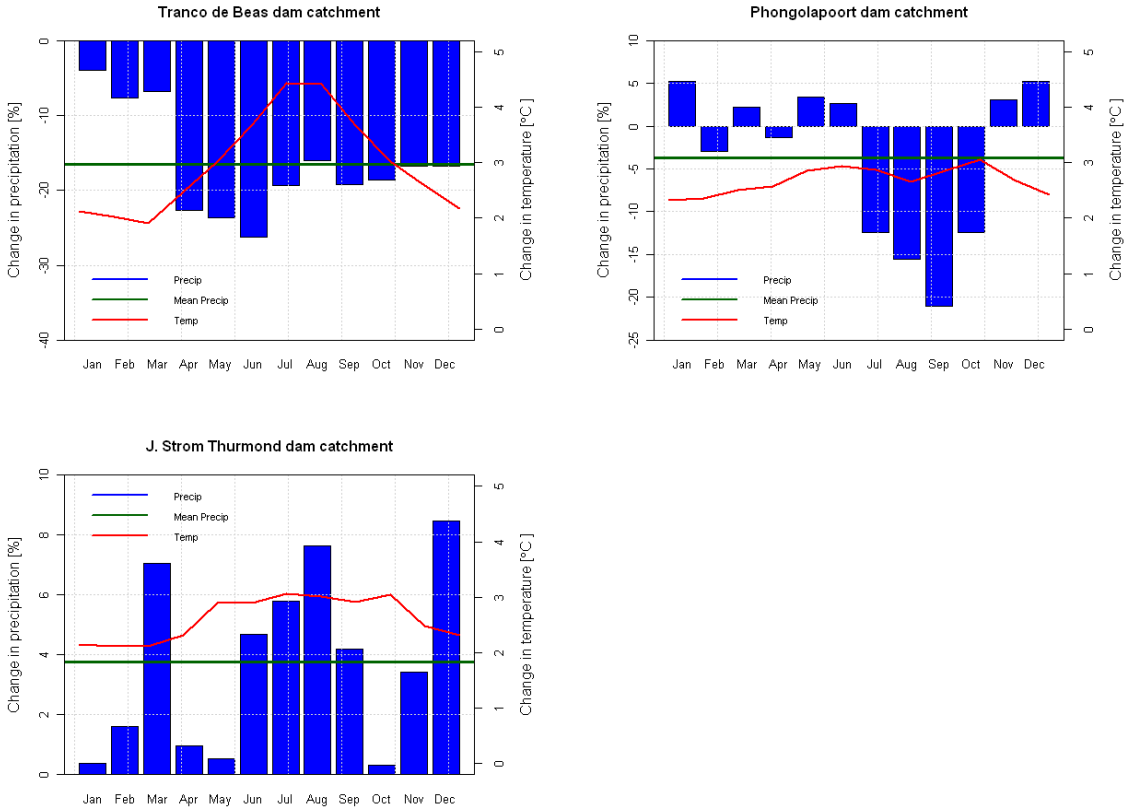

Figure 5.10 Projected changes in precipitation and temperature for dam catchments under mean of 5 GCM A1B scenario for the 2050s.

Figure 5.11 and 5.12 show the frequency histograms for precipitation and temperature change for the three case study dam catchments. Precipitation change in the J. Strom Thurmond dam catchment shows the greatest range while the Tranco de Beas dam catchment has the smallest range. The Phongolapoort dam catchment sees the greatest spatial variation in temperature change within the catchment with a range of 0.3 degrees Celsius. These differences however are the result of the downscaling approach used.

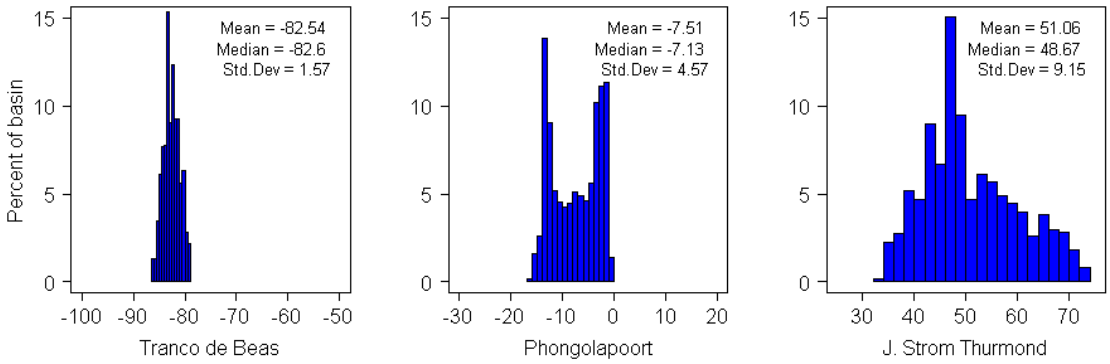

Figure 5.11 Frequency histograms for precipitation change for the dam catchments based on the mean of 5 GCM under the A1B scenario for the 2050s (mm/yr)

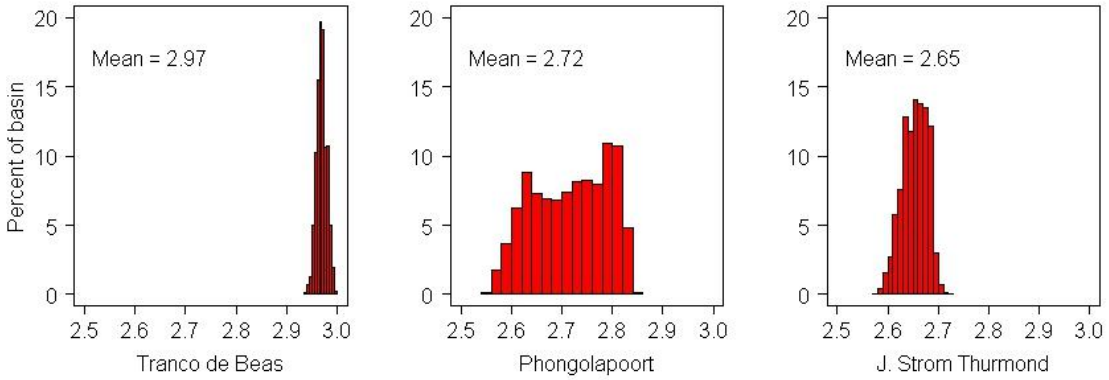

Figure 5.12 Frequency histograms for temperature change for the dam catchments based on the mean of 5 GCM under the A1B scenario for the 2050s (°C/yr)

5.2.3. Hydrological modeling

5.2.3.1. AguaAndes/Waterworld

In order to assess whether the projected changes in climatic inputs (precipitation and temperature) into the system will lead to changes in inflow of water into the dams, a spatial hydrological model is used. The model used is the FIESTA (Mulligan and Burke, 2005; Bruijnzeel *et al.,* 2011) model which is described in more detail below. The model is embedded within the framework of the policy support system AguaAndes/Waterworld (Mulligan, 2012d) and available at:

http://www.policysupport.org/waterworld which is an online policy support system initially developed for the Challenge Programme on Water and Food (CPWF) basin focal project for the Andes (BFP-ANDES). The system is called AguaAndes when used within the Andes mountain range and has been further developed for the 2nd phase of the CPWF in the COMPANDES project (www.benefitsharing.net). If the system is used outside of the Andes, it is referred to as WaterWorld. However, there is no difference in the underlying model, only the interface. The Policy Support System can be used to test the consequences of implementing land and water related policies. As well as an adapted version of the FIESTA hydrological model it incorporates other models for biophysical and socioeconomic processes as well as options for designing and implementing scenarios of change for climate and land use. The system runs on either 1-square km or 1-hectare resolution within 10-degree or 1-degree tiles respectively and can be applied anywhere globally as the underlying database (referred to as SimTerra) is global in extent. For one hectare simulations only the DEM and its derivatives have a resolution of 1 hectare with all other input data being sub-sampled from their native resolutions of between 250m and 1km. Furthermore, users can upload their own data if they have better resolution or more recent data than is provided with the PSS. For the analysis in this chapter, the model is run at 1-square kilometre spatial resolution so the dam catchments are contained within the model analysis extent of 10-degree latitude and longitude tiles. SimTerra is described in more detail in section 5.2.3.3.

5.2.3.2. FIESTA model

FIESTA, an acronym for Fog Interception for the Enhancement of Streamflow in Tropical Areas is a model developed by Mulligan and Burke in 2005 for the DfiD project FRP R7991 and was specifically designed to better understand the spatial and seasonal changes in water and evaporative losses as a result of conversion of cloud forest to pasture in tropical mountainous environments. The model is a process-based spatially distributed model that models the above-ground components of the water balance on a monthly time-step but also includes a diurnal time-step to characterize the average

daily dynamics within a month which is important for fog and evaporation calculations. Model calculations are carried out for one year of data using a long-term (50 years) climatology. Therefore this model is a static equilibrium model (see section 2.7.3)

FIESTA is a grid based model and can be run at a 1ha or 1km spatial resolution. There are no subsurface components since soil and base flow cannot be parameterized at these spatial scales due to a lack of data on subsurface properties. Runoff is approximated by routing the water balance down a stream flow network giving an indication of potential long term runoff with soil and groundwater stores in equilibrium. Since its development in 2005, the model has been updated a number of times and the latest version includes an energy budget based snow and ice model to model the contribution of snowmelt to runoff based on Walter *et al.,* (2005) which is described below. While originally developed for tropical cloud forests, the model is highly physically based and thus adaptable for assessing impacts of land cover and climate change on water production, particularly in mountainous areas. It has been applied in many regions of tropical Latin America as well as areas in Africa and Asia (Mulligan, 2012d).

Input data

As described above, the model can be run at 1ha or 1km spatial resolutions and requires a total of 146 digital maps (for v2.3) to run a simulation. It uses mean 50- year values of basic climate variables for every month as well as recent data for terrain (SRTM, Farr and Kobrick, 2000), climate (WorldClim, Hijmans *et al.,* 2005) and land cover (MODIS Vegetation Continuous Fields VCF2000; Hansen *et al.,* 2006). Table 5.4 gives an overview of the main input maps and their sources while section 5.2.3.3 describes the SimTerra database that contains all the necessary input data to drive the FIESTA model and other models contained in the AguaAndes/Waterworld policy support systems (see figure 5.13)

Table 5.4 Data sources for AguaAndes/WaterWorld (Source: Mulligan, 2012d)

Variable	**Units**	**Source**
Boundary layer wind direction (monthly)	degrees from N	Derived from BADC (2004)
Mean sea level pressure (monthly)	mb	derived from BADC (2004)
Elevation (SRTM1k)	metres (a.s.l)	Farr and Kobrick (2000)
Elevation	metres (a.s.l)	Jarvis *et al* (2008)
Air temperature (monthly)	deg. C	New *et al* (2003)
Wind speed (monthly)	m/s *10	New *et al* (2003)
Relative Humidity (monthly)	%	New *et al* (2003)
Mean annual temperature	deg. C	Hijmans *et al* (2005)
Mean monthly precipitation (monthly)	mm/month	Hijmans *et al* (2005)
Total annual precipitation	mm/year	Hijmans *et al* (2005)
Mean daily maximum temperature (monthly)	deg. C *10	Hijmans *et al* (2005)
Mean monthly temperature (monthly)	deg. C *10	Hijmans *et al* (2005)
Mean daily minimum temperature (monthly)	deg. C *10	Hijmans *et al* (2005)
Cloud frequency (DJF)	fraction	Mulligan (2006d)
Cloud frequency (JJA)	fraction	Mulligan (2006d)
Cloud frequency (MAM)	fraction	Mulligan (2006d)
Cloud frequency (SON)	fraction	Mulligan (2006d)
Mean annual cloud frequency	fraction	Mulligan (2006d)
Cloud frequency (monthly)	fraction	Mulligan (2006d)
Cloud frequency 00:00-06:00 hrs	fraction	Mulligan (2006d)
Cloud frequency 12:00-18:00 hrs	fraction	Mulligan (2006d)
Cloud frequency 18:00-24:00 hrs	fraction	Mulligan (2006d)
Cloud frequency 06:00-12:00 hrs	fraction	Mulligan (2006d)
Local drainage direction	direction	Mulligan (2009)
Cover of bare ground	percentage	Hansen *et al* (2006)
Cover of herb-covered ground	percentage	Hansen *et al* (2006)
Cover of tree-covered ground	percentage	Hansen *et al* (2006)
Daily temperature range (monthly)	deg C * 10	Hansen *et al* (2006)

Since the model is originally developed to model cloud water interception in cloud forests, there is a particular focus on capturing the contribution of fog to the water balance in addition to the rainfall. Fog inputs are calculated on the basis of wind speed, topographical exposure and vegetation structure. There are two functional vegetation types, forest and herbaceous cover. Furthermore, to indicate areas where vegetation

does not influence hydrology, a layer of bare soil is included. These layers are based on the MODIS vegetation continuous fields data product (Hansen *et al.,* 2006). Fog interception is calculated as a function of LAI and occurrence of ground-level cloud is derived from atmospheric cloud frequency based on a monthly and diurnal cloud climatology derived by Mulligan (2006d) from the MODIS MOD35 product. The impact of this cloud frequency on solar radiation is also calculated which in turn affects the potential and actual evapo-transpiration. AET also depends on the leaf area index and will be much reduced in areas with low vegetation cover. Snow and ice is accounted for in the model since version 2 and is calculated with a physical process based energy budget snowmelt model based on Walter *et al.,* (2005) which estimates parameters based on established relationships using only data on minimum and maximum temperatures, solar radiation and wind speed.

Using the calculations described above, for every pixel and for every time step, the water balance is calculated taking into account wind driven rain, fog, snow-melt and calculated values of evapo-transpiration based on topographic, climatic and vegetation properties (Mulligan and Burke, 2005) which is finally cumulated downstream along a stream flow network to give potential runoff values. A more in-depth description of the FIESTA model is given in Mulligan and Burke (2005), Bruijnzeel *et al.,* (2011) and Mulligan (2012d).

5.2.3.3. SimTerra

SimTerra (Mulligan, 2009) is a database of environmental variables available on a global scale at resolutions between 1-hectare and 1 km^2. The data have been generated or sourced from ground-based and remote sensing sources. The database is continuously expanded but currently contains 327 different maps for 162 variables that are biophysical (hydrological, climate, landscape and vegetation) and socio-economic (population, GDP, poverty, infrastructure, land use, crop types and irrigation). This dataset is the core of the AguaAndes/Waterworld policy support system and provides all the necessary input files to run the FIESTA model and other

models associated with the system with some of the variables available as monthly files and others as annual or seasonal input files. All maps in the database are in un-projected geographic coordinates and use the WGS84 datum. An overview of the maps necessary to run AguaAndes/WaterWorld in the system is given in appendix IV.

5.2.3.4. Snow and ice modelling

Since version 2.3 of the model, AguaAndes/WaterWorld contains a snow and ice model that can simulate the processes of melt water production, snow fall and snow pack. The model component is based on a full energy balance for snow accumulation and melting after Walter *et al.,* (2005) where parameters are either estimated using only the day of the year, the geographical location and maximum and minimum temperature or are available directly in the SimTerra database (e.g. cloudcover and wind speed). Initial monthly snow cover is based on MODIS snow cover data processed by Mulligan (2006a) and snow fall is assumed to occur where precipitation occurs at temperature below 0°C. Changes in melt water production and snow pack as a result of climate changes currently only take into account changes in temperature and precipitation as these are the only parameters that change for the climate change scenarios.

5.2.3.5. Soil erosion and sedimentation model

As of version 2.0 of the WaterWorld model, modules for soil erosion, soil deposition and transportation are included. The erosion model is based on the Thornes (1990) model defined as:

$$E = kQ^2S^{1.67}e^{-0.07V_c} \quad (5.1)$$

Where E is erosion (mm/hr), k is a soil erodibility coefficient which currently is a constant held at 0.2 throughout the model domain since there is no information on soils, Q is runoff (mm/hr) which is derived from the FIESTA model, S is the tangent of

the slope gradient which is derived from the SRTM DEM and Vc the vegetation cover (tree and herb functional type as %) which is based on the MODIS VCF data (Hansen *et al.,* 2006). Sediment transport is determined by the transport capacity Tc which is calculated according to stream power which is a function of runoff and slope (Kirkby, 1976):

$$T_c Q^{1.7} \sin(S)^{0.001} (1 - V_c) \quad (5.2)$$

Sediment transport S is a function of sediment inputs from upstream plus local erosion, P where these are less than the transport capacity. Finally sediment deposition occurs where S is greater than P until S=P.

It is important to recognize that this model for wash erosion on a monthly time-step does not capture impacts of extreme rainfall events and landslides. Both types of events may deliver much sediment to dams. However, since there is very little evidence upon which to project extreme event magnitudes and frequency, impacts of changing runoff can only be assessed based on the GCM results. Furthermore, impacts of climate change on vegetation cover are also not taken into account which may have consequences for the impacts of climate change on soil erosion.

5.2.3.6. Output data

The policy support system provides a range of annual and monthly output grid maps that can be downloaded from the system in various GIS formats or can be viewed online using the geo-browse functionality. Output maps include water balance, wind driven precipitation, fog deposition, actual evapo-transpiration and runoff as well as annual and monthly hillslope runoff, soil erosion and soil deposition and percentage of water that may be polluted as an indication of water quality. Snow pack water equivalent, snow fall and melt water production are available as monthly maps only.

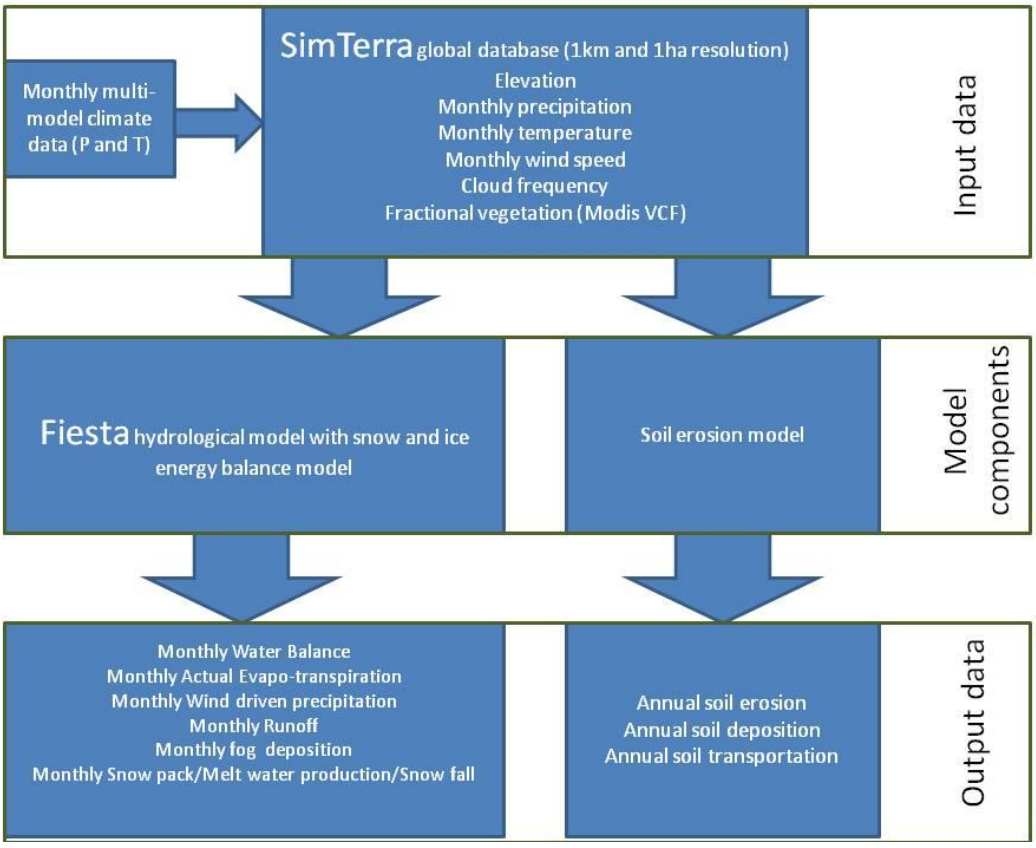

Figure 5.13 Overview of WaterWorld modelling framework with key inputs and outputs used in the analysis.

5.2.3.7. Validation

In the validation process for large scale models, as a result of the usually poor data availability for these models at this scale, the deficiencies measured are often derived from the data as well as from the model (Mulligan and Burke, 2005; Mulligan 2012). Significant uncertainties are present in some of the model inputs, especially rainfall, wind speed and wind direction, land cover and topography (Bruijnzeel *et al.,* 2011). However, the FIESTA model has been extensively validated with satisfactory results for Costa Rica (Mulligan and Burke, 2005) and Colombia (Sáenz, 2007) as well as for a number of other studies around the world (Mulligan, 2012d). Therefore, a comprehensive validation exercise for the three case studies is not carried out (largely because of a lack of good validation data), though, an attempt is made to address some of the input data uncertainties and validate the model outputs at the scale of the whole basin as specific data for the dam catchments proved difficult to obtain. It is

assumed that if the model performs well at the scale of the basin where the dam is located, this will also likely be the case for the dam catchment.

To see whether the FIESTA model performs well in modelling river flows within the case study basins, a validation was carried out by using measured average monthly river discharge values obtained from the RivDIS database available at: http://www.-eosdis.ornl.gov/rivdis/STATIONS.HTM (Vörösmarty *et al.,* 1998) for the Guadalquivir basin. Monthly stream flow data for the Savannah basin was obtained from the national water information system of the USGS (USGS, 2011) while monthly values for the Maputo basin were derived from the joint Maputo river basin water resources study carried out by Skoy Plancenter Ltd (Skoy Plancenter, 2009). The discharge data covers periods of at least 50 years with measurement periods between 1930-1984 for the Guadalquivir basin, 1930-2011 for the Savannah basin and 1929-1984 for the Maputo basin. Historical data on climate and data on reservoir building was obtained from various sources. Table 5.5 shows the obtained data, years available and sources for the validation data.

Table 5.5 Validation data

Basin	**Precipitation data years**	**Source**	**Flow data years**	**Source**	**First dams built**
Guadalquivir	1940-2010	Klein Tank *et al.,* 2002	1930-1984	Vörösmarty *et al.,* 1998	1946
Maputo	1920-2004	Skoy Plancenter 2009	1929-1968	Skoy Plancenter 2009	1966[2]
Savannah	1895-2010	USGS, 2011	1930-1984	USGS, 2011	1945

[2]source: http://www.dwaf.gov.za/maputobasinatlas/JMRBWRS_Atlas.html

Validation of flows and precipitation input

A validation of modelled versus observed stream flow for the basins was carried out by calculating the mean observed stream flow for the longest possible period before any dams were built in the river basins under study and compared with modelled baseline stream flow based on the WorldClim input precipitation for the period between 1950-2000. For all three case study basins this means that the modelled stream flow is based on a different time period than for the precipitation data. Since precipitation constitutes the largest input in the water balance model, an estimation of precipitation uncertainty is calculated by comparing the input WorldClim precipitation and the modelled wind driven precipitation with observed long term precipitation data for a number of stations within the catchments that are not part of the WorldClim database to ensure an independent sample.

5.3. Results

5.3.1. Validation results

Quadalquivir basin modelled runoff amounts to 428 mm/yr based on the WorldClim precipitation for the years 1950-2000 compared to measured runoff of 403 mm/yr at Alcala del Rio station for the years 1930-1945 which is the period before dam building began in the region. A difference of 5.8%. This difference might be the result of differences between the time period for the input precipitation data and validation flow data or it could be the result of an over-estimation of the precipitation input for the basin. To see whether this is the case, precipitation measurements at stations that are not included in the WorldClim dataset within the basin are compared to the WorldClim interpolated data and modelled wind driven rain values at those points.

There are six WorldClim stations that fall within the Guadalquivir basin with an additional eight stations around the edge. Measured station precipitation data for four stations not part of the WorldClim database for this basin was obtained from the European Climate Assessment and Dataset database (Klein Tank *et al.,* 2002) that is

available online at: http://eca.knmi.nl/ This database has daily climatic data available for 4822 meteorological stations throughout Europe and the Mediterranean.

Table 5.6. shows the measured and modelled precipitation at four stations in the Guadalquivir basin. The difference between observed and modelled rainfall is only 2.8% for the four stations studied. Therefore the difference in precipitation cannot explain the differences in the measured versus modelled flow so the model slightly over estimates flow for the full basin.

Table 5.6 Measured versus modelled rainfall for individual stations in Guadalquivir basin

Station	Latitude	Longitude	Altitude	Years	Measured (raw) rainfall (mm/yr)	Input WorldClim rainfall (mm/yr)	Difference measured WorldClim (mm/yr) (%)	Modelled wind driven rain	Difference measured wind driven (mm/yr) (%)
Sevilla	-5.88	37.42	34	1951-2010	576	580	4 (0.7)	580	4 (0.7)
Cordoba	-4.85	37.84	90	1960-2010	618	625	7 (1.1)	623	5 (0.8)
Granada Aeropuerto	-3.63	37.14	567	1940-2010	382	403	21 (5.5)	410	28 (7.3)
Jaen	-3.81	37.78	510	1942-1982	572	543	-29 (-5.1)	585	13 (2.2)
Mean	-	-	-	-	**537**	**538**	**0.8 (0.6)**	**550**	**12.5 (2.8)**

For the Maputo basin, the best available stream flow data records obtained are for the Usuthu river, hence this large river catchment was used for the validation of modelled stream flow in the basin. The total annual measured runoff for the Usuthu river at Frontera Oeste station for the period 1920-1966 amounts to 161 mm/yr and the modelled flow totals 315 mm/yr which is an overestimation of the annual yield by 96%. Measured precipitation data was obtained for seven stations in the basin and compared to the WorldClim interpolated input data and modelled wind driven precipitation for those points. The results can be found in table 5.6. There is a slight overestimation for four stations and a underestimation for three stations resulting in a mean difference for all stations of only 2.9% for input precipitation and 4.1% of modelled wind driven precipitation. However, the WorldClim station density at the

top of the basin where rainfall is highest (Amsterdam station), is very low (2 stations for an area of ~ 5000 km^2). Since the interpolated WorldClim rainfall shows a significant overestimation for this station (> 12%, see table 5.6), it is likely that rainfall is overestimated for this area which makes up around 25% of the Usuthu sub-basin. Apart from inaccuracies in precipitation input, differences in modelled flow can potentially be attributed to differences in calculated evapo-transpiration since this constitutes the second largest flux in the water balance calculation. Examining the simulated PET values for the basin reveal that the annual mean PET amounts to 1138 mm/yr (table 5.9) whereas Symons pan evaporation for the area is measured to be in the region of 1400 to 1600 mm/yr (Skoy Plancenter, 2009). This difference could be due to lower radiation receipt as a result of more cloud cover in the model from the MODIS cloud climatology (Mulligan, 2006d). Another explanation for the higher measured ET is that the area is characterised by high wind speeds with average daily runs between 230-240 km/day between September and December (Jaganyi *et al.,* 2008) that increase ET but are not accounted for in the model. Inaccurate flow gauge location information could also be a result of differences between observed and modelled flows as well as the method of measurement and differences in contributing area. Information on the quality of the observed runoff at this station is given in Skoy Plancenter (2009) which rates the quality as average. This is because the flow gauge consists of a wide rated section in a sandy river bed where it is likely that the cross-section of the river changes during high flow events which means new rating curves have to be developed after each high flow event. This was done for the period between 1963-1974 but not for earlier periods. Furthermore, since it is a large river, obtaining accurate current meter readings is difficult.

Table 5.7 Measured versus modelled rainfall for individual stations in Maputo basin

Station	Latidutde	Longitude	Altitude	years	Measured (raw) rainfall mm/yr	Input WorldClim rainfall mm/yr	Difference measured WorldClim (mm/yr) (%)	Modelled wind driven rain	Difference measured wind driven (mm/yr) (%)
Amsterdam	-26.26	30.67	1271	1920-1999	819	924	105 (12.8)	934	115 (14.0)
Vlakkloof Estate	-26.95	30.58	1381	1929-1990	906	870	-36 (-4.0)	877	-29 (-3.2)
Groot Rietvlei	-27.13	30.37	1311	1928-2003	770	818	48 (6.2)	819	49 (6.4)
Marthinusdrift	-27.52	30.72	1128	1953-2004	930	909	-21 (-2.3)	917	-13 (-1.4)
Nyonyane	-26.45	31.20	720	1920-1987	1104	1034	-70 (-6.3)	1023	-81 (-7.3)
Lauwsburg	-27.58	31.28	1250	1950-2002	808	886	78 (9.6)	898	90 (11.1)
Magugu	-27.15	32.01	610	1952-2004	770	800	30 (3.8)	840	70 (9.1)
Mean	-	-	-	-	**872**	**892**	**19.1 (2.9)**	**901**	**28.7 (4.1)**

Savannah basin modelled runoff amounts to 512 mm/yr based on precipitation input for the years 1950-1999 (WorldClim) versus measured 434 mm/yr of runoff at Clyo station (USGS station 02198500) for the period 1930-1945 before dam building in the region, which is a difference of 18%. The stream flow gauge is located 4 metres above sea level and is measured using a water level recorder. The quality of the data is considered to be good with the exception of daily discharge estimates (USGS, 2004). Precipitation data for 10 stations from within the Savannah basin has been obtained from the NOAA National Climatic Data Center (Menne *et al.,* 2005) of which 6 stations were in different locations than those used for WorldClim. The station long-term observed means were compared with WorldClim input precipitation and modelled wind driven precipitation (see table 5.8). The difference between measured and modelled precipitation for these locations are minimal. However, since the dataset of measured rainfall is sufficiently long it was possible to compare the measured 1930-1945 mean precipitation with the measured mean for the 1950-2000 period which is the time period used by the model. Precipitation for the 1930-1945 period amounted to 1177 mm/yr on average which is more than 100 mm less (-7.5%) compared to the measured precipitation for the period 1950-2000 and 9% less than the wind-driven

precipitation as calculated by the model. The difference in mean precipitation between the period used by the model and the period for the observed stream flow data can therefore partly explain the differences in modelled flow.

Table 5.8 Measured versus modelled rainfall for individual stations in Savannah basin

Station	Latitude	Longitude	Altitude	years	Measured (raw) rainfall mm/yr	Input WorldClim rainfall mm/yr	Difference measured WorldClim (mm/yr) (%)	Modelled wind driven rain	Difference measured wind driven (mm/yr) (%)
Greenwood	34.12	-82.17	187.5	1895-2010	1170	1204	34 (2.9)	1206	36 (3.1)
Warrenton	33.40	-82.62	149.4	1895-2010	1205	1211	6 (0.5)	1216	11 (0.9)
Aiken	33.49	-81.69	150	1895-2010	1184	1223	39 (3.3)	1217	33 (2.8)
Anderson	34.52	-82.66	243.8	1895-2010	1245	1273	28 (2.2)	1263	18 (1.4)
Clemson	34.66	-82.82	251.2	1895-2010	1342	1362	20 (1.5)	1375	33 (2.5)
Toccoa	34.57	-83.33	308.5	1895-2010	1487	1477	-10 (-0.7)	1499	12 (0.8)
Mean	-	-	-	-	**1272.2**	**1291.7**	**19.5 (1.6)**	**1296**	**23.8 (1.9)**

Overall, the validation results show that the model performs reasonably well in the Guadalquivir and Savannah basin but overestimates flow for the Maputo basin. This is most likely caused by an underestimation of the evapo-transpiration in the region. Mulligan and Burke (2005, p104) have described this characteristic of the model in dry cloud free lowlands in earlier validation studies in Costa Rica.

5.3.1.1. Validation of Potential Evapo-transpiration

Since precipitation inputs cannot fully explain the overestimation of flows in all three river basins, the modelled potential evapo-transpiration of WaterWorld was examined in more detail. Table 5.9 shows the results for a comparison exercise for PET using the observed FAO PET station data from the CLIMWAT dataset introduced in chapter 4 as a reference. This data is based on a Penman-Monteith interpretation of observed climatic parameters for 5500 meteorological stations around the world. More

information about this dataset and a map of spatial distribution of stations around the world can be found in appendix IV. The validation was carried out for all CLIMWAT station points that are contained within the 10-degree latitude and longitude tiles in which the basins lie. Mean elevation for the points in the Guadalquivir 10-degree tile is 350 metres whereas the mean elevation in the Guadalquivir basin is 580 metres. Mean elevation for the stations in the Maputo tile is 216 metres while the mean elevation in the Maputo basin is 850 metres. Mean elevation for the stations in the Savannah tile is 188 metres with a mean elevation in the Savannah basin of 192 metres. The results are given as the mean of points. The observed PET data was also compared to other estimated PET datasets as described in chapter 4.

Table 5.9 Potential evapo-transpiration validation for 10-degree tiles of case study basins. Methods are Penman-Monteith (PM), Hargreaves (Har), TEMP-PE (Oudin *et al.,* 2005b) and Fiesta (Mulligan and Burke, 2005)

		Guadalquivir			Maputo			Savannah		
latitude		35			-25			35		
longitude		-5			35			-85		
Nr of CLIMWAT stations in tile		31 (14)*			43 (43)			20 (9)		
	method	value	Mean dif	%	value	Mean dif	%	value	Mean dif	%
CLIMWAT PET	PM	1233	-	-	1441	-	-	1313	-	-
FAO pet (10')	PM	1348	115	9.3	1442	1	0.1	1212	-101	-7.7
MODIS PET	PM	2534	1301	105.5	2862	1421	98.6	1865	552	42.0
CIAT PET	Har	1264	31	2.5	1637	196	13.6	1244	-69	-5.3
WC TEMP-PET	TEMP-PE	1038	-195	-15.8	1396	-45	-3.1	979	-334	-25.4
FIESTA PET	FIESTA	785	**-448**	-36.3	1138	**-303**	-21.0	778	**-535**	-40.7

* Number in brackets is the number of stations used for validating the MODIS PET dataset as this dataset has no full global coverage

The FIESTA modelled PET underestimates PET for all three basins compared to the CLIMWAT data with differences ranging from -21% for the Maputo basin to -41% for

the Savannah basin. However, most of the other PET estimations are also lower than the CLIMWAT database which is most likely due to differences in the estimation method (see discussion in chapter 4). A more specific explanation as to why the FIESTA PET is lower than the other estimations is that it factors in cloud cover impacts on radiation where all the other methods use top-of-the-atmosphere solar radiation. However, if these effects are greater in the model than they should be then they could explain the apparent overestimation of stream flow in the basins.

5.3.2. Case study results

For each dam catchment, maps of elevation (SRTM) and vegetative land cover (herb and tree fraction) based on the MODIS VCF data (Hansen *et al.,* 2006) were created from the WaterWorld inputs as these characteristics can explain the spatial variability in other model outputs that have an impact on the water balance such as wind driven precipitation, actual evapo-transpiration and fog inputs. The key WaterWorld model outputs are then presented for every catchment for both the baseline and as the change from the baseline for the A1B climate scenario for the 2050s as an annual total or average. Examining the baseline results of the different components of the water balance on an annual basis highlights in which areas water is produced within a catchment and which are thus important when reviewing the management options that would be available to offset some of the impacts of climate change. To take into account the seasonal variability of the changes, monthly maps of water balance for each catchment are presented and results of the changes in inflow into the dam reservoirs on a monthly basis will be given. To characterize the seasonal variability in inflow into the dams, the coefficient of variation for the baseline and the climate scenario will be presented. Finally, results of the wash erosion model will be presented and changes of sediment delivery to the dam reservoirs will be given.

5.3.2.1. Tranco de Beas dam, Guadalquivir basin, Spain

Figure 5.14 shows the catchment characteristics for the Tranco de Beas dam in Spain with the dam location in the north-west corner of the catchment. The catchment has a

strong elevational gradient with elevation reaching 1860 m.a.s.l at the south east of the catchment quickly dropping to just over 600 m.a.s.l at the dam site. Vegetation in the catchment is dominated by herbaceous cover with a mean herb fraction of 76%. Trees are found mostly at lower elevation in the valley with a mean fraction over the catchment of 17% with the remaining land cover classed bare which is mostly at the highest elevations in the south-east of the catchment.

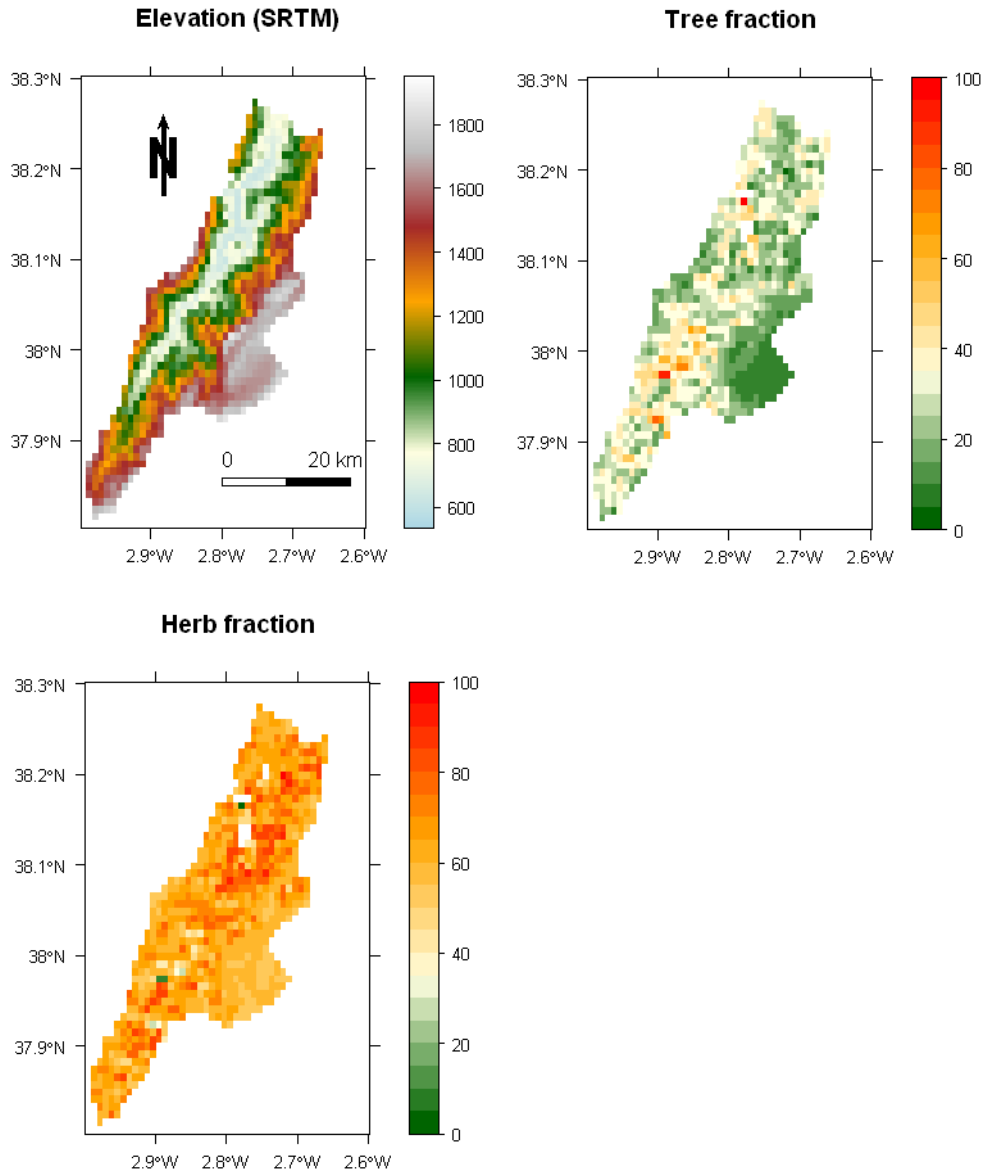

Figure 5.14 Catchment elevation based on SRTM DEM and herb and tree fractions based on MODIS VCF for the Tranco de Beas dam catchment, Spain.

Baseline results

The annual baseline model results shown in figure 5.15 show that both wind driven rainfall and actual evapo-transpiration are highly spatially variable within the dam catchment with rainfall varying between around 400 mm/yr to nearly 800 mm/yr and evapo-transpiration between 65 mm/yr to 550 mm/yr. Highest values for precipitation are found towards the south east of the catchment where elevation is highest. Highest values for AET are found at higher elevation. Mean AET over the catchment amounts to 208 mm/yr. Fog inputs are as expected dominated by trees and reach values of up to 35 mm/yr (6.5 % of rainfall), with a mean annual input of 25 mm (4.6% of rainfall). Snow occurs at the highest elevations above 1400 m.a.s.l which is mainly in the south east of the catchment with a mean annual snow pack of 6 mm and annual snow fall of 5.6 mm. Mean melt water contribution to the water balance amounts to 3.5 mm/yr. Finally, the resulting water balance shows that most of the water is produced towards the south east of the catchment at higher elevations where rainfall inputs are highest.

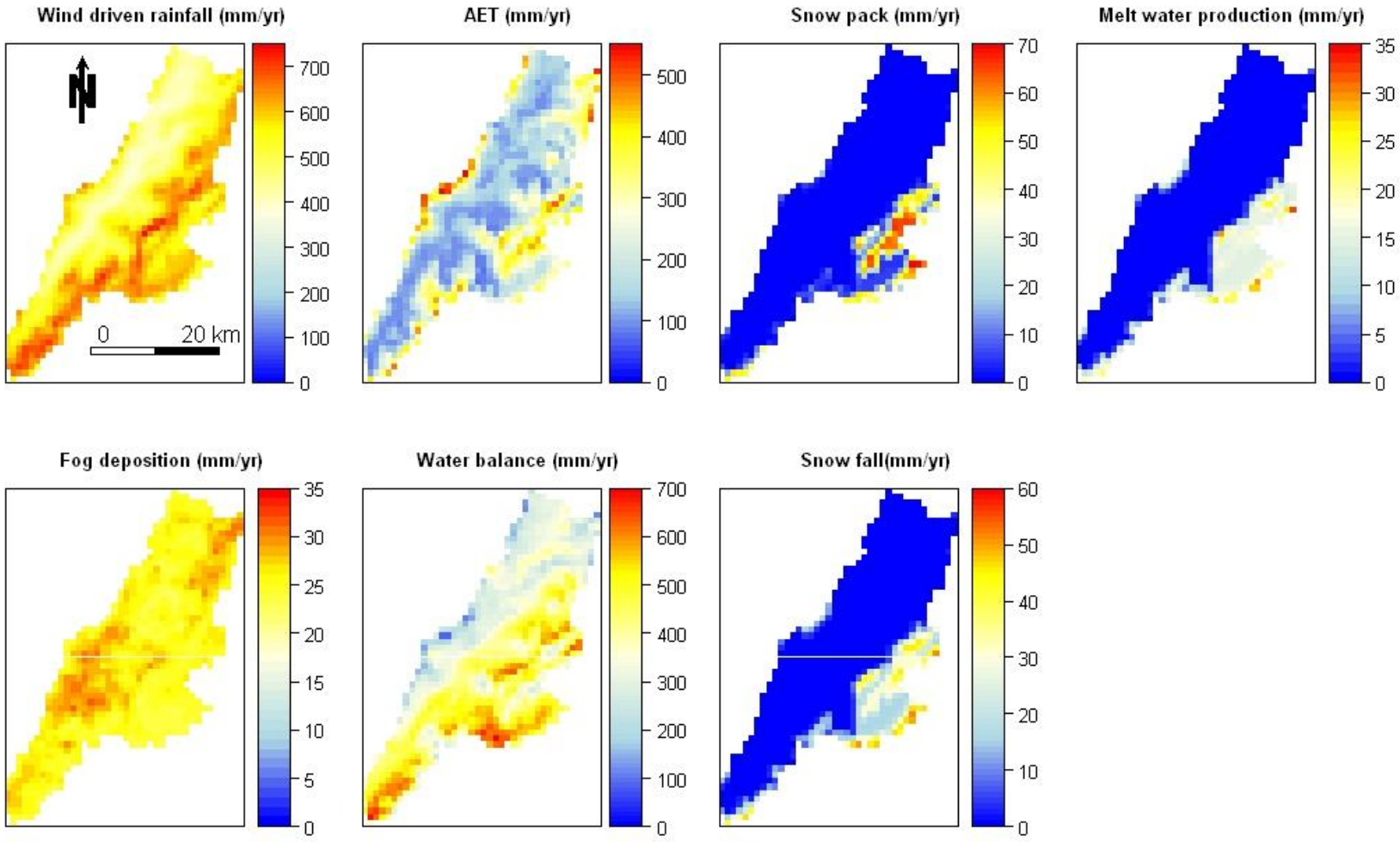

Figure 5.15 Annual baseline model results for wind driven rainfall, AET, water balance and fog inputs (mm) for Tranco de Beas dam catchment, Spain.

Scenario results

The climate scenario results shown as changes from the baseline in figure 5.16 show that the largest change in the water budget derives from changes in wind driven rainfall which -with the exception of a few cells- is projected to decrease for nearly the whole catchment as a result of a decrease in input precipitation. Mean decrease in wind driven rainfall for the catchments is 78 mm/yr. Actual evapo-transpiration on the other hand is projected to increase with 22 mm/yr on average as a result of increased temperature. Fog inputs decrease with 4 mm/yr on average as a result of the effects of increased temperature on the lifting condensation level for cloud formation. Changes in fog inputs seem to largely follow the spatial pattern of the elevation with greatest decrease at lower altitudes. Melt water changes are minimal with less than 1 mm/yr on average. As a result of these changes, the overall water balance decreases with approximately 110 mm/yr with around 70 % of this change deriving from a decrease in input precipitation and around 20% as a result of a increase in AET.

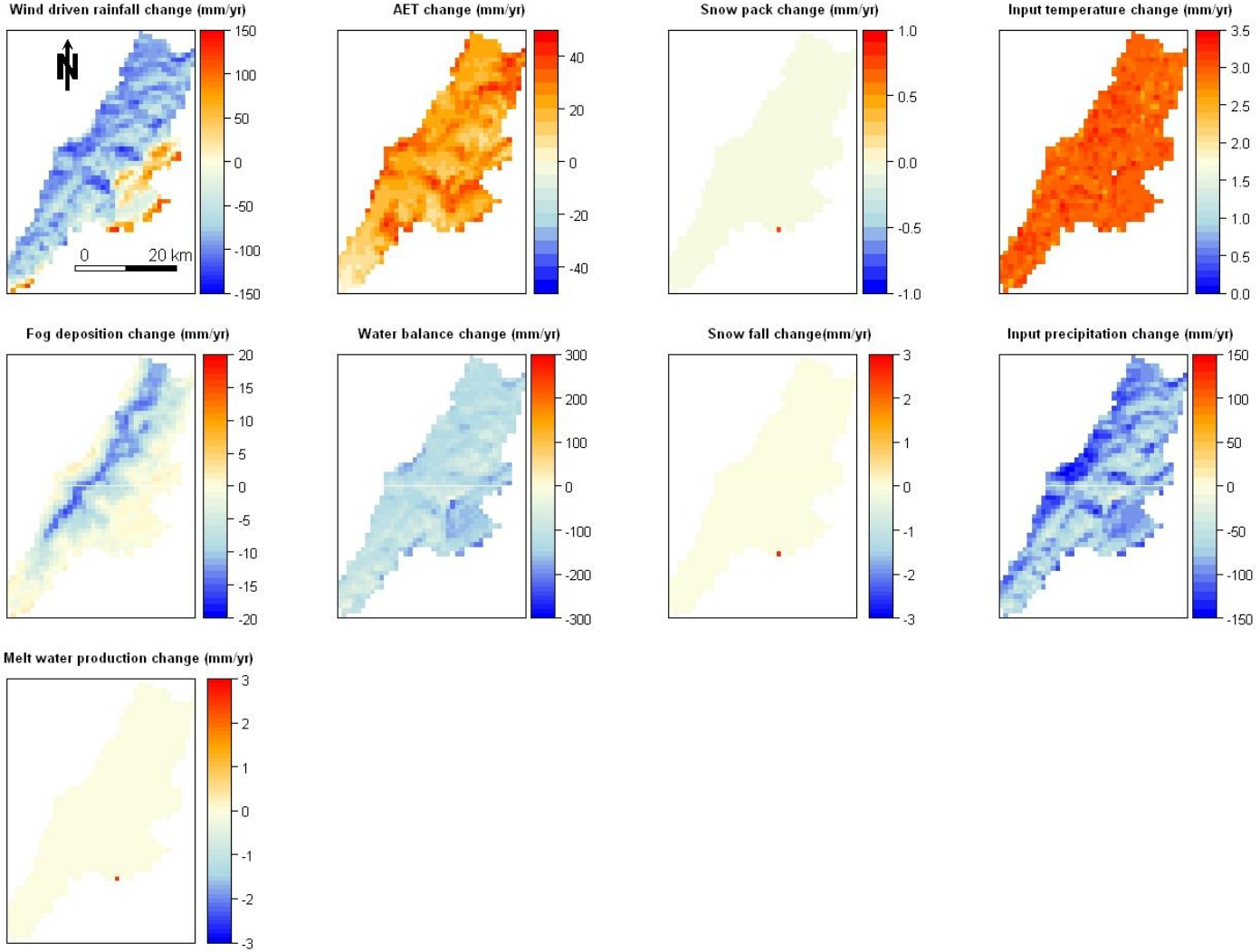

Figure 5.16 Annual modelled changes in wind driven rainfall, AET, water balance and fog inputs (mm) between WorldClim baseline climatology and mean of 5 GCM for A1B scenario for 2050s for Tranco de Beas dam catchment, Spain

Seasonal results

Figure 5.17 shows the spatial distribution of the changes in water balance on a monthly basis. Overall the catchment is drying for every month with considerable spatial variation in the winter months of December, January and February which is due to variability in changes in precipitation input for those months. Precipitation change in these winter months makes up for around 70% of the change in water balance. However, in the summer months of July and August when water balance changes are minimal as a result of very low precipitation input the contribution of AET change to the change in water balance exceeds 50%.

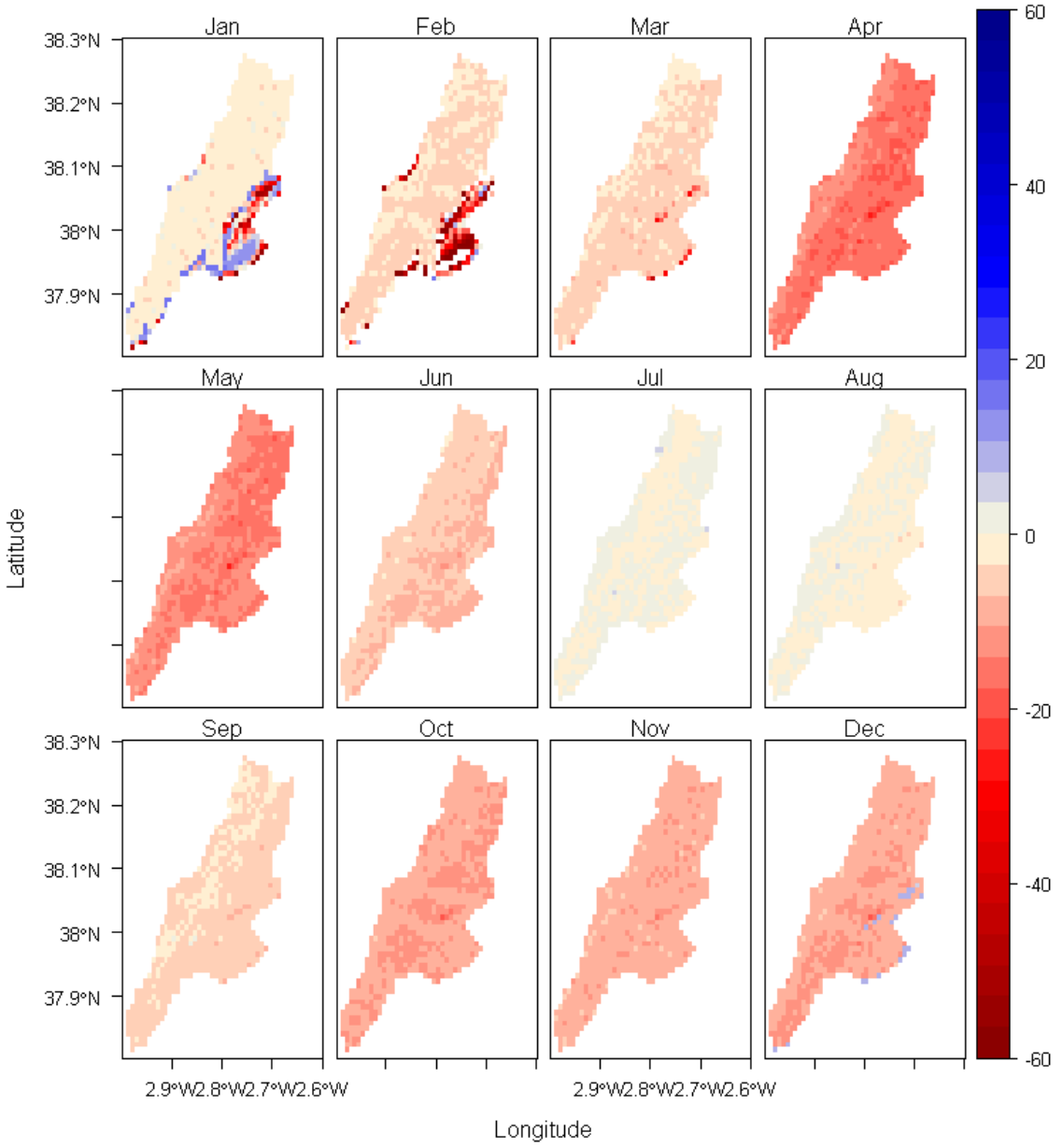

Figure 5.17 Monthly modelled changes in water balance for Tranco de Beas dam catchment in Guadalquivir river basin, Spain (mm) between A1B scenario using 5 GCM and WorldClim baseline climatology

Changes in inflow into the dam reservoir

Figure 5.18 shows the monthly baseline flow into the Tranco de Beas dam reservoir (a) and the projected changes in inflow under the climate change scenario (b). Simulated total annual baseline flow into the dam reservoir is 256 million m^3. The total storage volume of the Tranco de Beas reservoir is 500 million m^3 (ICOLD, 2003), therefore the reservoir storage relative to the baseline mean annual inflow is around 50%. However,

since the inflow is extremely low in the summer months of June to August (7.4 million m^3), reservoir storage has to be increased in the winter months to maintain operation throughout the summer. Under the A1B scenario simulation, inflow into the dam reservoir is projected to decrease by 42 million m^3 which equals a relative mean change in flow of nearly -17% or 8.4% of reservoir storage. There is a decrease of flow in every month but the most significant change in relative terms (up to -30%) is in the months of April to June with an absolute change for the month of April of 8.7 million m^3. The coefficient of variation, defined as the standard deviation divided by the mean of the monthly flow values increases slightly from 0.60 to 0.64 meaning the month-to-month flow becomes a little more variable throughout the year.

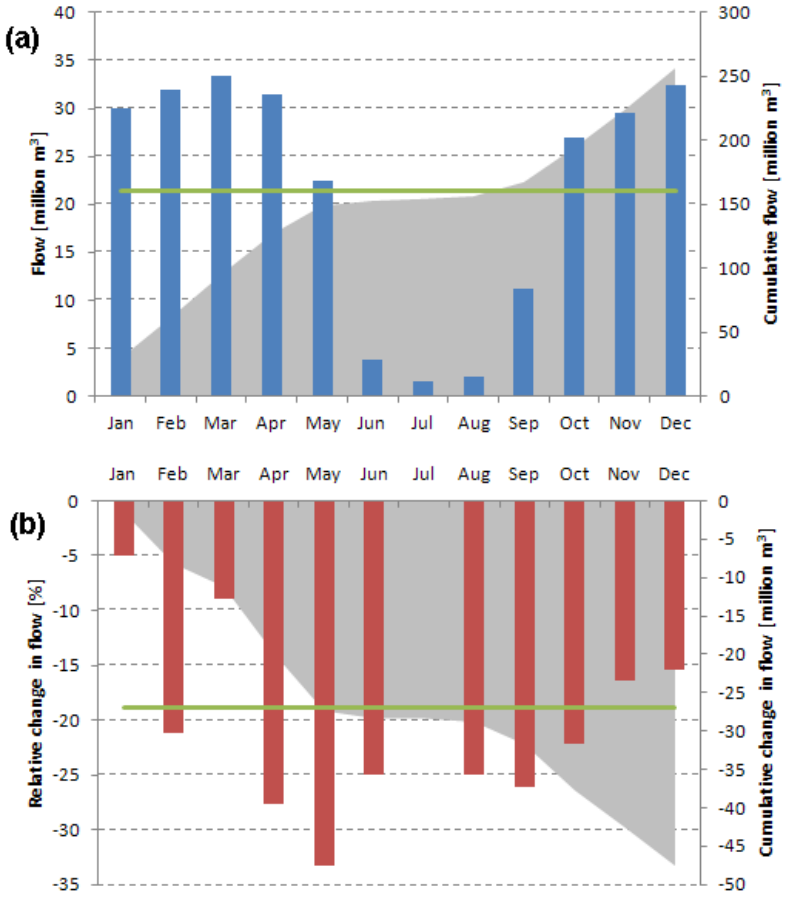

Figure 5.18 (a) Simulated monthly baseline and cumulative baseline flow into Tranco de Beas dam reservoir with mean flow (green line) of 21.4 Mm^3. (b) relative monthly and cumulative absolute change under the A1B scenario. The green line denotes the mean change over the year at -16.9%. Grey area represents the cumulative change.

Change in sediment delivery to the dam reservoir

Baseline simulated soil deposition within the Tranco de Beas dam catchment deriving from hillslopes and channels totals 536 tons/km^2/yr. Total simulated sediment delivery to the dam reservoir totals 90609 tons/yr for the baseline which is 0.02% of the reservoir storage capacity per year. These values are in line with reported figures for observed sedimentation at the Tranco de Beas reservoir by Cobo (2008) who estimated the total amount of sediment in the reservoir by comparing the inital volume of the reservoir with an estimation of the current volume using bathymetry and photogrammetry. This yielded a total sediment volume in the reservoir of 3.38 million m^3 accumulated over 45 years or 75088 tons/yr or a loss of storage of 0.02% per year. Under the 5 GCM A1B scenario, total soil deposition from hillslopes and channels is projected to increase by 21 tons/km^2/yr (4%) leading to a total increase in sediment delivery to the Tranco de Beas dam reservoir of 1845 tons/yr or 1.1%.

5.3.2.2. J. Strom Thurmond dam, Savannah basin, USA

Figure 5.19 shows the elevation and vegetative cover for the J. Strom Thurmond dam in the Savannah basin, USA. Elevation ranges from more than 1400 m.a.s.l. in the north-eastern located Appalachian mountains to 56 m.a.s.l. at the dam site. Vegetation in the catchment is dominated by tree cover with very high tree cover in the mountains. Overall, 50% of the catchment is covered with trees and 48% with herbaceous cover.

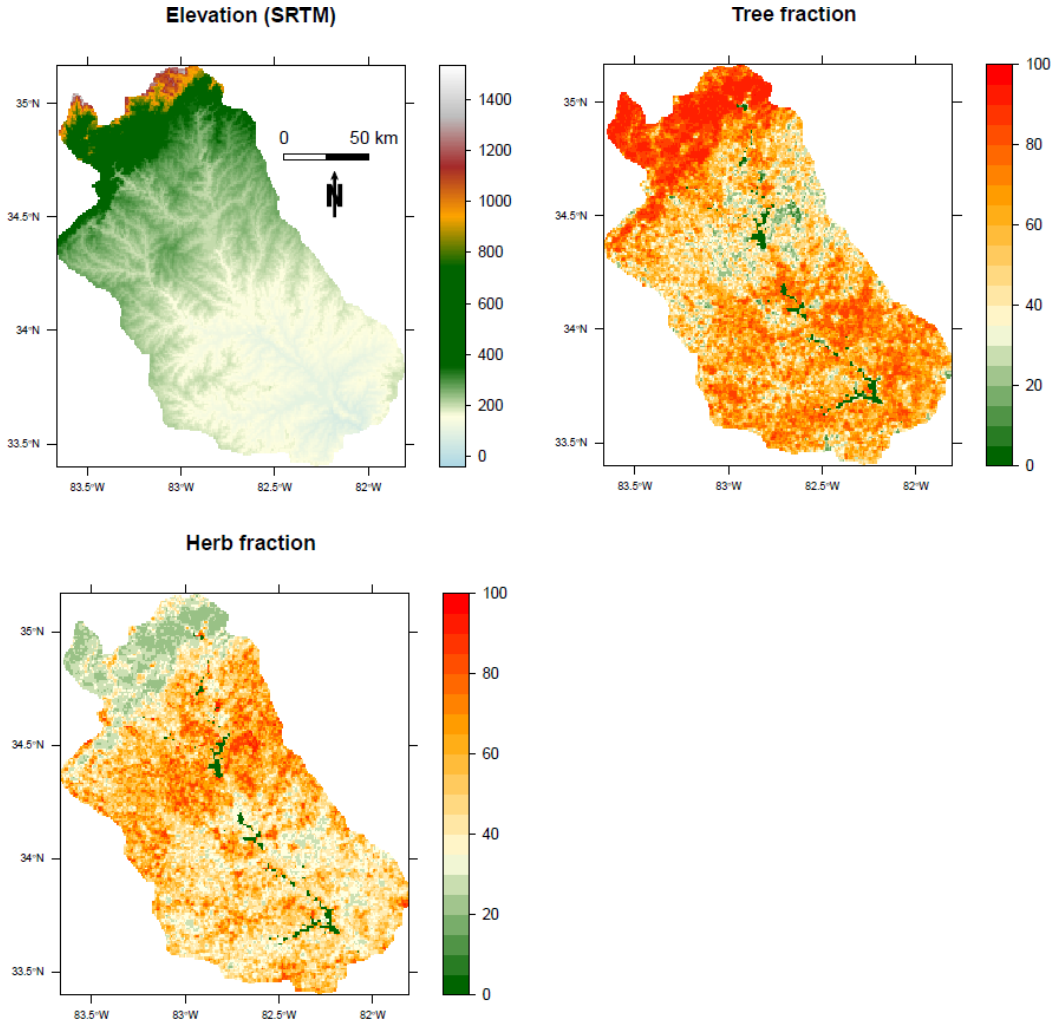

Figure 5.19 Catchment elevation based on SRTM and herb and tree fractions based on MODIS VCF for the J. Strom Thurman dam catchment, United States

Baseline results

The annual baseline model results for the J. Strom Thurmond dam catchment show an overall wind driven precipitation input into the catchment of 1310 mm/yr with noticeably higher values towards the north-east of the catchment in the Apalachian mountains. Vegetation in the catchment is also clearly defined by the mountains with mostly trees found at higher elevations and herbaceous cover at lower elevations (see figure 5.19) with a consequent influence upon actual evapo-transpiration and fog inputs. AET on average for the catchment amounts to 731 mm/yr and fog inputs are minimal with 11 mm/yr (0.8% of precipitation) on average. The resulting water balance is mostly dominated by precipitation inputs with very high values in the mountains

where inputs are high and AET is low. Mean annual snow pack is considerable in the mountains with values of up to 200 mm but since there is no snow at the lower elevations, the mean for the catchment is only 6 mm. Similarly, snow fall occurs only in the mountains with a catchment wide average of 4.5 mm/yr. Therefore snow melt contribution to the catchment wide water balance is small with less than 3 mm/yr. The resulting water balance amounts to 621 mm/yr for the catchment but with significantly higher values in the mountains (up to 2500 mm).

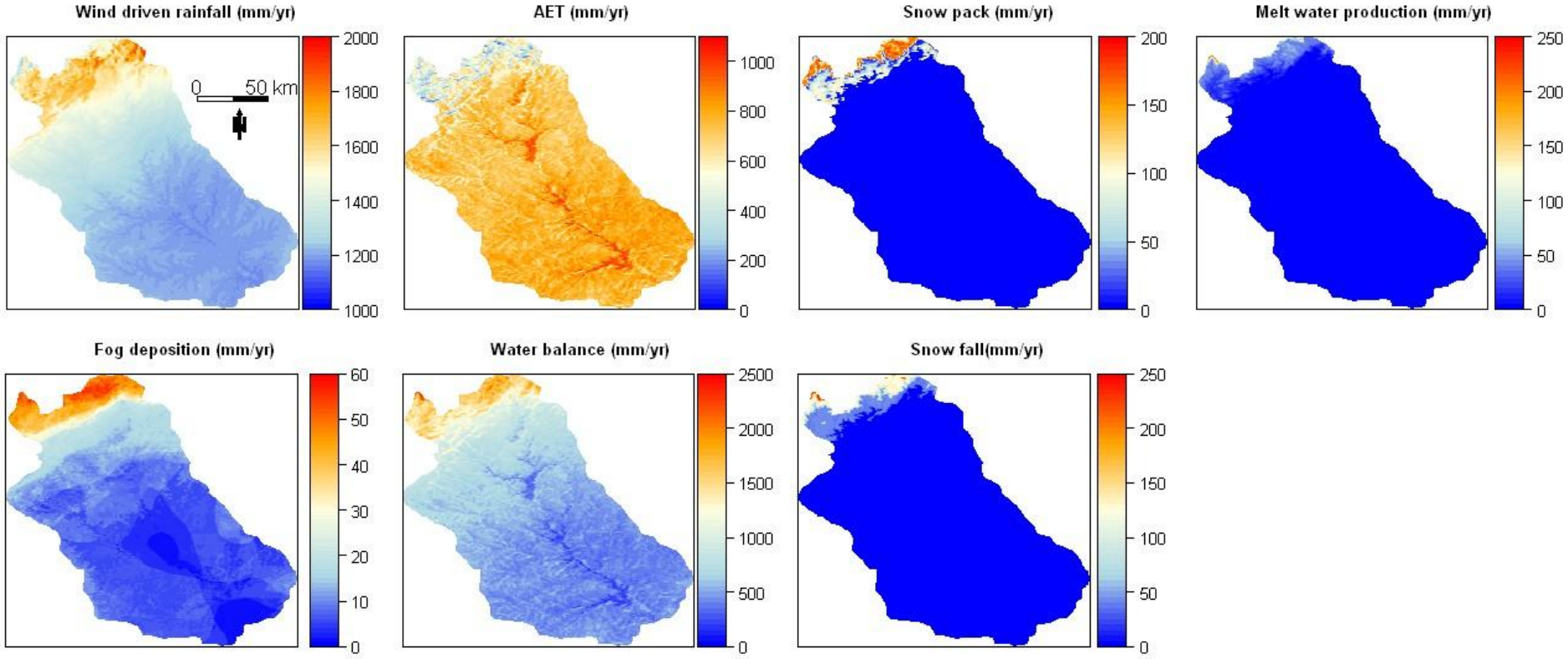

Figure 5.20 Annual baseline model results for wind driven rainfall, AET, water balance and fog inputs for J. Strom Thurmond dam catchment, United States

Scenario results

The scenario results for the J. Strom Thurmond dam catchment show a strong divide between a very strong increase in precipitation in the mountains of up to 650 mm/yr and a more modest increase at lower altitudes of around 40 mm/yr. This difference can be explained by differences between original low resolution high precipitation GCM values for the mountains and low precipitation GCM values in the lowlands and the downscaling approach taken. The delta method simply adds the mean change factor between GCM values for the future and a baseline to observed baseline climate (Fowler *et al.,* 2007), which means that there can be strong spatial differences as observed in figure 5.21.

AET changes are spatially variable with the greatest increase found in the river valley where land cover is bare (see figure 5.21) and some decrease in the mountains. On average though there is an increase over the catchment of 65 mm/yr. Changes in fog input are minor although the greatest changes take place in areas with very little fog input under the baseline conditions. Snow pack, snow fall and melt water changes show a localised increase in the mountains as a result of increased precipitation in areas that remain below 0°C under climate change, although melt water changes for a catchment as a whole are minor with 0.08 mm/yr. The resulting change in the water balance averages -36 mm/yr with the greatest changes (both positive and negative) taking place in the mountains and less spatial variation in the lowlands.

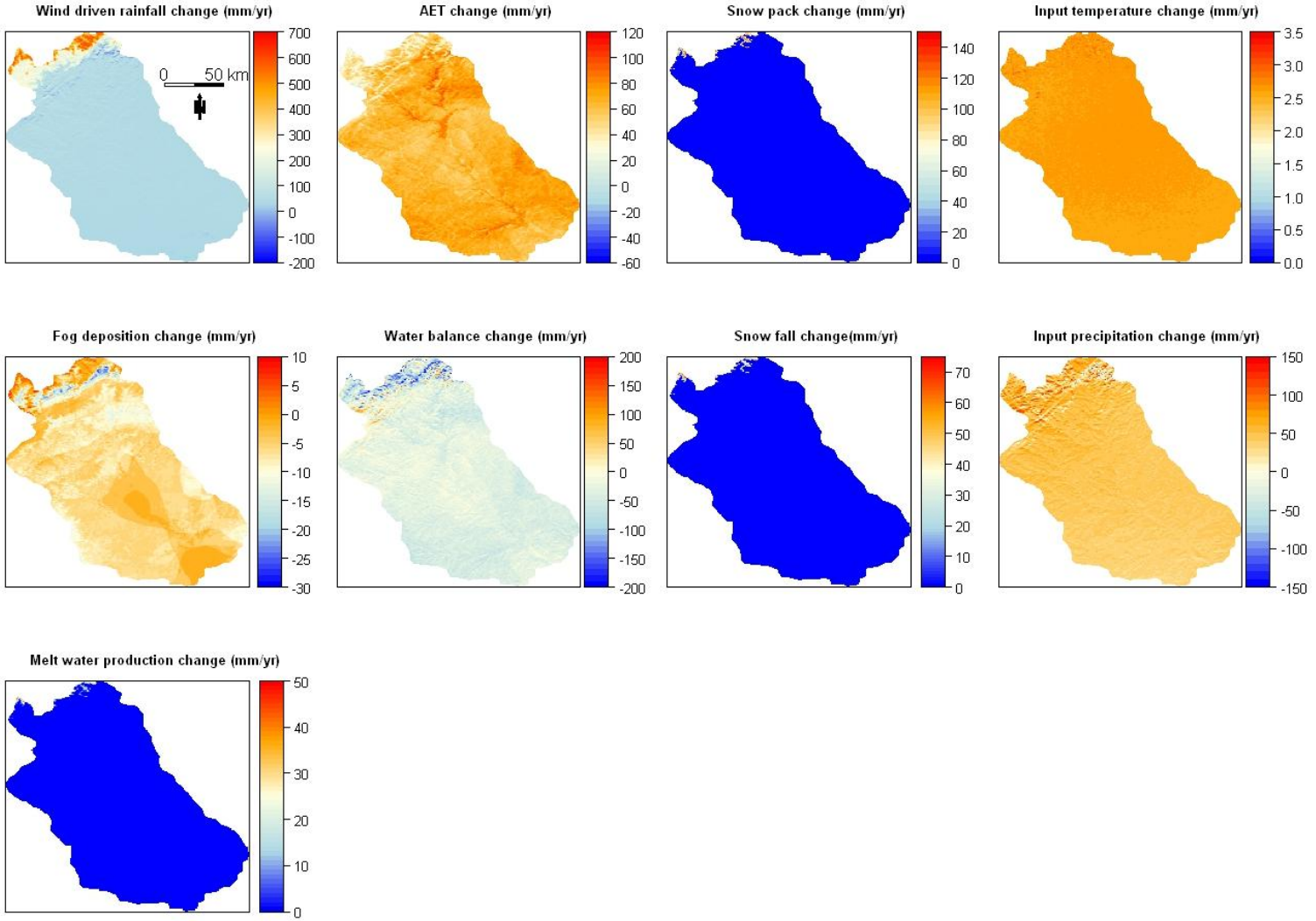

Figure 5.21 Annual modelled changes in wind driven rainfall, AET, water balance and fog inputs (mm) between WorldClim baseline climatology and mean of 5 GCM for A1B scenario for 2050s for J. Strom Thurmond dam catchment, USA

Seasonal results

Figure 5.22 shows the monthly progression of the water balance in the dam catchment. As clear from figure 5.21 the catchment overall yields less water under the A1B scenario. However, there are areas in the catchment that will on average over the year show a positive water balance. There is a strong spatial variation in the changes with some areas within the catchment at or near drying whilst other regions are wetting. Most notable changes are the strong increase and decrease in water balance for the Apalachian mountains for January and February. The strong decrease in water balance for the month of May is the result of a much higher increase of ET compared to other months and minimal change in precipitation. This increase in AET (80% of water balance change) can be explained by the increase in projected temperature for May (see figure 5.9) while precipitation change is minimal (< 1% of water balance). Overall, changes in the water balance are predominantly due to changes in AET. Only in the winter months of November to March changes in wind driven precipitation have a greater impact on the water balance.

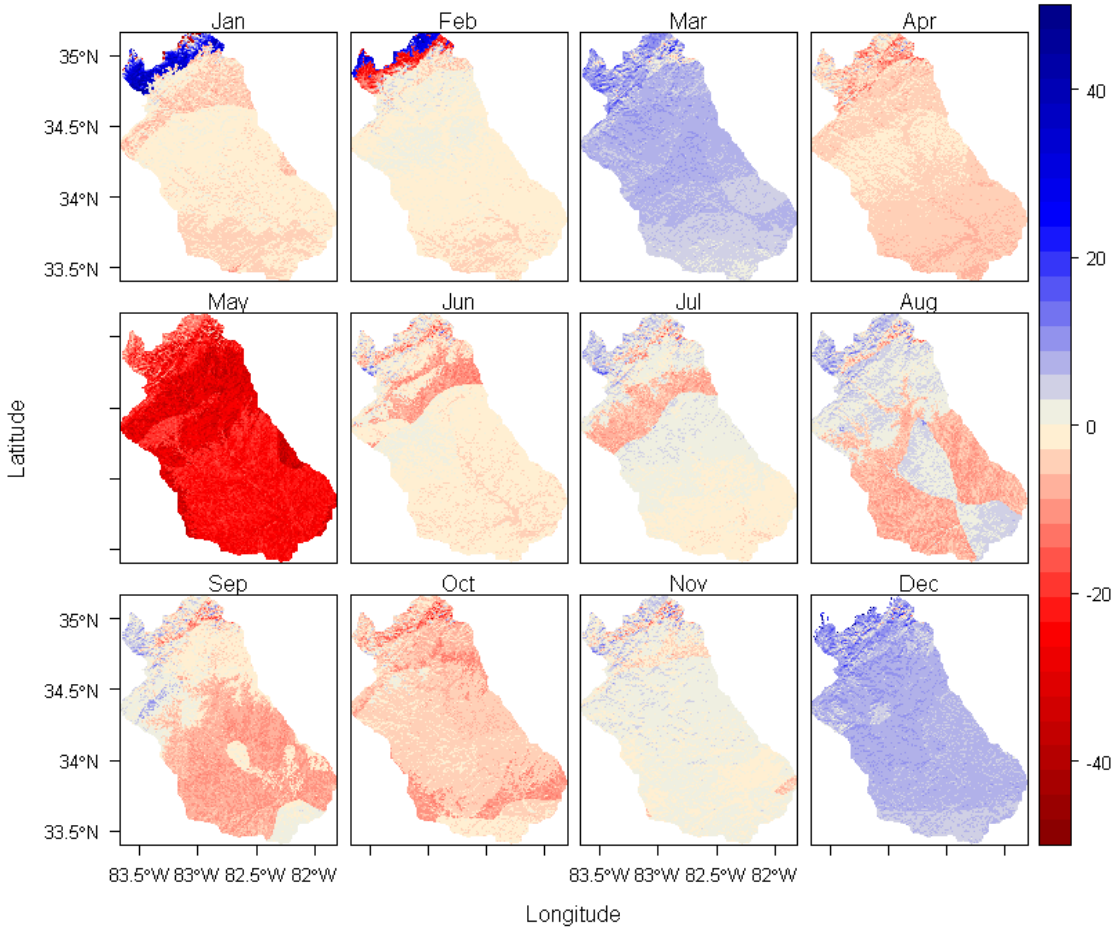

Figure 5.22 Monthly modelled changes in water balance for J. Strom Thurmond dam catchment in Savannah basin, USA (mm) between A1B scenario using 5 GCM and WorldClim baseline climatology

Change in inflow into the dam reservoir

Figure 5.23a shows the simulated monthly baseline inflow for the J. Strom Thurman dam reservoir. Annual simulated flow amounts to 7023 million m^3. The reservoir has a maximum storage capacity of 4712 million m^3 and a normal storage of 3096 million m^3 (NID, 2007). Therefore, the reservoir is capable of storing around 70% of the total annual inflow with inflow exceeding maximum storage from November to March. The annual relative change under the A1B scenario for the 2050s is projected to be negative with a catchment wide decrease in runoff of -1.8% and a cumulative annual change in inflow to the reservoir of -17.2 million m^3 (< 1% of total storage). The monthly changes are variable with a particularly strong difference between the months of March and April, June and July and again from November to December which follows the pattern of rainfall input change as can be seen from figure 5.21.

Coefficient of variation for the monthly flow increases from 0.4 to 0.5 meaning the month-to-month flow becomes more variable.

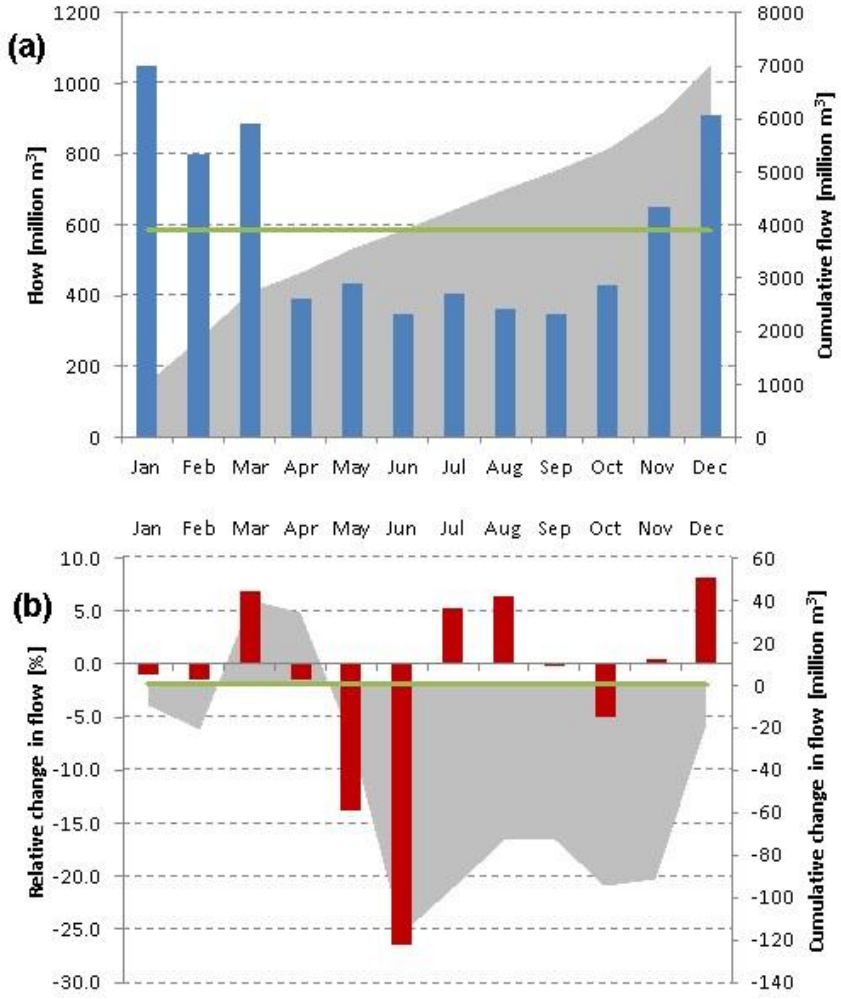

Figure 5.23 (a) Simulated monthly baseline and cumulative baseline flow into J. Strom Thurman dam reservoir with mean flow (green line) of 585 Mm^3. (b) relative monthly and cumulative absolute change under the A1B scenario. The green line denotes the mean change over the year at -1.8%. Grey area represents the cumulative change.

Change in sediment delivery to the dam reservoir

Baseline simulated sediment delivery to the dam reservoir amounts to 0.5 million tons/yr (0.013 % of the reservoir capacity) or a specific sediment yield of 33 tons/km^2/yr. No published figures for dam sedimentation for the reservoir could be found but yield estimates for the Savannah river are in the range of 43 ± 5.5

tons/km^2/yr (McKarney-Castle *et al.,* 2010). Under the 5 GCM A1B scenario, sediment delivery to the dam reservoir is projected to increase by 10125 tons/yr which is a increase of +1.8%.

5.3.2.3. Phongolapoort dam, Maputo basin, Africa

Figure 5.24 shows the catchment characteristics of the Phongolapoort dam catchment. Elevation ranges from 2200 m.a.s.l. to the west of the catchment gradually declining to 125 m.a.s.l. at the dam site. Vegetation in the catchment consists mainly of herbaceous cover with patches of tree cover. On average, 21% of the catchment is covered by trees and 76% with herbaceous cover. Tree cover upstream in the catchment consists mostly of commercial forestry which is estimated to abstract around 200 million m^3 of water each year (Jaganyi *et al.,* 2008) while sugar cane is the main commercial agricultural crop in the catchment.

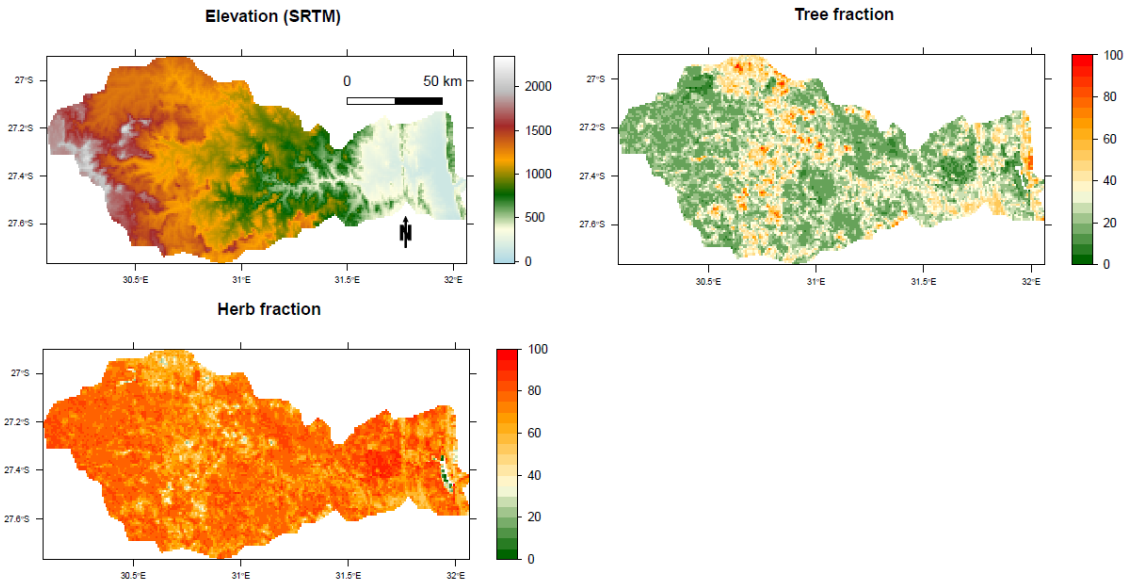

Figure 5.24 Catchment elevation based on SRTM and herb and tree fractions based on MODIS VCF for the Phongolopoort dam catchment, Maputo basin, Africa

Baseline results

Figure 5.25 shows the baseline model results for the Phongolapoort dam catchment in the Maputo basin. Wind-driven rainfall is highest towards the west of the catchment with altitudes between 1000 and 1500 m.a.s.l. and lowest near the dam site on the eastern border of the catchment. Average precipitation over the catchment amounts to 821 mm/yr. Actual evapo-transpiration is extremely spatially variable with values ranging from 112 to over a 1000 mm/yr but averaging 519 mm/yr. Fog inputs make up a considerable portion of the annual water balance with inputs up to 120 mm/yr for some areas and a catchment average of 42 mm/yr for the catchment. The resulting water balance is also highly spatially variable, mostly as a result of the spatial variability in rainfall and actual evapo-transpiration. The negative values towards the east of the catchment near the dam site are the result of local evapo-transpiration exceeding local rainfall and fog inputs and would thus have to be sustained by surface and sub-surface flows from upstream or from irrigation. The annual baseline water balance averages 344 mm/yr for the catchment.

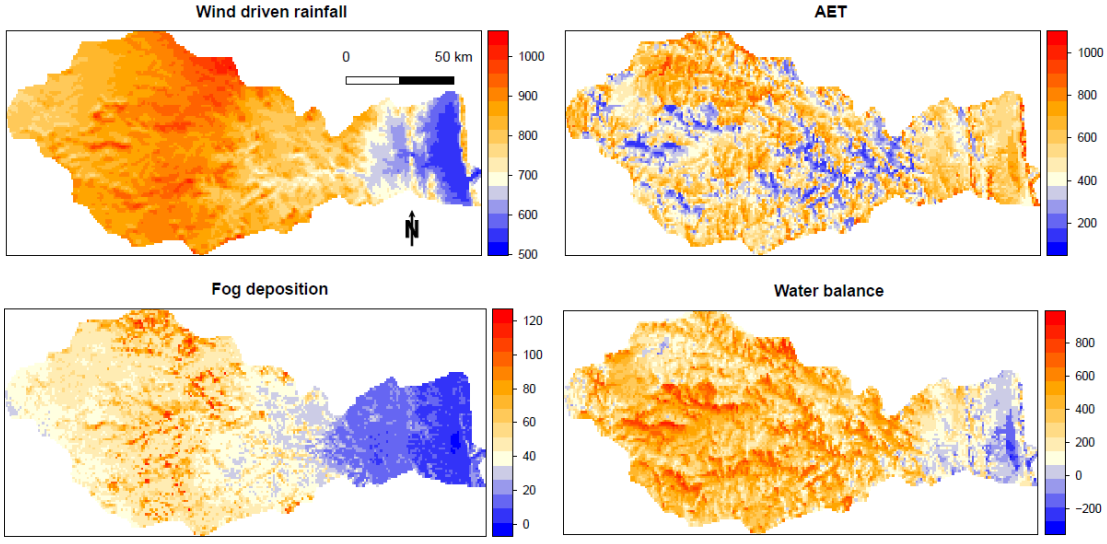

Figure 5.25 Annual baseline model results for wind driven rainfall, AET, water balance and fog inputs (mm) for Phongolapoort dam catchment, Maputo basin, Africa

Scenario results

Figure 5.26 shows the scenario results for the Phongolapoort dam catchment for the 5 GCM A1B scenario for the 2050s as difference from the WorldClim baseline and the changes in temperature and precipitation input into the model.

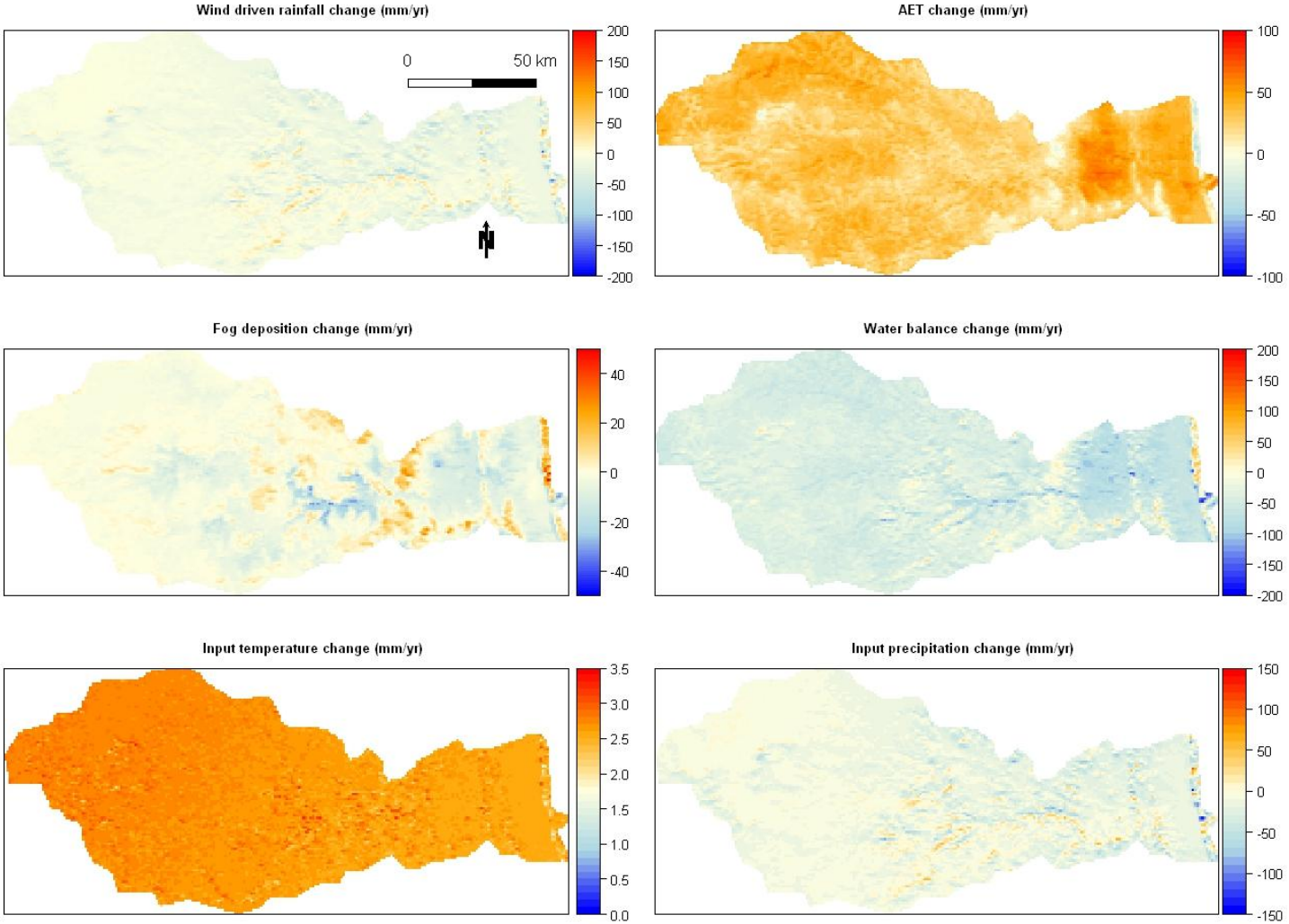

Figure 5.26 Annual modelled changes in wind driven rainfall, AET, water balance and fog inputs (mm) between WorldClim baseline climatology and mean of 5 GCM for A1B scenario for 2050s for Phongolapoort dam catchment, Africa

Changes in wind driven rainfall are spatially variable with values ranging from -215 mm/yr to 250 mm/yr. Overall there is a decrease in wind driven precipitation of 12 mm/yr over the catchment. AET changes are also spatially variable with an overall increase of 31 mm/yr. Changes in fog inputs are quite large for some cells because of a change in temperature-driven lifting condensation level but overall only amount to a decrease of 2 mm/yr over the catchment. As a result of the spatial variability in the above described changes, the resulting water balance shows a similar pattern with changes between -660 mm/yr to 530 mm/yr. However, the catchment average amounts to a decrease in water balance of no more than 42 mm/yr.

Seasonal results

Figure 5.27 shows the monthly progression of the water balance in the Phongolapoort dam catchment with wetting in the months November to January and drying from August to October. There are no strong differences between areas so wetting and drying appears to be reasonably uniform over the catchment compared with the other dam catchments examined. Changes in the water balance are mostly governed by changes in precipitation with the exception of the months March, April, June and November when changes in AET are greater than changes in wind driven precipitation. Overall though, changes in AET are of similar magnitude as changes in wind driven precipitation meaning both temperature and precipitation change have an equal impact on the water balance for this scenario.

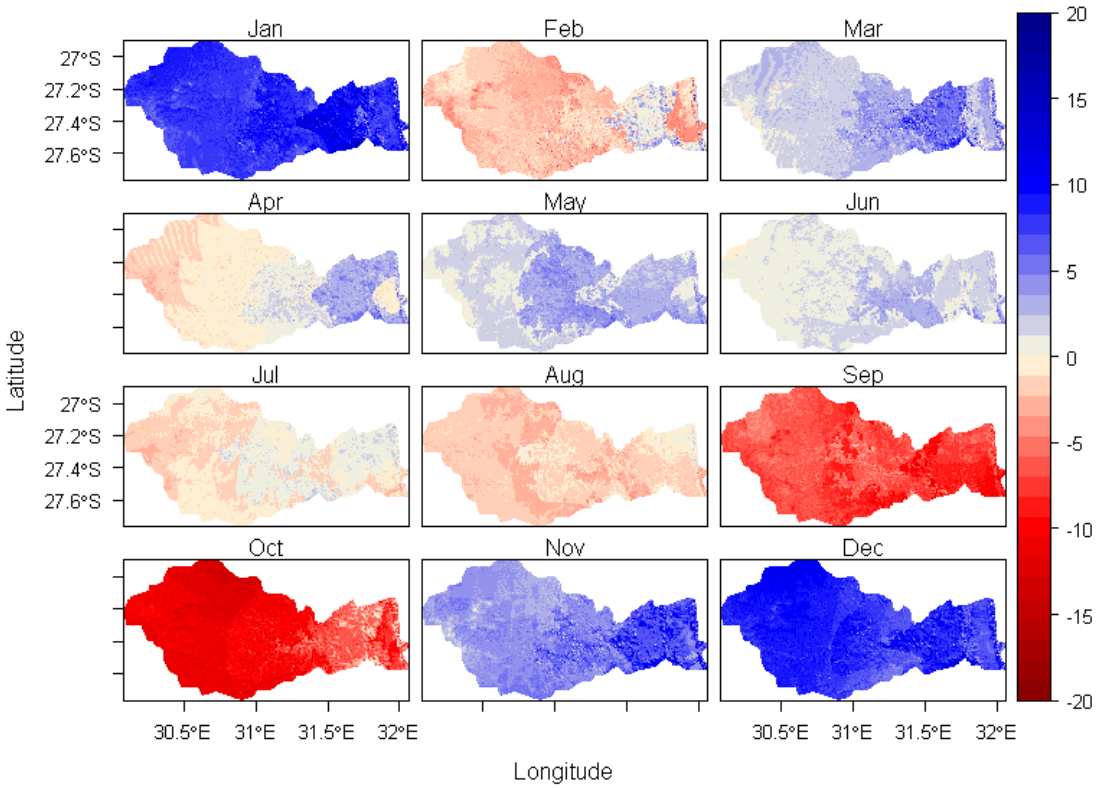

Figure 5.27 Monthly modelled changes in water balance for for Phongolapoort dam catchment in Maputo basin, South Africa (mm) between A1B scenario using 5 GCM and WorldClim baseline climatology

Change in inflow into the dam reservoir

Figure 5.28 shows the monthly simulated baseline flow into the Phongolapoort dam reservoir (a) and the projected changes in inflow under the climate change scenario (b). Simulated total annual baseline flow into the dam reservoir is 4694 million m^3. The total storage volume of the Phongolapoort dam reservoir is 2267 million m^3 (Skoy Plancenter, 2009), therefore the reservoir is capable of storing around 50% of annual flow. Monthly flow does not exceed maximum reservoir storage for any month. The relative annual simulated change under the A1B scenario is -10.5% with some monthly variation such as positive changes in the months of January, March, May and December and strong negative changes in the months of July, August and September. Annually, there is a negative change in the volume of water flowing into the dam reservoir with a decrease of nearly 200 million m^3 (9% of storage). The coefficient of

variation increases from 0.7 for the baseline to 0.8 under the A1B scenario indicating there is an increase in the month-to-month variability in the flow.

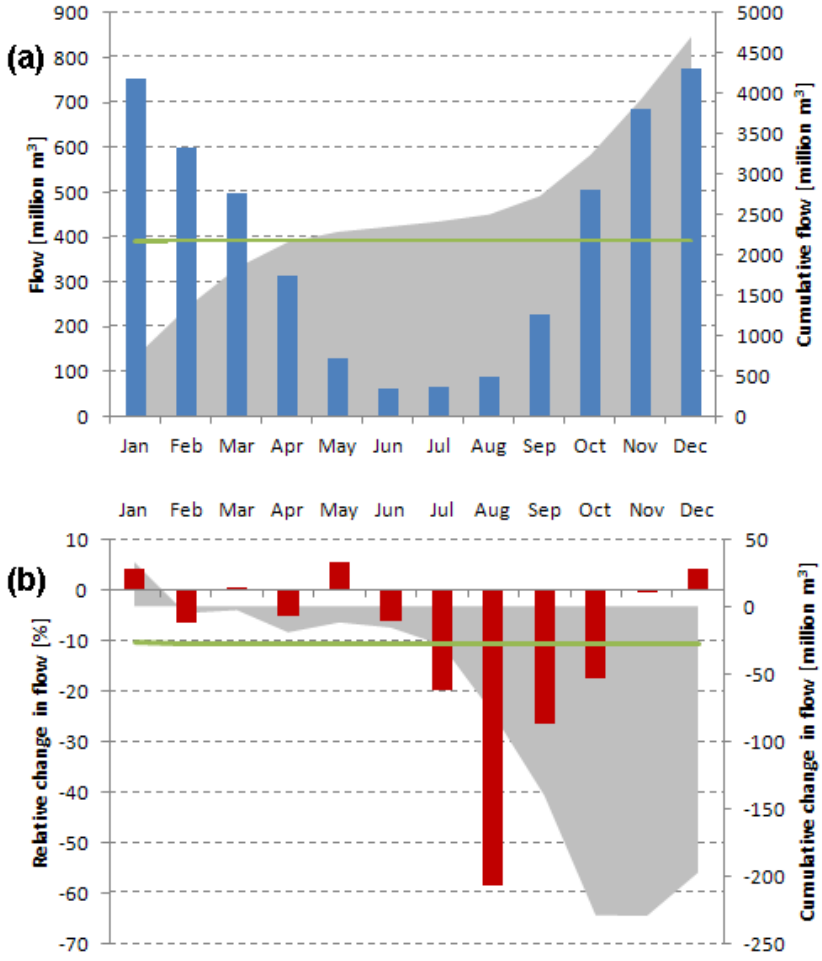

Figure 5.28 (a) Simulated monthly baseline and cumulative baseline flow into Phongolopoort dam reservoir with mean flow (green line) of 391 Mm^3. (b) relative monthly and cumulative absolute change under the A1B scenario. The green line denotes the mean change over the year at -10.5%. Grey area represents the cumulative change.

Change in sedimentation delivery to the dam reservoir

Baseline simulated sediment delivery to the dam reservoir amounts to 1.8 million tons/yr for the baseline which is a specific sediment yield of 298 tons/km^2/yr. With a total storage capacity in the reservoir of 2267 million m^3, this amounts to 0.08% of storage. Recorded sediment yields for the Phongolapoort dam between 1973 and 1984 (Skoy Plancenter, 2009) are higher with 446 tons/km2/yr or 3.4 million tons a

year, which is a yearly rate of 0.12% of storage capacity. Under the 5 GCM A1B scenario, sediment delivery to the dam is projected to increase by 0.25 million tons/yr to 2 million tons/yr, a change of +14%.

5.4. Discussion and conclusions

5.4.1. The AguaAndes/WaterWorld model

The key considerations for using the AguaAndes/WaterWorld model have been described in chapter 2. In the context of this chapter, it is very important that the model used can be applied in different climatic regions with no additional data requirements so the analysis can be extended to model other dam catchments contained in the global dam database in a consistent approach. Furthermore, the model should allow for easy implementation of land use and climate change scenarios with a focus on giving an indication of the direction and magnitude of a change in water balance as a result of a climate change scenario compared to a baseline simulation rather than being highly calibrated and used to predict water balance and runoff *per se*. The focus on examining differences between a baseline and scenario rather than absolute magnitudes means the model is less sensitive to error in the magnitude of input data but probably more sensitive to error in the representation of physical processes underlying the model (Mulligan and Burke, 2005; Mulligan, 2012d). Since the model is used for scenario analysis, it is important that the (known) physical basis of the model remains intact and thus the model is not calibrated as that would involve changing parameter values based on baseline data that might not be appropriate for future conditions for which calibration data is not available. However, this does require the model to perform well under baseline conditions in order to be able to interpret the output under scenario conditions with confidence.

5.4.2. Validation

The validation exercise carried out revealed that the model performs quite well for the Guadalquivir river with a slight overestimation of annual flow of 25 mm (5.8%). This

overestimation is attributed to an underestimation of PET and hence AET by the model. Compared to a Penman-Monteith estimation based on observed station data, PET estimations by AguaAndes/WaterWorld are some 36% lower for this basin. Since the model factors in cloud cover impacts on radiation, this difference could be attributed to the cloud cover data or to differences in estimation methods. However, Mulligan and Burke (2005, p104) have described underestimation of PET in an earlier validation study in Costa Rica for dry, cloud free lowlands.

Annual stream flow is also overestimated for the Savannah river with 78 mm (18%). Validation of precipitation input for the Savannah basin revealed that precipitation input for the observed stream flow period was 9% less than the wind driven precipitation used for the modelled stream flow and can thus explain some of this overestimation since precipitation is the largest flux in the water balance model. Also for this basin, simulated PET yielded lower values (-42%) than estimates based on observed data which could account for some of the difference. Another source of error could derive from the observed data. Even though the observed stream flow record used in the validation is classed as good (USGS, 2004), measurement errors are possible with the type of recorder used (Sauer and Turnipseed, 2010) as well as errors in conversion of runoff volumes to runoff depths which requires accurate drainage areas.

Simulated stream flow for the Usuthu river in the Maputo basin is also overestimated with nearly double that of the annual observed flow (154 mm, 96%). Again, for this basin, simulated PET was found to be lower than estimates based on observed data which can partly explain the discrepancy. In this basin though, observed evapo-transpiration could be higher than model estimates because of high wind speeds in the area (Jaganyi *et al.,* 2008). The most likely reason for the overestimation though is the overestimation of precipitation input for a large part (~25%) of this sub-basin. WorldClim interpolated data for the top of the basin is based on a very limited number of stations and comparison of the interpolated field with observed station data yielded

an overestimation of more than 12%. Furthermore, the quality of the observed flow data is rated as average and issues with this data have been reported (Skoy Plancenter, 2009) which could explain some of the differences and finally, inaccurate location information of the stream flow gauge can be the cause of a difference in contributing catchment area which is used for conversion of runoff volumes to runoff depths. For this sub-basin, the SRTM DEM derived catchment area for the Usuthu river up until the flow gauge in the Maputo basin yields 15,506 km^2 whereas the catchment area for the observed stream flow according to the runoff data (Skoy plancenter, 2009) amounts to some 5 % higher at 16,249 km^2.

The simulation results in the Maputo basin highlight possible errors with (a) the model used, (b) the input data used by the model or (c) both. Given the good validation results in this chapter for the Guadalquivir and Savannah basins as well as in other regions around the world (Mulligan and Burke, 2005; Saenz and Mulligan, 2007) it is possible that the model does not perform well in this type of environment or that there are serious deficiencies in the input and/or validation data. Since the AguaAndes/WaterWorld model is un-calibrated and uses global remotely sensed datasets, it is not expected to closely replicate observed runoff measured at a gauge. However, based on the above considerations, the model is considered robust enough to be suitable for the purpose of comparative climate change scenario analysis between basins. Furthermore, using a un-calibrated model in a comparative between-basin analysis as carried out in this chapter highlights the danger of using calibrated models with data for individual catchments as models may be fitted but they would not be as robust. Using globally consistent data sets with a globally applicable model such as WaterWorld therefore provides the opportunity to validate input datasets such as the Worldclim climatology which could be the scope of future work.
Furthermore, the ease of use as a web based tool with all data included and the global extent of the data make it easy to carry out this analysis for other dams within the $GOOD^2$ database as well as implement other scenarios of climate and/or land use changes.

5.4.3. Climate change scenario

The interpretation of the climate scenario in the model is limited to changes in mean monthly temperature and mean monthly precipitation since these data are routinely available from the GCMs. However, under different temperature conditions there will also be changes in relative humidity as this is dependent on air temperature which in turn will impact ET. Cloudiness, wind speed, direction and solar radiation are also likely to change. Furthermore, changes in climatic conditions will have an impact on vegetation such as shifts in growing seasons and type of vegetation which also have an impact on ET. These effects are not accounted for in the model but could have a significant impact on the resulting water balance under climate change. The following chapter will explore some of the model sensitivities to changes in relative humidity and vegetation in order to better understand the associated uncertainties.

5.4.4. Climate change impacts on dams

Simulated annual changes in the water balance of the Tranco de Beas dam catchment are dominated by a change in precipitation with a decrease on average of 78 mm with less change in evapo-transpiration (+22 mm). Changes in the annual water balance of the J. Strom Thurmond dam catchment and the Phongolapoort dam catchment are dominated by changes in evapo-transpiration with increases of 65 mm and 31 mm AET respectively. Annual wind driven precipitation for the J. Strom Thurmond dam catchment is projected to also increase by 61 mm and decrease overall for the Phongolapoort dam catchment by 12 mm. Simulated changes in annual fog inputs for all three catchments are modest with a decrease of between 2 and 6 mm. The Tranco de Beas catchment shows only a minor increase in ET despite having the greatest projected increase in temperature. This is due to the lack of vegetation in this catchment and the model assumption that AET is close to zero on completely un-vegetated ground. Overall, the Phongolapoort dam catchment has the smallest changes in precipitation input and change in ET, however since precipitation is projected to decrease and ET to increase, the catchment is projected to dry. The J. Strom Thurmond dam catchment on the other hand, sees quite a large increase in

precipitation combined with a increase in ET of equal or greater magnitude, the overall annual catchment wide change is a decrease in water balance of 36 mm. The Tranco de Beas dam catchment is most affected by the climate change due to an increase in ET combined with a decrease in precipitation, the overall catchment water balance decreases significantly with 120 mm/yr. Melt water contributions only play a role in the J. Strom Thurmond and Tranco de Beas dam catchments where some snow fall occurs at the highest elevations. However, baseline contributions are small for both catchments (3 and 3.5 mm/yr respectively) and changes in this contribution are less than 1 mm/yr for both catchments.

Changes in inflow into dam reservoirs

The impacts of climate change on the water balance of the dam catchments results in a strong mean simulated decrease in flow into the Tranco de Beas dam reservoir of nearly 17% with flow decreasing every month which is expected since precipitation input decreases for every month as well (see figure 5.10). There is very limited relative change in flow for the month of July since this is the driest month with very little baseline flow. The J. Strom Thurmond dam is simulated to receive slightly less water on an annual basis with a mean decrease in inflow of 1.8% with greatest decrease in the months of May and June as a result of relatively little change in precipitation for those months but strong increase in evapo-transpiration. The Phongolapoort dam is simulated to receive 10.5% less water on an annual basis, with greatest change between July and October which is following the changes in precipitation input for those months (see figure 5.10). All basins see an increase in month-to-month variability of flow though with the greatest change (10%) for the J. Strom Thurmond dam and the Phongolapoort dam. The latter dam however, already experiences highly seasonal flow under the baseline which is exacerbated by climate change.

The Tranco de Beas dam reservoir has a relatively large reservoir that is capable of storing double the simulated annual baseline flow. This means that this reservoir is less sensitive to changes in seasonal distribution of flow as it is capable of storing more

water. However, annual changes in flow as projected by this scenario will ultimately mean there will be a shortage of water to maintain dam operation. While climate change projections, particularly for precipitation are highly uncertain as described in section 4.2.2, all models agree on the direction of change for the area where the Tranco de Beas dam is located. Projected significant decreases in precipitation and increases in temperature for this area have also been found by Giorgi and Lionello, (2008) using 17 models for three SRES emission scenarios (A1B, A2 and B1) for the 2050s and 2100s and Gao *et al.,* (2006) using regional climate models. Therefore, warmer and drier conditions for this dam catchment are very likely hence adaptation measures should be considered. Some possible adaptation measures for the Guadalquivir basin as a whole are described in chapter 6.

The J. Strom Thurmond dam reservoir has relatively less storage capacity than the Tranco de Beas dam with a capacity of around 70% of simulated annual inflow. Projected changes in inflow for this catchment however are less than 1% of total storage meaning that the dam is more sensitive to changes in inflow but the magnitude of changes might also be less. However, uncertainty in the projections for this area is quite high with only three out of five GCM agreeing on the direction of change (see section 4.2.2) and a range between the models of 300-400 mm/yr for this scenario (see figure 4.1).

The Phongolapoort dam reservoir has a storage capacity of around 50% of simulated annual flow with monthly flow not exceeding a storage of 35%. The projected decrease in inflow for this reservoir amounts to 9% of the total storage volume. There is low between-model uncertainty in this area with all models agreeing on the direction of change and between-model range of precipitation projections is lower than 100 mm/yr.

Sedimentation

Simulated sedimentation rates are in the correct order of magnitude for all three basins with a slight underestimation for the J. Strom Thurmond and Phongolapoort dam reservoirs and an overestimation for the Tranco de Beas dam. Simulated changes as a result of climate change are highest for the Phongolapoort dam with 14% increase while increase in sedimentation at the J. Strom Thurmond and Tranco de Beas reservoirs is less than 2%. Total sedimentation rates for all three reservoirs remain reasonably low with less than 0.1% of reservoir storage capacity per year. It should be noted though that modelling soil erosion and sediment yield within catchments is challenging due to the usually high data requirements (in particular for soil, rainfall intensity and high resolution slope gradient) and difficulties with including all erosion and sediment transport processes (de Vente, 2009). The erosion and sediment transport model contained in WaterWorld is based on the Thornes (1990) erosion model which uses only four parameters and is therefore a good choice of model for larger spatial scales (Morgan and Nearing, 2011). However, to accurately model sedimentation rates within the catchment would require a more in-depth modelling exercise that would require specific catchment data on soil erodability, rainfall erosivity and processes other than wash (e.g. landslides) based on field observations and measurements. The modelled sediment yields in this chapter should therefore be interpreted with caution. Nevertheless, since the focus in this chapter is on understanding direction and relative magnitude of changes as a result of climate change, the model can be very useful in quickly determining these for a range of scenarios for different geographical areas and indicating the hotspots in the catchment that generate most of the change in erosion.

6. Case study basins sensitivity analysis using AguaAndes/WaterWorld

6.1. Introduction

This chapter aims to explore several features of the AguaAndes/WaterWorld modelling system to assess the sensitivity to climate change of key model outputs for the case study basins presented in chapter 5. Sensitivity of basins to climate change is assessed by applying simple climate change scenarios and examining the change in model outputs. Furthermore, to highlight how differences in geography between basins including factors such as terrain, vegetation and baseline climate affect the outcomes of the *same* climate change, an analysis is carried out whereby the same climate change (i.e. the same delta's between baseline and scenario climates) are applied to the different basins. This analysis helps in determining which characteristics of basins make them more or less sensitive to a given climate change and thus can be instrumental in better understanding the nature of climate change in basins and devising adaptation measures. Also, some model experiments have been carried out on changing land use to simulate the effects of hypothetical ecosystem-based adaptation interventions that can be taken in the river basins to mitigate the impacts of climate change.

6.2. Climate change sensitivity of basins

To assess how sensitive the basins are to a given climate change, a sensitivity analysis was carried out in which the WaterWorld model was run for a number of simple climate change scenarios. The output maps of calculated actual evapo-transpiration, wind driven precipitation, water balance and water balance seasonality were then sampled for 1000 randomly chosen points in the basins. These 1000 points were then plotted in order to create scatter graphs of changes in AET and wind driven precipitation and the impacts on the water balance and the seasonality of the water balance (see figures 6.1 to 6.6 and Appendix VI). Furthermore, relative and absolute

changes from the baseline were calculated as the mean of points and presented along with the standard deviation as a measure of uncertainty. Seasonality of water balance was calculated using a modified Walsh and Lawler (1981) seasonality index calculated by WaterWorld, which is defined as the sum of the absolute mean deviation of mean monthly water balance from the overall monthly mean divided by mean annual water balance. This results in an index ranging from 0 to 1 where values of 1 are extremely seasonal and low to zero values mean that there is hardly any seasonality or all months are equal. Tedesco *et al.,* (2008) found that this method does not produce different results compared to other measures of seasonality such as the Markham technique (Markham, 1970) when applied in Africa. Hence, since the Walsh and Lawler method is calculated by Water World this method for assessment of seasonality was used. The simple scenarios used in this analysis were a uniform change from the baseline in precipitation over the basins of +10% and -10% and a change in temperature of +2°C and -2°C, distributed evenly across all seasons. Baseline temperature and precipitation were based on the WorldClim (Hijmans *et al.,* 2005) baseline as described in chapter 5. This analysis was carried out for all three case study basins, representing three different geographical regions with very different characteristics.

6.2.1. Results

Table 6.1 to 6.3 show the results for this analysis as the mean absolute and relative change for 1000 random points in each basin. Scatter plots for run 1 (precipitation -10%) and run 2 (temperature + 2°C) are shown in figures 6.1 to 6.6 while scatter plots for the remaining runs are shown in Appendix VI. To ensure that a different sample size has no influence on the patterns of change, some plots were also created using samples of 5000 and 10000 points. These resulted in the same patterns of change, hence the remaining plots were carried out with a sample of 1000 points.

From tables 6.1 to 6.3 it can be seen that the Maputo basin is most sensitive to climate change in relative terms with a mean change in water balance up to +92% for a scenario with uniform change in precipitation of +10% combined with a temperature

change of -2°C (run 7) and the Guadalquivir basin is least sensitive in relative terms with a maximum change of +50% in mean water balance for the same scenario. Temperature changes have less influence on the water balance as expected but a uniform change of plus or minus 2°C still leads to a relative change in water balance of around 13% for the Guadalquivir basin, 23% for the Maputo basin but only around 6% for the Savannah basin. Relative water balance seasonality changes are also greatest in the Maputo basin with changes up to 17% compared to Guadalquivir and Savannah having changes between 4 and 6 percent. These differences between the basins are the result of differences in seasonal precipitation. Since the uniformly applied climate change scenario is a percentage of input precipitation, absolute changes will be greater for seasons with more rainfall. Temperature changes are absolute changes (+ and -2°C) and since the AET calculation is energy driven, changes in the basin are expected to be linear. For all three basins, these changes are between 4.5% and 4.9%. The direction of the change in seasonality is different for the Savannah basin compared to the two other basins showing a decrease in seasonality with increasing precipitation and increase in water balance seasonality for decreasing precipitation whereas the reverse is the case for the Guadalquivir and Maputo basins. This is the result of non-linear changes in water balance as a result of changes in precipitation for high elevation cells where part of the precipitation falls as snow (see figure 6.3). Due to reduced snowfall in the winter months, there is less melt water production and thus a further decrease in water balance for these months. The increased variability of the water balance means there is greater seasonality. The reverse is true for increases in precipitation. For the scenarios where input precipitation is not changed, there is no change in wind-driven precipitation for the Guadalquivir basin and the Maputo basin. However, the Savannah basin sees a change in wind-driven precipitation of -3% for a scenario with a decrease in temperature of -2°C. Again, this is the result of a change in the amount of precipitation that falls as rain versus snow where there is increased snow fall at higher elevations as a result of the decrease in temperature which means there is an effective reduction in precipitation and thus wind driven precipitation.

Table 6.1 List of sensitivity runs and mean absolute change, standard deviation and relative change for 1000 random points in the Guadalquivir basin

Run	P	T	Δ AET			Δ WindP			ΔWB			ΔSeas		
			mm	SD	%	mm	SD	%	mm	SD	%	index	SD	%
1	-10%	0	0	0	0	-56.1	11.4	-9.9	-56.3	11.4	-36	-0.009	0.003	-4.0
2	0	+2	19.4	8.3	4.5	0	0	0	-19.7	8.8	-12.6	0.003	0.001	0
3	-10%	+2	19.4	8.3	4.5	-55.8	13.6	-9.8	-76.1	15.4	-48.7	-0.009	0.003	-3.8
4	+10%	0	0	0	0	58.3	11.9	37.4	58.5	11.9	37.4	0.01	0.003	4.1
5	+10%	+2	19.4	8.3	4.5	58.7	15.9	10.3	38.8	13.7	24.8	0.001	0.002	4.15
6	0	-2	-19.9	8.6	-4.6	0	0	0	20.3	9.5	13	0	0	0
7	+10	-2	-19.9	8.6	-4.6	57.2	17.7	10.1	78.8	17.2	50.4	0.001	0.004	4.1
8	-10	-2	-19.9	8.6	-4.6	-57.0	18.1	-10.0	-36.0	12.8	-23.1	-0.001	0.003	-4.2

Table 6.2 List of sensitivity runs and mean absolute change, standard deviation and relative change for 1000 random points in the Maputo basin

Run	P	T	ΔAET			ΔWindP			ΔWB			ΔSeas		
			mm	SD	%	mm	SD	%	mm	SD	%	index	SD	%
1	-10%	0	0	0	0	-85.4	17.8	-12.2	-85.5	17.6	-65.7	-0.02	0.009	-14.7
2	0	+2	29.5	9.0	4.9	0	0	0	-30.1	9.2	-23.1	-0.005	0.003	-4.1
3	-10%	+2	29.5	9.0	4.9	-85.4	17.8	-12.2	-115.6	18.9	-88.8	-0.02	0.011	-17.6
4	+10%	0	0	0	0	88.9	18.6	12.7	88.9	18.4	68.3	0.02	0.006	16.5
5	+10%	+2	29.5	9.0	4.9	88.9	18.6	12.7	58.9	21.4	45.2	0.01	0.005	11.6
6	0	-2	-30.9	9.3	-5.1	0	0	0	30.9	9.3	23.7	0.006	0.003	4.9
7	+10	-2	-30.5	9.3	-5.1	88.9	18.6	12.7	119.9	19.5	92	0.03	0.008	7.05
8	-10	-2	-30.5	9.3	5.1	-85.4	17.8	-12.2	-54.6	20.9	-41.9	-0.01	0.005	-11.0

Table 6.3 List of sensitivity runs and mean absolute change, standard deviation and relative change for 1000 random points in the Savannah basin

Run	P	T	Δ AET			Δ WindP			Δ WB			Δ Seas		
			mm	SD	%	mm	SD	%	mm	SD	%	index	SD	%
1	-10%	0	0	0	0	-144.3	17.5	-11.2	-144.3	21.1	-26.0	0.007	0.002	4.5
2	0	+2	35.2	5.3	4.7	14.3	66	1.1	-34.2	12.6	-6.2	0.004	0.003	2.2
3	-10%	+2	35	5.3	5.4	-130	53.0	-10.1	-184	17.1	-27	0.01	0.004	5.6
4	+10%	0	0	0	0	146.4	18.2	12.9	148	21.9	42.5	-0.007	0.003	-3.9
5	+10%	+2	34.8	5.3	4.7	162.2	83.2	14	108.7	32.1	31.1	-0.005	0.004	-3.2
6	0	-2	-36.2	5.4	-4.8	-37.4	91.4	-2.9	32.8	21.3	5.9	-0.004	0.007	-2.7
7	+10	-2	-36.2	5.4	-4.8	105	85.1	8.2	179.7	22.4	32.4	-0.009	0.007	-5.9
8	-10	-2	-36.2	5.4	-4.8	-176.4	97.8	-13.8	-110.8	34.4	-20.0	0.003	0.008	1.6

Examining the scatter graphs in figures 6.1 to 6.6 and Appendix VI it can be seen that the Guadalquivir and Maputo basins have similar responses to the climate change scenarios in the sensitivity analysis. The Savannah basin sample however shows a different pattern with regard to precipitation changes with a non-linear relationship between changes in precipitation and water balance which is due to reduced snowfall and associated snow melt in the winter months as described above. Moreover, quite a number of cells show a change in wind driven precipitation for the scenarios with no change in input precipitation (runs 2 and 6). This is because more of the rain is falling as snow (see figures VI.18 and VI.22). Actual evapo-transpiration changes are mostly linear showing a decrease in water balance with an increase in AET (figures 6.4 to 6.6). However at the highest elevation cells in the Savannah basin (figure 6.6) a increase in water balance with increase in AET can be observed which is the result of increased temperature and hence an increase in snow melt constituting a greater contribution to the water balance than the loss through evapo-transpiration. Water balance seasonality increases more for the lowlands because at these elevations, there is no cloud water interception which acts as a buffer during the dry season and is unaffected by changes in precipitation. This effect ensures that montane seasonality is more stable. This is particularly the case in areas where cloud water interception makes up a significant proportion of precipitation inputs in the dry season which is the case for the Maputo basin (see figures 6.2 and 6.5).

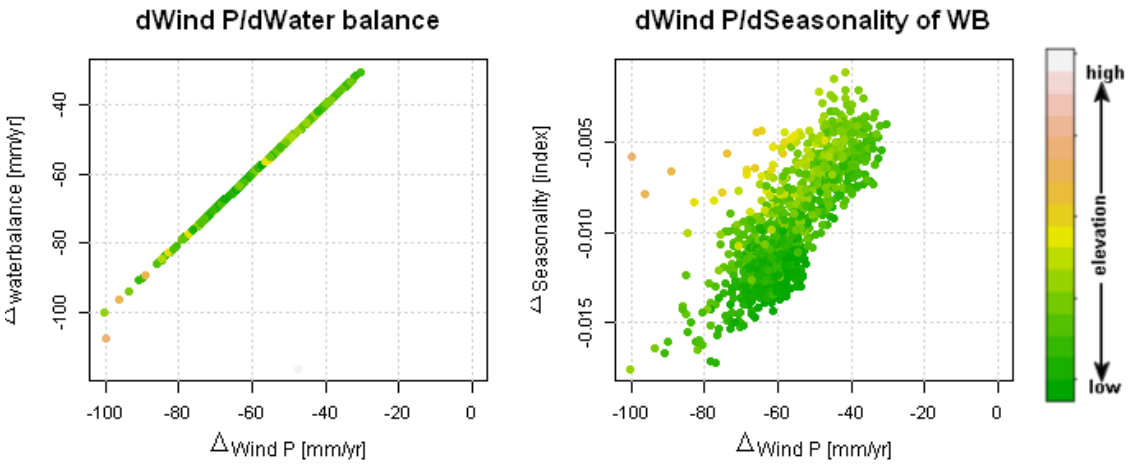

Figure 6.1 Water balance and water balance seasonality sensitivity for sensitivity run 1 Guadalquivir basin (precipitation -10% temperature no change).

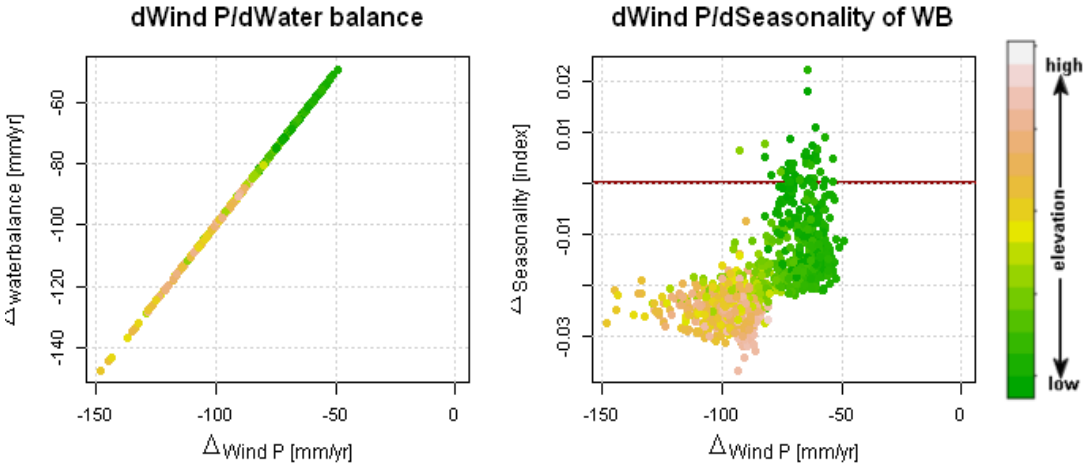

Figure 6.2 Water balance and water balance seasonality sensitivity for sensitivity run 1 Maputo basin (precipitation -10% temperature no change).

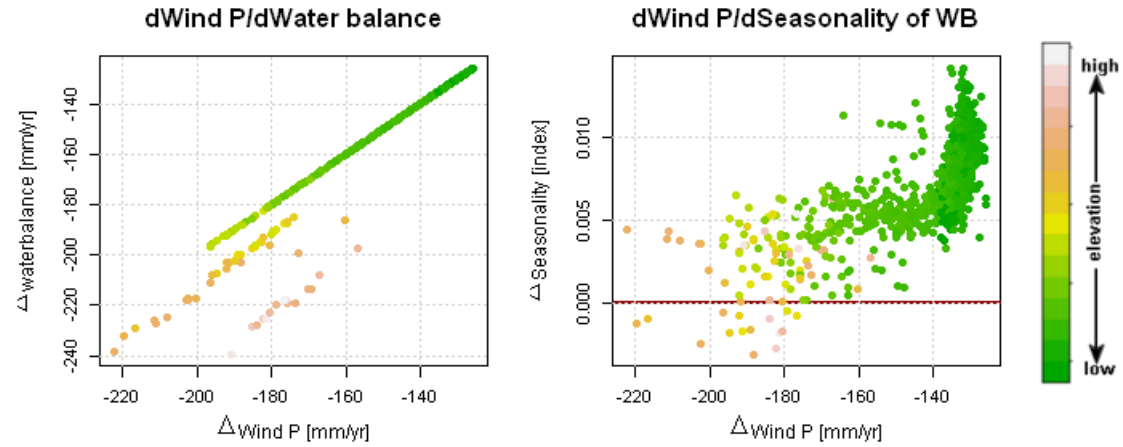

Figure 6.3 Water balance and water balance seasonality sensitivity for sensitivity run 1 Savannah basin (precipitation -10% temperature no change).

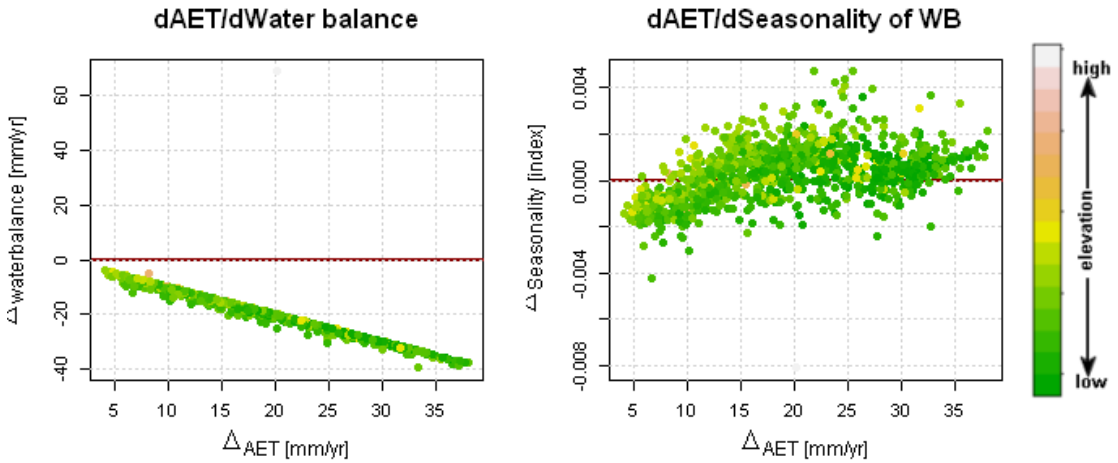

Figure 6.4 Water balance and water balance seasonality sensitivity for sensitivity run 2 Guadalquivir basin (precipitation no change, temperature +2°C).

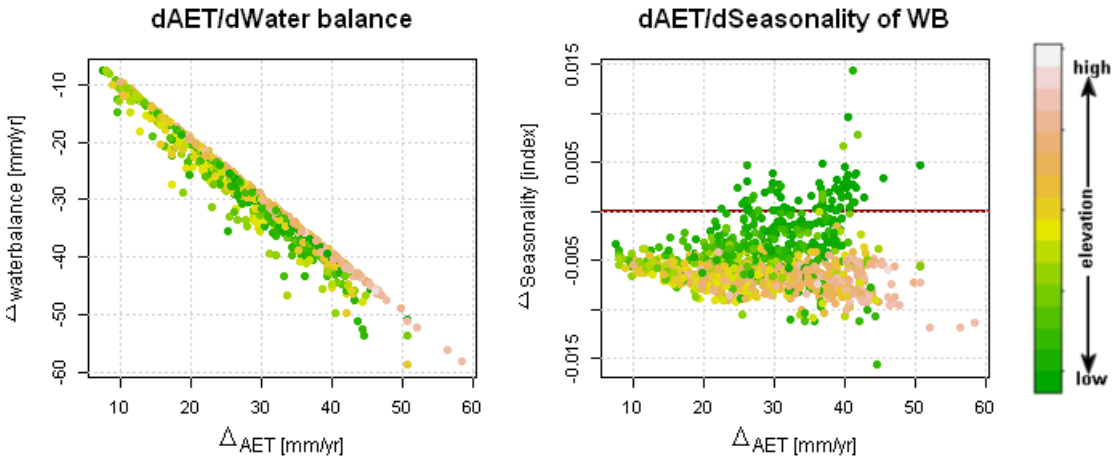

Figure 6.5 Water balance and water balance seasonality sensitivity for sensitivity run 2 Maputo basin (precipitation no change, temperature +2°C).

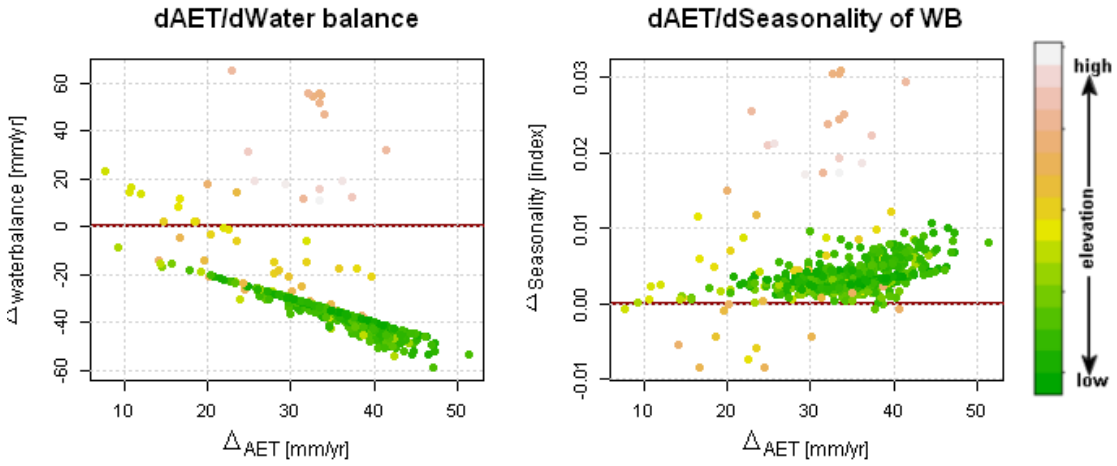

Figure 6.6 Water balance and water balance seasonality sensitivity for sensitivity run 2 Savannah basin (precipitation no change, temperature +2°C).

6.3. Cross-basin climate change analysis

As the case study basins are all located in geographically different areas, inter-basin comparison of the impacts of climate change also incorporates differences in specific basin characteristics. The hydrological consequences of climate change on dam catchments are mostly the result of between-basin differences in rainfall change which means that some of the effects of differing hydrology in the basins are less apparent. To be able to highlight how differences in basin geography such as terrain, vegetation

and baseline climate affect the outcomes of the same climate change, a hypothetical analysis is carried out whereby the same climate change (i.e. the same deltas) were applied to all the different basins. This analysis helps in determining what characteristics of basins make them more or less sensitive to a given climate change and thus can be instrumental in devising adaptation measures in basins.

6.3.1. Methodology

The analysis was carried out in a similar fashion to the initial climate change assessment in chapter 5 using the AguaAndes/Waterworld model. The 5 GCM scenario for A1B for the 2050s for the Guadalquivir basin was used as the reference climate change scenario and the WorldClim temperature and precipitation (Hijmans *et al.,* 2005) for this basin as the baseline. In order to be able to apply the same climate change to different basins, the monthly delta's for temperature and precipitation for this basin were extracted using ArcMap, and the statistics (min, max and standard deviation) for these grids were calculated. Uniform random monthly rasters with a ten degree spatial extent were then created based on these statistics and applied to the baseline monthly WorldClim grids for precipitation and temperature for each basin. This retains the statistical distribution of the deltas but loses the spatial structure and autocorrelation. These monthly grids for temperature and precipitation were then uploaded to the system as ARCASCII's as a climate change policy exercise. After the creation of monthly grids for temperature and precipitation based on climate change delta's, monthly relative humidity input data was also adjusted as a change in temperature can have a effect on relative humidity which in turn affects actual evapo-transpiration through a change in vapour pressure. Monthly relative humidity (RH) files for each case study basin based on New *et al.,* (2003), which are used as input to AguaAndes/WaterWorld were downloaded from the system, and processed in ArcMap whereby a set of algorithms derived from Mulligan and Burke (2005) was used to adjust the RH values to the changes in temperature under climate change. Firstly the new saturated vapour pressure (mb) was calculated based on the climate change scenario temperature using the following equation:

$$es_{cc} = \exp\left(26.66082 - 0.0091379024 \times (\text{temp}_{cc} + 273.15) - \left(\frac{6106.396}{\text{temp}_{cc} + 273.15}\right)\right) \quad (6.1)$$

Where es_{cc} is the saturated vapour pressure (mb) and $temp_{CC}$ is the scenario temperature (°C). Then the vapour pressure was calculated based on the baseline relative humidity using the saturated vapour pressure for the baseline temperature:

$$e = \frac{RH}{100} \times es_{baseline} \quad (6.2)$$

Where e is the vapour pressure (mb), RH is the baseline relative humidity (%) and $es_{baseline}$ is the saturated vapour pressure for the baseline temperature. Finally, the new relative humidity was calculated using the vapour pressure for the baseline but saturated vapour pressure for the climate change scenario. Baseline vapour pressure was used since it is not possible to calculate RH for the scenario otherwise since this depends on temperature and dewpoint.

$$RH_{new} = \frac{e}{es_{cc}} \times 100 \quad (6.3)$$

Once this procedure was carried out for all input months, the grids were uploaded to the system using the 'change input map' facility. Subsequently the model was then run for each basin using the same climate change delta's for temperature and precipitation and adjusted relative humidity input data. These model runs were then compared and the output analysed It should be noted that this analysis does not include other likely changes as a result of climate change such as solar radiation and cloudiness that would impact the hydrology of the basins. Table 6.4 gives the descriptive statistics for the annual climate change scenarios used in this analysis.

Table 6.4 Descriptive statistics for projected change between 1950-2000 and 2050 based on 5 GCM for A1B scenario for the Guadalquivir basin

	Mean	Max	Min	Standard deviation
Precipitation (mm)	-97	-131	-78	10.7
Temperature (°C)	2.9	3.1	2.7	0.08

6.3.2. Results

Figure 6.7 shows the resulting change in evapo-transpiration for all three basins, along with the tree and herb fractions derived from the MODIS VCF data (Hansen *et al.,* 2006) and figure 6.8 shows the frequency distribution of the changes in evapo-transpiration. Overall, ET change for the Savannah basin is most significant with losses of up to 10 mm/yr and a mean change of 0.5 mm/yr. The Maputo basin also has some areas with changes up to 10 mm/yr but has the lowest overall change with a mean of only 0.02 mm/yr. Changes in the Guadalquivir basin show a greater spatial distribution with changes throughout the basin although maximum changes are no more than 5 mm/yr and a mean change of 0.25 mm/yr. Therefore, between basin differences are small with the greatest change in basins that have the highest tree cover (Savannah and Maputo basins).

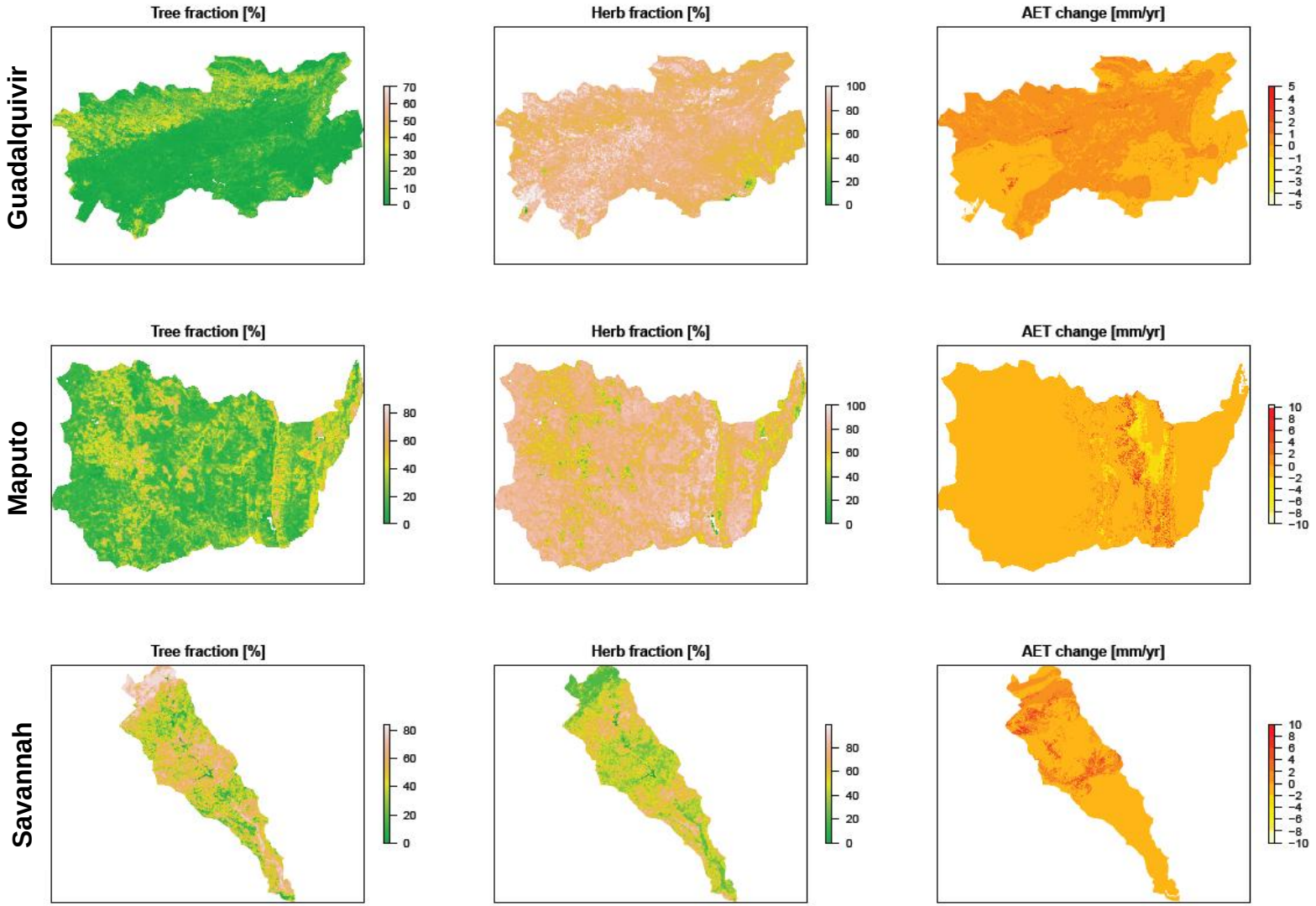

Figure 6.7 Tree and herb fraction (%) based on MODIS VCF data (Hansen et al., 2006) and changes in evapo-transpiration (mm/year) for the three case study basins for generalised climate change scenario

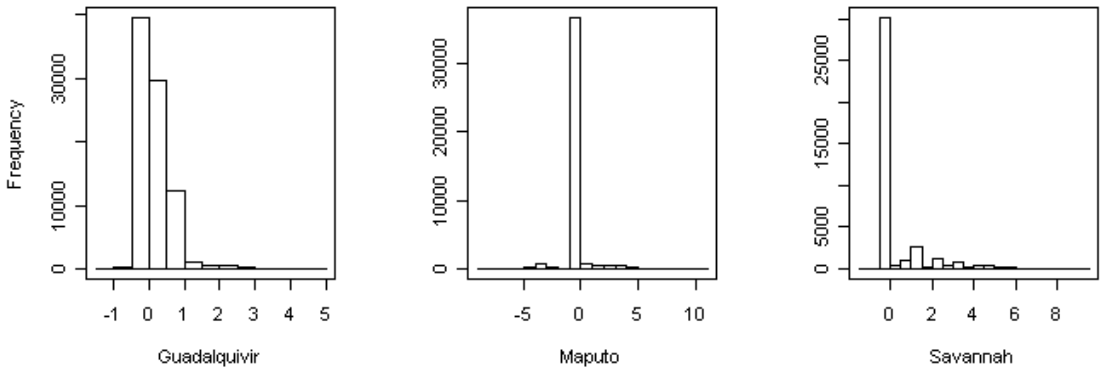

Figure 6.8 Frequency distribution of change in evapo-transpiration for three case study basins (mm/year)

Figure 6.9 shows the scatter plots of the scenario input precipitation versus the modelled wind-driven precipitation for each basin under the generalised climate change scenario and figure 6.10 shows the annual changes in wind driven precipitation along with digital elevation models of these basins. All basins show an overall decrease in wind driven rainfall. However, the high altitude area at the top of the Savannah basin shows a significantly positive change in wind driven rainfall as well as some of the higher altitude areas in the Guadalquivir basin which is the result of a smaller proportion of input precipitation falling as snow due to increased temperatures which means the wind driven rainfall will increase for those areas. Changes for the Maputo basin are uniform over the basin with a mean decrease in rainfall of around 107 mm a year, mostly at higher elevations in the basin. Mean decrease in wind-driven rainfall for the Guadalquivir basin is 101 mm/yr and for the Savannah basin 96 mm/yr.

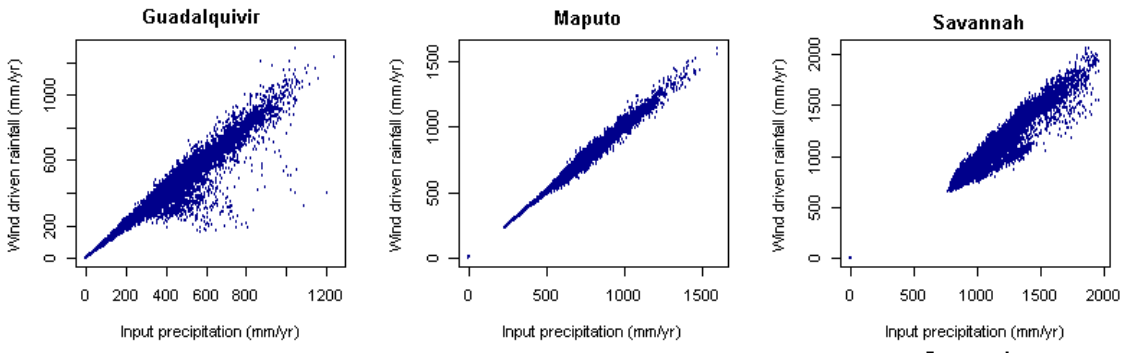

Figure 6.9 Scatter plots of input precipitation and annual modelled wind driven precipitation for three case study basins

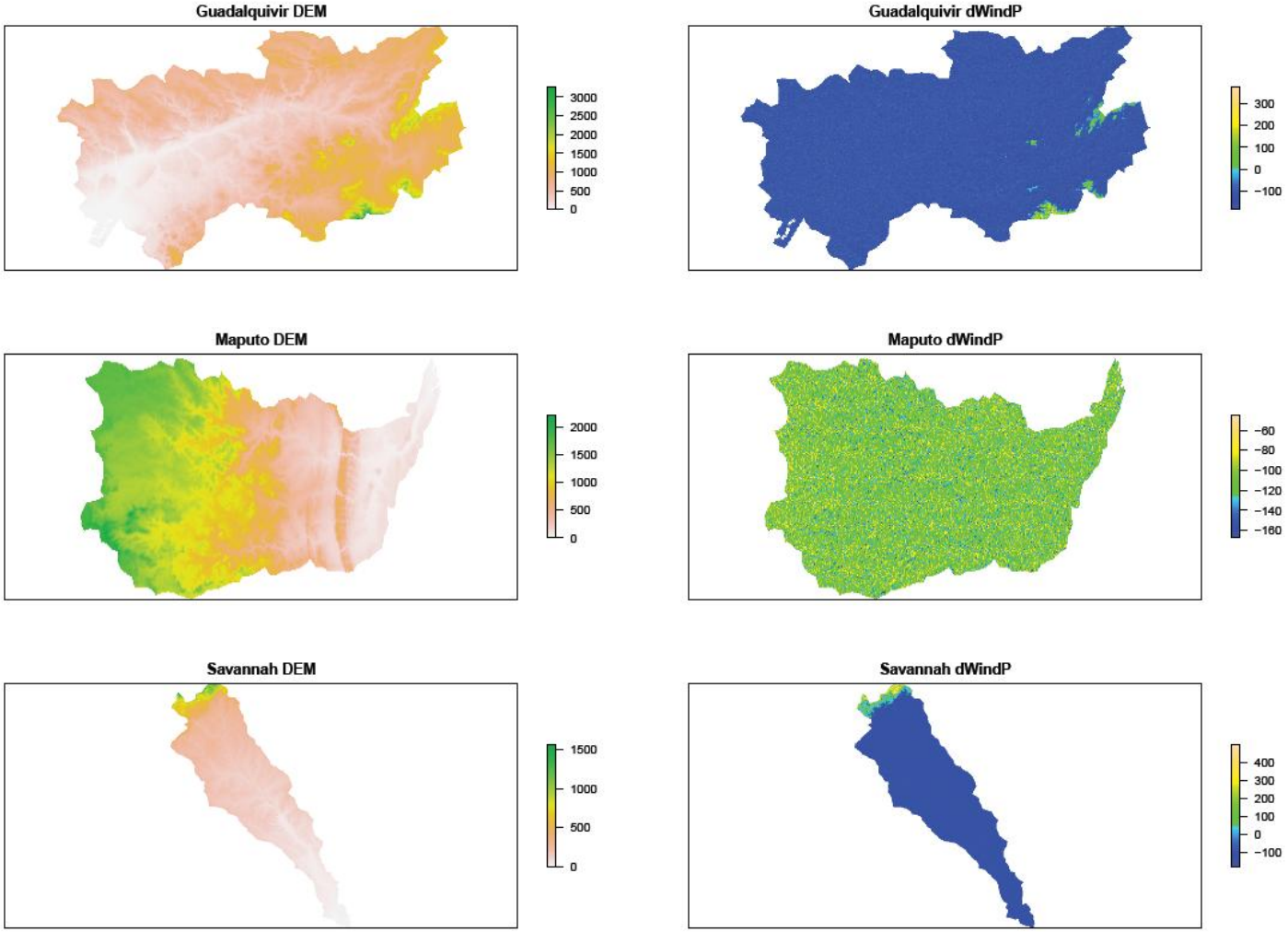

Figure 6.10 Changes in wind-driven rainfall for the three case study basins in mm/year for a generalised scenario

Figure 6.11 shows the changes in water balance and frequency distributions of these changes for the case study basins. Overall, as a result of the reduced precipitation, combined with minor changes in evapo-transpiration, all basins show an overall decrease in water balance. However, some areas at higher altitudes in the basins show a greater decrease in water balance despite having an increase in wind-driven precipitation. This is the result of decreased snowfall and snow melt in those areas that overall results in a net decrease of water balance. Changes in water balance mostly reflect the changes in precipitation since the AET changes are relatively small. All three basins thus show a similar response to a generalised scenario with some spatial differences in evapo-transpiration as a result of differences in vegetation. However, the changes in evapo-transpiration are smaller than when simulated with only changing temperature leaving relative humidity to baseline values (see table 6.1 to 6.3) which highlights the limitations of only using changes in temperature and precipitation for climate change impact analysis. Between basin differences in response to changes in precipitation are also minimal with only high altitude, snow dominated areas showing differences in wind-driven precipitation due to a shift from snowfall to rain, hence these changes are driven by temperature change. The resulting between basin water balances are therefore also very similar with differences due to changes in melt water at higher altitudes.

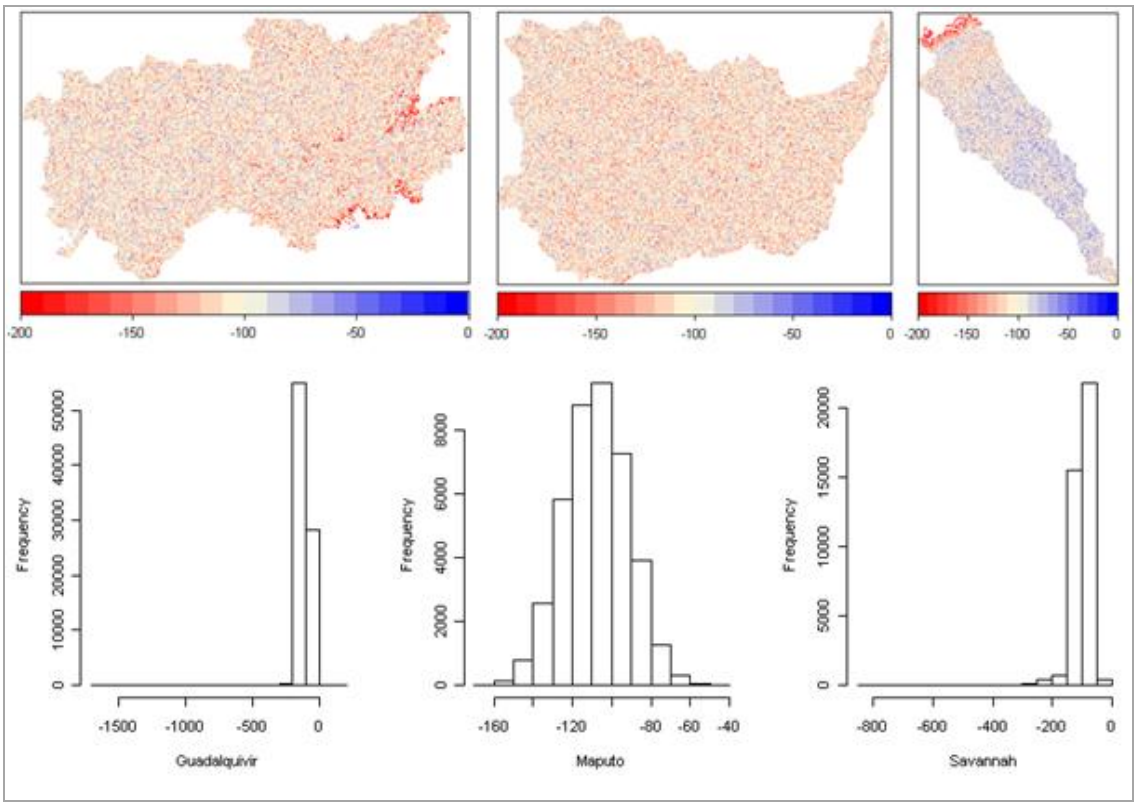

Figure 6.11 Changes in water balance for the three case study basins for a generalised scenario (mm/yr) (top) and frequency distributions of change in water balance (mm/yr) (bottom)

6.4. Sensitivity to vegetation change

The climate change analysis in the large dam catchments carried out in chapter 5, assumes that impacts of climate change are solely confined to changes in temperature and precipitation. However, climate change will most likely also have a impact on land cover with changes in the coverage, distribution and types of vegetation occurring which in turn will affect the hydrological response to a changing climate. To assess to what extent changes in vegetative cover affect the climate change response of hydrological fluxes as simulated under changes of precipitation and temperature alone, a sensitivity analysis was carried out in which the vegetative cover used as input by the model was varied, thus reflecting the effects of wetting and drying as a result of vegetation.

This sensitivity analysis was carried out by varying the percentage covers of the three vegetation types in the model; herb, tree and bare based on the MODIS vegetation

continuous fields dataset (Hansen *et al.,* 2006) in four different scenarios as described in table 6.5. This can be done using the policy exercises - land use change functionality of the AguaAndes/WaterWorld model. The results are then compared to the run for the mean of 5 GCM A1B scenario climate change to see which land management scenario would exacerbate or cancel out the effects of the projected climate change. The analysis was carried out for all three basins for four different land cover scenarios. The scenarios are applied on a pixel basis over the basins and represent the following changes in land management: afforestation, increase in agriculture, mosaic where all land classes are mixed equally and finally degradation. The percentage changes in the three land classes for the model for the four scenarios are given in table 6.5

Table 6.5 Vegetation sensitivity percentage changes in land use classes from baseline

Sensitivity Run	**Tree (% change)**	**Herb (% change)**	**Bare (% change)**	**Management**
1	70	20	10	Afforestation
2	20	70	10	Agriculture
3	33.3	33.3	33.3	Mosaic
4	10	20	70	Degradation

6.4.1. Results

Table 6.6 shows the results for the vegetation sensitivity runs for the three case study basins as the mean change of 1000 randomly sampled points in the basins for annual water balance change from the baseline in absolute and relative terms and relative change in water balance seasonality. Scatter plots of changes in water balance and water balance seasonality as a result of changes in land cover are shown in figures 6.12 to 6.14 for scenario 1 while the remaining scenarios are shown in Appendix VII. The sensitivity of the model to changes in land cover indicate that the Guadalquivir basin is most sensitive to changes in land cover with the greatest increase in water balance in relative terms under a scenario of land degradation, which is essentially a reduction of vegetation cover, as well as the greatest decrease for a scenario of afforestation. Since the projected climate change for this basin results in a significant decrease of water

(-96% for sample of points), any land use scenario that reduces the water use by vegetation, will have a counter effect on the impacts of climate change. The Maputo basin is least sensitive to changes in land cover in relative terms with a maximum increase in water balance of 3.5% under a degradation scenario and only the afforestation scenario has a moderate negative impact on the water balance. Also for this basin the A1B projected change in water balance is negative meaning that in order to offset some of this climate change impact, measures that reduce the water use within the basin are favourable. The Savannah basin is only moderately affected by an afforestation scenario with a reduction in water balance of -3.9%. All other scenarios increase the water balance. Also for this basin, the A1B scenario projects a decrease in the water balance meaning management options that reduce the water use in the basin are more favourable. Water balance seasonality is set to decrease for all scenarios for the Savannah basin but increases for an afforestation scenario for the Guadalquivir basin as well as for an agriculture scenario for the Maputo basin. Figure 6.15 shows the spatial distribution of the percentage change of tree, herb and bare land cover versus the percentage change of water balance for scenario 1. This helps identify those areas within the catchments where land management interventions will have most impact as high values mean that there is a greater change in water balance for every percent change in land cover.

Table 6.6 Results for vegetation sensitivity runs for three case study basins as mean change from the baseline for 1000 randomly sampled points in the basins

Run	**ΔTree (%)**	**Δ Herb (%)**	**Δ Bare (%)**	**ΔWater balance**			**ΔWater balance A1B**		**Δ Water balance Seasonality**
Guadalquivir				mm	SD	%	mm	%	%
1	60.9	-56.9	-3.5	-70.2	54.3	-44.7			5.6
2	10.7	-6.9	-3.5	-15.7	25.2	-9.5	-151	-96	-0.6
3	24	-43.6	19.8	8.4	26.7	5.3			-3.5
4	-0.7	-56.9	56.5	82.8	45.4	52.7			-13.5
Maputo									
1	46.7	-54	7.26	-3.7	16.7	-0.5			-0.74
2	-3.2	-3.96	7.26	3.0	6.6	0.4	-27.3	-3.8	0.6
3	10.08	-40.66	30.57	11.2	7.1	1.6			-0.22
4	-13.2	-53.96	67.26	25.2	12.3	3.5			-0.2
Savannah									
1	20.5	-28.8	9.7	-20.2	37.3	-3.9			-5.1
2	-29.5	21.2	9.7	73.3	38.1	14.0	-36.8	-6.4	-18.1
3	-16.2	-15.5	33	99.4	41.1	19.0			-24.8
4	-39.5	-28.8	69.7	215	59.9	41.0			-42.7

Examining the scatter plots in figures 6.12 to 6.14, it can be seen that changes in water balance for the Maputo basin (figure 6.13) are smaller compared to the other basins. Furthermore, while the Guadalquivir and the Savannah basins have more or less linear responses to vegetation changes with increases in tree cover leading to decreases in water balance, the opposite is the case for high altitude areas in the Maputo basin. This is the result of increased cloud water interception at high altitude by the increased tree cover that contributes to the water balance. Since cloud water interception is localized to highly exposed areas, not all high altitude cells show an increase in water balance.

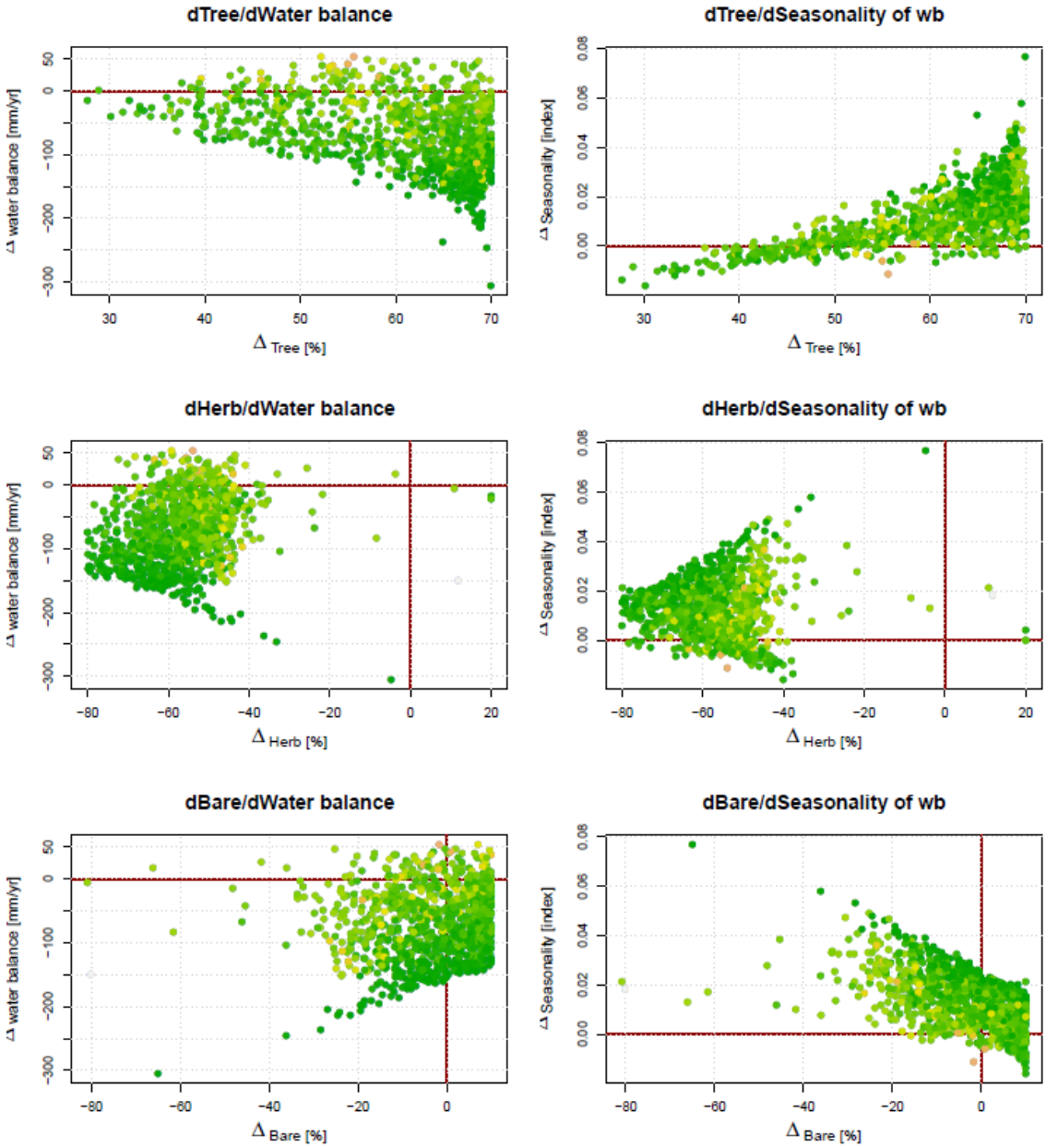

Figure 6.12 Water balance and water balance seasonality changes with changes in per-pixel vegetation functional types of tree (top), herb (middle) and bare (bottom) land cover for sensitivity run 1 (tree 70%, herb 20% and bare 10%) from the MODIS VCF baseline for the Guadalquivir basin.

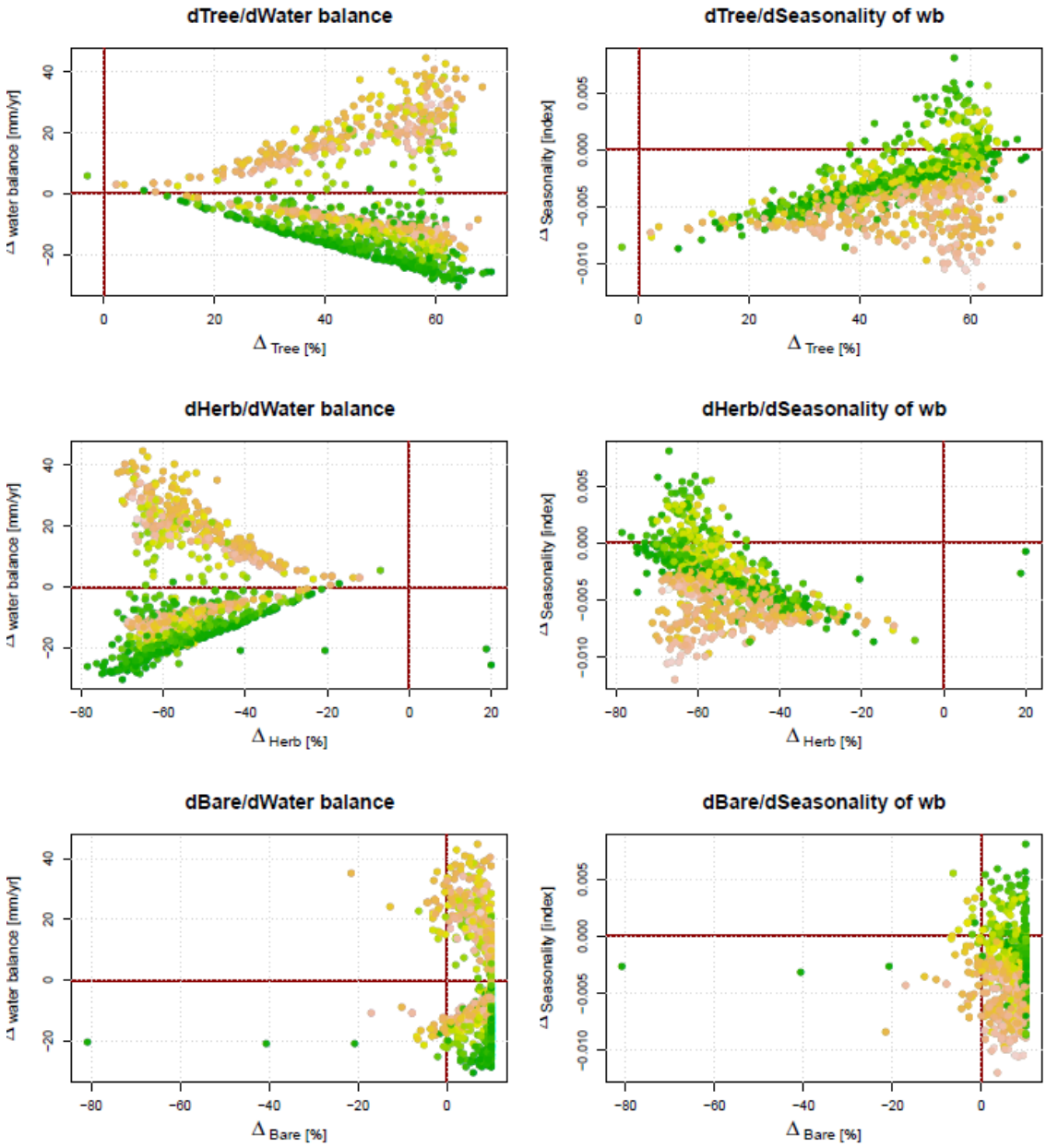

Figure 6.13 Water balance and water balance seasonality changes with changes in per-pixel vegetation functional types of tree (top), herb (middle) and bare (bottom) land cover for sensitivity run 1 (tree 70%, herb 20% and bare 10%) from the MODIS VCF baseline for the Maputo basin.

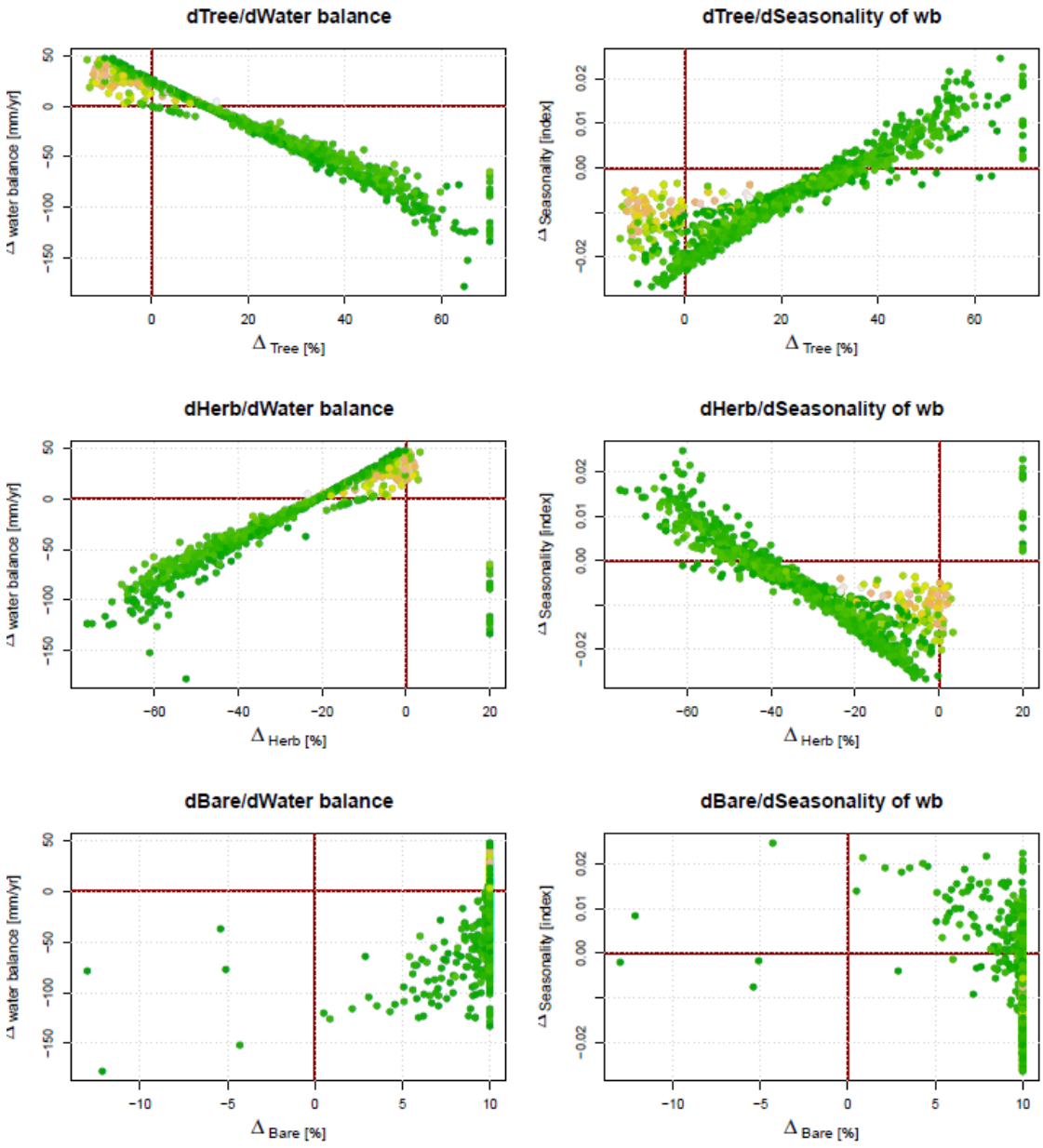

Figure 6.14 Water balance and water balance seasonality changes with changes in per-pixel vegetation functional types of tree (top), herb (middle) and bare (bottom) land cover for sensitivity run 1 (tree 70%, herb 20% and bare 10%) from the MODIS VCF baseline for the Savannah basin.

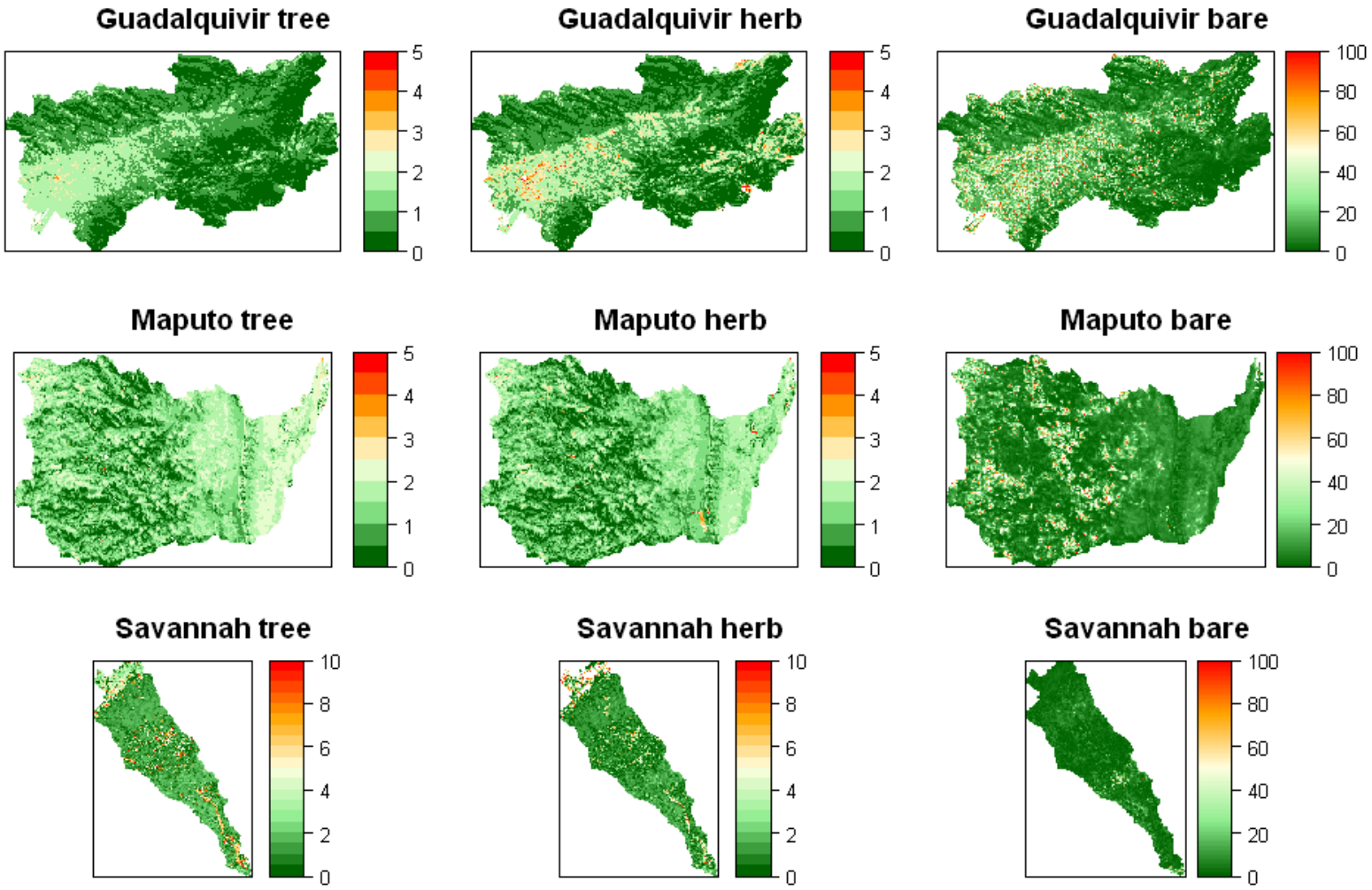

Figure 6.15 Spatial distribution of percentage change in water balance as a percentage change of land cover type for tree, herb and bare land cover types for all three case study basins

6.5. Discussion and conclusions

6.5.1. climate change sensitivity of basins

Sensitivity to climate change of the case study basins introduced in chapter 5 was assessed using the policy exercises - simple climate change scenario feature of WaterWorld. Climate change scenarios of +/- 10% precipitation and +/- 2°C temperature applied uniformly over the basins were run in AguaAndes/WaterWorld and results are presented as mean changes between the scenario and the WorldClim baseline for 1000 random chosen points in each basin for water balance and water balance seasonality. The results indicate that the Maputo basin is most sensitive to climate change with relative mean change in water balance up to 92% for a drying scenario of -10% precipitation and +2°C temperature change and the Guadalquivir basin is least sensitive with maximum relative change of 50% for the same scenario. Relative seasonality changes are also greatest in the Maputo basin with relative changes up to 17% compared to Guadalquivir and Savannah that only have changes between 4 and 6 percent for the same seasonality of climate change. It should be noted though that since the uniformly applied climate change scenario is a percentage of input precipitation, absolute changes will be greater for seasons with more rainfall. The Savannah basin, unlike the Guadalquivir and Maputo, shows a non-linear change in water balance for a sample of 1000 points with changes in input precipitation and temperature. Changes in precipitation lead to changes in the amount of snow fall and thus snow melt contribution while changes in temperature change result in changes in the proportion of input precipitation falling as snow versus rain.

Relevance to dams

With the Maputo basin being the most sensitive to changes in precipitation and temperature, the dams in this basin are more sensitive to a change in climate in terms of their water resources. However, the mean of 5 GCM A1B scenario projects a decrease in water balance for the same sample points of -3.8% (see table 6.6) with high between-model agreement as can be seen in section 4.2.2. Therefore, whilst

sensitivity is higher, actual changes might be smaller in magnitude. In contrast, the Guadalquivir basin shows a projected decrease in water balance for the sample points of -96%. This basin also has high between-model agreement on the direction (and magnitude) of the projected changes as can be seen in section 4.2.2 and 4.2. Projected significant decreases in precipitation and increases in temperature for this area have also been found by Giorgi and Lionello, (2008) using 17 models for three SRES emission scenarios (A1B, A2 and B1) for the 2050s and 2100s and Gao *et al.,* (2006) using regional climate models. The relative certainty of the changes combined with a relatively high sensitivity to those changes therefore put this basin at very high risk from climate change. Finally, the Savannah basin is projected to be more specifically affected by climate change with reduced snowfall in the mountains leading to a decrease in seasonal snow melt. This seasonal change is particularly important for dams that rely on winter storage. Projections for this region however are less in agreement with only three models agreeing on the direction of change for the A1B scenario (see section 4.2.2).

6.5.2. Cross-basin climate change analysis

To be able to highlight how differences in basin geography such as terrain, vegetation and baseline climate affect the outcomes of the same climate change, an analysis was carried out whereby the same climate change (i.e. the same deltas for temperature and precipitation) were applied to the three case study basins. Moreover, relative humidity was also adjusted to avoid the change in temperature having a significant, unintended change on humidity. The results show that using this scenario yields to only minor differences in evapo-transpiration between the basins as a result of water availability and to more significant differences in precipitation in higher altitude areas for the Guadalquivir and Savannah basins as a result of rainfall/snow dynamics. However, no significant differences in water balance were determined for these basins which mean that the climate change impacts as determined by the hydrological model are mostly driven by changes in precipitation. However, even though the changes in evapo-transpiration are small, the simulated changes are smaller than when

simulated with only changing temperature and leaving the relative humidity to baseline values. This highlights the limitations of only using changes in temperature and precipitation in climate impact analysis. As well as changes in relative humidity, climate change can also impact the cloud base altitude (Still et al., 1999) generally leading to increased cloud base altitude at higher elevations.

6.5.3. Sensitivity to vegetation change

The final sensitivity analysis for this chapter involved using the policy exercises - change land use functionality of WaterWorld to assess to what extent changes in vegetative cover affect the climate change response as simulated under changes of precipitation and temperature alone. The results indicate that the Guadalquivir basin is most sensitive to changes in land use and the Maputo basin least sensitive. A scenario of afforestation (70% tree) decreases water balance in all three basins and a scenario of land degradation (70% bare) has the greatest positive impact on water balances.

Changes in land use could therefore potentially offset some of the climate change impacts in the basins. For the Guadalquivir basin, where a high percentage of the land cover consists of herb fraction (77%), i.e. agriculture, of which a great proportion is irrigated, a change in agricultural practices and less water consuming irrigation is potentially the best adaptation measure to the projected decrease in water. Agricultural water use in the basin currently is around 86% of total water consumption with around 12% of the basin being irrigated (Gaeckler *et al.,* 2007) of which olive groves, cotton and rice are the main consumers. Measures such as moving from flooding irrigation to sprinkle irrigation and using waste water for intensive irrigation are already part of water policy in the basin, however in order to cope with the projected future water stress, more adaptation measures are necessary.

The Maputo basin, like the Guadalquivir basin is mostly dominated by herb fraction (74%). Current land use in the area is mainly agricultural with the sector using 64% of total available water (SADC, 2010). The model simulations have shown that a change in

land use to more trees at higher elevations can increase the water balance in these areas as a result of increased fog interception. An increase in tree cover at those high altitude areas where fog occurs would therefore be a suitable measure. Increasing tree cover also has the added benefit of reducing erosion. Possible locations are identified by those areas where the greatest positive change in water balance can be achieved (see figure 6.15).

The Savannah basin has a much higher tree fraction compared to the two other basins (49% tree, 49% herb) which means that current water use is high. A change towards more agriculture has therefore a greater impact on the water balance as compared to the other two basins. As discussed above though, climate change projections for this area have greater uncertainty with not all GCM agreeing on the direction of change which means that it is more difficult to decide on adaptation measures.

Thus far, the potential adaptation measures have focused on the projected climate change for the 2050s. However, it has been shown for some areas (Mulligan, 2011) that the direction of climate change can reverse when looking further into the future. An initial analysis of model runs for the mean of 5 GCM A1B scenario for the 2080s showed that the projected climate change is of similar direction as for the 2050s for all basins although magnitudes do change (i.e. Maputo water balance -44%, Savannah water balance - 19%). Therefore adaptation measures can be implemented over a longer time-frame.

While the assessment of sensitivity based on the three functional vegetation types is very useful in quickly determining patterns of change and comparing basins, a full analysis of possible adaptation measures through land management should take into account all current and possible vegetation (crop) types within the basins since particularly seasonal changes in demand can make a great difference to the overall water budget. Furthermore, it should be noted that the climate change projections are based on multi-GCM means. The results of individual model projections or different set of models may change the magnitude (Maputo and Guadalquivir basins) or direction

(Savannah basin) of the changes which means adaptation measures need to be flexible.

7. Impacts of climate change on Cañón del Pato HEP station, Santa basin, Peru

7.1. Introduction

This chapter describes the application of the AguaAndes/WaterWorld model to the Santa river basin in the Peruvian Andes. This basin is part of the Challenge Program on Water and Food COMPANDES (www.benefitsharing.net) project that aims to develop mechanisms for benefit sharing that can improve productivity and reduce water conflicts in basins throughout the Andes. Part of this project is the further development of the web based AguaAndes/WaterWorld policy support system in order to provide information and understanding of biophysical processes, hydrology and impacts of climate- and land use changes and management interventions and improve the hydro-literacy of local stakeholders and organisations within the basin.

This chapter aims to apply some of the capabilities of AguaAndes/WaterWorld and its climate change scenario analysis in a real world case study basin. The first part of this chapter describes a validation of the AguaAndes/WaterWorld model in the Santa river basin using two different precipitation input datasets (WorldClim and TRMM). The model was then used to assess the potential impacts of climate change on the Cañón del Pato hydroelectric power station located in the Santa basin using eight different climate change scenarios. The climate change scenarios used are part of the AguaAndes/WaterWorld policy exercise functionality and are based on downscaled multi-GCM means for two different SRES emission scenarios (A1B and A2A) for the 2050s from the IPCC AR4. Since the Santa basin is located in the Peruvian Andes, the water supply is influenced by melt water from glaciers in the mountains. To address the importance of melt water as a contributor to the water supply, changes in mean snow pack, melt water production and snow fall as a result of climate changes will be assessed. Furthermore, changes in total flow through the Cañón del Pato HEP station as well as changes in sediment delivery as a result of climate changes will be described.

Finally, the impact of initial conditions for snow and ice cover on model outputs has been assessed using a model spin-up procedure. Since AguaAndes/WaterWorld is a an equilibrium rather than a transient model (i.e. changes for any given scenario are changes between a baseline and a scenario run), any simulated changes as a result of climate change do not take into account changes in initial storage conditions for the model year, i.e. initial storage conditions are the same as for the baseline. This aspect is important in climate change analysis as particularly stores of snow and ice are expected to decrease over time with projected increases in temperature and the transience of these decreases may extend beyond a model year.

7.2. The Rio Santa basin

7.2.1. Study site

Location and topography

The Rio Santa basin is located in Peru, in the Ancash regional administrative area about 400 km north of the capital Lima. The basin has a total drainage area of around 12,200 km^2 and a total length of 316 km which makes it the second largest river and most regular flowing Peruvian river to flow into the Pacific ocean (Mark *et al.,* 2010). The river originates at lake Conococha at an altitude of 4080 m.a.s.l. and then runs north in the Callejon de Huaylas valley which is located between de Cordilleras Blanca and Negra mountain ranges, it then turns west at the confluence with the Rio Manta towards the city of Chimbote at the Pacific coast (McKinney, 2011). The Cordillera Blanca is the world's most extensive tropical mountain range with about one quarter of all tropical glaciers (more than 600 km^2) and over 30 peaks that are higher than 6000 m.a.s.l. (Kaser *et al.,* 2003; Vuille *et al.,* 2008). Of the 23 tributary streams of the Rio Santa, 20 originate from the glaciers of the Cordillerra Blanca, making glacier melt an important contributor to the Rio Santa discharge, particularly in the dry season. Conservative estimates of this contribution by Mark *et al.,* (2005) indicate that about two-thirds of the dry season flow of the Rio Santa in the Huaylas valley originates in

the Cordillera Blanca with 40% of the total flow coming from glacier melt. Figure 7.1 shows the location of the Santa basin in Peru, the location of the Cañón del Pato hydroelectric power facility and the elevation in the basin.

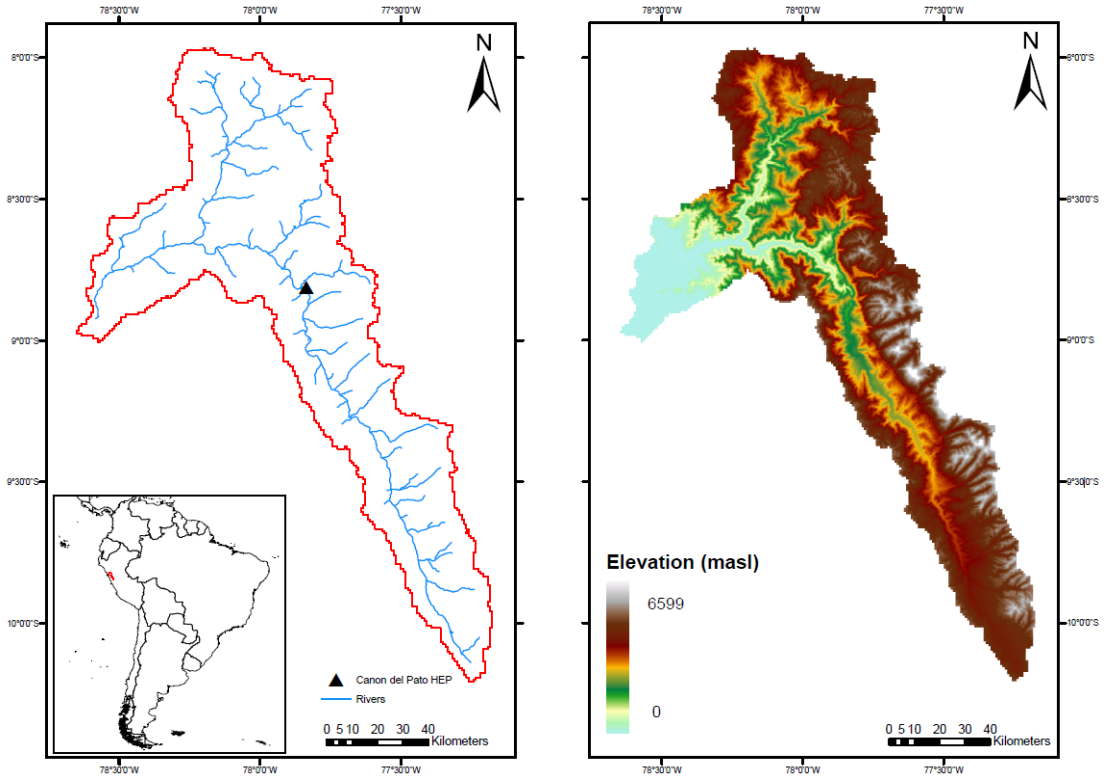

Figure 7.1 Location of Santa basin in Peru (left inset), Santa basin with river system and location of Cañón del Pato HEP (left) and map showing elevation in the basin ranging from sea level to nearly 6600 m.a.s.l. in the Eastern Cordillera Blanca (right) based on SRTM data.

7.2.2. Current and recent climate

Temperature

Temperature in the area is dominated by the Intertropical Convergence Zone (ITCZ) and trade winds leading to only small variations in annual air temperature seasonality (Mark *et al.,* 2005; Maurer, 2009). There are six WorldClim temperature stations in the Santa basin with another two within a 25 km radius. Mean annual temperature in the basin based on these stations is 9.6°C with a mean monthly minimum of 8.2°C in August and a mean monthly maximum of in 10.9 °C in March.

Precipitation

More than eighty percent of precipitation falls in the wet season between October and May when the ITCZ is in the region (Mark *et al.,* 2005; Mark *et al.,* 2010). In the dry season, the ITCZ moves north of the region (McKinney, 2011). The Cordillera Blanca acts as a barrier between the humid Amazon and the extremely dry coastal region with the Amazonian side being up to three times wetter than the Pacific side (Racoviteanu *et al.,* 2008). There are fifteen WorldClim precipitation stations in the Santa basin with another eleven within a 25 km radius. Average precipitation for the basin amounts to 548 mm a year however, this is extremely spatially variable with the highest precipitation found along the Cordillera Blanca and the lowest in the dry coastal region.

Recent climate changes

A temperature increase of around 0.35/0.39 degree Celsius per decade has been found in central Peru between 1951 and 1999 based on 29 temperature stations (Mark, 2005) while Vuille *et al.,* (2008) using 279 temperature stations found 0.10 degrees Celsius increase per decade between 1939 and 2006 for the tropical Andes between 1 deg N and 23 deg S, leading to an overall temperature increase of nearly 0.7 degrees since 1939.

Clear recent trends in precipitation have not been found, partly as a result of the lack of long period, high-quality precipitation records. Vuille *et al.,* (2003) analyzed 42 precipitation stations in the region and only found 5 with a significant increase and 2 with a significant decrease in annual precipitation with no clear dependence on elevation. Some other studies though have found clear precipitation increases from mostly the Eastern slopes of the Andes (Vuille *et al.,* 2003).

Water resources and land use

The basin can roughly be divided into three zones based on elevation: the high mountains above 2000 metres, the Callejon de Huaylas valley between 1000 and 2000

metres and the coastal region below 1000 metres. The highland areas mostly support subsistence farming and grazing. Land use in the Callejon de Huaylas valley mostly consists of small irrigated farming and the coastal region is dominated by large commercial irrigated agriculture in the Chavimochic and Chinecas project areas. Furthermore, the coastal cities of Chimbote and Trujillo further north are dependent on water from the Rio Santa for their drinking water supplies.

Hydropower

The Cañón del Pato hydroelectric power plant is located near the end of the Callejon de Huaylas valley just before the Santa river turns west (see figure 7.1). It started operations in 1958 with 50 megawatts installed capacity which gradually increased to 263 MW currently (McKinney, 2011). The facility uses run-of-the-river flow from the river Santa as well as releases from four lakes in the Cordillera Blanca (Paron, Cullicocha, Aguaschocha and Rajucolta). These glacial lakes can provide up to 60 million m^3 of flow in the dry season with Lake Paron at an altitude of 4100 m.a.s.l. being the largest and most important contributing lake. The dam catchment measures 4561 km^2. Figure 7.2 shows the catchment characteristics of the Cañón del Pato dam catchment. Elevation ranges from 6508 m.a.s.l. in the Eastern Cordillera Blanca of the catchment gradually declining to 1685 m.a.s.l. at the dam site. Vegetation in the catchment consists mainly of herbaceous cover with patches of tree cover. On average, 8% of the catchment is covered by trees and 64% with herbaceous cover with the remainder classified as bare. Many of the trees found at these high altitudes are Polylepis trees, which are part of the rose family. This species is frequently harvested for firewood leaving only small remaining pockets in the area. Overgrazing in the area has caused an additional deforestation. There have been conservation efforts in the area but these have mostly failed because of a lack of stakeholder input and buy-in (McKinney, 2011). Farming in the area is mostly subsistence farming with farmers growing typical Andean crops such as potatoes, corn, quinoa, barley, wheat, oca and olluco.

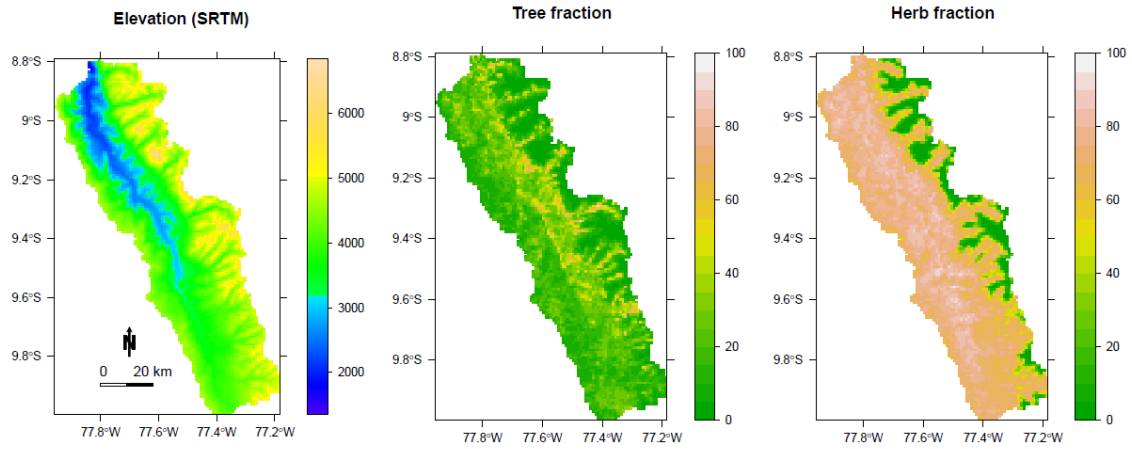

Figure 7.2 Catchment elevation based on SRTM and Tree and Herb fractions based on MODIS VCF for the Cañón del Pato dam catchment, Santa basin, Peru.

7.3. Methodology

The web based AguaAndes/WaterWorld policy support system as described in chapter 5 was applied to the Santa river basin in order to model the impacts of a range of climate change scenarios on the Cañón del Pato hydroelectric power station. The first step in the analysis was to run a baseline simulation at 1-km spatial resolution. This analysis then served as a basis for model validation and a static baseline to which the scenario outputs can be compared.

In order to validate the model, observed stream flow records were obtained through the COMPANDES project with original data supplied by the Peruvian institute of natural resources (INRENA) . Observed stream flow records were available for 16 sub catchments within the Santa basin for measurement periods ranging from 9 to 57 years. Since only the approximate locations of the stream flow gauging stations were known and the model was run at 1-km spatial resolution resulting in a rather coarse stream flow network, a manual adjustment of the stream flow locations to their corresponding locations on the Hydrosheds DEM derived stream flow network was necessary. This was done in ArcMap GIS. The uncertainty in moving of the gauging stations to the nearest location on this network has implications for the modelled stream flow that can explain (minor) differences in modelled and observed flow.

For the baseline simulation, the model was run with two different input precipitation datasets. The default WorldClim precipitation data based on a 1950-2000 long term monthly mean (Hijmans *et al.,* 2005) and a TRMM (Tropical Rainfall Measuring Mission) monthly precipitation climatology based on the TRMM 2B31 dataset for the years 1997-2006 developed by Mulligan, (2006b). The WorldClim precipitation is based on an interpolation of fifteen stations for the ten degree tile that contains the Santa basin.

Table 7.1 shows the results for the stream flow validation for both precipitation climatologies for all available observed stream flow stations (16 stations) and for stations that have an average annual flow of at least 5 $m^3 s^{-1}$ (8 stations). The results for all stations using the WorldClim climatology are also split into wet and dry seasons. The modelled annual stream flow shows a good fit with observed data for all stations (R^2 = 0.84) but particularly for the stations with higher flow rates (R^2 = 0.99) using WorldClim precipitation. The model slightly underestimates flow (bias -2.5%) for the larger stations though as well as for the wet season (bias -7.2%) but slightly overestimates flow for the dry season (bias 6.7%). Validation results based on TRMM rainfall show a slightly less good fit. Seasonally, using the WorldClim rainfall climatology both wet and dry season show a good fit as well. There is no spatial pattern in the errors found at individual stations with flow at some of the smaller stations either over- or underestimated.

Table 7.1 AguaAndes/WaterWorld validation results for 16 sub-catchments (total) and 8 sub-catchments with an average flow above 5 m^3s^{-1} for annual and wet- and dry season flow in the Santa basin, Peru

	Annual WorldClim rainfall		Annual TRMM Rainfall		Wet season WorldClim rainfall	Dry season WorldClim rainfall
Statistics	Q total (m^3s^{-1})	Q>5 ($m^3 s^{-1}$)	Q total (m^3s^{-1})	Q>5 (m^3s^{-1})	Q total (m^3s^{-1})	Q total (m^3s^{-1})
Observed mean (m^3s^{-1})	34.5	46.3	34.5	57.9	35.0	14.4
Modelled mean (m^3s^{-1})	29.9	48.9	24.8	40.1	43.0	7.5
Modelled SD (m^3s^{-1})	54	71.6	47	58.1	85.9	13.6
Bias (m^3s^{-1})	4.6	-2.5	9.7	17.3	-7.2	6.7
Mean Absolute Error (MAE)	8.5	3.6	10.7	17.9	7.2	6.7
Root mean Squared Error (RMSE)	318.7	32.9	373.8	274.1	14.2	18.7
R^2	0.84	0.99	0.80	0.73	0.96	0.98
Modified index of agreement (d_1)	0.90	0.97	0.87	0.84	0.90	0.71
Modified coefficient of efficiency (E_1)	0.81	0.73	0.76	0.71	0.80	0.53

7.3.1. Climate change projections

As described in chapters two and four, there is great uncertainty in projection of precipitation by GCMs, which is particularly the case for highly heterogeneous landscapes such as the Andes mountain range (Buytaert et al*.,* 2009; Ramirez and Jarvis, 2010). Since precipitation constitutes the main flux in the water balance model, these uncertainties are critical. To address some of this uncertainty, a range of climate change scenarios will be used for the analysis in this chapter. By using the mean of 24 GCM for the SRES A1B scenario and 17 for the SRES A2A emission scenario, the central tendency of the projections will be represented. Since the central tendency might not be the best model available, the AguaAndes/WaterWorld model will also be run with the mean of all available GCM projections plus and minus one standard deviation of the inter-GCM variability of temperature and precipitation to capture the variability in

the GCM projections. Finally, the model will also be run with the mean of 5 GCM for the A1B and A2A emission scenarios in order to compare inter-emission scenario differences. The GCMs used in the analysis are the downscaled (1-km spatial resolution) GCMs that are freely available from CIAT (2010) for the 2050s that have been discussed in more detail in chapter 4. The characteristics of these GCM can be found in Appendix VIII.

Table 7.2 shows an overview of all climate change scenarios used to drive the AguaAndes/WaterWorld model in this chapter with the mean change for precipitation and temperature compared to the WorldClim baseline for the Cañón del Pato dam watershed.

Table 7.2 Climate change scenarios used in analysis. All projections are means for the 2041-2060 period (2050s)

Scenario	**Number of GCM**	**Mean P change (mm/yr)**	**CV of P change (%)**	**Mean T change (°C)**
A1B mean	24	101	-4.7	1.9
A1B mean+ SD	24	349	-12.6	2.3
A1B mean- SD	24	-147	11.6	1.4
A2A mean	17	118	-15.2	2.5
A2A mean +SD	17	306	-30.9	3.5
A2A mean - SD	17	-67	11.1	1.6
A1B	5	44	0.2	2.6
A2A	5	87	-4.2	2.3

Figure 7.3 shows the monthly change in precipitation and temperature from the baseline climatology for the Cañón del Pato dam watershed for all climate change scenarios for the 2050s. Seasonal variation in temperature projections is greater for the mean of 17 GCM A2A scenarios than for the A1B 24 GCM scenarios while the reverse is the case for the 5 GCM scenarios, which also show a greater change compared to the baseline meaning the 5 GCM are at the higher end of the projections. Precipitation change for the A1B 24 mean GCM scenario is also less seasonal than the

A2A 17 GCM scenario with the latter showing a sharp increase in the dry season from May to October. These projections contradict claims from the literature that most AR4 GCMs project increased precipitation in the wet season and decrease in the dry season in the region (Vera *et al.,* 2006; McKinney, 2011) although these experiments were carried out with a different set of models and for a different time-period (CNRM_CM3, GFDL_CM2, IPSL_CM4, ECHAM5_MPI/OM (2 runs), GISS-EH (3 runs), MIROC_3.2 (3 runs), MRI_CGFM2.3.2 (5 runs), A1B, 2070s). Hence, the discrepancy can be explained by the number and type of GCMs used in the analysis since particularly precipitation projections show great differences between GCMs as described in chapter 4.

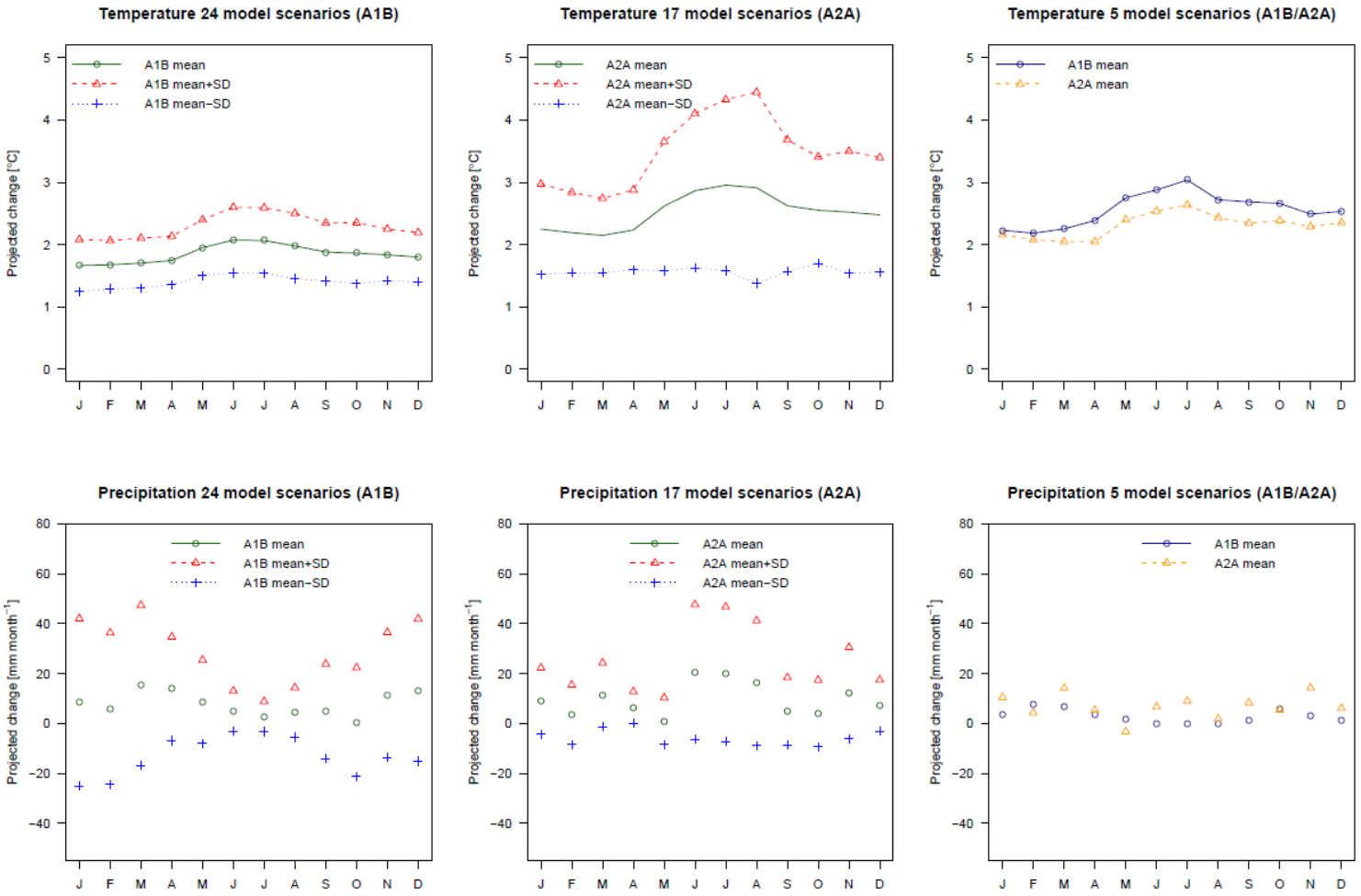

Figure 7.3 Graphs of variability in the scenario projections for monthly temperature and precipitation anomalies for the Santa basin, Peru for the 2050s. Scenarios as defined in text.

7.4. Results and discussion

This section describes the results of the AguaAndes/WaterWorld equilibrium modelling analysis for the Cañón del Pato HEP catchment in the Rio Santa basin. Results are shown as annual changes from the WorldClim climatic baseline for wind driven precipitation, actual evapo-transpiration, fog inputs, snow fall, melt water and water balance for all scenarios. To examine the seasonal changes, spatial maps of water balance, melt water production, snow fall and snow pack water equivalent are plotted for all scenarios. To assess the impact of climate change on the Cañón del Pato HEP facility, changes in stream flow and inputs of sediment will be described for all scenarios. Finally, the results of the model spin-up effects will be described and discussed.

7.4.1. Annual changes

Figure 7.4 shows the results for wind driven precipitation, actual evapo-transpiration, fog inputs, snow fall, melt water and water balance for the WorldClim climatic baseline. Figures 7.5 to 7.12 show the spatial annual changes in wind driven precipitation, actual evapo-transpiration, fog inputs, snow fall, melt water and water balances for all climate change scenarios. Table 7.3 shows the annual changes from the WorldClim baseline as mean values for the catchment while figure 7.13 presents these mean annual changes as bar charts. All scenarios with the exception of the A1B 24 -SD scenario show an overall increase in wind driven rainfall which is expected based on the precipitation and temperature projections shown in figure 7.3. High localised changes in wind driven precipitation are mostly the result of increased temperature decreasing the amount of input precipitation falling as snow and hence increasing the amount of precipitation falling as rain. This effect can be observed for all scenarios where there is a clear increase in wind driven precipitation on the high altitude areas of the Cordillera Blanca towards the eastern side of the catchment which are the same areas where snowfall is projected to decrease. Also, since there is no snowfall on the ridges of the Cordillera Negra, no spatially explicit increase in wind driven precipitation can be observed.

The projected decrease in precipitation under the A1B 24 - SD scenario can be observed in the valley towards the lower end of the catchment (figure 7.7). It can be observed that some of the highest areas in the Cordillera Blanca see a decrease in wind driven precipitation even though surrounding ridges experience a marked increase. Increased snow fall in those areas is responsible for the increase. Since temperature at these high altitudes does not drop below 0°C, even under the climate change scenario, increases in input precipitation will lead to more snowfall while at lower altitudes, precipitation falling as snow under the baseline now falls as rain.

Mean AET changes are positive for all scenarios which is also expected since temperature is projected to increase which changes vapour pressure and in turn potential evapo-transpiration. Since there are no changes in vegetated land cover (the MODIS VCF fractions), the LAI remains the same and hence actual evapo-transpiration will increase with increasing temperature. There are however considerable spatial variations in AET changes, with decreases for all scenarios around the edge of the catchment and increases in the lower parts of the catchment in the valleys. The spatial variation in AET can be explained by the smoothing interpolation applied to the GCM temperature grids that have less spatial variation than the baseline WorldClim temperature grids which leads to shifts in magnitude and direction of changes and thus spatial variation in these changes even though the mean annual change is positive for the catchment.

Mean fog deposition changes are limited for all scenarios with the A2A 17 + SD scenario showing the greatest change with -2 mm/yr with baseline fog inputs around 15 mm/yr. Changes in fog deposition are the result of changes in lifting condensation level as a result of the changes in temperature which results in more capture on exposed ridges in the band between the former and new lifting condensation levels while a decrease in fog interception occurs as a result of a rise in the cloud base level. This is particularly clear for the A1B 24 GCM scenarios (figures 7.5-7.7) where a clear

increase on some ridges of the Cordillera Blanca and localised decreases in the Cordillera Negra can be observed.

Table 7.4 shows the annual changes in melt water production, snow fall and mean snow pack water equivalent for all scenarios. As observed in figures 7.5 to 7.12, there is a mean annual decrease in melt water production for all scenarios. Due to increased temperatures, higher snow melt is expected in some areas, however a decrease in annual melt is observed which is the result of increased temperature leading to decreased snowfall and more precipitation falling as rain instead. The increase in temperature means there is a larger area where snowmelt can take place but since there is a decrease in snow fall, there is less snow to melt during the warmer periods of the year. Mean annual snow pack shows a slight increase over the catchment for the A1B 24 and A1B 24 + SD scenarios and a slight decrease for all other scenarios because the changes in melting and in snowfall balance out. Increase in mean snowpack is the result of strong localised increases in snow fall as can be observed for instance in figure 7.16 where some of the highest peaks and glaciers receive considerably more snow fall in the wet season. However, most areas in the Cordillera Blanca see a reduction in the snow pack. A decrease in snow pack as a result of climate change has already been observed in the area with Racoviteanu *et al.,* (2008) describing the decrease of glaciers in the Cordillera Blanca with -0.68% per year over the period 1970-2003. While melting of the glaciers can add to the water balance in the short term, it also carries with it increased risks of longer term water shortage and so called glacial lake outburst floods or GLOFS. Indeed, in 2010 extensive flooding was caused by such a lake flood in the Santa basin which destroyed at least 50 homes (McKinney, 2011). Since melt water production in the model combined melt from fresh snow fall as well as glacial melt, the magnitude of glacial melt cannot be established since the reduction in melt seen is mostly attributable to reductions in snow fall. This means that reductions in snowmelt are as much a function of changes in precipitation as they are of changes in temperature. Since changes in precipitation as a result of

climate change in this area are highly uncertain, (Buytaert *et al.,* 2010), the resulting impacts on changes in melt water are also highly uncertain.

Water balance changes are dominated by changes in wind-driven rainfall and show an increase for all scenarios with the exception of the lower end of projection scenario A1B 24 - SD as this scenario projects a decrease in input precipitation. Combined with increases in AET and decreases in melt water this results in a overall decrease in water balance. All other scenarios show overall increases in water balance with some localised decreases which can be explained by a decrease in snow melt for those areas.

Table 7.3 Annual changes from the WorldClim baseline for wind driven precipitation, actual evapo-transpiration, fog deposition, snow fall, melt water production and water balance under the climate change scenarios as mean values for the dam catchment

	Wind driven precipitation change				AET change				Fog deposition change				Melt water change				Water balance change			
Scenario	**Mean**	**Min**	**Max**	**SD**	**Mean**	**Min**	**Max**	**SD**	**Mean**	**Min**	**Max**	**SD**	**Mean**	**Min**	**Max**	**SD**	**Mean**	**Min**	**Max**	**SD**
A1B 24	220	-893	1279	246	9	-47	76	14	0	-14	12	3	-50	-1496	382	143	83	-482	510	80
A1B 24 - SD	-21	-893	909	242	7	-53	71	14	0	-13	12	3	-50	-1496	409	144	-164	-738	203	84
A1B 24 + SD	469	-892	1648	257	12	-41	82	13	0	-14	11	3	-52	-1496	327	143	900	255	2700	255
A2A 17	211	-270	1067	181	10	-7	8	1	0	-7	8	1	-36	-892	462	92	111	-199	456	48
A2A 17 - SD	28	-556	885	167	5	-104	52	18	0	-7	9	1	-43	-1059	633	102	-72	-430	192	41
A2A 17 + SD	420	0	1411	219	15	-84	74	16	-2	-9	6	2	-36	-808	532	89	293	5	723	71
A1B 5	157	-357	1047	201	11	-94	62	17	0	-7	8	2	-42	-951	478	100	35	-313	380	50
A2A 5	185	-357	1077	186	10	-96	60	17	0	-7	9	2	-38	-942	600	96	80	-255	441	51

Table 7.4 Annual changes from the WorldClim baseline for melt water production, snowfall and snow pack water equivalent under the climate change scenarios as mean values for the Cañón del Pato dam catchment (mm)

	Melt water production				**Snowfall**				**Snow pack**			
Scenario	**Mean**	**Min**	**Max**	**SD**	**Mean**	**Min**	**Max**	**SD**	**Mean**	**Min**	**max**	**SD**
A1B 24	-50.14	-1495.7	382.2	143.2	-50.2	-1541.2	402.9	139.2	0.76	-140.1	798.8	56.3
A1B 24 + SD	-50.2	-1495.7	409.3	144.3	-50	-1541.2	433.6	139.4	1.8	-140.1	798.9	58.5
A1B 24 - SD	-52.0	-1495.7	327.4	142.5	-52.4	-1541.2	331.6	139.5	-0.61	-140.1	800.9	53.7
A2A 17	-36.4	-891.8	461.5	92.3	-37.6	-900.8	470.1	92.9	-2.7	-95.7	350.9	19.4
A2A 17 + SD	-43.3	-1058.5	632.6	102.3	-43.8	-976.8	645.9	99.8	-1.2	-89.1	628.6	34.2
A2A 17 - SD	-36.2	-808.4	532.4	89.1	-37.4	-840.3	537.5	90.5	-4.1	-103.3	206.3	14.3
A1B 5	-42.1	-951.3	477.9	100.3	-43.4	-959.5	484.6	101.2	-3.8	-111.7	414.8	20.5
A2A 5	-37.7	-941.7	599.5	95.5	-38.8	-952.8	607.9	96.1	-3.1	-110.5	351.9	18.9

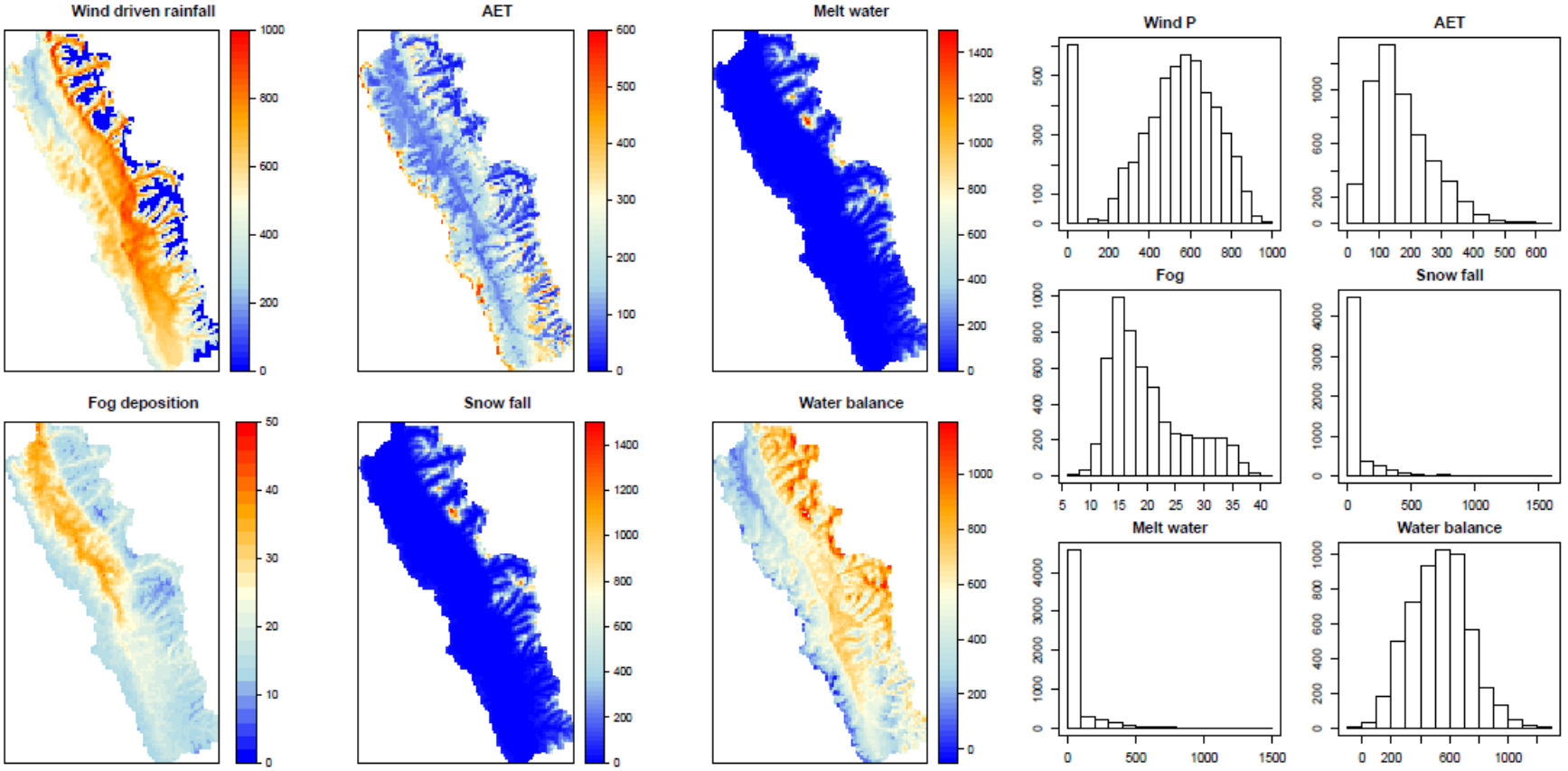

Figure 7.4 Annual wind driven rainfall, actual evapo-transpiration, melt water production, fog deposition, snow fall and water balance for the baseline (WorldClim) simulation for the Cañón del Pato HEP catchment.

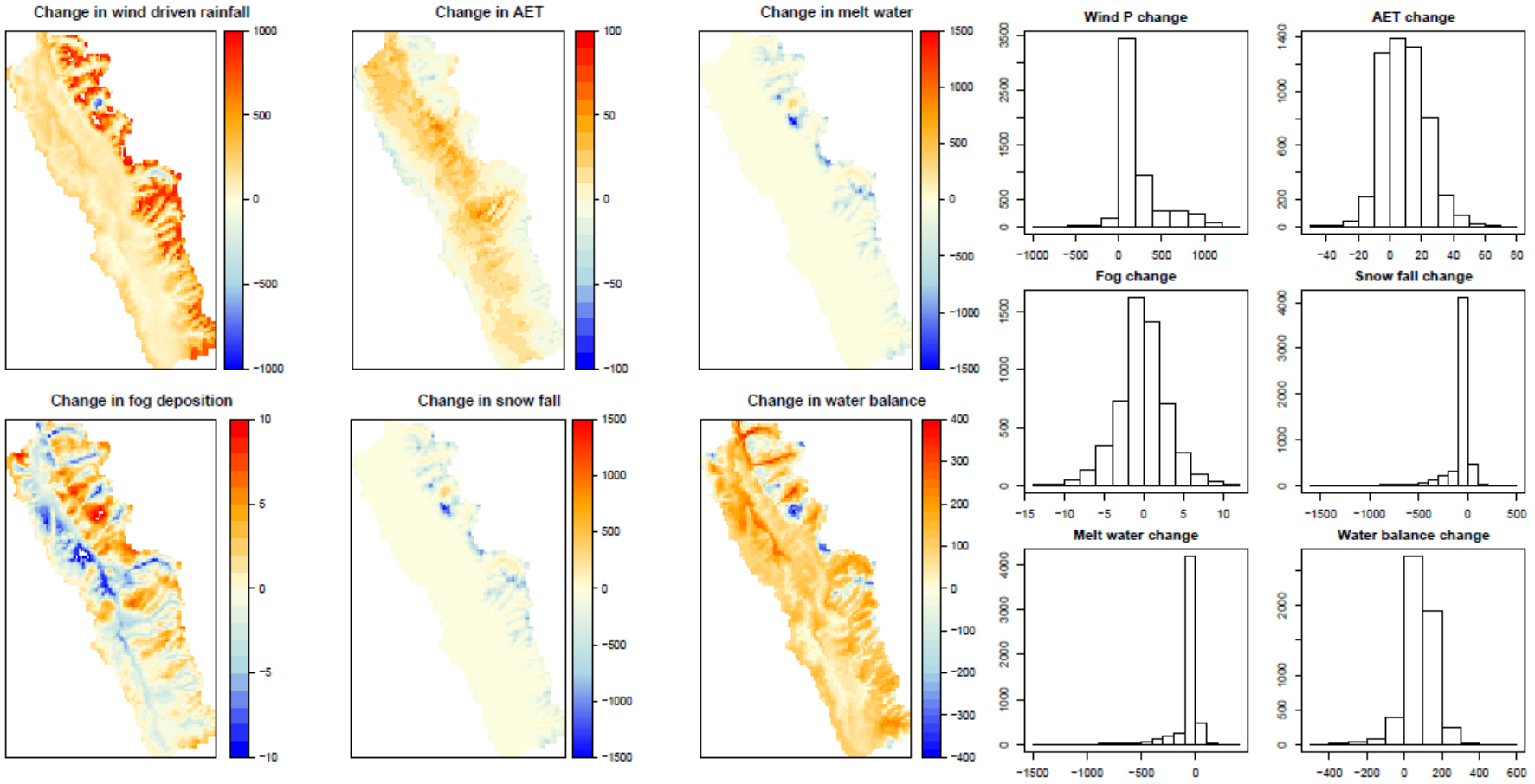

Figure 7.5 Annual projected changes from the WorldClim baseline for wind driven rainfall, actual evapo-transpiration, melt water production, fog deposition, snow fall and water balance under the A1B 24 GCM scenario for the 2050s for the Cañón del Pato catchment.

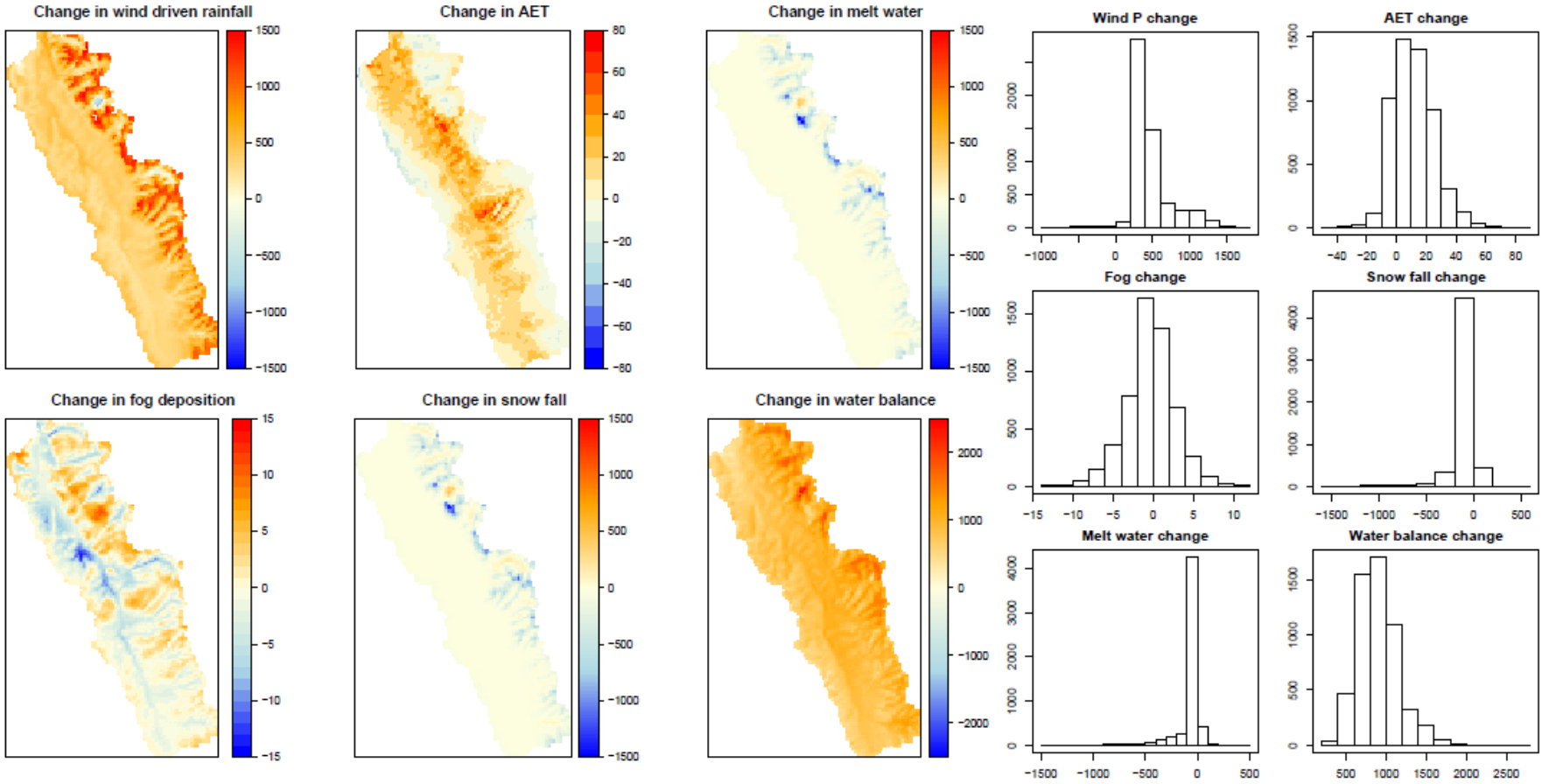

Figure 7.6 Annual projected changes from the WorldClim baseline for wind driven rainfall, actual evapo-transpiration, melt water production, fog deposition, snow fall and water balance under the A1B 24 GCM + SD scenario for the 2050s for the Cañón del Pato HEP catchment.

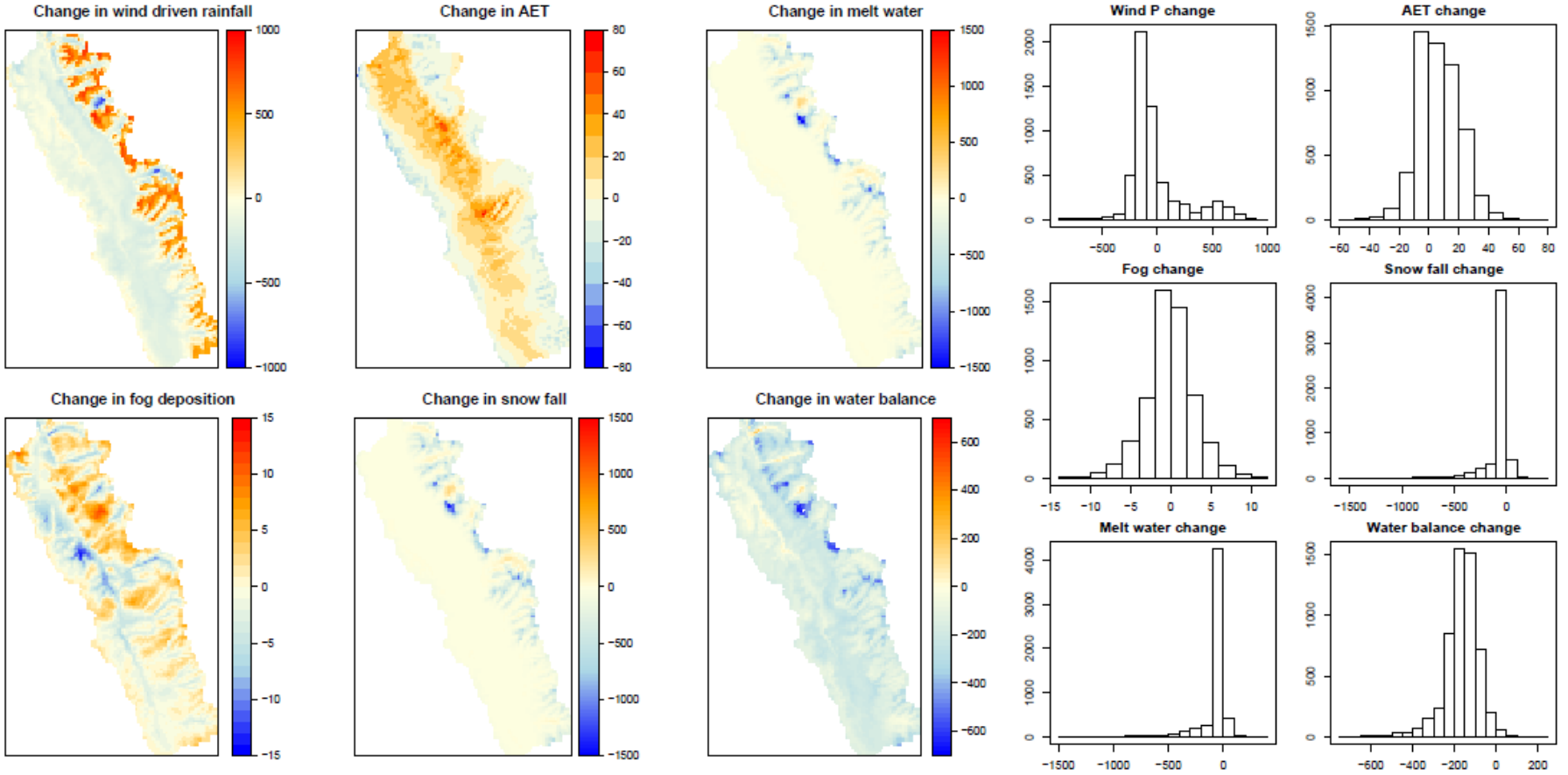

Figure 7.7 Annual projected changes from the WorldClim baseline for wind driven rainfall, actual evapo-transpiration, melt water production, fog deposition, snow flal and water balance under the A1B 24 GCM - SD scenario for the 2050s for the Cañón del Pato HEP catchment.

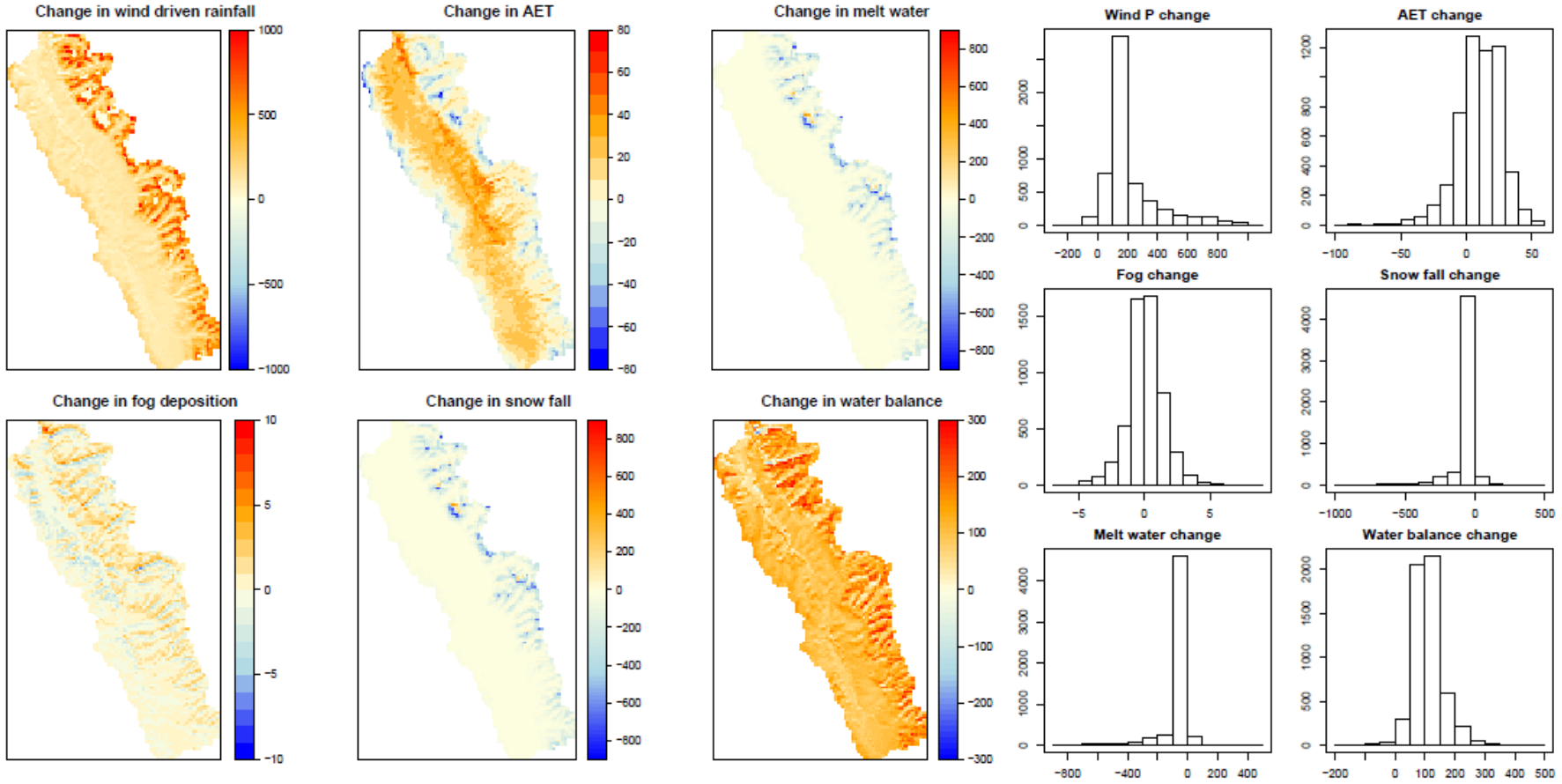

Figure 7.8 Annual projected changes from the WorldClim baseline for wind driven rainfall, actual evapo-transpiration, fog deposition and water balance under the A2A 17 GCM scenario for the 2050s for the Cañón del Pato HEP catchment.

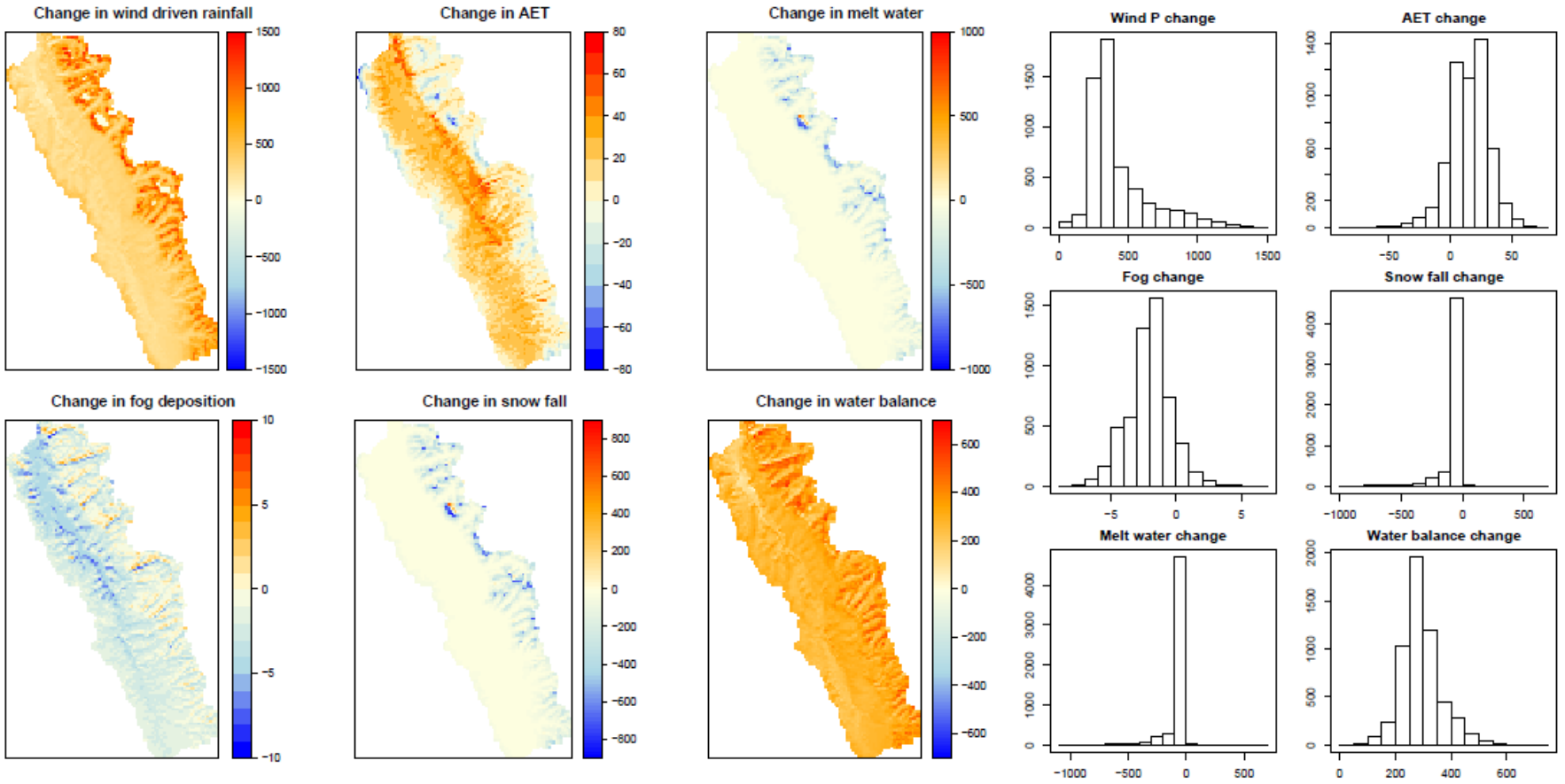

Figure 7.9 Annual projected changes from the WorldClim baseline for wind driven rainfall, actual evapo-transpiration, melt water production, fog deposition, snow fall and water balance under the A2A 17 GCM + SD scenario for the 2050s for the Cañón del Pato HEP catchment.

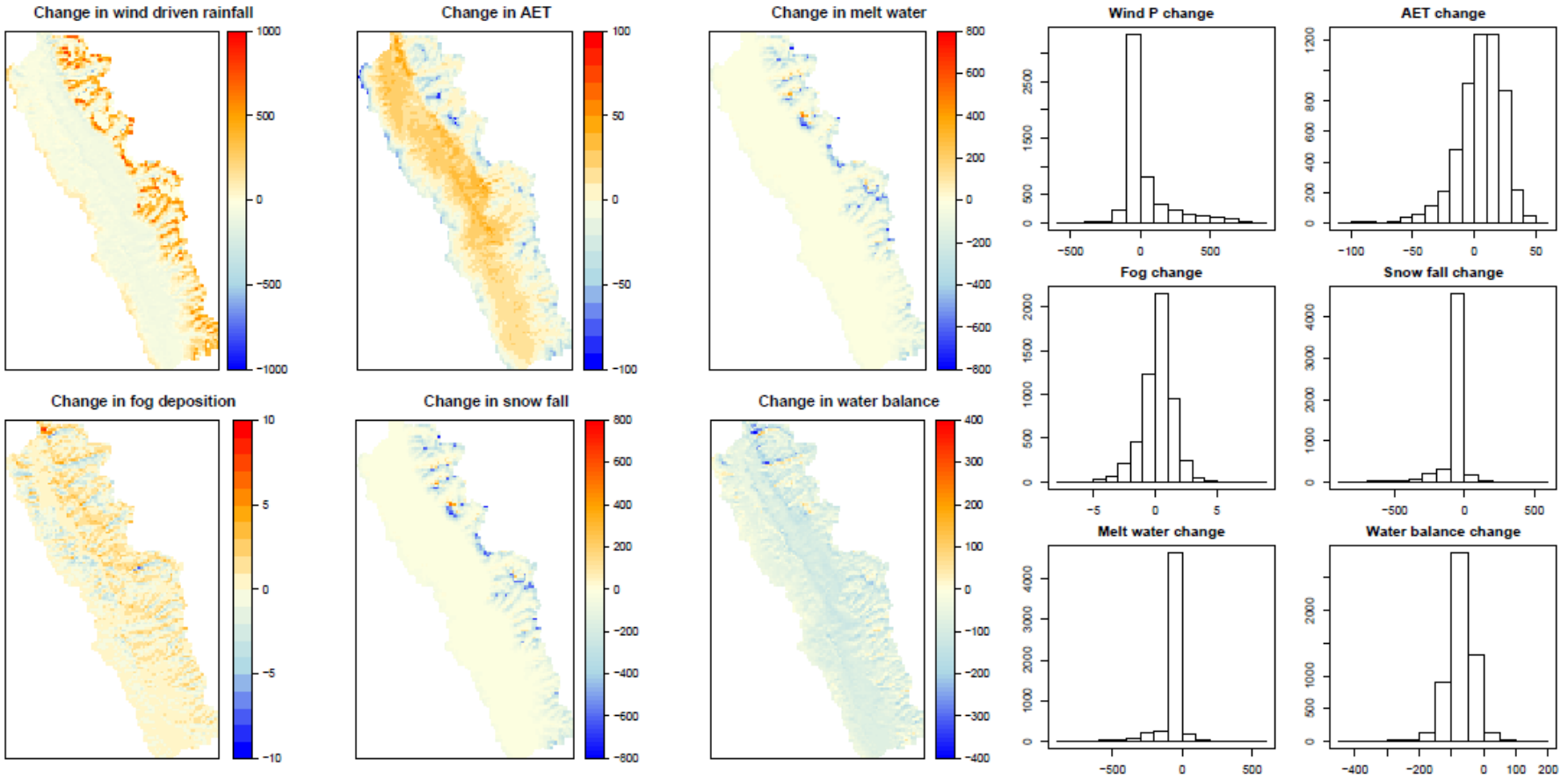

Figure 7.10 Annual projected changes from the WorldClim baseline for wind driven rainfall, actual evapo-transpiration, melt water production, fog deposition, snow fall and water balance under the A2A 17 GCM - SD scenario for the 2050s for the Cañón del Pato HEP catchment.

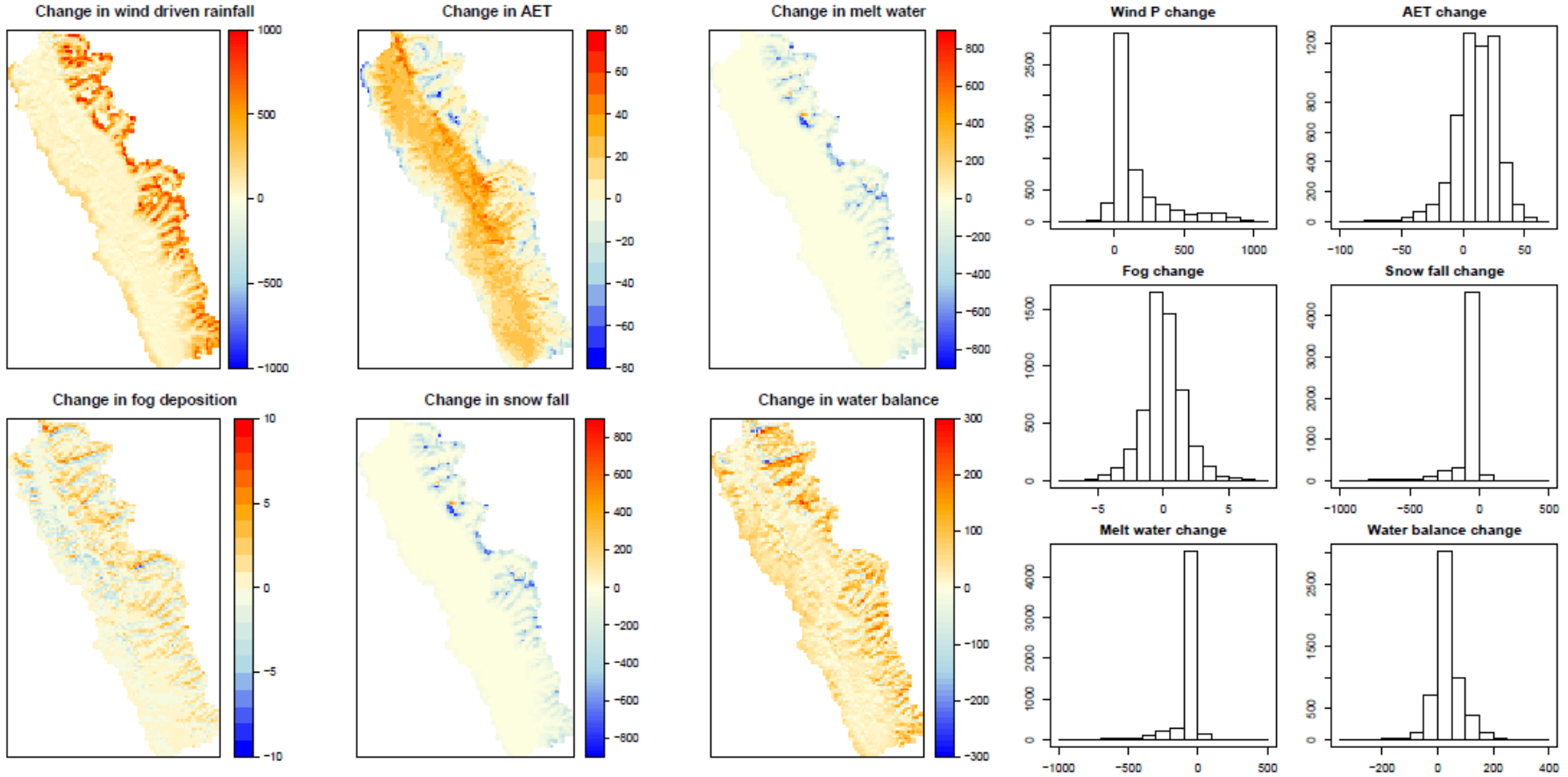

Figure 7.11 Annual projected changes from the WorldClim baseline for wind driven rainfall, actual evapo-transpiration, melt water production, fog deposition, snow fall and water balance under the A1B 5 GCM scenario for the 2050s for the Cañón del Pato HEP catchment.

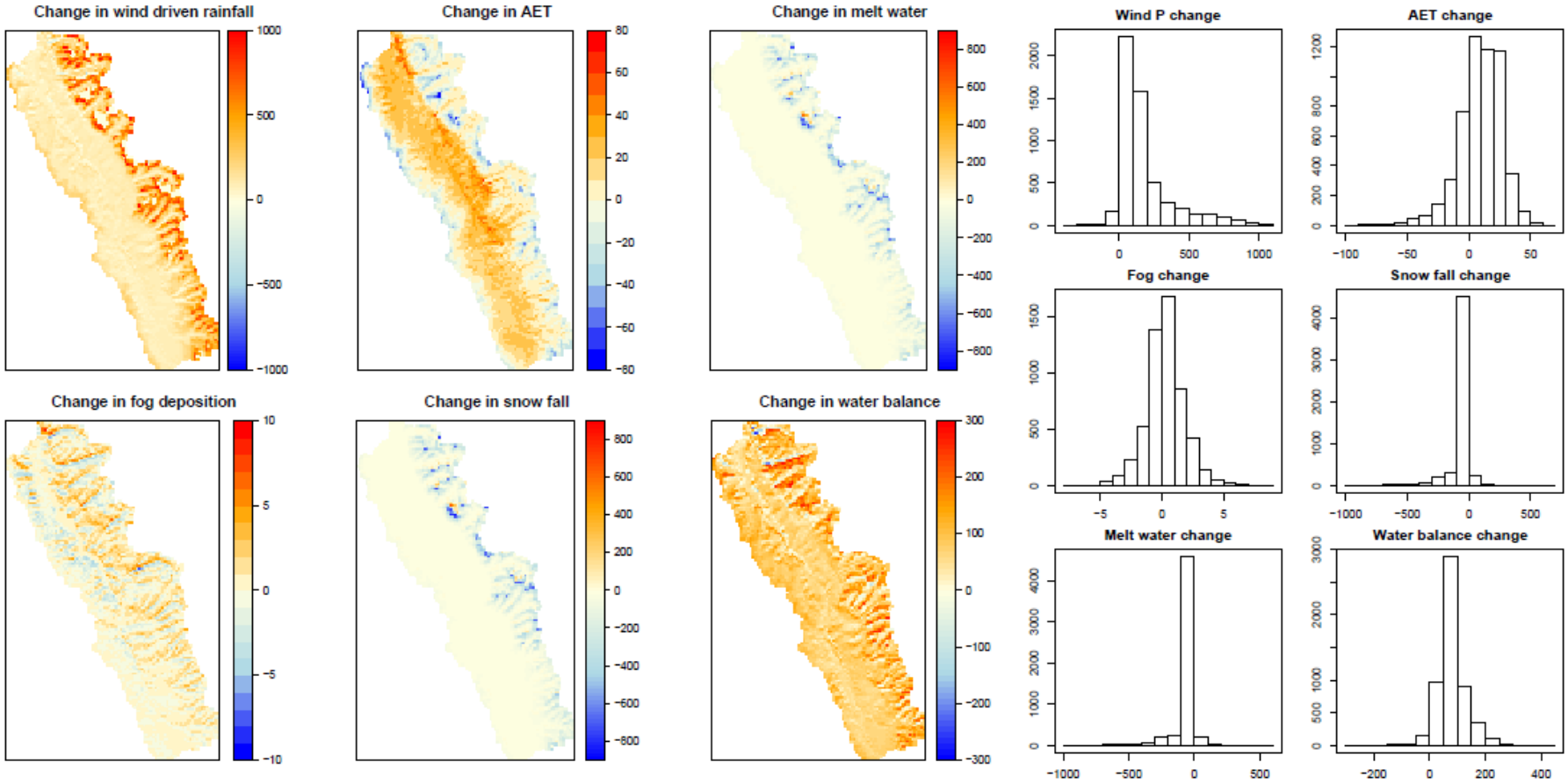

Figure 7.12 Annual projected changes from the WorldClim baseline for wind driven rainfall, actual evapo-transpiration, melt water production, fog deposition, snow fall and water balance under the A2A 5 GCM scenario for the 2050s for the Cañón del Pato HEP catchment.

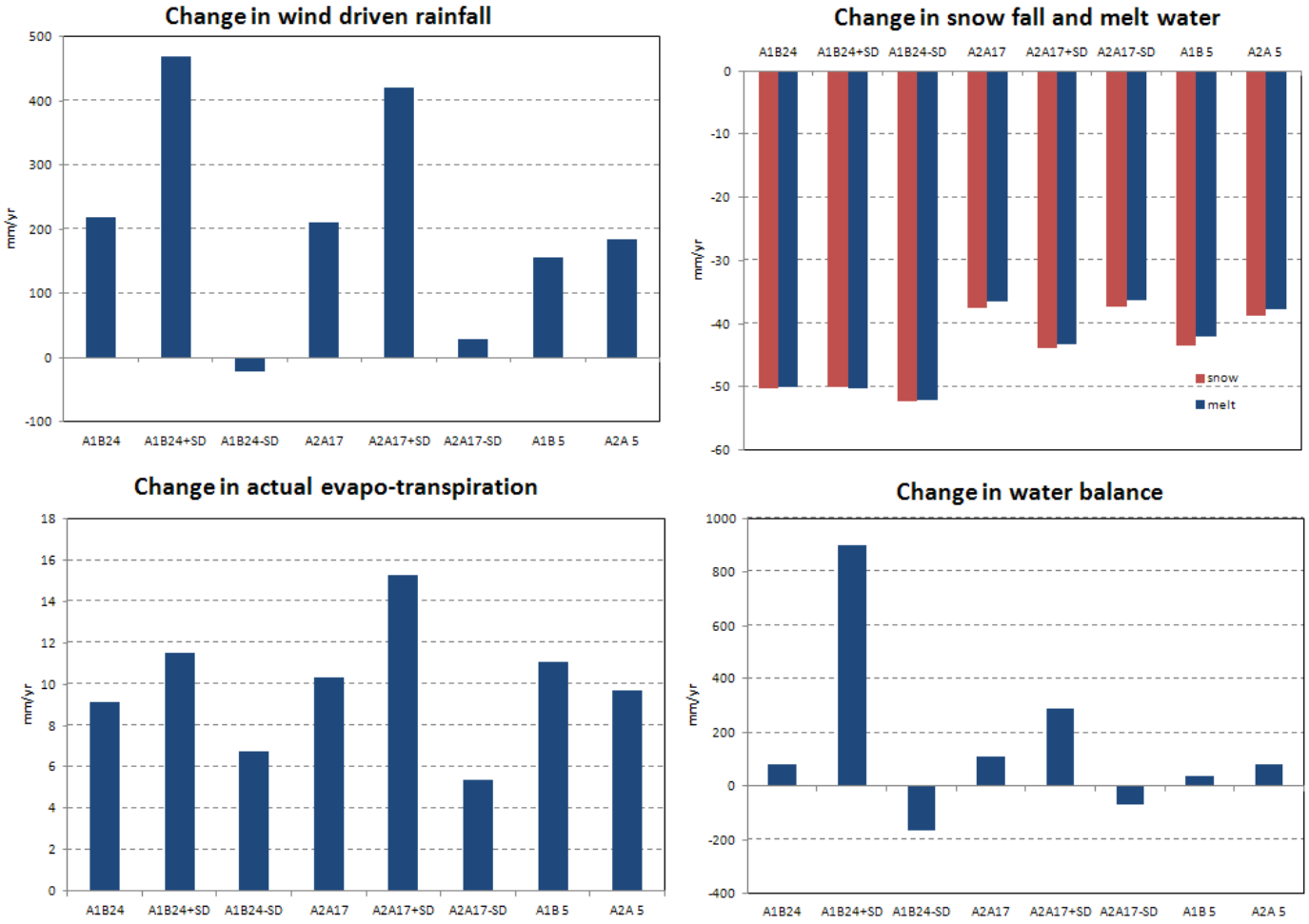

Figure 7.13 Mean annual catchment wide changes from the WorldClim climatology baseline for wind driven rainfall, evapo-transpiration, snowfall, melt water production and water balance for Cañón del Pato HEP catchment for all eight climate change scenarios.

7.4.1.1. Seasonal changes

To assess the magnitude of the contribution of melt water to the total water balance throughout the year, wind driven rainfall, actual evapo-transpiration and melt water production are averaged over the catchment for every month for every scenario. Under the baseline, total melt water contribution amounts to 35% of the total annual water balance, surpassing precipitation inputs in the dry season from May to August. Therefore, changes in melt water production can have significant impacts on the water balance, particularly in the dry season. Figure 7.14 shows the mean relative changes over the catchment of wind driven precipitation, evapo-transpiration and melt water production. The contribution of fog to the changes in water balance are minimal as can be seen in table 7.3 and is therefore not included in this analysis.

The results show that changes in evapo-transpiration are minimal compared to changes in precipitation and melt water production. Melt water production shows a decrease for all scenarios in both wet and dry seasons for all A1B scenarios but a slight increase for A2A scenarios in the dry season. This is due to a slight increase in snow fall because of greater precipitation and thus snowpack for these months as can be observed in the monthly plots of snow fall (figures 7.18, 7.20, 7.22, 7.24, 7.26, 7.28, 7.30 and 7.32). For all scenarios, the greatest changes take place in the dry season with sharp increases in precipitation, particularly in June and July. It should be noted however that these are relative changes. Since baseline precipitation in the dry season only amounts to 55 mm or 9% of the annual total, with only 4 mm in June and 3 mm in July, the projected changes in wind driven precipitation do not add significantly to the overall annual water balance but do significantly contribute to water availability in the dry season.

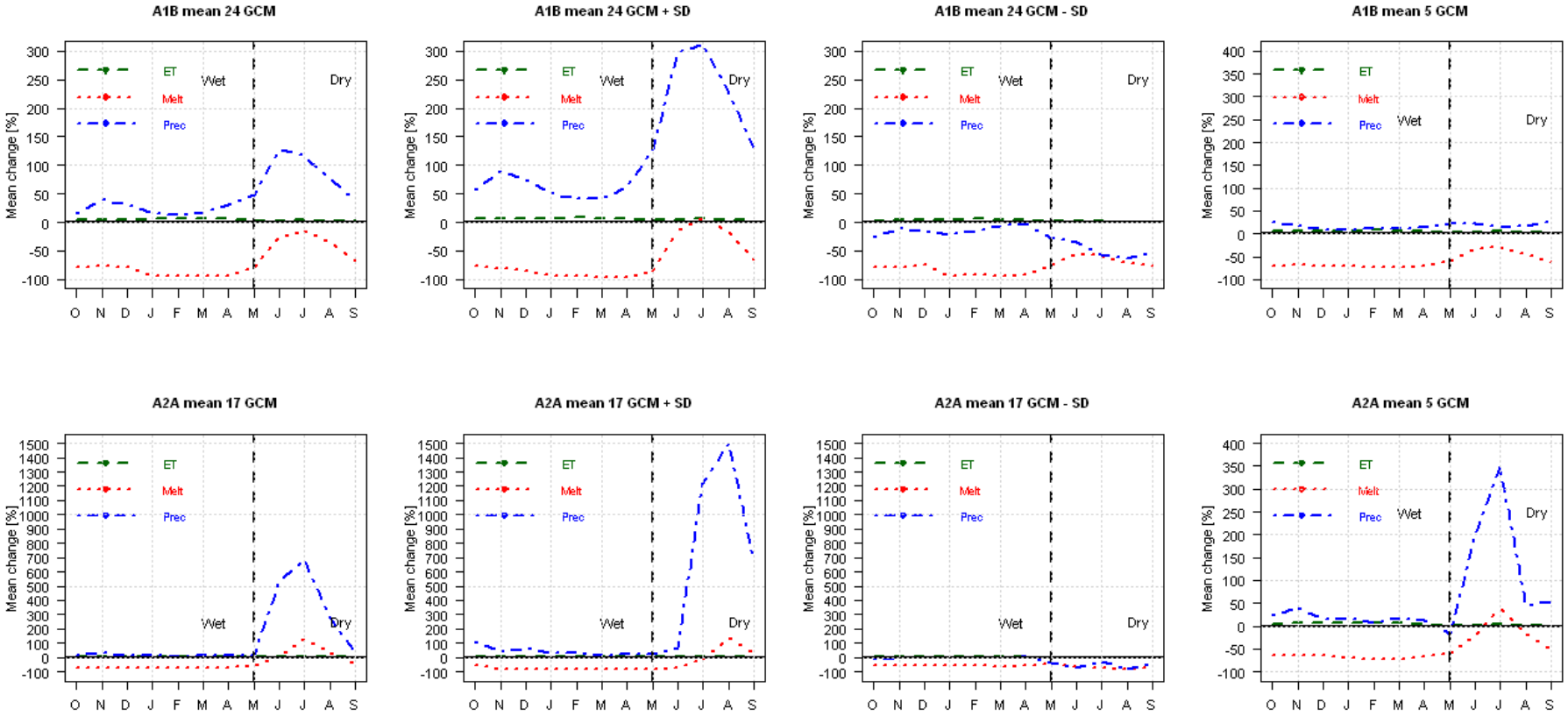

Figure 7.14 Mean relative change from the baseline for actual evapo-transpiration, melt water production and modelled wind driven precipitation for Cañón del Pato HEP catchment for all climate change scenarios

Figures 7.17 to 7.32 show the monthly spatial changes in water balance, melt water production, snow fall and snow pack water equivalent for all scenarios while the monthly spatial results for the baseline are shown in figure 7.15 and 7.16. Mean monthly changes over the Cañón del Pato HEP catchment are summarized in figure 7.33. It can be observed that the greatest changes in water balance take place in the eastern Cordillera Blanca with some areas wetting but most of the mountain range drying in the wet season. This is most likely the result of negative changes in melt water production as discussed in section 7.4.1. and can be observed in the monthly plots of melt water production. In the dry season from May to September, these areas show very little change for the A1B scenarios but are wetting for A2A scenarios, particularly for the A2A 17 GCM scenario as a result of increased rainfall in these months. Spatial changes in the valley are mostly uniform for all scenarios apart from the top north end of the catchment, close to the hydropower facility where changes are minimal.

The spatial distribution of changes in snow fall are very similar for all scenarios with decreases for nearly the full extent of the Cordillera Blanca with the exception of some small high ridges and glaciers discussed earlier where a increase is observed. There are also decreases along the edge for the full length of the western Cordillera Negra. All decreases can be explained by increases in temperature leading to a shift from snow fall to rainfall.

Changes in snow pack water equivalent show a similar spatial distribution as the changes in snow fall with decreases along the whole of the eastern Cordillera Blanca and some localised high altitude areas where increases can be observed.

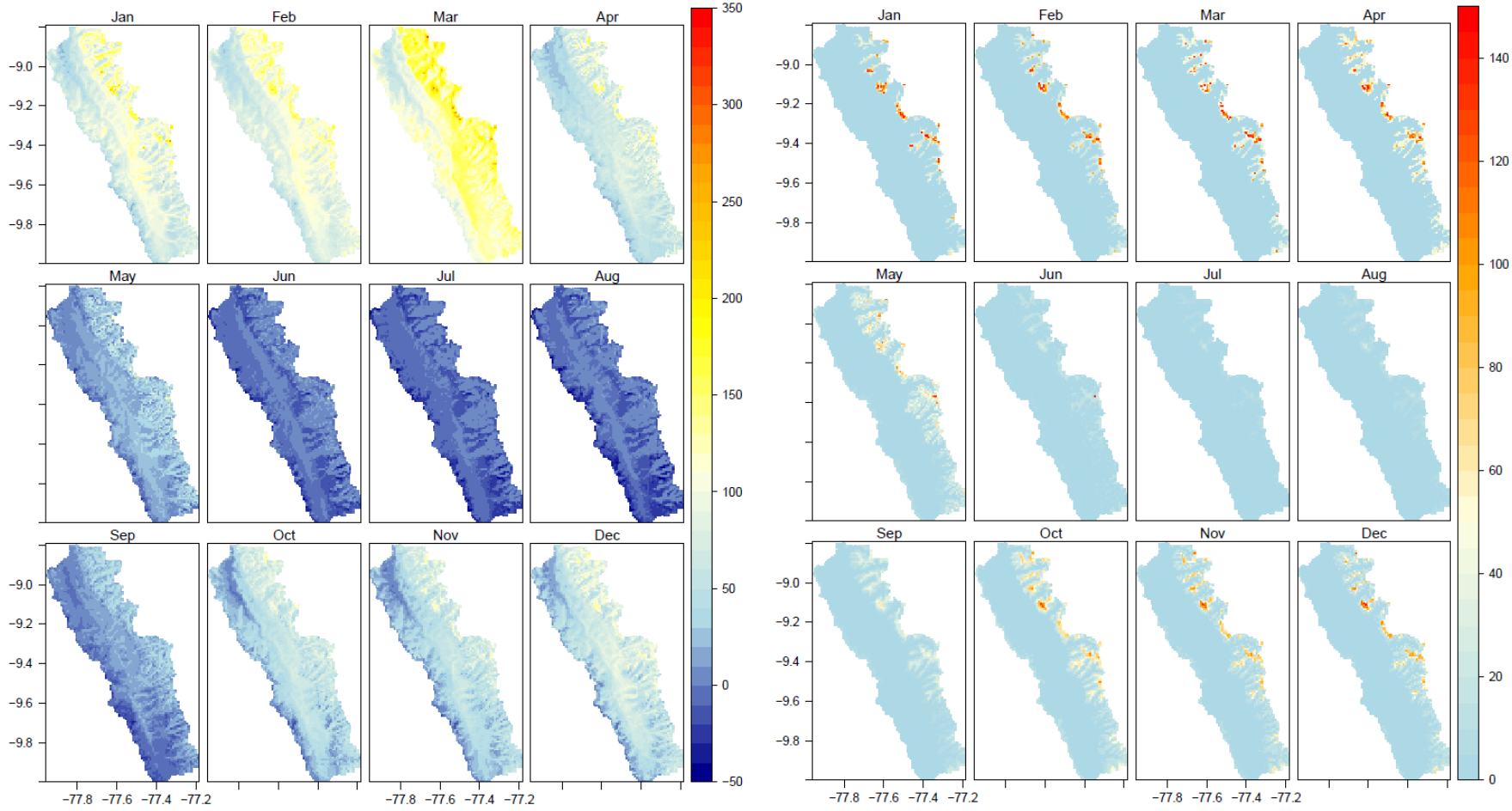

Figure 7.15 Monthly progression of water balance (left) and melt water production (right) in the Cañón del Pato HEP catchment for the WorldClim baseline (mm)

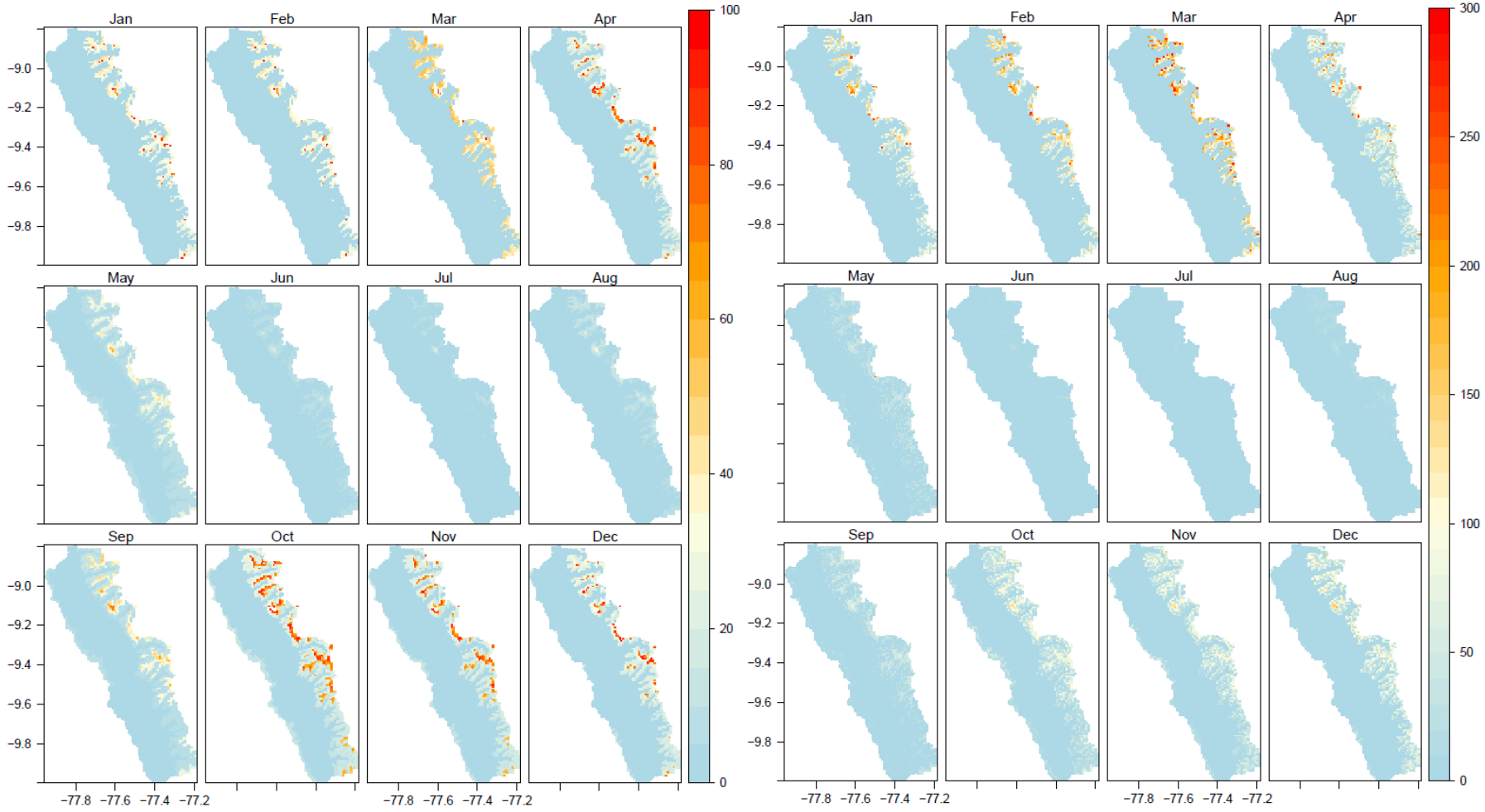

Figure 7.16 Monthly progression of snow fall (left) and mean snow pack water equivalent (right) in the Cañón del Pato HEP catchment for the WorldClim baseline (mm)

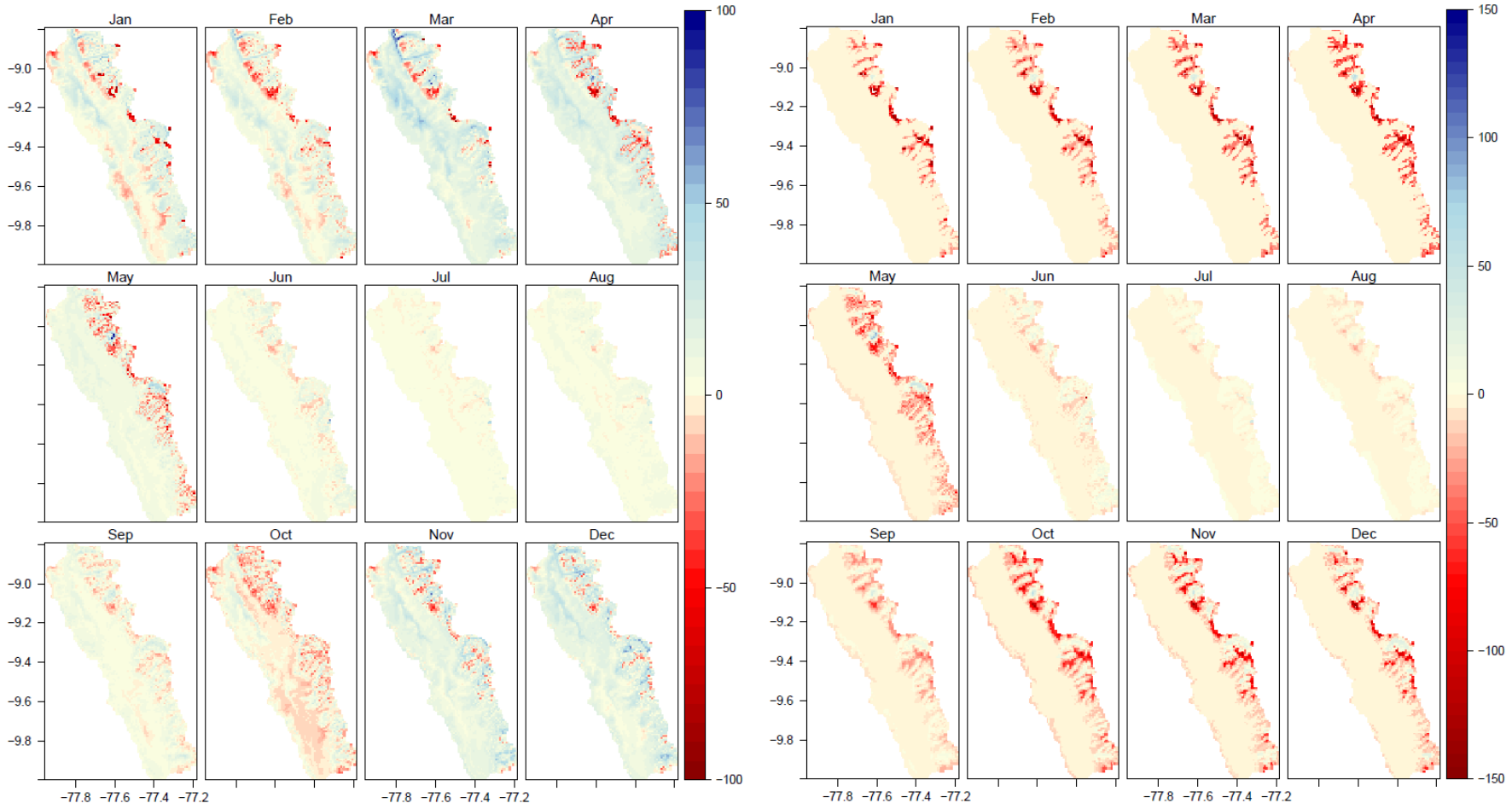

Figure 7.17 Monthly progression of change in water balance (left) and melt water production (right) in the Cañón del Pato HEP catchment under the A1B mean of all models scenario for 24 GCM (mm)

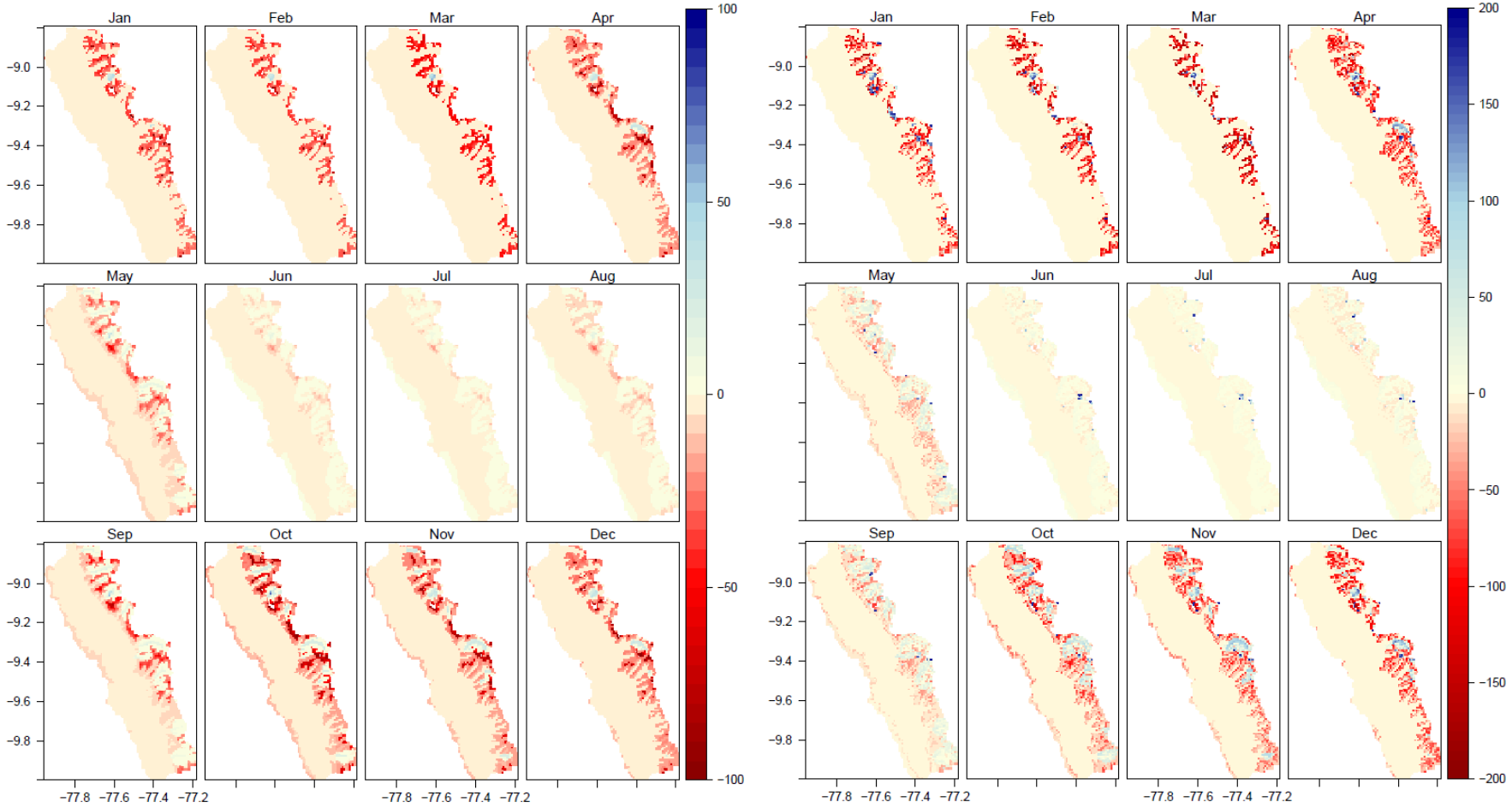

Figure 7.18 Monthly progression of change in snow fall (left) and mean snow pack water equivalent (right) in the Cañón del Pato HEP catchment under the A1B mean of all models scenario for 24 GCM (mm)

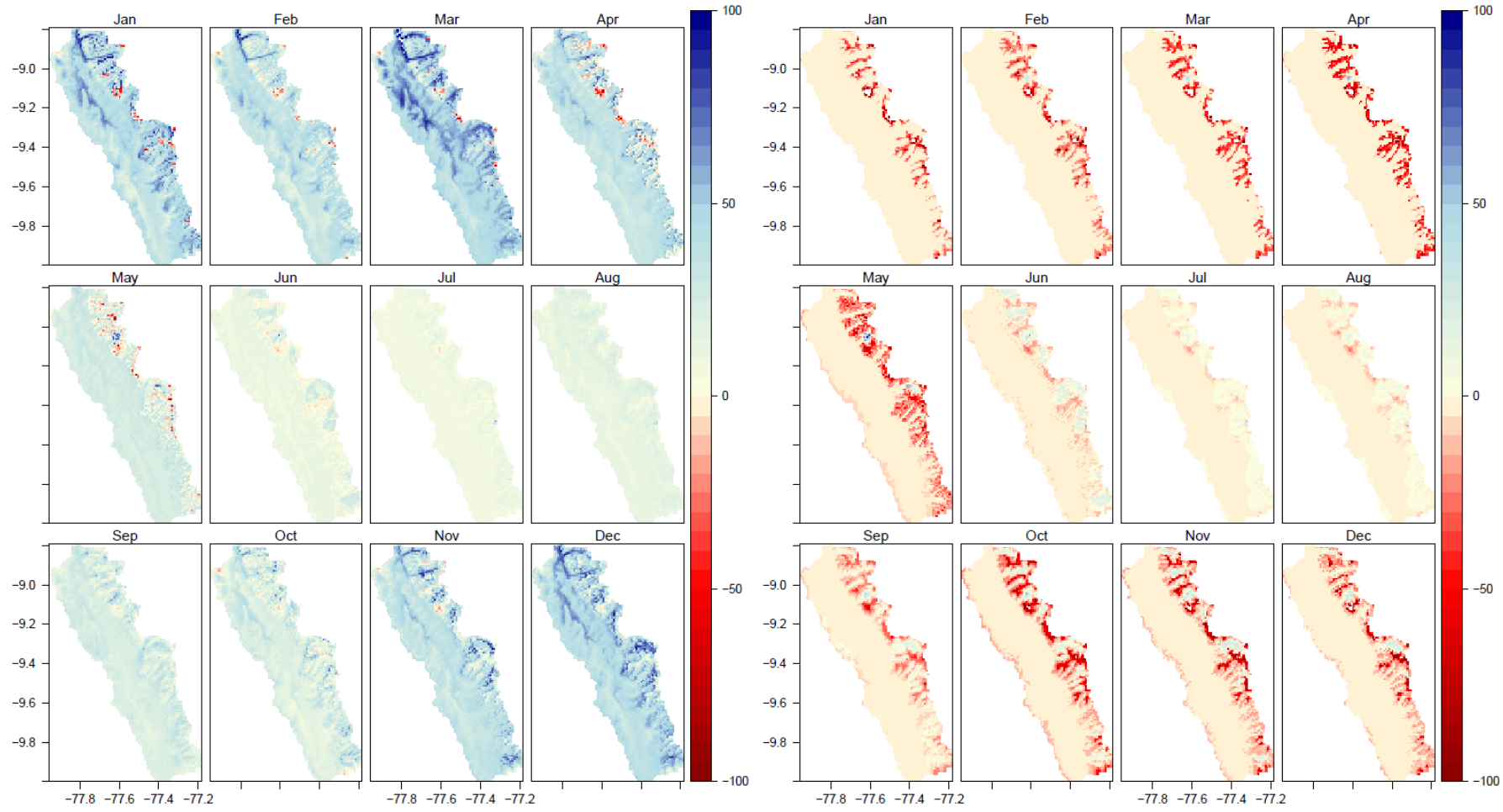

Figure 7.19 Monthly progression of change in water balance (left) and melt water production (right) in the Cañón del Pato HEP catchment under the A1B mean of all models + one SD scenario for 24 GCM (mm)

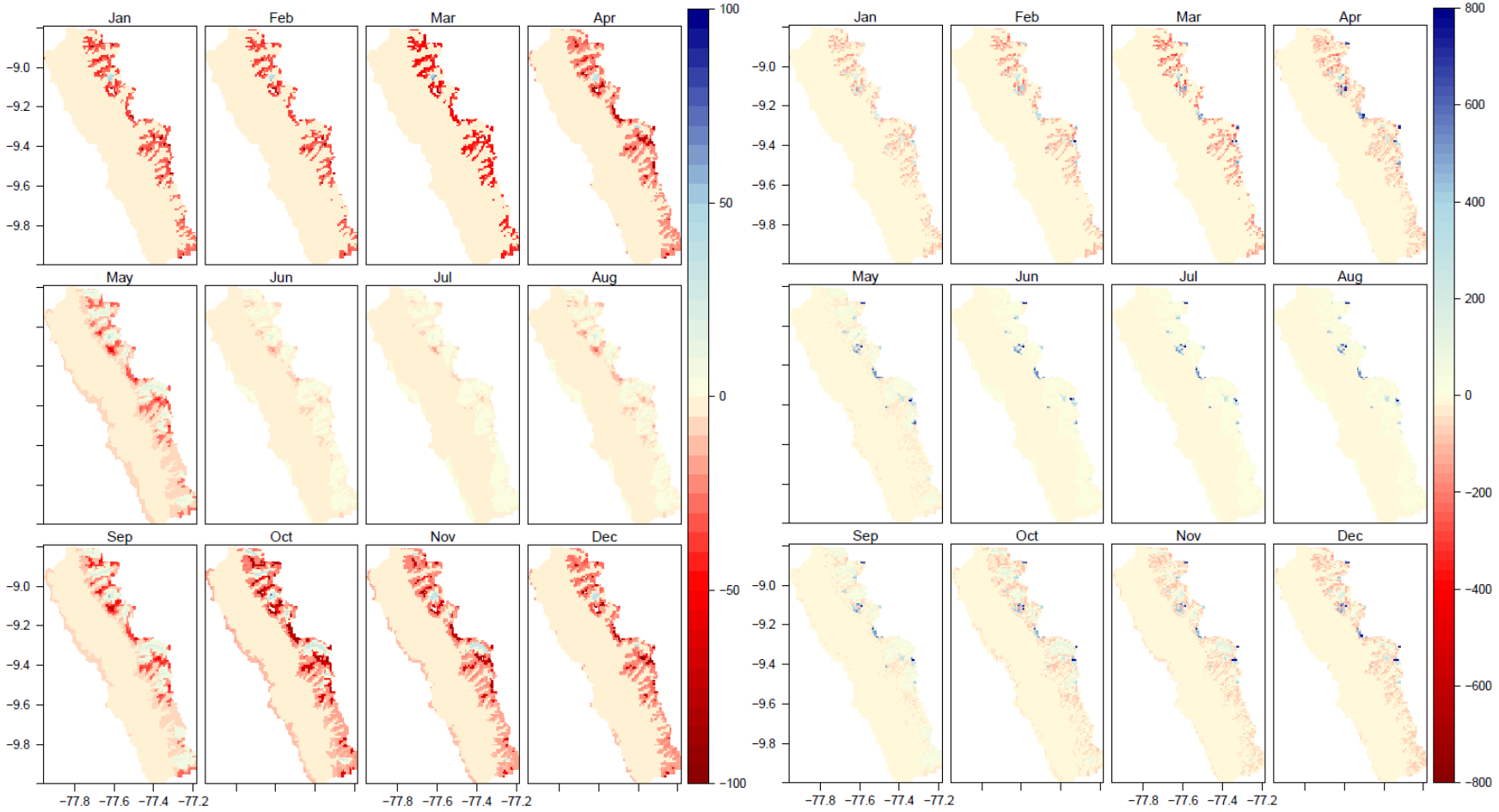

Figure 7.20 Monthly progression of change in snow fall (left) and mean snow pack water equivalent (right) in the Cañón del Pato HEP catchment under the A1B mean of all models scenario + one SD for 24 GCM (mm)

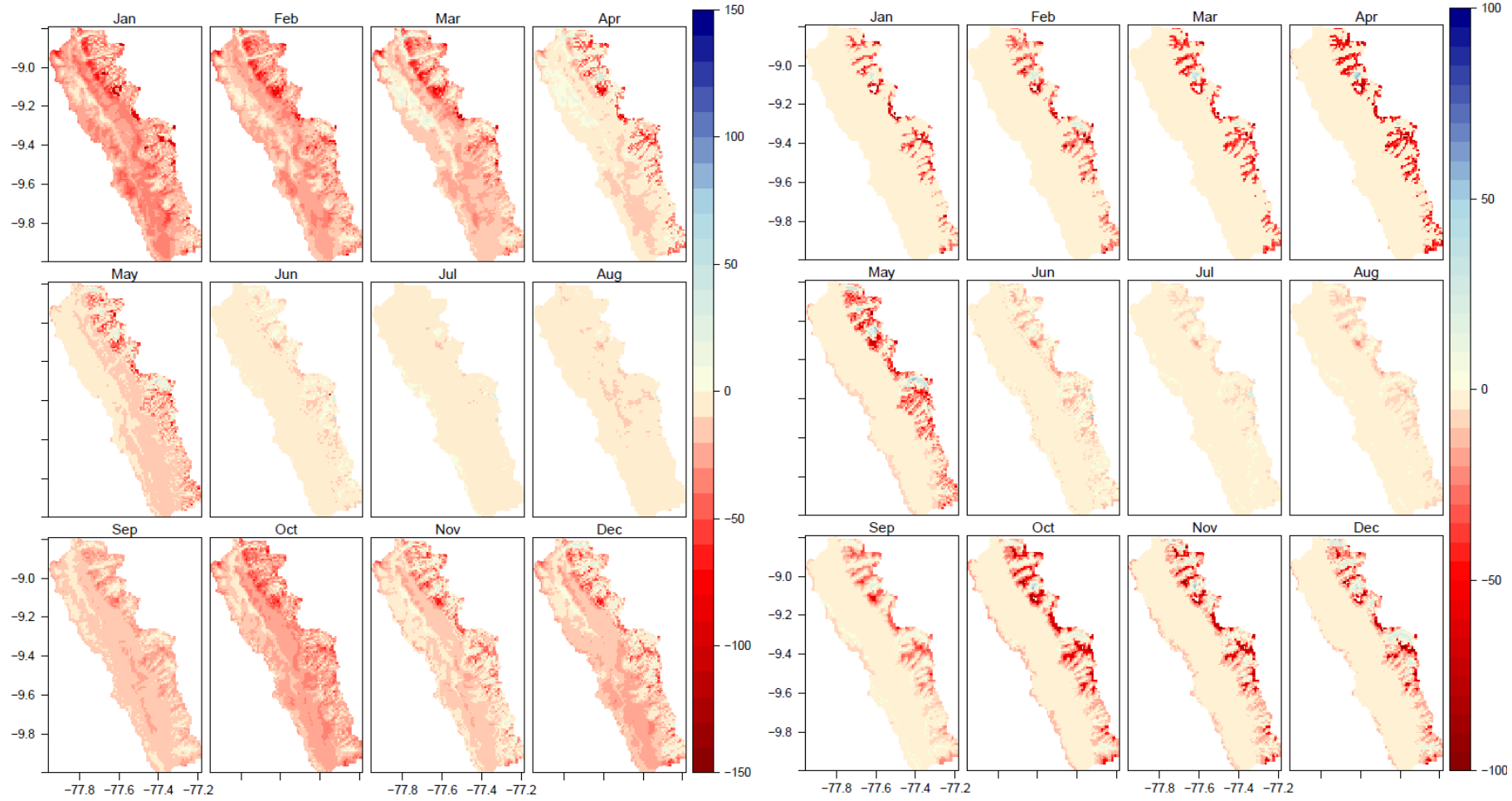

Figure 7.21 Monthly progression of change in water balance (left) and melt water production (right) in the Cañón del Pato HEP catchment under the A1B mean of all models - one SD scenario for 24 GCM (mm)

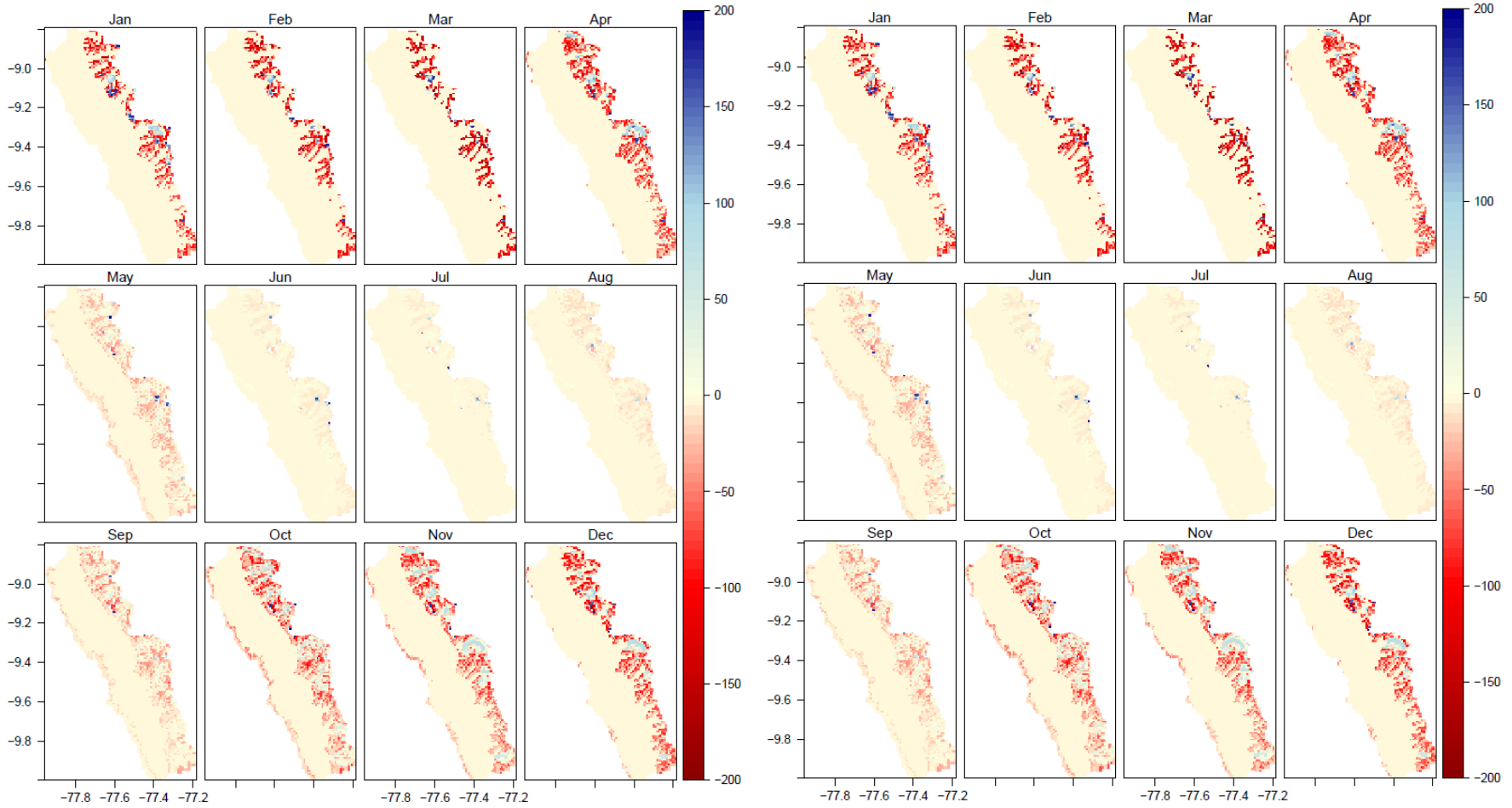

Figure 7.22 Monthly progression of change in snow fall (left) and mean snow pack water equivalent (right) in the Cañón del Pato HEP catchment under the A1B mean of all models scenario - one SD for 24 GCM (mm)

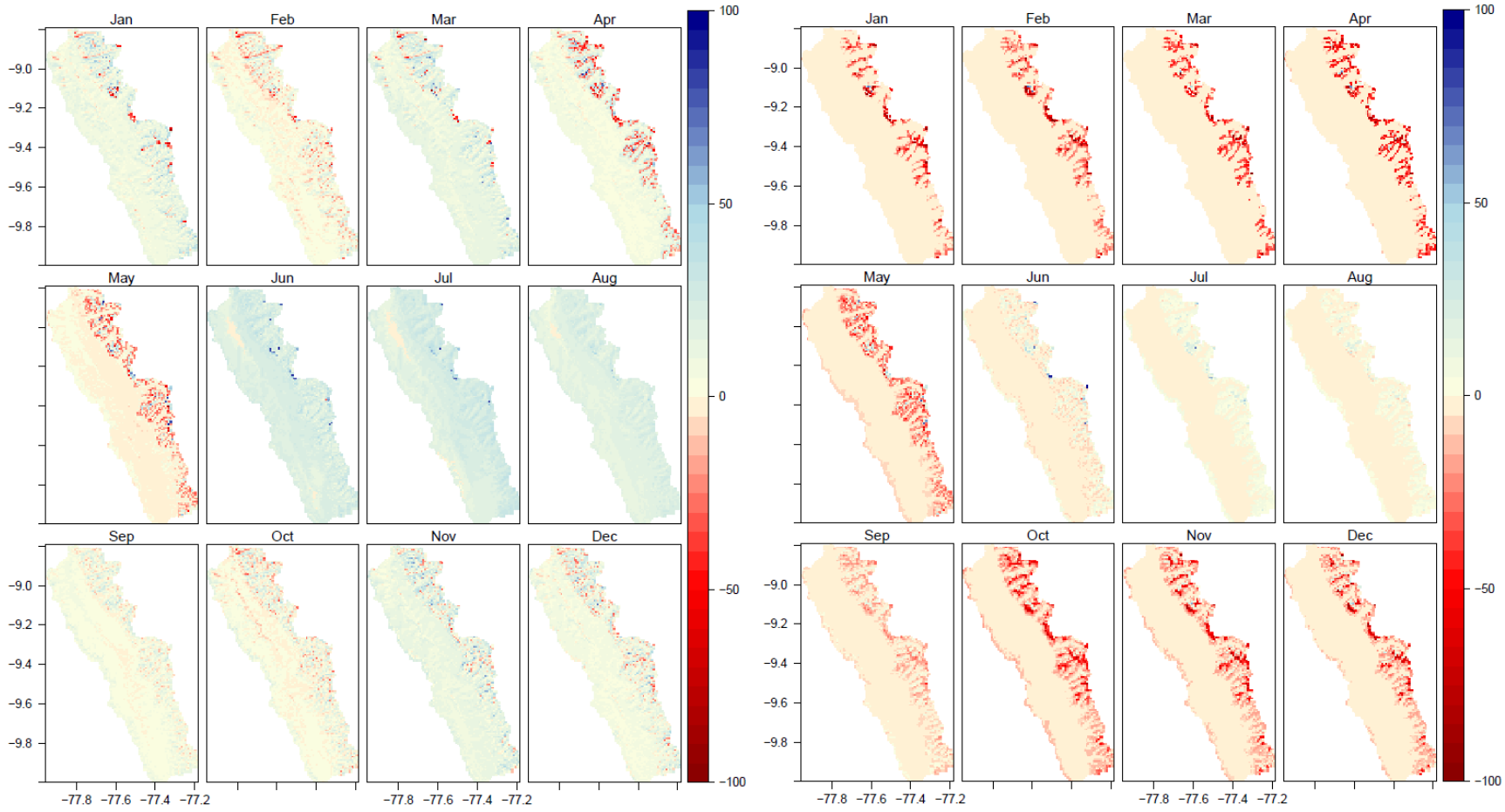

Figure 7.23 Monthly progression of change in water balance (left) and melt water production (right) in the Cañón del Pato HEP catchment under the A2A mean of all models scenario for 17GCM (mm)

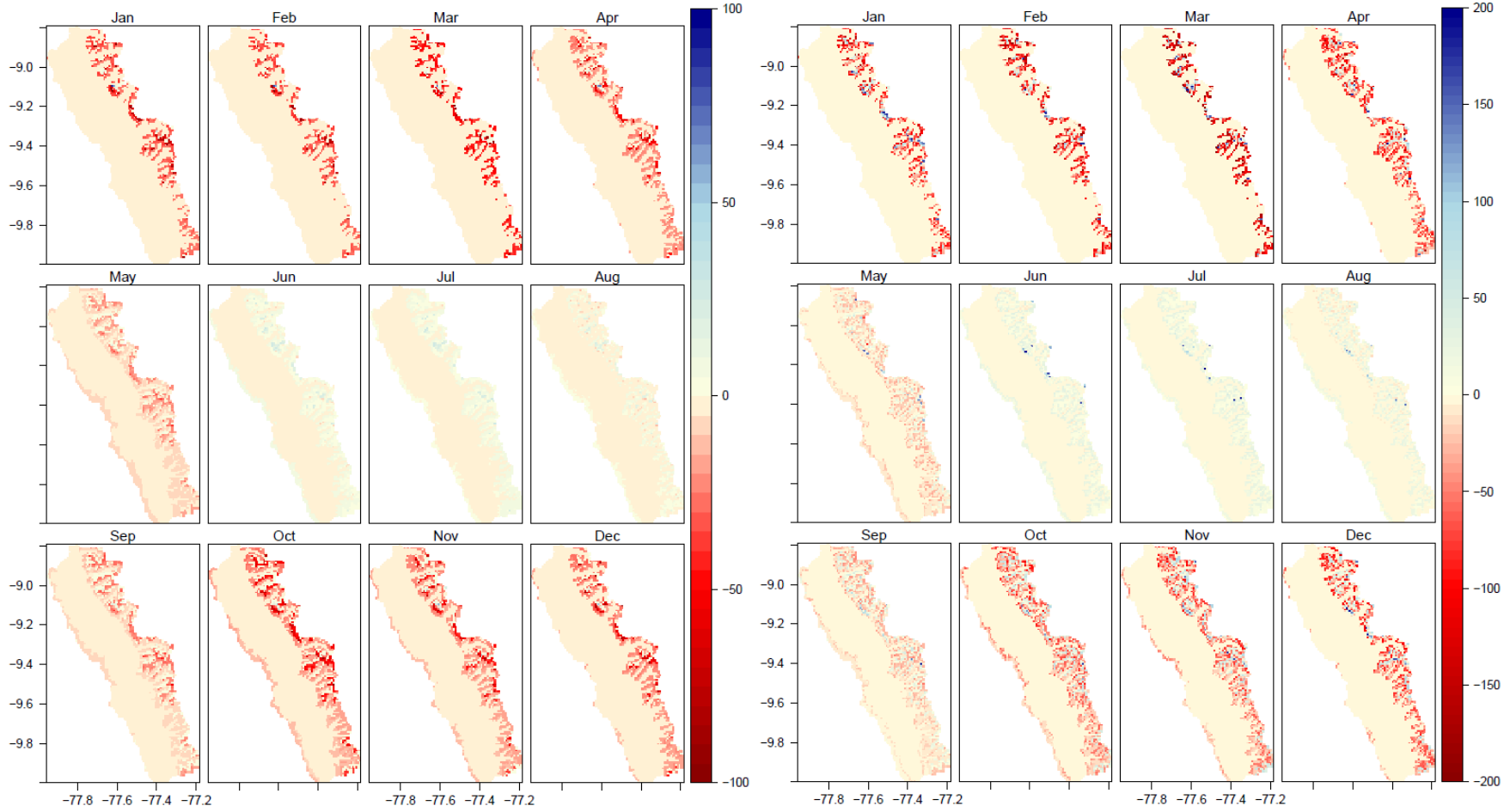

Figure 7.24 Monthly progression of change in snow fall (left) and mean snow pack water equivalent (right) in the Cañón del Pato HEP catchment under the A2A mean of all models scenario for 17GCM (mm)

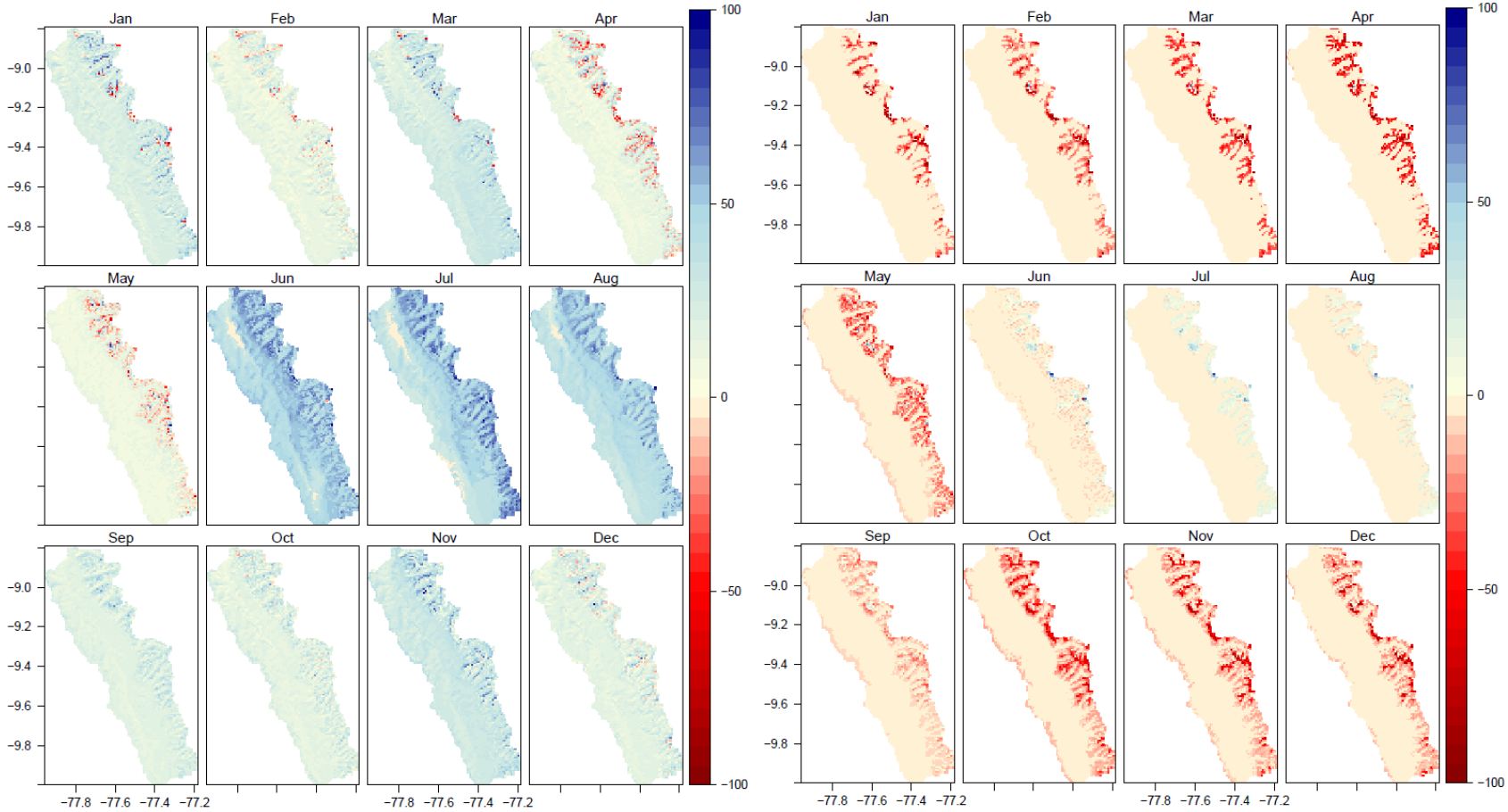

Figure 7.25 Monthly progression of change in water balance (left) and melt water production (right) in the Cañón del Pato HEP catchment under the A2A mean of all models + one SD scenario for 17GCM (mm)

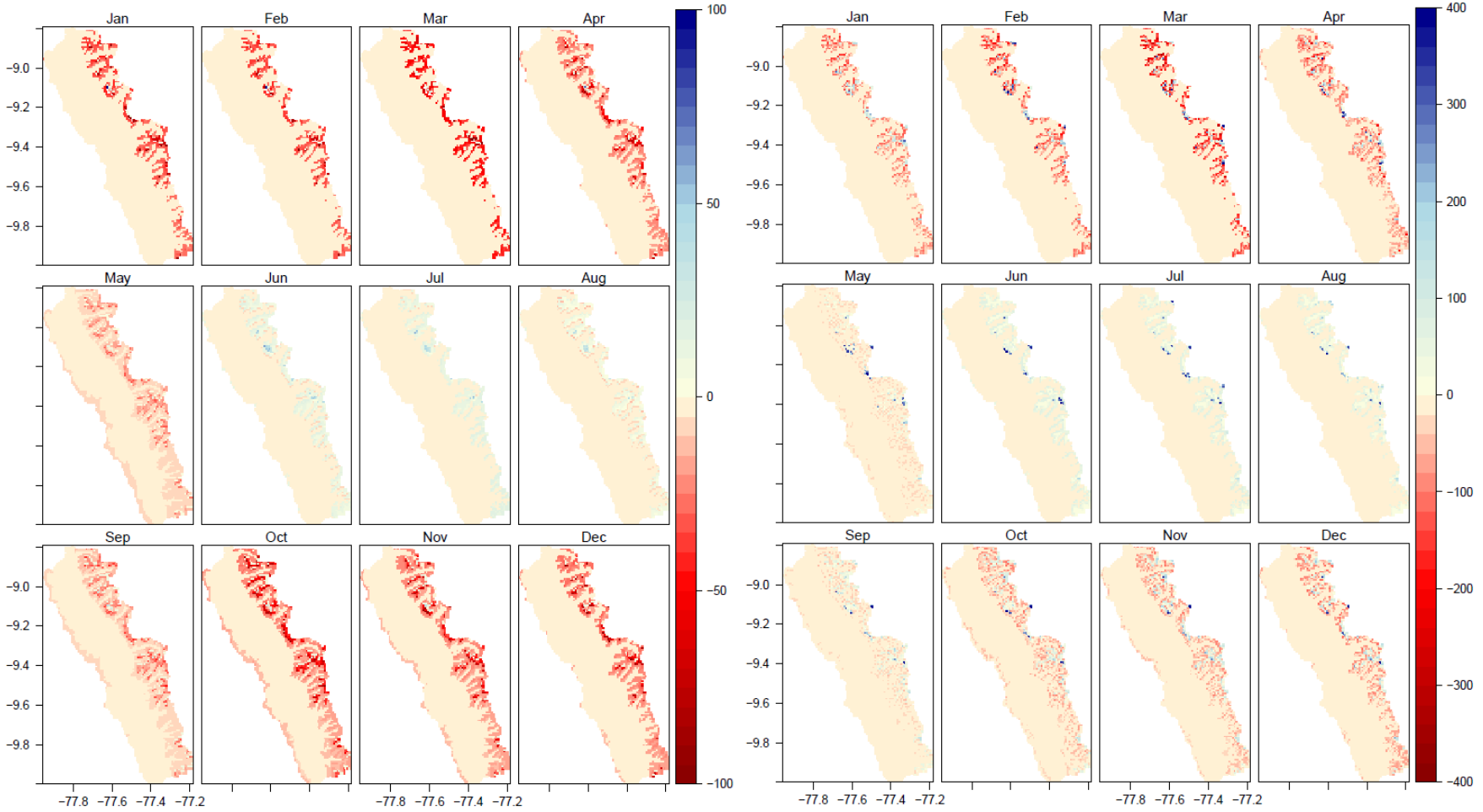

Figure 7.26 Monthly progression of change in snow fall (left) and mean snow pack water equivalent (right) in the Cañón del Pato HEP catchment under the A2A mean of all models + one SD scenario for 17GCM (mm)

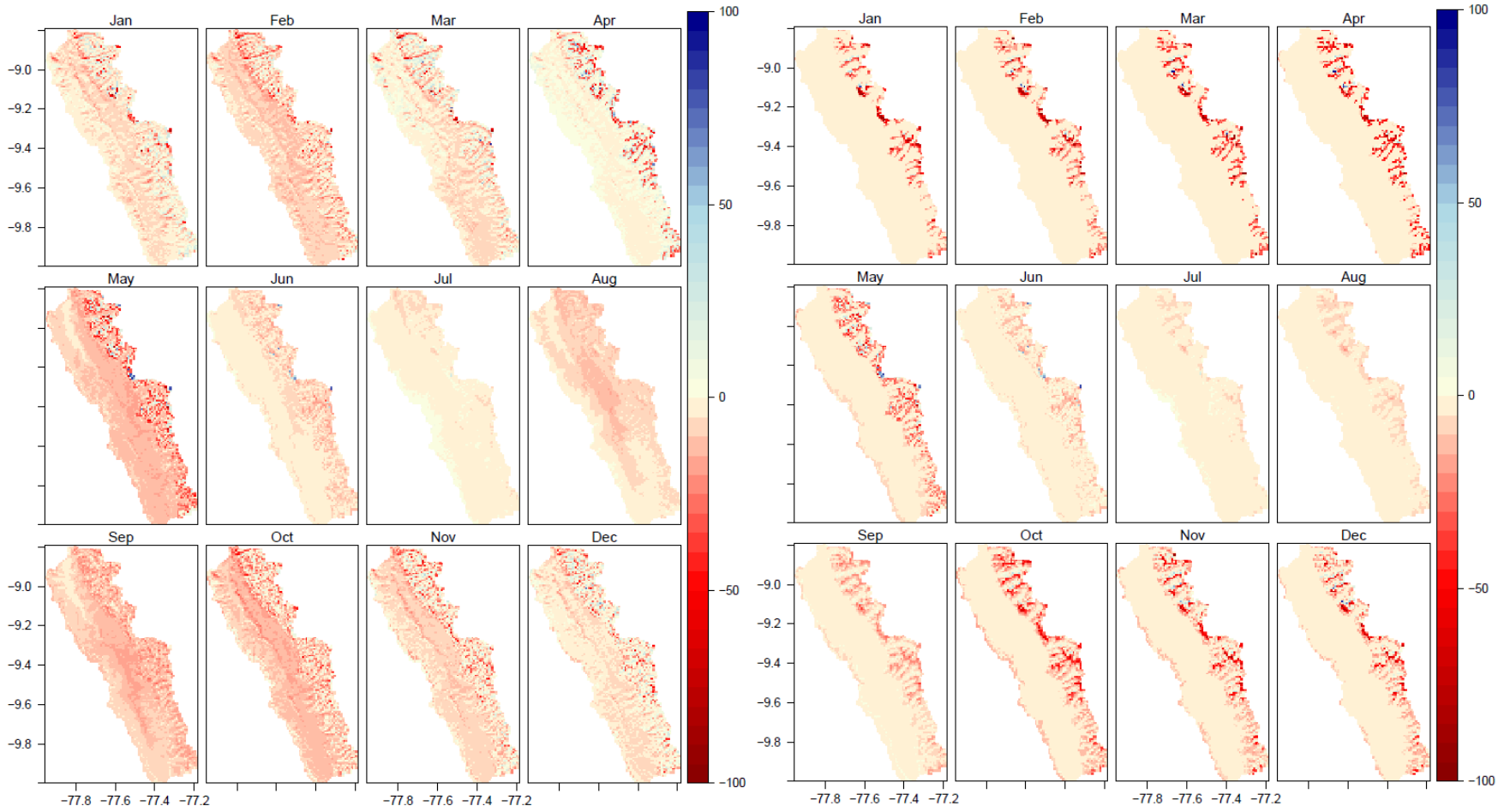

Figure 7.27 Monthly progression of change in water balance (left) and melt water production (right) in the Cañón del Pato HEP catchment under the A2A mean of all models - one SD scenario for 17GCM (mm)

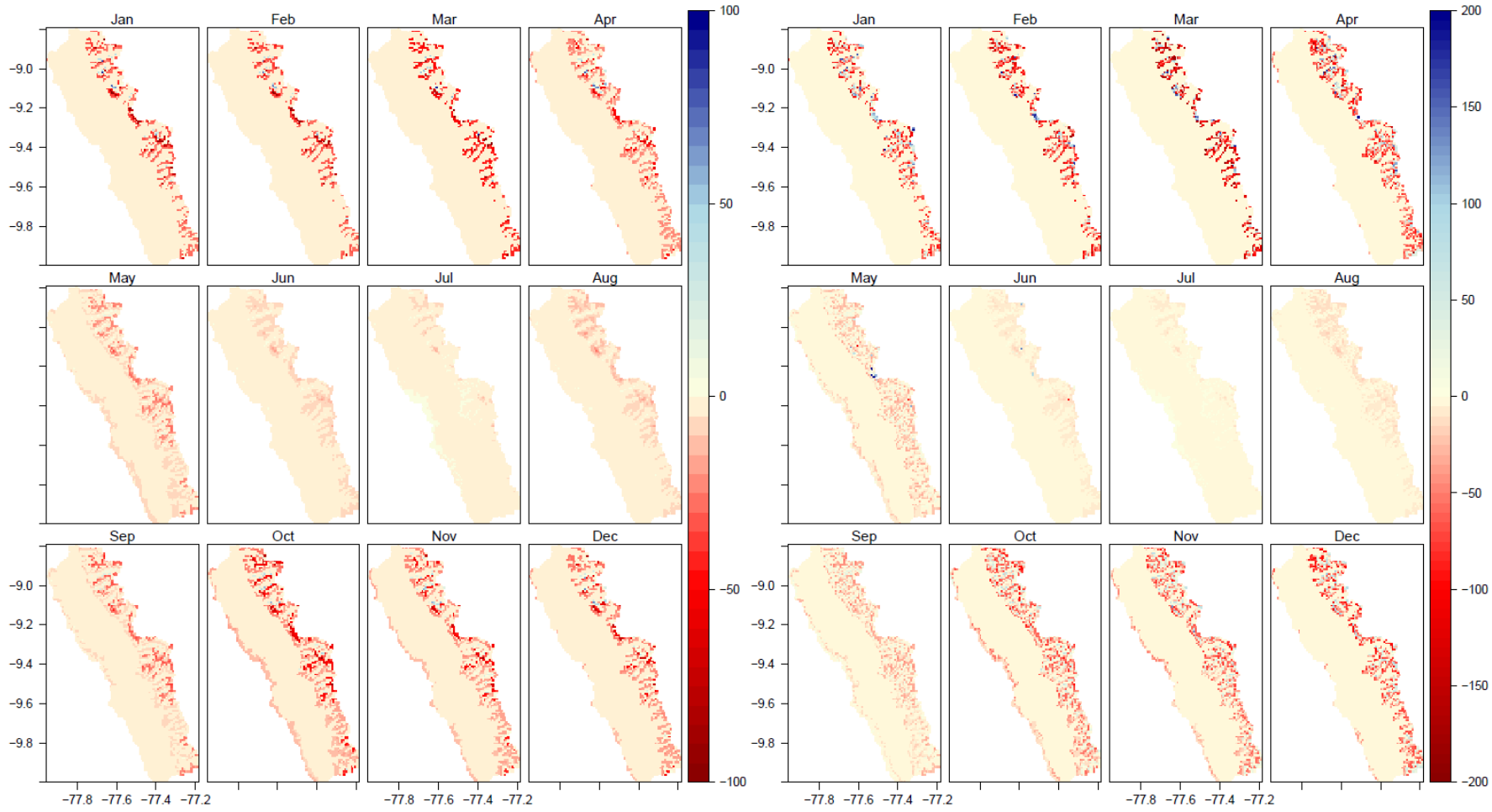

Figure 7.28 Monthly progression of change in snow fall (left) and mean snow pack water equivalent (right) in the Cañón del Pato HEP catchment under the A2A mean of all models - one SD scenario for 17GCM (mm)

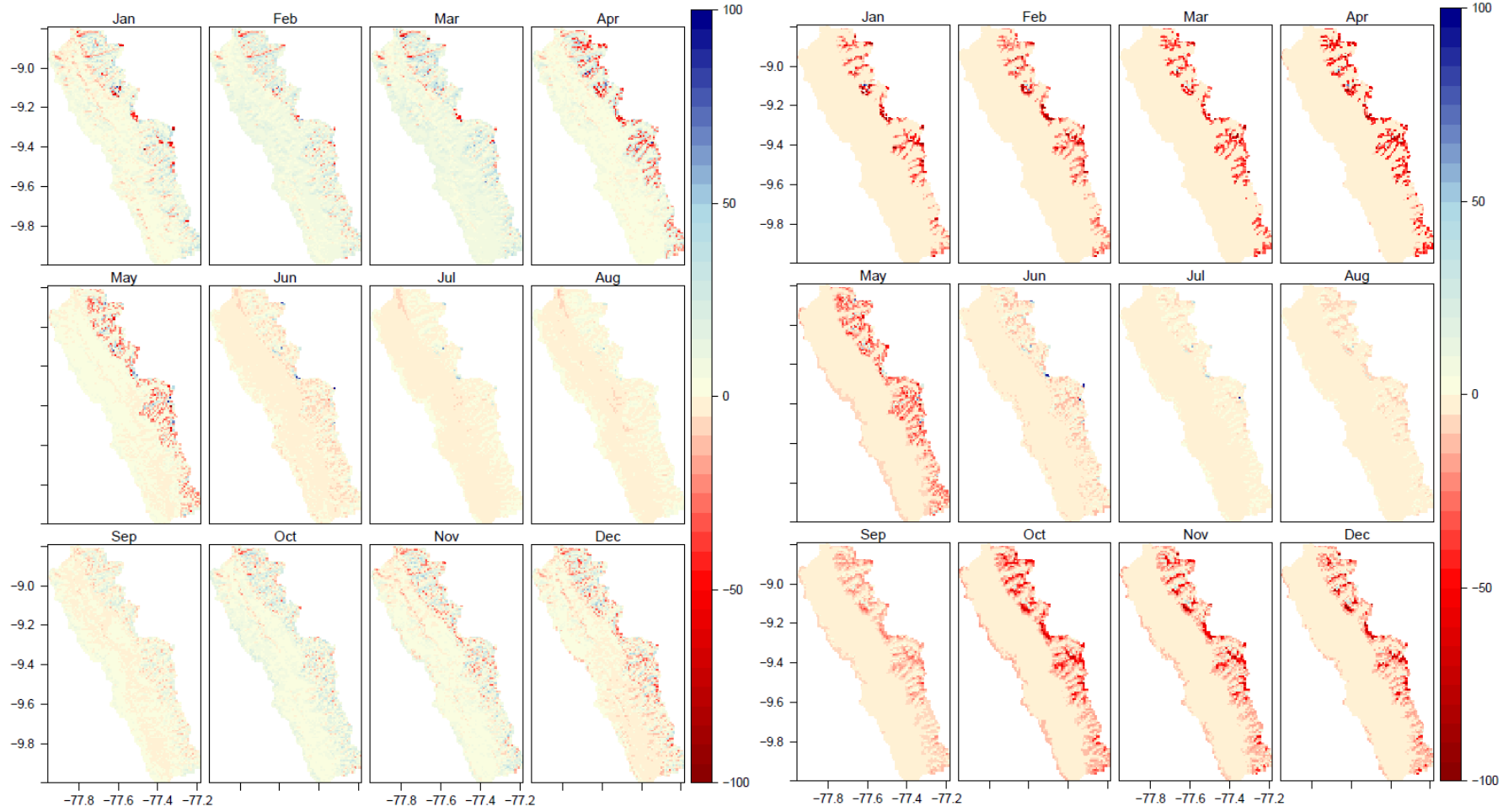

Figure 7.29 Monthly progression of change in water balance (left) and melt water production (right) in the Cañón del Pato HEP catchment under the A1B mean scenario for 5 GCM (mm)

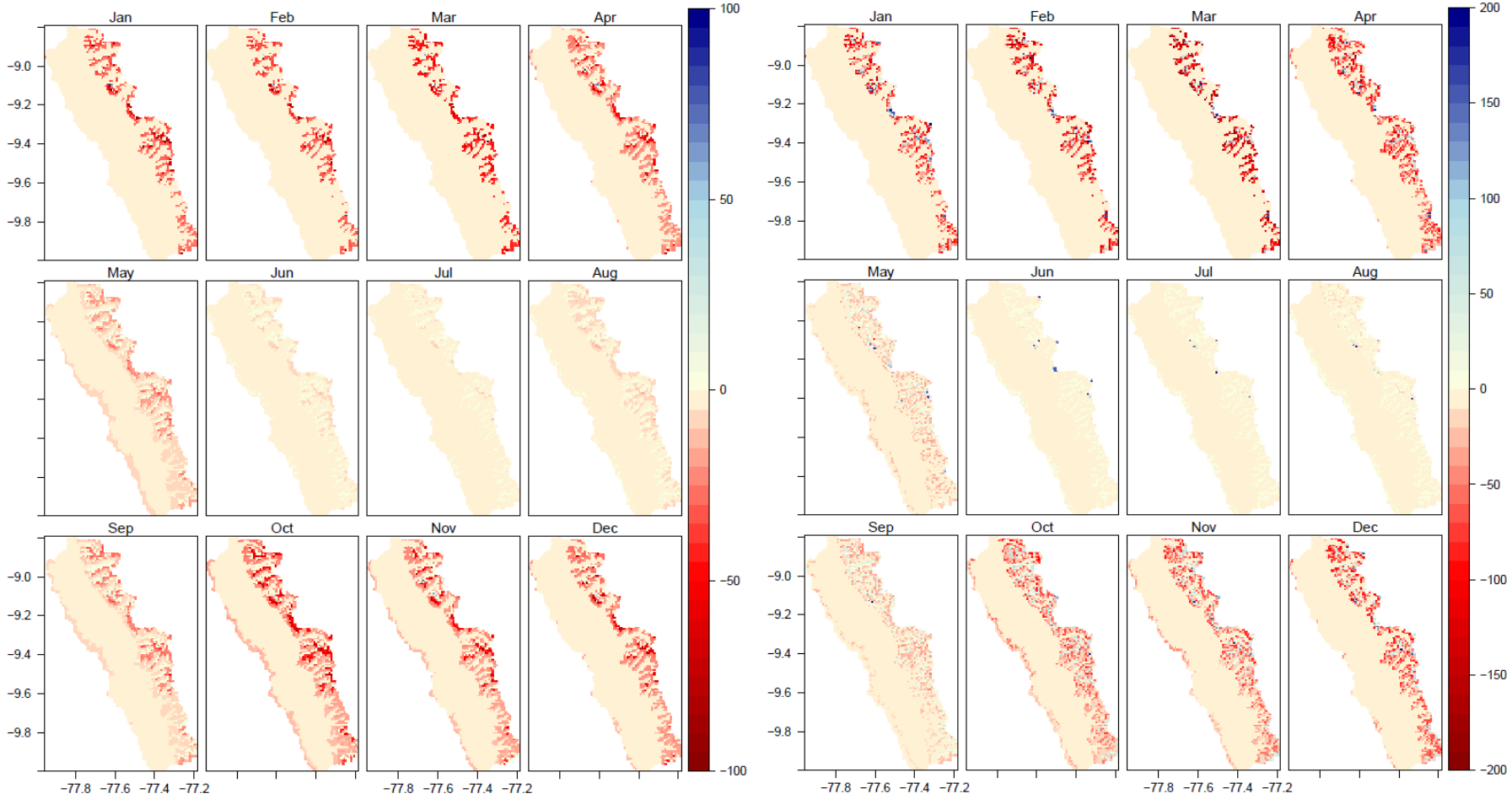

Figure 7.30 Monthly progression of change in snow fall (left) and mean snow pack water equivalent (right) in the Cañón del Pato HEP catchment under the A1B mean scenario for 5 GCM (mm)

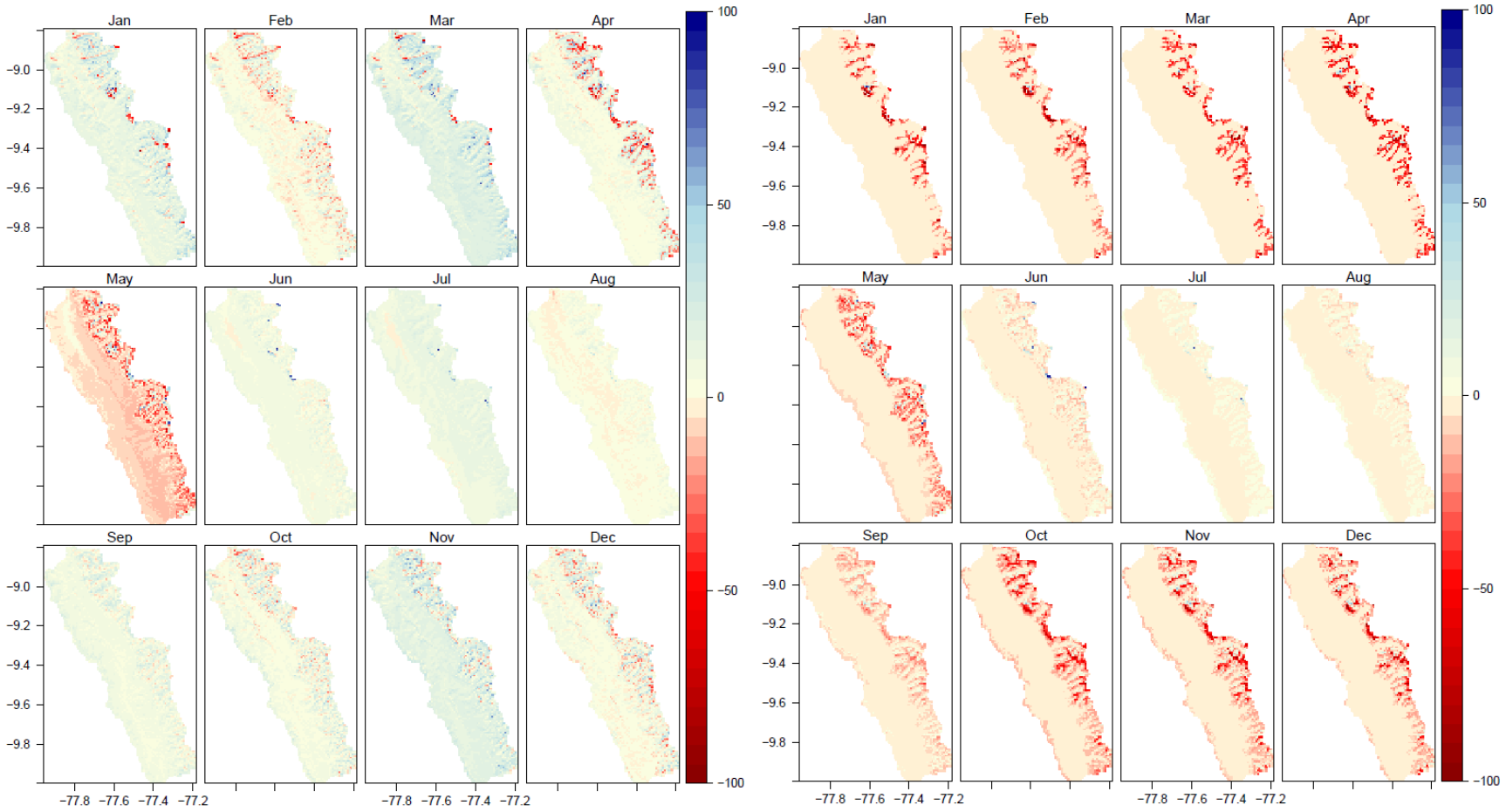

Figure 7.31 Monthly progression of change in water balance (left) and melt water production (right) in the Cañón del Pato HEP catchment under the A2A mean scenario for 5 GCM (mm)

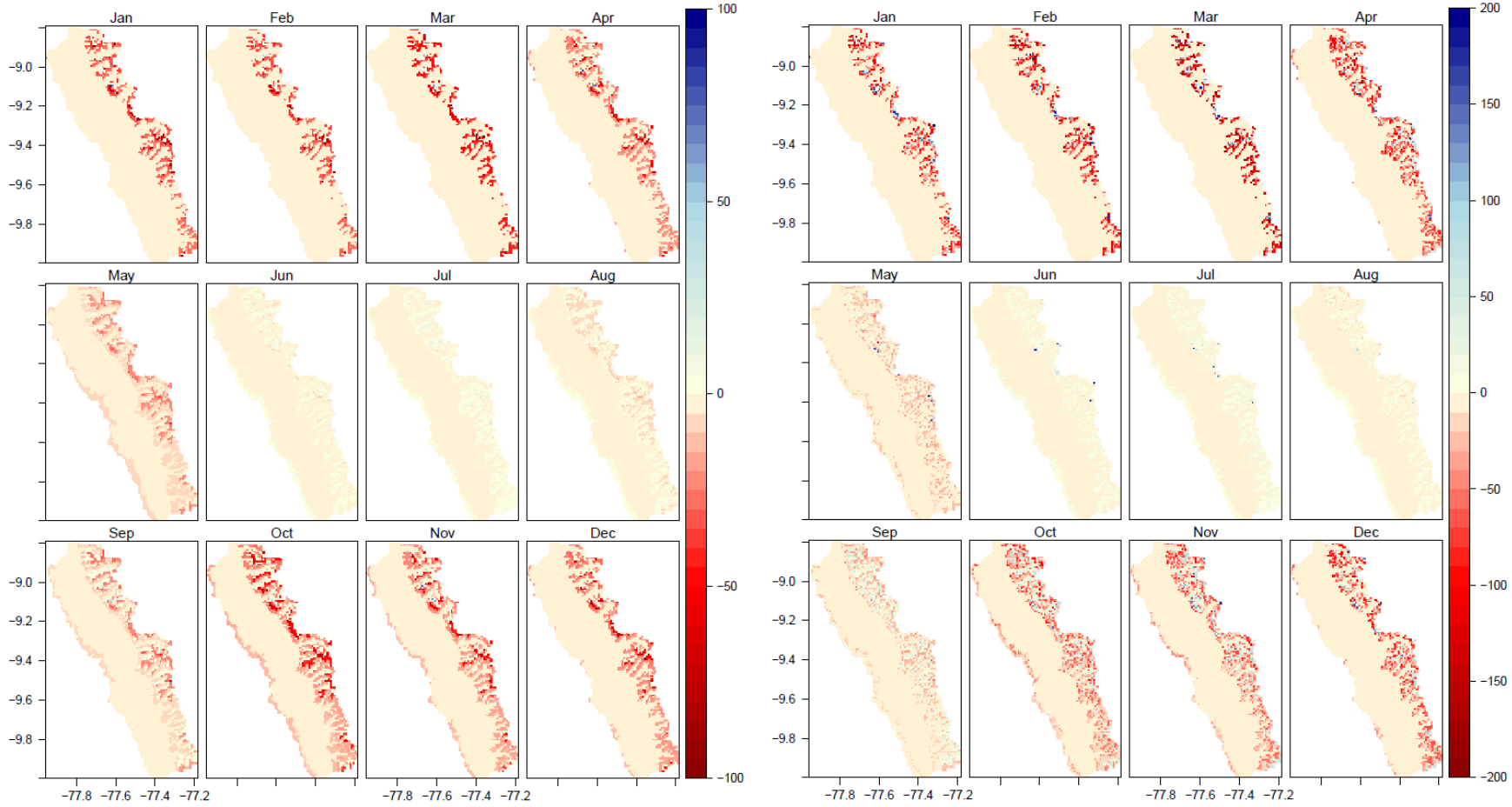

Figure 7.32 Monthly progression of change in snow fall (left) and mean snow pack water equivalent (right) in the Cañón del Pato HEP catchment under the A2A mean scenario for 5 GCM (mm)

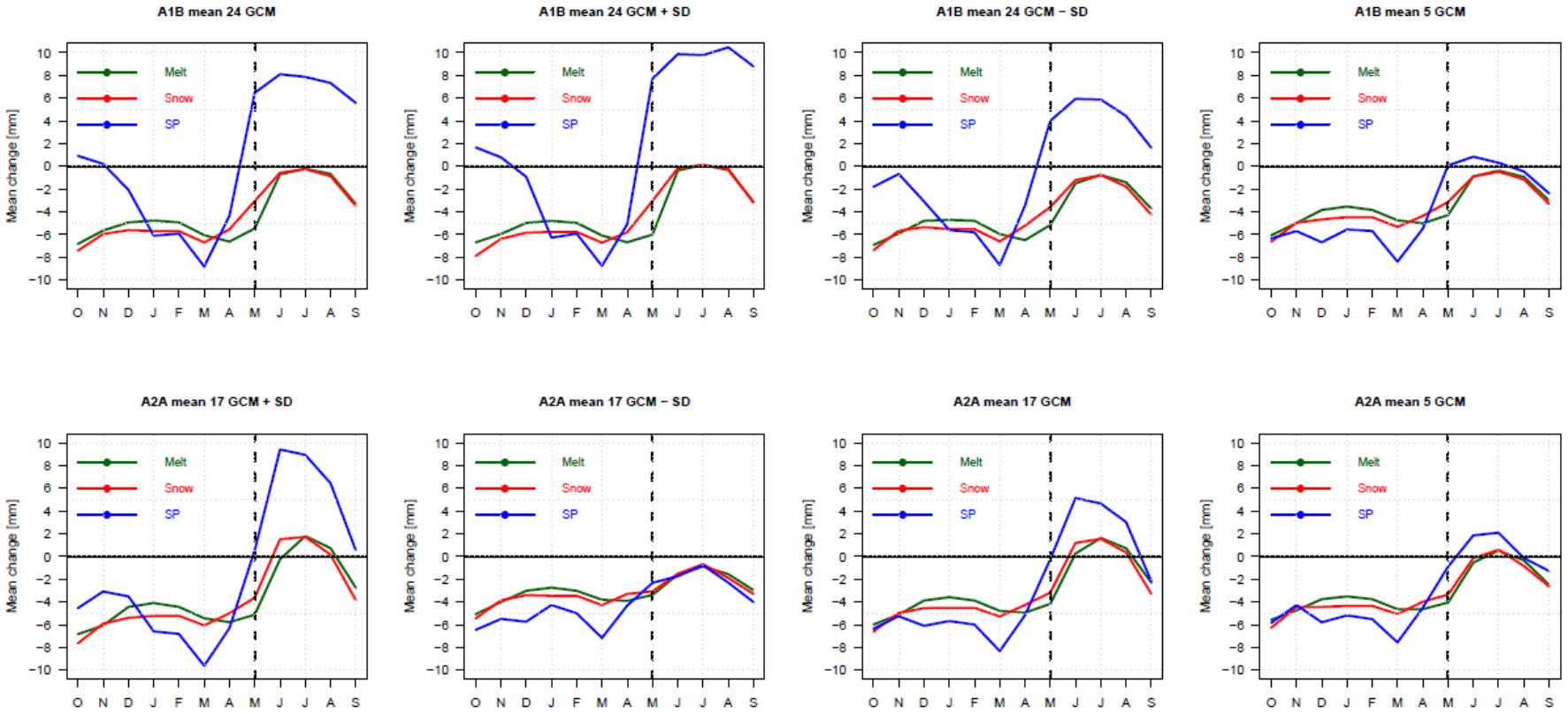

Figure 7.33 Mean monthly change in the Cañón del Pato HEP catchment for melt water production, snow fall and snow pack between the baseline and the climate change scenarios for the 2050s.

7.4.1.2. Change in flow through Cañón del Pato HEP

Figure 7.34 shows the monthly relative changes in flow through the Cañón del Pato HEP station in the Santa basin as the change between the climate change scenarios and the WorldClim baseline as simulated by the AguaAndes/WaterWorld model while table 7.5 summarizes the annual results. The balance between contributions to the water balance from changes in wind driven precipitation and snow melt is also shown.

Change in total annual yield through the HEP facility for all multi model mean scenarios is positive with the exception of the A1B 24 - SD scenario which is at the lower end of projections showing an absolute annual decrease with -479 Mm^3. This is the result of a decrease in input precipitation which also increases the contribution of melt water to the change. Comparing the four multi-model mean scenarios (A1B 24, A2A 17, A1B 5 and A2A 5) shows that the A2A scenarios have a slightly greater impact on stream flow than the A1B scenarios which is the result of greater changes in the wet season. Changes in precipitation dominate the changes in water balance for most scenarios showing an increase in the contribution of precipitation with respect to the baseline. The exception to this are the scenarios that see a reduction or very small increase in precipitation (-SD scenarios). Since projected changes in precipitation are highly uncertain as described in section 7.4.1, these results should be interpreted with caution. However, using a range of climate change scenarios based on different numbers of GCM and for different emission pathways has provided a way of dealing with some of that uncertainty. Particularly the use of plus and minus one standard deviation of the mean in the scenarios gives a good indication of upper and lower bounds of projections. Since seven out of the eight used climate change scenarios agree on the direction of change for the Cañón del Pato HEP station, there is good reason to accept that changes in the flow through the power station will increase on an annual basis. The magnitude of the changes however remains uncertain although all mean GCM scenarios project annual increases in the region of 20 to 30%.

Increases in flow during the wet period have also been found by Vergara *et al.,* (2011) using an ensemble of 16 GCM for the A1B and B1 emission scenarios for the 2030s with minor decreases in flow in the dry season as a result of projected decrease in

precipitation and Juen *et al.,* (2007) describing an increase in flow from Cordillera Blanca basins with more than 20% in the wet season and a decrease in the dry season with about the same percentage using simple uniform climate scenarios based on 4 different emission pathways for the 2050s. In contrast, in the same report an annual decrease in flow at Cañón del Pato is projected for the 2050s based on trend analysis and extrapolation of historical flow records that show a decrease in precipitation for the region. However, due to lack of sufficiently long observational records, the trends were based on only a limited number of stations (10) that span a much larger area.

Generally though, the various studies and the results presented in this chapter indicate an annual increase in flow through the Cañón del Pato HEP station due to increased annual precipitation. Seasonal changes are more uncertain however, since the lower end of projections (-SD scenarios) show a decrease in precipitation for the dry season which is also found in some of the studies describe above. Since the Cañón del Pato hydro-electric power station operates as a run-of-the river station, changes in the seasonal distribution of water means the facility is even more dependent on seasonal storage provided by the 4 glacial lakes described in section 7.2.2. Possible reductions in dry season flow would exacerbate competition between agricultural and hydropower use while increases in the wet season might cause problems such as flooding and increased risk of landslides.

Table 7.5 Annual absolute and relative changes in flow through Cañón del Pato HEP station for baseline and climate change scenarios and percentage deriving from precipitation and melt water.

Scenario	**Flow through HEP (Mm^3/yr)**	**% change**	**Prec (%)**	**Melt (%)**
Baseline	2458	-	70	30
A1B 24	5901	24	80	20
A1B 24 + SD	1705	69.4	90	10
A1B 24 - SD	-479	-19.5	30	70
A2A 17	820	33.4	85	15
A2A 17 + SD	1563	63.6	92	8
A2A 17 - SD	111	4.5	40	60
A1B 5	540	21.9	78	12
A2A 5	766	31.1	83	17

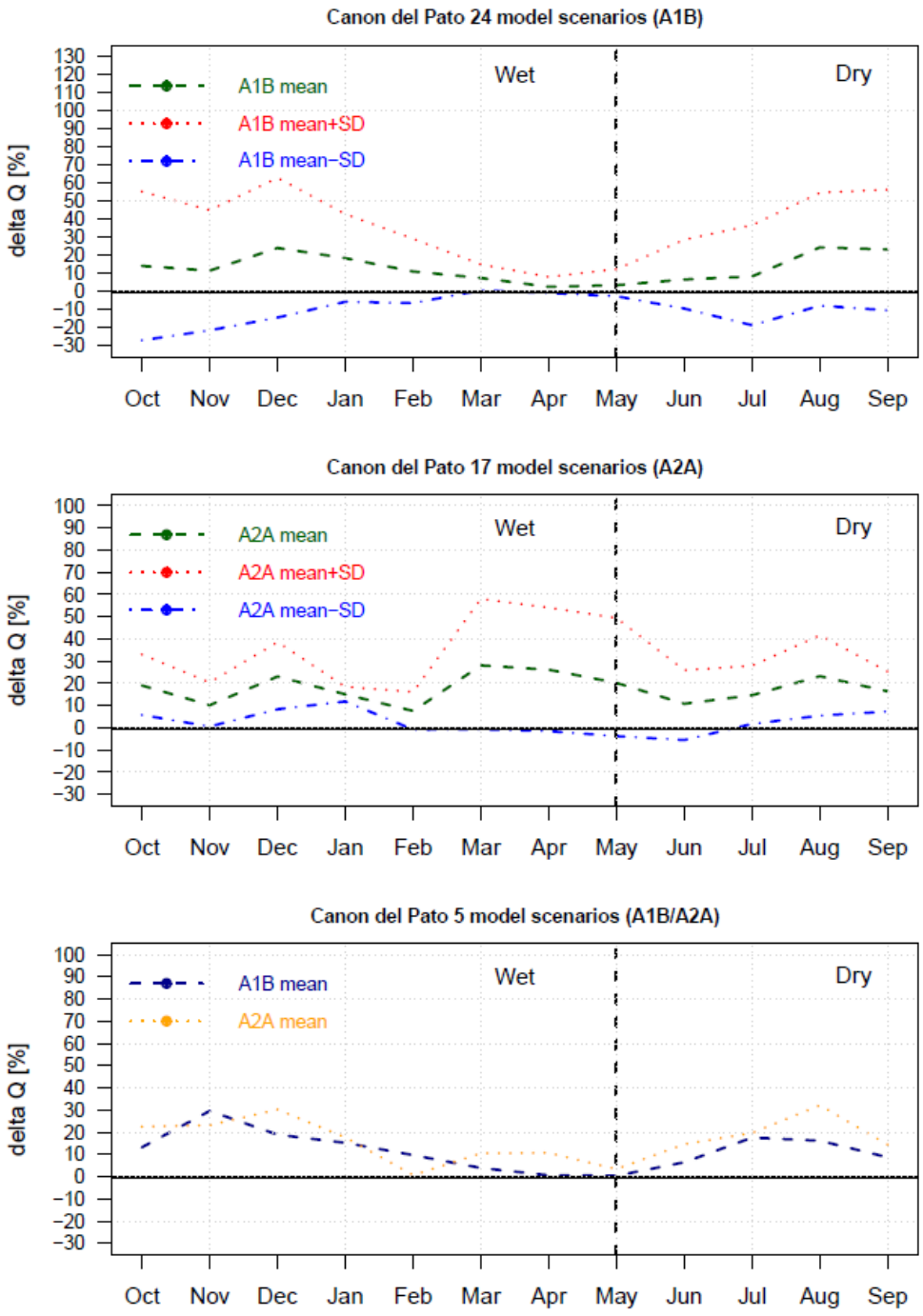

Figure 7.34 Relative changes in flow through Cañón del Pato HEP station for mean and +/ - SD scenarios for 24 GCM under the A1B emission scenario for 2050s (top), mean and +/- SD scenarios for 17 GCM under the A2A emission scenario for 2050s (middle) and for mean of 5 GCM for both A1B and A2A emission scenario for the 2050s (bottom).

7.4.1.3. Sedimentation

To assess the changes in sedimentation transport at the Cañón del Pato HEP facility under the different climate change scenarios, the AguaAndes/WaterWorld sedimentation model output was analysed at the point of the dam. The erosion and sedimentation model is described in more detail in section 5.2.3.5. Table 7.6 shows the results for the annual change in sedimentation transport from the baseline simulation at the HEP facility for all climate change scenarios used in this chapter. High levels of suspended sediment are a problem for the power plant as it can damage the turbines which are costly to replace and often mean the plant cannot run at full capacity.

Table 7.6 Change in sedimentation rates at Cañón del Pato HEP facility for all climate change scenarios

Scenario	A1B 24	A1B 24 +SD	A1B 24 - SD	A2A 17	A2A 17 +SD	A2A 17 - SD	A1B 5	A2A 5
Tonnes (x1000)	1454.8	5985.2	-1972.9	1259.3	3768.4	-600.9	800.6	1329.7
% change	24.4	100.5	-33.1	21.1	63.3	-10.1	13.4	22.3

All scenarios show considerable change compared to the baseline with only the scenarios at the lower end of the projections (- one SD) showing a decrease in sedimentation. The A1B mean scenario using 24 GCM has a greater impact than the A2A mean scenario with 17 GCM. However, the reverse is true for the scenarios that include the same 5 GCM which is an indication of the variability in the multi-GCM mean scenarios and therefore a clear reminder of the uncertainty between GCMs which should be taken into account when choosing GCMs for use in future impact analysis. The differences between the scenarios can be explained by the differences in precipitation and associated runoff.

As described in section 5.2.3.5. it should be noted that this wash erosion model does not capture impacts of heavy rainfall events or landslides. Such events however can have a significant impact on the total sedimentation flows, particularly in steep gradient areas such as the Santa basin. Indeed, according to Vilimek *et al* (2000) the

area is highly unstable after the 1970 earthquake which became apparent in 1998 when dozens of landslides were observed with a high risk of future occurrences of these type of events (Klimes *et al.,* 2009). The observed and projected glacial recession in the catchment (Mark *et al.,* 2010) can cause additional sediment flow as a result of exposing more soft material to heavy rains while glacial lake outburst floods would cause large landslides. Increased sediment flow is also possible as a result of glacial recession exposing more soft material to heavy rains. Furthermore, glacier recession increases the risk of glacial lake outburst floods that can cause landslides and hence significant sediment transport.

7.4.1.4. Impacts of store

To assess what the impact is of the initial conditions of the storage component snow and ice in the model, a number of iterative model runs was carried out whereby the model was run with different number of iterations. This allows for repeating the model with the 50-year climatology but using the store values at the end of each year as the initial conditions for the start of the following year. This modelling procedure is known as 'spin up'. This assessment is particularly important when looking at impacts of climate change as snow and ice stores may take more than one simulation year to come to an equilibrium with the new climate and the contribution of snow and ice to stream flow can be significant, particularly in the dry season.

The Santa basin tile (10 degree latitude/longitude) was run for a total of 20 iterations using the baseline WorldClim climatology and total annual values for snow pack water equivalent, melt water and water balance were calculated. Figure 7.35 shows the number of iterations versus the annual total for the tile.

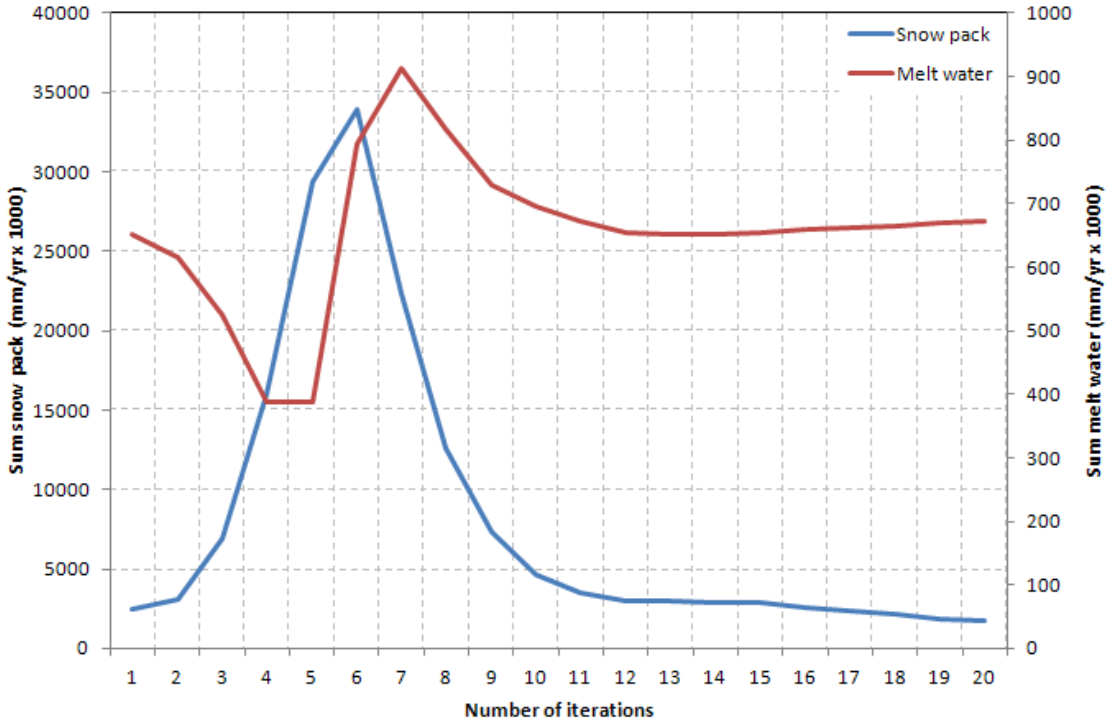

Figure 7.35 Results spin up procedure AguaAndes/WaterWorld for total annual snow pack and melt water for 10 degree latitude/longitude tile, Peru

The results show that for the tile as a whole, snow pack gradually increases during the first six iterations after which it decreases again before levelling out around the 12th time-step at a value similar to the initial condition. Snowmelt decreases during the first five iterations after which it peaks at seven iterations and then slowly decreases again and levelling out around the 12th iteration at about the level of the first iteration. The results indicate that in the case of this tile, increased snowfall increases the snow pack during a model year. This happens up to a tipping point in the snow and ice model energy balance calculation whereby at a certain threshold of snow pack water equivalent, melt production increases and reduces the snow pack again. Changes in water balance as a result of iterations follow the same pattern as changes in snow pack water equivalent meaning that for this area, model equilibrium values are close to those when running the model for only one year which means that running the model for only one year for the baseline and scenario does not significantly affect outcomes.

7.5. Conclusion

This chapter assessed the impacts of climate change on the Cañón del Pato HEP station in the Santa basin in Peru using some of the built in climate change scenarios in the AguaAndes/WaterWorld model. The model was validated against observed stream flow data for 16 stations in the Rio Santa basin using simulations based on two different precipitation climatologies based on WorldClim data and TRMM rainfall. The model validation showed a good fit with observed data for all stations (R^2= 0.84) with a particularly good fit for stations with flow rates of more than 5 m^3s^{-1} (R^2=0.99) using WorldClim precipitation. The model slightly underestimates flow (bias -2.5%) for the larger stations though as well as for the wet season (bias -7.2%) but slightly overestimates flow for the dry season (bias 6.7%). Validation results for the TRMM precipitation showed a slightly less good fit (R^2=0.8) with an overestimation of flow for all stations.

Simulations for eight different climate change scenarios for the Cañón del Pato HEP catchment were carried out using the AguaAndes/WaterWorld policy exercises functionality. Four of the climate change scenarios that were used were based on multi-GCM means for two different SRES emission scenarios (A1B and A2A) for the 2050s with the other four scenarios representing the upper and lower bounds of two of the multi-GCM mean projections as the mean plus one standard deviation and the mean minus one standard deviation. The model simulations show that mean annual wind driven precipitation for the Cañón del Pato catchment increases compared to the WorldClim baseline for seven of the eight climate change scenarios used. Actual evapo-transpiration in the catchment increases for all scenarios and changes in fog inputs are negative for some and positive for others but are minimal for all scenarios used. With the exception of the scenarios representing the lower bounds of the climate change projections (- one SD) all scenarios show an increase in mean annual water balance as a result of the increases in precipitation. The greatest changes in water balance take place in the eastern Cordillera Blanca mountain range. Mean melt water production is projected to decrease under all scenarios as a result of decreases

in snow fall due to higher temperatures. Decreases in melt water in the dry season are compensated by increases in rainfall giving an overall increase in dry season water balance for all mean and mean + SD scenarios.

As a result of the simulated increases in overall water balance, stream flow through the Cañón del Pato HEP facility is projected to increase for all mean and mean + SD scenarios with up to 63% for the upper end of projections and around 20-30% for all mean scenarios. The contribution of melt water to stream flow is projected to decrease for all mean and mean + SD scenarios which means that water resources in the area are more dominated by precipitation, particularly in the dry season. The results are in line with previous observations in the catchment by Vergara *et al.,* (2011) and Juen *et al.,* (2007) that describe an increase in wet season flow for the 2030s and 2050s respectively. However, both these studies also observe a minor decrease in flow in the dry season as a result of decreased melt not compensated for by changes in precipitation whereas in this study, increase in dry season precipitation is greater than loss in melt for most scenarios.

A number of authors have addressed the changes in contribution of glacier melt to the stream flow in the catchment as a result of climate change which are particularly important in the dry season (Mark, *et al.,* 2010; Bury *et al.,* 2010; Chevallier *et al.,* 2011). However, as this study shows, the extent to which this will lead to a decrease in flow depends on the changes in precipitation. As described in section 7.3.1 projections of precipitation by GCMs are highly uncertain in general and even more so in highly heterogeneous landscapes such as the Andes mountain range (Ramirez and Jarvis, 2010; Buytaert et al*.,* 2009. Therefore, climate change adaptation measures should account for this uncertainty, particularly with respect to possibly more variable and unreliable stream flow in the dry season. Possible adaptation measures identified by McKinney *et al.,* (2011) are to increase or develop more and better storage and distribution systems which could include small reservoirs, modified lakes and

household-scale water storage. Also, changes in irrigation practices and shifts in crop types and varieties could potentially result in a decrease in water demand.

Sedimentation transport through the HEP station is projected to increase for all mean and mean + SD scenarios with up to 100% for the upper end of projections and increases between 13-25% for the mean scenarios as a result of increased precipitation and runoff. High sediment rates already cause considerable damage to the turbines at the Cañón del Pato HEP facility, making costly repairs necessary. Increased loads as a result of climate change would therefore mean significant additional running costs for the power plant with associated costly down-times to replace the turbines. However, even more damaging to the operation of the power plant is the possibility of landslides and high rainfall events that can bring vast numbers of sediment to the plant or even block the flow of the river.

Based on the validation of stream flows it can be concluded that the AguaAndes/WaterWorld model performs well in the Rio Santa basin under current conditions. The inclusion of multi-model mean GCM scenarios in the model makes it easy to explore different futures and the inclusion of upper and lower bounds to the climate change scenarios as represented by the plus and minus one standard deviation provide a useful uncertainty range proving that modelling results based on these GCM scenarios should be interpreted with caution as the direction of changes can switch between upper and lower bounds of the mean GCM scenarios.

8. Summary, conclusions and future research recommendations

8.1. Key findings

This thesis has presented some significant developments in the context of a method for assessment of global water resources in watersheds of dams under climate change. The main findings of this thesis are summarised below:

1. The co-development of a global geo-referenced database of dams (GOOD^2) containing more than 36,000 dams as well as the extraction of the watersheds of these dams showing that 18% of all global land drains into a dam.

2. Nearly all large dam catchments globally are projected to be affected by climate change with nearly 70% of dam catchments drier than the 1960-1990 baseline on an annual basis under a mean of 5 GCM scenario for the A1B scenario for the 2050s and more than 40% of catchments projected to be drier under the A2A scenario.

3. Under the A1B scenario, a total of 740 million people are projected to be affected by drying in the dam watersheds while 423 million people are affected by wetting. Under the A2A scenario, these numbers are 788 million and 370 million respectively. Hence, 60 to 70% of people living in dam catchments, are likely to experience drier conditions.

4. The AguaAndes/WaterWorld model presents a novel approach to the assessment of climate impacts on water resources of dams as the model physically based yet can be run using globally available datasets. Therefore, the model can be applied anywhere in the world and similar analysis for other dams in the GOOD^2 database can be carried out with relative ease.

5. Applying the AguaAndes/WaterWorld water balance model to three dam impacted case study basins has shown that the model performs well in simulating baseline measured flows for the Savannah and Guadalquivir basin but less so for the Maputo basin. However, the model is considered to be robust enough to be suitable for the purpose of comparative climate change scenario analysis between basins.

6. Based on eight different climate scenarios for the 2050s and AguaAndes/WaterWorld model simulations, it is likely that there will be an annual and wet season increase in flow through the Cañón del Pato hydropower facility in the Santa basin, Peru with a greater proportion coming from precipitation than snow melt compared to what is currently the case.

8.2. Impacts

The results from this study have shown that nearly all dam catchments are projected to be affected by climate change. However, some regions are more affected than others. There are a number of climate change vulnerabilities identified by the IPCC at different scales and for different systems, processes or groups. For instance global social systems such as food supply and freshwater resources are vulnerable while more regionally, melting of inter-tropical glaciers and drying in North Africa and the Mediterranean have been identified as key vulnerabilities. Moreover, extreme events such as floods in mid to high latitude areas and droughts in mid-latitude continental areas are projected to increase in frequency and intensity (IPCC, 2007). Dams play a critical role in many of these vulnerabilities and this study has highlighted some of them. For instance, the large number of dams in the Mediterranean are projected to be severely impacted by drier conditions whereas snow and glacier-fed basins as found in Pakistan, Nepal and in the Andes are projected to receive more water with substantial changes in timing of flows.

8.3. Aim and objectives

The main aim of the research discussed in this thesis was to assess the effects of climate change in the watersheds of global dams on water resources delivered to those dams and then to examine the implications of climate change for a number of these dams in more detail, with specific focus on the Andes mountain range in South America. To address this, the following specific objectives were formulated:

1) help complete a global geo-referenced database of dams and extract the individual hydrologically correct watersheds of those dams
2) create global high resolution multi-model climate change grids for temperature and precipitation for two different emission scenarios for the 2050s
3) assess the impact of projected climate change (temperature and precipitation) on the watersheds of global dams in terms of changes in available water
4) model the impact of climate change on a number of large dams in different climate regions using the WaterWorld model (Mulligan, 2012d)
5) Test the sensitivity of this model for a number of model outputs and inputs
6) Compare the model against the best available field data for baseline (current) conditions
7) Apply the model to the Santa basin in Peru to assess the impacts of climate change on a small hydro-electric power plant

The following section will provide a synthesis of the main results in this thesis presented in chapter 3 to 7 by addressing each of the stated objectives above. Furthermore, limitations to the research and recommendations for future research will be given.

8.4. Summary, conclusions and recommendations for future research

The first objective of this study was to help develop a global geo-referenced database of dams (GOOD^2) and extract the watersheds of these dams. Work on this database started in 2006 and lasted until 2009. Most of the pan-tropical zone between 23.5 degrees north and 35.5 degrees south was digitised by Leo Saénz while Arnout van Soesbergen did most of the area north and south of this region with additions from Mark Mulligan at various locations throughout the globe. The pan-tropical dam database or KCL Geo-referenced Tropical Dams Database (KCL GTDD) has been published separately (Saénz, 2011; Saénz and Mulligan, 2012) so the global database should be seen as an extension to the pan-tropical dam database. Using a Google Earth GEOWIKI to locate and digitize the dams has proven to be an excellent tool for this kind of data collection although low-resolution imagery and cloud cover at the time of digitising probably resulted in a lack of representation of small dams in some areas. The resulting database currently holds 36,194 dams with most dams found in Asia (18,066) followed by South America (6,203) and North America (5,562). Current estimates and reported figures for the number of large dams around the globe range between 40,000 - 50,000 (World Commission on Dams, 2000; ICOLD, 2003; Lehner and Döll, 2004;) with an additional possible 800,000 small dams (McCully, 1996). Since most of the dams in the GOOD^2 database are large dams, there is reasonable confidence that the database captures most of the existing large dams, particularly since a number of reported dams are auxiliary dams or run-of-the river dams that are not included in the GOOD^2 database but are also not relevant to the type of water resources assessment carried out here. Using GIS techniques, the watershed for each individual dam was extracted. These watersheds proved to be highly accurate when compared to reported figures from various sources (R^2 = 0.98, n = 362). All dam catchments combined cover around 18% of the total global land mass with 32% of all tropical land mass contributing to flow into dams.

The GOOD^2 database is a valuable addition to environmental databases and has been used to model potential impacts of land use and climate change on access and supply

of freshwater and has the potential to be used for a range of other studies dealing with hydrological impacts in relation to dams. However, in order to guarantee an up-to-date database that can be used for a large number of studies, the following recommendations are being made:

- Since finishing the database in 2009, only minor updates have been made. It is recommended that the database be updated for all those areas that now have higher resolution imagery in Google Earth as well as areas that are known to have high rates of dam building (i.e. China, India and parts of Africa) to make sure the latest large dams are included.

- The database makes no distinction between reservoir dams and run-of-the-river dams which means that some of the large catchments in the database could be the result of run-of-the-river dams. This is an important distinction for studies into freshwater resources. Therefore, for future updates, it is recommended that these attributes are added to the database.

The second objective of this thesis was to create global high resolution multi-model climate change grids for temperature and precipitation for two different emission scenarios for the 2050s that could then be used to assess the impact of projected climate change (temperature and precipitation) on the watersheds of global dams in terms of changes in available water (objective 3) and also to model the impact of climate change on a number of large dams in different climate regions using the WaterWorld model (Mulligan, 2012d) (objective 4).

The climate grids created were based on the output of 5 GCM (CCCMA_CGCM31, CSIRO_MK30, IPSL_CM4, MPI_ECHAM5, UKMO_HADCM3) from the AR4 for the SRES A1B and A2A emission scenarios for the 2050s downscaled using the delta method by CIAT (2010). Using the WorldClim climatology (Hijmans *et al.,* 2005) as a baseline, changes in temperature and precipitation were assessed as well as between-model

uncertainty. In terms of precipitation, the greatest disagreement between models can be found in the humid tropics for both emissions scenarios as a result of very high precipitation in these areas and the inability of GCMs to capture the complex atmospheric dynamics. Significant differences were also observed in areas with strong altitudinal gradients such as the Andes mountain range, an effect also described by Buytaert *et al.,* (2010) and attributable to the differing coarse resolutions between models that fail to accurately take into account elevation gradients and thus neglect orographic precipitation events. Between-model agreement on temperature change was found to be much higher although ranges are higher in the more northern latitudes for both scenarios.

The climate change grids were used to create projected global water balances using a temperature based PET method based on a method suggested by Oudin *et al.,* (2005). This method of estimating PET made it possible to calculate PET for the climate change scenarios using only mean monthly temperature data. Compared to other PET calculation approaches and observational data around the globe the derived PET yielded satisfactory results. AET values were obtained by incorporating data from a multi-sensor daily remotely sensed soil moisture product (Owe *et al.,* 2008) reprocessed into a mean monthly soil moisture climatology (Mulligan, 2012b) assuming soil moisture in future periods will be the same as for the baseline.

Applying the changes in water balance to the dam catchments for both scenarios showed that nearly all dam catchments are projected to be affected by climate change with nearly 70% of dam catchments drier than the baseline for the A1B scenario and more than 40% of catchments drier than the baseline for the A2A scenario. Seasonally, under the A1B scenario, dam catchments are projected to become drier while an increase is observed for many catchments under the A2A scenario. Projected changes in reservoir water level for fifty nine individual dams were assessed based on the water balance changes and assuming the total water yield within their catchments is routed down to the reservoir, hence there is no allowance for changes in catchment sub-

surface storage processes (i.e. assuming that storage equilibrates over the time periods under investigation). Nevertheless, this method can be used to quickly assess the potential for change in freshwater provision and hydropower production under different climate change projections and can easily be extended and applied to other dams in the GOOD^2 database. The results of this analysis showed that average reservoir level changes for the A1B scenario are -6 metres for drying catchments and +3.1 metres for wetting catchments and -3.8 metres and +8 metres for the A2A scenario for drying and wetting respectively. In general, dams that have a small reservoir volume to catchment area ratio (i.e. small reservoirs served by large catchments) are more vulnerable to climate changes. Seasonal changes in water delivery to a dam reservoir can have a greater impact than annual changes to the operation of a dam. Some dams are projected to have an additional dry-wet season difference of more than 25 metres (Sera da Mesa dam, Brazil, High Aswan dam, Egypt) increasing the dry-wet season difference in reservoir water level with 35% and 50% respectively which means these dams will have to change the way they operate to cope with these changes which in turn could have impacts on their downstream environments.

Under the A1B scenario, a total of 740 million people are projected to be affected by drying in the dam watersheds while 423 million people are affected by wetting. Under the A2A scenario, these numbers are 788 million and 370 million respectively. This means that 60 to 70 percent of people living in dam catchments, are likely to experience drier conditions which could affect them directly through a decrease in access to water but also indirectly through reduced dam output in terms of hydropower or freshwater for irrigation.

The analysis of impacts of climate change in dam catchments using the GOOD^2 database yielded some interesting results and is the first such assessment of impacts of climate change aggregated over dam catchments on a global scale. Nevertheless, the following observations could be the focus of additional research:

- The work has focused on using a multi-model mean for the climate change scenarios. While this is an accepted method to deal with GCM uncertainty (Tebaldi, 2010; Buytaert, 2009), the sensitivity of the impacts based on these scenarios is unknown. Therefore, to test if changes in direction and magnitude exist between models, the analysis would have to be carried out using the individual climate models separately.

- Uncertainties also arise from the chosen method to calculate PET for the water balance. The sensitivity of the results to the chosen method could be assessed by using different PET estimations as well as using different precipitation climatologies (such as TRMM) and soil moisture climatologies.

Objective 4 of this thesis was to model the impact of climate change on a number of large dams in different climate regions using the WaterWorld model (Mulligan, 2012d). The selection of large dams to be included in this analysis was based on a multi-criteria analysis ranking three river basins into high, medium and low climate change impact and subsequently selecting a large dam to be analysed within each of these river basins. The selected dam catchments were the Tranco de Beas dam catchment in the Guadalquivir basin in Spain, the J. Strom Thurmond dam catchment in the Savannah basin in the USA and the Phongolapoort dam catchment in the Maputo river basin in South Africa/Mozambique. A validation of stream flows was carried out at the scale of the basin for reasons of data availability. The results of the validation showed the model performs well for the Savannah and Guadalquivir basins but overestimates annual flow for the Maputo river basin. This overestimation is attributed to a number of reasons including overestimation of rainfall input, underestimation of water loss through evapo-transpiration and possible errors in observed data. Impacts of climate change projections on inflow into dam reservoirs was assessed by running the WaterWorld model with the 5 GCM mean scenarios for the A1B scenario for the 2050s and comparing the results with a baseline run based on the WorldClim climatology.

The simulation results show that annual inflows into the reservoirs decrease for all three analysed dam catchments with -17% for the Tranco de Beas dam catchment, -10.5% for the Phongolapoort dam catchment and -1.8% for the J. Strom Thurmond dam catchment.

All three catchments are also projected to have greater month-to-month variability in stream flow as indicated by an increase in their respective monthly stream flow coefficient of variation. The decrease in annual flows is consistent with the results of the much simpler water balance analysis carried out in chapter 4. The extent to which these changes have an impact on reservoir operation and dam safety depends on the total storage to annual flow ratio. The J. Strom Thurmond dam is capable of storing 70% of simulated baseline annual inflow compared to 50% for the Phongolapoort dam and 200% for the Tranco de Beas dam which means that the Phongolapoort dam is most sensitive to changes in inflow although given the overestimation of the model for this basin, the storage to inflow ratio is likely to be higher for this reservoir. The magnitude of changes in inflow as a result of climate change for these reservoirs is subject to uncertainty in the climate change projections and the hydrological model. This study showed there is high between model agreement for the Mediterranean area where the Tranco de Beas dam is located with other studies using different scenarios, time-periods and GCM also agreeing on a warmer and drier future (Gao *et al.,* 2006; Giorgi and Lionello, 2008). Similarly for the area where the Phongolapoort dam is located there is high between-model agreement and low range of precipitation projections for the scenario used. For the area where the J. Strom Thurmond dam is located though, the uncertainty in precipitation predictions is higher with only three out of five models agreeing on the direction of change. Projected changes in precipitation for this area are small however which means the projected change in water balance is mostly driven by changes in AET whereas changes for the other two dams are mostly driven by precipitation changes. However, since uncertainty with respect to (precipitation) projections in GCMs is high and precipitation is the largest flux in the water balance, the results of any hydrological impact assessment using

these projections should be interpreted with caution and sensitivity to differences in input climatology based on GCM should be assessed. Furthermore, this study used climate change data that was downscaled from GCMs using the delta or change factor method to drive the hydrological model. Various studies however have indicated that the choice of downscaling method can have an effect on the outcome of a water resource impact study (e.g. Andreasson *et al.,* 2003; Coulibaly et al*.,* 2005; Diaz-Nieto and Wilby, 2010; Buytaert *et al.,* 2010) which can result in differences in projected magnitude or even a shift in direction of change (Fowler, 2007). Uncertainties also relate to the time-step used in the analysis. This study uses monthly means based on long-term climatologies. However, changes in extreme events such as rainfall intensity can have a greater impact on water resources than more gradual changes potentially causing dam breaches or problems downstream due to changes in timing of release flows. Changes in extreme events are expected but are very difficult to project (IPCC, 2012).

To assess how sensitive the case study basins are to climate change, the WaterWorld model was run with simple climate change scenarios that were uniform in magnitude and direction for each basin. The results of this analysis showed that the Maputo basin is most sensitive (greatest change in water balance) to climate change (defined as temperature and precipitation change) in relative terms although since the scenario is defined as a percentage change in precipitation, absolute changes will be greater for seasons (and basins) with more rainfall. Projected changes for this basin based on the 5 GCM mean for A1B and A2A for the 2050s scenarios are the lowest of all three basins with high between-model agreement. Therefore, while sensitivity of this basin might be highest, actual changes might be smaller in magnitude because of lower expected climate change. The basins were also compared in terms of their sensitivity to changes in vegetation in order to simulate possible eco-system based adaptation measures. In general, increases in tree cover result in a decreased water balance because of higher ET while the opposite is true for a reduction in tree cover. An interesting exception to this was found for high altitude areas in the Maputo basin where increased tree cover

resulted in a increase in water balance as a result of increased cloud water interception in excess of the higher ET.

Even though AguaAndes/WaterWorld is uncalibrated and uses global, remotely sensed datasets, based on the validation results in this thesis and in previous studies, the model is considered to be robust enough to be suitable for the purpose of comparative climate change scenario analysis between basins as carried out in this thesisFurthermore, using a un-calibrated model in a comparative between-basin analysis as carried out in this thesis highlights the danger of using calibrated models with data for individual catchments as models may be fitted to data but they would not be as robust to scenarios of change. Using globally consistent data sets with a globally applicable model such as WaterWorld therefore provides the opportunity to validate input datasets such as the Worldclim climatology. In addition, the fact that it can be applied globally makes it easy to carry out similar analysis for other dams within the GOOD^2 database. Furthermore, being able to use your own data and the built-in capabilities for climate and land use change scenario analysis make the system flexible enough for a much wider range of analysis. With respect to objectives 4 and 5 of this thesis, the following recommendations for further research are being made:

- Since the projected changes in the case study basins are modelled using the multi-model GCM mean, results of individual model projections or different set of models may change the magnitude or direction of the changes. It is therefore advisable to run a sensitivity analysis using individual model projections and/or different sets of scenarios.

- With the exception of the cross-basin climate change sensitivity analysis (section 6.3) all climate change projections and impact results are based on changes in temperature and precipitation only. Even though, precipitation changes are likely to dominate most climate change impacts, it would be good to test the model sensitivity to other parameters that are potentially influenced by climate change

such as solar radiation, wind speeds, relative humidity, cloud frequency and temperature range).

- In order to fully evaluate possible eco-system based interventions in the case study basins that could potentially offset the climate change impacts, more vegetation land cover types should be taken into account. Such an analysis could assess the potential for climate change adaptation through agriculture.

The final objective (objective 7) of this thesis was to apply the AguaAndes/WaterWorld model to the Santa basin in Peru to assess the impacts of climate change on the Cañón del Pato hydro-electric power plant. The Santa basin is interesting because of the importance of snow and ice on the basin hydrology and inputs to the HEP plant. The model was first validated against observed stream flow data for 16 stations in the Santa basin (objective 6) using WorldClim and TRMM rainfall climatologies. The model validation showed a good fit with observed data for all stations (R^2= 0.84) with a particularly good fit for stations with flow rates of more than 5m^3s^{-1} (R^2=0.99) using WorldClim precipitation. The model slightly underestimates flow (bias -2.5%) for the larger stations as well as for the wet season (bias -7.2%) but slightly overestimates flow for the dry season (bias 6.7%). Validation results for the TRMM precipitation showed a slightly less good fit (R^2=0.8) with an overestimation of flow for all stations. Since uncertainty in GCM projections is high, particularly for rainfall, more climate change scenarios including the plus and minus one standard deviation of the mean of all models were used in this study. The scenarios used where: A1B mean of 24 models, A2A mean of 17 GCM, A1B mean of 5 GCM, A2A mean of 5 GCM, A1B mean of 24 GCM + one standard deviation, A2A mean of 17 GCM plus one standard deviaton, A1B mean of 24 GCM minus one standard deviation and finally A2A mean of 17 GCM minus one standard deviation. The last four scenarios represent the high and low end of projections. All scenarios were projections for the 2050s. The location of the hydropower facility in the Andes mountain range means that snow fall and melt water dynamics are likely to be important in the assessment of water resources. The

simulation results show that the contribution of melt water to the water balance decreases for all scenarios as a result of decreases in snow fall and thus snow area due to higher temperatures. Annual precipitation is projected to increase for all scenarios leading to a simulated increase in water balance and an increase in flow through the Cañón del Pato HEP facility with between 20-30% for all mean scenarios and up to 60% for the high end scenarios. Annual increases in flow as a result of climate change have also been observed in other studies (Juen *et al.,* 2007; Vergara *et al.,* 2011) although some of these project decreases in the dry season, the difference in projected change for the dry season between this study and others can be attributed to greater projected increase of rainfall in this season that compensates for the decrease in melt. Simulation of sedimentation inputs through the HEP station show an increase of between 13-25% for all mean scenarios as a result of increased precipitation and runoff. However, landslides and high rainfall events that are not modelled could be far more important in sediment delivery and are likely to increase in the future (Klimes *et al.,* 2009)

Based on these results it can be concluded that even though there is high uncertainty in precipitation projections for this area it is likely that there will be an annual and wet season increase in flow with a greater proportion coming from precipitation than snow melt compared with what is currently the case. Changes in the dry season are more uncertain however with flow becoming possibly more variable and unreliable. The development of more and better storage and distribution systems such as small reservoirs, modified lakes and household-scale water storage could provide the necessary storage to maintain water supply throughout the dry season. Alternatives that decrease water demand in the dry season should also be investigated. Possibly through changes in irrigation practices and shift in crop types and varieties.

References

Aerts., J. C. J. H., Kriek, M., Schepel, M. 1999. STREAM (Spatial Tools for River Basins and Environment and Analysis of Management Options): 'Set up and Requirements'. *Physics and chemistry of the earth, parts A/B/C,* 24**,** 591-595.

Alcamo, J., Döll, P., Henrichs, T., Kaspar, F., Lehner, B., Rösch, T., Siebert, S. 2003. Development and testing of the WaterGAP 2 global model of water use and availability. *Hydrological Sciences,* 48**,** 317-337.

Alexander, L. V., Zhang, X., Peterson, T. C., Ceasar, J., Gleason, B., Tank, A. K., Haylock, M., Collins, D., Trewin, B., Rahimzadeh, F., Tagipour, A., Ambenje, P., Kumar, K. R., Revadekar, J., Griffiths, G., Vincent, L., Stephenson, D., Burn, J., Aguilar, E., Brunet, M., Taylor, M., New, M., Zhai, P., Rusticucci, M., Vazques-Aguirre, J. L. 2006. Global observed changes in daily climate extremes of temperature and precipitation. *Journal of Geophysical Research*.

Allen, R. G., Pereira, L. S., Raes, D., Smith, M. 1998. Crop evapotranspiration: guidelines for computing crop requirements. Irrigation and drainage paper No. 56, FAO, Rome, Italy.

Andreasson, J., Bergstrom, S., Carlsson, B., Graham, L. P. 2003. The effect of downscaling techniques on assessing water resources impacts from climate change scenarios. *Water Resources Systems. Water Resources Systems Water Availability and Global Change. Proceedings of symposium HS02a held during IUGG2003 at Sapporo, July 2003*.

AQUASTAT 2006. FAO's Information System on Water and Agriculture. [Online]. Available from: http://www.fao.org/nr/water/aquastat/main/index.stm [accessed 21 August 2012].

Arnell, N.W., Hulme, M. 2000. Implications of climate change for large dams and their management. Thematic Review II.2 prepared as an input to the World Commission on Dams. Cape Town: World Commission on Dams.

Arnell, N.W., Osborn, T. 2006. Interfacing climate and impacts models in integrated assessment modelling. *Tyndall Centre Technical Report 52.*

Arnell, N. W. 2004. Climate change and global water resources: SRES emissions and socio-economic scenarios. *Global Environmental Change,* 14**,** 31-52.

Arora, V. K. 2000. Streamflow simulations for continental-scale river basins in a global atmospheric general circulation model. *Advances in Water Resources,* 24**,** 775-791.

Arora, V. K., Boer, G. J. 1999. A variable velocity flow routing algorithm for GCMs. *Journal of Geophysical Research,* 104.

BADC 2004. Global mean sea-level pressure dataset. [online] Available at: http://badc.nerc.ac.uk/browse/badc/ukmo-gmslp.

Bahremand, A., De Smedt, F., Corluy, J., Liu, Y. B., Poorova, J., Velcicka, L., Kunikova, E. 2006. Application of WetSpa model for assessing land use impacts on floods in the Margecany-Hornad watershed, Slovakia.

Barbier, E. B., Thompson, J. R. 1998. The value of water: floodplain versus large-scale irrigation benefits in Northern Nigeria. *Royal Swedish Academy of Sciences, Ambio,* 27**,** 434-440.

Bhat, A., Blomquist, W. 2004. Policy, politics and water management in the Guadalquivir river basin, Spain. *Water Resources Research,* 40**,** 1-11.

Birkingshaw, S. J., James, P., Ewen, J. 2010. Graphical user interface for rapid set-up of SHETRAN physically based river catchment model. *Environmental modelling and software,* 25**,** 609-610.

Blenkinsop, S., Fowler, H.J. 2007. Changes in European drought characteristics projected by the PRUDENCE regional climate models. *International journal of climatology,* 27**,** 1595-1610.

Block, P. J., Strzepek, K., Rajagopalan, B. 2007. Integrated management of the Blue Nile basin in Ethopia. Hydropower and irrigation modeling. *IFPRI Discussion Paper 00700.* International Food Policy Research Institute.

Bonell, M. 2010. The impacts of global change in the humid tropics: selected rainfall-runoff issues linked with tropical forest-land management. *Irrig Drainage Syst,* 24**,** 279-325.

Brown, C., Wilby, R.L. 2012. An alternative approach to assessing climate risks. Eos Trans. AGU*,* 93 (41)**,** 401.

Bruijnzeel, L. A., Mulligan, M., Scatena, F. N. 2011. Hydrometeorology of tropical montane cloud forests: emerging patterns. *Hydrological Processes,* 25**,** 465-198.

Burke, E. J., Brown, S.J.., Christidis, N. 2006. Modeling the recent evolution of global drought and projections for the twenty-first century with the Hadley centre climate model. *Journal of hydrometeorology,* 7**,** 1113-1125.

Bury, J., Mark, B. G., McKenzie, J. M., French, A., Baraer, M., In Huh, K., Zapata Luyo, M. A., Gomez Lopez, R. J. 2010. Glacier recession and human vulnerability in the Yanmarey watershed of the Cordillera Blanca, Peru. *Climatic Change,* 105**,** 179-206.

Buytaert, W., Celleri, R., Timbe, L. 2009. Predicting climate change impacts on water resources in the tropical Andes: effects of GCM uncertainty. *Geophysical Research Letters,* 36.

Buytaert, W., Dewulf, A., Urrutia, R., Karmalker, A., Celleri, R. 2010. Uncertainties in climate change projections and regional downscaling in the tropical Andes: implications for water resources management. *Hydrol. Earth Syst. Sci,* 14**,** 1247-1258.

Caesar, J., Alexander, L. 2006. Large-scale changes in observed daily maximum and minimum temperatures: creation and analysis of a new gridded data set. *Journal of Geophysical Research,* 111.

CBDB 2008. Dams. Rio de Janeiro: Brazilian Committee on Dams. [Online] Available at: http://www.cbdb.org.br/ingles/indexe.htm. [Accessed 10 April 2012].

CGIAR-CSI 2010. Global geospatial potential evapotranspiration and aridity index. Methodology and dataset description.[Online] Available at: http://www.cgiar-csi.org/data/item/51-global-aridity-and-pet-database [accessed 15 May 2012].

Chevallier, P., Pouyaud, B., Suarez, W., Condom, T. 2011. Climate change threats to environment in the tropical Andes: glaciers and water resources. *Reg Environ Change,* 11.

Chormanski, J., Michalowski, R. 2011. Hydrological catchment model WetSpa-SGGW integrated with a calculation module in ArcGIS environment. *Scientific Review - Engineering and Environmental Sciences,* 53**,** 196-206.

Christensen, N., Lettenmaier, D. P. 2006. A multimodel ensemble approach to assessment of climate change impacts on the hydrology and water resources of the Colorado River basin. *Hydrology and Earth System Sciences Discussions,* 3**,** 3727-3770.

Christensen, N. S., Wood, A. W., Voisin, N., Lettenmaier, D. P., Palmer, R. N. 2004. The effects of climate change on the hydrology and water resources of the Colorado river basin. *Climatic Change,* 62**,** 337-363.

CIAT 2010. GCM downscaled GCM data portal [online database] available at: http://www.ccafs-climate.org/data/.

CIESIN 2005. Center for International Earth Science Information Network (CIESIN), Columbia University; and Centro Internacional de Agricultura Tropical (CIAT) Gridded Population of the World, Version 3 (GPWv3): Population Density Grid. Palisades, NY: Socioeconomic Data and Applications Center (SEDAC), Columbia University. Available at http://sedac.ciesin.columbia.edu/gpw. .

Cloke, H. 2012. Modelling climate impact on floods with ensemble climate projections. *Quarterly journal of the royal meteorological society*

Cobo, R. 2008. Los sedimentos de los embalses Espanoles. *Ingenieria del Agua,* 15.

Coulibaly, P., Dibike, Y. B., Anctil, F. 2005. Downscaling precipitation and temperature with temporal neural networks. *Journal of Hydrometeorology,* 6**,** 483-496.

COVENPRE 2008. Grandes Presas de Venezuela. Comité Venezolano de Grandes Presas. Caracas. Venezuela.

Covey, C., AchutaRao, K. M., Cubasch, U., Jones, P., Lambert, S. J., Mann, M. E., Phillips, T. J., Taylor, K. E. 2003. An overview of results from the Coupled Model Intercomparison Project. *Global and planetary change,* 37**,** 103-133.

Darwall, W., Smith, K., Lowe, T., Vié, J.-C. 2005. The status and distribution of freshwater biodiversity in eastern Africa. *In:* IUCN SSC Freshwater biodiversity assessment programme. Gland, S. (ed.). Cambridge, UK.

De Roo, A. P. J., Wesseling, C. G., Van Deursen, W. P. A. 2000. Physically based river basin modelling within a GIS: the LISFLOOD model. *Hydrological Processes,* 14**,** 1981-1992.

De Smedt, F., Yongbo, L., Gebremeskel, S. 2000. Hydrologic modeling on a catchment scale using GIS and remote sensed land use information. *In:* Brebbia, C. A. (ed.) *Risk Analysis II.* Southampton, Boston: WTI Press.

de Vente, J. 2009. *Soil erosion and sediment yield in Mediterranean geoecosystems.* PhD thesis, Katholieke Universiteit Leuven.

de Vente, J., Poesen, J., Arabkhedri, M., Verstraeten, G. 2007. The sediment delivery problem revisited. *Progress in physical geography,* 31**,** 155-178.

DHI Software 2007. MIKE SHE user manual. Volume 1: user guide. DHI Software.

Diaz-Nieto, J., Wilby, R. L. 2005. A comparison of statistical downscaling and climate change factor methods: impacts on low flows in the river Thames, UK. *Climatic Change,* 69**,** 245-268.

Digitalglobe 2010. Quickbird imagery [Online] Available at: www.digitalglobe.com.

Diodato, N., Bellocchi, G. 2009. Environmental implications of erosive rainfall across the Mediterranean. *In:* Halley, G. T. & Fridian, Y. T. (eds.) *Environmental Impact Assessments.* Nova Science Publishers, Inc.

Elshamy, M. E., Seierstad, I. A., Sorteberg, A. 2008. Impacts of climate change on Blue Nile flow using bias corrected GCM scenarios. *Hydrology and Earth System Sciences Discussions,* 5**,** 1407-1439.

ESRI 2010. Environmental Systems Research Insitute, ArcGIS Desktop version 9.3. .

Ewen, J., Parkin, G., O'Connell, P. E. 2000. SHETRAN: distributed river basin flow and transport modeling system. *Journal of hydrologic engineering*.

FAO 2004. Global map of monthly reference evapotranspiration - 10 arc minutes. [online] available at: http://www.fao.org/geonetwork/srv/en/main.home [accessed 15 July 2012].

FAO 2009. CLIMWAT 2.0 for CROPWAT Water development and management unit & climate change and bioenergy unit FAO [online] Available at: http://www.fao.org/nr/water/infores_databases_climwat.html [accessed 6 June 2012].

Farr, T. G., Kobrick, M. 2000. Shuttle Radar Topography Mission produces a wealth of data. *American Geophysical Union, EOS,* 81**,** 583-585.

Fealy, R., Sweeney, J. 2007. Statistical downscaling of precipitation for a selection of sites in Ireland employing a generalised linear modelling approach. *International Journal of Climatology,* 27.

Fearnside, P. M. 2012. Carbon credit for hydroelectric dams as a source of greenhouse-gas emissions: the example of Brazil's Teles Pires dam. *Mitig Adapt Strateg Glob Change*.

Fearnside, P. M., Pueyo, S. 2012. Greenhouse-gas emissions from tropical dams. *Nature climate change,* 2**,** 382-384.

Federer, C. A., Vörösmarty, C., Fekete, B. 1996. Intercomparison of methods for calculating potential evaporation in regional and global water balance models. *Water Resources Research,* 32**,** 2315-2321.

Fowler, H. J., Blenkinsop, S., Tebaldi, C. 2007. Linking climate change modelling to impacts studies: recent advances in downscaling techniques for hydrological modelling. *International Journal of Climatology,* 27**,** 1547-1578.

Freeman, T. 1996. What is imaging radar? . Jet Propulsion Laboratory.

Fyllas, N. M., A.Y., T. 2009. Simulating vegetation shifts in north-eastern Mediterranean mountain forests under climate change scenarios. *Global ecology and biogeography,* 18**,** 64-77.

Gaeckler, M., Vervier, P., Arguelles, A., Cifuentes, V. 2007. Experiences in analysis of pressures and impacts from agriculture on water resources and developing a related programme of measures. *In:* Cherlet, M. (ed.). Institute for environment and sustainability.

Gao, H., Shi, X., Zhu, C., Bohn, T. J., Su, F., Sheffield, M. P., Lettenmaier, D. P., Wood, E. F. 2010. Water budget record from Variable Infiltration Capacity (VIC) model. *Algorithm theoretical basis document for terrestrial water cycle data records*.

Gao, X., Pal, J. S., Giorgi, F. 2006. Projected changes in mean and extreme precipitation over the Mediterranean region from a high resolution double nested RCM simulation. *Geophysical Research Letters,* 33.

Gassman, P. W., Reyes, M. R., Green, C. H., Arnold, J. G. 2007. The soil and water assessment tool: historical development, applications, and future research directions. *Am. Soc of agricultural and biological engineers,* 50**,** 1211-1250.

Ghasimi, R. 1994. Tajikistan. World Bank Discussion paper No 257S Worldbank.

Giorgi, F., Lionello, P. 2008. Climate change projections for the Mediterranean region. *Global and Planetary Change,* 63**,** 90-104.

GLCF 2007. Global Land Cover Change Facility (GLCF). [Online] Available at: www.landcover.org. [Accessed 10 April 2012].

Gleckler, P. J., Taylor, K. E., Doutriaux, C. 2008. Performance metrics for climate models. *Journal of Geophysical Research*.

Google Earth 2009. [online] available at: earth.google.com

Graf, W. L. 1999. Dam nation: a geographic census of American dams and their large-scale hydrologic impacts *Water Resources Research,* 35**,** 1305-1311.

Graham, D. N., Butts, M. B. 2005. Flexible integrated watershed modeling with MIKE-SHE. *In:* Singh, V. P. F., D.K. (ed.) *Watershed models.* CRC Press.

GRDC 2007. Major river basins of the world / Global Runoff Data Centre. Koblenz, Germany: Federal Institute of Hydrology (BfG).

Hamlet, A. F., Lettenmaier, D. P. 1999. Effects of climate change on hydrology and water resources in the Columbia river basin. *Journal of the American Water Resources Association,* 35.

Hansen, M., DeFries, R., Townshend, J. R., Carroll, M., Dimiceli, C., Sohlberg, R. 2006. Vegetation Continuous Fields MOD44B, 2001 percent tree cover, collection 3, University of Maryland, College Park, Maryland.

Hargreaves, G. H. 1975. Moisture availability and crop production. *Transactions of the American society of agricultural engineers,* 18**,** 980-984.

Harrison, G. P., Wallace, H. W. W. A. R. 2003. Climate change impacts on financial risk in hydropower projects. *IEE Transactions on Power Systems,* 18.

Harrison, G. P., Whittington, H. W. 2002a. Susceptibility of the Batoka Gorge hydroelectric scheme to climate change. *Journal of Hydrology,* 264**,** 230-241.

Harrison, G. P., Whittington, H. W. 2002b. Vulnerability of hydropower projects to climate change. *IEE Proceedings Generation Transmission Distribution,* 149.

Harrison, G. P., Whittington, H. W., Wallace, A. R. 2003. Climate change impacts on financial risk in hydropower projects. *IEE Transactions on Power Systems,* 18.

Heinz Center 2003. Dam removal research: status and prospects. *In:* Graf, W. L. (ed.). Washington, D.C.: Heinz Center.

Hijmans, R. J., Cameron, S. E., Parra, J. L., Jones, P. G., Jarvis, A. 2005. Very high resolution interpolated climate surfaces for global land areas. *International Journal of Climatology,* 25**,** 1965-1978.

Hirabayashi, Y., Kanae, S., Emori, S., Oki, T., Kimoto, M., 2008. Global projections of changing risks of floods and droughts in a changing climate. *Journal of hydrological sciences,* 53**,** 754-772.

ICOLD 2003. World Register of Dams. Paris, France: International Commission on Large Dams.

IPCC 2007. Climate change 2007: synthesis report. International Panel on Climate Change. [online] Available from: http://www.ipcc.ch/pdf/assessment-report/ar4/syr/ar4_syr_spm.pdf [accessed 24 June 2009].

IPCC 2012. Managing the risks of extreme events and disasters to advance climate change adaptation. *A Special Report of Working Groups I and II of the Intergovernmental Panel on Climate Change [Field, C.B., V. Barros, T.F. Stocker, D. Qin, D.J. Dokken, K.L. Ebi, M.D. Mastrandrea,K.J. Mach, G.-K. Plattner, S.K. Allen, M. Tignor, and P.M. Midgley (eds)]. Cambridge University Press, Cambridge, UK, and New York, NY, USA, 582 pp.*

Jaganyi, I., Salagae, M., Matiwane, N. 2008. Integrating floodplain livelihoods into a diverse rural economy by enhancing co-operative management: a case study of the Pongolo floodplain system, South Africa, WRC Report No 1299/1/08 Water Research Commission Pretoria.

Jarvis, A., Reuter, H. I., Nelson, A., Guevara, E. 2008. Hole-filled SRTM for the globe version 4, available from teh CGIAR-CSI SRTM 90m Database: http://srtm.csi.cgiar.org.

Jones, R. N. 2000. Analysing the risk of climate change using an irrigation demand model. *Climate Research,* 14**,** 89-100.

Juen, I. 2007. Modelling observed and future runoff from a glacierized tropical catchment (Cordillera Blanca, Peru). *Global and planetary change,* 59**,** 37-48.

Kaser, G., Juen, I., Georges, C., Gomez, J., Tamayo, W. 2003. The impact of glaciers on the runoff and the reconstruction of mass balance history from hydrological data in the tropical Cordillera Blanca, Peru. *Journal of Hydrology,* 282**,** 130-144.

Kay, A. L., Davies, H. N. 2008. Calculating potential evaporation from climate model data: a source of uncertainty for hydrological climate change impacts. *Journal of hydrology,* 358**,** 221-239.

Keiser, J., De Castro, M. C., Maltese, M. F., Bos, R., Tanner, M., Singe, B. H., Utzinger, J. 2005. Effect of irrigation and large dams on the burden of malaria on a global and regional scale. *Am. J. Trop. Med. Hyg,* 72**,** 392-406.

Kharrufa, N. S. 1985. Simplified equation for evapotranspiration in arid regions. *Beitrage zur hydrologie, Sonderheft 5,* 1.

Kingston, D. G., Taylor, R. G. 2010. Sources of uncertainty in climate change impacts on river discharge and groundwater in a headwater catchment of the Upper Nile basin, Uganda. *Hydrol. Earth Syst. Sci,* 14.

Kirkby, M. J. 1976. Hydrological slope models: the influence of climate. *In:* Derbyshire, E. (ed.) *Geomorphology and climate.* John Wiley.

Klein Tank, A. M. G., Wijngaard, J. B., Können, G. P., Böhm, R., Demarée, G., Gocheva, A., Mileta, M., Pashiardis, S., Hejkrlik, L., Kern-Hansen, C., Heino, R., Bessemoulin, P., Müller-Westermeier, G., Leitass, A., Bukantis, A., Aberfeld, R., Van Engelen, A. F. V., Forland, E., Mietus, M., Coelho, F., Mares, C., Razuvaev, V., Nieplova, E., Cegnar, T., Antonio López, J., Dahlström, B., Moberg, A., Kirchhofer, W., Ceylan, A., Pachaliuk, O., Alexander, O. V., Petrovic, P. 2002. Daily dataset of 20th-century surface air temperature and precipitation series for the European Climate Assessment. . *International Journal of Climatology,* 22**,** 1441-1453.

Klimes, J., Vilimek, V., Omelka, M. 2009. Implications of geomorphological research for recent and prehistoric avalanches and related hazards at Huascaran, Peru. *Natural hazards,* 50**,** 193-209.

Kramer, A. 2003. Managing freshwater ecosystems of international water resources - the case of the Maputo river in Mozambique. *Working paper on management in environmental planning*.

Kundzewicz, Z. W., Mata, L. J., Arnell, N. W., Döll, P., Kabat, P., Jiménez, B., Miller, K. A., Oki, T., Şen, Z., Shiklomanov, I. A. 2007. Freshwater resources and their management. Climate Change 2007: Impacts, Adaptation and Vulnerability. Contribution of Working Group II to the Fourth Assessment Report of the Intergovernmental Panel on Climate Change. *In:* M.L. Parry, O. F. C., J.P. Palutikof, P.J. van der Linden, C.E. Hanson (ed.). Cambridge: IPCC.

Langedijk, R. A. 1984. Salt intrusion in the river Maputo: field survey and one-dimensional modelling. Delft: Delft University of Technology, Dep. of civil engineering.

Lehner, B., Czisch, G., Vassolo, S. 2005. The impact of global change on the hydropower potential of Europe: a model-based analysis. *Energy Policy,* 33**,** 839-855.

Lehner, B., Döll, P. 2004. Development and validation of a global database of lakes, reservoirs and wetlands. *Journal of Hydrology,* 296**,** 1-22.

Lehner, B., Döll, P., Alcamo, J., Henrichs, T., Kaspar, F. 2006. Estimating the impact of global change on flood and drought risks in Europe: a continental integrated analysis . *Climatic Change,* 75**,** 273-299.

Lehner, B., Reidy Liermann, C., Revenga, C., Vorosmarty, C., Fekete, B., Crouzet, P., Doll, P., Endejan, M., Frenken, K., Magome, J., Nillsson, C., Robertson, J. C., Rodel, R., Sindorf, N., Wisser, D. 2011. High-resolution mapping of the world's reservoirs and dams for sustainable river-flow management. *Frontiers in Ecology and Environment*.

Lehner, B., Verdin, K., Jarvis, A. 2008a. HydroSHEDS Technical documentation version 1.1.

Lehner, B., Verdin, K., Jarvis, A. 2008b. New global hydrography derived from spaceborn elevation data. *Eos, Transactions.* AGU.

Lenton, T.M., Held, H., Kriegler, E., Hall, J.W., Lucht, W., Rahmstorf, S., Schellnhuber, H.J. 2008. Tipping elements in the Earth's climate system. *Proceedings of the national academy of sciences,* 105**,** 1786-1793.

Liu, Y. B., Gebremeskel, S., De Smedt, F., Pfister, L. 2002. Prediction of floods with the WetSpa model. *Annals of the Warsaw Agricultural University - SGGW, Land reclamation,* 33**,** 71-80.

Livers, J. T. 1942. Some limitations to use of coefficient of variation. *Agricultural and applied economics association,* 24**,** 892-895.

Lowe, J. A., Hewit, C. D., Van Vuuren, D. P., Johns, T. C., Stehfest, E., Royer, J. F., Van der Linden, P. J. 2009. New study for climate modeling, analyses, and scenarios. *Eos Trans. AGU,* 90.

Magome, J., Ishidaira, H., Takeuchi, K. 2006. Unpublished dataset. University of Yamanashi, Japan.

Mann, M. E., Jones, P. D. 2003. Global surface temperatures over the past two millenia. *Geophysical Research Letters,* 30.

Mark, B. G. 2010. Climate change and tropical Andean glacier recession: evaluating hydrologic changes and livelihood vulnerability in the Cordillera Blanca, Peru. *Annals of the Association of American geographers*.

Mark, B. G., Bury, J., McKenzie, J. M., French, A., Baraer, M. 2010. Climate change and tropical andean glacier recession: evaluating hydrologic changes and livelihood vulnerability in the cordillera blanca, Peru. *Annals of the Association of American geographers,* 100**,** 1-12.

Mark, B. G., McKenzie, J. M., Gomez, J. 2005. Hydrochemical evaluation of changing glacier meltwater contribution to stream discharge: Callejon de Huaylas, Peru. *Hydrological Sciences,* 50.

Markham, C. G. 1970. Seasonality of precipitation in the United States. *Annals of the Association of American geographers,* 60**,** 593-597.

Markoff, M. S., Cullen, A. C. 2008. Impact of climate change on Pacific Northwest hydropower. *Climatic Change,* 87**,** 451-469.

Maurer, D. 2009. *Past and future runoff from glacier-covered tropical catchment basins in the Cordillera Blanca, Peru. A modeling approach based on IPCC scenarios. .* MSc thesis, University of Innsbruck.

Maurer, D., Adam, J. C., Wood, A. W. 2009. Climate model based consensus on the hydrologic impacts of climate change to the Rio Lempa basin of Central America. *Hydrol. Earth Syst. Sci,* 13**,** 183-194.

Maurer, E. P. 2007. Uncertainty in hydrologic impacts of climate change in the Sierra Nevada, California under two emissions scenarios. *Climatic Change,* 82**,** 309-325.

McCarney-Castle, K., Voulgaris, G., Kettner, A. J. 2010. Analysis of fluvial suspended sediment load contribution through anthropocene history to the south Atlantic bight coastal zone, U.S.A. *Journal of Geology,* 118**,** 399-416.

McCartney, M., King, J. 2011. Use of decision support systems to improve dam planning and dam operation in Africa. *CPWF R4D series.* CPWF.

McCully, P. 1996. *Silenced Rivers: the ecology and politics of large dams,* London, Zed Books.

McKerchar, A., Shankar, U., Hicks, M. 2005. Water harvesting: an ideal use of floodwaters? *Water and atmosphere,* 13.

McKinney, D. C., Anderson, G., Byers, A. 2011. Adaptation to climate change: case study - glacial retreat and adaptation options in Peru's rio Santa basin. International Resources Group (IRG).

Meehl, G. A., Stocker, T. F., Collins, W. D., Friedlingstein, P., Gaye, A. T., Gregory, J. M., Kitoh, A., Knutti, R., Murphy, J. M., Noda, A., Raper, S. C. B., Watterson, I. G., Weaver, A. J., Zhao, Z.-C. 2007. Global Climate Projections: Climate Change 2007: The Physical Science Basis. Contribution of Working Group I to the Fourth Assessment Report of the Intergovernmental Panel on Climate Change. *In:* Solomon, S., Qin, D., Manning, M., Chen, Z., Marquis, M., Averyt, K. B., Tignor, M. & Miller, H. L. (eds.). Cambridge: IPCC.

Menne, M. J., William, C. N. j., Vose, R. S. 2005. NOAA National Climatic Data Center Asheville.

Middelkoop, H., Daamen, K., Gellens, D., Grabs, W., Kwadijk, J. C. J., Lang, H., B.W.A.H.Parmet, Schädler, B., Schulla, J., Wilke, K. 2001. Impact of climate change on hydrological regimes and water resources management in the Rhine basin. *Climatic Change,* 49**,** 105-128.

Mimikou, M. A., Baltas, E. A. 1997. Climate change impacts on the reliability of hydroelectric energy production. *Hydrological Sciences Journal,* 42**,** 661-678.

Minville, M., Brissette, F., Krau, S., Leconte, R. 2009. Adaptation to climate change in the management of a Canadian water-resources system exploited for hydropower. *Water Resources Management*.

Monteith, J. L. 1965. Evaporation and environment. *Symposia of the Society for Experimental Biology,* 19**,** 205-234.

Morgan, R. P. C., Nearing, M. 2011. *Handbook of erosion modelling*.

Moss, R. H., Edmonds, J. A., Hibbard, K. A., Manning, M., Rose, S. K., Van Vuuren, D. P., Carter, T. R., Emori, S., Kainuma, M., Kram, T., Meehl, G. A., Mitchell, J. F. B., Nakicenovic, N., Riahi, K., Smith, S. J., Stouffer, R. J., Thomson, A. M., Weyant, J. P., Wilbanks, T. J. 2010. The next generation of scenarios for climate change research and assessment. *Nature,* 463.

MRC 2008. Mainstream dams. Mekong River Commission [Online] Available at: http://www.mrcmekong.org/about_mrc.htm#MRC [accessed 10 September 2009].

Mu, Q., Zhao, M., Running, S. W. 2011. Improvements to a MODIS global terrestrial evapotranspiration algorithm. *Remote sensing of environment,* 115**,** 1781-1800.

Mulligan, M. 2006a. Estimates mean snow water equivalent. Available at: http://www.policysupport.org/simterra.

Mulligan, M. 2006b. Global Gridded 1km TRMM Rainfall Climatology and Derivatives. Version 1.0. Database: http://geodata.policysupport.org/2b31climatology

Mulligan, M. 2006c. GNS places database. [Online] Available from: http://geodata.policysupport.org/places [Accesses 20 August 2012].

Mulligan, M. 2006d. MODIS MOD35 pan-tropical cloud climatology. Version 1. September 2006 [online] Available at:http://www.ambiotek.com/clouds.

Mulligan, M. 2006e. Processed coastline and water bodies dataset from NASA SRTM Water Body Data.Version 1.0. Database [online] available from: http://geodata.policysupport.org/swbd.

Mulligan, M. 2007. Terrascope : a Google Earth Implementation of the Landsat geocover datasets. Version 1.0.[online] available from: http://geodata.policysupport.org/terrascope.

Mulligan, M. 2009. SimTerra: a gridded global database of climate, terrain and land cover maps at 1 km and 100 m resolution for modelling studies [online]. Available from www.policysupport.org/simterra.

Mulligan, M. 2011. Climate change and environmental drivers. *The 3rd International Forum on Water and Food.* Tshwane, South Africa.

Mulligan, M. 2012a. GOOD2 Dam reservoir areas. Calculated using SWBD dataset and Global dams database (Mulligan et al., 2009).

Mulligan, M. 2012b. Mean monthly soil moisture climatology based on VUA soil moisture dataset (Owe et al., 2008).

Mulligan, M. 2012c. MODIS long term monthly mean PET data 1984-2006 based on MODIS MOD16 (Mu et al., 2011).

Mulligan, M. 2012d. WaterWorld: a self-parameterising, physically-based model for application in data-poor but problem-rich environments globally (in review). *Hydrology Research*.

Mulligan, M., Burke, S. M. 2005. FIESTA Fog Interception for the Enhancement of Streamflow in Tropical Areas. Final technical report for AMBIOTEK contribution to DFID FRP R7991.

Muñoz, J. R., Sailor, D. J. 1998. A modelling methodology for assessing the impact of climate variability and climatic change on hydroelectric generation. *Energy Conversion and Management,* 39**,** 1459-1469.

Murphy, N. 2010. *An analysis of hydrological model undertainty at the local stage of a climate change impact assessment in the Suir catchment.* Master of Literature Degree, National university of Ireland.

Nakicenovic, N., Alcamo, J., Davis, G., de Vries, B., Fenhann, J., Gaffin, S., Gregory, K., Grubler, A., Jung, T. Y., Kram, T., Emilio la Rovere, E., Michaelis, L., Mori, S.,

Morita, T., Pepper, W., Pitcher, H., Price, L., Riahi, K., Roerhl, A., Rogner, H. H., Sankovski, A., Schlesinger, M., Shukla, P., Smith, S., Swart, R., van Rooyen, S., Victor, N., Dadi, Z. (eds.) 2000. *Special report on emissions scenarios,* Cambrige: Cambridge University Press.

NASA 2005. SRTM Water Body Data (SWBD) v.2.0 [online] Available at: http://www2.jpl.nasa.gov/srtm/ [Accessed May 2010].

National register of large dams in India 2009. National register of large dams in India. [online] Available at: http://www.indiaenvironmentportal.org.in/files/National%20Register%20of%20Large%20Dams%202009.pdf [Accessed: 02 February, 2010]

Neitsch, S. L., Arnold, J. G., Kiniry, J. R., Williams, J. R. 2005. Soil and Water Assessment Tool Theoretical Documentation. Temple, Texas.

Nelson, E., Mendoza, G., Regetz, J., Polasky, S., Tallis, H. T., Cameron, D., Chan, K. M., Daily, G. C., Goldstein, J., Kareivar, P. M., Lonsdorf, E., Naidoo, R., Ricketts, T., Shaw, M. R. 2009. Modeling multiple ecosystem services, biodiversity conservation, commodity production, and tradeoffs at landscape scales. *Frontiers in Ecology and Environment,* 7**,** 4-11.

New, M., Hulme, M., Jones, P. D. 2000. Global 30-year mean monthly climatology 1901-1960. Data set.

New, M., Lister, D., Hulme, M., Makin, I. 2003. A high-resolution data set of surface climate over global land areas. *Climate Research,* 21**,** 1-25.

NID 2007. National Inventory of Dams. [online] Available at: http://geo.usace.army.mil/pgis/f?p=397:1:0.

Nijssen, B., O'Donnel, G. M., Hamlet, A. F., Lettenmaier, D. P. 2001. Hydrologic sensitivity of global rivers to climate change. *Climatic Change,* 50**,** 143-175.

Nilsson, C., Reidy, C. A., Dynesius, M., Revenga, C. 2005. Fragmentation and flow regulation of the world's large river systems. *Science,* 308.

O'Callaghan, J. F., Mark, D. M. 1984. The extraction of drainage networks from digital elevation data. *Computer Vision, Graphics, and Image Processing,* 28**,** 323-344.

Oki, T., Kanae, S. 2006. Global hydrological cycles and worl water resources. *Science,* 313**,** 1068.

Oudin, L., Hervieu, F., Michel, C., Perrin, C., Andréassian, V., Anctil, F., Loumagne, C. 2005a. Which potential evapotranspiration input for a lumped rainfall-runoff model? Part 2 - towards a simple and efficient potential evapotranspiration model for rainfall-runoff modelling. *Journal of hydrology,* 303**,** 290-306.

Oudin, L., Michel, C., Anctil, F. 2005b. Which potential evapotranspiration input for a lumped rainfall-runoff model? Part 1 - Can rainfall-runoff models effectively handle detailed potential evapotranspiration inputs? *Journal of Hydrology,* 303**,** 275-289.

Owe, M., de Jeu, R., Holmes, T. 2008. Multisensor historical climatology of satellite-derived global land surface moisture. *Journal of Geophysical Research,* 113.

Palmer, M. A., C.A. Reidy Liermann, Nilsson, C., Flörke, M., J. Alcamo, P. Sam Lake, bond, N. 2008. Climate change and the world's river basins: anticipating management options. *Frontiers in Ecology and Environment,* 6.

Palmieri, A., Shah, F., Dinar, A. 2001. Economics of reservoir sedimentation and sustainable management of dams. *Journal of Environmental Management,* 61**,** 149-163.

Payne, J. T., Wood, A. W., Hamlet, A. F., Palmer, R. N., Lettenmaier, D. P. 2004. Mitigating the effects of climate change on the water resources of the Columbia river basin. *Climatic Change,* 62**,** 233-256.

PCRaster 2008. PCRaster environmental modelling software. [Online] Available at: pcraster.geo.uu.nl.

Penman, H. L. 1948. Natural evaporation from open water, bare soil and grass. *Proceedings of the Royal Society of London,* 193**,** 120-146.

Petts, G. E. 1984. *Impounded rivers: perspectives for ecological management,* Chichester, John Wiley and Sons.

Pierce, D. W., Barnett, T. P., Santer, B. D., Gleckler, P. J. 2009. Selecting global climate models for regional climate change studies. *Proc. National Academy of Science USA,* 106**,** 8441-8446.

Porretta-Brandyk, L., Chormanski, J., Ignar, S., Okruszko, T., Brandyk, A., Szymczak, T., Krezalek, K. 2011. Evaluation and verification of the WetSpa model based on selected rural catchments in Poland. *Journal of water and land development***,** 115-133.

Power technology. 2012. *Guri hydroelectric power plant, Orinoco, Venezuela. Available at: http://www.power-technology.com/projects/gurihydroelectric/* [Online]. [Accessed 30 August 2012].

Priestley, C. H. B., Taylor, K. E. 1972. On the assessment of surface heat flux and evaporation using large-scale parameters. *Monthly weather review,* 100**,** 81-92.

Racoviteanu, A. E., Arnaud, Y., Williams, M. W., Ordonez, J. 2008. Decadal changes in glacier parameters in the Cordillera Blanca, Peru, derived from remote sensing. *Journal of Glaciology,* 54**,** 499-510.

Ramankutty, N., Evan, A. T., Monfreda, C., Foleyet, J. A. 2008. Farming the planet:1. Geographic distribution of global agricultural lands in the year 2000. *Global biogeochemical cycles,* 22.

Ramirez, J., Jarvis, A. 2010a. Disaggregation of global circulation model outputs.

Ramirez, J., Jarvis, A. 2010b. Disaggregation of Global Circulation Model outputs. Decision and policy analysis working paper no.2 Available at: http://www.ccafs-climate.org/media/ccafs_climate/docs/Disaggregation-WP-02.pdf.

Reichler, T., Kim, J. 2008. How well do coupled models simiulate today's climate. *Bull Am Meteorol Soc.,* 89.

Reidy Liermann, C. 2007. *Ecohydrologic impacts of dams: a global assessment.* Doctoral, Umea University.

Rödel, R., Hoffmann, T. 2005. Quantifying the efficiency of river regulation. *Advances in Geosciences,* 5**,** 75-82.

Rosenzweig, C., Strzepek, K. M., Major, D. C., Iglesias, A., Yates, D. N., McCluskey, A., Hillel, D. 2004. Water resources for agriculture in a changing climate: international case studies. *Global Environmental Change,* 14**,** 345-360.

SADC 2010. SADC economic accounting of water use project Maputo River basin pilot report [online] Available at: http://www.sadcwateraccounting.org/_system/writable/DMSStorage/811en/SADC-EAW%20Maputo%20Pilot%20Report.pdf.

Sáenz, L. 2007. A detailed scientific analysis of the impact of land use change on water resource provision to Bogota D.C. and implications for the development of pes schemes. Unpublished MSc thesis, department of Geography, Kings College London.

Sáenz, L. L. 2011. *Understanding the impact of conservation of cloud forests on water inputs to dams.* PhD, Kings College London.

Sáenz, L. L., Mulligan, M. 2012. The role of tropical montane cloud forests on water inputs to tropical dams and implications of their continuing loss. Submitted.

Sauer, V., Turnipseed, D. P. 2010. Stage measurement at gaging stations: U.S. Geological survey techniques and methods book 3, chap. A7, 45p. [online] Available at: http://pubs.usgs.gov/tm/tm3-a7/.

Schaefli, B., Hingray, B., Musy, A. 2007. Climate change and hydropower production in the Swiss Alps: quantification of potential impacts and related modelling uncertainties. *Hydrology and Earth System Sciences,* 11**,** 1191-1205.

Scherrer, S. C., Appenzeller, C., Liniger, M. A., Schär, C. 2005. European temperature distribution changes in observations and climate change scenarios. *Geophysical Research Letters,* 32.

Schiermeier, Q. 2008. Purification with a pinch of salt. Nature*,* 452.

Schneider, S. H. 1983. CO_2, climate and society: a brief overview. *In:* Chen, R. S., Boulding, E. M. & Schneider, S. H. (eds.) *Social science research and climatic change: an interdisciplinary appraisal.* Dordrecht: D. Reidel Publishing.

Scudder, T. 2005. *The future of large dams: dealing with social, environmental, institutional and political costs,* London, Earthscan.

SEPREM 2010. Spanish society on dams and reservoirs, SEPREM. [Online] Available at: www.seprem.es [Accessed 24 March, 2010].

Serra, P., Pons, X., Sauri, D. 2008. Land-cover and land-use change in a Mediterranean landscape: a spatial analysis of driving forces integrating biophysical and human factors. *Applied Geography,* 28**,** 189-209.

Sieber, J., Purkey, D. 2007. WEAP: Water Evaluation and Planning System. User Guide. Somerville, MA: Stockholm Environment Institute, U.S. Center.

Skoy Plancenter 2009. Joint Maputo river basin water resources study. [online] Available at: http://www.dwaf.gov.za/maputobasinatlas/JMRBWRS_Atlas.html Accessed: 15 Oct 2010.

Stainforth, D. A., Downing, T. E., Lopez, R. W. A., New, M. 2007. Issues in the interpretation of climate model ensembles to inform decisions. *Philos. Trans. R. Soc***,** 2163-2177.

Stanley, D. J., Warne, A. G. 1998. Nile Delta in its destruction phase. *Journal of Coastal Research,* 14**,** 794-825.

STARDEX 2006. Stardex STatistical and Regional dynamical Downscaling of EXtremes for European regions. [Online] Available from: http://www.cru.uea.ac.uk/cru/research/stardex/.

Sternberg, R. 2009. Hydropower's future, the environment, and global energy systems. *Renewable and sustainable energy reviews*.

Still, C.J., Foster, P.N., Schneider, S.H. 1999. Simulating the effects of climate change on tropical montane cloud forests. *Nature,* 398**,** 608-610.

Strahler, A. N. 1952. Dynamic basis of geomorphology. *Geological Society of America Bulletin,* 63**,** 923-938.

Tallis, H. T., Polasky, S. 2009. Mapping and valuing Ecosystem Services as an approach for conservation and natural-resource management. *The year in ecology and conservation biology,* 1162**,** 265-283.

Tallis, H. T., Ricketts, T., Ennaanay, D., Nelson, E., Vigerstol, K., Mendoza, G., Wolny, S., Olwero, N., Aukema, J., Foster, J., Forrest, J., Cameron, D. 2008. InVEST 1.003 beta user's guide. The natural capital project, Stanford.

Tebaldi, C., Knutti, R. 2007. The use of multi-model ensemble in probabilistic climate projections. *Philos. Trans. R. Soc,* 365**,** 2053-2075.

Tebaldi, C., Knutti, R. 2010. Climate models and their projections of future changes. *In:* D, L. & Burke, M. (eds.) *Climate change and food security: adapting agriculture to a warmer world.*

Tedesco, P. A., Hugueny, B., Oberdorff, T., Durr, H. H., Merigoux, S., de Merona, B. 2008. River hydrological seasonality influences life history strategies of tropical riverine fishes. *Oecologia,* 156**,** 691-702.

Teutschbein, C., Seibert, J. 2010. Regional climate models for hydrological impact studies at the catchment scale: a review of recent modeling strategies. *Geography Compass,* 4/7**,** 834-860.

Thornes, J. B. 1990. *The interaction of erosional and vegetational dynamics in land degradation: spatial outcomes,* New York, John Wiley and Sons Ltd.

Thorntwaite, C. 1948. An approach toward a rational classification of climate. *Geogr. Rev.,* 38**,** 55-94.

Todd, M. C., Taylor, R. G., Osborn, T., Kingston, D., Arnell, N., Gosling, S. N. 2010. Quantifying the impact of climate change on water resources at the basin scale on five continents - a unified approach. *Hydrol. Earth Syst. Sci,* 7**,** 7485-7519.

Trenberth, K. E., Jones, P. D., Ambenje, P., R. Bojariu, D. E., Tank, A. K., Parker, D., Rahimzadeh, F., Renwick, J. A., Rusticucci, M., Soden, B., Zhai, P. 2007. Observations: Surface and Atmospheric Climate Change: Climate Change 2007: The Physical Science Basis. Contribution of Working Group I to the Fourth Assessment Report of the Intergovernmental Panel on Climate Change. *In:* Solomon, S., Qin, D., Manning, M., Chen, Z., Marquis, M., Averyt, K. B., Tignor, M. & Miller, H. L. (eds.). Cambridge: IPCC.

UN 2012. UN Energy Statistics Database 2012 [Online] Available at: data.un.org [Accessed 8 May 2012].

USACE 2006. United States Army Corps of Engineers: National Inventory of dams. [online] Available at: http://geo.usace.army.mil/pgis/f?p=397:1:0.

USGS 2004. Information about water year 2004. Available online: http://ga2.er.usgs.gov/LibAreportPDF/2004/Discharge/sp02198500.pdf.

USGS 2011. National Water Information System [online] Available at: http://waterdata.usgs.gov/nwis Accessed: 10 January 2011.

Van Deursen, W. P. A. 1995. *Geographical Information Systems and Dynamic Models Development and application of a prototype spatial modelling language.* PhD thesis, University of Utrecht.

VanRheenen, N. T., Wood, A. W., Palmer, R. N., Lettenmaier, D. P. 2004. Potential implications of pcm climate change scenarios for Sacramento-San Joaquin river basin hydrology and water resources. *Climatic Change,* 62**,** 257-281.

Vera, C., Silvestri, G., Liebmann, B., Gonzales, P. 2006. Climate change scenarios for seasonal precipitation in South America from IPCC-AR4 models. *Geophysical Research Letters,* 33.

Verburg, P. H., Eickhout, B., Van Meijl, H. 2008. A multi-scale, multi-model approach for analyzing the future dynamics of European land use. *Annals of regional science,* 42**,** 55-77.

Vergara, W., Deeb, A., Leino, I., Kitoh, A., Escobar, M. 2011. Assessment of the impacts of climate change on mountain hydrology. Washington: The World Bank and ESMAP.

Vicuna, S., Leonardson, R., Hanemann, M. W., Dale, L. L., Dracup, J. A. 2008. Climate change impacts on high elevation hydropower generation in California's Sierra Nevada: a case study in the upper American river. *Climatic Change,* 87.

Vilimek, V., Zapata, M. L., Stemberk, J. 2000. Slope movements in the Callejon de Huaylas, Peru. *Acta Unversitatis Carolinae,* 35**,** 39-51.

Vogiatzakis, I. N., Mannion, A. M., Griffiths, G. H. 2006. Mediterranean ecosystems: problems and tools for conservation. *Progress in Physical Geography,* 30**,** 175-200.

Vörösmarty, C. J., Fekete, B., Tucker, B. A. 1998. Global river discharge, 1807-1991, version 1.1 (RivDIS) dataset. Available online: http://www.daac.ornl.gov. Oak Ridge National Laboratory Distributed Active Archive Center, Oak Ridge, Tennessee.

Vörösmarty, C. J., Meybeck, M., Fekete, B., Sharma, K., Green, P., Syvitski, J. P. M. 2003. Anthropogenic sediment retention: major global impact from registered river impoundments. *Global and planetary change,* 39**,** 169-190.

Vuille, M., Francou, B., Wagnon, P., Juen, I., Kaser, G., Mark, B. G., Bradley, R. S. 2008. Climate change and tropical Andean glaciers: Past, present and future. *Earth Science Reviews,* 89**,** 79-96.

Vuille, M., Werner, R. S., Bradley, R. S., Keimig, F. 2003. 20th century climate change in the tropical Adnes: observations and model results. *Climatic Change,* 59**,** 75-99.

Wada, Y., Van Beek, L.P.H., Van Kempen, C.H., Reckman, J.W.T.M., Vasak, S., Bierkens, M.F.P. 2010. Global depletion of groundwater resources. *Geophysical Research Letters,* 37.

Walsh, R. P. D., Lawler, D. M. 1981. Rainfall seasonality: description, spatial patterns and change through time. *Weather,* 36**,** 201-209.

Walter, M. T., Brooks, E. S., McCool, D. K., King, L. G., Molnau, M., Boll, J. 2005. Process based snowmelt modelling: does it require more input data than temperature-index modelling? *Journal of Hydrology,* 300**,** 65-75.

Wang, Z.-M., Batelaan, O., De Smedt, F. 1996. A distributed model for water and energy transfer between soil, plants and atmosphere (WetSpa). *Phys. Chem. Earth,* 21**,** 189-193.

WaterWorld 2012. WaterWorld Policy Support System [online] Available at: www.policysupport.org [accessed 24 Sep 2012].

World Commission on Dams (eds.) 2000. *Dams and development: a new framework for decision-making,* London: Earthscan.

Wesseling, C. G., D., K., Burrough, P. A., Van Deursen, W. P. A. 1996. Integrating dynamic environmental models in GIS: the development of a dynamic modelling language. *Transactions in GIS,* 1**,** 40-48.

Wetterhal, F, Pappenberger, F., He, Y., Freer, J., Cloke, H.L., 2012. Conditioning model output statistics of regional climate model precipitation on circulation patterns. *Nonlinear processes in geophysics (in press)*.

Wigmosta, M. S., Vail, L., Lettenmaier, D. P. 1994. A distributed hydrology-vegetation model for complex terrain. *Water Resources Research,* 30**,** 1665-1679.

Wilby, R. L. 2005. Uncertainty in water resource model parameters used for climate change impact assessment. *Hydrological Processes,* 19**,** 3201-3219.

Wilby, R. L., Charles, S. P., Zorita, E., Timbal, B., Whetton, P., Mearns, L. O. 2004. Guidelines for use of climate scenarios developed from statistical downscaling methods.

Worldbank 2012. World Development Indicators 2012 [Online] Available at: http://data.worldbank.org/data-catalog/world-development-indicators [Accessed 7 May 2012].

WWF 2004. Rivers at Risk. Dams and the future of freshwater ecosystems. WWF/WRI.

Yang, W., Andreasson, J. Graham, L.P., Olsson, J. Rosberg, J. Wetterhall, F. 2010. Distribution based scaling to improve the usability of RCM regional climate model projections for hydrological climate change impact studies. *Hydrology research,* 41**,** 211-229.

Yates, D. N., Sieber, J., Purkey, D., Lee, A. H. 2005. WEAP21 - A demand, priority-, and preference-driven water planning model Part 1: model characteristics. *Water International,* 30**,** 487-500.

Appendices

Appendix I: Dam validation data

Dam ID	*Dam*	*Country*	*Area GOOD^2 (2011) km^2*	*Reported catchment area km^2*	*Difference with reported area (%)*
1	Bouroumi	Algeria	195	150	23.1
2	Deurdeur	Algeria	413	468	-13.3
3	Lekhal	Algeria	177	189	-6.8
4	Durlassboden	Austria	74	75	-1.4
5	Xingo	Brazil	613065	608700	0.7
6	Tucuri	Brazil	761113	758000	0.4
7	Itaipu	Brazil	902004	820000	10.0
8	Foz do Areia	Brazil	36358	29800	22.0
9	Embarrocado	Brazil	44465	29000	53.3
10	Segredo	Brazil	41358	34100	21.3
11	Nova Ponte	Brazil	16960	15300	10.8
12	Furnas	Brazil	57665	50464	14.3
13	Sao Simao	Brazil	185743	171000	8.6
14	Machadinho	Brazil	38260	32000	19.6
15	ITA	Brazil	54378	44500	22.2
16	Itaparica	Brazil	586391	592000	-0.9
17	Corumba	Brazil	29620	27800	6.5
18	Mirimbondon	Brazil	115216	116700	-1.3
19	Tres Iramos	Brazil	69801	69900	-0.1
20	Salto Santiago	Brazil	53133	43900	21.0
21	Miranda	Brazil	20492	17000	20.5
22	Tres Marias	Brazil	50053	50600	-1.1
23	Nova Avanhandava	Brazil	60077	62300	-3.6
24	Dosspat	Bulgaria	369	432	-16.9
25	Ogosta	Bulgaria	1002	985	1.7
26	Jrebchevo	Bulgaria	1351	1372	-1.6
27	Yasna Poliana	Bulgaria	52	50	3.1
28	Bebresh	Bulgaria	79	69	12.7

29	Malko Sharkovo	Bulgaria	183	187	-2.4
30	Gorni Dabnik	Bulgaria	39	39	1.0
31	Bagre	Burkina Faso	32714	33500	-2.3
32	Guavio	Colombia	1368	1350	1.3
33	Betania	Colombia	12957	13572	-4.5
34	Salvajina	Colombia	3640	3652	-0.3
35	Esmeralda	Colombia	2443	2403	1.7
36	Urra 1	Colombia	4659	4600	1.3
37	Miel I	Colombia	770	7700	-90.0
38	Alto Anchicaya	Colombia	374	380	-1.6
39	Porce II	Colombia	3353	3000	11.8
40	Prado	Colombia	1597	1400	14.1
41	Santa Rita	Colombia	1314	1250	5.1
42	Rio Grande II	Colombia	1150	1400	-17.9
43	Guillermo CAno	Colombia	446	428	4.2
44	Santa Rita (Dike I)	Colombia	1314	1250	5.1
45	Santa Rita (Dike II)	Colombia	1314	1250	5.1
46	Neusa	Colombia	134	145	-7.6
47	Troneras	Colombia	373	396	-5.8
48	Calima	Colombia	315	315	0.0
49	Punchina	Colombia	613	592	3.5
50	Playas	Colombia	161	202	-20.3
51	Regadera	Colombia	146	150	-2.7
52	La Fe	Colombia	146	78	87.2
53	D'Inga	Congo (DRC)	3765224	3800000	-0.9
54	Nzilo	Congo (DRC)	17740	17551	1.1
55	Nzeke	Congo (DRC)	18324	18338	-0.1
56	Mobaye	Congo (DRC)	399570	400000	-0.1
57	Koni	Congo (DRC)	14576	12960	12.5
58	Ruzizi I	Congo (DRC)	7466	6884	8.5
59	Ruzizi II	Congo (DRC)	7466	7000	6.7
60	Mwadinguisha	Congo (DRC)	13060	12889	1.3
61	Prancevici	Croatia	3006	3850	-28.1
62	Razovac	Croatia	1379	1400	-1.5
63	Botonega	Croatia	80	73	9.3

64	Yermasoyia	Cyprus	167	157	6.0
65	Asprokremmos	Cyprus	216	224	-3.7
66	Kalavasos	Cyprus	110	96	12.7
67	Akhna	Cyprus	31	30	2.9
68	Evretou	Cyprus	92	91	1.1
69	Stanovice	Czech Republic	92	92	-0.4
70	Klicava	Czech Republic	76	80	-4.9
71	Svihov	Czech Republic	1169	1178	-0.8
72	Nechranice	Czech Republic	3428	3590	-4.7
73	High Aswan Dam	Egypt	3068155	2200000	39.5
74	Vouglans	France	1301	1120	13.9
75	Serre Poncon	France	3585	3600	-0.4
76	Sarrans	France	2466	2540	-3.0
77	Grandval	France	1766	1782	-0.9
78	Le Chastang	France	4164	4127	0.9
79	Saint Etienne Cantales	France	754	691	8.4
80	Enchanet	France	452	452	-0.1
81	Villerest	France	6345	6520	-2.8
82	Tolla	France	127	132	-4.3
83	Les Fades	France	1292	1300	-0.6
84	Alesani	France	57	55	3.5
85	Bleiloch	Germany	1233	1240	-0.6
86	Hohenwarte	Germany	1566	1657	-5.8
87	Schwammenauel	Germany	425	288	32.2
88	Pohl	Germany	148	160	-8.2
89	Eibenstock	Germany	156	200	-28.5
90	Kremasta	Greece	3546	3570	-0.7
91	Kastraki	Greece	4078	4118	-1.0
92	Kolka	Iceland	1590	1520	4.4
93	Srisailam	India	203552	206242	-1.3
94	Nagarjuna Sagar	India	215734	215192	0.3

95	Sholayar	India	188	122	54.1
96	Koyna	India	906	891	1.7
97	Bhadra	India	2076	1968	5.5
98	Ukai	India	60748	62225	-2.4
99	Upper Aliyar	India	120	121	-0.8
100	Upper Bhavani	India	37	34	8.8
101	Parambikulam	India	268	231	16.0
102	Balimela	India	5000	4910	1.8
103	Mettur	India	40923	42215	-3.1
104	Kadana	India	25654	25520	0.5
105	Cirata	Indonesia	4063	4119	-1.4
106	Wadaslintang	Indonesia	148	196	-24.5
107	Batu Tegi	Indonesia	392	420	-6.7
108	Mrica	Indonesia	1116	1022	9.2
109	Jatiluhur	Indonesia	4420	4500	-1.8
110	Wonorejo	Indonesia	110	126	-12.7
111	Saguling	Indonesia	2427	2283	6.3
112	Karan Kates	Indonesia	2037	2050	-0.6
113	Lahor	Indonesia	164	160	2.5
114	Bili Bili	Indonesia	370	384	-3.6
115	Koto Panjang	Indonesia	334	334	0.0
116	Kedung Ombo	Indonesia	633	614	3.1
117	Sempor	Indonesia	41	43	-4.7
118	Riam Kanan	Indonesia	1116	1043	7.0
119	Sermo	Indonesia	20	22	-9.1
120	Selorejo	Indonesia	220	236	-6.8
121	Wlingi	Indonesia	2940	2890	1.7
122	Sigura Gura	Indonesia	3160	3730	-15.3
123	Mamak	Indonesia	90	101	-10.9
124	Sampean baru	Indonesia	739	735	0.5
125	Garung	Indonesia	60	47	27.7
126	Bening	Indonesia	76	90	-15.6
127	Pacal	Indonesia	76	90	-15.6
128	Sengguruh	Indonesia	2037	1659	22.8
129	Pengga	Indonesia	382	340	12.4

130	Way rarem	Indonesia	336	328	2.4
131	Pieve di Cadore	Italy	787	819	-4.0
132	Salto	Italy	926	741	20.0
133	Cantoniera	Italy	2028	2056	-1.4
134	Place Moulin	Italy	77	74	3.9
135	Forte Buso	Italy	68	66	2.9
136	Kossou	Ivory Coast	152	150	1.3
137	Buyo	Ivory Coast	48615	46000	5.7
138	Ayame I	Ivory Coast	9001	9320	-3.4
139	Ayame	Ivory Coast	9103	9320	-2.3
140	Tabbo	Ivory Coast	60803	58700	3.6
141	Tagokura	Japan	712	702	1.4
142	Takami	Japan	276	283	-2.5
143	Miboro	Japan	383	396	-3.4
144	Sakuma	Japan	3807	3827	-0.5
145	Ogochi	Japan	268	263	1.9
146	Okutadami	Japan	429	426	0.7
147	Katse	Lesotho	2355	1866	26.2
148	Ghan	Libya	636	650	-2.2
149	Tikves	Macedonia	5362	5361	0.0
150	Kalimanci	Macedonia	1121	1100	1.9
151	Varahina	Madagascar	397	336	18.2
152	Kenyir	Malasya	2580	7000	-63.1
153	Temengor	Malasya	3396	2830	20.0
154	Batang	Malasya	1103	2175	-49.3
155	Pedu	Malasya	253	283	-10.6
156	kenering	Malasya	6595	8950	-26.3
157	Jor	Malasya	1115	1104	1.0
158	Jor II	Malasya	1115	1104	1.0
159	batu	Malasya	99	195	-49.2
160	Sultan abu Bakar	Malasya	983	983	0.0
161	Bersia	Malasya	5595	5280	6.0
162	Klang gates	Malasya	311	311	0.0
163	Chenderoh	Malasya	9514	14700	-35.3
164	Mahang	Malasya	48	50	-4.0

165	Al Wahda	Marocco	2679	6200	-131.4
166	Carhuacocha	Peru	4346	4000	8.7
167	Roznow	Poland	4129	4865	-17.8
168	Tresna	Poland	1039	1030	0.9
169	Czorsztyn-Niedzica	Poland	1003	1147	-14.4
170	Goczalkowice	Poland	584	523	10.4
171	Jeziorsko	Poland	8747	9063	-3.6
172	Porabka	Poland	1094	1076	1.6
173	Chancza	Poland	475	490	-3.2
174	Klimkowka	Poland	212	210	0.9
175	Miranda do Douro	Portugal	63214	63500	-0.5
176	Salamonde	Portugal	601	642	-6.8
177	Alqueva	Portugal	53841	55000	-2.2
178	Canicada	Portugal	826	860	-4.1
179	Maranhao	Portugal	2461	2282	7.3
180	Vilar	Portugal	369	359	2.7
181	Azibo	Portugal	108	91	15.7
182	Funcho	Portugal	245	200	18.4
183	Guilhofrei	Portugal	123	122	1.2
184	Aguieira	Portugal	3239	3113	3.9
185	Siriu	Romania	700	680	2.9
186	Cincis	Romania	323	301	6.8
187	Irkutsk	Russia	596860	604300	-1.2
188	Goedertrouw	South Africa	1620	1280	26.6
189	Paris	South Africa	2137	1700	25.7
190	Blyderiverspoor	South Africa	2551	2176	17.2
191	Fika-Patso	South Africa	82	85	-3.5
192	Inanda	South Africa	5282	1172	350.7
193	Sandile	South Africa	431	348	23.9
194	Hartebeespoort	South Africa	4205	4110	2.3
195	Thabina	South Africa	177	30	490.0
196	Bridle drift	South Africa	1647	1176	40.1
197	Kat River	South Africa	232	258	-10.1
198	Kogelberg	South Africa	241	179	34.6
199	Loskop	South Africa	13886	12285	13.0

200	Injaka	South Africa	1984	210	844.8
201	Kwena	South Africa	1198	698	71.6
202	Groendal	South Africa	395	282	40.1
203	Driekoppies	South Africa	1037	900	15.2
204	Knellpoort	South Africa	821	776	5.8
205	Xonxa	South Africa	2022	1486	36.1
206	Los Peares	Spain	4569	4553	0.4
207	Susqueda	Spain	1558	1775	-13.9
208	Valdecanas	Spain	36363	36540	-0.5
209	El Atazar	Spain	982	946	3.7
210	Almendra	Spain	7433	7100	4.5
211	Tous Spain	Spain	19529	17821	8.7
212	Aldeadavila	Spain	71133	73458	-3.3
213	La Fernandina	Spain	744	663	10.9
214	Guadalmena	Spain	1277	1323	-3.6
215	Contreras	Spain	3321	3331	-0.3
216	Benageber	Spain	3461	3495	-1.0
217	Giribaile	Spain	1717	1634	4.8
218	Tranco de Beas	Spain	613	550	10.3
219	El Cenajo	Spain	2264	1273	43.8
220	Camarasa	Spain	2842	2850	-0.3
221	Itoiz	Spain	444	510	-14.9
222	Quentar	Spain	90	102	-13.8
223	Canales	Spain	187	176	5.8
224	Bao	Spain	689	726	-5.4
225	Las Portas	Spain	137	168	-22.6
226	La Cohilla	Spain	88	91	-3.4
227	San Esteban	Spain	5900	7216	-22.3
228	Eume	Spain	390	500	-28.2
229	Santa Ana	Spain	1752	1758	-0.3
230	La Vinuela	Spain	96	119	-23.8
231	El Limonero	Spain	146	166	-13.9
232	San Clemente	Spain	140	152	-8.6
233	Vicatoria	Sri Lanka	1792	1869	-4.1
234	Randenigala	Sri Lanka	2248	2305	-2.5

235	Kotmale	Sri Lanka	578	545	6.1
236	Senanayaka Samudra	Sri Lanka	967	983	-1.6
237	Maduru Oya	Sri Lanka	469	453	3.5
238	Mousakelle	Sri Lanka	108	128	-15.6
239	Udawalawe	Sri Lanka	1162	1162	0.0
240	Muruthawela	Sri Lanka	116	110	5.5
241	Nalanda	Sri Lanka	441	123	258.5
242	Huruluwewa	Sri Lanka	595	197	202.0
243	Inginimitiya	Sri Lanka	510	550	-7.3
244	Bowatenna	Sri Lanka	422	479	-11.9
245	Iranamadu	Sri Lanka	581	581	0.0
246	Kandalma	Sri Lanka	482	482	0.0
247	Kantalai	Sri Lanka	419	482	-13.1
248	Morawewa	Sri Lanka	75	93	-19.4
249	Pdayaviya	Sri Lanka	532	532	0.0
250	Mahakanadarawa	Sri Lanka	323	323	0.0
251	Kalawewa	Sri Lanka	850	827	2.8
252	Unnichchai	Sri Lanka	252	271	-7.0
253	Hackren	Sweden	1206	1153	4.4
254	Flasjon	Sweden	1709	1489	12.9
255	Krokstrommen	Sweden	9655	9440	2.2
256	Ligga	Sweden	9260	10260	-10.8
257	Balforsens	Sweden	12013	11535	4.0
258	Rossens	Switzerland	954	954	0.0
259	Mauvoisin	Switzerland	106	114	-7.6
260	Marmorera	Switzerland	89	89	0.0
261	Contra	Switzerland	228	233	-2.2
262	Bhumibol	Thailand	27192	26386	3.1
263	Srinagarind	Thailand	6896	10880	-36.6
264	Sidi Salem	Tunesia	17764	18000	-1.3
265	Bir M'Che	Tunesia	1519	1260	17.1
266	Ataturk	Turkey	99084	98000	1.1
267	Dicle	Turkey	3055	3216	-5.3
268	Godet	Turkey	985	686	30.4
269	Hasan ugurlu	Turkey	35769	35900	-0.4

270	Menzelet	Turkey	8615	8430	2.1
271	Sariyar dam	Turkey	46275	41778	9.7
272	Keban	Turkey	72514	64100	11.6
273	Karacaorren-1	Turkey	17020	5446	68.0
274	Kirazdere	Turkey	205	258	-25.9
275	Salto Grande	Uruguay	248738	244036	1.9
276	Cosntitucion	Uruguay	68096	62950	8.2
277	Doctor Gabriel Terra	Uruguay	39926	39700	0.6
278	Rincon of baygorria	Uruguay	45643	43900	4.0
279	Paso Severino	Uruguay	3648	2385	53.0
280	Oroville	USA	9004	9352	-3.9
281	Shasta dam	USA	18673	17262	7.6
282	Folsom	USA	4854	4856	0.0
283	Pardee	USA	1509	1492	1.1
284	Arrowrock	USA	6154	5698	7.4
285	Boundary	USA	70917	65268	8.0
286	Summersville	USA	2321	2080	10.4
287	Round Butte	USA	21896	19461	11.1
288	Glen Canyon	USA	276988	280587	-1.3
289	Lucky Peak	USA	6902	6941	-0.6
290	Flaming Gorge	USA	39089	38850	0.6
291	Fontana	USA	3817	4069	-6.6
292	Blue Mesa	USA	8930	8987	-0.6
293	Abiquiui	USA	5451	5558	-2.0
294	Navajo	USA	8315	8262	0.6
295	Watauga	USA	1289	1212	6.0
296	Trinity	USA	1744	1792	-2.8
297	Diablo	USA	2605	2857	-9.7
298	Anderson Ranch	USA	2514	2486	1.1
299	Libby	USA	33858	23271	31.3
300	Terminus	USA	1451	1450	0.0
301	Success	USA	1021	1005	1.6
302	Isabella	USA	5248	5372	-2.4
303	San Clemente	USA	298	323	-8.4
304	New Hogan	USA	922	940	-2.0

305	Sugar Pine	USA	29	34	-17.2
306	Our House	USA	404	375	7.2
307	Stockton	USA	2926	3004	-2.7
308	Arkabutla	USA	2577	2590	-0.5
309	Sardis	USA	3991	4001	-0.3
310	Grenada	USA	3472	3418	1.6
311	Nockamixon	USA	161	189	-17.5
312	Union Lake	USA	550	564	-2.5
313	Ashokan	USA	578	663	-14.7
314	Downsville	USA	963	962	0.1
315	East Sidney	USA	269	264	1.9
316	Gainer memorial	USA	285	240	15.5
317	Aziscohos	USA	546	554	-1.5
318	Wolcott	USA	338	348	-3.0
319	Flagstaff	USA	1260	1336	-6.0
320	Moxie	USA	215	230	-7.0
321	Hatfield	USA	2961	3341	-12.8
322	Ute	USA	22369	28852	-29.0
323	Santa Rosa	USA	6814	6304	7.5
324	Vail	USA	833	793	4.8
325	Santiago Creek	USA	161	163	-1.5
326	Hemet Lake	USA	169	173	-2.4
327	Sutherland	USA	140	151	-7.9
328	Big Tujungano 1	USA	211	212	-0.4
329	Littlerock	USA	152	164	-7.9
330	Santa Felicia	USA	1043	1091	-4.6
331	Nacimiento	USA	853	839	1.6
332	Antelope	USA	178	183	-2.9
333	Red Rock	USA	118	112	5.1
334	Applegate	USA	567	577	-1.8
335	Dorena	USA	689	686	0.4
336	Fern Ridge	USA	762	712	6.6
337	Carty Reservoir	USA	152	168	-10.7
338	La Grande	USA	794	756	4.7
339	Glines Canyon	USA	636	635	0.2

340	Wynoochee	USA	105	106	-1.2
341	Guri	Venezuela	85511	85000	0.6
342	La Honda	Venezuela	1352	4900	-72.4
343	Macagua	Venezuela	92279	95000	-2.9
344	Maticora	Venezuela	2418	2490	-2.9
345	Atarigua	Venezuela	2867	2732	4.9
346	Carauchi	Venezuela	90911	91000	-0.1
347	Tiznados	Venezuela	1482	1490	-0.5
348	Agua Viva	Venezuela	4557	4436	2.7
349	Socuy	Venezuela	612	509	20.2
350	Machango	Venezuela	574	586	-2.0
351	Lagartijo	Venezuela	362	302	19.9
352	Turimique	Venezuela	576	565	1.9
353	Los Algarrobos	Venezuela	577	565	2.1
354	Masparro	Venezuela	533	500	6.6
355	Pao-cachinche	Venezuela	3446	1211	184.6
356	Dos Cerritos	Venezuela	925	910	1.6
357	Kariba	Zambia	697935	514892	35.5
358	Zervreila	Zwitzerland	65	64	0.8

Appendix II: Number of dams per country and country area draining into dam

Name of country	Area(km^2)	Nr of dams	% of country area that runs into dam
ARMENIA	29509.38	4	100.0
BURUNDI	24836.97	3	100.0
LIECHTENSTEIN	0.00	0	100.0
RWANDA	25348.88	1	100.0
UGANDA	240680.39	3	100.0
LESOTHO	30340.47	6	99.7
CONGO, THE DRC	2344648.83	36	99.3
ZAMBIA	747294.21	104	99.1
ANDORRA	0.00	1	99.0
BURKINA FASO	273762.00	104	93.5
CONGO	338339.14	2	90.1
SWITZERLAND	42550.31	63	88.7
SYRIA	184547.19	42	83.3
MALAWI	125495.75	26	81.6
BELARUS	205528.10	12	77.9
SUDAN	2510787.96	7	77.8
KYRGYZSTAN	199188.72	16	74.3
TOGO	58568.02	2	74.3
BENIN	120517.41	4	73.5
SPAIN	512601.84	407	73.4
ZIMBABWE	386551.54	1067	72.2
CANADA	10022976.22	175	71.0
TANZANIA	943295.48	32	69.9
GHANA	241527.97	6	68.4
TURKEY	778858.54	335	68.2
ANGOLA	1247522.09	33	66.8
CENTRAL AFRICAN REPUBLIC	622098.01	2	65.6
UKRAINE	597344.95	86	64.8
THAILAND	516378.31	256	58.6

SOUTH AFRICA	1212987.13	1355	57.5
GEORGIA	69231.38	8	57.1
UNITED STATES	9489566.62	4014	56.2
JORDAN	91920.39	4	55.3
GUINEA	247429.15	4	54.6
MEXICO	1952898.37	1017	53.7
CAMEROON	478385.55	8	53.2
URUGUAY	176325.42	323	52.7
POLAND	313969.05	47	52.4
KENYA	593123.75	61	47.5
COTE D'IVOIRE	326745.76	42	46.7
INDIA	3178010.36	6665	46.4
IRAQ	443686.75	12	46.3
CHINA	9425845.98	8742	46.0
ETHIOPIA	1259920.53	17	45.6
SWAZILAND	17914.82	12	45.3
MALI	1251432.39	5	45.1
EL SALVADOR	24031.97	2	43.5
MONGOLIA	1561400.24	2	43.0
NIGER	1190267.27	5	41.2
MACEDONIA, THE FORMER YUGOSLAV REPUBLIC	25850.07	13	40.9
ROMANIA	236303.44	150	39.2
BRAZIL	8520377.30	5305	38.8
KOREA, DEMOCRATIC PEOPLE'S REPUBLIC OF	126289.65	121	38.5
AZERBAIJAN	85181.37	10	36.9
CZECH REPUBLIC	78148.54	35	35.8
BELGIUM	30128.25	8	34.2
VIETNAM	328026.27	431	33.5
LEBANON	9844.78	1	33.4
SRI LANKA	64716.49	160	33.2
CAMBODIA	181989.07	16	32.4
NIGERIA	910614.33	74	31.2
SINGAPORE	247.81	4	31.0
LATVIA	66067.30	5	30.2
MOROCCO	416438.78	54	29.1

ALBANIA	29624.51	29	29.0
PORTUGAL	93291.28	111	28.9
FINLAND	334434.77	36	27.4
NEPAL	150439.19	11	27.2
SWEDEN	442661.86	69	25.8
AFGHANISTAN	635129.82	5	25.7
TAJIKISTAN	142568.23	5	25.5
PUERTO RICO	8093.08	16	24.4
MOLDOVA, REPUBLIC OF	33502.14	8	24.4
BOSNIA AND HERZEGOVINA	50400.55	14	24.2
LAO PEOPLE'S DEMOCRATIC REPUBLIC	234933.00	13	24.1
KAZAKHSTAN	2720323.79	107	23.6
CUBA	112670.31	274	23.3
IRAN	1625527.93	51	22.8
SLOVAKIA	46762.94	11	22.6
NAMIBIA	818406.05	78	22.6
AUSTRIA	83697.04	26	22.3
WESTERN SAHARA	268271.01	1	22.1
SLOVENIA	19046.83	7	20.8
ITALY	305106.06	223	20.0
BULGARIA	110837.46	51	19.3
DOMINICAN REPUBLIC	50126.99	14	19.0
KOREA, REPUBLIC OF	96122.53	109	19.0
PAKISTAN	803188.11	63	18.8
YUGOSLAVIA	98684.53	39	18.3
FRANCE	586124.93	260	18.3
VENEZUELA	923248.62	200	18.1
BOTSWANA	578743.10	12	17.1
EGYPT	989725.33	4	15.8
SAUDI ARABIA	1979754.85	9	15.4
GREECE	135224.22	28	15.3
COSTA RICA	52971.29	19	14.8
MYANMAR	656434.03	76	14.6
ERITREA	0.00	2	14.6
ARGENTINA	2776226.11	186	14.0

HAITI	28209.87	3	14.0
LUXEMBOURG	2440.48	4	13.1
CROATIA	58655.63	17	13.1
HONDURAS	111048.05	5	12.4
RUSSIAN FEDERATION	16631081.45	192	12.3
ALGERIA	2294283.34	55	12.0
GUATEMALA	109727.90	4	11.7
NEW ZEALAND	269451.11	58	11.5
MOZAMBIQUE	773082.57	24	11.4
LIBERIA	94214.99	1	10.7
LITHUANIA	68044.62	11	10.5
TUNISIA	164371.21	52	10.3
CYPRUS	10649.45	9	9.8
PANAMA	77126.29	9	9.8
TAIWAN, PROVINCE OF CHINA	37593.69	21	9.2
JAPAN	380746.16	368	9.1
SURINAME	144337.57	4	8.9
ECUADOR	261483.19	14	8.9
UZBEKISTAN	446023.87	27	8.8
MACAU	0.00	2	8.3
GERMANY	362300.62	135	8.2
FRENCH GUIANA	83835.86	1	7.0
AUSTRALIA	7738144.13	583	6.3
CHILE	746801.54	35	6.2
IRELAND	69522.48	8	5.8
MALAYSIA	328056.48	47	5.0
UNITED KINGDOM	247320.03	255	4.6
GABON	269668.88	2	4.6
BANGLADESH	141216.80	2	4.6
PARAGUAY	401654.62	3	4.0
COLOMBIA	1137440.43	105	4.0
BHUTAN	39048.15	0	3.8
TURKMENISTAN	469241.51	3	3.8
NETHERLANDS	33760.45	1	3.8
NORWAY	375352.75	29	3.2

PHILIPPINES	308612.32	22	3.2
YEMEN	376787.75	2	3.0
NICARAGUA	128890.63	4	2.4
ICELAND	102016.89	4	2.1
PERU	1305870.11	17	1.6
MADAGASCAR	590309.04	18	1.4
MAURITANIA	1038638.42	2	1.3
ISRAEL	21817.93	5	1.1
INDONESIA	1908515.47	71	1.1
ISLE OF MAN	247320.03	1	0.9
HUNGARY	91887.99	8	0.9
SENEGAL	192109.84	1	0.8
CHAD	1281375.14	0	0.4
PAPUA NEW GUINEA	472595.01	2	0.3
SOLOMON ISLANDS	33421.29	1	0.3
BOLIVIA	1092978.78	6	0.2
ESTONIA	45134.51	1	0.2
BELIZE	21172.06	1	0.1
LIBYA	1639164.31	3	0.1
BRUNEI DARUSSALAM	6234.89	1	0.1
GUINEA-BISSAU	34604.57	0	0.1
GUYANA	204997.51	1	0.1
EAST TIMOR	0.00	1	0.0
SIERRA LEONE	71512.28	1	0.0
SOMALIA	637787.70	1	0.0
DENMARK	43740.27	2	0.0
AMERICAN SAMOA	457.07	0	0.0
ANGUILLA	116.13	0	0.0
ANTARCTICA	0.00	0	0.0
ANTIGUA AND BARBUDA	583.78	0	0.0
ARUBA	284.04	0	0.0
BAHAMAS	18724.76	0	0.0
BAHRAIN	897.96	0	0.0
BAKER-HOWLAND-JARVIS	44.15	0	0.0
BARBADOS	506.41	0	0.0

BERMUDA	108.68	0	0.0
BRITISH INDIAN OCEAN TERRITORY	527.51	0	0.0
CANADA	10022976.22	0	0.0
CAPE VERDE	6263.43	0	0.0
CAYMAN ISLANDS	432.94	0	0.0
CHRISTMAS ISLAND	19.77	0	0.0
COCOS (KEELING) ISLANDS	16.98	0	0.0
COMOROS	2178.39	0	0.0
COOK ISLANDS	111.14	0	0.0
DJIBOUTI	21570.32	0	0.0
DOMINICA	852.95	0	0.0
EQUATORIAL GUINEA	28413.55	0	0.0
FALKLAND ISLANDS (MALVINAS)	11861.45	0	0.0
FAROE ISLANDS	1531.99	0	0.0
FIJI	19834.63	0	0.0
FRENCH POLYNESIA	1422.92	0	0.0
FRENCH SOUTHERN TERRITORIES	6952.47	0	0.0
GAMBIA	10603.45	0	0.0
GREENLAND	2109392.91	0	0.0
GRENADA	355.37	0	0.0
GUADELOUPE	1741.28	0	0.0
GUAM	695.38	0	0.0
GUERNSEY	107.93	0	0.0
JAMAICA	11136.68	0	0.0
JERSEY	150.16	0	0.0
JOHNSTON ATOLL	9489566.62	0	0.0
KINGMAN REEF - PALMYRA ATOLL	9489566.62	0	0.0
KIRIBATI	2911.60	0	0.0
KUWAIT	16286.71	0	0.0
MALDIVES	2074.18	0	0.0
MALTA	352.56	0	0.0
MARSHALL ISLANDS	280.72	0	0.0
MARSHALL ISLANDS	5741.86	0	0.0
MARTINIQUE	1406.02	0	0.0
MAURITIUS	2619.44	0	0.0

MAYOTTE	603.24	0	0.0
MICRONESIA, FEDERATED STATES OF	282.09	0	0.0
MIDWAI ISLANDS	50.51	0	0.0
MONACO	0.00	0	0.0
MONTSERRAT	583.78	0	0.0
NAURU	31.30	0	0.0
NETHERLANDS ANTILLES	1358.24	0	0.0
NEW CALEDONIA	586124.93	0	0.0
NIUE	524.27	0	0.0
NORFOLK ISLAND	127.31	0	0.0
NORTHERN MARIANA ISLANDS	1139.05	0	0.0
OMAN	320200.23	0	0.0
PALAU	837.93	0	0.0
PALESTINE	7920.05	1	0.0
QATAR	10834.61	0	0.0
REUNION	2842.84	0	0.0
SAINT HELENA	247320.03	0	0.0
SAINT KITTS AND NEVIS	197.28	0	0.0
SAINT LUCIA	877.68	0	0.0
SAINT PIERRE AND MIQUELON	384.75	0	0.0
SAINT VINCENT AND THE GRENADINES	584.77	0	0.0
SAN MARINO	328.52	0	0.0
SAO TOME AND PRINCIPE	1561.16	0	0.0
SEYCHELLES	1776.17	0	0.0
SOUTH GEORGIA AND THE SOUTH SANDWICH ISL	5443.94	0	0.0
TONGA	1636.61	0	0.0
TRINIDAD AND TOBAGO	4948.04	0	0.0
TURKS AND CAICOS ISLANDS	1202.66	0	0.0
TUVALU	189.27	0	0.0
UNITED ARAB EMIRATES	94648.13	0	0.0
VANUATU	13722.84	0	0.0
VATICAN CITY (HOLY SEE)	0.00	0	0.0
VIRGIN ISLANDS	652.38	0	0.0
VIRGIN ISLANDS (U.S.)	652.38	0	0.0
WAKE ISLAND	53.02	0	0.0

WALLIS AND FUTUNA ISLANDS	96.41	0	0.0
WESTERN SAMOA	2768.80	0	0.0

Appendix III: Country dependency on dams

Country	% irrigated cropland	% HEP
Afghanistan	33.8	66.9
Albania	50.5	98.1
Algeria	6.9	0.7
Angola	2.2	96.2
Argentina	5.4	25.6
Armenia	51.5	29.4
Australia	5.4	4.7
Austria	0.3	60.6
Azerbaijan	70.5	10.3
Bahamas, The	8.3	N/A
Bahrain	66.7	N/A
Bangladesh	56.1	4.2
Barbados	29.4	N/A
Belarus	2.3	0.1
Belgium	4.7	2.1
Belize	2.9	82.1
Benin	0.4	0.7
Bhutan	23.5	100.0
Bolivia	4.1	36.6
Bosnia and Herzegovina	0.3	34.3
Botswana	0.3	N/A
Brazil	4.4	79.8
Brunei	5.6	N/A
Bulgaria	16.6	7.3
Burkina Faso	0.5	21.9
Burma	17.0	N/A
Burundi	1.6	98.2
Cambodia	7.0	3.1
Cameroon	0.4	76.2
Canada	1.5	58.7
Cape Verde	6.1	N/A

Central African Republic	0.1	81.5
Chad	0.8	N/A
Chile	82.4	40.5
China	47.2	16.9
Colombia	24.0	82.8
Congo, Democratic Republic of the	0.1	99.4
Congo, Republic of the	0.4	81.3
Costa Rica	20.6	78.0
Côte d'Ivoire	1.1	32.7
Croatia	0.7	43.2
Cuba	23.0	0.8
Cyprus	25.6	N/A
Czech Republic	0.7	2.8
Denmark	19.7	0.1
Dominican Republic	17.2	11.2
Ecuador	34.8	60.7
Egypt	99.9	10.9
El Salvador	5.0	34.2
Eritrea	3.7	N/A
Estonia	0.7	0.3
Ethiopia	2.5	87.3
Fiji	1.1	85.7
Finland	2.9	22.1
France	13.3	11.9
French Polynesia	4.0	30.6
Gabon	1.4	43.8
Gambia, The	0.6	N/A
Georgia	44.0	84.8
Germany	4.0	4.2
Ghana	0.5	74.1
Greece	37.9	6.5
Guatemala	6.3	42.6
Guinea	5.4	52.9
Guinea-Bissau	4.6	N/A
Guyana	29.4	N/A

Haiti	8.4	37.2
Honduras	5.6	35.0
Hungary	4.8	0.5
India	32.9	13.6
Indonesia	12.4	7.7
Iran	40.2	2.2
Iraq	58.6	1.5
Israel	45.8	0.0
Italy	25.7	14.8
Jamaica	8.8	2.0
Japan	54.7	7.7
Jordan	28.6	0.4
Kazakhstan	15.7	9.3
Kenya	2.0	40.4
Korea, North	50.3	N/A
Korea, South	47.6	N/A
Kuwait	72.2	N/A
Kyrgyzstan	76.0	90.4
Laos	16.5	86.2
Latvia	2.1	58.9
Lebanon	33.2	3.5
Lesotho	0.9	100.0
Liberia	0.5	N/A
Libya	21.9	N/A
Lithuania	0.5	7.1
Macedonia, Republic of	9.0	N/A
Madagascar	30.6	54.2
Malawi	2.2	85.7
Malaysia	4.8	7.6
Mali	4.9	55.3
Malta	18.2	N/A
Mauritania	9.8	N/A
Mauritius	20.8	3.2
Mexico	23.2	15.1
Moldova	14.0	N/A

Mongolia	7.0	N/A
Morocco	15.4	6.7
Mozambique	2.6	99.9
Namibia	1.0	67.5
Nepal	47.1	99.6
Netherlands	60.2	0.1
New Caledonia	100.0	24.5
New Zealand	8.5	51.0
Nicaragua	2.8	15.9
Niger	0.5	N/A
Nigeria	0.8	27.1
Oman	90.0	N/A
Pakistan	82.0	30.3
Panama	6.2	61.8
Paraguay	2.1	100.0
Peru	27.8	58.7
Philippines	14.5	16.5
Poland	0.8	1.8
Portugal	27.3	15.9
Puerto Rico	36.0	0.7
Qatar	61.9	N/A
Romania	31.3	26.5
Russia	3.7	16.0
Rwanda	0.6	36.3
Saint Lucia	16.7	N/A
Saint Vincent and the Grenadines	7.1	24.5
São Tomé and Príncipe	18.2	N/A
Saudi Arabia	42.7	N/A
Senegal	4.8	N/A
Serbia and Montenegro	0.9	27.1
Sierra Leone	4.7	31.7
Slovakia	12.7	14.6
Slovenia	1.5	24.5
Somalia	18.7	4.6
South Africa	9.5	1.6

Spain	20.4	8.3
Sri Lanka	38.8	41.8
Sudan	10.7	32.4
Suriname	75.0	53.9
Swaziland	26.0	38.1
Sweden	4.3	46.1
Switzerland	5.8	55.0
Syria	24.3	7.0
Tajikistan	68.3	98.1
Tanzania	3.6	60.1
Thailand	28.2	4.8
Togo	0.3	74.0
Trinidad and Tobago	3.3	N/A
Tunisia	8.0	0.3
Turkey	20.0	16.8
Turkmenistan	79.4	0.0
Uganda	0.1	71.3
Ukraine	6.6	6.0
United Arab Emirates	29.9	N/A
United Kingdom	3.0	2.4
United States	12.5	6.5
Uruguay	14.9	51.4
Uzbekistan	84.9	23.0
Venezuela	16.9	72.8
Vietnam	33.7	35.6
Yemen	33.0	N/A
Zambia	3.0	99.7
Zimbabwe	5.2	53.4

Appendix IV: FAO CLIMWAT 2.0 for CROPWAT

Source: FAO 2009. CLIMWAT 2.0 for CROPWAT Water development and management unit & climate change and bioenergy unit FAO. Available at: http://www.fao.org/nr/water/infores_databases_climwat.html

CLIMWAT is a climatic database to be used in combination with the computer program CROPWAT. and allows the calculation of crop water requirements, irrigation supply and irrigation scheduling for various crops for a range of climatological stations worldwide. CLIMWAT 2.0 for CROPWAT is a joint publication of the Water Development and Management Unit and the Climate Change and Bioenergy Unit of FAO. CLIMWAT 2.0 offers observed agroclimatic data of over 5000 stations worldwide distributed as shown below.

.

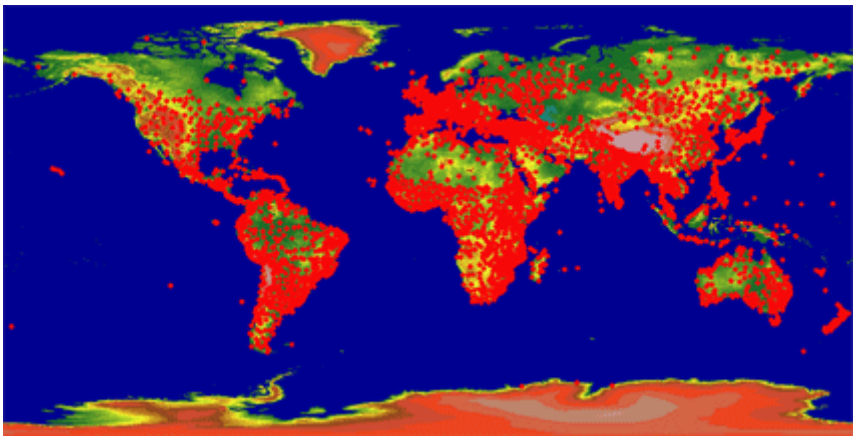

IV.1 Location of stations included in CLIMWAT 2.0

CLIMWAT provides long-term monthly mean values of seven climatic parameters, namely:

- Mean daily maximum temperature in °C
- Mean daily minimum temperature in °C
- Mean relative humidity in %
- Mean wind speed in km/day
- Mean sunshine hours per day

- Mean solar radiation in MJ/m2/day
- Monthly rainfall in mm/month
- Monthly effective rainfall in mm/month
- Reference evapotranspiration calculated with the Penman-Monteith method in mm/day.

The data can be extracted for a single or multiple stations in the format suitable for their use in CROPWAT. Two files are created for each selected station. The first file contains long-term monthly rainfall data [mm/month]. Additionally, effective rainfall is also included calculated and included in the same file. The second file consists of long-term monthly averages for the seven climatic parameters, mentioned above. This file also contains the coordinates and altitude of the location.

All station information is drawn from the database of The Agromet Groupof FAO.
All variables, except potential evapotranspiration, are direct observations or conversions of observations. Original data coming from a large number of meteorological stations as included in CLIMWAT, could not be uniform. For example, humidity and radiation can be expressed through different variables. With respect to humidity, data can be provided as relative humidity, dew point temperature or water vapour pressure. These three variables can be uniquely converted into each other if the mean temperature is known. However, if humidity is measured and provided in more than one of these variables, the actual numbers would not necessarily be in line. In this case it is necessary to decide which variable to use. When compiling CLIMWAT, it was decided to use water vapour pressure as a core variable and only where it is not available, use dew point temperature and relative humidity. However, there is a risk that the provided value of vapour pressure is higher than the one that is possible to obtain, given the mean temperature. The original databases were crosschecked for this possible inconsistency and one of the other variables was used in the few cases where it occurred.

The same problem arises with radiation. Instead of the solar energy flux at the surface often only sunshine hours or sunshine fraction are recorded, both of which though can be converted to radiation. In order to calculate evapotranspiration using the Penman-Monteith method, both radiation and sunshine fraction are necessary. To keep both these values in agreement the observed radiation was used as base variable and the sunshine fraction was estimated from it. When only the sunshine fraction (or hours) has been observed it was used to estimate radiation. If both (fraction and radiation) are observed radiation was preferred. As a result, the provided relative humidity and sunshine hours are often deduced from observations of vapour pressure and radiation, even if the former are observed. The procedure, however, ensures that the different expressions are coherent.

In compiling the data, an effort was made to cover the period 1971 - 2000, but when data for this period were not available, any recent series that ends after 1975 and that has at least 15 years of data have been included. Some of the series are "broken", but they nevertheless have at least 15 years of data (e.g. 1961-70 and 1992-2000).
We prepared the dataset and the extraction software with great care and made every effort to provide reliable data. However, we cannot guarantee that all the observations that went into the procedure are free of errors.

Appendix V: SimTerra database parameters

Table V.1 SimTerra database parameters used in AguaAndes/WaterWorld

Map name	Variable	Source Citation
2, blwind1 – blwind12	Boundary layer wind direction January to December	derived from UK Meteorological Office, Hadley Centre, CSIRO (Scientific and Industrial Research for Australia), Australia and NIWA (National Institute of Water and Atmospheric Research), New Zealand. Met Office - Global Mean Sea-Level Pressure datasets (GMSLP and HadSLP1), [Internet]. British Atmospheric Data Centre, 2000, Date of citation. Available from http://badc.nerc.ac.uk/data/gmslp/
14, gmslp1 – gmslp12	Mean sea level pressure January to December	derived from UK Meteorological Office, Hadley Centre, CSIRO (Scientific and Industrial Research for Australia), Australia and NIWA (National Institute of Water and Atmospheric Research), New Zealand. Met Office - Global Mean Sea-Level Pressure datasets (GMSLP and HadSLP1), [Internet]. British Atmospheric Data Centre, 2000, Date of citation. Available from http://badc.nerc.ac.uk/data/gmslp/
26, hysh1kdem	Elevation (hydro1k)	Lehner, B., Verdin, K., Jarvis, A. (2008): New global hydrography derived from spaceborne elevation data. Eos, Transactions, AGU, 89(10): 93-94
32, ueatmp1 – ueatmp12	Air temperature January to December	Mark New, David Lister, Mike Hulme and Ian Makin (2003) A high-resolution data set of surface climate over global land areas. Climate Research, 2000, Vol 21, pg 1-25
44, ueawnd1 – ueawnd12	Wind speed January to December	Mark New, David Lister, Mike Hulme and Ian Makin (2003) A high-resolution data set of surface climate over global land areas. Climate Research, 2000, Vol 21, pg 1-25
56, uearh1 – uearh12	Relative Humidity January to December	Mark New, David Lister, Mike Hulme and Ian Makin (2003) A high-resolution data set of surface climate over global land areas. Climate Research, 2000, Vol 21, pg 1-25
68, wcmeantemp (map)	Mean annual temperature	Hijmans, R.J., S.E. Cameron, J.L. Parra, P.G. Jones and A. Jarvis, 2005. Very high resolution interpolated climate surfaces for global land areas. International Journal of Climatology 25: 1965-1978
69, wcprec1 – wcprec12	Mean monthly precipitation January to December	Hijmans, R.J., S.E. Cameron, J.L. Parra, P.G. Jones and A. Jarvis, 2005. Very high resolution interpolated climate surfaces for global land areas. International Journal of Climatology 25: 1965-1978
81, sumrain (map)	Total annual precipitation	Hijmans, R.J., S.E. Cameron, J.L. Parra, P.G. Jones and A. Jarvis, 2005. Very high resolution interpolated climate surfaces for global land areas. International Journal of Climatology 25: 1965-1978

82, wctmax1 – wctmax12	Mean daily maximum temperature January to December	Hijmans, R.J., S.E. Cameron, J.L. Parra, P.G. Jones and A. Jarvis, 2005. Very high resolution interpolated climate surfaces for global land areas. International Journal of Climatology 25: 1965-1978
94, wctmean1 – wctmean12	Mean monthly temperature January to December	Hijmans, R.J., S.E. Cameron, J.L. Parra, P.G. Jones and A. Jarvis, 2005. Very high resolution interpolated climate surfaces for global land areas. International Journal of Climatology 25: 1965-1978
106, wctmmin1 – wctmmin12	Mean daily minimum temperature January to December	Hijmans, R.J., S.E. Cameron, J.L. Parra, P.G. Jones and A. Jarvis, 2005. Very high resolution interpolated climate surfaces for global land areas. International Journal of Climatology 25: 1965-1978
118, modisclddjf (map)	Cloud frequency (DJF)	Mulligan, M. (2006) MODIS MOD35 pan-tropical cloud climatology.Version 1. September 2006. http://www.ambiotek.com/clouds
119, modiscldjja (map)	Cloud frequency (JJA)	Mulligan, M. (2006) MODIS MOD35 pan-tropical cloud climatology.Version 1. September 2006. http://www.ambiotek.com/clouds
120, modiscldmam (map)	Cloud frequency (MAM)	Mulligan, M. (2006) MODIS MOD35 pan-tropical cloud climatology.Version 1. September 2006. http://www.ambiotek.com/clouds
121, modiscldson (map)	Cloud frequency (SON)	Mulligan, M. (2006) MODIS MOD35 pan-tropical cloud climatology.Version 1. September 2006. http://www.ambiotek.com/clouds
122, mcloud (map)	Mean annual cloud frequency	Mulligan, M. (2006) MODIS MOD35 pan-tropical cloud climatology.Version 1. September 2006. http://www.ambiotek.com/clouds
123, mcloud1 – mcloud12	Cloud frequency January to December	Mulligan, M. (2006) MODIS MOD35 pan-tropical cloud climatology.Version 1. September 2006. http://www.ambiotek.com/clouds
135, mcloud0-6 (map)	Cloud frequency 00:00-06:00 hrs	Mulligan, M. (2006) MODIS MOD35 pan-tropical cloud climatology.Version 1. September 2006. http://www.ambiotek.com/clouds
136, mcloud12-18 (map)	Cloud frequency 12:00-18:00 hrs	Mulligan, M. (2006) MODIS MOD35 pan-tropical cloud climatology.Version 1. September 2006. http://www.ambiotek.com/clouds
137, mcloud18-24 (map)	Cloud frequency 18:00-24:00 hrs	Mulligan, M. (2006) MODIS MOD35 pan-tropical cloud climatology.Version 1. September 2006. http://www.ambiotek.com/clouds
138, mcloud6-12 (map)	Cloud frequency 06:00-12:00 hrs	Mulligan, M. (2006) MODIS MOD35 pan-tropical cloud climatology.Version 1. September 2006. http://www.ambiotek.com/clouds
165, clone (map)	Study area	Mulligan, M. (2009) SimTerra : A consistent global gridded database of environmental properties for spatial modelling. http://www.ambiotek.com/simterra

166, lddhysh1k (map)	Local drainage direction	Lehner, B., Verdin, K., Jarvis, A. (2008): New global hydrography derived from spaceborne elevation data. Eos, Transactions, AGU, 89(10): 93-94
167, vcfbare2000 (map)	Cover of bare ground	Hansen, M., R. DeFries, J.R. Townshend, M. Carroll, C. Dimiceli, and R. Sohlberg (2006), Vegetation Continuous Fields MOD44B, 2001 Percent Tree Cover, Collection 4, University of Maryland, College Park, Maryland, 2001.
168, vcfherb2000 (map)	Cover of herb-covered ground	Hansen, M., R. DeFries, J.R. Townshend, M. Carroll, C. Dimiceli, and R. Sohlberg (2006), Vegetation Continuous Fields MOD44B, 2001 Percent Tree Cover, Collection 4, University of Maryland, College Park, Maryland, 2001.
169, vcftree2000 (map)	Cover of tree-covered ground	Hansen, M., R. DeFries, J.R. Townshend, M. Carroll, C. Dimiceli, and R. Sohlberg (2006), Vegetation Continuous Fields MOD44B, 2001 Percent Tree Cover, Collection 4, University of Maryland, College Park, Maryland, 2001.
170, cloudfreq1 – cloudfreq12	Cloud frequency January to December	Wylie, D.P., W. P. Menzel, H. M. Woolf, K. I. Strabala, 1994: Four Years of Global Cirrus Cloud Statistics Using HIRS., J. of Climate, 7, 1972-1986
184, cellarea (map)	Cell area	Mulligan, M. (2009) SimTerra : A consistent global gridded database of environmental properties for spatial modelling. http://www.ambiotek.com/simterra
196, damid (map)	Dams	Mulligan, M., Saenz, L. and van Soesbergen, A. (2011) Development and validation of a georeferenced global database of dams. Submitted Water Resources Research. http://www.ambiotek.com/dams
256, roads (map)	Roads (GAUL)	UN FAO UN FAO GIEWS World road trails. Whole world's roads and railways .
273, all_mines (map)	Presence of mines	Mulligan, M. (2010) A combined global database of mines. http://www.ambiotek.com/mines
274, oilandgas (map)	Presence of oil and gas wells	Mulligan, M. (2010) A combined global database of oil and gas wells. http://www.ambiotek.com/oilandgas
301, watbal (map)	Water balance (WorldClim rainfall -ET)	Mulligan,M., Luis Leonardo Saenz Cruz, Jorge Pena-Arancibia, Myles Fisher (2010) Water Availability and use across the CPWF basins. Water International. Accepted
311, convclone (map)	Study area (CN)	Mulligan, M. (2009) SimTerra : A consistent global gridded database of environmental properties for spatial modelling. http://www.ambiotek.com/simterra
321, initial_swe (map)	Mean snow water equivalent	Mulligan, M (2011) Estimates mean snow water equivalent. http://www.ambiotek.com/simterra
327, pov_pc (map)	Percentage of population considered..	Elvidge *et al* (2006) A global poverty map from satellite data. http://www.ngdc.noaa.gov/dmsp/pubs/Poverty_index_20061227_a.pdf

Appendix VI: Model sensitivity to climate change

Guadalquivir basin

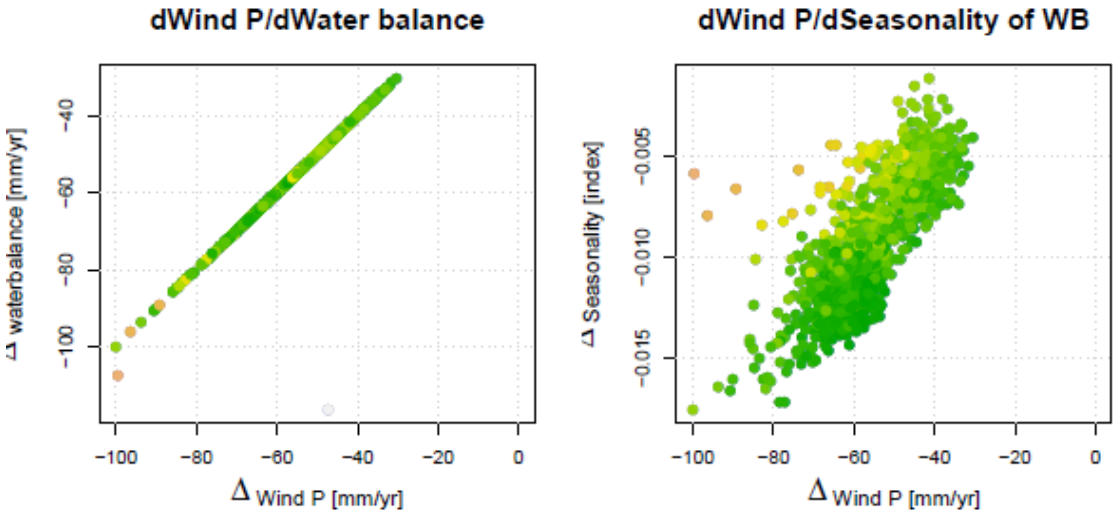

Figure VI.8.1 Water balance and water seasonality sensitivity run 1 Guadalquivir basin (precip -10%, Temp no change)

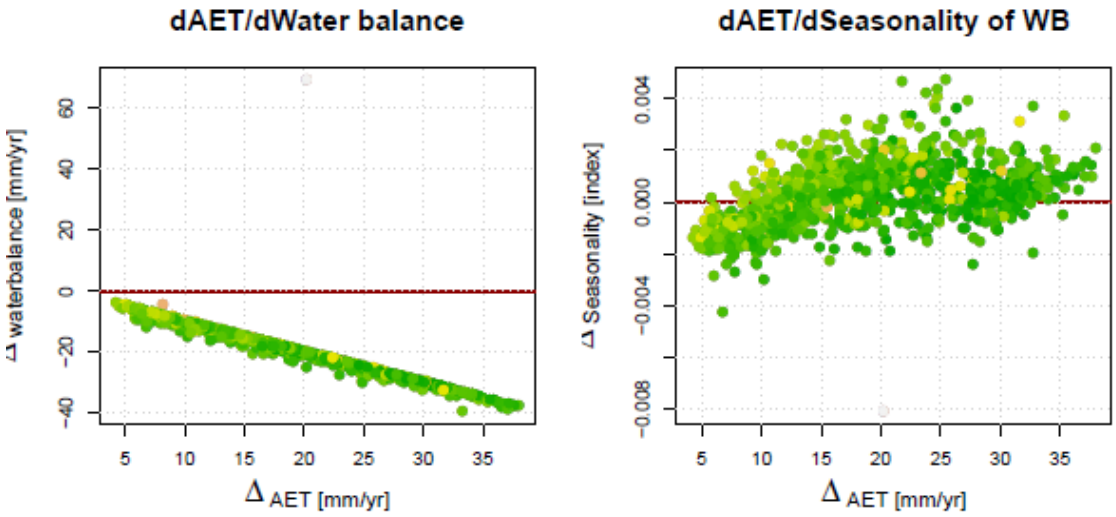

Figure VI.8.2 Water balance and water seasonality sensitivity run 2 Guadalquivir basin (Temp +2°C, Precip no change).

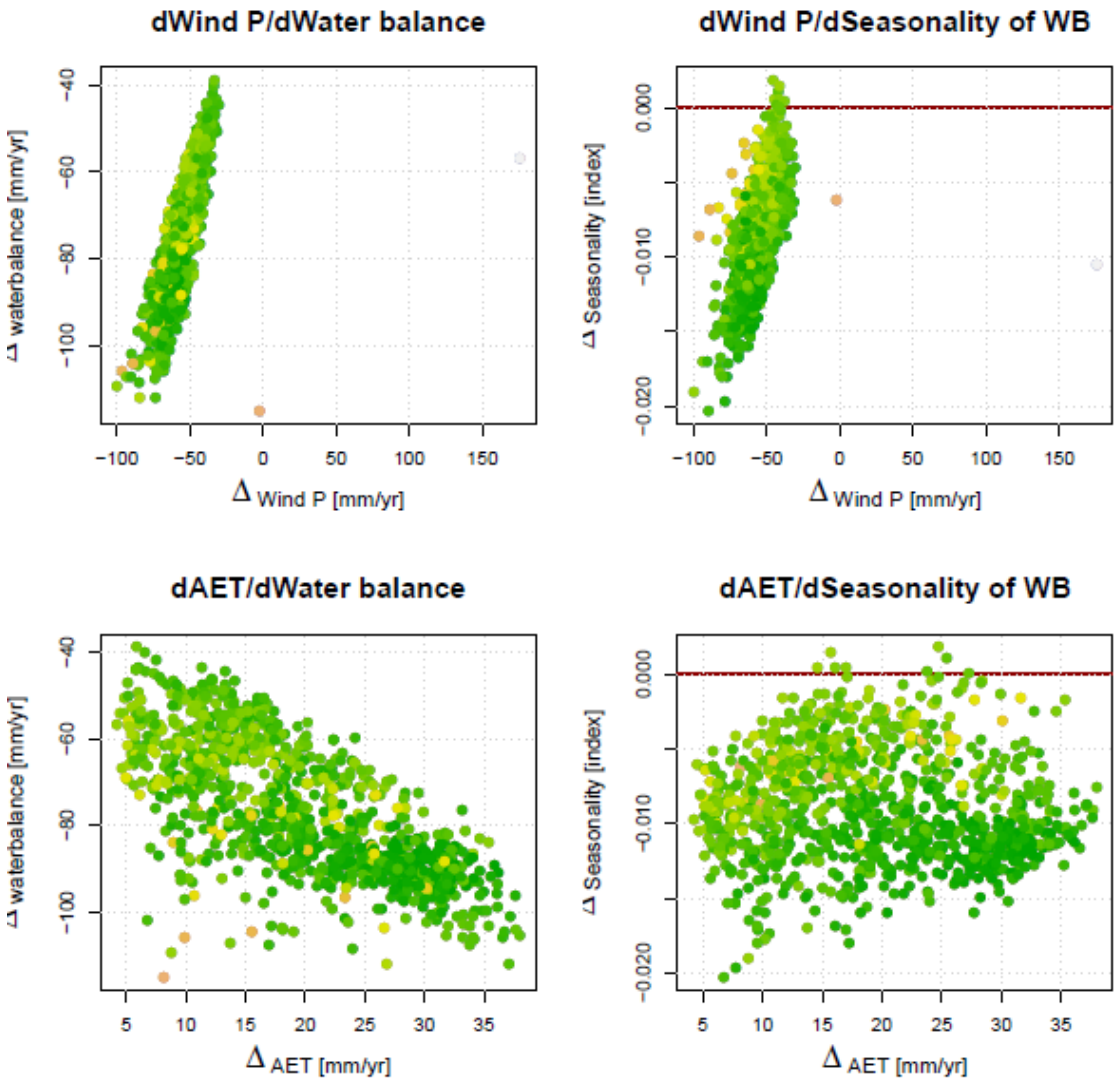

Figure VI.8.3 Water balance and water seasonality sensitivity run 3 Guadalquivir basin (Temp -2°C, Precip -10%)

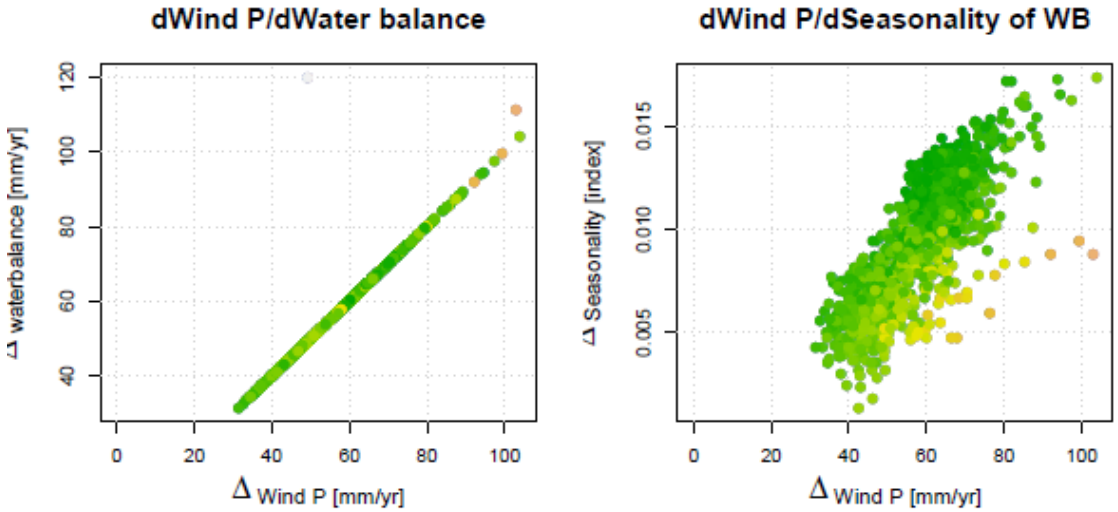

Figure VI.8.4 Water balance and water seasonality sensitivity run 4 Guadalquivir basin (precip +10%, Temp no change)

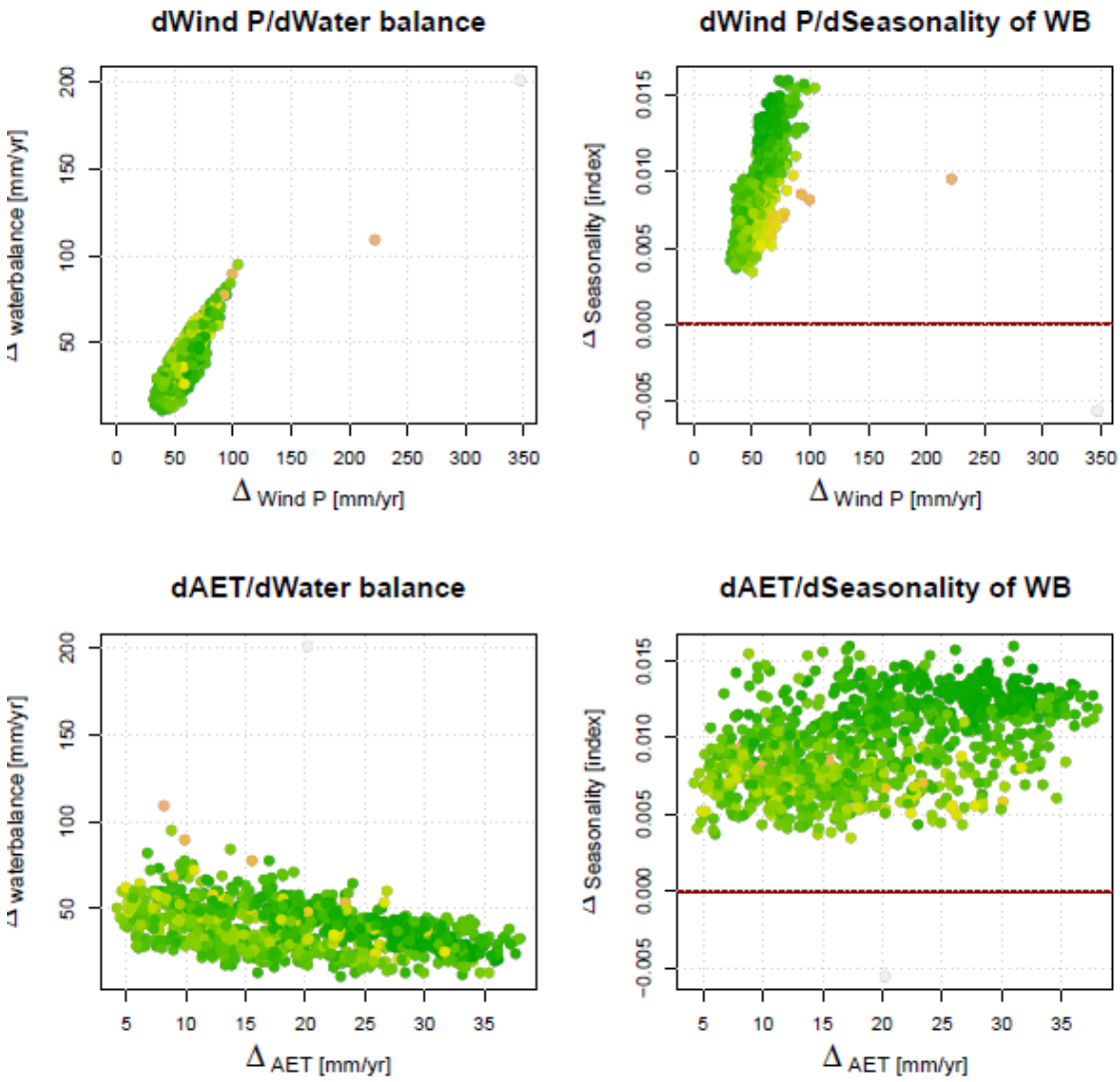

Figure VI.8.5 Water balance and water balance seasonality sensitivity run 5 Guadalquivir basin (precip +10%, temp +2°C)

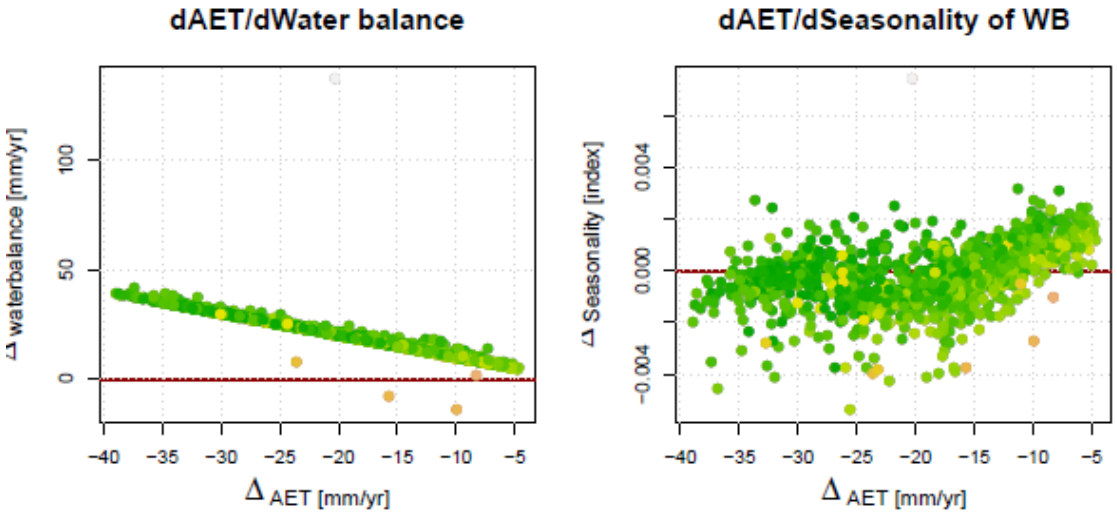

Figure VI.8.6 Water balance and water seasonality sensitivity run 6 Guadalquivir basin (precip no change Temp -2°C)

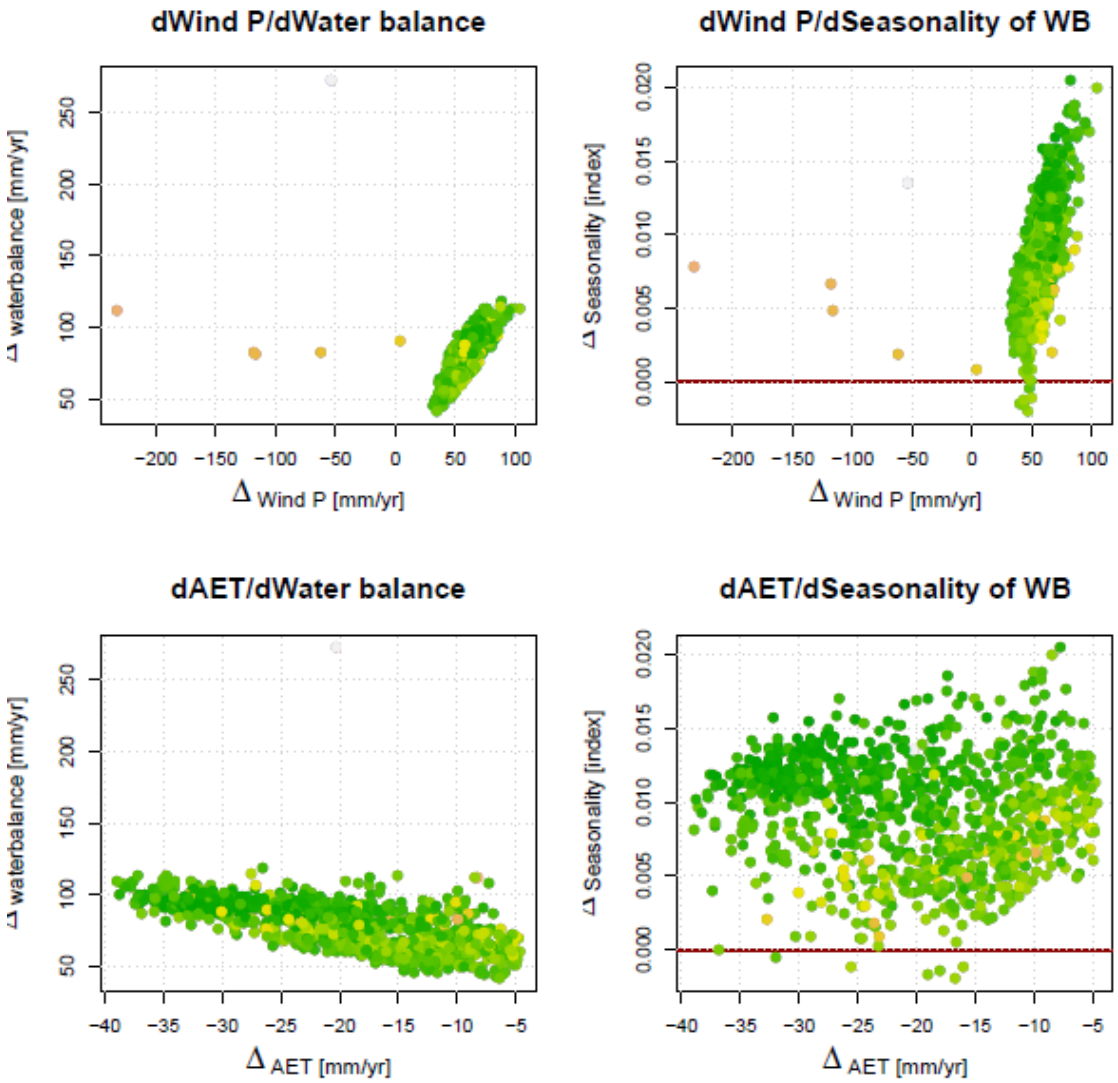

Figure VI.8.7 Water balance and water seasonality sensitivity run 7 Guadalquivir basin (precip +10, change Temp -2°C)

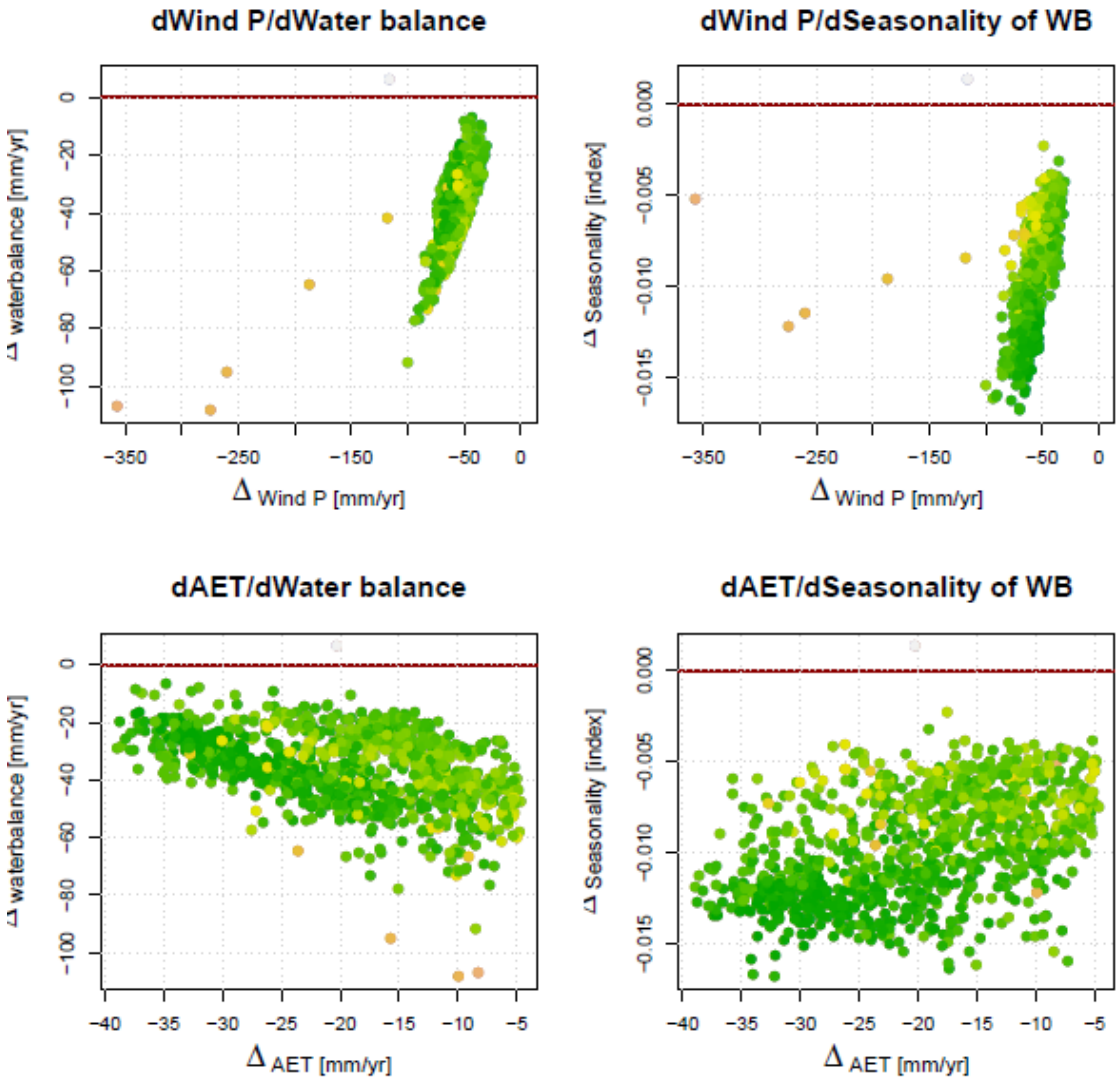

Figure VI.8.8 Water balance and water seasonality sensitivity run 8 Guadalquivir basin (precip -10, change Temp -2°C)

Maputo basin

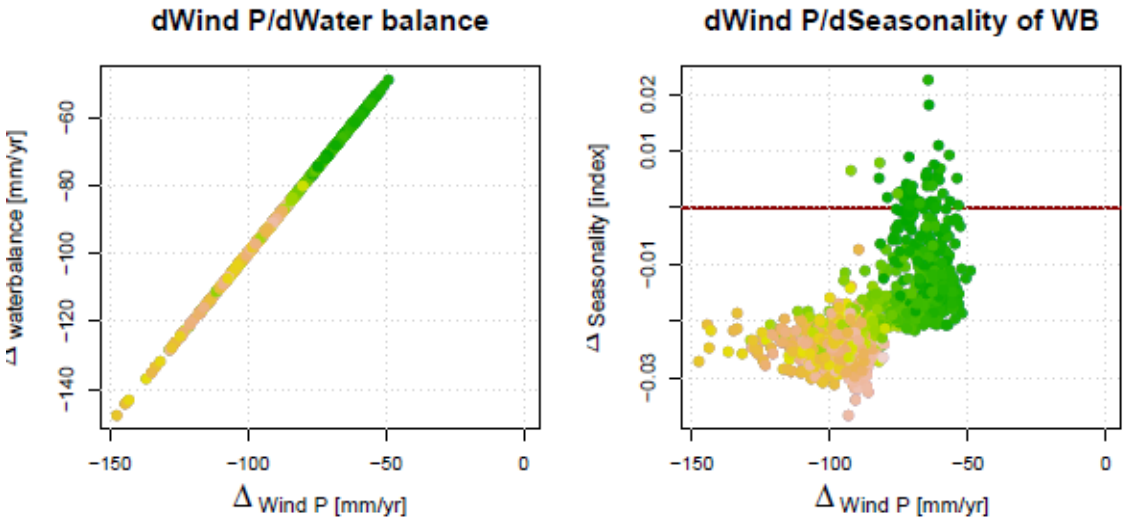

Figure V.8.9 Water balance and water seasonality sensitivity run 1 Maputo basin (precip -10%, change Temp no change)

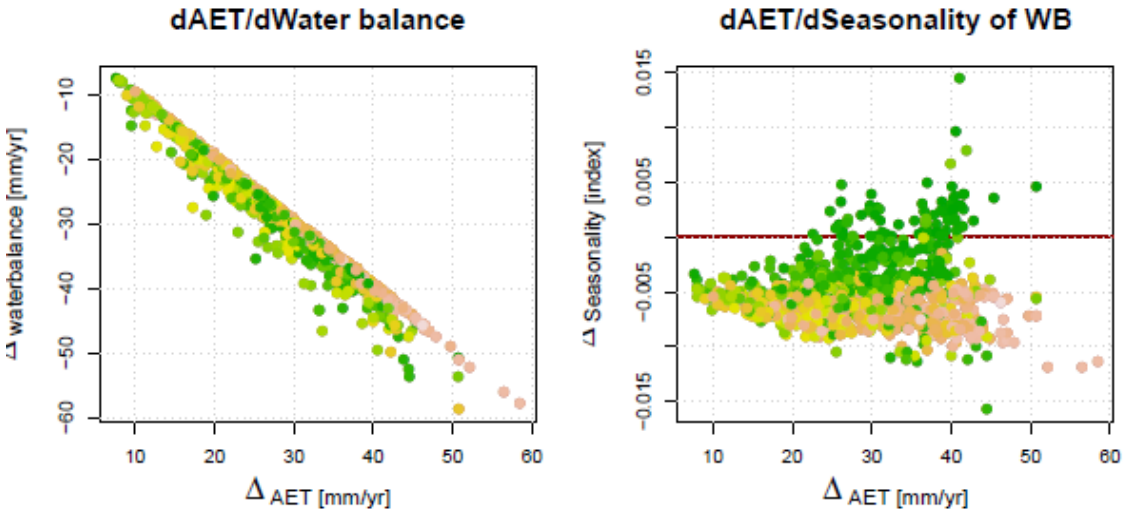

Figure VI.8.10 Water balance and water seasonality sensitivity run 2 Maputo basin (precip no change, Temp +2°C)

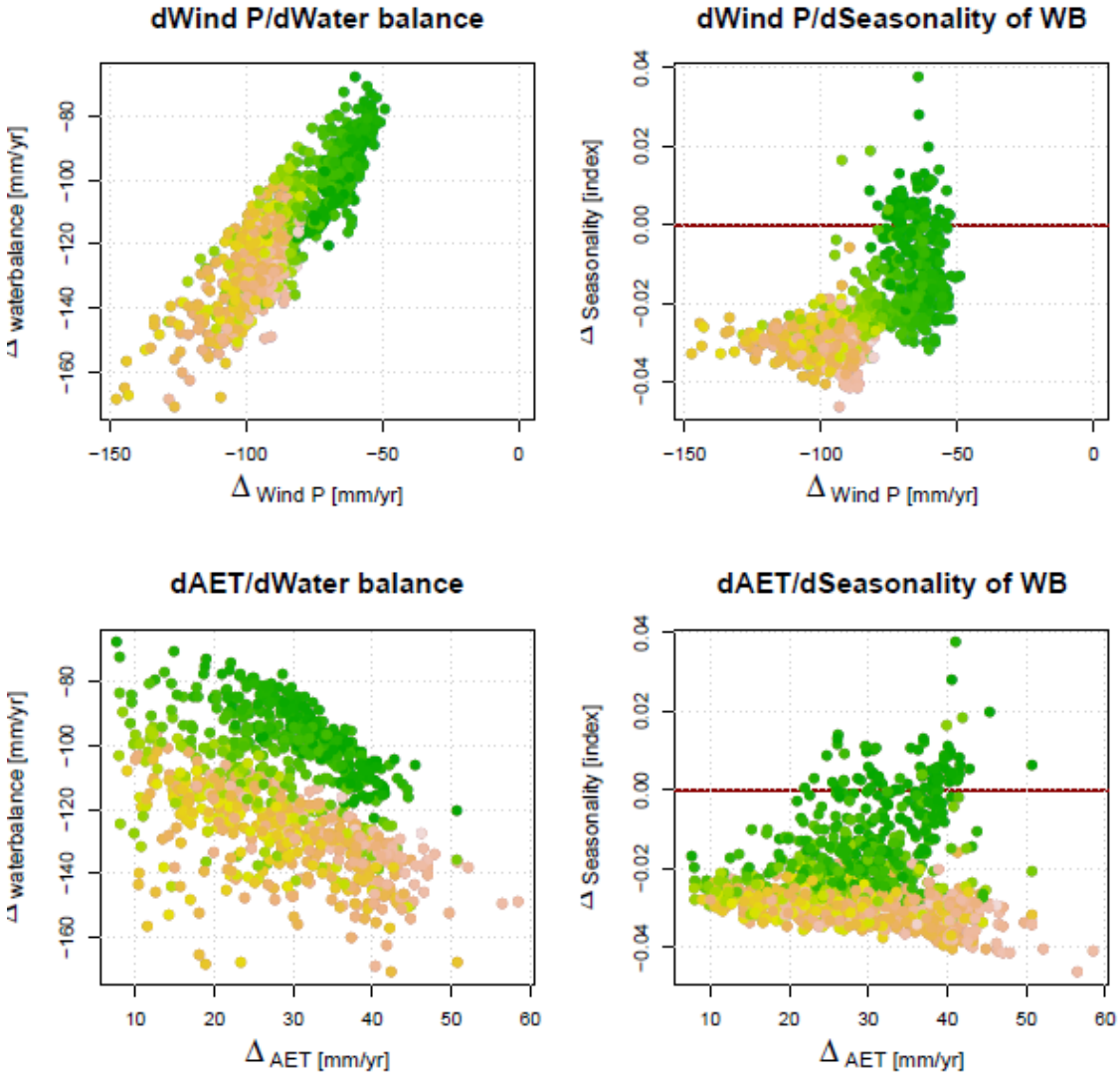

Figure VI.8.11 Water balance and water seasonality sensitivity run 3 Maputo basin (precip -10%, change Temp +2°C)

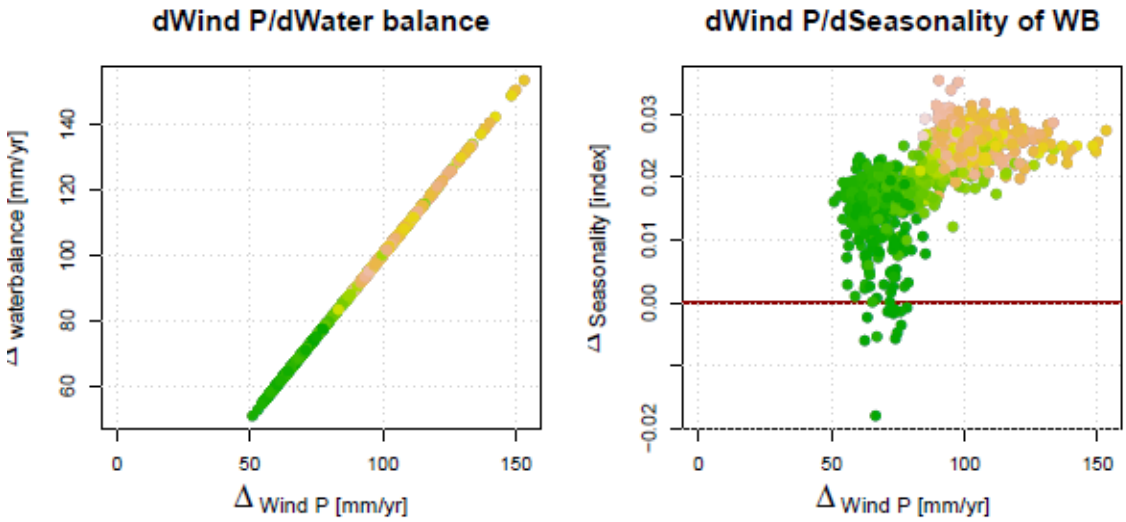

Figure VI.8.12 Water balance and water seasonality sensitivity run 4 Maputo basin (precip +10%, Temp no change)

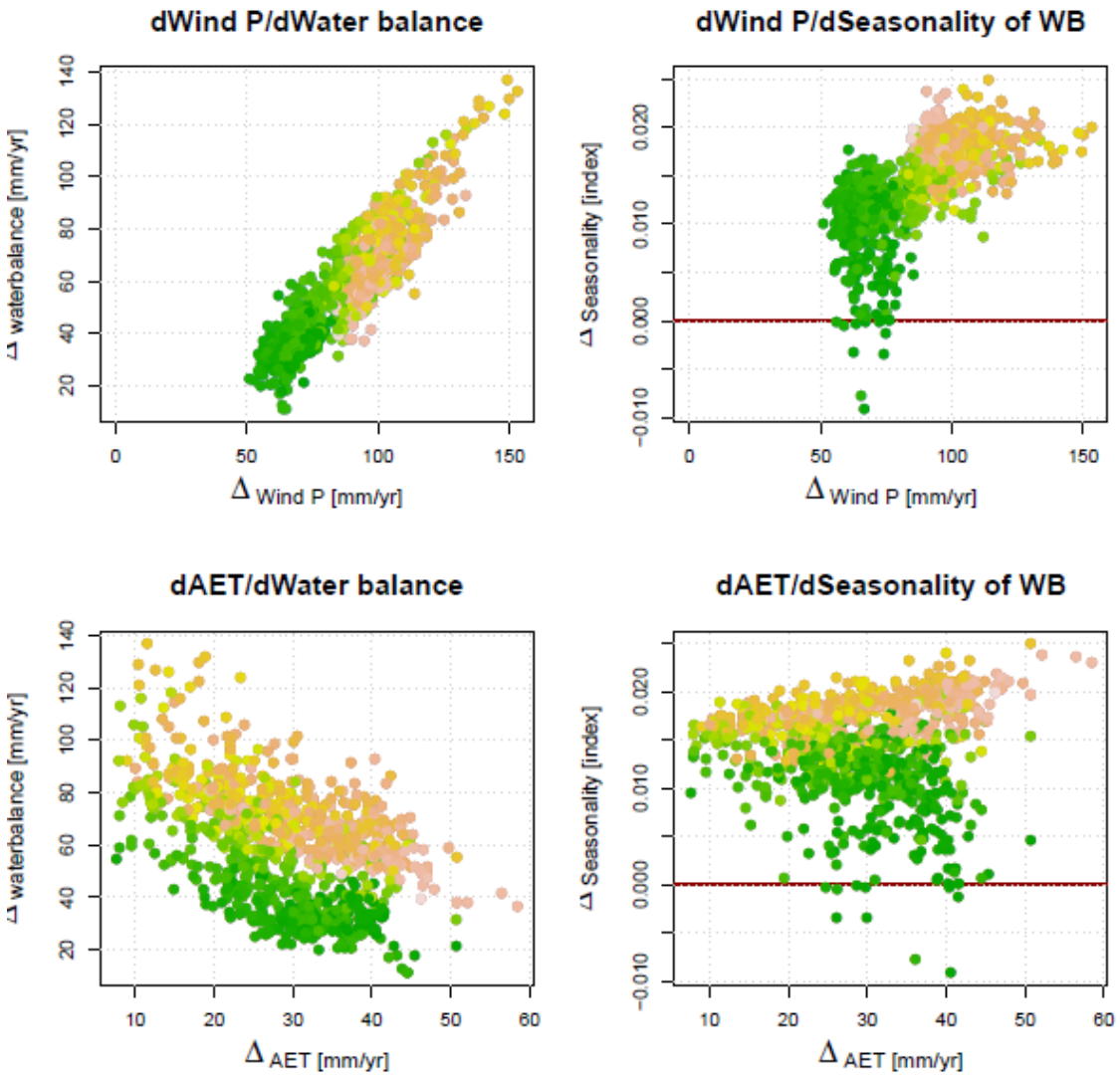

Figure VI.8.13 Water balance and water seasonality sensitivity run 5 Maputo basin (precip +10%, Temp +2°C)

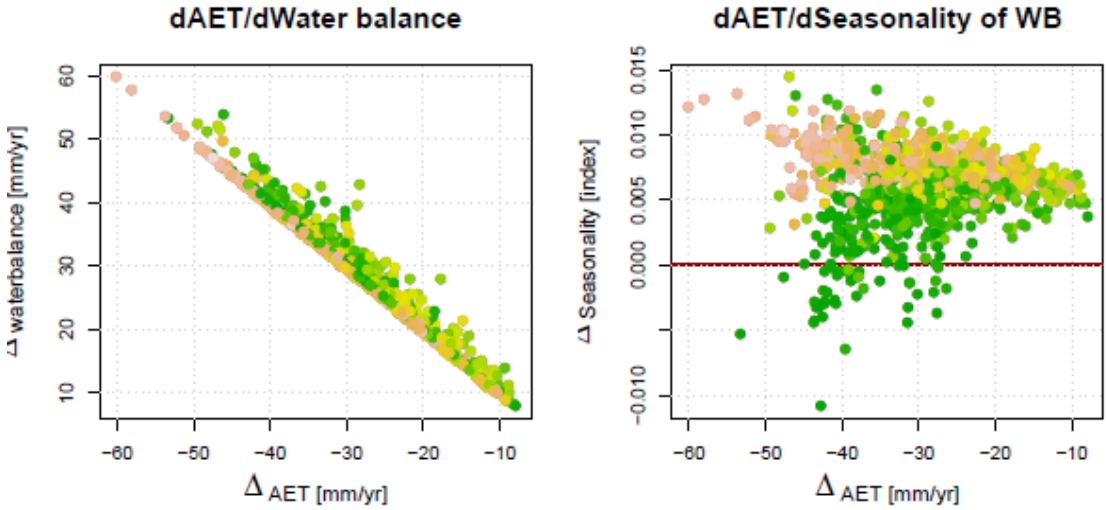

Figure VI.8.14 Water balance and water balance seasonality sensitivity run 6 Maputo basin (precip no change, Temp -2 degrees C)

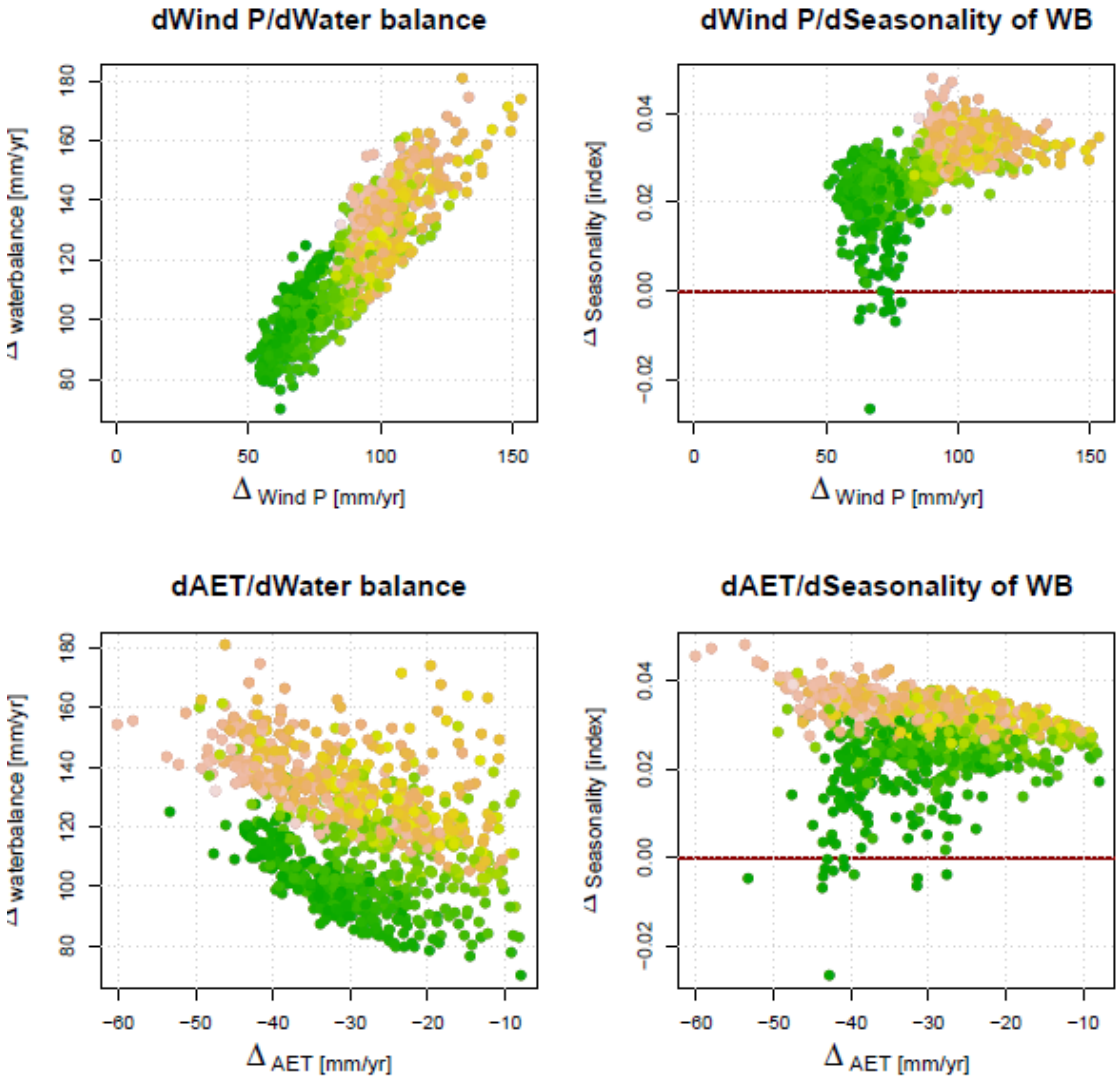

Figure VI.8.15 Water balance and water seasonality sensitivity run 7 Maputo basin (precip +10%, Temp -2 degrees C)

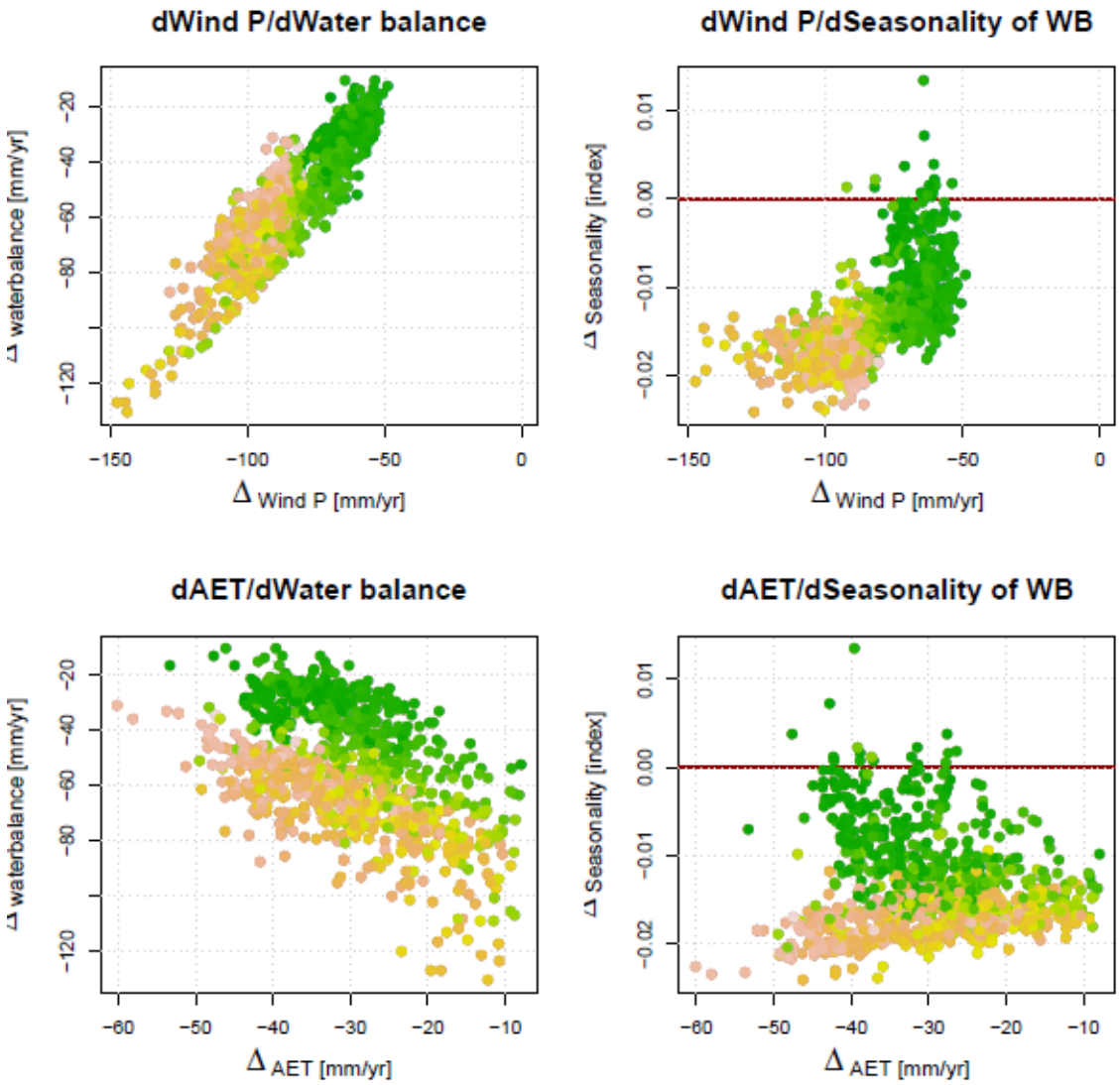

Figure VI.8.16 Water balance and water seasonality sensitivity run 8 Maputo basin (precip -10%, Temp -2 degrees C)

Savannah basin

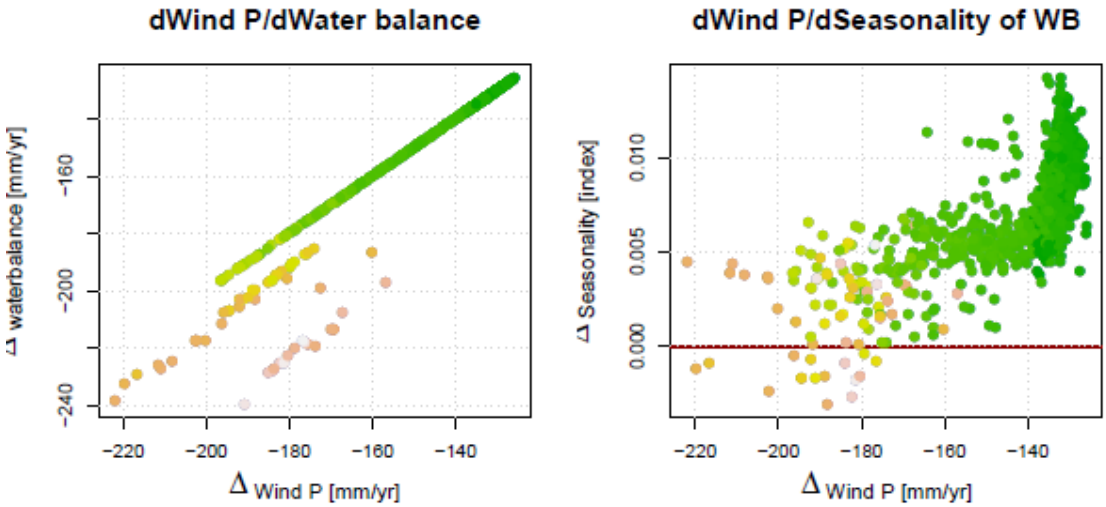

Figure VI.8.17 Water balance and water seasonality sensitivity run 1 Savannah basin (precip -10%, Temp no change)

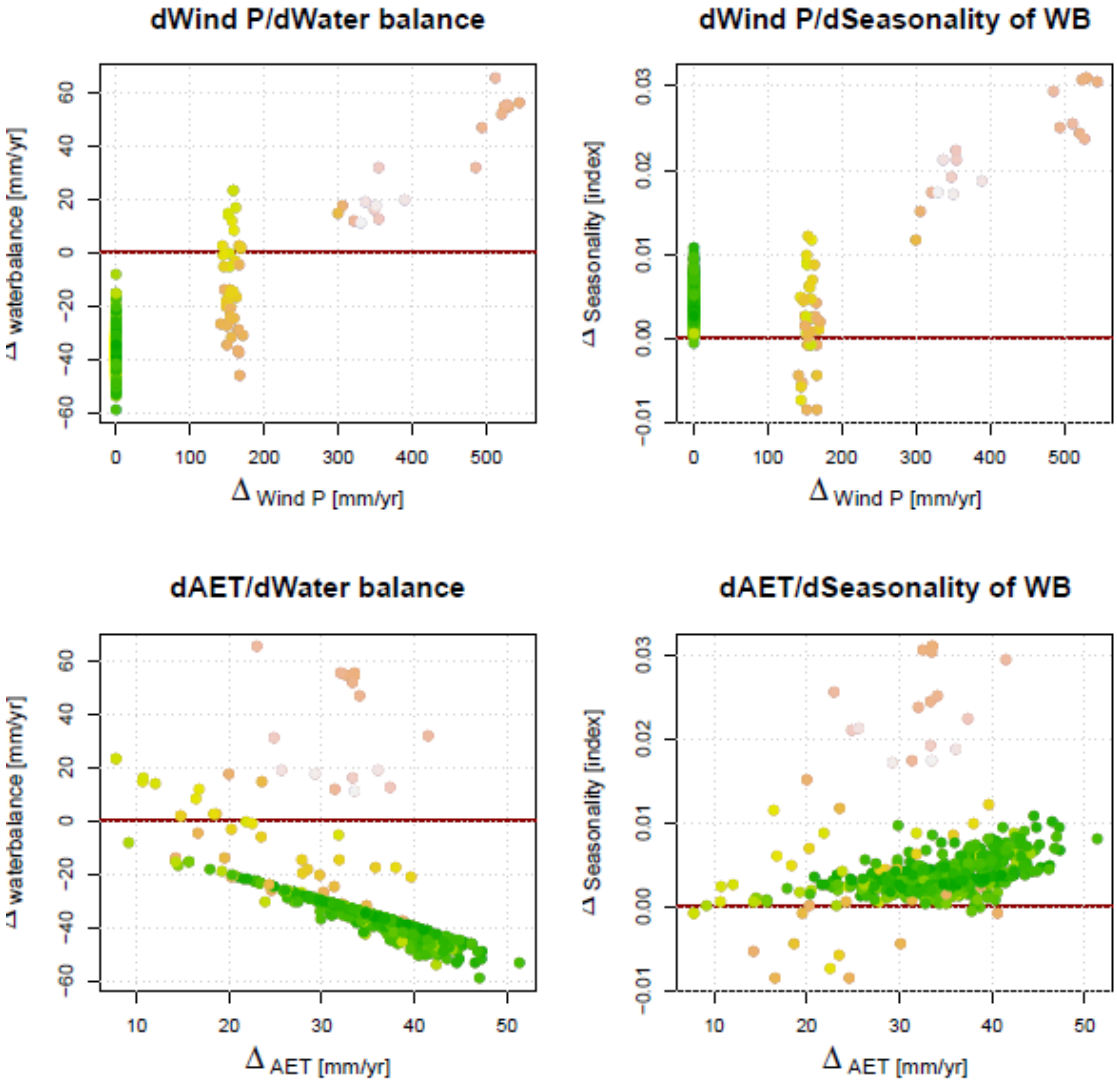

Figure VI.8.18 Water balance and water seasonality sensitivity run 2 Savannah basin (precip no change, Temp +2 degrees C)

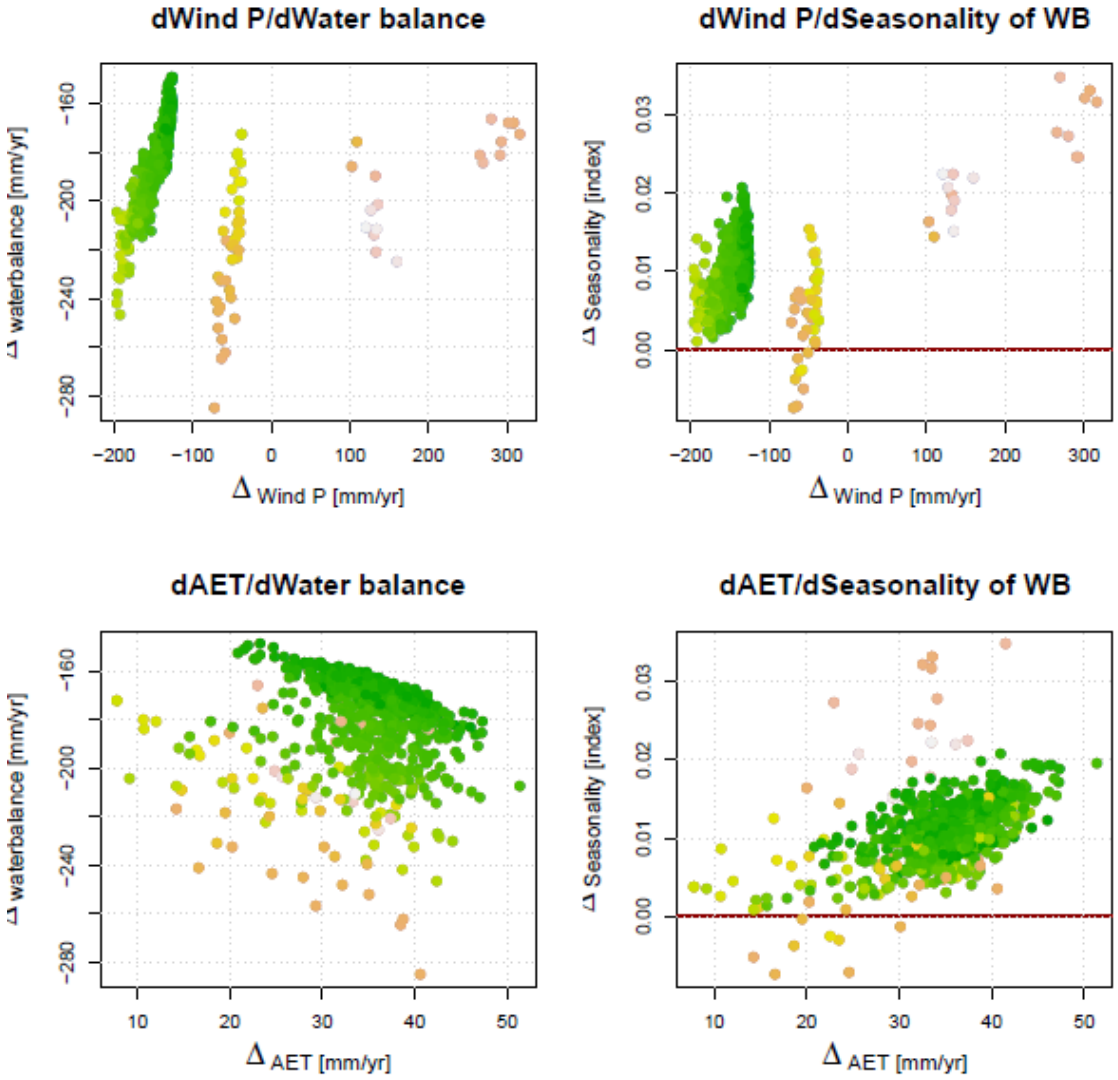

Figure VI.8.19 Water balance and water seasonality sensitivity run 3 Savannah basin (precip -10%, Temp +2 degrees C)

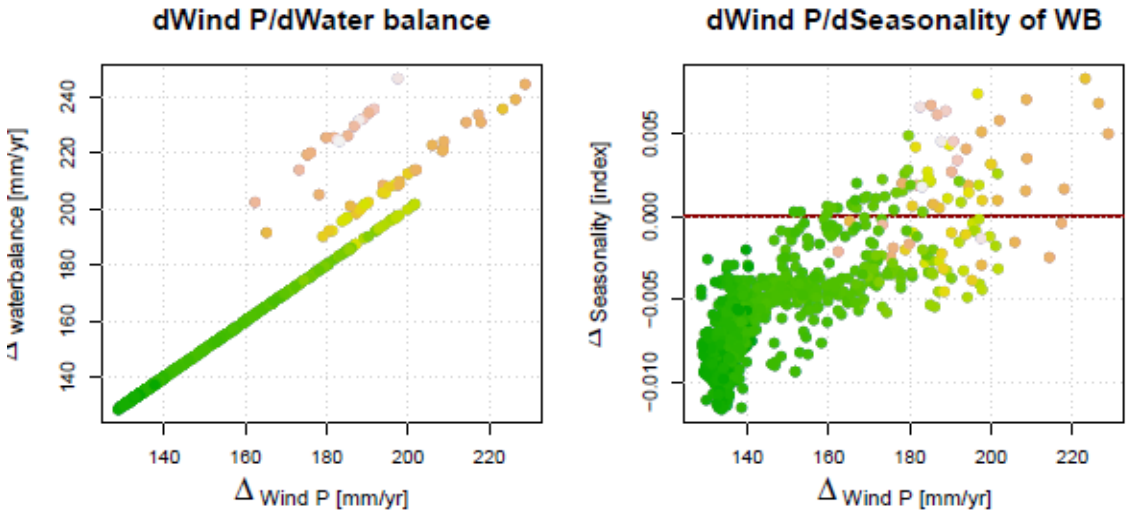

Figure VI.8.20 Water balance and water seasonality sensitivity run 4 Savannah basin (precip +10%, Temp no change)

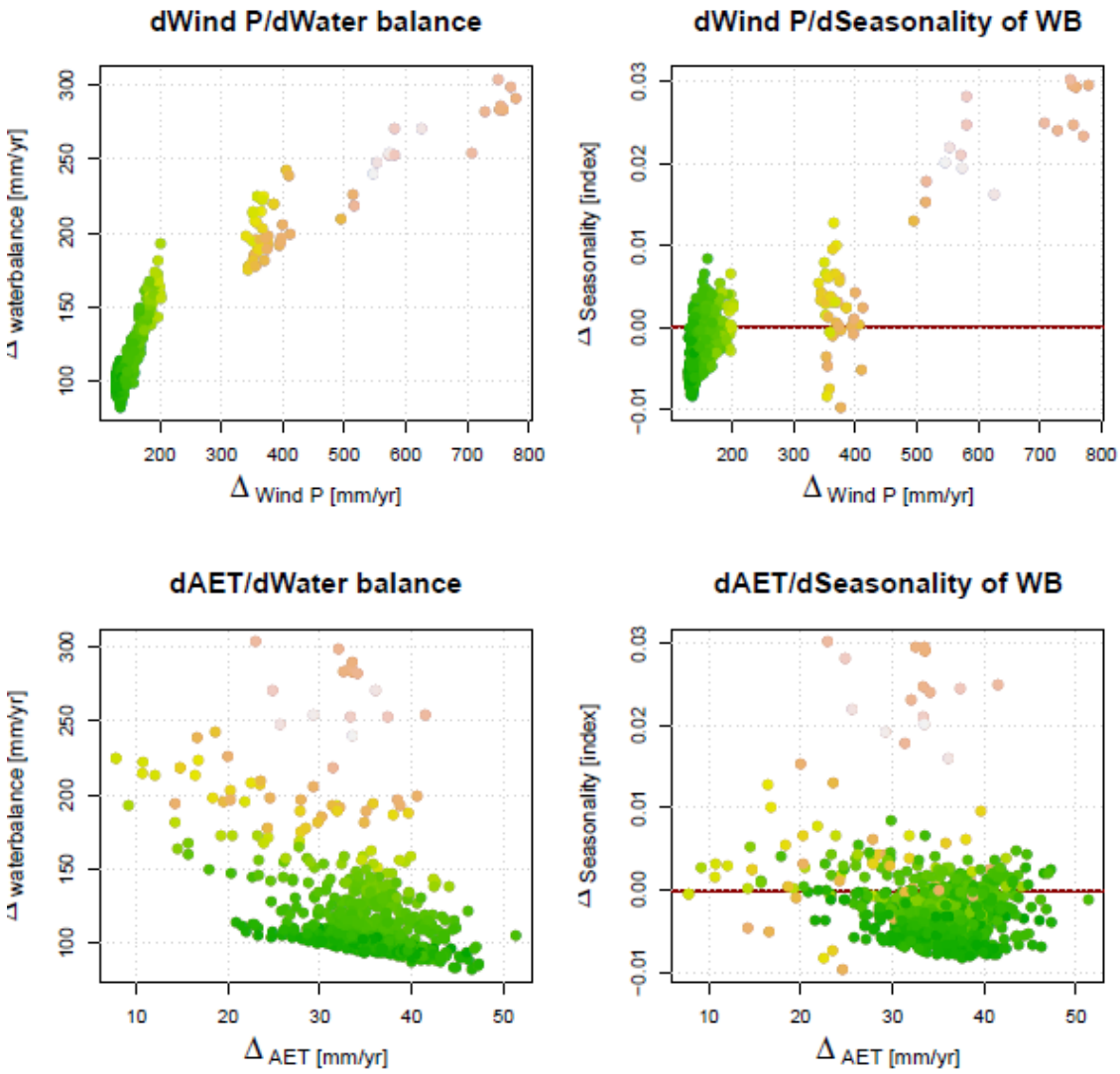

Figure VI.8.21 Water balance and water balance seasonality sensitivity run 5 Savannah basin (precip +10%, Temp+2 degrees C)

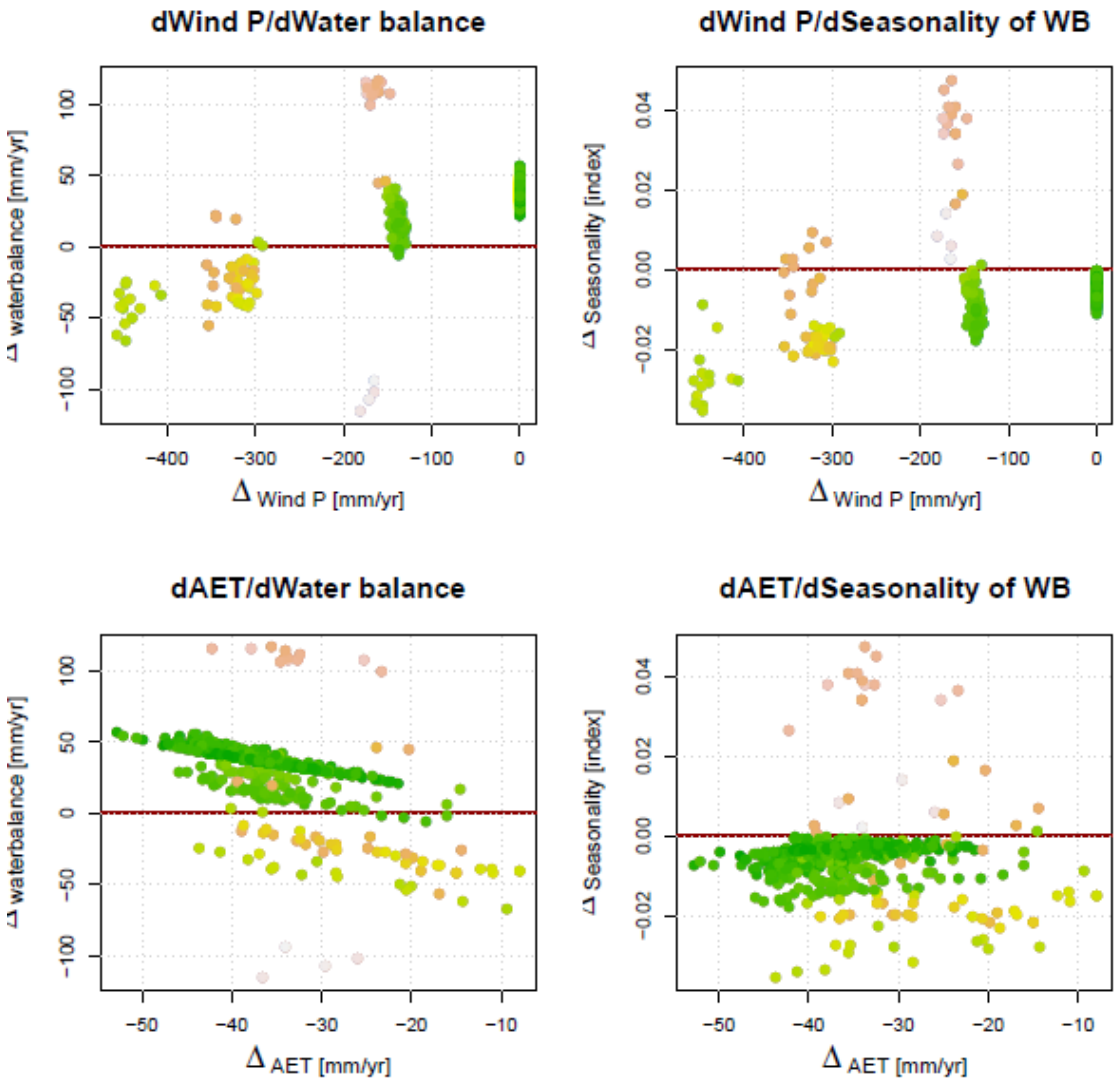

Figure VI.8.22 Water balance and water seasonality sensitivity run 6 Savannah basin (precip no change, Temp -2 degrees C)

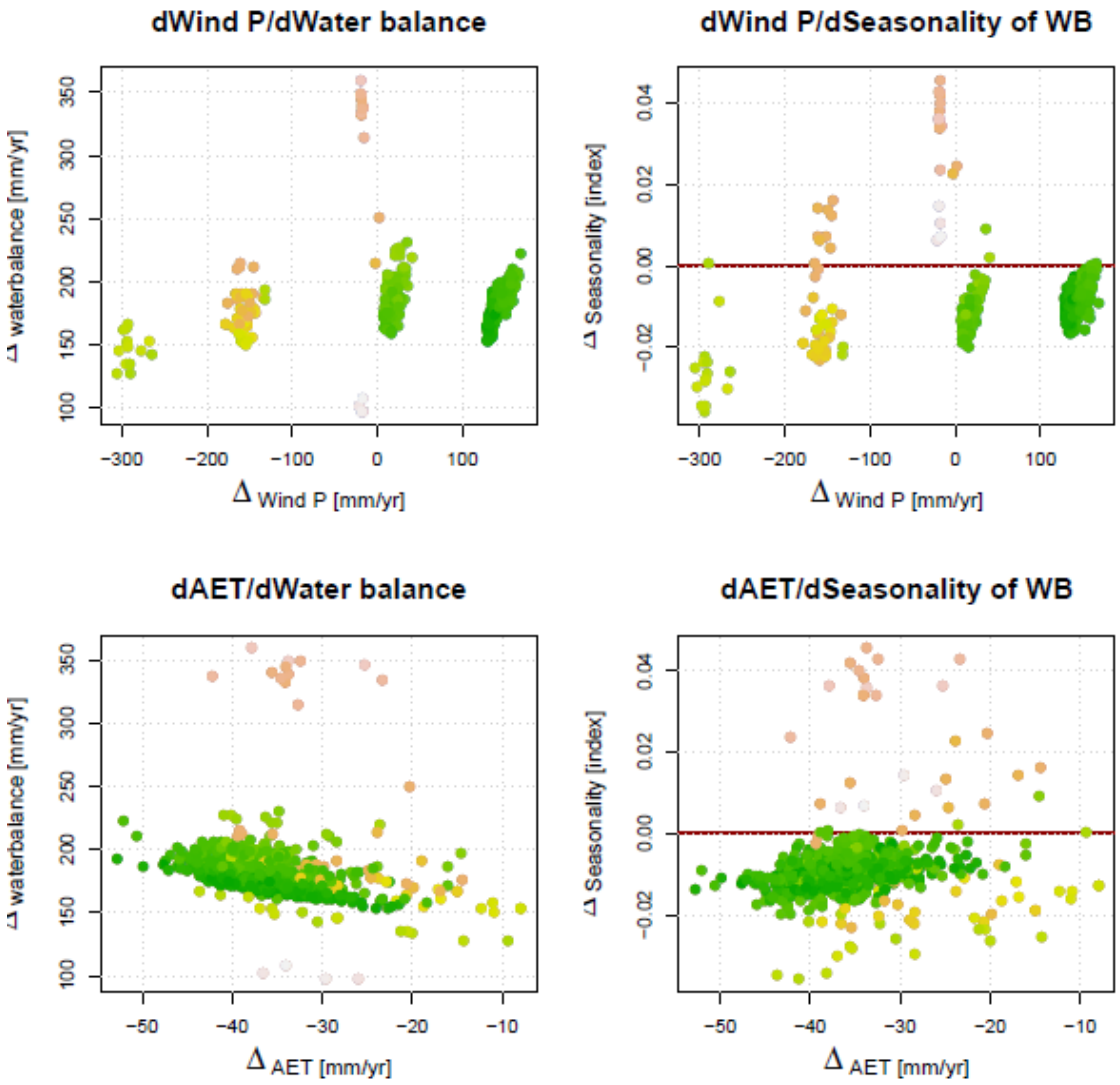

Figure VI.8.23 Water balance and water seasonality sensitivity run 7 Savannah basin (precip +10%, Temp-2 degrees C)

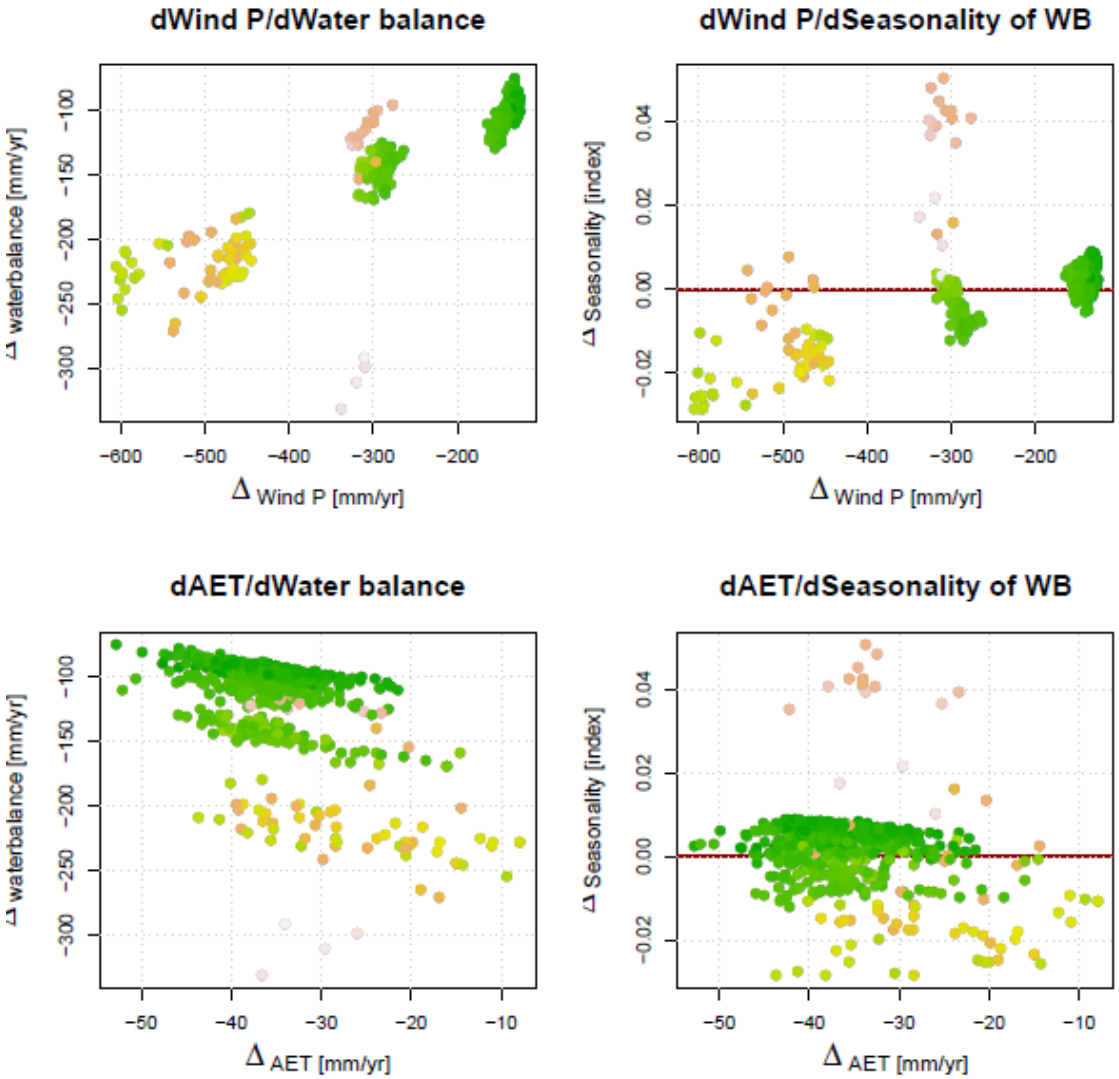

Figure VI.8.24 Water balance and water balance seasonality sensitivity run 8 Savannah basin (precip -10%, Temp-2 degrees C)

Appendix VII: Model sensitivity to vegetation changes

Table VII.1 Percentage change for functional land cover types for vegetation sensitivity runs and corresponding management type

Sensitivity Run	Tree %	Herb %	Bare %	Management
1	70	20	10	Afforestation
2	20	70	10	Agriculture
3	33.3	33.3	33.3	Mosaic
4	10	20	70	Degradation

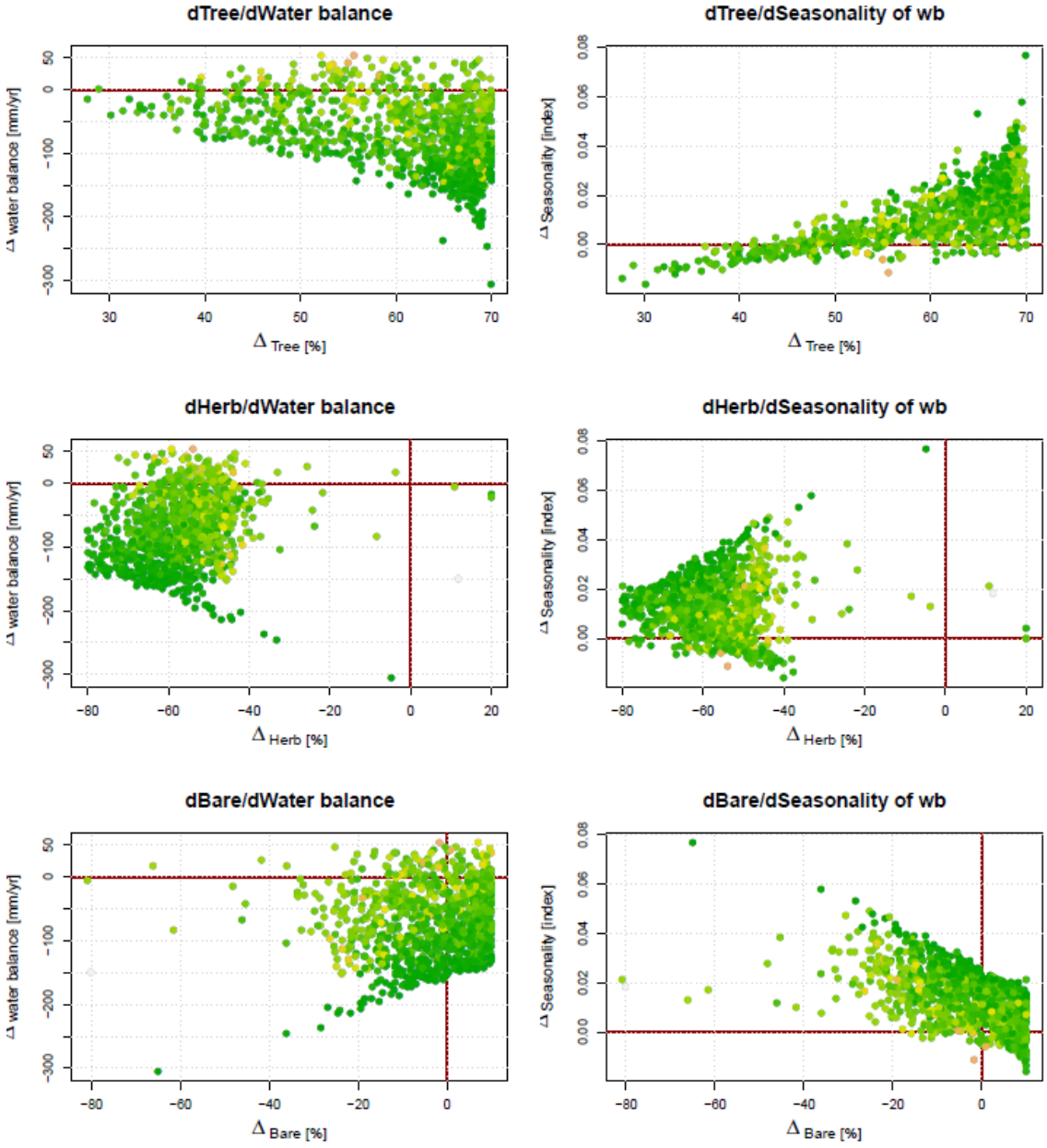

Figure VII.1 Run 1 Guadalquivir vegetation sensitivity analysis. Tree 70%, Herb 20% and Bare 10%

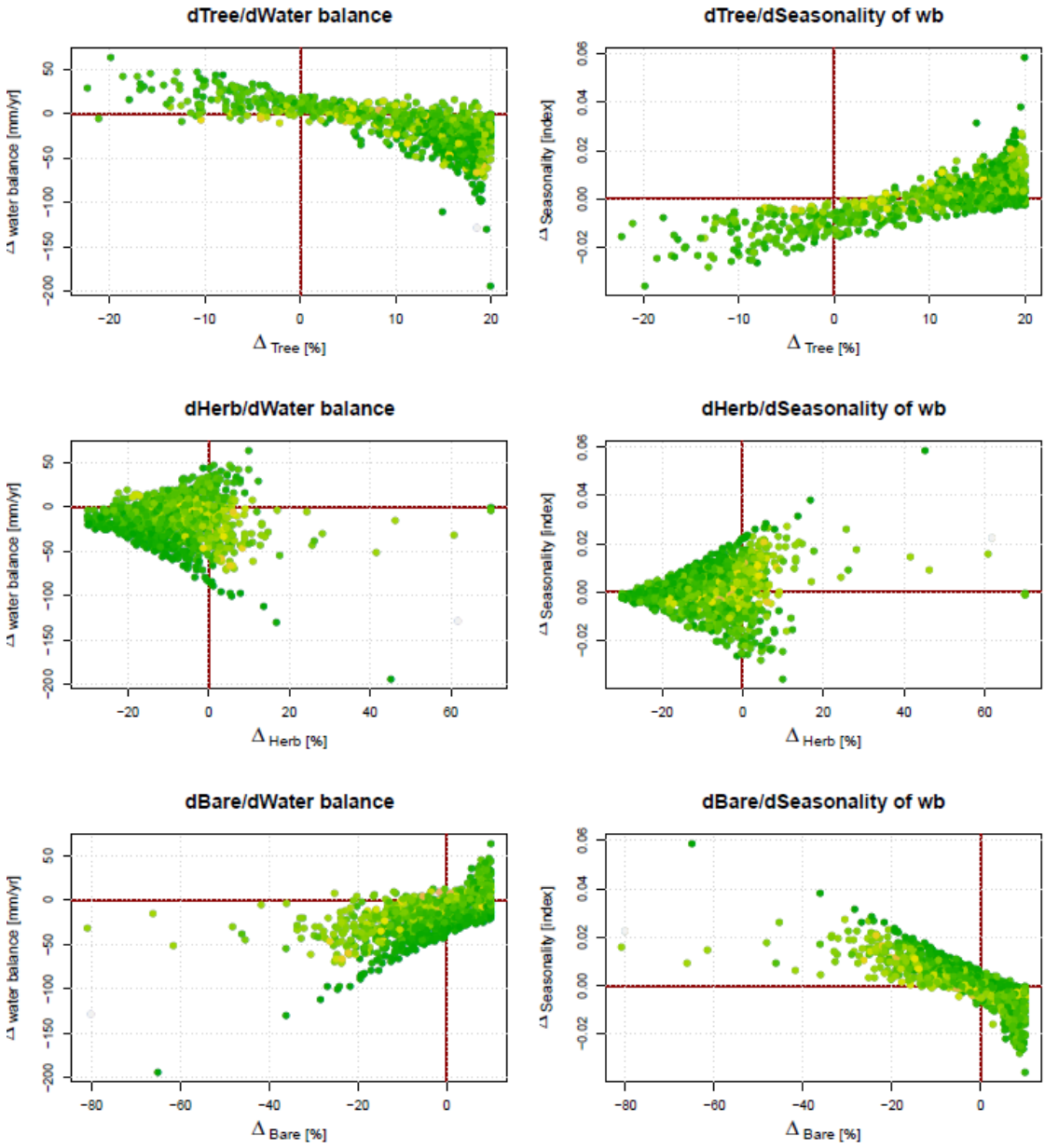

Figure VII.2 Run 2 vegetation sensitivity analysis Guadalquivir basin. Tree 20%, Herb 70% and Bare 10%

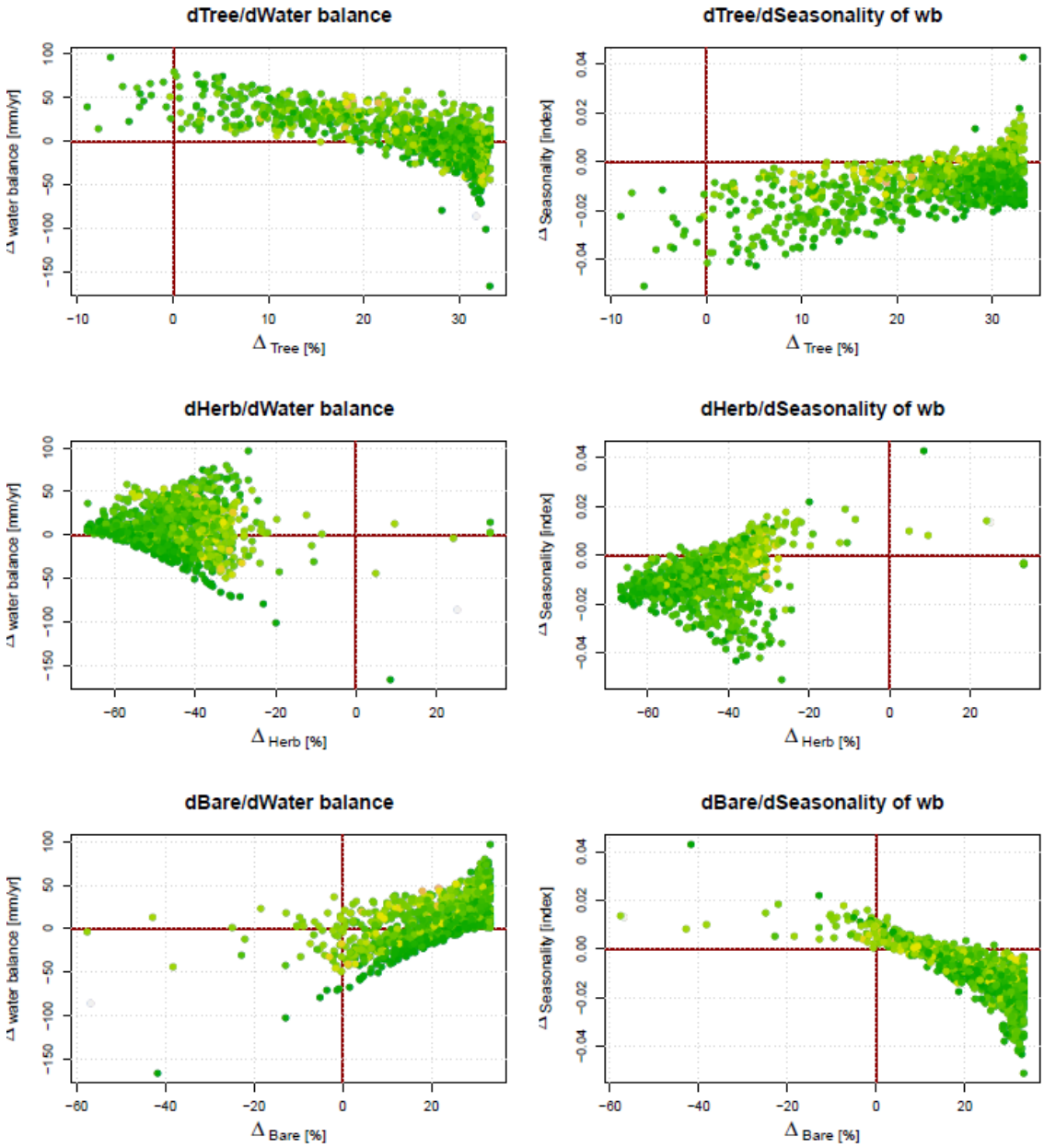

Figure VII.3 Run 3 vegetation sensitivity analysis Guadalquivir basin. Tree 33.3%, Herb 33.3% and Bare 33.3%

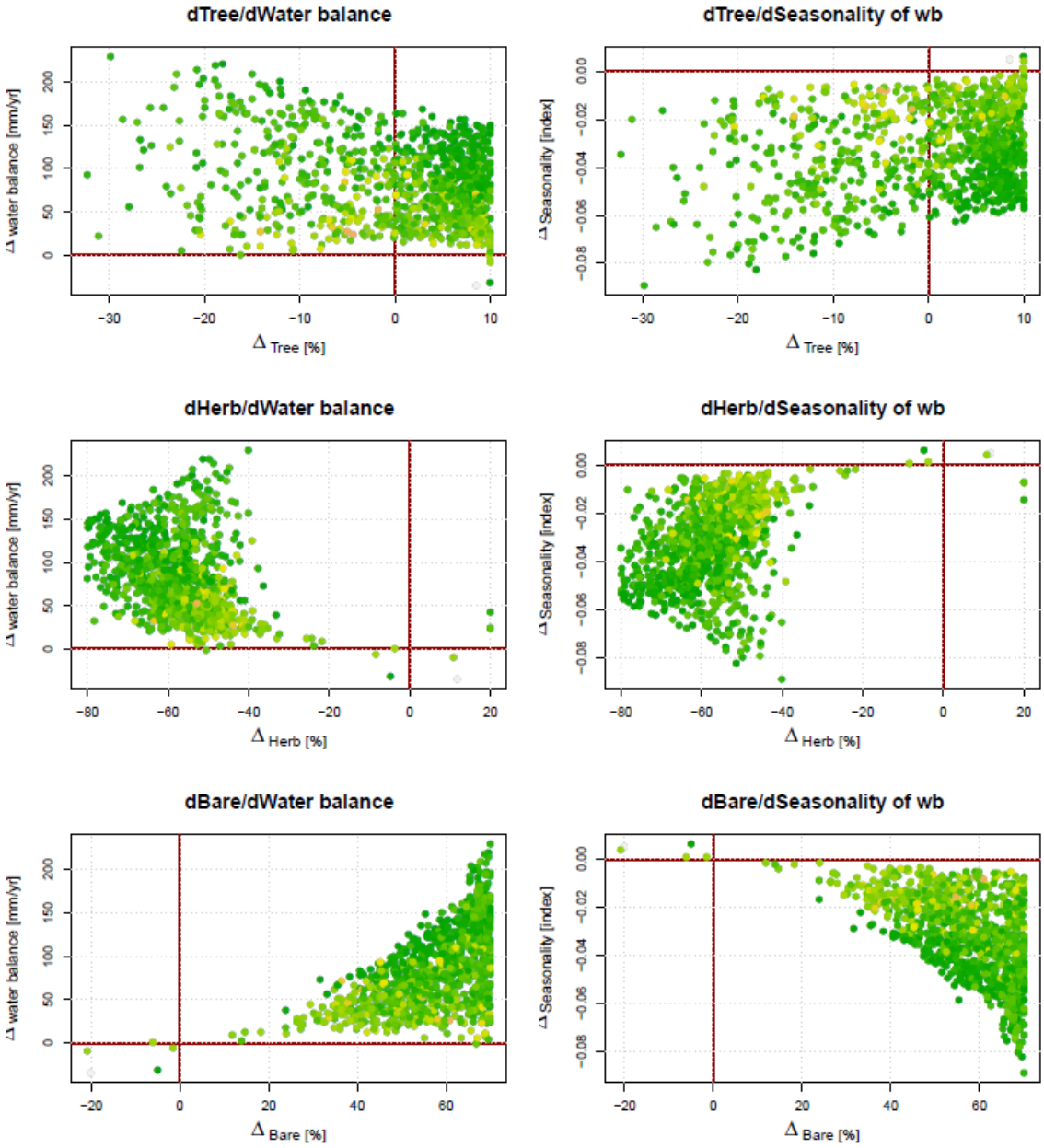

Figure VII.4 Run 4 vegetation sensitivity analysis Guadalquivir basin. Tree 10%, Herb 20% and Bare 70%

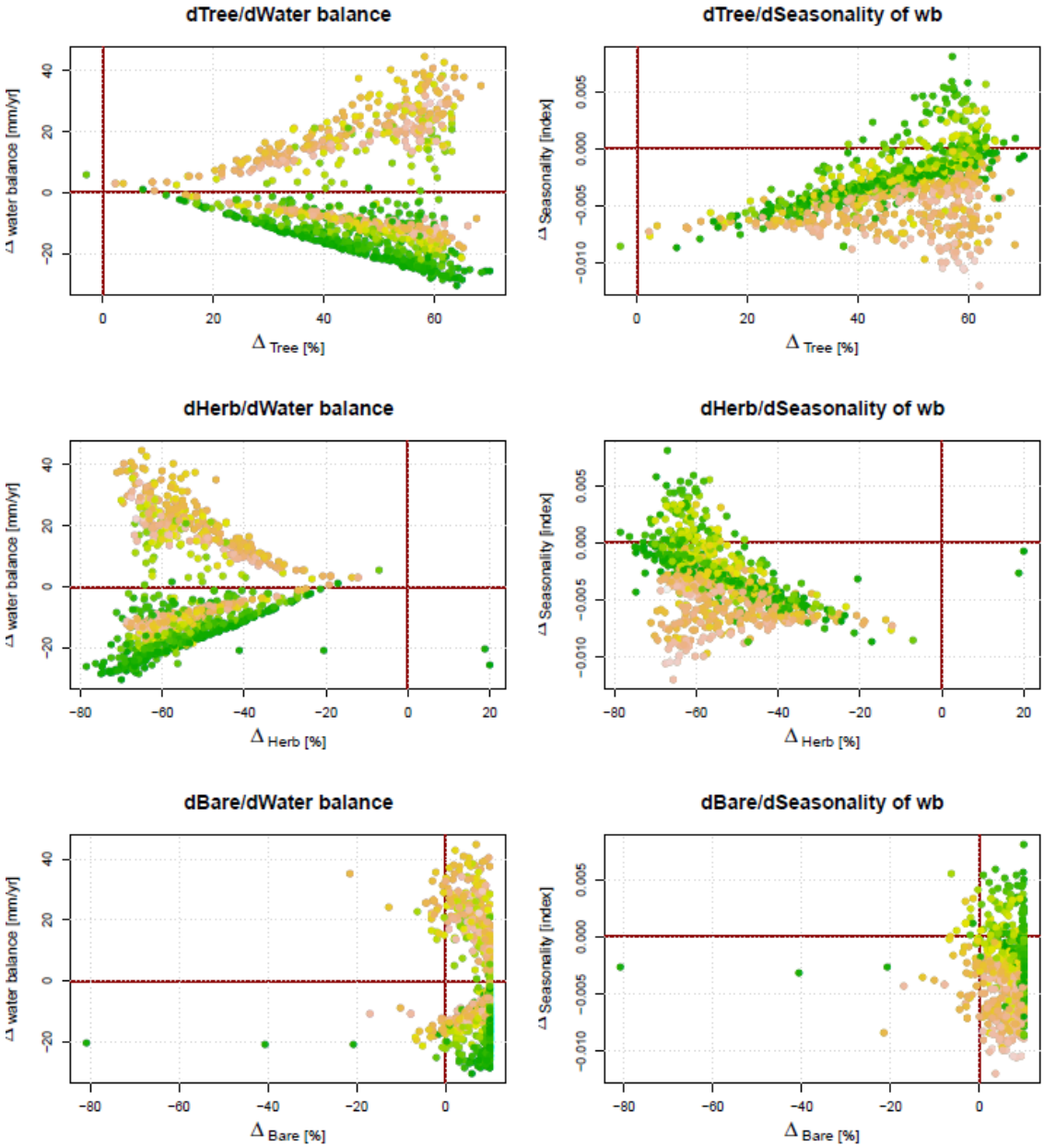

Figure VII.5 Run 1 vegetation sensitivity analysis Maputo basin. Tree 70%, Herb 20% and Bare 10%

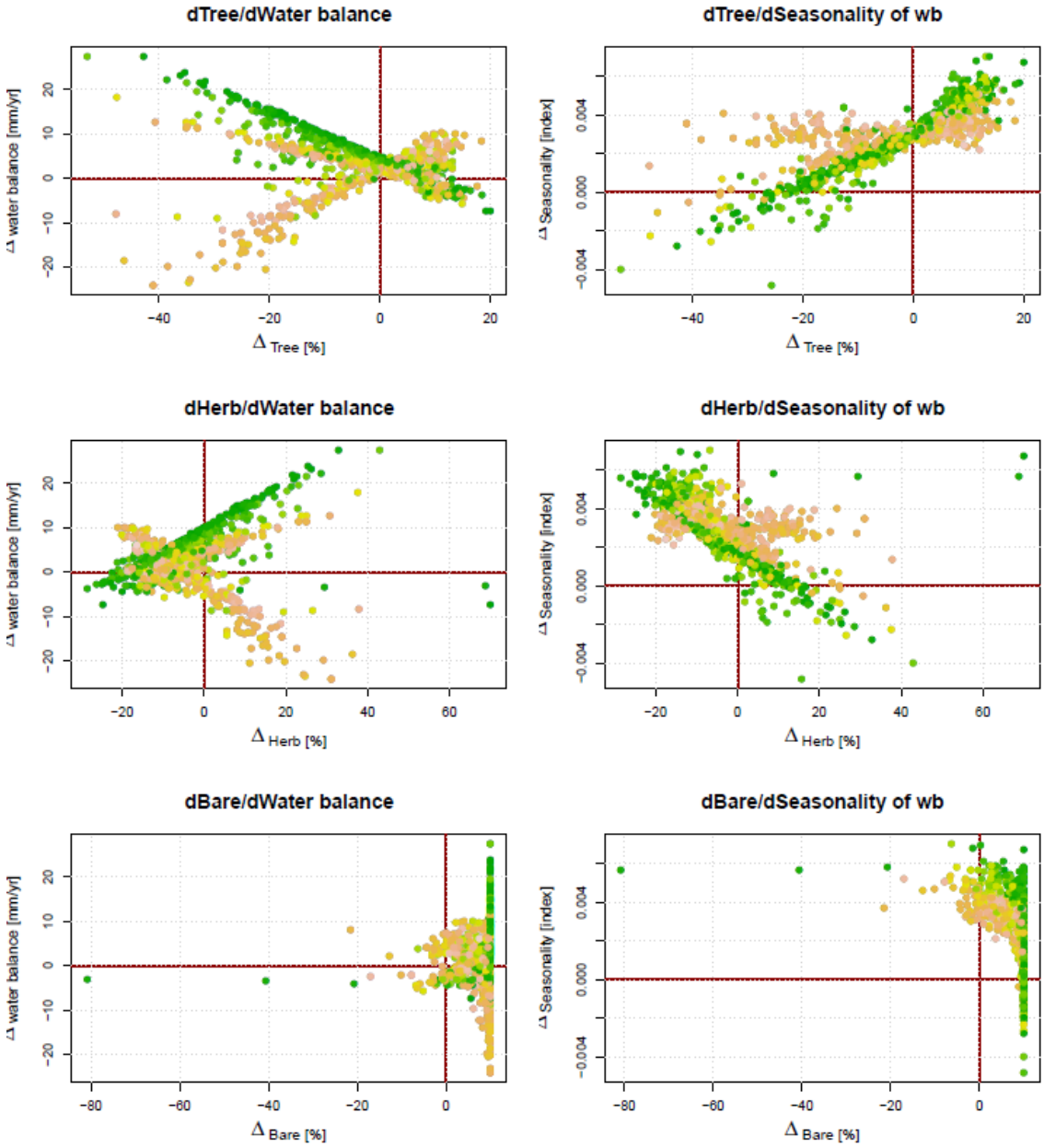

Figure VII.6 Run 2 vegetation sensitivity analysis Maputo basin. Tree 20%, Herb 70% and Bare 10%

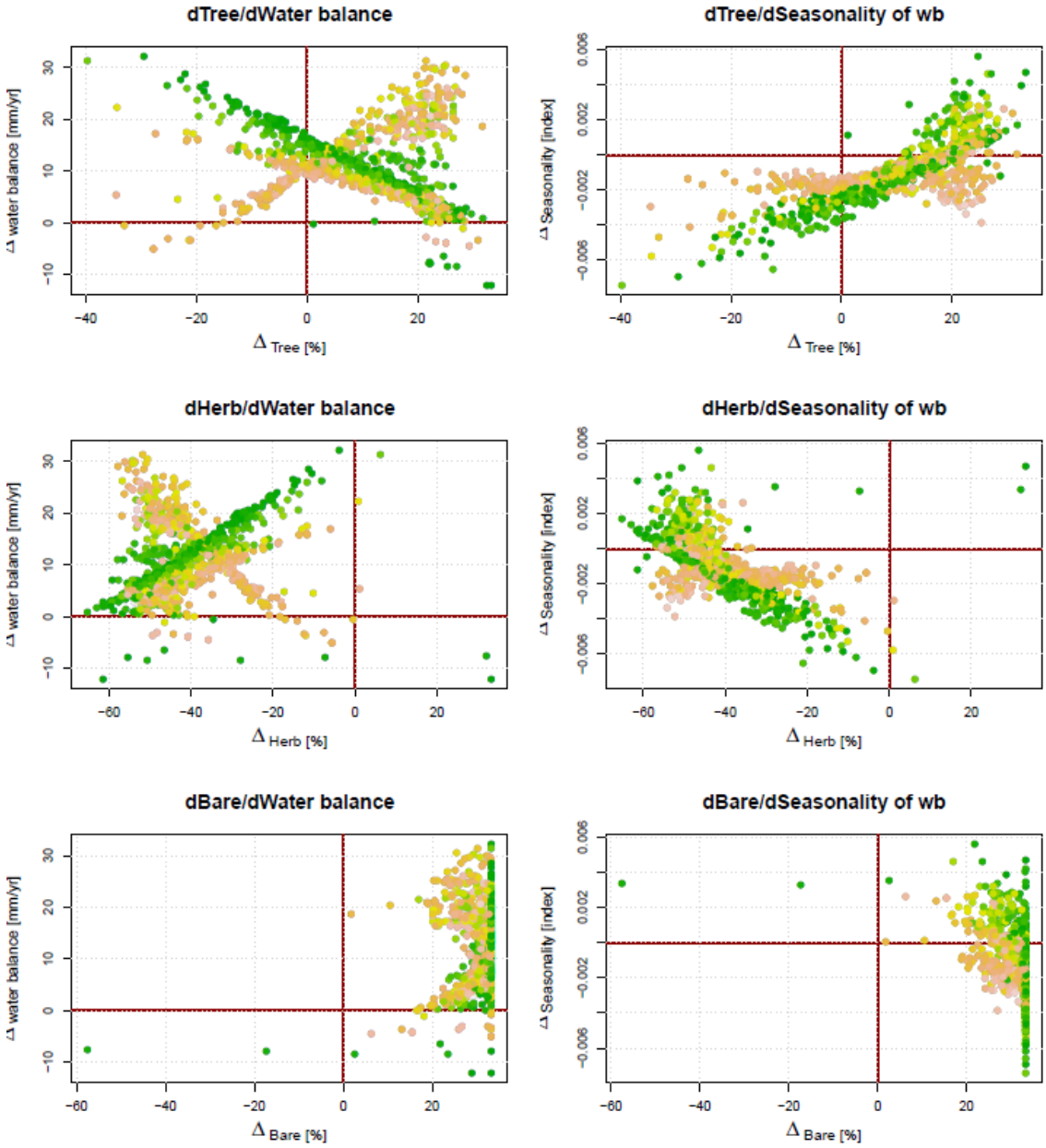

Figure VII.7 Run 3 vegetation sensitivity analysis Maputo basin. Tree 33.3%, Herb 33.3% and Bare 33.3%

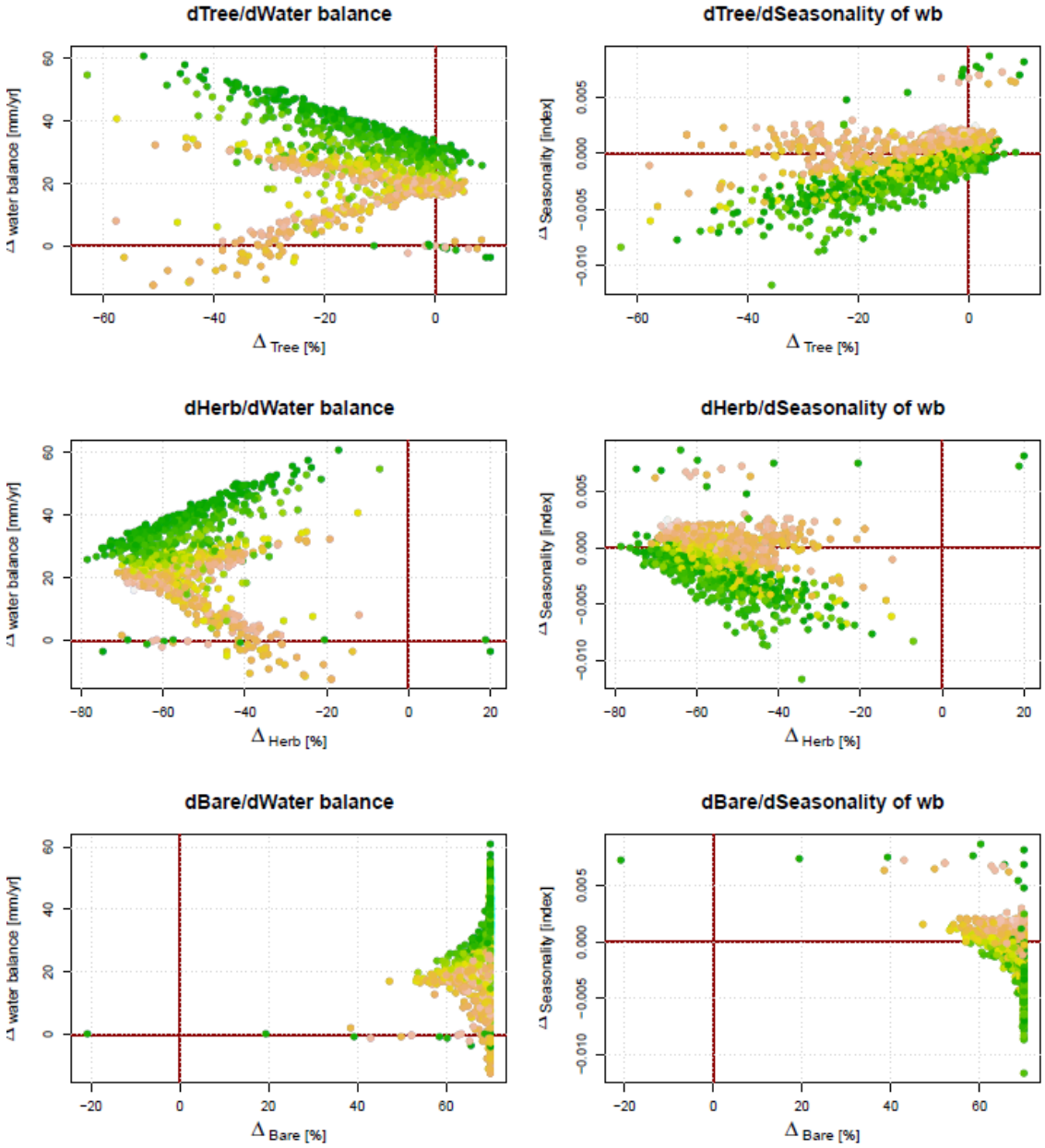

Figure VII.8 Run 4 vegetation sensitivity analysis Maputo basin. Tree 10%, Herb 20% and Bare 70%

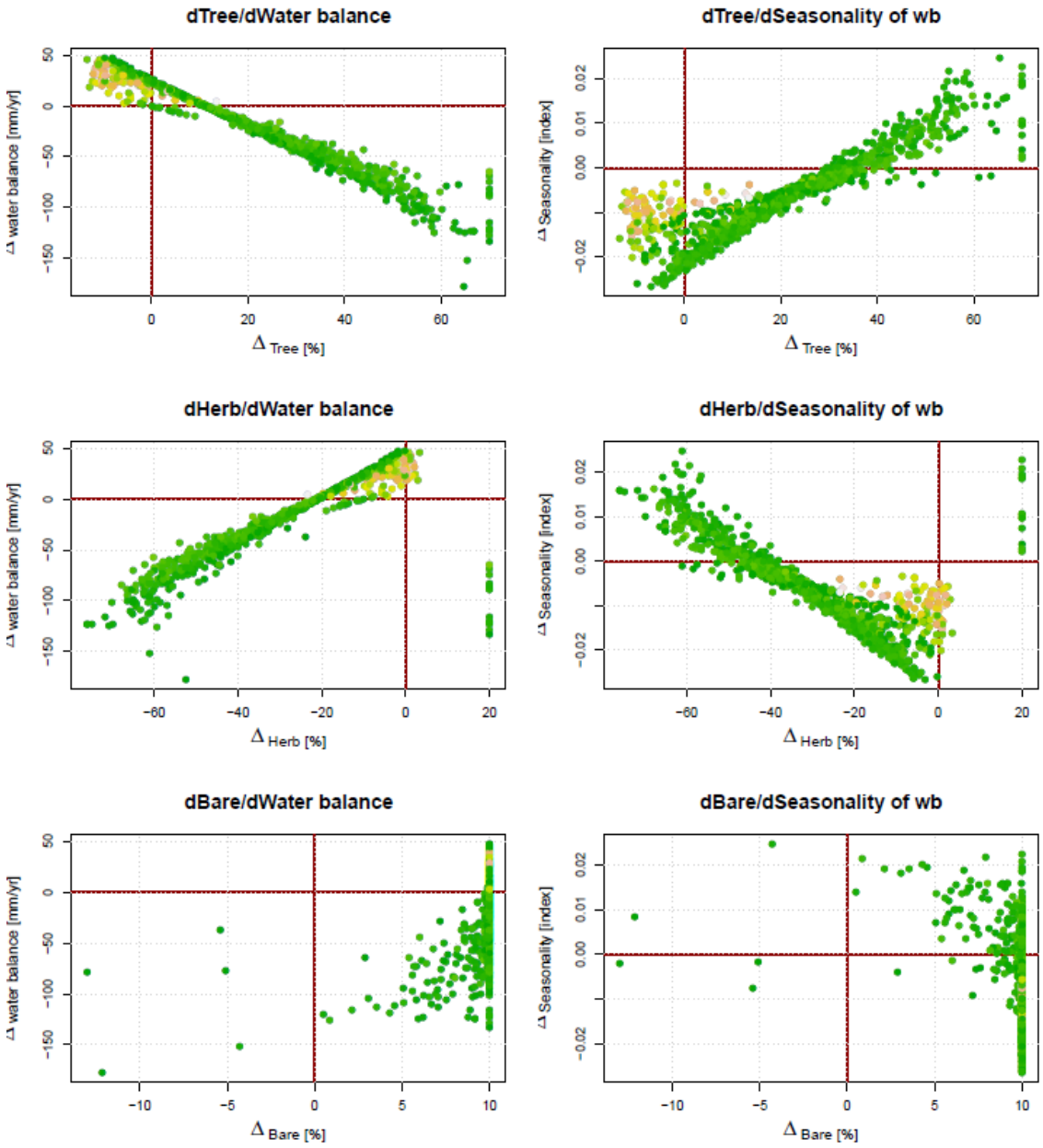

Figure VII.9 Run 1 vegetation sensitivity analysis Savannah basin. Tree 70%, Herb 20% and Bare 10%

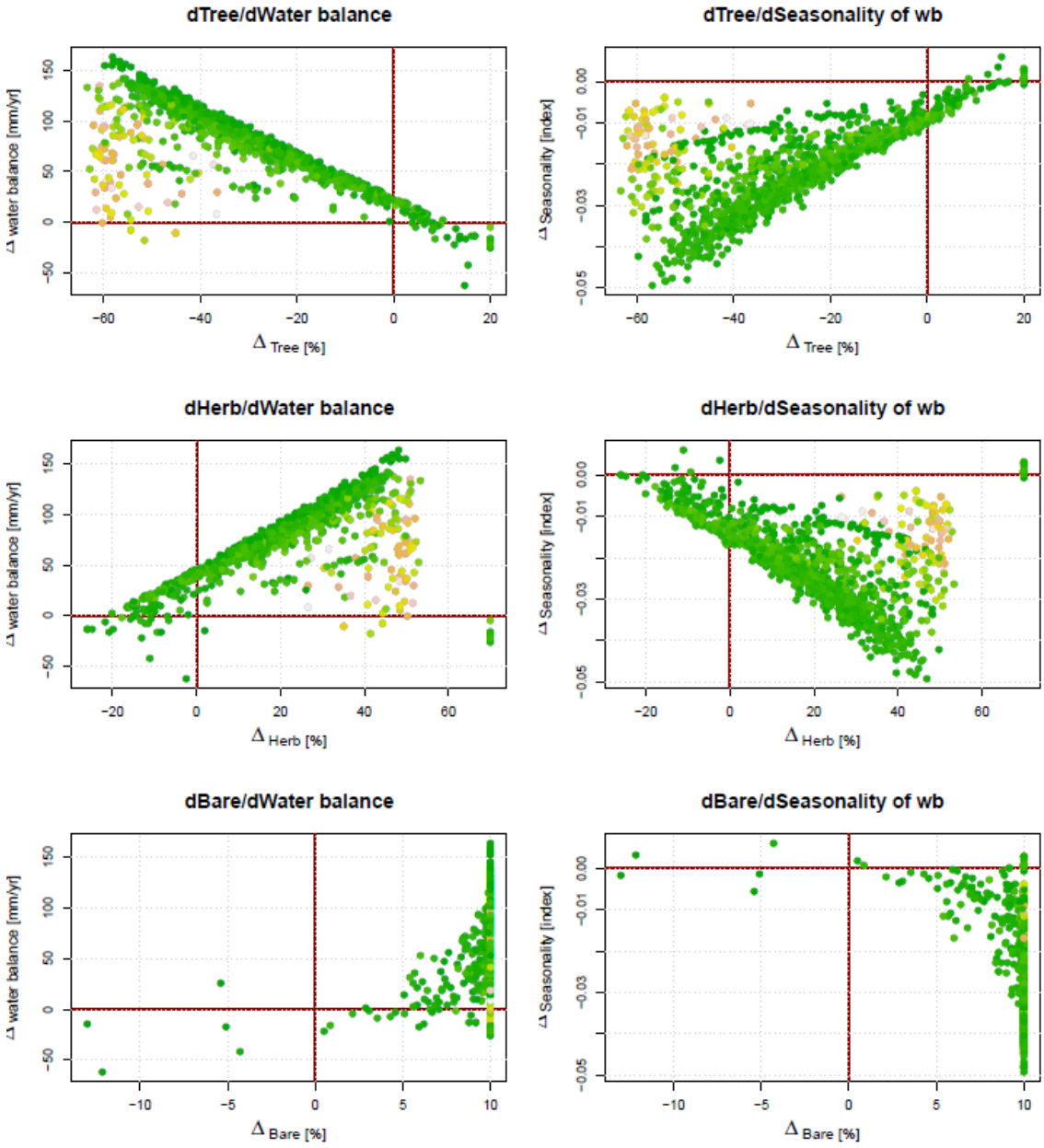

Figure VII.10 Run 2 vegetation sensitivity analysis Savannah basin. Tree 20%, Herb 70% and Bare 10%

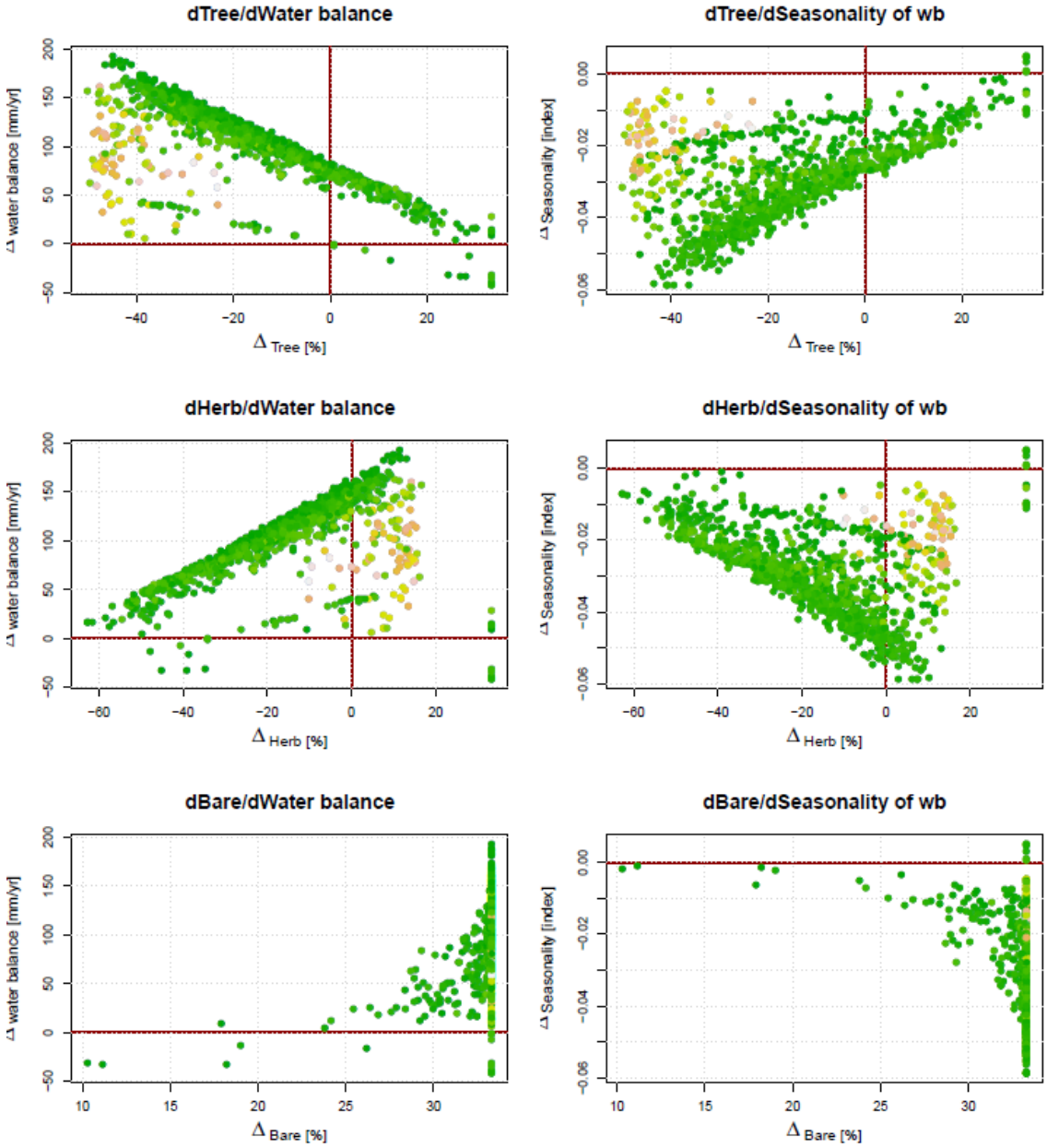

Figure VII.11 Run 3 vegetation sensitivity analysis Savannah basin. Tree 33.3%, Herb 33.3% and Bare 33.3%

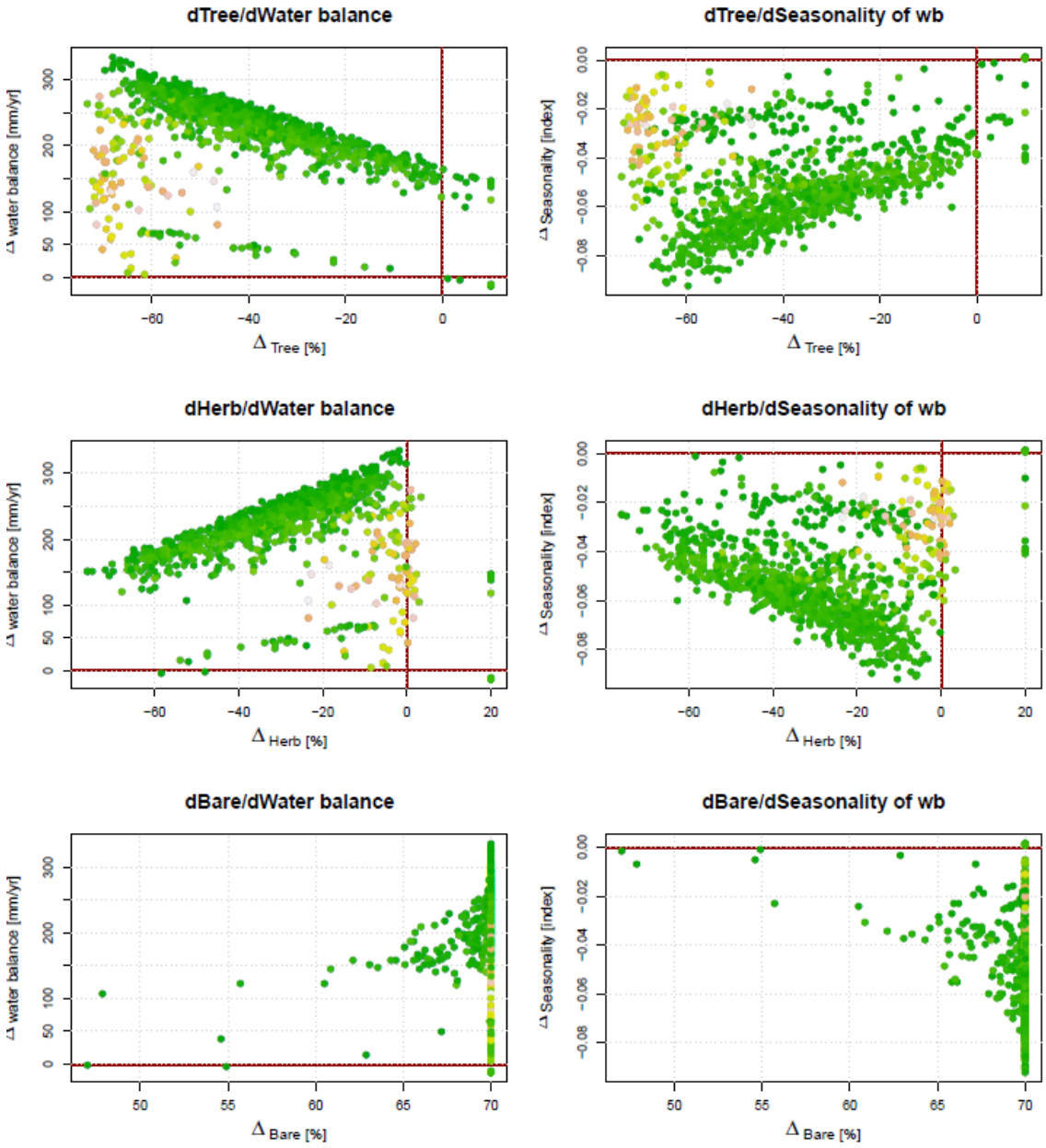

Figure VII.12 Run 4 vegetation sensitivity analysis Savannah basin. Tree 10%, Herb 20% and Bare 70%

Appendix VIII: GCM specifications

Table VII.1 Available GCMS and original resolution of the CIAT climate dataset (source: Ramirez and Jarvis, 2010)

Model	Country	Atmosphere	Ocean	Reference
BCCR-BCM2.0	Norway	T63, L31	1.5x0.5, L35	N/A
CCCMA-CGCM3.1 (T47)	Canada	T47 (3.75x3.75), L31	1.85x1.85, L29	Scinocca et al. (2008)
CCCMA-CGCM3.1 (T63)	Canada	T63 (2.8x2.8), L31	1.4x0.94, L29	Scinocca et al. (2008)
CNRM-CM3	France	T63 (2.8x2.8), L45	1.875x(0.5-2), L31	Salas-Mélia et al. (2005)
CSIRO-Mk3.0	Australia	T63, L18	1.875x0.84, L31	Gordon et al. (2002)
CSIRO-Mk3.5	Australia	T63, L18	1.875x0.84, L31	Gordon et al. (2002)
GFDL-CM2.0	USA	2.5x2.0, L24	1.0x(1/3-1), L50	Delworth et al. (2004)
GFDL-CM2.1	USA	2.5x2.0, L24	1.0x(1/3-1), L50	Delworth et al. (2004)
GISS-AOM	USA	4x3, L12	4x3, L16	Russell et al. (1995)
GISS-MODEL-EH	USA	5x4, L20	5x4, L13	Schmidt et al. (2005)
GISS-MODEL-ER	USA	5x4, L20	5x4, L13	Schmidt et al. (2005)
IAP-FGOALS1.0-G	China	2.8x2.8, L26	1x1, L16	Yu et al. (2004)
INGV-ECHAM4	Italy	T42, L19	2x(0.5-2), L31	Gualdi et al. (2006)
INM-CM3.0	Russia	5x4, L21	2.5x2, L33	Diansky et al. (2002)
IPSL-CM4	France	2.5x3.75, L19	2x(1-2), L30	Marti et al. (2005)
MIROC3.2-HIRES	Japan	T106, L56	0.28x0.19, L47	Hasumi and Emori (2004)
MIROC3.2-MEDRES	Japan	T42, L20	1.4x(0.5-1.4), L43	Hasumi and Emori (2004)
MIUB-ECHO-G	Germany/Korea	T30, L19	T42, L20	Grötzner et al. (1996)
MPI-ECHAM5	Germany	T63, L32	1x1, L41	Jungclaus et al. (2005)
MRI-CGCM2.3.2A	Japan	T42, L30	2.5x(0.5-2.0)	Yukimoto et al. (2001)
NCAR-CCSM3.0	USA	T85L26, 1.4x1.4	1x(0.27-1), L40	Collins et al. (2005)
NCAR-PCM1	USA	T42 (2.8x2.8), L18	1x(0.27-1), L40	Washington et al. (2000)
UKMO-HADCM3	UK	3.75x2.5, L19	1.25x1.25, L20	Gordon et al. (2002)
UKMO-HADGEM1	UK	1.875x1.25, L38	1.25x1.25, L20	Johns et al. (2006)